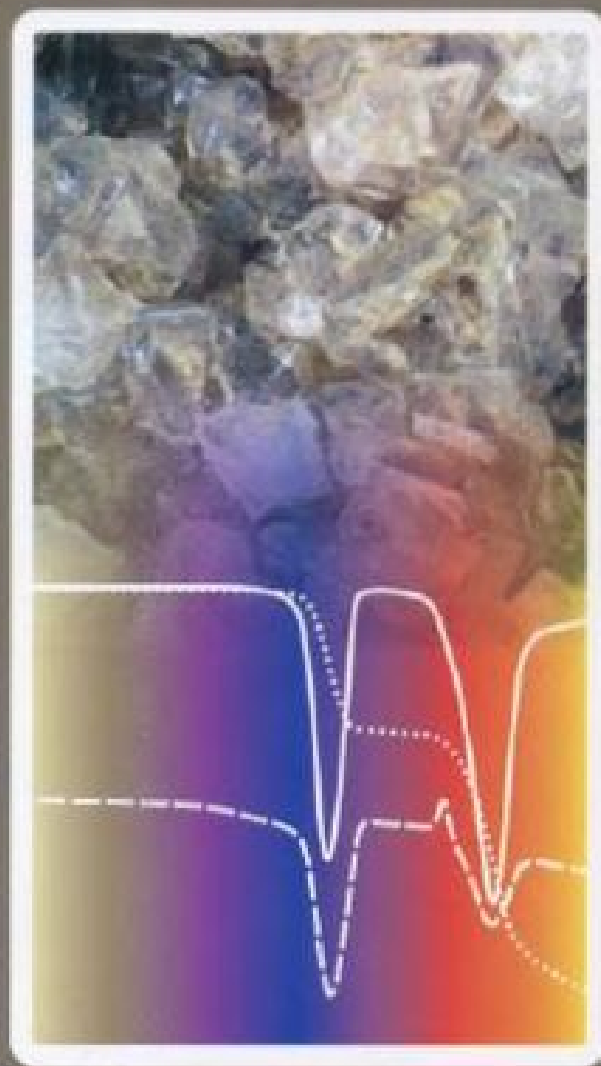


**Mária Földvári**

Handbook of  
thermogravimetric system of minerals  
and its use in geological practice



**Budapest, 2011**



Occasional Papers of the Geological Institute of Hungary,  
volume 213

# Handbook of thermogravimetric system of minerals and its use in geological practice

Mária Földvári

BUDAPEST, 2011

© Copyright Geological Institute of Hungary (Magyar Állami Földtani Intézet), 2011

All rights reserved! Minden jog fenntartva!

*Serial editor — Sorozatszerkesztő*

GYULA MAROS

*Reviewer — Lektor:*

GYÖRGY LIPTAY

*English text — Angol szöveg:*

MÁRIA FÖLDVÁRI

*Linguistic reviewer — Nyelvi lektor:*

MCINTOSH WILLIAM RICHÁRD

*Technical editor — Műszaki szerkesztő*

OLGA PIROS, DEZSŐ SIMONYI

*DTP*

DEZSŐ SIMONYI, OLGA PIROS,

*Cover design — Borítóterv*

DEZSŐ SIMONYI

*Printing house — Nyomda:*

Innova-Print Kft.

Published by the Geological Institute of Hungary — Kiadja a Magyar Állami Földtani Intézet

*Responsible editor — Felelős kiadó*

TAMÁS FANCSIK

director — igazgató

This book has been subsidized by the Committee on Publishing Scientific Books and Periodicals  
of Hungarian Academy of Sciences

A könyv a Magyar Tudományos Akadémia Könyv- és Folyóiratkiadó Bizottságának  
támogatásával készült

ISBN 978-963-671-288-4

# CONTENTS

Index of Figures .....	7
Index of Tables .....	11
Preface .....	13
<b>Measurement methods and system of thermal reaction of minerals</b> .....	15
Introduction to the thermoanalytical methods .....	16
Thermoanalytical techniques .....	16
Differential Thermal Analysis (DTA) .....	16
Thermogravimetry (TG) .....	17
Evolved Gas Analysis (EGA) .....	17
Derivative technique .....	17
Multiple techniques .....	17
Experimental conditions .....	17
Thermoanalytical parameters .....	17
Nomenclature of DTA and TG curves .....	18
Description of the shape of thermoanalytical curves (DTA, DTG) .....	19
Calibration .....	19
Temperature and DTA calibration .....	19
Evaluation of DTA peak resolution .....	20
Other materials usually used for calibration .....	20
Heat of reaction ( $\Delta H$ ) .....	20
TG calibration .....	20
DTG calibration .....	20
Effects influencing thermoanalytical curves .....	20
Standardization .....	21
Recommendations of ICTA Nomenclature Committee for reporting Thermal Analysis results .....	21
Thermogravimetric investigation techniques and methods .....	22
Techniques .....	22
Quantitative determination based on mass-change .....	22
Derivative Thermogravimetry (DTG, DDTG) .....	23
Sample controlled Thermal Analysis (or controlled rate Thermal Analysis) .....	23
Coupled simultaneous techniques, EGA methods .....	24
Methods .....	25
Calculation of virtual kinetic parameters .....	25
Corrected decomposition temperature .....	26
Supplementary methods .....	27
Characteristic thermal reactions of mineral groups .....	27
Thermal activity of minerals .....	27
System of thermal decomposition reactions .....	28
Water in minerals. Dehydration .....	28
Adsorbed water .....	29
Interlayer waters bond by phyllosilicates .....	29
“Zeolitic water” .....	36
Water in amorphous phases .....	36
Water found in completely confined internal spaces .....	37
Water bound in solid solution .....	38
Crystal hydrates (constitutional water in water-bearing carbonate, sulphate, phosphate and salt minerals) .....	38
Thermal dissociation .....	40
Other thermal reactions with mass change (sublimation, oxidation, reduction) .....	43

Other thermal reactions without mass change .....	44
Solid-phase structural decomposition .....	44
Polymorphic transition .....	44
Melting .....	45
Curie point .....	45
Solid phase reaction .....	46
<b>Thermogravimetric curves and their interpretation by stoichiometric processes of minerals .....</b>	<b>47</b>
1. Native elements .....	48
1.1. Sulphur: S .....	48
1.2. Graphite C .....	48
1.2.1. Analysis in air .....	48
1.2.2. Analysis in oxygen .....	49
2. Sulphides .....	49
2.1. Pyrite $\text{FeS}_2$ .....	52
2.2. Cinnabar $\text{HgS}$ .....	53
2.3. Galena $\text{PbS}$ .....	54
2.4. Sphalerite $\text{ZnS}$ .....	54
2.5. Other chalcogenide minerals .....	54
3. Oxides .....	55
3.1. Silica minerals .....	55
3.1.1. Quartz $\text{SiO}_2$ .....	55
3.1.2. Opal $\text{SiO}_2 \cdot n\text{H}_2\text{O}$ .....	56
3.1.3. Other silica minerals .....	56
3.2. Iron oxides .....	57
3.2.1. Magnetite $\text{Fe}_3\text{O}_4$ .....	57
3.2.2. Hematite $\text{Fe}_2\text{O}_3$ .....	57
3.2.3. "Ferrihydrite $\text{Fe}^{3+}_{4-5}(\text{OH}, \text{O})_{12} (2.5\text{Fe}_2\text{O}_3 \cdot 4.5\text{H}_2\text{O}$ or $\text{Fe}_5\text{HO}_8 \cdot 4\text{H}_2\text{O}$ )" .....	57
3.3. Manganese oxides .....	60
3.3.1. Pyrolusite $\text{MnO}_2$ .....	60
3.3.2. Other manganese oxides .....	60
3.4. Other oxides .....	61
4. Hydroxides .....	61
4.1. Simple hydroxides .....	61
4.1.1. Gibbsite $\text{Al}(\text{OH})_3$ .....	61
4.1.2. Nordstrandite $\text{Al}(\text{OH})_3$ .....	62
4.1.3. Brucite $\text{Mg}(\text{OH})_2$ .....	63
4.1.4. Portlandite $\text{Ca}(\text{OH})_2$ .....	63
4.1.5. Other simple hydroxides .....	63
4.2. Oxides containing Hydroxyl (oxyde-hydroxides) .....	64
4.2.1. Goethite $\alpha\text{-FeOOH}$ .....	64
4.2.2. Lepidocrocite $\gamma\text{-FeOOH}$ .....	65
4.2.3. Manganite $\gamma\text{-MnOOH}$ .....	65
4.2.4. Boehmite $\gamma\text{-AlOOH}$ .....	66
4.2.5. Diaspore $\alpha\text{-AlOOH}$ .....	66
4.2.6. Alumogel $\text{AlOOH} \cdot n\text{H}_2\text{O}$ .....	67
4.3. Hydroxide containing multiple cations .....	67
4.3.1. Lithiophorite $(\text{Al}, \text{Li})(\text{OH})_2 \cdot \text{MnO}_2$ .....	67
4.4. Other hydroxides .....	67
4.5. References for bauxite .....	67
5. Silicates .....	68
5.1. Phyllosilicates .....	68
5.1.1. The 1:1 layer type clay minerals .....	68
5.1.1.1. Kaolinite subgroup .....	68
5.1.1.1.1. Kaolinite (kaolinite-T) $\text{Al}_2\text{Si}_2\text{O}_5(\text{OH})_4$ .....	68
5.1.1.1.2. Dickite (kaolinite-2M) $\text{Al}_2\text{Si}_2\text{O}_5(\text{OH})_4$ .....	70
5.1.1.1.3. Fireclay (kaolinite-1M <sub>d</sub> ) $\text{Al}_2\text{Si}_2\text{O}_5(\text{OH})_4 \cdot n\text{H}_2\text{O}$ ( $n < 2$ ) .....	70
5.1.1.1.4. Halloysite $\text{Al}_2\text{Si}_2\text{O}_5(\text{OH})_4 \cdot 2\text{H}_2\text{O}$ .....	71
5.1.1.1.5. Allophane non-crystalline $m\text{Al}_2\text{O}_3 \cdot n\text{SiO}_2 \cdot p\text{H}_2\text{O}$ or $\text{Al}_2\text{O}_3 \cdot (\text{SiO}_2)_{1.3-2} \cdot (\text{H}_2\text{O})_{2.5-3}$ .....	71
5.1.1.2. Serpentine subgroup .....	72
5.1.2. 2:1 layer type clay minerals .....	74
5.1.2.1. Pyrophyllite-Talc group .....	75

5.1.2.1.1. Pyrophyllite $\text{Al}_2\text{Si}_4\text{O}_{10}(\text{OH})_2$	75
5.1.2.1.2. Talc $\text{Mg}_3\text{Si}_4\text{O}_{10}(\text{OH})_2$	76
5.1.2.2. Smectite group	76
5.1.2.2.1. Montmorillonite $(\text{Na,Ca})_{0.3}(\text{Al,Mg})_2\text{Si}_4\text{O}_{10}(\text{OH})_2 \cdot n(\text{H}_2\text{O})$	76
5.1.2.2.1.1. Ca-montmorillonite	76
5.1.2.2.1.2. Na-montmorillonite	78
5.1.2.2.1.3. "Abnormal montmorillonites"	78
5.1.2.2.2. Beidellite $(\text{Na,Ca})_{0.5}\text{Al}_2(\text{Si}_{3.5}\text{Al}_{0.5})\text{O}_{10}(\text{OH})_2 \cdot n(\text{H}_2\text{O})$	80
5.1.2.2.3. Nontronite $(\text{Na,Ca})_{0.3}\text{Fe}^{3+}_2(\text{Si,Al})_4\text{O}_{10}(\text{OH})_2 \cdot n(\text{H}_2\text{O})$	80
5.1.2.2.4. Saponite $(\text{Na,Ca})_{0.3}(\text{Mg,Fe}^{2+})_3(\text{Si,Al})_4\text{O}_{10}(\text{OH})_2 \cdot 4(\text{H}_2\text{O})$	80
5.1.2.3. Vermiculite group $(\text{Mg,Fe}^{2+},\text{Al})_3(\text{Al,Si})_4\text{O}_{10}(\text{OH})_2 \cdot n(\text{H}_2\text{O})$	81
5.1.2.4. Mica group	82
5.1.2.4.1. Muscovite $\text{KAl}_2[\text{AlSi}_3\text{O}_{10}(\text{OH,F})_2]$	82
5.1.2.4.2. Biotite $\text{K}(\text{Mg,Fe}^{2+})_3[\text{AlSi}_3\text{O}_{10}](\text{OH,F})_2$	82
5.1.2.5. Hydromica (clay-mica, interlayer-deficient mica) group	83
5.1.2.5.1. Illite $\text{K}_{0.65}[\text{Al,Mg,Fe}]_2\text{Al}_{0.65}\text{Si}_{3.35}\text{O}_{10}(\text{OH})_2 \cdot \text{H}_2\text{O}$ or $(\text{K,H}_3\text{O})\text{Al}_2(\text{Si}_3\text{Al})\text{O}_{10}(\text{H}_2\text{O,OH})_2$	83
5.1.2.5.2. Hydromuscovite (sericite)	84
5.1.2.5.3. Glauconite $(\text{K,Na})(\text{Fe}^{3+},\text{Al,Mg})_2(\text{Si,Al})_4\text{O}_{10}(\text{OH})_2 \cdot \text{H}_2\text{O}$	84
5.1.2.6. Chlorite group (2:1 layer with interlayer hydroxide sheet/ or 2:1:1/or 2:2 layer type)	85
5.1.2.7. Interstratified or mixed-layer minerals	86
5.1.2.7.1. Regularly interstratified minerals	86
5.1.2.7.1.1. Rectorite (1:1 interstratification of dioctahedral paragonite-smectite) $(\text{Na,Ca})\text{Al}_4(\text{Si,Al})_8\text{O}_{20}(\text{OH})_4 \cdot 2\text{H}_2\text{O}$	86
5.1.2.7.1.2. Tosudite (1:1 interstratification of dioctahedral chlorite-smectite)	86
5.1.2.7.2. Randomly interstratified minerals	87
5.1.2.7.2.1. Illite-montmorillonite	87
5.1.2.7.2.2. Chlorite-vermiculite	87
5.1.2.7.2.3. Talc-saponite	87
5.1.2.8. Pseudo-layer silicates	88
5.1.2.8.1. Palygorskite $[(\text{Mg,Al,Fe})_2\text{Si}_4\text{O}_{10}(\text{OH}) \cdot 4\text{H}_2\text{O}]$	88
5.1.2.8.2. Sepiolite $\text{Mg}_4\text{Si}_6\text{O}_{15}(\text{OH})_2 \cdot 6(\text{H}_2\text{O})$	89
5.1.2.9. Phyllosilicate two-dimensional infinite sheets with other than six-membered rings	89
5.1.2.9.1. Apophyllite $\text{KCa}_4(\text{Si}_4\text{O}_{10})_2(\text{F,OH}) \cdot 8(\text{H}_2\text{O})$	89
5.1.2.9.2. Prehnite $\text{Ca}_2\text{Al}_2\text{Si}_3\text{O}_{10}(\text{OH})_2$	90
5.1.2.9.3. Tobermorite $\text{Ca}_3(\text{OH})_2\text{Si}_6\text{O}_{16} \cdot 4\text{H}_2\text{O}$	90
5.2. Nesosilicates	91
5.2.1. Topaz $\text{Al}_2\text{SiO}_4(\text{F,OH})_2$	91
5.2.2. Epidote $\text{Ca}_2(\text{Fe}^{3+},\text{Al})\text{Al}_2(\text{SiO}_4)(\text{Si}_2\text{O}_7)\text{O}(\text{OH})$	91
5.2.3. Vesuvianite $\text{Ca}_{10}(\text{Mg,Fe})_2\text{Al}_4(\text{SiO}_4)_5(\text{Si}_2\text{O}_7)_2(\text{OH,F})_4$	92
5.2.4. Zunyite $\text{Al}_{13}\text{Si}_5\text{O}_{20}(\text{OH,F})_{18}\text{Cl}$	92
5.2.5. Katoite $\text{Ca}_3\text{Al}_2(\text{SiO}_4)_3 \cdot \text{Ca}_2\text{Al}_2(\text{OH})_{12}$	93
5.3. Sorosilicates (and Cyclosilicates)	93
5.3.1. Hemimorphite $\text{Zn}_4((\text{Si}_2\text{O}_7)(\text{OH})_2 \cdot \text{H}_2\text{O})$	93
5.3.2. Axinite $\text{Ca}_2(\text{Fe}^{2+},\text{Mg,Mn})\text{Al}_2\text{BO}_3\text{Si}_4\text{O}_{12}(\text{OH})$	93
5.3.3. Tourmaline $((\text{Na,Ca})(\text{Li,Mg,Fe}^{2+}\text{Al})_3(\text{Al,Fe}^{3+})_6(\text{B}_3\text{Si}_6\text{O}_{27}(\text{O,OH,F})_4)$	94
5.4. Inosilicates	94
5.4.1. Amphiboles $(\text{Ca,Na,K})_{0-3}[(\text{Mg,Fe,Mn,Al,Ti})_{5-7}(\text{Si,Al})_8\text{O}_{22}(\text{O,OH,F})_2]$	94
5.4.2. Charoite $\text{K}_5\text{Ca}_8(\text{Si}_6\text{O}_{15})_2(\text{Si}_2\text{O}_7)\text{Si}_4\text{O}_9(\text{OH,F}) \cdot 3(\text{H}_2\text{O})$	94
5.5. Tectosilicates	95
5.5.1. Zeolites	95
5.5.1.1. Zeolites with Chains of 4-membered rings, $\text{Al}_2\text{Si}_2\text{O}_{10}$	95
5.5.1.1.1. Natrolite $\text{Na}_2[\text{Al}_2\text{Si}_3\text{O}_{10}] \cdot 2\text{H}_2\text{O}$	95
5.5.1.1.2. Gonnardite (tetranatrolite) $(\text{Na,Ca})_{6-8}[(\text{Al,Si})_{20}\text{O}_{40}] \cdot 12\text{H}_2\text{O}$	96
5.5.1.1.3. Mesolite $\text{Na}_2\text{Ca}_2[\text{Al}_6\text{Si}_9\text{O}_{30}] \cdot 8\text{H}_2\text{O}$	96
5.5.1.1.4. Thomsonite $\text{NaCa}_2[\text{Al}_5\text{Si}_5\text{O}_{20}] \cdot 6\text{H}_2\text{O}$	97
5.5.1.1.5. Scolecite $\text{Ca}[\text{Al}_2\text{Si}_3\text{O}_{10}] \cdot 3\text{H}_2\text{O}$	98
5.5.1.1.6. Edingtonite $\text{Ba}[\text{Al}_2\text{Si}_3\text{O}_{10}] \cdot 4\text{H}_2\text{O}$	98
5.5.1.2. Zeolites with chains of single connected 4-membered rings	98
5.5.1.2.1. Analcime $\text{Na}[\text{AlSi}_2\text{O}_6] \cdot \text{H}_2\text{O}$	98
5.5.1.2.2. Laumontite $\text{Ca}[\text{Al}_2\text{Si}_4\text{O}_{12}] \cdot 4-4.5\text{H}_2\text{O}$ (fully hydrated laumontite)	99
5.5.1.3. Zeolites with chains of double-connected 4-membered rings	100

5.5.1.3.1. Gismondine $\text{Ca}[\text{Al}_2\text{Si}_2\text{O}_8] \cdot 4.4\text{--}4.5\text{H}_2\text{O}$	100
5.5.1.3.2. Phillipsite $(\text{K}, \text{Na}, \text{Ca})_4[(\text{Si}, \text{Al})_{16}\text{O}_{32}] \cdot 12\text{H}_2\text{O}$	100
5.5.1.3.3. Harmotome $\text{Ba}_2(\text{Ca}_{0.5}\text{Na})[\text{Al}_6\text{Si}_{10}\text{O}_{32}] \cdot 12\text{H}_2\text{O}$	101
5.5.1.4. Zeolites with chains of 5-membered rings	101
5.5.1.4.1. Mordenite $(\text{Na}, \text{Ca}, \text{K})_6[\text{AlSi}_5\text{O}_{12}]_8 \cdot 28\text{H}_2\text{O}$	101
5.5.1.5. Zeolites with sheets of 4–4–1–1 structural units	102
5.5.1.5.1. Heulandite $(\text{Ca}, \text{Na}, \text{K}, \text{Sr})_9[(\text{Si}, \text{Al})_{36}\text{O}_{72}] \cdot n\text{H}_2\text{O}$ ( $n=22\text{--}26$ )	102
5.5.1.5.2. Clinoptilolite $(\text{K}, \text{Na}, \text{Ca})_6[(\text{Si}, \text{Al})_{36}\text{O}_{72}] \cdot n\text{H}_2\text{O}$ ( $n=20\text{--}24$ )	103
5.5.1.5.3. Stilbite $(\text{Na}, \text{Ca})_9[\text{Si}, \text{Al}]_{36}\text{O}_{72} \cdot 27\text{--}30\text{H}_2\text{O}$	104
5.5.1.6. Zeolites with cages and double cages of 4-, 6- and 8-membered rings.	104
5.5.1.6.1. Gmelinite $\text{Na}_8[\text{Al}_8\text{Si}_{16}\text{O}_{48}] \cdot 21.5\text{H}_2\text{O}$ or $\text{K}_8[\text{Al}_8\text{Si}_{16}\text{O}_{48}] \cdot 23.5\text{H}_2\text{O}$ or $\text{Ca}_4[\text{Al}_8\text{Si}_{16}\text{O}_{48}] \cdot 23.5\text{H}_2\text{O}$	104
5.5.1.6.2. Erionite $\text{Na}_{10}[\text{Al}_{10}\text{Si}_{26}\text{O}_{72}] \cdot 24.6\text{H}_2\text{O}$ or $\text{K}_{10}[\text{Al}_{10}\text{Si}_{26}\text{O}_{72}] \cdot 32\text{H}_2\text{O}$ or $\text{Ca}_5[\text{Al}_{10}\text{Si}_{26}\text{O}_{72}] \cdot 31\text{H}_2\text{O}$	105
5.5.1.6.3. Chabasite $(\text{Ca}_{0.5}, \text{Na}, \text{K})_4[\text{Al}_4\text{Si}_8\text{O}_{24}] \cdot 12\text{H}_2\text{O}$	105
5.5.1.6.4. Faujasite $(\text{Na}, \text{Ca}, \text{Mg})_2[(\text{Si}, \text{Al})_{12}\text{O}_{24}] \cdot n\text{H}_2\text{O}$ ( $n \approx 16$ )	106
5.5.1.7. Thermoanalytical data of other zeolites	106
5.5.2. Other tectosilicates	107
6. Carbonates	107
6.1. Water free simple carbonates	107
6.1.1. Calcite $\text{CaCO}_3$	108
6.1.2. Magnesite $\text{MgCO}_3$	109
6.1.3. Rhodochrosite $\text{MnCO}_3$	109
6.1.4. Siderite $\text{FeCO}_3$	109
6.1.5. Cerussite $\text{PbCO}_3$	110
6.2. Water free double carbonates	111
6.2.1. Dolomite $\text{MgCa}(\text{CO}_3)_2$	111
6.2.2. Huntite $\text{Mg}_3\text{Ca}(\text{CO}_3)_4$	113
6.2.3. Ankerite (real) $(\text{Mg} > \text{Fe}), \text{Ca}(\text{CO}_3)_2$	114
6.2.4. Ferrous dolomite	114
6.2.5. Kutnahorite (real) generally $(\text{Mn} > \text{Mg}, \text{Ca}, \text{Fe}), \text{Ca}(\text{CO}_3)_2$	115
6.3. Waterfree carbonates without additional anions	116
6.3.1. Kalicinite $\text{KHCO}_3$	116
6.3.2. Teschemacherite $(\text{NH}_4)\text{HCO}_3$	116
6.4. Waterfree carbonates with additional anions	117
6.4.1. Malachite $\text{Cu}_2(\text{OH})_2\text{CO}_3$	117
6.4.2. Azurite $\text{Cu}_3((\text{OH})\text{CO}_3)_2$	117
6.4.3. Dawsonite $\text{Na}_3\text{Al}(\text{CO}_3)_3 \cdot 2\text{Al}(\text{OH})_3$	117
6.5 Water-bearing carbonates	117
6.5.1. Nesquehonite $\text{MgCO}_3 \cdot 3\text{H}_2\text{O}$ or $\text{Mg}(\text{HCO}_3)(\text{OH}) \cdot 2(\text{H}_2\text{O})$	117
6.5.2. Hydromagnesite $3\text{MgCO}_3 \cdot \text{Mg}(\text{OH})_2 \cdot 3\text{H}_2\text{O}$	118
6.5.3. Dypingite $\text{Mg}_5(\text{CO}_3)_4(\text{OH})_2 \cdot 5\text{H}_2\text{O}$	118
6.5.4. Hydrotalcite $\text{Mg}_6\text{Al}_2(\text{CO}_3)(\text{OH})_{16} \cdot 4(\text{H}_2\text{O})$	118
6.6. Other carbonates	119
7. Sulphates	121
7.1. Waterfree sulfates	122
7.1.1. Mascagnite $(\text{NH}_4)_2\text{SO}_4$	122
7.2. Water-bearing sulfates with mono cation	122
7.2.1. Chalcantite $\text{CuSO}_4 \cdot 5\text{H}_2\text{O}$	122
7.2.2. Melanterite $\text{FeSO}_4 \cdot 7\text{H}_2\text{O}$	123
7.2.3. Rozenite $\text{FeSO}_4 \cdot 4\text{H}_2\text{O}$	123
7.2.4. Szomolnokite $\text{FeSO}_4 \cdot \text{H}_2\text{O}$	124
7.2.5. Alunogen $\text{Al}_2(\text{SO}_4)_3 \cdot 17\text{H}_2\text{O}$	124
7.2.6. Hexahydrate $\text{MgSO}_4 \cdot 6\text{H}_2\text{O}$	124
7.2.7. Gypsum $\text{CaSO}_4 \cdot 2\text{H}_2\text{O}$	125
7.3. Water-bearing sulfates with several different cations	125
7.3.1. Römerite $\text{Fe}^{2+}\text{Fe}^{3+}_2(\text{SO}_4)_4 \times 14\text{H}_2\text{O}$	125
7.3.2. Voltaite $\text{K}_2\text{Fe}^{2+}_2\text{Fe}^{3+}_3\text{Al}(\text{SO}_4)_{12} \cdot 18(\text{H}_2\text{O})$	126
7.3.3. Halotrichite $\text{Fe}^{2+}\text{Al}_2(\text{SO}_4)_4 \cdot 22(\text{H}_2\text{O})$	126
7.3.4. Potassium-alum $\text{KAl}(\text{SO}_4)_2 \cdot 12\text{H}_2\text{O}$	126
7.3.5. Tschermigite $(\text{NH}_4)\text{Al}(\text{SO}_4)_2 \cdot 12\text{H}_2\text{O}$	127
7.4. Waterfree sulfates with additional anions	127
7.4.1. Alunite $\text{KAl}_3(\text{SO}_4)_2(\text{OH})_6$	127

7.4.2. Jarosite $\text{KFe}_3(\text{SO}_4)_2(\text{OH})_6$ .....	128
7.5. Water-bearing sulfates with additional anions .....	128
7.5.1. Aluminite $\text{Al}_2(\text{SO}_4)(\text{OH})_4 \cdot 7\text{H}_2\text{O}$ .....	128
7.5.2. Fibroferrite $\text{Fe}^{3+}(\text{SO}_4)(\text{OH}) \cdot 5\text{H}_2\text{O}$ .....	129
7.5.3. Copiapite $(\text{Fe}^{2+}, \text{Mg})(\text{Fe}^{3+}, \text{Al})_4(\text{SO}_4)_6(\text{OH})_2 \cdot 20\text{H}_2\text{O}$ .....	129
8. Phosphates, arsenates, vanadates .....	130
8.1. Hydrated phosphates .....	130
8.1.1. Vivianite $\text{Fe}^{2+}_3(\text{PO}_4)_2 \cdot 8\text{H}_2\text{O}$ .....	130
8.2. Anhydrous phosphates containing hydroxyl .....	130
8.2.1. Lazulite $(\text{Mg}, \text{Fe})\text{Al}_2(\text{PO}_4)_2(\text{OH})_2$ .....	130
8.2.2. Gorceixite $\text{BaAl}_3(\text{PO}_4)(\text{PO}_3\text{OH})(\text{OH})_6$ .....	131
8.3. Water-bearing phosphates with additional anions .....	131
8.3.1. Diadochite $\text{Fe}^{3+}_2(\text{PO}_4)(\text{SO}_4)(\text{OH}) \cdot 6\text{H}_2\text{O}$ .....	131
8.4. Hydrated arsenates .....	132
8.4.1. Kaňkite $\text{Fe}^{3+}\text{AsO}_4 \cdot 3.5\text{H}_2\text{O}$ .....	132
9. Borates .....	133
10. Halides .....	133
10.1. Halite $\text{NaCl}$ .....	133
10.2. Bischofite $\text{MgCl}_2 \cdot 6\text{H}_2\text{O}$ .....	134
11. Organic minerals .....	134
11.1. Whewellite $\text{Ca}(\text{C}_2\text{O}_4) \cdot \text{H}_2\text{O}$ (calcium oxalate monohydrate) .....	134
11.2. Humboldtine (Oxalite) $\text{Fe}^{2+}(\text{C}_2\text{O}_4) \cdot 2\text{H}_2\text{O}$ .....	134
12. Organic materials .....	135
12.1. Determination of the coalification of organic matter content of the sample .....	135
12.2. Proximate (immediate) analysis of coal .....	135
13. Investigation of rocks .....	136
13.1. Perlite .....	136
13.2. Phase analysis .....	137
14. Special geological applications .....	138
References .....	141
Mineral and rock indexes .....	177

## Index of Figures

Figure 1. Formalized DTA curve .....	18
Figure 2. Formalized TG curve .....	18
Figure 3. Determination of peak resolution .....	20
Figure 4. TG curve of calcite (Triassic limestone, Gerecse Mts, Hungary) .....	22
Figure 5. TG base line and TG curves of $\text{CuSO}_4 \cdot 5\text{H}_2\text{O}$ (after BALCEROVIAK 1988) .....	23
Figure 6. TG and DTG curves of the dehydration of $\text{CuSO}_4 \cdot 5\text{H}_2\text{O}$ .....	23
Figure 7. Separation of the overlapped reactions of boehmite and kaolinite by DDTG (bauxite, Nyirád, Hungary) .....	23
Figure 8. Separation of the overlapped reactions of boehmite and kaolinite by Q-DTG (bauxite, Nyirád, Hungary) .....	23
Figure 9. Separation of the overlapping reactions of kaolinite and siderite by thermo-gas-titrimetric determination of siderite .....	24
Figure 10. a)DEGAS — thermogravimetry in vacuum and release of $\text{CO}_2$ , water and hydrocarbons of a kaoline from Washington County, b) TG-DTG plot of a kaolin sample (K2) in He and air at a heating rate of $20^\circ\text{C min}^{-1}$ (after CARLEER et al. 1998), c) Ion-chromatograms (GC-MS) of gases released by heating of the same sample above in air, below in He as a function of temperature (after CARLEER et al. 1998) .....	25
Figure 11. Calculation of virtual kinetic parameters from T, TG and DTG curve .....	25
Figure 12. PA curve of well-ordered kaolinite from Mesa Alta (based on data measured by SMYKATZ-KLOSS 1974) .....	26
Figure 13. Indirect parameters for the characterisation of materials .....	26
Figure 14. Quarry sap on bentonite sample (from Buru, Romania) and the same sample 4 months later .....	29
Figure 15. Q-TG curve of Na-montmorillonite .....	30
Figure 16. Dehydration of Cs-montmorillonite .....	30
Figure 17. Dehydration of K-montmorillonite .....	31
Figure 18. Dehydration of sodium activated montmorillonite .....	31
Figure 19. Dehydration of Ag-montmorillonite .....	31
Figure 20. DTG curve of the two-step dehydration of Li-montmorillonite .....	31
Figure 21. IR spectra of Li-montmorillonite samples in OH stretching regions: unheated and after heating for 24h at $300^\circ\text{C}$ . (after MADEJOVÁ et al. 1999) .....	31
Figure 22. DTG and DDTG curves of Ba-montmorillonite dehydration .....	32

Figure 23. DTG and DDTG curves of Hg-montmorillonite dehydration .....	32
Figure 24. DTG curve of dehydration of Ca-montmorillonite (Kuzmice, Slovakia) .....	32
Figure 25. DTG and DDTG curves of dehydration of Ca-montmorillonite (Egyházaskesző, Hungary) .....	32
Figure 26. Interlayer cation contents of smectites in the samples from Hole 735B of Ocean Drilling Program (after ALT, BACH 2001) .....	33
Figure 27. Thermoanalytical curves of fresh Mn-montmorillonite .....	33
Figure 28. Thermoanalytical curves of the same Mn-montmorillonite three years later .....	33
Figure 29. DTG curve of dehydration of Mg-montmorillonite .....	33
Figure 30. DTG curve of dehydration of Al-montmorillonite .....	34
Figure 31. DTA curves of dehydration of Al-montmorillonite treated with solutions of various pH values (after MAFTULEAC et al. 2002) .....	35
Figure 32. Dehydration temperature and “PA curve” of montmorillonites based on the measurement of 382 different natural samples .....	35
Figure 33. Dehydration temperature and “PA curve” of illites and glauconites .....	35
Figure 34. Dehydration temperature and “PA curve” of different kind of zeolites .....	36
Figure 35. Q-TG curve of mordenite .....	36
Figure 36. TG and DTG curves of perlite (Lehotka, Slovakia) .....	37
Figure 37. DTG and TG curves of perlite series in Borehole Kishuta-1 .....	37
Figure 38. PA curve of opals .....	37
Figure 39. Decrepitation of barite (open crucible, curve 1) .....	37
Figure 40. Evolution of water bound as solid solution from aragonite .....	38
Figure 41. Dehydration of $\text{CuSO}_4 \cdot 5\text{H}_2\text{O}$ examined by dynamic (curves 1–2) and “quasi-isothermal” (curve 3) heating techniques using open and labyrinth crucibles .....	38
Figure 42. Dehydration of $\text{MgSO}_4 \cdot 7\text{H}_2\text{O}$ examined by dynamic (curves 1–2) and “quasi-isothermal” (curve 3) heating techniques using open (curves 1–2) and labyrinth crucibles (curve 3) .....	39
Figure 43. Dehydration of gypsum ( $\text{CaSO}_4 \cdot \text{H}_2\text{O}$ ) under dynamic heating .....	39
Figure 44. Dehydration of gypsum ( $\text{CaSO}_4 \cdot \text{H}_2\text{O}$ ) under “quasi-isothermal” and “quasi-isobaric” conditions .....	39
Figure 45. PA curves of the first and the second reaction of water escape from gypsum .....	39
Figure 46. (001) projection of the unit cell of palygorskite (BRADLEY 1940) .....	40
Figure 47. PA curves of the different water types in palygorskite .....	40
Figure 48. TG, DTG, and DTA curves of colemanite (WACŁAWSKA et al. 1988) .....	40
Figure 49. Decomposition temperature versus electronegativity .....	41
Figure 50. Comparison of the decomposition temperature of single and double carbonates .....	41
Figure 51. $\text{H}_2$ - and $\text{H}_2\text{O}$ -release from standard kaolinite KGa-1, Georgia, USA .....	41
Figure 52. Q-TG curve of portlandite .....	42
Figure 53. Q-TG curve of calcite .....	42
Figure 54. TG and DTG curve of chalcantite under dynamic heating (a), TG curve of chalcantite under quasi-static circumstances (b) .....	42
Figure 55. Q-TG curves of dehydroxylation processes of boehmite, kaolinite and pyrophyllite. ....	43
Figure 56. TG and DTG curve of mixture of calcite and dolomite .....	43
Figure 57. TG curve of mixture of dolomite and calcite under quasi-static circumstances .....	43
Figure 58. Aluminite Borehole Csordakút-421, 38.2–38.3 m (Hungary) .....	46
Figure 59. Calcite impurities in an aluminite sample Borehole Csordakút-421, 38.8–38.9 m (Hungary) .....	46
Figure 1.1. Thermoanalytical curves of sulphur .....	48
Figure 1.2.1. Graphite oxidation in air .....	48
Figure 1.2.2. Graphite oxidation in oxygen (DTA, TG, DTG, TGT and DDTG curves) .....	49
Figure 2.1.1. DTA, TG and DTG curves of the complex reactions of a sample with relatively high pyrite content .....	49
Figure 2.1.2. DTA, TG and DTG curves of the oxidation of pyrite in oxygen .....	52
Figure 2.1.3. DTA, TG and DTG curves of the disproportion of pyrite in nitrogen .....	52
Figure 2.2. Oxidation and sublimation of cinnabar .....	53
Figure 2.3. Thermoanalytical curves of galena .....	53
Figure 2.4. Thermoanalytical curves of sphalerite .....	54
Figure 3.1.1. Thermoanalytical curves of quartz .....	54
Figure 3.1.2. Thermoanalytical curves of opal .....	56
Figure 3.2.1. Oxidation reaction of magnetite .....	56
Figure 3.2.3a. Surface structural model for ferrihydrite. (MANCEAU, GATES 1995) .....	57
Figure 3.2.3b. Derivatogram of ferrihydrite .....	58
Figure 3.3.1. Derivatogram of pyrolusite .....	59
Figure 4.1.1a. Thermogravimetric curves of natural gibbsite .....	60
Figure 4.1.1b. PA curve of natural gibbsite .....	61
Figure 4.1.1c. Thermogravimetric curves of artificial gibbsite .....	61

Figure 4.1.2. Thermogravimetric curves of a sample containing nordstrandite .....	62
Figure 4.1.3. Thermogravimetric curves of a sample containing brucite .....	63
Figure 4.1.4. Thermogravimetric curves of a sample containing portlandite .....	63
Figure 4.2.1a. Thermogravimetric curves of a sample containing goethite .....	64
Figure 4.2.1b. Temperature of dehydration peak, the shift of $d_{111}$ X-ray reflection and the wave number of the deformation band around $900\text{ cm}^{-1}$ as function of the aluminium content of goethite (after JÓNÁS, SOLYMÁR 1970b) ..	64
Figure 4.2.1c. Thermogravimetric curves of a sample containing alumo-goethite .....	64
Figure 4.2.2. Thermogravimetric curves of a sample containing lepidocrocite .....	65
Figure 4.2.3. Thermogravimetric curves of a sample containing manganite .....	65
Figure 4.2.4. Thermogravimetric curves of a sample containing boehmite .....	66
Figure 4.2.5a. Thermogravimetric curves of a sample containing diaspore .....	66
Figure 4.2.5b. PA curves of Hungarian diaspore and boehmite minerals from bauxite .....	66
Figure 4.3.1. Thermogravimetric curves of a sample containing lithiophorite .....	67
Figure 5.1.1.1.1a. Thermoanalytical curves of kaolinite .....	68
Figure 5.1.1.1.1b. Thermoanalytical parameters used for the determination of the crystallinity of kaolinite from the DTA curve .....	69
Figure 5.1.1.1.1c. Indirect parameters for the characterisation of kaolinite .....	69
Figure 5.1.1.1.1d. Thermoanalytical parameters used for the the determination of the crystallinity of the kaolinite from the DTG curve .....	70
Figure 5.1.1.1.2. Thermoanalytical curves of dickite .....	70
Figure 5.1.1.1.3. Thermoanalytical curves of fireclay .....	70
Figure 5.1.1.1.4. Thermoanalytical curves of halloysite .....	71
Figure 5.1.1.1.5. Thermoanalytical curves of an allophane containing sample .....	71
Figure 5.1.1.2a. Thermal reaction schemes of reaction sequences of Mg-chrysotile. According to BALL, TAYLOR (1963), BRINDLEY, HAYAMI (1965), and MARTIN (1977). Summarized by MACKENZIE and MEINHOLD (1994) .....	73
Figure 5.1.1.2b Schematic representation of proposed chrysotile reaction sequences according to MACKENZIE, MEINHOLD (1994). .....	73
Figure 5.1.1.2c. Thermoanalytical curves of chrysotile .....	73
Figure 5.1.1.2d. Thermoanalytical curves of lizardite .....	74
Figure 5.1.1.2e. Thermoanalytical curves of “hydroantigorite” .....	74
Figure 5.1.2.1.1. Thermogravimetric curves of pyrophyllite .....	75
Figure 5.1.2.1.2. Thermogravimetric curves of a talc containing sample .....	76
Figure 5.1.2.2.1.1a. Typical thermogravimetric curves of primary Ca-montmorillonite .....	77
Figure 5.1.2.2.1.1b. Derivatogram of sample containing montmorillonite .....	77
Figure 5.1.2.2.1.1c. Quantitative determination using ethylenglycole .....	77
Figure 5.1.2.2.1.2. Typical thermogravimetric curves of primary Na-montmorillonite .....	78
Figure 5.1.2.2.1.3a. Thermogravimetric curves of an “abnormal montmorillonite” with double dehydroxylation ..	78
Figure 5.1.2.2.1.3b. Thermogravimetric curves of an “abnormal montmorillonite” with a low temperature dehydroxylation .....	79
Figure 5.1.2.2.1.3c. DTA curve of a Wyoming-type montmorillonite .....	79
Figure 5.1.2.2.1.3d. DTA curve of a Cheto-type montmorillonite .....	79
Figure 5.1.2.2.2. Thermogravimetric curves of iron beidellite .....	80
Figure 5.1.2.2.3. Thermogravimetric curves of nontronite .....	80
Figure 5.1.2.2.4a. Thermogravimetric curves of saponite .....	80
Figure 5.1.2.2.4b. Thermogravimetric curves of iron-saponite .....	81
Figure 5.1.2.3. Thermoanalytical curves of vermiculite .....	81
Figure 5.1.2.4.1a. Unpulverised sample containing muscovite .....	82
Figure 5.1.2.4.1b. Effects of dry grinding on muscovite .....	82
Figure 5.1.2.4.1c. Thermogravimetric curves of same muscovite pulverised under methanol .....	82
Figure 5.1.2.4.2a. Thermogravimetric curves of fresh biotite .....	83
Figure 5.1.2.4.2b. Signal of the initial chloritization of a biotite separate. ....	83
Figure 5.1.2.5.1. Thermogravimetric curves of illite containing sample .....	84
Figure 5.1.2.5.2. Thermogravimetric curves of a hydromuscovite containing sample .....	84
Figure 5.1.2.5.3. Thermogravimetric curves of a glauconite separate .....	84
Figure 5.1.2.6a. Typical thermoanalytic curves of primary chlorite .....	85
Figure 5.1.2.6b. Typical thermoanalytic curves of sedimentary chlorite .....	85
Figure 5.1.2.7.1.1. Thermoanalytic curves of K-rectorite (allevardite) .....	86
Figure 5.1.2.7.1.3. Thermoanalytic curves of tosudite .....	86
Figure 5.1.2.7.2.1. Thermoanalytic curves of interstratified illite/montmorillonite .....	87
Figure 5.1.2.7.2.2. Thermoanalytic curves of interstratified chlorite-vermiculite .....	87
Figure 5.1.2.7.2.3. Thermoanalytic curves of interstratified talc-saponite .....	87

Figure 5.1.2.8.1. Thermogravimetric curves of a palygorskite-bearing sample	88
Figure 5.1.2.8.2. Thermoanalytic curves of sepiolite	89
Figure 5.1.2.9.1. Thermoanalytic curves of apophyllite	89
Figure 5.1.2.9.2. Thermoanalytic curves of prehnite	90
Figure 5.1.2.9.3. Thermoanalytic curves of tobermorite	90
Figure 5.2.1. Thermoanalytic curves of a topaz-bearing sample	91
Figure 5.2.2. Thermogravimetric curves of an epidote-bearing sample	91
Figure 5.2.3. Thermoanalytic curves of a vesuvianite-bearing sample	92
Figure 5.2.4. Thermoanalytic curves of a zunyite-bearing sample	92
Figure 5.2.5. Thermogravimetric curves of katoite	93
Figure 5.3.2. Thermogravimetric curves of ferroaxinite	93
Figure 5.3.3. Thermoanalytical curves of a tourmaline (dravite)-bearing sample	94
Figure 5.4.2. Thermogravimetric curves of charoite	95
Figure 5.5.1.1.1. Thermogravimetric curves of natrolite	96
Figure 5.5.1.1.4. Thermoanalytic curves of a thomsonite-bearing sample with gonnardite? impurities	97
Figure 5.5.1.2.1. Thermogravimetric curves of analcime	99
Figure 5.5.1.2.2. Thermoanalytical curves of laumontite (leonhardite?)	100
Figure 5.5.1.3.2. Thermogravimetric curves of phillipsite	101
Figure 5.5.1.4.1. Thermogravimetric curves of mordenite	102
Figure 5.5.1.5.2. Thermogravimetric curves of clinoptilolite	103
Figure 5.5.1.5.3. Thermoanalytical curves of stilbite	104
Figure 5.5.1.6.3. Thermoanalytical curves of chabasite	106
Figure 6.1.1a. Thermogravimetric curves of calcite	108
Figure 6.1.1b. Thermogravimetric curves of a strongly weathered calcite	108
Figure 6.1.2. Thermogravimetric curves of magnesite	109
Figure 6.1.3. Thermogravimetric curves of rhodochrosite	109
Figure 6.1.4a. Thermoanalytical curves of siderite	110
Figure 6.1.4b. Superposition of the endothermic and exothermic reactions on the DTA curve of siderite	110
Figure 6.1.5. Thermoanalytical curves of cerussite	111
Figure 6.2.1a. Thermogravimetric curves of dolomite	111
Figure 6.2.1b. Thermogravimetric curves of dolomite in loess	112
Figure 6.2.1c. Thermogravimetric curves of dolomite in palaeosoil	112
Figure 6.2.1d. Thermogravimetric curves of “protodolomite” (Mg-poor dolomite) bearing rock with halite content	113
Figure 6.2.1e. Thermogravimetric curves of the previous sample after washing by distilled water	113
Figure 6.2.1f. Thermogravimetric curves of high magnesium calcite and Ca-dolomite (“protodolomite”)	113
Figure 6.2.2. Thermogravimetric curves of huntite	113
Figure 6.2.3. Thermoanalytical curves of real ankerite	114
Figure 6.2.4a. Thermogravimetric curves of ferrous dolomite with higher iron content	114
Figure 6.2.4b. Thermogravimetric curves of ferrous dolomite	115
Figure 6.2.4c. Thermogravimetric curves of ferrous dolomite with low iron content	115
Figure 6.2.5. Thermogravimetric curves of kutnahorite	115
Figure 6.3.1. Thermoanalytical curves of kalicinite	116
Figure 6.3.2. Thermogravimetric curves of teschemacherite	116
Figure 6.4.1. Thermogravimetric curves of malachite	117
Figure 6.4.3. Thermoanalytical curves of dawsonite	117
Figure 6.5.1. Thermogravimetric curves of dypingite	118
Figure 7.1.1. Thermoanalytical curves of a mascagnite bearing sample	122
Figure 7.2.1. Thermogravimetric curves of chalcantite	122
Figure 7.2.2. Thermoanalytical curves of melanterite	123
Figure 7.2.3. Thermoanalytical curves of rozenite	123
Figure 7.2.4. Thermoanalytical curves of szomolnokite bearing sample	124
Figure 7.2.5. Thermogravimetric curves of alunogen	124
Figure 7.2.6. Thermogravimetric curves of hexahydrate	125
Figure 7.2.7. Thermogravimetric curves of a gypsum bearing sample	125
Figure 7.3.1. Thermoanalytical curves of römerite	125
Figure 7.3.2. Thermogravimetric curves of voltaite	126
Figure 7.3.3. Thermoanalytical curves of halotrichite	126
Figure 7.3.4. Thermogravimetric curves of potassium-alum	127
Figure 7.3.5. Thermogravimetric curves of tschermigite	127
Figure 7.4.1. Thermoanalytical curves of alunite	128
Figure 7.4.2. Thermoanalytical curves of a jarosite bearing sample	128

Figure 7.5.1. Thermoanalytical curves of an aluminite bearing sample .....	128
Figure 7.5.3. Thermoanalytical curves of copiapite .....	129
Figure 8.1.1. Thermoanalytical curves of vivianite .....	130
Figure 8.2.1. Thermoanalytical curves of lazulite .....	131
Figure 8.2.2. Thermoanalytical curves of gorceixite .....	131
Figure 8.3.1. Thermoanalytical curves of diadochite .....	132
Figure 8.4.1. Thermoanalytical curves of kaňkite .....	132
Figure 10.1a. Thermoanalytical curves of halite .....	133
Figure 10.1b. Thermoanalytical curves of an admixture of epsomite and halite .....	133
Figure 11.1. Thermoanalytical curves of whewellite .....	134
Figure 11.2. Thermoanalytical curves of humboldtine .....	135
Figure 12.1. DTA curves of 20 mg coal sample diluted by 980 mg $\text{Al}_2\text{O}_3$ .....	135
Figure 12.2. Characterisation of coal by thermogravimetric analysis .....	136
Figure 13.1. Thermogravimetric curves of perlite .....	136
Figure 13.2. Quantitative evaluation of a bauxite sample .....	137
Figure 14.6b. Weathering (palaeoclimate) curve of a loess section in Borehole Üveghuta–22 (Hungary), based on the molecular and hydroxide water content measured from TG curves. ....	138
Figure 14.7. Relationship between the interlayer water content and the metasomatic alteration temperature in the Borehole Pázmánd–2, Hungary .....	139
Figure 14.8a. Characteristic thermal decomposition temperature for kaolinite of different genesis compared to Mesa Alta kaolinite .....	139
Figure 14.8b. Characteristic thermal parameters for kaolinite of different diagenetic stage compared to hydrothermal kaolinite .....	139
Figure 14.8c. Peak temperature of exothermic reaction for kaolinite of different genesis .....	140
Figure 14.12a. $\delta^{13}\text{C}$ and $\delta^{18}\text{O}$ values .....	140
Figure 14.12b. Corrected decomposition temperature of travertine sample from different localities .....	140

### Index of Tables

Table 1. Individual thermoanalytical techniques .....	16
Table 2. Dimensions of thermoanalytical parameters (the recommended SI symbols should be used) .....	18
Table 3. Conventions of recording .....	18
Table 4. Empirical parameters for the description of peak shape .....	19
Table 5. Available Certified Reference Materials .....	19
Table 6. Proposed standard conditions of the thermoanalytical investigation of minerals (by SMYKATZ-KLOSS 1974) .....	21
Table 7. Proposed standard conditions of the treatment (by SMYKATZ-KLOSS 1974) .....	21
Table 8. Schema of thermo-gas-titrimetric determination of different components .....	24
Table 9. Joint use of instrument-based mineralogical phase analytical methods (DTA-TG, XRD, IR) .....	27
Table 10. Chemical and physical thermal reaction types and their appearance on thermoanalytical curves .....	28
Table 11. The most frequent types of occurrence of water in minerals and their most characteristic thermoanalytical features .....	28
Table 12. Measurement parameters of the bentonite sample from Buru, Romania .....	29
Table 13. Hydration enthalpies ( $\Delta H_{\text{hyd}}$ ) of metal cations .....	30
Table 14. Characteristic data of the monovalent and bivalent interlayer cations. ....	33
Table 15. Probable state of active centres of Al-montmorillonite treated with solutions of various pH values. ....	34
Table 16. Temperature of decomposition depending on the electronegativity .....	40
Table 17. Temperature of decomposition of hydroxide in different types of structures depending on the electronegativity .....	42
Table 18. Characteristic evaporation and sublimation temperature of minerals .....	43
Table 19. Characteristic temperatures of the oxidation and the reduction of minerals .....	43
Table 20. Types of solid-phase structural decomposition and crystallization of new phases .....	44
Table 21. Characteristic temperatures of polymorphic transition of minerals .....	44
Table 22. Characteristic melting points of minerals .....	45
Table 23. Curie point of minerals .....	46
Table T2a. Oxidation of the most common simple sulphide minerals in order of temperature ( $^{\circ}\text{C}$ ) .....	50
Table T2b. Principal modes of oxidation of pyrite .....	50
Table T2c. Further reactions of sulphides. ....	51
Table T3.1. Thermal reactions of silica minerals .....	55
Table T3.2.3. DTA reaction of synthetic iron oxide gels .....	59
Table T3.3.2. Thermal reactions of other manganese oxides .....	60
Table T4.1. Dehydroxylation process of simple hydroxide minerals .....	61

Table T.4.2. Dehydroxylation of oxyhydroxide minerals .....	64
Table T5.1.1. Thermoanalytical data of 1:1 layer type clay minerals .....	68
Table T5.1.1.1a, b. Characterisation of kaolinite types based on different DTA parameters .....	69
Table T5.1.1.2a. Characteristic peak temperatures of Mg-serpentines based on different references .....	72
Table T5.1.1.2b. Temperature interval data of Mg-serpentines .....	72
Table T5.1.2. Thermoanalytical data of the main 2:1 layer type clay minerals .....	74
Table T5.1.2.5. Composition of the members of the muscovite-illite series .....	83
Table T5.1.2.6. Thermoanalytical data of the main 2:1:1 layer type phyllosilicates .....	85
Table T5.1.2.8.1. Dehydration temperature of water evaluated from palygorskite on the basis of published data ..	88
Table T5.1.2.8.2. Steps of the water escape from sepiolite based on published data .....	89
Table T5.2. Dehydroxylation temperature of some mesosilicates .....	91
Table T5.5.1.1.1. Thermoanalytical data of natrolite .....	95
Table T5.5.1.1.2. Thermoanalytical data of gonnardite .....	96
Table T5.5.1.1.3. Thermoanalytical data of mesolite .....	96
Table T5.5.1.1.4. Thermoanalytical data of thomsonite .....	97
Table T5.5.1.1.5. Thermoanalytical data of scolecite .....	98
Table T5.5.1.1.6. Thermoanalytical data of edingtonite .....	98
Table T5.5.1.2.1. Thermoanalytical data of analcime .....	98
Table T5.5.1.2.2. Thermoanalytical data of laumontite .....	99
Table T5.5.1.3.1. Thermoanalytical data of gismondine .....	100
Table T5.5.1.3.2. Thermoanalytical data of phillipsite .....	101
Table T5.5.1.3.3. Thermoanalytical data of harmotome .....	101
Table T5.5.1.4.1. Thermoanalytical data of mordenite .....	102
Table T5.5.1.5.1. Thermoanalytical data of heulandite .....	102
Table T5.5.1.5.2. Thermoanalytical data of clinoptilolite .....	103
Table T5.5.1.5.3. Thermoanalytical data of stilbite .....	104
Table T5.5.1.6.1. Thermoanalytical data of gmelinite .....	105
Table T5.5.1.6.2. Thermoanalytical data of erionite .....	105
Table T5.5.1.6.3. Thermoanalytical data of chabasite .....	105
Table T5.5.1.6.4. Thermoanalytical data of faujasite .....	106
Table T5.5.1.7. Thermoanalytical data of other zeolites .....	106
Table T6.1a. The most important reactions of simple carbonate minerals .....	107
Table T6.1b. Further reactions of simple carbonates .....	108
Table T6.2. The main reactions of double carbonate minerals .....	111
Table 6.2.1. Composition of carbonate in loess and palaeosoil analysed by different methods .....	112
Table T6.5.1. Thermal reactions of nesquehonite .....	117
Table 6.5.2. Thermal reactions of hydromagnesite .....	118
Table T6.5.4. Thermal reactions of hydrotalcite .....	118
Table T6.6. Thermal reaction of other carbonates according to data of BECK (1950) .....	119
Table T7a. The main reactions of the most frequent simple sulphate minerals .....	121
Table T7b. Further reactions of sulphates .....	121
Table T7.1.1. Reaction of mascagnite according to the literature .....	122
Table T12.2. Characterisation of coal by thermogravimetric analysis .....	136
Table T13.2a. Evaluation by the measured data .....	137
Table T13.2b. Comparison the results of different investigations .....	137
Table T14.8. Characteristic thermal parameters of crystallinity for kaolinite of different genesis .....	139

## PREFACE

Thermal analysis plays a specific role in the identification and quantitative determination of mineral components of rocks. In spite of the fact that minerals were the first group of materials studied regularly by using thermoanalytical methods, the potential offered by these methods is still not fully utilized in the field of earth sciences. The range of thermoanalytical methods applied in earth sciences is rather wide. Most works are based on DTA. DTA data provide indirect analytical information on a material and the quantification of a reaction is limited. From quantitative phase analysis point of view it is very important that thermogravimetric measurements give direct and absolute values for thermal reactions making stoichiometric calculation possible. Both DTA (Differential Thermal Analysis) and TG (Thermogravimetry) are undoubtedly the most widespread methods, whereas the rest are normally applied rather occasionally, to find solution to specific problems only.

Thermogravimetry dates back to the work of TALABOT who in 1833 equipped a laboratory with thermobalances for quality control of Chinese silk. Thermogravimetric analysis of the minerals and rocks has been applied systematically since the mid 1960s. Derivatography, the technique of simultaneous thermal analytical measurement developed by PAULIKS was a combination of TG and DTA. The measure the rate of change of the sample property with temperature, later the sample controlled thermal analysis or controlled rate thermal analysis (quasi-thermogravimetry) and the computerized new generation of these equipments received the possibility to the author during 40 years to analyze about 30 000 geological samples. The experiences of this long time permit of the systematization of the thermal reactions of the minerals and made reasonable the compilation of this book. Handbook for geological samples based on thermogravimetry earlier only the otherwise excellent publication by TODOR in 1972.

Mária FÖLDVÁRI

**MEASUREMENT METHODS AND SYSTEM OF  
THERMAL REACTIONS OF MINERALS**

# INTRODUCTION TO THE THERMOANALYTICAL METHODS

The International Confederation for Thermal Analysis and Calorimetry has published several recommendations for the nomenclature, standardizing and publishing of results of thermal analysis.

## Thermoanalytical techniques

Thermal analysis is a group of analytical techniques in which physical properties or chemical reactions of a substance are measured as a function of temperature. The classification of the individual thermoanalytical techniques are summarised in Table 1.

**Table 1.** Individual thermoanalytical techniques

Property	Technique	Abbreviation	Notes
Heat	Calorimetry		
Temperature	Thermometry		May also be described as heating or cooling curves
Temperature Difference	Differential Thermal Analysis	DTA	Temperature difference between a sample and a reference material
Heat Flow Rate	Differential Scanning Calorimetry	DSC	Heat flow rate difference between a sample and a reference material
Mass	Thermogravimetry or Thermogravimetric Analysis	TG TGA	
Dimensional and Mechanical	Dynamic Mechanical Analysis	DMA	Modulies are determined
	Thermomechanical Analysis	TMA	Deformation of the substance under compression, tension, flexure, torsion or elasticity
	Thermomodilatometry, • linear • volumetric	TD	Dimensions are measured
Electrical	Dielectric Thermal Analysis	DEA	Dielectric Constant/Dielectric Loss measured
	Thermally Stimulated Current	TSC	Current
Magnetic characteristics	Thermomagnetometry	TM	Magnetic susceptibility
Gas flow	Evolved Gas Analysis	EGA	The nature and/or amount of gas/vapour is determined • volume • heat-conductivity
	• gasvolumetry		
	• thermogastitrimetry,	TGT	• nature and amount by titration
	• mass spectrometry	MS	• nature and amount by mass spectrometer
	• high temperature IR spectrometry	HTIR	• nature and amount by IR spectrometry
Pressure	Emanation Thermal Analysis	ETA	Trapped radioactive gas within the sample released and measured
	Thermomanometry	TM	Evolution of gas is detected by pressure change
Optical characteristics	Thermobarometry		Pressure exerted by a dense sample on the walls of a constant volume cell is studied
	Thermooptometry thermophotometry • thermorefractometry		(Thermomicroscopy) • measurement of total light • determination of refractive index • determination of reflection
	• dynamic reflection spectrometry Thermoluminescence	DRS TL	• emission of light
Acoustic	Thermosonimetry		• sound emitted by the substance
	Thermoacoustometry		• imposed acoustic waves after passing through the substance
Structure	Thermodiffractometry		Compositional or chemical nature of the sample are studied
	Thermospectrometry	HTIRA	High temperature X-ray analysis Measured of light of specific wavelength(s)
Reactions in solution	Thermometric titrimetry		

## Differential thermal analysis (DTA)

A technique in which the temperature difference between a substance and a reference material is measured as a function of temperature whilst the substance and reference material are subjected to the same controlled temperature programme.

The technique requires the use of a reference material, which is a known substance, usually inactive thermally (inert material) over the temperature range interest. Important features of the reference material are that the thermal characteristic (specific heat, conductivity etc.) and the particle size should be very similar to that of the sample.

The most commonly used reference materials:

- calcined  $\alpha$ - $\text{Al}_2\text{O}_3$ ,
- calcined  $\text{MgO}$ ,
- a part of the of the sample precalcined to 1000 °C,
- calcined quartz-free kaolinite,
- quartz.

### **Thermogravimetry (TG)**

A technique in which the mass of a substance is measured as a function of temperature while the substance is subjected to a controlled temperature programme.

### **Evolved Gas Analysis (EGA)**

A technique in which the nature and/or amount of volatile product(s) released by a substance are/is measured as a function of temperature whilst the substance is subjected to a controlled temperature programme.

### **Derivative technique**

The derivative technique yields the first derivative of the original thermal curve with the respect to either time or temperature. It may be possible to measure the rate of property change. These curves give a higher resolution and present more accurately the specific temperature characteristics. The derivative curves obtained by using different instrumental techniques or by computerized derivation. If necessary the second derivative of the primary curves may also be displayed by deriving (e.g.  $\text{TG} \rightarrow \text{DTG} \rightarrow \text{DDTG}$  or  $\text{DTA} \rightarrow \text{DDTA}$ ).

### **Multiple techniques**

- Simultaneous techniques: application of two or more techniques to the same sample at the same time (e.g. simultaneous thermogravimetry and differential thermal analysis in derivatograph).
- Coupled simultaneous techniques: application of two or more techniques to the same sample when two instruments are connected through an interface (e.g. differential thermal analysis and mass spectrometry).
- Combined techniques: application of two or more techniques using separate samples for each technique.

## **Experimental conditions**

Thermal measurements can be carried out:

#### **1. With different heating techniques:**

##### **a) Under dynamic temperature change:**

- heating:
  - linear or constant rate e.g. temperature/time curve is linearly programmed.
- cooling:
  - according to heat-incapacity of the furnace,,
  - programmed (cooling rate less than the heat-incapacity of the furnace).

##### **b) Under static conditions:**

- isothermal,
  - quasi isothermal (at a quasi equilibrium condition i.e. self regulation by the constant partial pressure of the volatile products, Q-TG, Q-DTG, Q-DTA etc.),
  - special quasi isothermal (at a quasi equilibrium condition combined by timing).
- ##### **c) Combined.**

#### **2. Under different types of gas atmosphere: air, oxygen, nitrogen, argon, helium (20% $\text{O}_2$ , 80% He) or in vacuum.**

## **Thermoanalytical parameters**

The following tables summarise the principles of the most important definitions which are used in earth sciences and in this book (Table 2, 3).

**Table 2.** Dimensions of thermoanalytical parameters (the recommended SI symbols should be used)

Abbreviation	Parameter	Symbol	Units
T	temperature	T	°C or K
t	time	t	s (min, h)
q	heat of reaction	$\Delta H$	joule/mg
DT	heating rate	$B=dT/dt$	°C/min, Ks <sup>-1</sup>
DIA	differential thermal analysis curve	$\Delta I$	°C
TG	mass, thermogravimetry curve	m	mg or %
DTG	derivative thermogravimetry curve	$dm/dt$ or $dm/dT$	mg/min or mg/°C
TGI	thermogravimetry curve	v	cm <sup>3</sup> or ml
DTGI	derivative thermogravimetry curve	$dv/dt$ or $dv/dT$	cm <sup>3</sup> /min or ml/°C
DEGAS	gas release	m/z	-
	order of reaction	n	-
	activation energy	E	kJoule/mol
	fraction reacted	$\alpha$	%

**Table 3.** Conventions of recording

Curve	Ordinate	Abscissa
TG	mass decreasing downwards	t or T increasing from left to right
DTG	mass losses downwards	
Q-TG	mass decreasing downwards	
DT	$dT/dt$	
DIA	endothermic reaction downwards	

## Nomenclature of DTA and TG curves

A formalized DTA curve is shown in Figure 1.

Base line: AB and DE correspond to the portion or portions of the DTA curve for which  $\Delta T$  is approximately zero.

Peak: BCD is that portion of the DTA curve which departs from and subsequently returns to the base line.

Initial temperature: B (characteristic reaction temperature) determination is approximate

Final temperature: D (the sample again has the same temperature as the inert material,  $\Delta T = 0$ ).

Peak temperature: point of intersection of CF and the temperature axis (maximum rate of reaction) can be measured quite accurately.

Endothermic peak: is a peak where the temperature of the sample falls below that of the reference material ( $\Delta T$  is negative).

Exothermic peak: is a peak where the temperature of the sample rises above that of the reference material ( $\Delta T$  is positive).

Peak width (reaction temperature range): B'D' is the time or temperature interval between the points of departure from and return to the base line.

Peak width at half height: reaction width at  $\Delta T/2$ .

Peak height: CF is the distance vertical to the time or temperature axis, between the interpolated base line and the peak tip.

Peak area: BCDB is the area enclosed between the peak and the interpolated base line. There are several ways to interpolate the base line. (Later Figure 6 gives only an example.) Locations of B and D depend on the method of interpolation of the base line (reaction heat  $\Delta H$ ).

Extrapolated onset: G is the point of intersection of the tangent drawn at the point of greatest slope on the leading edge of the peak (BC) with the extrapolated base line.

Base line of DTA curve is where  $\Delta T$  is zero.

Base line shift:  $\gamma$  difference between the specific heat of the original sample and its reaction product.

All definitions refer to a single peak such as that shown in Figure 1; multiple peak system, showing shoulders or more than one maximum or minimum, can be considered to result from the superposition of single peaks.

While the true characteristic reaction temperature can be determined only approximately, the peak temperature can be measured quite accurately.

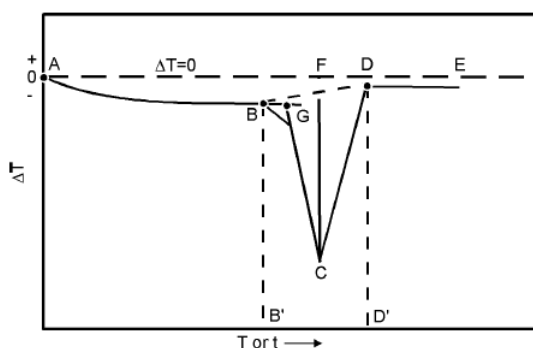


**Figure 1.** Formalized DTA curve

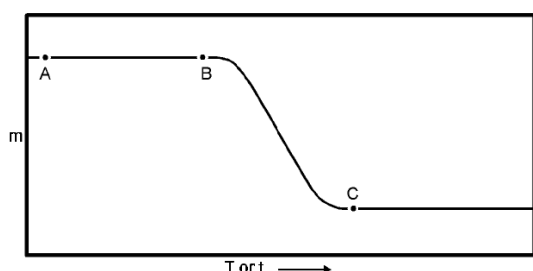


**Figure 2.** Formalized TG curve

A formalized TG curve is shown in Figure 2.

Plateau: AB is that part of the TG curve where the weight is essentially constant.

Initial temperature ( $T_i$ ) B is the temperature (on the Celsius or Kelvin scales) at which the cumulative weight reaches a magnitude that the thermobalance can detect.

Final temperature ( $T_f$ ) C is the temperature (on the Celsius or Kelvin scales) at which the cumulative weight reaches a maximum.

The reaction interval is the temperature difference between  $T_f$  and  $T_i$  as defined above.

All definitions refer to a single-step process, multistage processes can be considered as resulting from a series of single-step processes.

## Description of the shape of thermoanalytical curves (DTA, DTG)

Parameters (Table 4) characterize the four empirical properties of a peak:

1. position of the peak along the temperature axis: such as  $T_{(max)}$ ,  $T_{(\alpha)}$
2. width:  $\Delta T(\alpha_2, \alpha_1)$ ,  $W_T$ ,
3. asymmetry:  $a_{(max)}$ ,  $R_{(\alpha)}$  etc.
4. sharpness/flatness of the peak: U etc.

Form: shoulder.

**Table 4.** Empirical parameters for the description of peak shape

Parameter	Description
$T_{(max)}$	temperature of the peak maximum
$T_{(\alpha)}$	temperature relevant to a particular reacted fraction ( $\alpha$ )
$T(i_1), T(i_2)$	temperature of inflexion points
$\Delta T(\alpha_2, \alpha_1) = T_{(i_2)} - T_{(i_1)}$	width
$W_T = (d\alpha/dT)^{-1}_{max}$	reciprocal of the maximum rate of transformation
$U = \frac{\Delta T(0.8, 0.2)}{W_T}$	max 0.6
$R_{(\alpha)} = \frac{\Delta T(\alpha, 0.2)}{\Delta T(0.8, 0.2)}$	sharpness

## Calibration

The apparatus should be calibrated before starting investigations and later after almost 200 runs.

### Temperature and DTA calibration

Based on the recommendation of ICTA (International Confederation for Thermal Analysis) Committee on Standardization solid I  $\nabla$  solid II first order phase transitions would be preferable for use in dynamic DTA (Table 5).

**Table 5.** Available Certified Reference Materials

Material	Initial (on set) temperature °C	Peak temperature °C	Heats of transition joule/mg (peak area)	NBS-ICTA*
KNO <sub>3</sub>	128	135	0.0546	GM-758
KClO <sub>4</sub>	299	309	0.1008	GM-758
Ag <sub>2</sub> SO <sub>4</sub>	424	433	0.0252	GM-759
SiO <sub>2</sub>	571	574	0.0105	GM-759
K <sub>2</sub> SO <sub>4</sub>	582	588	0.0462	GM-759
K <sub>2</sub> CrO <sub>4</sub>	665	673	0.0546	GM-759
BaCO <sub>3</sub>	808	819	0.0840	GM-760
SrCO <sub>3</sub>	928	938	0.1344	GM-760

\*National Bureau of Standards

## Evaluation of DTA peak resolution

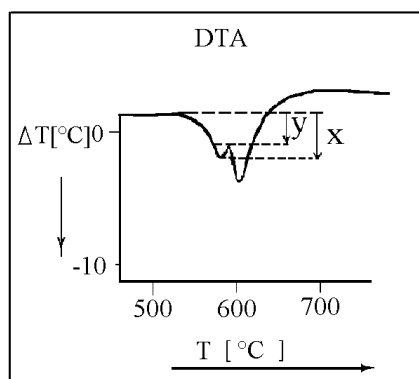


Figure 3. Determination of peak resolution

4:1 mixture (by weight) of  $\text{SiO}_2$  and  $\text{K}_2\text{SO}_4$

$\Delta T/\text{dt } 10^\circ\text{Cmin}^{-1}$

Reactions:

1. at  $574^\circ\text{C}$ : transition of  $\alpha$ -quartz  $\rightarrow$   $\beta$ -quartz,

2. at  $583^\circ\text{C}$ : transition of  $\text{K}_2\text{SO}_4$  rhombic  $\rightarrow$   $\text{K}_2\text{SO}_4$  hexagonal value of the resolution:

$$\text{percent resolution} = \left[ 100 \cdot \left( 1 - \frac{y}{x} \right) \right],$$

where  $x$  = the height of  $\text{SiO}_2$  peak,

$y$  = the minimum deviation the experimental curve from the base-line in region between the peaks.

## Other materials usually used for calibration

### Heat of reaction ( $\Delta H$ )

$\text{C}_{12}\text{H}_{22}\text{O}_{11}$  (sacharose = cane sugar) during the reaction:  $\text{C}_{12}\text{H}_{22}\text{O}_{11} + 12\text{O}_2 \rightarrow 12\text{CO}_2 + 11\text{H}_2\text{O}$ .

During the reaction the combustion heat (peak area) 16.51 joule/mg.

### TG calibration

$\text{KHCO}_3$  at  $170^\circ\text{C}$  (heating rate:  $5^\circ\text{Cmin}^{-1}$ )  $\text{KHCO}_3 \rightarrow \text{CO}_2 + \text{H}_2\text{O} + \text{K}_2\text{CO}_3$ .

Theoretical mass loss based on the reaction is 31%.

### DTG calibration

Total evaporation of methanol ( $\text{CH}_3\text{OH}$ ).

## Effects influencing thermoanalytical curves

In thermal analysis the influence of all the apparative and preparative factors is much greater than in other mineralogical techniques (e.g. X-ray method):

### 1. Experimental conditions

— Apparative factors:

- heating rate (with increasing heating rate peak temperature shifts higher and,
- shape of DTA peak also changes),
- sample arrangement,
- furnace atmosphere,
- shape of crucible,
- thermocouple, etc.

— Preparation:

- packing density,
- grain size,
- amount of the sample,
- humidity of the air in the laboratory (dehydration of clay minerals), etc.

### 2. Properties of the substance

Reasons of the drift of base line in DTA curves:

- differences in heat conductivity and heat capacity of the sample and inert substance (partial elimination: mixing the sample with inert material or reducing the sample amount),
- difference between the specific heat of the original sample and its reaction product,
- imperfect centring of the sample holder in the furnace.

## Standardization

Consequences of influencing experimental conditions: As much as possible the mineralogical thermoanalytical investigation should be made under standard conditions (Table 6 and 7) to get comparable and reproducible results.

**Table 6.** Proposed standard conditions of the thermoanalytical investigation of minerals (by SMYKATZ-KLOSS 1974)

Experimental agent	Criterion
Amount of sample material	100 mg+20 mg Al <sub>2</sub> O <sub>3</sub> (mixed)
Reference material	150 mg annealed Al <sub>2</sub> O <sub>3</sub>
Grain size of sample material	Clay minerals: 0.6–2 µ Ø Other material: 60–200 µ Ø
Furnace atmosphere	air, without any current or turbulence
Thermocouple	Pt-PtRh10, 0.1–0.3 mm Ø
Heating rate	10 °C/min
Packing density	Loose packed, no pressing

**Table 7.** Proposed standard conditions of the treatment (by SMYKATZ-KLOSS 1974)

Hardness	Mohs	Grinding method
very hard sample	>6.5	3 min. grinding by hand in a corundum mortar
hard sample	4.5–6.5	1 min. grinding in an agate mill (machine) at low velocity (500 g volume, 3 balls of <2.5 cm Ø)
soft sample	<4.5	2 min. pulverizing by hand in agate mortar

In the case of investigating a series of similar samples it is absolutely necessary to analyse always under the same conditions. Each published thermoanalytical curve should be completed by the information on all conditions of the analysis.

## Recommendations of ICTA Nomenclature Committee for reporting thermal analysis results

— Identification of all substances (sample, reference, diluent) by a definitive name, an empirical formula, or equivalent compositional data.

— The origin of all substances, details of their histories, pre-treatment and chemical purities, so far as these are known.

— Measurement of the average rate of linear temperature change over the temperature range involving the phenomena of interest. Non-linear temperature programming should be described in detail.

— Identification of the sample atmosphere by pressure, composition and purity; whether the atmosphere is static, self-generated, or dynamic through or over the sample. Where applicable, the ambient atmospheric pressure and humidity should be specified. If the pressure is other than atmospheric, full details of the method of control should be given.

— A statement of the dimensions, geometry and material of the sample holder (open, closed).

— A statement of the method of loading (quasi-static, dynamic) where applicable.

— Identification of the abscissa scale in terms of time or of temperature at a specific location. Time or temperature should be plotted to increase from left to right.

— Information about the methods applied to identify intermediates or final products.

— Faithful reproduction of all origin records.

— Identification of the apparatus used by type and/or commercial name

*The following additional details are also necessary in the report of DTA data:*

— Wherever possible, each thermal effect should be identified and supplementary supporting evidence stated.

— Sample weight and dilution of the sample, particle size.

— Use of grinding apparatus, size fractionation methods.

— Geometry and materials of the thermocouples and the location of the differential and temperature-measuring thermocouples.

— The ordinate scale should indicate deflection per degree Centigrade at a specified temperature. Preferred plotting will indicate upward deflection as a positive temperature differential, and downward deflection as a negative temperature differential, with respect to the reference. Deviations from this practice should be clearly marked.

*The following additional details are also necessary in the report of TG data:*

— A statement of the sample weight and weight scale for the ordinate. Weight loss should be plotted as a downward trend and deviation from this practice should be clearly marked. Additional scales (e.g. fractional decomposition, molecular composition) may be used for the ordinate when desired.

— If derivative thermogravimetry is employed, then method of obtaining the derivative should be indicated and the units of the ordinate specified.

The following additional details are also necessary in the report of each EGA or EGD record:

— Method (MS, GC, specific detector).

— Interface (time delay, trapping).

— A clear statement of the temperature environment of the sample during reaction.

— Identification of the ordinate scale in specific terms where possible. In general, increasing concentration of evolved gas should be plotted upwards. Deviations from these practices should be clearly marked.

*Data acquisition and manipulation by computers:*

— How many bits A/D conversion?

— It should be possible to view the raw data prior to any smoothing.

— Equations used in the derivation of properties need to be either given in the handbook or references to the literature are required. An example is the form of the equation used in kinetic analysis.

— How often the signal sampled? How many points are averaged? What base line treatment is actually used?

\*\*\*

References for thermoanalytical methods: 50, 142, 237, 509, 554, 555, 556, 632, 671, 691, 692, 698, 724, 725, 727, 842, 877, 879, 1006, 1193, 1194

## THERMOGRAVIMETRIC INVESTIGATION TECHNIQUES AND METHODS

### Techniques

#### Quantitative determination based on mass-change

Quantitative determination methods applied in thermal analysis can be based upon the measurement of DTA peak areas using calibration curves, whereas in the case of decomposition reactions they can be performed by applying the PA (Proben Abhängigkeit = curve of sample amount dependence) curves using the logarithmic relation between the temperature of the decomposition reaction and concentration. However, these methods offer the possibility of semi-quantitative estimation, only. The most suitable methods for quantitative determination are measurements based on mass-changes in the course of decomposition (possibly oxidation and reduction) processes. The advantage of this method is, as compared to any other instrument-based methods of phase analysis, that directly obtained parameters, each with absolute value are used. Within the accuracy range of the analytical balance applied for plotting the TG curves, thermogravimetry may represent one of the

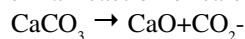
most precise analytical methods. Here, from the mass-change in a given reaction, and with the knowledge of thermochemical reaction equation the mass percent ratio can be determined for the mineral component in the sample.

The stoichiometric factor introduced for quantitative determination is as follows:

$$f = \frac{M}{m},$$

where M = molecular mass of the mineral,  
m = mass-change during the given reaction.

Theoretical thermal reaction of calcite (Figure 4):



Molar mass    100        56    44

Stoichiometric factor: 2.27.

Calcite content in the sample of Figure 4 = 99%.

Accuracy of determination based on thermogravimetric

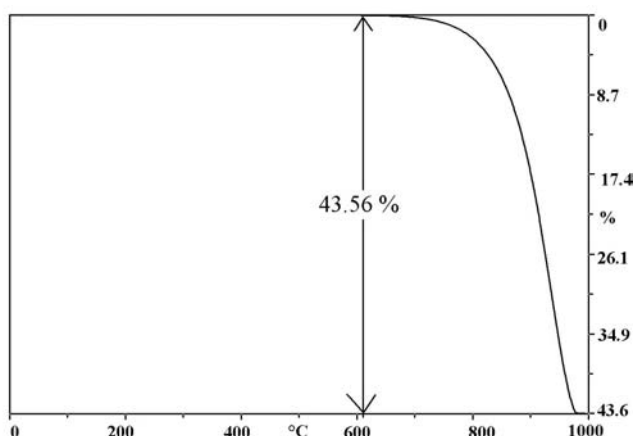


Figure 4. TG curve of calcite (Triassic limestone, Gerecse Mts, Hungary)

measurement and the limits of phase detection are different for each mineral. In a multicomponent system the accurate determination of the composition is more difficult than others. For instance, although the weight change of a sample can be found out by means of thermobalance with an accuracy of + 0.1%, the amounts of the individual components of minerals can be determined often only with accuracy lower by several orders of magnitude. This fact attributed to three causes.

The most frequent and difficult problem is caused by the circumstance that the individual mineral components decompose closely after one another. Whereas in a favourable case the overlapping of the decomposition only decreases the accuracy of the determination, under disadvantageous conditions it may totally hinder even the identification of the components.

Theoretically, minerals, for which the stoichiometric factor of the decomposition reaction is the lowest, can be determined with the highest accuracy. For reactions with high stoichiometric factors, the small mass-change and the eventual measurement errors multiplied due to the factor may reduce considerably the accuracy of the measurement and in this case all we can obtain is a semi-quantitative estimation.

In accordance with the above statements, the different minerals can be arranged in the following order:

- I. Sublimatory minerals (sulphur, cinnabar)    f=1,
- II. Sulphates (determined from  $\text{SO}_3$ )            f=2–6,  
    Hydroxides (determined from  $\text{H}_2\text{O}$ )        f=1.5–10,  
    Carbonates (determined from  $\text{CO}_2$ )        f=2–10,
- III. Phosphates (determined from  $\text{H}_2\text{O}$ )        f=2–20,  
    Zeolites    f=4–15,  
    Phyllosilicates                                  f=7–30,
- IV. Certain neso-, soro- and inosilicates        f>20.

Accuracy of determination is also influenced by the question whether the reaction is really of stoichiometric type, or not. Examples for varying, non-stoichiometrical reactions are represented by the decomposition of gibbsite or by the decomposition reaction of siderite. Determination can also be influenced by the possible substitution within the minerals, and the lack of its knowledge will make the stoichiometric calculation inaccurate.

Substitutions should be frequently recognized for phyllosilicates, but are also frequent among carbonates and other minerals.

The reliability of accuracy of measurement is higher if the mineral concerned has more than one reaction suitable for determination.

If the furnace is heated up the TG curve moves in the direction of mass increase (sample mass is constant). In the initial period of heating (up to 100–150 °C) this change is rapid, slowing and becoming smaller later (Figure 5). The reason is the convections stream, the changes and the density changes of the gas medium inside the furnace (buoyancy). It is evident that neglecting these changes will cause inevitable errors in the interpretation of TG data. Changes in the TG curve (base line) are not large in absolute scale but they — especially in case of a little amount of sample — are perceptible and correctable.

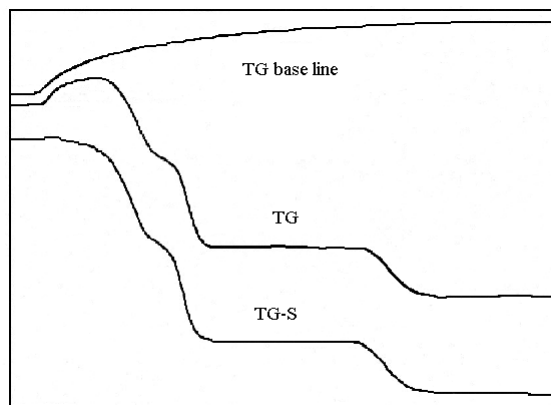


**Figure 5.** TG base line and TG curves of  $\text{CuSO}_4 \cdot 5\text{H}_2\text{O}$  (after BALCEROVIAK 1988)

TG=measured, TG-S = corrected TG curve

### Derivative Thermogravimetry (DTG, DDTG)

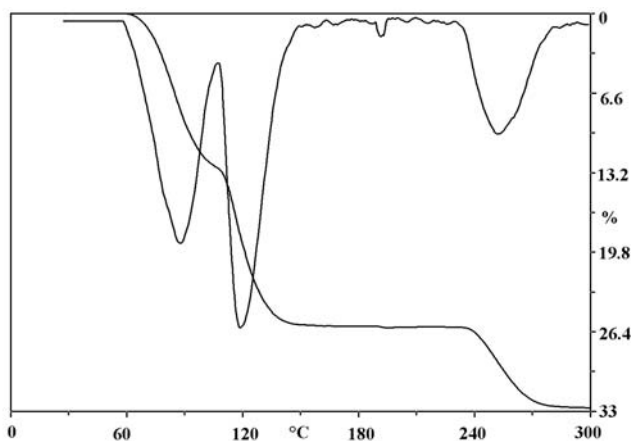


**Figure 6.** TG and DTG curves of the dehydration of  $\text{CuSO}_4 \cdot 5\text{H}_2\text{O}$

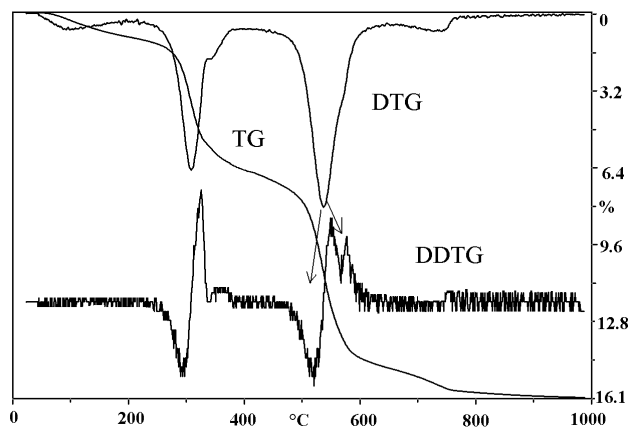


**Figure 7.** Separation of the overlapped reactions of boehmite and kaolinite by DDTG (bauxite, Nyírád, Hungary)

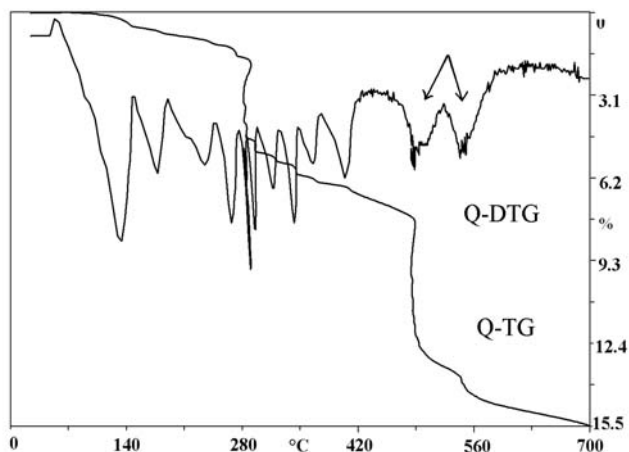
Resolution of the individual steps of more complex TG curves can be improved by examining the derivative DTG curves (Figure 6). The DTG curve is the representation of the rate of weight loss. The DTG peaks indicate the specific temperatures characteristic of the different mineral components more accurately than the TG curve. The DTG peak indicates characteristic decomposition temperatures.

The second derivate of thermogravimetric curve (DDTG) gives new possibilities for detailed investigations. The method is useful for the separation of overlapping reactions with good results. Decompositions of boehmite and kaolinite often overlap between 400 and 650 °C (Figure 7).

### Sample controlled Thermal Analysis (or controlled rate Thermal Analysis)

Instead of linear heating more complex temperature programmes can be applied. Beside the isotherm, the combination of linear and isotherm used frequently the different methods of constant rate programs. For the regulation the pressure or the mass-change of evolved gas can be used (ROUQUEROL 1970, 1973, PAULIK, J., PAULIK, F. 1971a, b, PAULIK, F., PAULIK, J. 1972, 1973).

**Figure 8.** Separation of the overlapped reactions of boehmite and kaolinite by Q-DTG (bauxite, Nyírád, Hungary)



In the case of derivatograph a specially designed crucible is used, where a self-generated atmospheric pressure surrounds the sample which in this way decomposes under “quasi-isothermal–quasi-isobaric” conditions. As soon as a mass-change begins and reaches a given value the heating stops. This controlling cycle is repeated over-and-over until the end of the reaction.

These methods make the shapes of thermal curves independent of the effects of experimental conditions by eliminating the effects of heat and gas transfer, helping to separate the overlapping reactions (Figure 8), to characterise the types or to interpret the mechanism and kinetics of a reaction.

### Coupled simultaneous techniques, EGA methods

Thermal analytic techniques (DTA, TG) can detect only thermal effects or mass-changes, but do not identify decomposition products. Simultaneous TG, DTG and DTA examinations may be supplemented by EGA. Different kinds of evolved gas analysis (EGA) methods may help to determine the nature and amount of the evolved product or separate such overlapped reactions of gas products. The most frequent components of decompositions are water,  $\text{CO}_2$  and  $\text{SO}_3$  ( $\text{SO}_2$ ).

A simple EGA method is the continuous and selective water detector where a hygroscopic reagent absorbs the water from the evolved gas mixture and other gases do not interfere. Quantitation is based on the calibration of detected curves. The device can be modified with “hopcalite” catalyst for the continuous determination of  $\text{CO}$ , and of soda lime for  $\text{CO}_2$  determination.

Another indirect chemical EGA method is thermo-gas-titrimetry (TGT) (Table 8, Figure 9). The thermogastitric method is based on the selective direct determination of  $\text{SO}_3$  and  $\text{CO}_2$  evolved from the heated sample and the indirect analysis of

**Table 8.** Schema of thermo-gas-titrimetric determination of different components

Atmosphere pH	In oxygen	In nitrogen	Differential curves ( $\text{O}_2\text{-N}_2$ )
9.3	$\text{CO}_2$ , $\text{SO}_3$ , $\text{C}_{\text{org}}$ , S	$\text{CO}_2$ , $\text{SO}_3$	$\text{C}_{\text{org}}$ , S
4.0	$\text{SO}_3$ , S	$\text{SO}_3$	S
Differential curves pH(9.3)–pH(4.0)	$\text{CO}_2$ , $\text{C}_{\text{org}}$	$\text{CO}_2$	$\text{C}_{\text{org}}$

water. The thermogas-titrimetric adapter under  $\text{O}_2$  or  $\text{N}_2$  atmosphere as a carrier gas transporter collects the released gases quantitatively and absorbs them in water therefore the pH of the water is changed. This is sensed by a glass and a reference electrode couple. As soon as the pH of the solution begins to deviate from the preselected value, the automatic burette begins to operate, adding NaOH titrant to the absorption liquid so that the pH of this stays constant and titrates the gases in

this way continuously and automatically. The volume of titrant consumed, recorded as a function of the temperature, yields the TGT curve.

The most effective and fastest method of gas analysis is mass spectrometry during which the investigation of the products of thermal analysis was carried out in vacuum (Figure 10a).

At the TG-GC-MS coupling, the evolved gases are collected in a cooled solution of dichloromethane. After the thermal treatment, the absorption solution is analyzed by GC-MS. Individual components are identified by their mass spectra (Figure 10b, c).

During the TG-FTIR analysis TG follows changes in mass of the sample as a function of temperature and/or time. This analysis gives characteristic information about the composition of the measured sample, in particular the amounts of the various components. The gases evolved from a sample during thermal analysis are passed through a heated tube from the thermal analyser to an internal gas cell in the Infrared spectrometer, where a gas spectrum is recorded. This enables the identification of gases released directly from the sample or during thermal treatment.

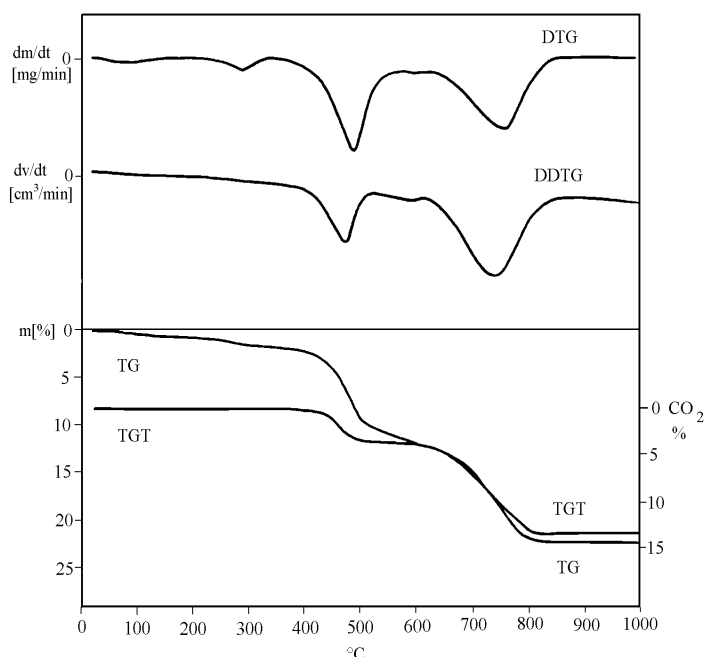


**Figure 9.** Separation of the overlapping reactions of kaolinite and siderite by thermo-gas-titrimetric determination of siderite

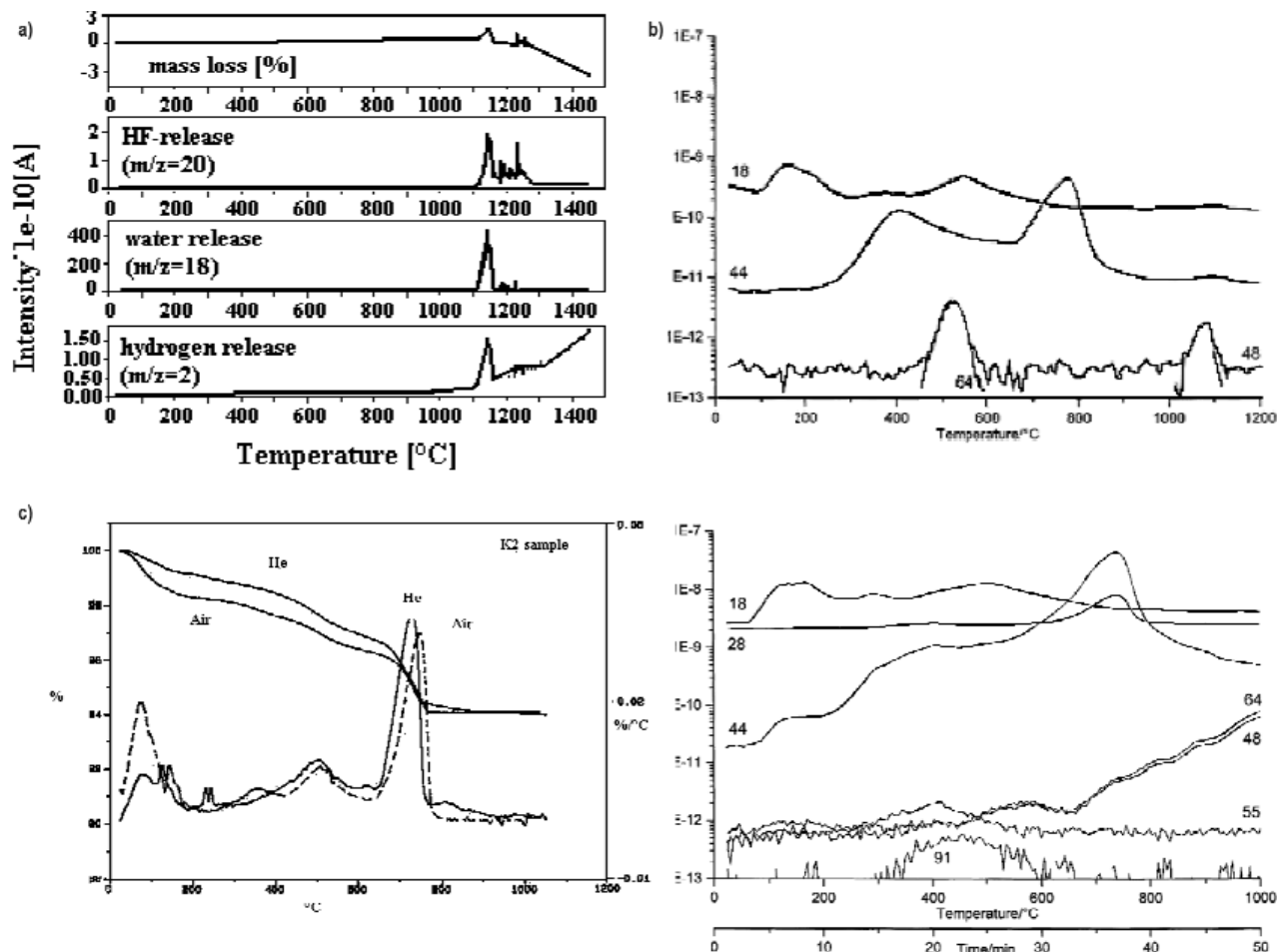


**Figure 10.** a) DEGA — thermogravimetry in vacuum and release of  $\text{CO}_2$ , water and hydrocarbons of a kaoline from Washington County (kaolinite 97%, anatase 2.5%, crandallite 0.5%) (website [www.igw.uni-jena.de/mineral/start.html](http://www.igw.uni-jena.de/mineral/start.html) 2005–09–26), b) TG-DTG plot of a kaolin sample (K2) in He and air at a heating rate of  $20\text{ }^\circ\text{C min}^{-1}$  (after CARLEER et al. 1998), c) Ion-chromatograms (GC-MS) of gases released by heating of the same sample above in air, below in He as a function of temperature. Selected mass-ions:  $18\text{H}_2\text{O}$ ,  $44\text{CO}_2$ , 48 and  $64\text{SO}_2$ , 55 aliphatic hydrocarbons, 91 aromatic hydrocarbons (after CARLEER et al. 1998)

Other applications in material research and environmental applications have been described demonstrating the possibility of the combination of TG with relevant detection systems for qualitative and quantitative analyses of the gases evolved by materials.

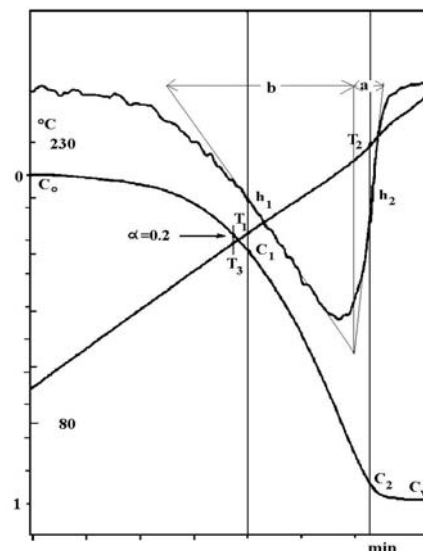
## Methods

### Calculation of virtual kinetic parameters

Calculation of characteristic kinetic parameters of thermal reactions from thermoanalytical curves started about 40 years ago. A great variety of calculation methods were developed in the past time and there is great discussion about the applicability of the methods. Frequent questions in the thermoanalytic literature are the mathematical procedures and their physico-chemical interpretation. Independently of the rigorous physico-chemical meaning, the virtual kinetic parameter triplets [reaction order ( $n$ ), activation energy ( $E$ ) and preexponential factor ( $\lg A$ )] may be suitable for the numerical characterization of the reaction investigated and for comparison of samples examined in series. For the software of the computerized Derivatograph a simple method has been developed for the estimation of the formal-kinetic parameters (ARNOLD et al. 1987) and (Figure 11) respectively.

**Figure 11.** Calculation of virtual kinetic parameters from T, TG and DTG curve

$h_i$  = value of the derived weight change ( $\text{dm}/\text{dt}$ ) at the selected points ( $\text{mg}/\text{min}$ ),  $a_i$  = degree of conversion at the selected points,  $T_i$  = temperatures related to the given points (K),  $C_i$  = measured weight at the given point (mg)



The virtual (partial) reaction order calculated by the Kissinger method:

$$n = 1.26 (a/b)^{1/2},$$

where a and b are represent sections of the DTG baseline before and after the DTG peak maximum (cut out of the abscisse meaning the time axis, of tangents drawn at the inflection point of sections preceeding and following the maximum of DTG peak) after KISSINGER (1957).

The activation energy (kJmol<sup>-1</sup>) according ARNOLD et al. (1987):

$$E = \frac{[\ln(1 - \alpha_1) - \ln(1 - \alpha_2)]}{(1/T_1 - 1/T_2)} \cdot R,$$

where

a = fraction reacted,

T<sub>i</sub> = temperatures of the half values of the DTG curve (in degrees Kelvin),

R = universal gas constant (kJmol<sup>-1</sup>deg<sup>-1</sup>).

The given software performs calculations at a decomposition ratio of 20 and 80%.

The computation method yields acceptable results only for one step processes. In the case of overlapping processes of several steps, the calculated parameters have no sense.

### Corrected decomposition temperature

There is a well-known fact that the peak temperature of a decomposition process due to the partial pressure of the decomposed gas or vapour product depends among others on its amount (ROWLAND, LEWIS 1951, ROBERTSON et al. 1954, PAULIK, F. et al. 1961, LANGER, KERR 1967). The relation between peak temperature and concentration is logarithmic. Based on this connection for the semiquantitative determination of different minerals from the DTA curve the so-called PA (Proben Abhängigkeit = curves of sample amount dependence) curves (Figure 12) were introduced by (SMYKATZ-KLOSS 1974).

$$T = c \cdot (\log M + T_1),$$

where

T = measured temperature,

M = quantity of investigated phase,

T<sub>1</sub> = temperature of the decomposition of 1 mg of the phase,

c = specific constant of reaction.

The use of corrected (or interpolated) decomposition temperature allows eliminating the temperature differences of a given reaction caused by the different quantity of the phases participating in the reaction. An extrapolation of the measured peak temperature considering the mass change during the decomposition process measured on the TG curve compared to a

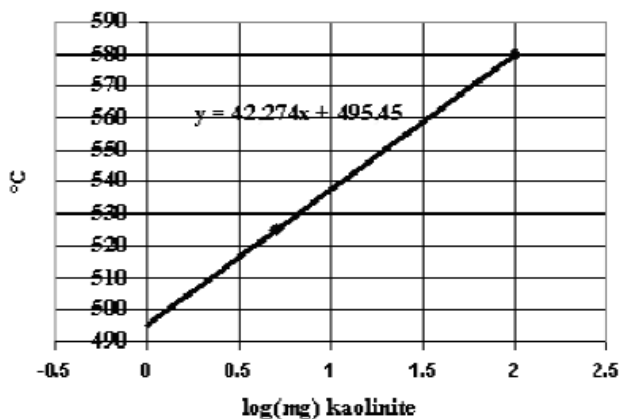


Figure 12. PA curve of well-ordered kaolinite from Mesa Alta (based on data measured by SMYKATZ-KLOSS 1974)

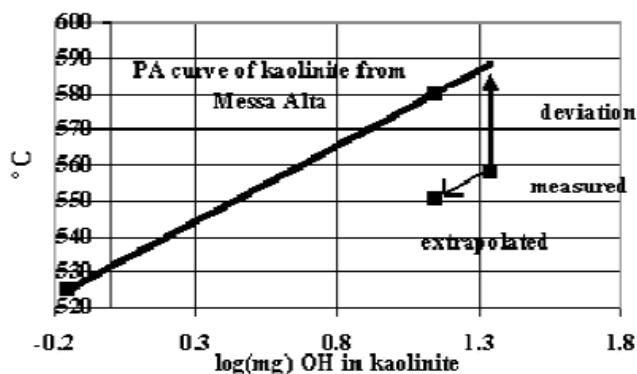


Figure 13. Indirect parameters for the characterisation of materials extrapolated decomposition temperature=peak temperature of 13.95 mg OH of 100 mg of an investigated kaolinite, deviation = peak temperature difference between 100 mg kaolinite from Mesa Alta and kaolinite examined)

standard quantity of the decomposed products makes the peak temperature data suitable for direct characterization and comparison (FÖLDVÁRI 1999). From the differences between the measured and the comparative standard decomposition temperatures (Figure 13) conclusions on other facts which influence the decomposition temperature (crystallinity, substitution, different geological process as weathering, diagenesis etc.) may be drawn.

\*\*\*

References for thermogravimetric methods: 28, 49, 83, 101, 142, 154, 278, 322, 325, 326, 389, 474, 477, 543, 544, 572, 620, 621, 622, 624, 645, 762, 809, 822, 823, 824, 826, 829, 832, 835, 837, 843, 844, 845, 849, 850, 908, 917, 918, 923, 1006, 1064, 1195

## Supplementary methods

Application of different atmospheres in the measurement may also render a great help. Oxygen atmosphere contributes to the improvement of the oxidation and combustion processes, and to their restriction to a narrower temperature range, whereas the application of inert atmosphere may enable to eliminate the oxidation process from the thermal curve.

Another alternative is represented by the different procedures based on treatment e.g.:

- acidic dissolution of carbonates from the sample,
- NaOH treatment for the separation of goethite and hydrargillite (which removes gibbsite but does not affect goethite),
- treatment of organic materials with  $H_2O_2$ ,
- catalytic agent to enhance a reaction (combustion increasing catalytic agent) (REISZ, INCZÉDY 1979),
- additive provoking solid phase reaction to influence a process (e.g. the addition of MgO or CaO in order to shift the disturbing decomposition reaction of sulphates [sulphides] into higher temperature ranges),
- treatment for the identification and quantitative determination of minerals. The best known ones are those applied for the identification of clay minerals (e.g. piperidine), and the ethylene glycol treatment, the latter being used also for the quantitative determination of swelling clay minerals (FIEDLER, WAGNER 1967).

The different kinds of methods used for phase analysis of rocks are partly complementary to one another and partly serve for the verification of one another (FÖLDVÁRI, FARKAS 1985) and Table 9 respectively.

**Table 9.** Joint use of instrument-based mineralogical phase analytical methods (DTA-TG, XRD, IR)

Evaluation type	X-ray diffraction	Thermogravimetry	IR-spectroscopy
Qualitative analysis, identification of minerals	generally (suitable for detecting all crystalline phases)	partial (only the thermally active minerals)	restricted
Quantitative determination	relative method	absolute method (based on the stoichiometry of mass change)	based on calibration curves of the individual minerals
	semi-quantitative	the accuracy of the measurement may vary from mineral to mineral.	restricted
Individual mineral properties (submineralogical features)	substitution, degree of crystallinity, polytype modification, grain size	substitution, degree of crystallinity, polytype modification	substitution, degree of crystallinity, polytype modification

Although the determination of the individual properties of different minerals, in a stricter sense, is not included within the range the phase analysis, it should be noted that the thermoanalytical methods may be, and in several cases are, more effective for the identification of the submineralogical properties (substitution, polytype, degree of crystallization etc.).

References: 310, 329, 902

## CHARACTERISTIC THERMAL REACTIONS OF MINERAL GROUPS

### Thermal activity of minerals

The range of applicability of this method is limited by the fact that it can be applied only for thermally active minerals, since a considerable part of minerals do not show any thermal reaction in response to heating. Conditions under which rocks or their minerals were developed usually determine their thermal activity. Igneous rocks and their minerals developed at a high temperature do not have any thermal reactions when analyzed within the standard temperature range (up to 1000–1500 °C). Igneous minerals association formed at a lower temperature i.e. in response to postmagmatic activity, or transformed at a lower temperature, sedimentary rocks, and minerals of metamorphic rocks developed at a lower temperature and in lower pressure range have thermal effects suitable also for analytical purposes. Thus it implies that there are rocks in which no mineral component can be identified. For the major part of rocks only a certain portion of rock-forming minerals can be analyzed by using methods of thermal analysis, whereas 100 percent of mineral phases can be determined in the case of a few rocks only.

The types of thermal reaction of minerals and the form they appear on DTA and TG curves are summarized in Table 10.

Some of the reaction types (structural transformation, melting temperature etc.) appear within well recorded narrow temperature ranges, irrespective of the conditions of analysis and other factors. These reactions, however, have a general low thermal intensity and are not accompanied by changes in mass.

The temperature of decomposition reactions that are most suitable for the identification and the quantitative determination of minerals is, however, highly sensitive to both the material properties and the conditions of the analysis. This fact, though it offers several advantages, as compared to other methods, is somewhat disadvantageous for thermal analysis. The reason of the present situation, i.e. thermal analysis plays a minor role, as compared to its capacities, is that the reaction temperatures, most suitable for the analysis can be specified in a less exact manner than other parameters used in other analytical methods (X-ray diffraction, infrared spectroscopy, etc.) and therefore their application requires greater routine. Standardization of conditions of

**Table 10.** Chemical and physical thermal reaction types and their appearance on thermoanalytical curves

Reaction type				DTA	TG
1. Chemical reactions	Thermal decomposition	dehydration		endothermic	mass-loss
		dehydroxylation		endothermic	mass-loss
		thermal dissociation		endothermic	mass-loss
		solid phase structural decomposition		endothermic	-
	Oxidation			exothermic	mass-change
	Reduction			endothermic	mass-loss
	Solid phase reaction, double decomposition			exothermic	mass-change possible
2. Physical reactions	structural transition			endothermic	
	formation of new solid phase			exothermic	-
	phase transition (state change)	melting		endothermic	
		sublimation		endothermic	mass-loss
	decrepitation			-	mass-loss
	magnetic changes			endothermic	signal deviation possible

the analysis (rate of heating, method of temperature measurement, quantity of samples, the atmosphere applied, etc.) may restrict, to some extent, the temperature range in which the decomposition reaction concerned may appear.

In spite of difficulties the decomposition reactions accompanied by change in mass are considered to be most suitable for the identification and quantitative determination of minerals. There are cases when other reactions accompanied by mass change, e.g. oxidation, reduction or sublimation, have to be relied upon. The other types of reaction are regarded in this system as complementary information only and for minerals having only these reactions no quantitative determination is generally undertaken.

## System of thermal decomposition reactions

The decomposition reactions can be divided into several groups:

— Dehydration processes. These processes react upon heating by the escape of water originally bounded in the structure in the form of  $H_2O$  molecules.

— Thermal dissociation processes. In this case the components escaping in course of the decomposition are not found in molecular form (ready for decomposition) in the structure, but are in ionic form bounded by strong ionic-covalent forces.

A transition is represented between these two groups by the dehydroxylation processes, in the course of which, although water escapes from the structure in response to heating, its original bonding in the structure is similar to that of the second group.

## Water in minerals. Dehydration

Water is the most frequent decompositions product which can be bound many ways with different forces in the various minerals. The kinetic and mechanism of water release and the temperatures and the temperature intervals of the reaction differ widely. Molecular water can be bound in minerals in two fundamentally different manners; by adsorption forces on

**Table 11.** The most frequent types of occurrence of water in minerals and their most characteristic thermoanalytical features

Type and location of water				Bonding types	Form of water elements	Factors governing quantity of water	Reaction of water removal	Temperature of water removal	Character of water escape	Influence of water on structure
Bound on surface	Adsorbed on external surfaces			van der Waals forces	$H_2O$	Surface polarity and external conditions	Desorption	40–100 °C	Non-equilibrium process, non-isothermal under quasi-equilibrium conditions	No structure-determining function
	In open internal spaces	Interlayer In channels	Internal space decreases	Free or physically adsorbed water (van der Waals)	Mainly $H_2O$ , OH traces Mainly $H_2O$ , some OH (mainly on AlO, tetrahedra)	Size and features of surface of internal space		Wide temperature range, depending on physical and energetical conditions		
Bound in internal spaces		In internal spaces of natural glasses or amorphous structures	↓	(forces or H-bonding), capillary condensation	Mainly OH, further $H_2O$ layers		Decrepitation	Temperature of the emergence of incision	Explosion like for nonpurified sample	No structure-determining function
	In closed internal spaces	Inclusions In lattice elements	Primary in mineral Enclosed by heating		Liquid or gaseous $H_2O$ molecules "Solid solution" as compound crystal	Size of internal space		Temperature of the rearrangement of lattice elements	Non-isothermal	
	Cation hydrate sheet					Cation hydration energy		Depending on the hydration's energy of cation		
Covalently bound	Crystal water			Coordinate H-bonding around the cations	$H_2O$ molecules		Thermal dissociation (dehydroxylation)	Depending on phase equilibrium	Equilibrium process, isothermal under quasi-equilibrium conditions	Except for last molecule essentially no structure determining function
	Structural OH ions			Ionic-covalent bonding	OH ions	Stoichiometric		Depending on electronegativity and on position in lattice structure	Essentially isothermal, for complex structures non-isothermal due to diffusion	Structure-determining

the different surfaces of the structure (value of bonding energy 1–40 kJoule/mol) or by something stronger coordination forces around certain cations of the structure. Water is the decomposition product of dehydroxylation too. The Table 11 lists the decomposition processes accompanied by the escape of water, and the most important features of these processes. It is clearly shown in the Tables, that the different types of water form continuous sequences.

References: 323, 336

### Adsorbed water

Minerals are capable of binding different amounts of water, both on their external and on their internal surfaces, namely on the surface of the internal channels or other cavities of the crystal. A typical example for water adsorbed on external and internal surfaces of minerals is provided by silicates that contain  $\text{SiO}_4$  and especially  $\text{AlO}_4$  tetrahedra. The polar ions or atomic groups on the surface of a solid, bind the polar water molecules by van der Waals forces. It is an interaction between the O atoms of the siloxane or Si-O-Al groups and the water hydrogen. The interaction depends on the Si-O-Si angle. The most hydrophil character has an angle  $<109^\circ$ . The hydrophilicity of a Si-O-Al group is higher as compared to a Si-O-Si group. The resulting monomolecular layer also creates a new polar surface, which permits the oriented adsorption of further molecule sequences. Properties of the adsorbed water molecules differ from the properties of the molecules in bulk liquid water only in the first nanometre from the clay surface which is equal to approx. three monolayers. Water and the silicate together form a solid phase. The most difficult type to remove the water stuck directly on the solid surfaces of minerals. Sorbed metal on the external surface of montmorillonite only with few  $\text{H}_2\text{O}$  molecules are hydrated.

Another possibility for water adsorption is the edge surface of the disrupted aluminosilicate layer where the exposed functional groups are very active. When these activated groups are in contact with water chemisorption may occur and this “broken bond surface” is covered with amphoteric surface hydroxyls mainly in the form of silanol, aluminol or magnesol. During water adsorption water-hydroxyl bonds are formed.

The linkage may be on the external surface of minerals (so-called sticking water), or can appear on the surface of the internal spaces formed by the structure of minerals. Practically, binding of water on the internal surfaces is the same as described above, if the available internal space is large enough. These internal surfaces and cavities may be of different shape and size and these can influence significantly the types of binding.

The escape of the free liquid “sticking” water as a colloid system from the surface is at lower temperature compared to the interlayer water (Figure 14, Table 12). In the case of the air-dried sample water bounded to the external surfaces as a solid phase may be seen at the low temperature size of the dehydration peak.

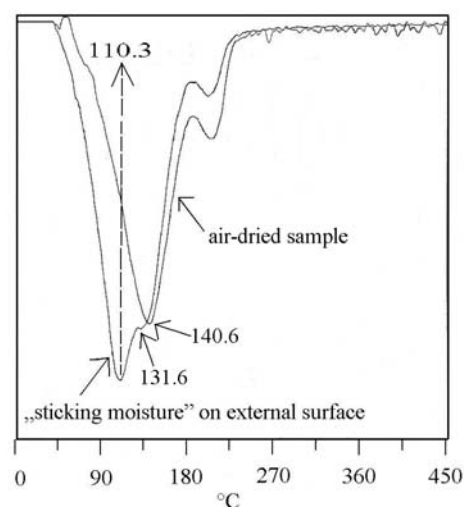


**Figure 14.** Quarry sap on bentonite sample (from Buru, Romania) and the same sample 4 months later

**Table 12.** Measurement parameters of the bentonite sample from Buru, Romania

Sample condition	Sample mass (mg)	Mass loss (%)	Measured peak temperature I (°C)	Measured peak temperature II (°C)	Corrected peak* temperature I (°C)	Corrected peak* temperature II (°C)
Sample with quarry sap	113	13.1	110.3	131.6	119	145
Air-dried sample	158.1	7.58		140.6		146

\*Corrected to 18 mg mass of water.

The external surface area for most natural smectites is less than 20% of the internal surfaces. The binding energy of water on the external surfaces of clay minerals about  $1.5 \pm 1$  kJ/mol.

### Interlayer waters bond by phyllosilicates

In the minerals of the smectite group a small amount of tetrahedral Si atoms is substituted by Al, and/or the octahedral Al atoms are substituted by atoms of lower oxidation number. Therefore there is an abundance of negative ions in the crystal-forming layer complex, which can be balanced by an interlayer, regularly exchangeable cation and by water. This water has no structure determining function; the escape of water is non-equilibrium process. The reaction under quasi-equilibrium condition is non-isotherm (Figure 15).

Fine structure of water in the interlayer space divided into three zones has different water structure (YARIV 1992). Two zones contain ordered water. The first one is the layer at the flat oxygen planes which border the interlayer space ( $A_0$ ). The nature of the oxygen plane depends on the charge of the silicate layer and the octahedral substitution. Predominantly the Si-

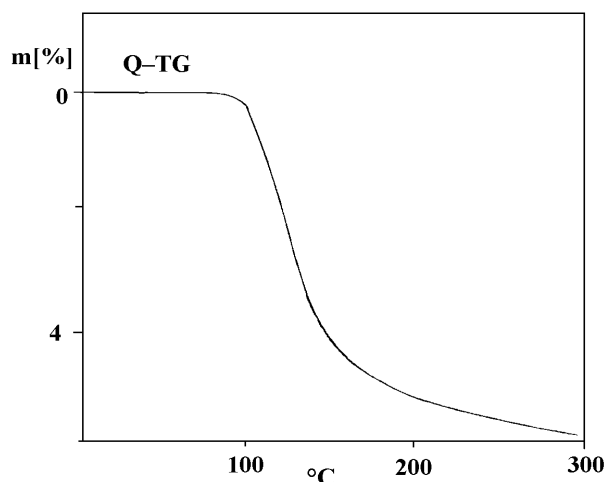


Figure 15. Q-TG curve of Na-montmorillonite

O-Al groups of the oxygen plane at tetrahedral substitution can form hydrogen bonds with water molecules. The second type is the hydration zone of the interlayer cation which is the result of ion-water electrostatic interaction. Each ion is surrounded by a cosphere in which the organisation of water molecules differs from that in the outside ( $A_m$ ). The hydrations energy of an exchangeable cation depends on its size, charge and on its electronegativity (Table 13). The nature of the exchangeable cation markedly influences the low-temperature peak system.

The third zone having a low degree of order serves a bridge between the two first zones ( $B_{om}$ ).

The bond energy of water in the interlayer space is about  $7.5 \pm 3$  kJ/mol and in the interlayer space with cation 7.8–12.1 kJ/mol.

The loss of sorbed water gives a large peak system at a low temperature on the thermogravimetric curve. The form of endothermic effects can be of simple or double character depending on the nature of exchange cations. Montmorillonite with different cations in the interlayer space may have different interlayer distance. If the basal spacing found between 9.8–10 Å water molecules are adsorbed mainly on the outer surface of the 2:1 phyllosilicates (hydromicas). Until the formation is a monolayer, the basal spacing is about 12.2–12.4 Å. When the basal spacing is between 14.5–15 Å it indicates that a second water layer is formed in the interlayer space.

The montmorillonite saturated with monovalent cation has only a single thermal dehydration peak. The amount of water is about 7%, due to water form the monolayer in the interlayer space ( $d(001) = 12$ –12.6 Å). The hydration number of the metal is 3 or 4 and it has a triangular or square flat coordination parallel to the layers.

The Cs in the interlayer space has no  $A_m$  zone due to its low electric charge and large size. But two  $Cs^+$  — two water complexes are so strongly bound that they are observed as a unit. The DTG peak is symmetric (Figure 16), based on the investigation of 10 different samples with  $\alpha_{(max)}$  between 46–52% (average 47%), basal spacing between 12.28–12.49 Å measured by X-ray diffraction. Monte Carlo (MC) and molecular dynamics (MD) modelling techniques suggest that, in stable Cs-smectite the interlamellar water content is less than a monolayer. Cs-montmorillonite, containing 1/3 and 2/3 water monolayer is the “12 Å Cs-smectite”, 1/3 monolayer is the most likely stable water content (Figure 16).

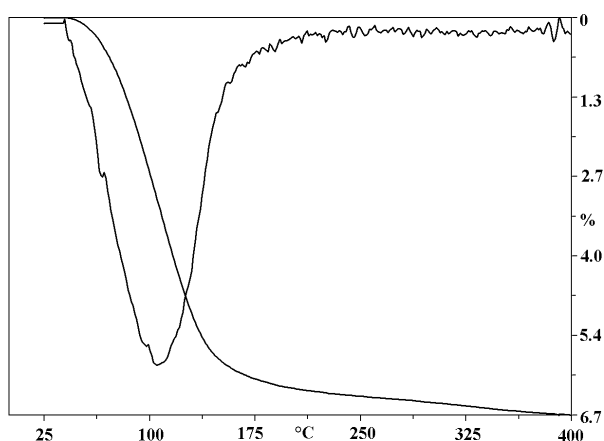


Figure 16. Dehydration of Cs-montmorillonite

Table 13. Hydration enthalpies ( $\Delta H_{hyd}$ ) of metal cations (data are taken from WULFSBERG 1987)

Charge	Hydration enthalpies (kJ/mol)					
	electronegativity<1.5			electronegativity>1.5		
	ion	radius	$\Delta H_{hyd}$	ion	radius	$\Delta H_{hyd}$
1	Cs	181	-263			
	Rb	166	-296	Tl	164	-326
	K	152	321			
	Na	116	405	Ag	129	475
	Li	90	515	Cu	91	594
	H		-1091			
2	Ba	149	1304			
	Sr	132	-1445	Pb	133	-1480
	Ca	114	-1592	Cd	109	-1806
				Cr	94	1850
				Mn	97	1845
				Fe	92	-1920
	Mg	86	-1922	Co	88	-2054
				Ni	83	-2106
				Cu	91	2100
				Zn	88	2044
3				Fe	78	-4376
4	Ce	101	-6489	Al	67	4660

stable Cs-smectite the interlamellar water content is less than a monolayer. Cs-montmorillonite, containing 1/3 and 2/3 water monolayer is the “12 Å Cs-smectite”, 1/3 monolayer is the most likely stable water content (Figure 16).

Montmorillonite saturated by K or Na shows an asymmetric dehydration peak (Figures 17, 18).

They have only a small water sheet. Their ion-water interactions (coordinative bond) are slightly lowers than that of the water-water interaction (hydrogen bond in water is stronger than most other intermolecular forces because every water molecule is H-bond with four other molecules).

In the case of K-montmorillonite based on investigated 13 different samples with  $\alpha_{(max)}$  between 49–67% (average 60%), basal spacing between 12.07–12.85 Å (monolayer) measured by X-ray diffraction.

Measurement data for 23 Na-montmorillonite samples with  $\alpha_{(max)}$  between 50–73% (average 65%), basal spacing between

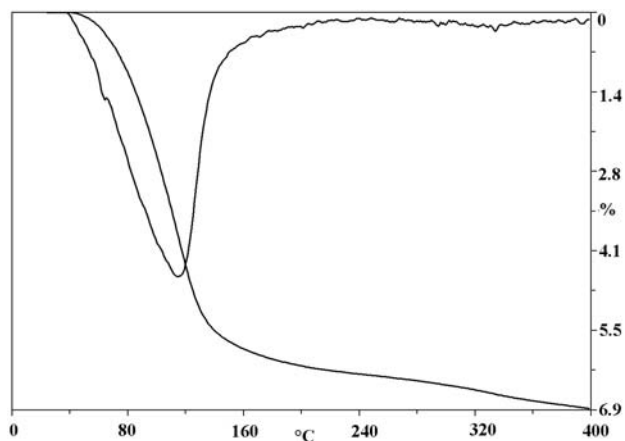


Figure 17. Dehydration of K-montmorillonite

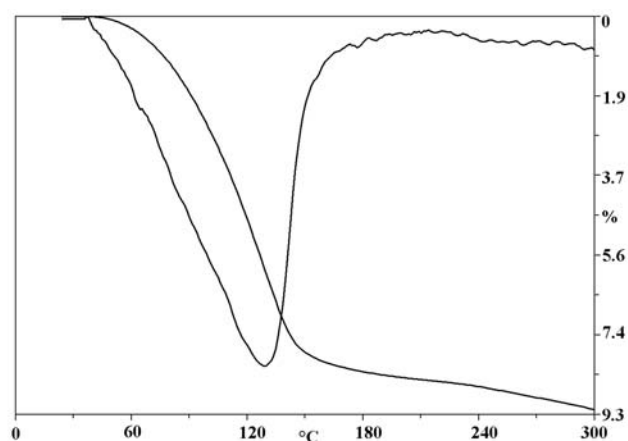


Figure 18. Dehydration of sodium activated montmorillonite

11.43–13.24 Å (monolayer) measured by X-ray diffraction. There was some difference between the shape of dehydration peak of activated [ $\alpha_{(\max)}$  between 50–70% (average 63%)] and of the seven natural ( $\alpha_{(\max)}$  between 68–73% (average 71%) Na-montmorillonites.

At the Ag saturated montmorillonite where the electrostatic bonding is something larger as at Na the curve of dehydration is symmetric (Figure 19) (Ion-water interaction is probably equal to the water-water interaction). Measurement data:  $\alpha_{(\max)}$  51% “d value” 12.6 Å (monolayer). The exothermal reaction at 361 °C refers to the oxidation of metallic silver.

Dehydration of Li saturated montmorillonite appears to be anomalous, because it gives a double peak (Figure 20). The high temperature peak corresponds to the water escaping from the cation hydrate sheet. This separate peak has several possible explanations: (1) the hydration energy of Li is higher compared to other monovalent cations. (2) Li is small enough to be organized in the interlayer close to the oxygen plates, and it forms higher energy sites for water adsorption. Li-montmorillonite has the highest water content among the monovalent saturated montmorillonites. Measurement data reflect these special behaviours. For 16

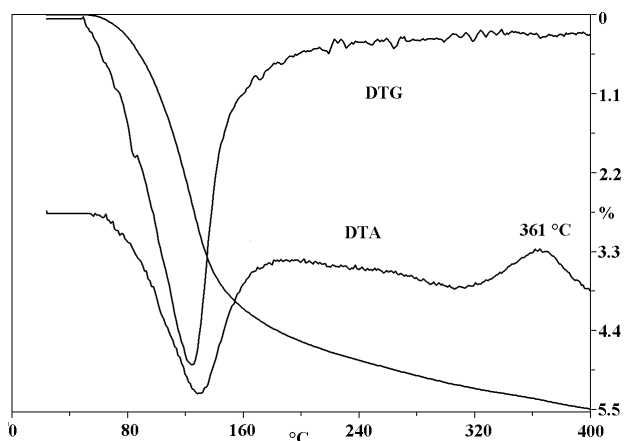


Figure 19. Dehydration of Ag-montmorillonite

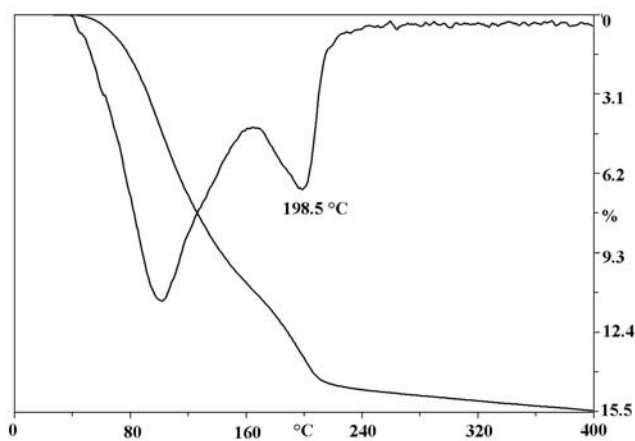


Figure 20. DTG curve of the two-step dehydration of Li-montmorillonite

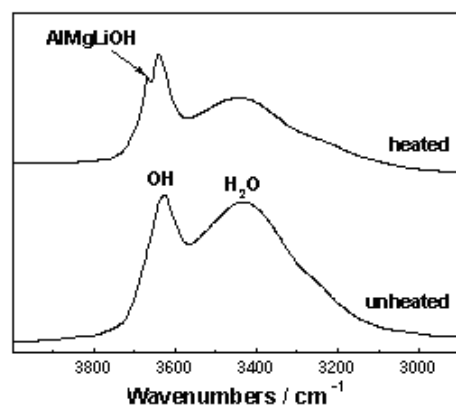


Figure 21. IR spectra of Li-montmorillonite samples in OH stretching regions: unheated and after heating for 24h at 300 °C (after MADEJOVÁ et al. 1999)

Li-montmorillonite samples with  $\alpha_{(\max)}$  between 21–36% (average 31%), basal spacing between 12.16–15.45 Å measured by X-ray diffraction (the structure of interlayer water in Li-montmorillonite can be either two- or one-layer hydrates depending on the circumstances, for example on humidity).

When Li-saturated montmorillonite is heated to 200–300 °C, the Li ions migrate from inter-layer positions to sites in the layer structure. Li<sup>+</sup> gets fixed in two different sites: (1) in the pseudohexagonal holes of the tetrahedral sheet, and (2) in the previously vacant octahedra, creating local trioctahedral domains. Analysis of the FTIR spectra in the MIR regions with the AlMgLiOH stretching band at 3668 cm<sup>-1</sup> of Li-montmorillonite heated up to 300 °C is presented in Figure 21.

The montmorillonite saturated with bivalent cation has generally a double peak of dehydration. Water content of the montmorillonite is about 14–15% corresponding to the double layer of the octahedral coordination of hydration water of Me<sup>2+</sup>.

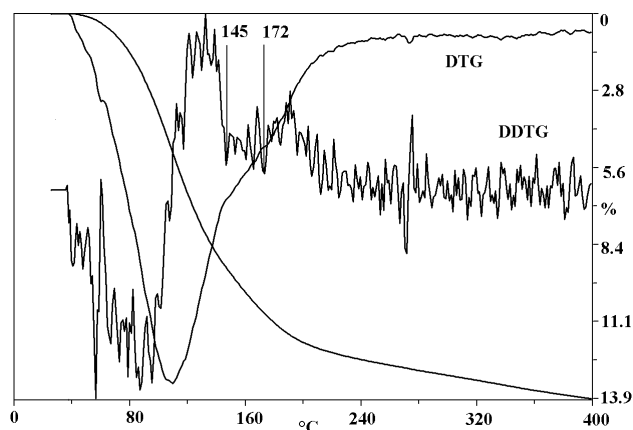


Figure 22. DTG and DDTG curves of Ba-montmorillonite dehydration

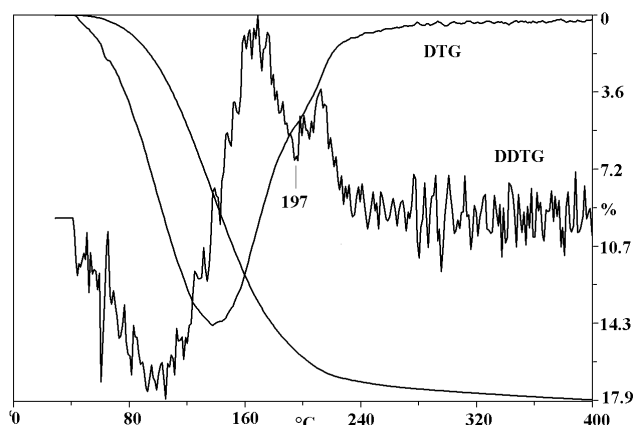


Figure 23. DTG and DDTG curves of Hg-montmorillonite dehydration

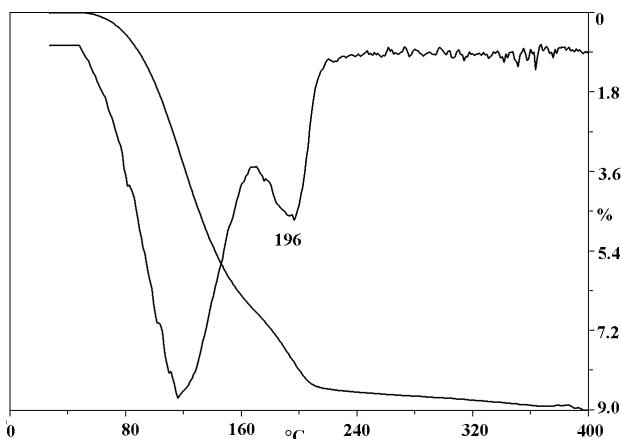
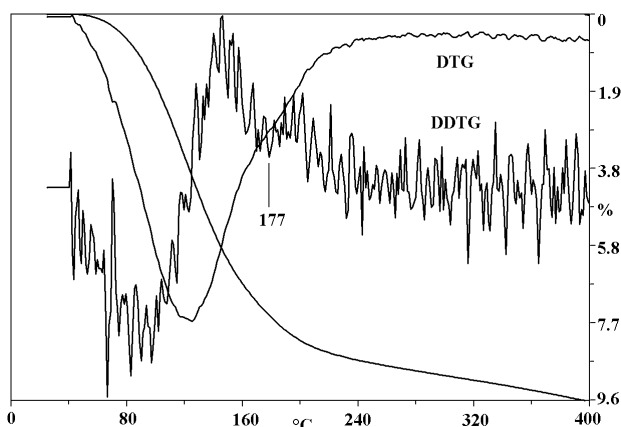


Figure 24. DTG curve of dehydration of Ca-montmorillonite (Kuzmice, Slovakia)



The dehydration peak of Ba saturated montmorillonite shows only a shoulder about 150–170 °C on the higher temperature side of the reaction. The second reaction may be better seen on the second derivate curve (Figure 22). Characteristic measurement data of 13 investigated samples are:  $\alpha_{(\max)}$  between 32–42% (average 38%), the basal spacing between 14.24–16.23 Å measured by X-ray diffraction (corresponding to the 2-layer hydrate).

Similar thermogravimetric picture may be seen in the case of Hg saturated montmorillonite, but the peak on the DDTG curve corresponding to the higher hydrations energy is at a somewhat higher temperature (Figure 23). Basal spacing is 15.54 Å (double layer) measured by X-ray diffraction.

In normal case the DTG curve of Ca-montmorillonite shows two separate steps of dehydration (Figure 24). Measurement data of 13 natural and one Ca saturated samples are:  $\alpha_{(\max)}$  between 36–51% (average 42%), basal spacing between 14.52–15.72 Å (corresponding to the 2-layer hydrate) measured by X-ray diffraction.

Sometimes the DTG curve of natural montmorillonite is less characteristic. The basal space [d(001) 16.04 Å] is corresponding to the double water layer but the hydrate sheet of the cation may be seen only on DDTG curve (Figure 25). The explanation can be that the interlayers of natural montmorillonites are usually not homoionic (Figure 26).

Manganese (II) ion adsorbed in the interlayer space of montmorillonite has a greater hydration energy than Ca has, therefore the elimination of water coordinated to manganese ion takes place at a higher temperature, at about 240–250 °C. Measurement data of 4 Mn saturated samples are:  $\alpha_{(\max)}$  between 30–42% (average 36%), basal spacing between 14.56–15.07 Å measured by X-ray diffraction (corresponding to 2-layer hydrate). The observed exothermic reaction is the oxidation of manganese (II) to manganese (IV) (Figure 27).

Manganese (II) ion adsorbed in the interlayer space of the montmorillonite oxidizes spontaneously to manganese (IV) under atmospheric conditions. The peak of the second dehydration in DTG curve cannot be observed practically and the exothermic oxidation is not observed on the DTA curve of the old manganese-montmorillonite (Figure 28). The basal spacing of montmorillonite (001) determined by X-ray diffraction is very similar for both the fresh (15.1 Å) and old (14.8 Å) samples.

Dehydration of Mg-montmorillonite is a well distinguished two-step reaction. The peak of the dehydration of the water coordinated to magnesium is to be seen at about 245–255 °C (Figure 29). Measurement data of 10 Mg saturated samples are:  $\alpha_{(\max)}$  between 44–57% (average 48%), basal spacing measured by X-ray diffraction between 14.63–16.25 Å (corresponding to 2-layer hydrate).

The characteristic data of different monovalent and bivalent interlayer cations are summarised in Table 14.

Copper sorption on montmorillonite may include several processes with different characteristics; therefore both thermal and X-ray diffraction data with great discrepancies have been described. For example: “original Ca-montmoril-

Figure 25. DTG and DDTG curves of dehydration of Ca-montmorillonite (Egyházaskesző, Hungary)

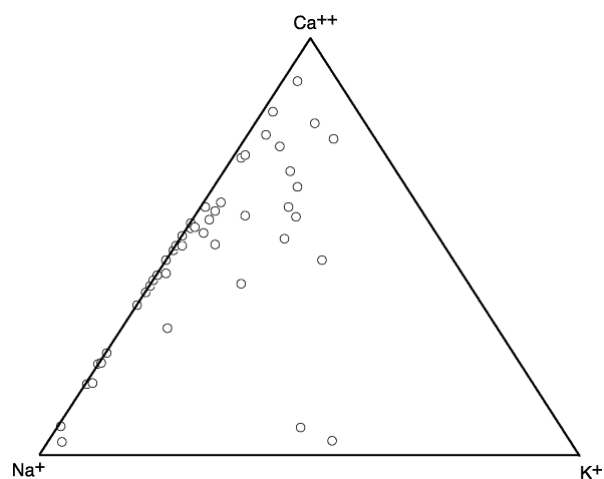


**Figure 26.** Interlayer cation contents of smectites in the samples from Hole 735B of Ocean Drilling Program (after ALT, BACH 2001)

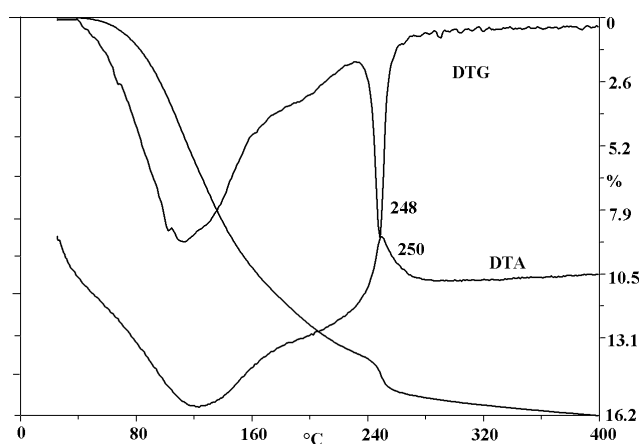


**Figure 27.** Thermoanalytical curves of fresh Mn-montmorillonite

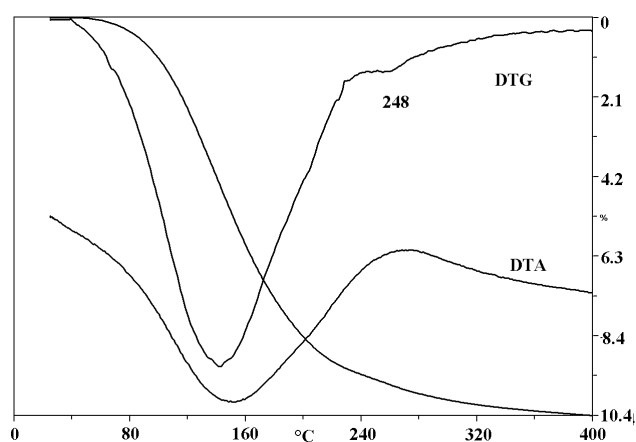


**Figure 28.** Thermoanalytical curves of the same Mn-montmorillonite three years later

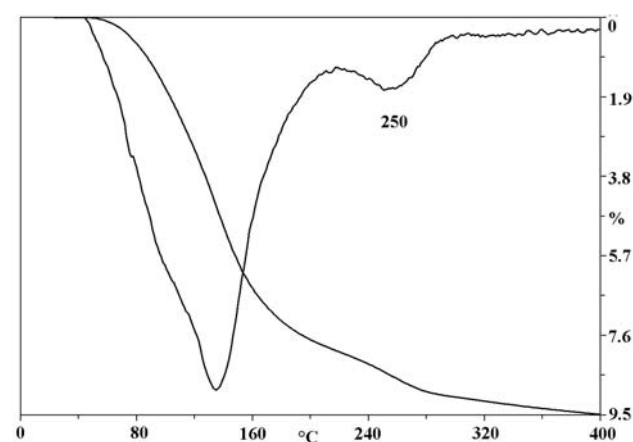


**Figure 29.** DTG curve of dehydration of Mg-montmorillonite

**Table 14.** Characteristic data of the monovalent and bivalent interlayer cations

Cation	Piece	Ionradius Å	Ionpotencial	Hydration enthalpy kJ/mol	$\alpha$ %	DTG peak of cation sheet °C	DDTG peak of cation sheet °C	d(001) Å
Monovalent								
Cs	10	1.81	0.55	-263	47			12.4
K	13	1.52	0.66	-321	60			12.27
Na	23	1.16	0.86	405	65			
Ag <sup>+</sup>	1	1.29	0.78	-475	51			
Li	16	0.9	1.11	-515	31	188		13.76
Bivalent								
Ba	13	1.49	1.34	-1304	38	147	152	15.58
Hg	1	1.16	1.72	1480	49		197	15.54
Ca	14	1.14	1.75	-1592	42	192		15.22
Mn	4	0.97	2.25	-1845	36	246		14.78
Mg	10	0.86	2.33	1922	48	245		15.05

Ionite treated with different concentrations of  $\text{CuSO}_4$ -solution show that adsorption of copper causes collapse in the structure from 14.71 Å to 12.75 Å (Kiss et al. 1997); or “Copper-bearing montmorillonite (Cu-MMT) was produced by  $\text{Cu}^{2+}$  cation exchange reaction. X-ray diffraction analysis showed that the (001) basal spacing of the MMT crystal lattice increased from 1.544 to 1.588 nm after  $\text{Cu}^{2+}$  exchange. This indicated that  $\text{Cu}^{2+}$  entered into interlayer position of MMT as a hydrated cation” (XIA et al. 2004). The movement of  $\text{Cu}^{2+}$  as a small cation from the interlayer into the 2:1 layer of montmorillonite upon heating is possible (d 12.4 → 9.5 Å) (HELLER-KALLAI, MOSER 1995).

The discrepancies can be explained by several reasons. There is heterogeneity of the sites for the adsorption of Cu. At low ionic strength, results suggest that Cu is sorbing in the interlayer and maintains its hydration sphere. At high ionic strength, Cu atoms are excluded from the interlayer and sorbed primarily on the silanol and aluminol functional groups of the montmorillonite (STRAWN et al. 2004). Cu adsorption may take place on edges or plains of montmorillonite

(UNDABEYTIA et al. 2002). Some  $\text{Cu}^{2+}$  ions seemed to replace the original interlayer metal cations and some entered into the hexagonal cavities. A small fraction of  $\text{Cu}^{2+}$  ions penetrated into the octahedral vacancies (HE et al. 2001).

The adsorption of copper depends on several other factors. In the Cu-smectite at a very low humidity the hydration number is below 4 (monolayer) (YARIV 1992). The adsorption of copper depends too on the concentration of the solution and on the concentration of the background electrolyte. The basal spacing of the Cu-montmorillonite depends on the Cu concentration of the ion and the pH (NÉMETH 2003). Copper forms  $\text{CuOH}^+$  at higher pH (STADLER, SCHINDLER 1993). The amount of fully hydratable  $\text{Cu}^{2+}$ -ions ( $[\text{Cu}(\text{H}_2\text{O})_6]^{2+}$ ) in interlayer positions depends on increasing time of treatment (PLÖTZE, EMMERICH 2004).

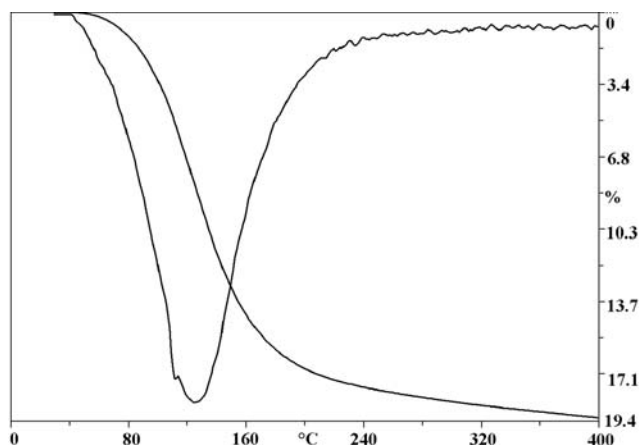


Figure 30. DTG curve of dehydration of Al-montmorillonite

The trivalent Al in the exchanged montmorillonite has a greater polarizing power. Therefore the  $A_m$  zone of Al extends over large areas. Since the total number of Al ions in the interlayer is only the third of the number of monovalent ions, the total area occupied by  $A_m$  is comparatively small, leaving space for the formation of zones  $B_{om}$  and  $A_o$ . The dehydration effect on the thermogravimetric curve is double corresponding to the bind of water molecules in various ways (Figure 30). The d-value of the montmorillonite (001) basal spacing for the presented sample is 15.76 Å, the water content is somewhat higher as earlier (19.5%).

The hydrolyzed state depends on pH. At higher pH gibbsite-like (gibbsite or nordstrandite: X-ray reflections at 4.86 and 4.36 Å, DUBBIN et al. 1994) and pseudoboehmite (X-ray reflection at 6.4 Å, BRYDON, KODAMA 1966) groups are present in the interlayer. According to MAFTULEAC et al. (2002) the endothermal effect of Al-montmorillonite is changed dependent on pH (Table 15 and Figure 31).

Table 15. Probable state of active centres of Al-montmorillonite treated with solutions of various pH values

pH interval	d(001) (nm)	Water quantity of the first endothermal effect (%)	Water quantity of the second endothermal effect (%)	Quantity of released water (%)	Interlaminary exchangeable cations
0.9	1.32	7.5	10	17.5	$\text{Al}(\text{H}_2\text{O})_6 \cdot m\text{H}_2\text{O}$
1	1.32	7.5	10	17.5	$\text{Al}(\text{H}_2\text{O})_6 \cdot m\text{H}_2\text{O}$
1.05	1.33	7.5	10	17.5	$\text{Al}(\text{H}_2\text{O})_6 \cdot m\text{H}_2\text{O}$
1.85	1.49	7.5	10	17.5	$\text{Al}(\text{H}_2\text{O})_6 \cdot m\text{H}_2\text{O}$
2.3	1.53	8	10	18	$\text{Al}(\text{H}_2\text{O})_6 \cdot m\text{H}_2\text{O}$ and $\text{Al}(\text{OH})(\text{H}_2\text{O}) \cdot n\text{H}_2\text{O}$
3.5	1.53	10	7	17	$\text{Al}(\text{H}_2\text{O})_6 \cdot m\text{H}_2\text{O}$ and $\text{Al}(\text{OH})(\text{H}_2\text{O}) \cdot n\text{H}_2\text{O}$
4.15	1.53	10.5	7.5	18	$\text{Al}(\text{H}_2\text{O})_6 \cdot m\text{H}_2\text{O}$ $\text{Al}(\text{OH})(\text{H}_2\text{O}) \cdot n\text{H}_2\text{O}$ and $\text{Al}(\text{OH})_3 \cdot (\text{H}_2\text{O})_4 \cdot k\text{H}_2\text{O}$
4.4	1.53	11	7	18	$\text{Al}(\text{H}_2\text{O})_6 \cdot m\text{H}_2\text{O}$ $\text{Al}(\text{OH})(\text{H}_2\text{O}) \cdot n\text{H}_2\text{O}$ and $\text{Al}(\text{OH})_3 \cdot (\text{H}_2\text{O})_4 \cdot k\text{H}_2\text{O}$
4.6	1.53	11	6	17	$\text{Al}(\text{H}_2\text{O})_6 \cdot m\text{H}_2\text{O}$ $\text{Al}(\text{OH})(\text{H}_2\text{O}) \cdot n\text{H}_2\text{O}$ and $\text{Al}(\text{OH})_3 \cdot (\text{H}_2\text{O})_4 \cdot k\text{H}_2\text{O}$
5.1	1.31	11	6	17	$\text{Al}(\text{H}_2\text{O})_6 \cdot m\text{H}_2\text{O}$ $\text{Al}(\text{OH})(\text{H}_2\text{O}) \cdot n\text{H}_2\text{O}$ and $\text{Al}(\text{OH})_3 \cdot (\text{H}_2\text{O})_4 \cdot k\text{H}_2\text{O}$

The relatively weak bonding of the water bound by adsorptive forces in the inner spaces of the montmorillonites shows the temperature values of the PA curve (Figure 32).

Halloysite has a kaolinite structure layer with a layer of water (2.9 Å) in the interlayer space. The layer thickness is therefore, 10 Å. The interlayer water in the lattice of halloysite where the layers curve and form a tubular structure due to the different size between the tetrahedral and octahedral layers (the smaller octahedric layer to the inside of the curve), each layer is separated by a monolayer (sometimes by two layers) of water.

The interlayer water is weakly bound. YARIV, SHOVAL (1975) showed that water molecules inside the interlayer space of halloysite are oriented toward the hydroxyl plane with the negative oxygens of water molecules but do not form hydrogen bond with OH-groups of the hydroxyl plane as the basal hydroxyls of the layer are very weak proton donors. Positive hydrogens are oriented toward the oxygen plane, but there is no localized interaction between water molecules and the basal sheets. Instead, hydrogen bonds occur between water molecules forming water clusters.

Examinations of GIESE, COSTANZO (1986) indicated that the water in 10 Å hydrate is of two types in equal quantity. One type (termed hole water) is closed into the ditrigonal holes of the silica tetrahedral and forms hydrogen bonds to the tetra-

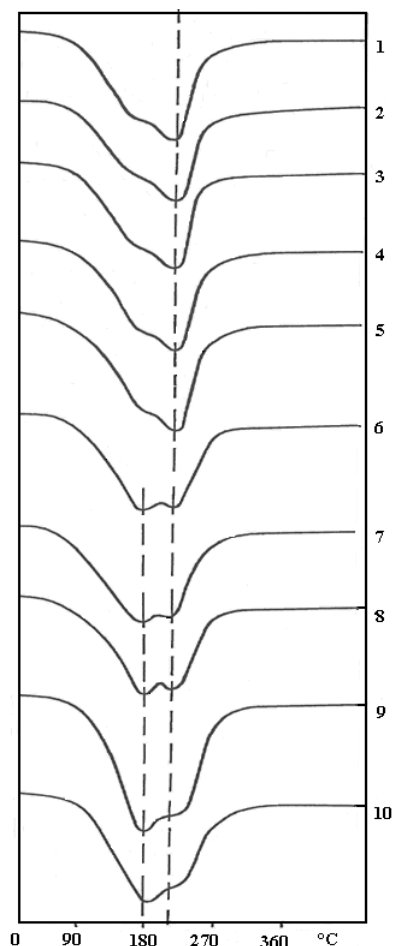


**Figure 31.** DTA curves of dehydration of Al-montmorillonite treated with solutions of various pH values (after MAFTULEAC et al. 2002)

hedral basal oxygen. The second type (termed associated water) lies at a different level in the structure that is farther from the tetrahedral sheet than the hole water. Associated water molecules donate hydrogen bonds to adjacent hole water molecules and receive hydrogen bond from three hydroxyls of the octahedral sheet.

There is some uncertainty in the published data regarding the way the molecular water is held in the illite itself.

“The breadth of the loss of molecular water over a wide range of temperatures corresponds to a similar distribution of intermolecular and binding forces between the polar water molecule and the clay composition (structural, sorbed or both?)” (EARNST 1991a).

The molar proportion of structurally bound  $H_2O$ ,  $H_2O^+$ , shows a strong negative correlation with the sum  $K+Na+Rb+Cs+Ca+Ba+0.33(F+Cl)$ , which demonstrates that the  $H_2O^+$  excess over that required for full occupancy of halogen-OH sites is chiefly bound in interlayer sites of alkali-deficient micas.

A phengitic component is present in which substitution of  $R^{2+}$  cations for octahedral Al is balanced by the addition of tetrahedral Si beyond the ideal Si:Al ratio

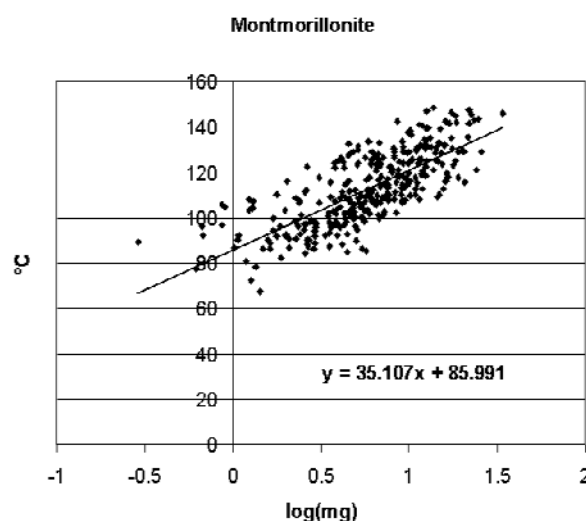


**Figure 32.** Dehydration temperature and “PA curve” of montmorillonites based on the measurement of 382 different natural samples

of 3:1 for muscovite. This substitution gives the octahedral sheet an overall negative charge of about 0.2 to 0.3 per formula unit. Interlayer vacancies or water molecules amounting to about 0.2 to 0.4 atoms per formula unit are compensated by additional tetrahedral Si cations beyond those required by the phengitic component.

There are three models for incorporation of  $H_2O$  in interlayer sites:

(1) neutral interlayer  $H_2O$  molecules as a consequence of fewer interlayer cations, (GRIM 1953), and molecular water in the micas is in the hexagonal cells non-occupied by potassium ions (BILONIZHKA 2001).

(2) a medium amount of K is replaced in illite by interlayer hydronium (oxonium or hydroxonium) ions,  $H_3O^+$  (BROWN, NORRISH 1952), and

(3) as a combination of  $H_2O$  and  $H_3O^+$ . Investigations of LOUCKS (1991) indicate that hydronium ion is a substantial interlayer site occupant in white micas formed in acidic to neutral pH environments at temperatures below about 450 °C. Neutral  $H_2O$  molecules occupy a significant fraction of interlayer sites in pedogenic and diagenetic illites and some hydrothermal sericites. Occurrence of vacant interlayer sites is virtually nonexistent.

The high pressure differential thermal analysis and resonating proton model do not support the  $H_3O^+$  model (MILLER et al. 1991a, b).

The force of bonding seems to be lower as in the case of montmorillonites (Figure 33).

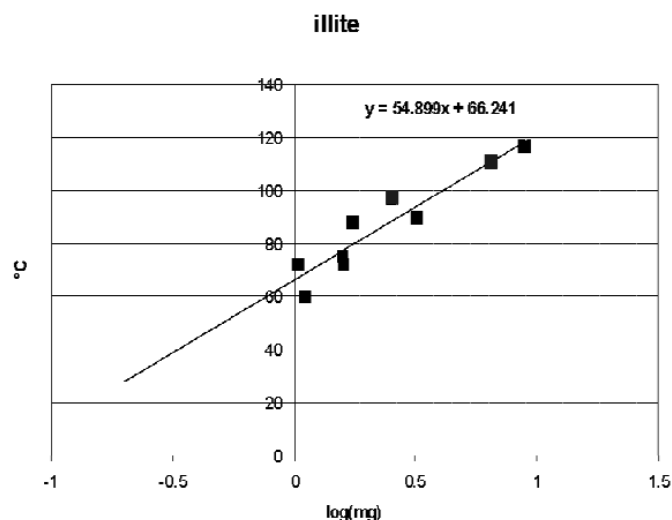


**Figure 33.** Dehydration temperature and “PA curve” of illites and glauconites

References: 15, 35, 36, 94, 97, 137, 143, 213, 226, 262, 270, 271, 333, 337, 386, 400, 425, 432, 436, 450, 480, 481, 497, 550, 570, 600, 673, 703, 704, 744, 745, 776, 788, 876, 884, 894, 914, 1023, 1034, 1046, 1047, 1074, 1076, 1099, 1174, 1177, 1178

## “Zeolitic water”

In zeolites and in the structure of some other minerals (e.g. aluminite, palygorskite etc.) the so-called “zeolitic water” is found in channels formed by the  $\text{SiO}_4$  and  $\text{AlO}_4$  tetrahedra, where it can move more-or-less freely. Relatively free movement is possible in wide channels, whereas narrower channels or capillaries impede movements, and water is adsorbed on the surface, e.g. mainly bound to the  $\text{AlO}_4$  tetrahedra, partly in the form of OH-groups. The escape temperature of the latter is higher, than that of molecular water. The nature of the internal space depends on the system of interconnecting channels. Three types of channel systems are identified from this point of view (BRECK 1974):

- One-dimensional system not permitting the intersection of the channel (for example analcime).
- Two-dimensional systems (for example natrolite, mordenite).
- Three-dimensional system type has two variants. In one type, channels are equidimensional; free diameter of all the channels is equal (for example: chabasite). The second type consists of three-dimensional intersecting channels, but the channels are not equidimensional; the diameter depends upon the crystallographic direction.

Internal spaces may be capillaries of extensive internal surfaces, and in this case capillary condensation plays a prominent role in water binding. These surfaces are covered by an  $\text{H}_2\text{O}$  monomolecular layer, which often belongs to the neighbouring surfaces. In such cases water is bound relatively stronger to the polar solid surface. Zeolites with high kinetic diameter (for clinoptilolite  $3.5 \text{ \AA}$ , free aperture of main channels for mordenite  $6.7 \times 7 \text{ \AA}$ , for chabasite  $3.7\text{--}4.2 \text{ \AA}$ , for stilbite  $4.1 \times 2 \text{ \AA}$ ) have

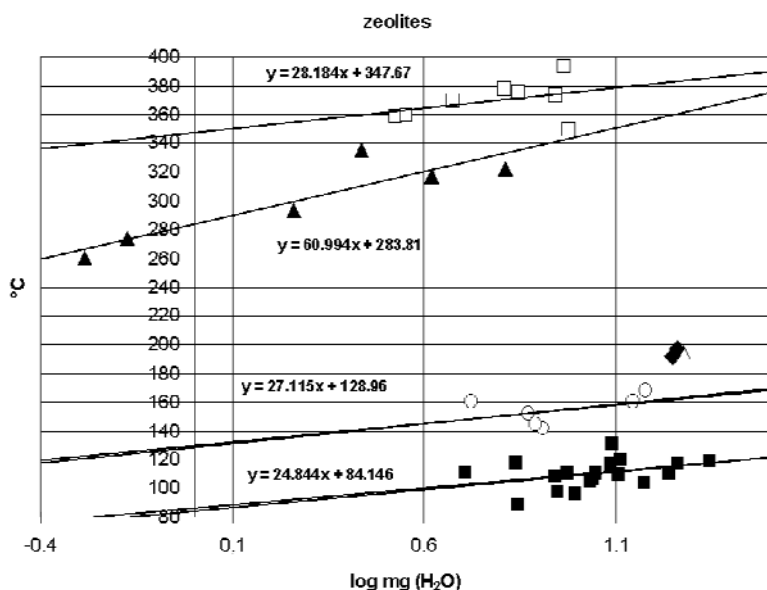


**Figure 34.** Dehydration temperature and “PA curve” of different kind of zeolites (clinoptilolite ■, mordenite ○, stilbite ◆, chabasite △, analcime ▲, natrolite □)

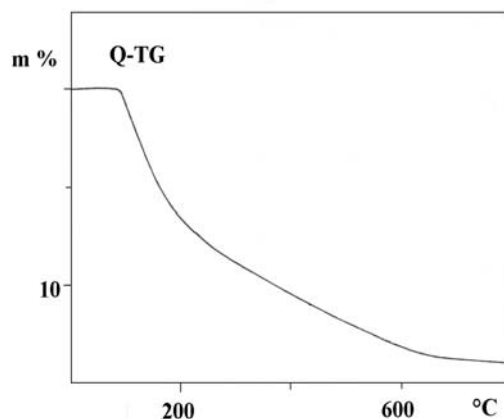


**Figure 35.** Q-TG curve of mordenite

the main dehydration temperature lower than  $200 \text{ }^\circ\text{C}$  and at zeolites with low kinetic diameter (for example analcime and natrolite  $2.6 \text{ \AA}$ ), the dehydration temperature is higher than  $250 \text{ }^\circ\text{C}$  (Figure 34).

Zeolitic water is bound in adsorptive way and has no structure determining role. Most zeolites may be dehydrated without the major alteration of their crystal structure. The loss of adsorbed water from the internal spaces due to heating is not an equilibrium reaction and the dehydration curves from quasi-isothermal heating techniques are always non-isothermal essentially (Figure 35).

References: 121, 582

## Water in amorphous phases

In materials with less ordered structure (short or intermediate range order  $5\text{--}15 \text{ \AA}$ ) internal spaces can be found generally. Natural glassy rocks and amorphous formations often contain water bound similarly to zeolitic water. In glassy rocks, most of this water is bound in OH form either as single hydroxyl (silanol) groups, or as pairs of hydroxyls.

The network forming the glassy rock is composed primarily of  $\text{SiO}_4$  and to a much lesser extent of  $\text{AlO}_4$  tetrahedra to which OH-groups are bound free or they bridge the  $\text{SiO}_4$  tetrahedra by hydrogen-bonds. If the internal space is large enough further water molecules can be hydrogen-bonded to the OH layers of the surface to permit this. Such binding is weaker, its elimination taking place at a lower temperature.

The quantity of water on the external surfaces and in the open internal spaces bound by adsorptive forces depends on the size and shape of these spaces as well as on the polarity of the surface and accordingly change the binding forces in the above mentioned ways. Water is bound by different energies and thermoanalytical curves usually reveal its steady loss over

a wide temperature range as poorly defined features (Figure 36). The bond on the surface of alumina (alumogel,  $\text{AlO}(\text{OH})\cdot\text{H}_2\text{O}$ , or  $\text{Al}_2\text{O}_3\cdot n\text{H}_2\text{O}$ ) or hydrous iron oxide of short range order (ferrihydrite, protoferrihydrite, formula variable) may be compared to the broken octahedral sheet of clay minerals, whereas the surface of amorphous silica (opal  $\text{SiO}_2\cdot n\text{H}_2\text{O}$ ) or aluminosilicate [allophane  $(\text{Al}_2\text{O}_3)(\text{SiO}_2)_{1.3-2.5}(\text{H}_2\text{O})$ ] may be compared to the broken tetrahedral sheet. Water can be bound also on the defect sites on the surface.

The quantity of water, bound in this way, cannot be expressed by stoichiometric means frequently, although the quantity is fairly well determined by the type of the structure. During drying the originally X-ray amorphous began to take on a definite form (often zeolite-like structure).

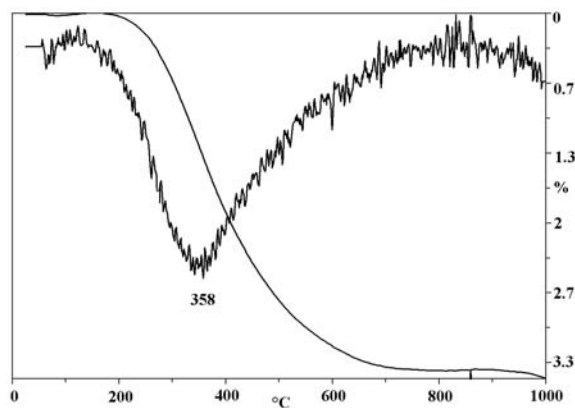


Figure 36. TG and DTG curves of perlite (Lehotka, Slovakia)

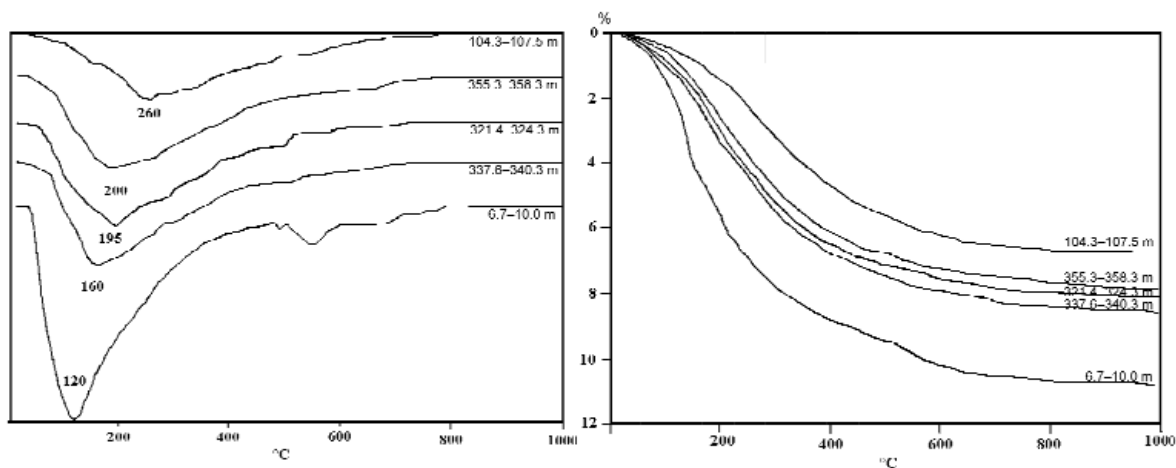


Figure 37. DTG and TG curves of perlite series in Borehole Kishuta-1

The higher water content escapes at a lower temperature, i.e. the smaller internal space bind the water stronger (Figure 37)

The influence of the size of internal spaces on the force of binding may be followed in the “PA curve” of the opal (Figure 38). The curve is opposing compared to other (stoichiometric) water quantity – temperature curves.

References: 507, 646, 658

### ***Water found in completely confined internal spaces***

Minerals sometimes contain water as an occlusion. Inclusion water involves the most primitive form of water in minerals. The included water at its emergence filled the cavity totally, and then, upon cooling, its volume decreased, allowing it to move freely, like a level. In the course of heating, at the temperature of the emergence of the inclusion, the liquid expands again to fill the whole hole, then, on further heating, its volume increases further, and the crystal bursts (decrepitation) and the sample sputtered from the sample holder. The phenomenon cannot be detected when a covered crucible is used since the amount of occluded water is several orders of magnitude smaller than that of solid particles expelled from the open crucible (see barite in Figure 39). This phenomenon can only be observed with non-powdered samples, because most occlusions are destroyed by powdering.

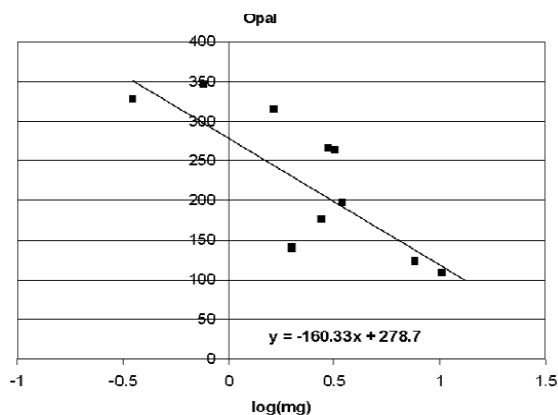


Figure 38. PA curve of opals

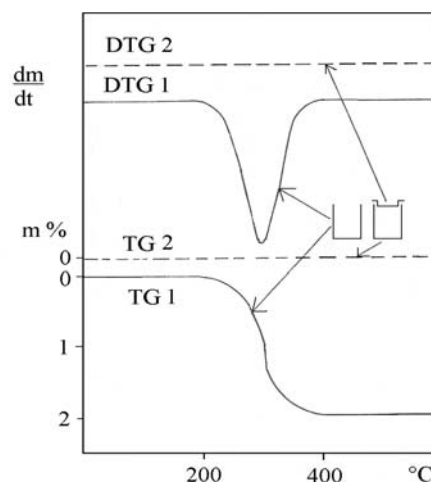


Figure 39. Decrementation of barite (open crucible, curve 1)

## Water bound in solid solution

Here, the ions do not occupy the entire space, thereby permitting the presence of 2–3 water molecules. Escape from their fixed position is possible only if the process of self-diffusion process within the crystal reaches a considerable rate. The rapid departure of such water can also be caused by a structural modification of the mineral (see aragonite in Figure 40).

In the case of zeolites and perlites some water can also be closed at the decomposition of the structure due to heating, as a silicate melt. In this case water escapes at a temperature higher than 900 °C.

References: 72, 323, 336, 819

## Crystal hydrates (constitutional water in water-bearing carbonate, sulphate, phosphate and salt minerals)

Crystal hydrate is an integral and stoichiometric part of the given structure. Crystal water is bonded generally by coordination forces which can be explained by the fact that cations within an aqueous solution coordinate water molecules that are incorporated into the lattice as aquo-complexes in the course of mineral precipitation. They often play a role of size control, e.g. sulphate minerals can form with a smaller cation, if size difference is compensated by water.

The larger part of this water does not have a structure determining function by itself as it is located in the second coordination sphere of the cations, however, the escape of water may result in the rearrangement of the structure. When heated, this water generally escapes at low temperatures, in several water molecules, in more-or-less overlapping stages. The dehydration of crystal water, in most cases is an isothermal process striving for equilibrium, i.e. the equilibrium of the reaction depends only on the gaseous product of the decomposition, i.e. on the partial pressure of water (Figure 41, 42, 43, 44). Due to these facts, discrepancies are to be found among the reported data. The dehydration of the crystal hydrate is complicated by other accompanying processes, as melting, liquid phase forming etc.

In the structure of the chalcantite  $\text{CuSO}_4 \cdot 5\text{H}_2\text{O}$  four water molecules are coordinated around the  $\text{Cu}^{2+}$  cation, the fifth molecule of water coordinated only by other water molecules or oxygens. During dehydration the first two moles are lost, then another two moles, and finally one mol water. The first two processes are isothermal while the departure of the last water molecule is non-isothermal (Figure 41).

The dehydration of epsomite ( $\text{MgSO}_4 \cdot 7\text{H}_2\text{O}$ ) is process of several steps under dynamic heating conditions that are influenced by the circumstances. The last molecule of water has a special contact with the cation and escapes at separately higher temperature. Intermediate monohydrate has not the same structure as natural monohydrate (kieserite) but a metastable phase. Similar reactions are at other crystal hydrates with more water molecule (melanterite, morenosite, goslarite, etc.)

The  $\text{MgSO}_4 \cdot 7\text{H}_2\text{O}$  lost the greater part of its crystal water content under quasi isothermal – quasi isobaric conditions at 105 °C, and the last molecule of water from the monohydrate escaped finally at 310–330 °C (Figure 42).

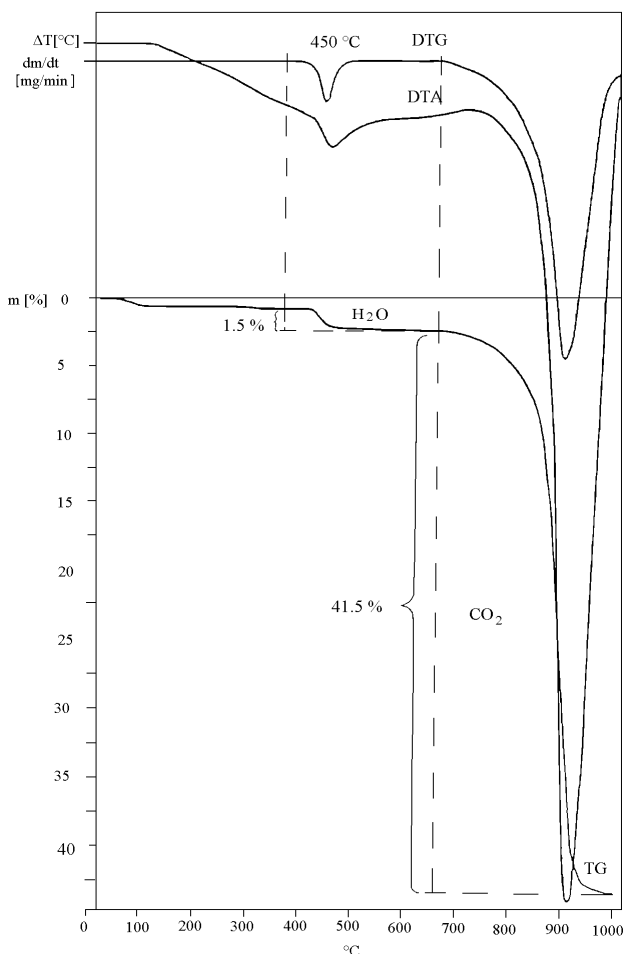


Figure 40. Evolution of water bound as solid solution from aragonite

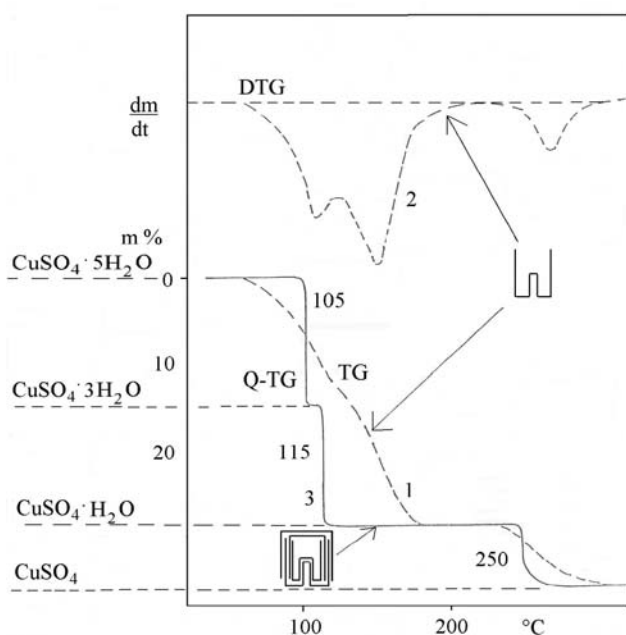
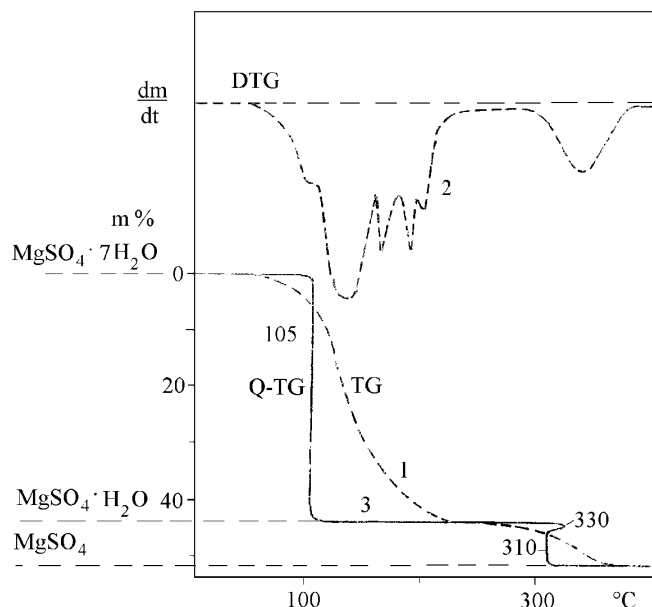
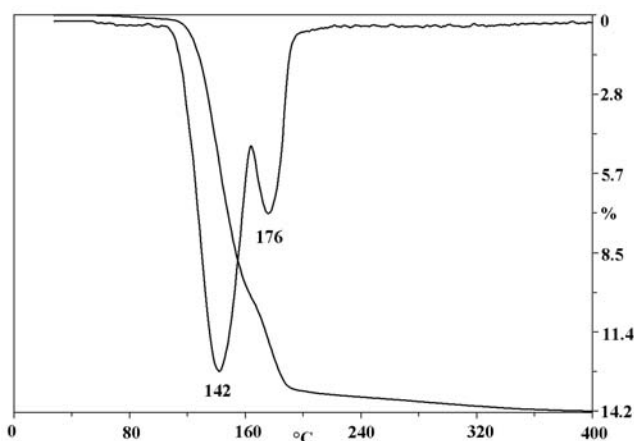


Figure 41. Dehydration of  $\text{CuSO}_4 \cdot 5\text{H}_2\text{O}$  examined by dynamic (curves 1–2) and "quasi-isothermal" (curve 3) heating techniques using open and labyrinth crucibles



**Figure 42.** Dehydration of  $\text{MgSO}_4 \cdot 7\text{H}_2\text{O}$  examined by dynamic (curves 1–2) and “quasi-isothermal” (curve 3) heating techniques using open (curves 1–2) and labyrinth crucibles (curve 3)



**Figure 43.** Dehydration of gypsum ( $\text{CaSO}_4 \cdot \text{H}_2\text{O}$ ) under dynamic heating  
Mass loss at the first step: 10.14%, at the second step: 3.48%

PAULIK, F., PAULIK, J. (1986) and EMONS et al. (1990) found two other steps at 115 and 150 °C which can be explained by that liquid phase is formed in the labyrinth crucible under quasi-isotherm heating, and this may cause the formation of three intermediates.

One part of the crystal hydrate has a structure determining function because it appears in the first coordination sphere of the cation (e.g. kieserite, HEIDE 1965a). Dehydration of kieserite takes place at a temperature about 50 °C higher as that of the intermediate monohydrate.

Water in gypsum is real constitutional water. In the gypsum crystal structure, calciums are coordinated by six oxygens from sulphate ( $\text{SO}_4$ ), and by two oxygens from water ( $\text{H}_2\text{O}$ ). Two sheets of sulphates are bound together by calciums forming double sheet layers. At each side of these layers are water molecules forming weak hydrogen bonds to the next layer in the structure.

Dehydration is a two-step process (Figures 43, 44). One part of the process of water loss takes place with a significant delay owing to the formation of protracted nucleus. The forming of a hemihydrate phase may not be explained by different bounding of water molecules.

Data of PA curves of gypsum show the difference between the bonding energy crystal water and that of adsorption water (see Figure 32, 33 and 45).

Similar water type is found in the structure of palygorskite apart from zeolitic water at the end position of pyroxene chains (Figure 46, 47 — see in detail in chapter 5.1.2.8.1 Palygorskite).

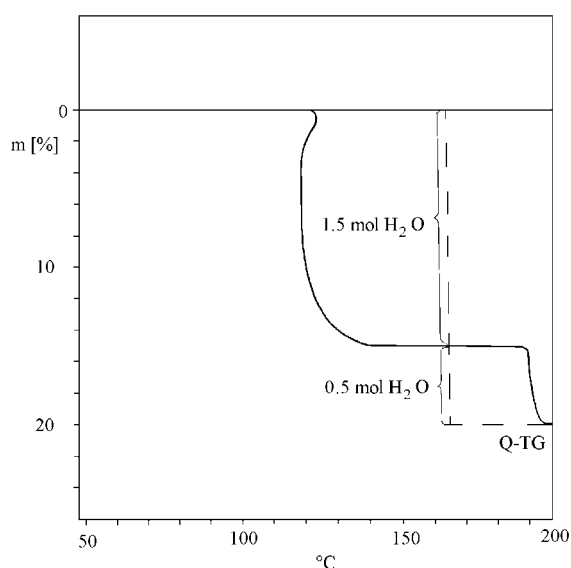


**Figure 44.** Dehydration of gypsum ( $\text{CaSO}_4 \cdot \text{H}_2\text{O}$ ) under “quasi-isothermal” and “quasi-isobaric” conditions

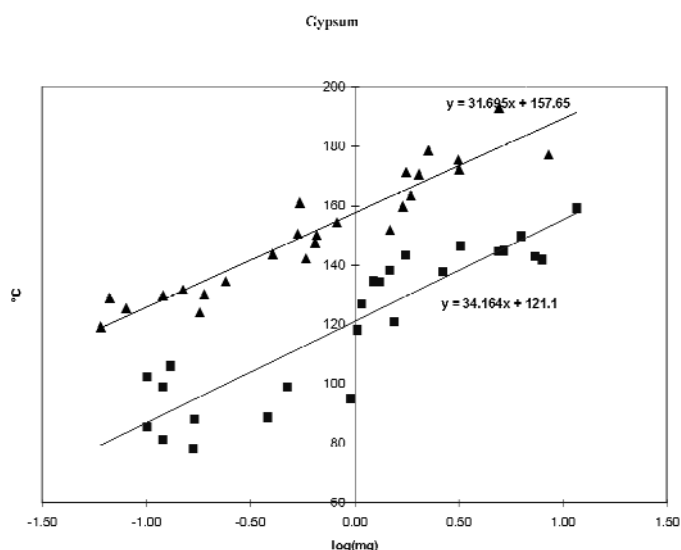


**Figure 45.** PA curves of the first (■) and the second (▲) reaction of water escape from gypsum

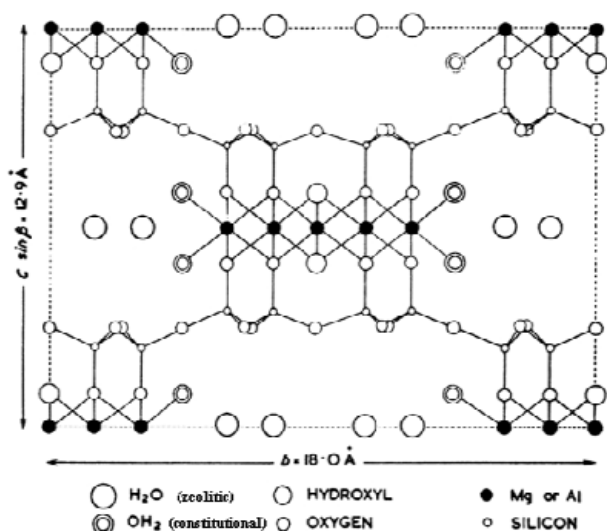


**Figure 46.** (001) projection of the unit cell of palygorskite (BRADLEY 1940)

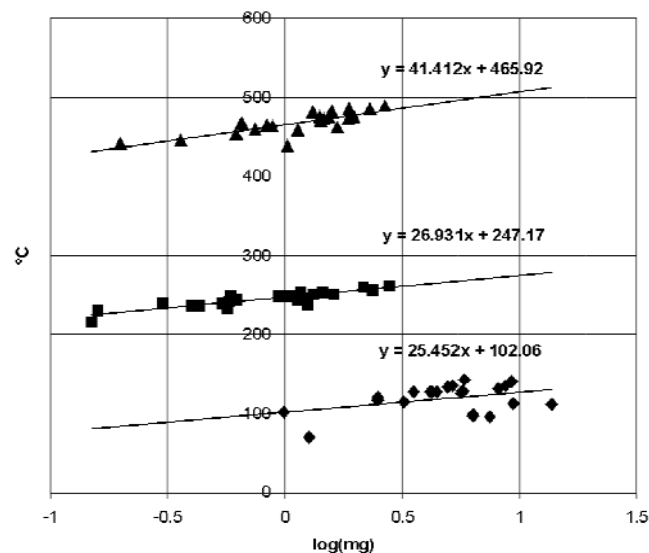


**Figure 47.** PA curves of the different water types in palygorskite

In some cases one part of molecular waters is not linked directly to cations (“free water” or “zeolitic water”), but bound by hydrogen bonding with the structure (e.g. aluminite).

References: 112, 283, 454, 455, 456, 457, 458, 461, 462, 463, 467, 472, 475, 826, 840, 841, 851

### Thermal dissociation

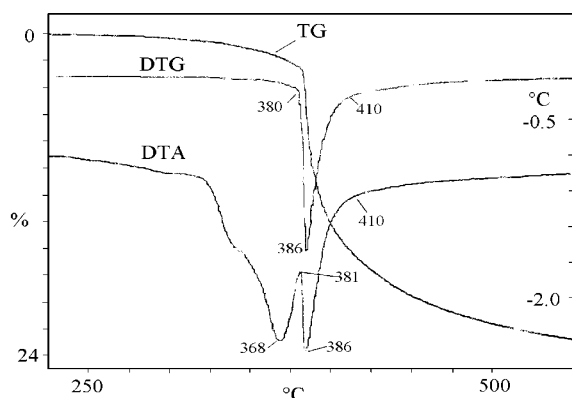


**Figure 48.** TG, DTG, and DTA curves of colemanite (WACŁAWSKA et al. 1988)

The components escaping in the course of thermal dissociation form an integral part of the structure. They are not present in molecular form in the structure, which explains why the mechanism of thermal dissociation consists of two phases:

- Formation of the escaping components (ionic → molecular form):
- in case of hydroxides: proton accommodation,
- for carbonates, sulphates etc.: oxygen rejection.
- Loss of decomposition product.

The two processes generally overlapped on the thermal curves. WACŁAWSKA et al. (1988) investigated the thermal dehydroxylation of colemanite  $[\text{Ca}_2\text{B}_6\text{O}_{18}(\text{OH})_6 \cdot 2\text{H}_2\text{O}]$  that represents a rare case with distinct separation of  $\text{H}_2\text{O}$  formation (DTA peak) and removal of water molecules (DTA and DTG peaks) from the mineral (Figure 48).

In the case of thermal dissociation reactions, the process is influenced by lattice structure features and by the compound instead of the thermodynamic phase-equilibrium because of the much stronger (85–550 kJoule/mol) ionic or covalent bonds in the structure. Among these factors bonding strength should be mentioned first. Table 16 and Figure 49 show clearly, that a decrease in electronegativity of cation, in connection with the same anion results in an increase of bonding strength and accordingly in an increase of dissociation temperature.

**Table 16.** Temperature of decomposition depending on the electronegativity

Cation	Electronegativity	Dehydroxylation		Calcination		Sulphate dissociation	
		°C	hydroxides	°C	carbonates	°C	sulphates
$\text{NH}_4$						460	mascagnite
B	2	160	sassolite				
Cu(2)	2			400	azurite	820	chalcantite
Bi	1.9			450	bismutite	800	bieberite
Fe(3)	1.9	195	bernalite			830	jarosite
Fe(2)	1.8			550	siderite	750	melanterite
Ni	1.8					860	morenosite
Cd	1.7			470	otavite		
Pb(2)	1.6			400	cerussite	890	anglesite
Zn	1.6			490	smithsonite	905	goslarite
Al	1.5	310	gibbsite			870	alunogen
Mn(3)	1.5						
Mn(2)	1.4			600	rhodochrosite	990	mallardite
Mg	1.2	450	brucite	670	magnesite	1070	kieserite
Ca	1	530	portlandite	950	calcite	1200	anhydrite
Sr	1			1180	strontianite	1180	celestine
Na	0.9			1150	natrite		
Ba	0.85			1200	witherite		
K	0.8					>1200	

In the case of the anions, electronegativity values of oxygen of the anion related towards the external cations are of similar effect. That is why, as it is shown in the Table 16, the compounds of the same cation with different anions show also a definite order of stability. The order given by the electronegativity values can be further refined by considering the valency and ionic potential.

Data based on the average of values published in the books of MACKENZIE 1957b, 1962, 1970, TSVETKOV et al. 1964, TODOR 1972, IVANOVA et al. 1974, SMYKATZ-KLOSS 1974.

Decomposition temperature of a given binding is also determined by the lattice structure. On the above basis it can be stated that a binding is decomposed at a higher temperature if within a more complex structure. The phenomenon is the result of several factors. On the one hand, the part of the structure not participating directly in the bond has an indirect impact on the bond strength and the stability of the structure.

The characteristic first peak of the double carbonates is always at higher temperature than the same decomposition in the single carbonates (Figure 50).

The possibility of the necessary diffusion in the course of the decomposition process is also influenced by the structure. Table 16 shows the temperature of the escape of OH-groups for minerals of different structure. For hydroxide the diffusion takes place in both stages of the decomposition (proton migration, escape of water molecules). In the case of isolated OH-groups, the protons show a smaller tendency to form H<sub>2</sub>O molecules. In this case, the formation of H<sub>2</sub> as the product of imperfect reaction might be possible (Figure 51).

For molecule development with oxygen rejection, of course, the process will take place in in-place manner; therefore diffusion plays a role only in the removal of the escaping component from the crystal lattice. In the case of hydroxides the structure may determine the number and distance of OH-groups yielding water during thermal dissociation and their position within the lattice structure may influence the development of decomposition temperature, as well. Dehydroxylation process of phyllosilicates reflects well their structural differences. The fact that the majority of the OH-groups are found on the surface of the layers, for 1:1 phyllosilicates, whereas within the layer complex for 2:1 phyllosilicates, is also reflected by the thermal curves of phyllosilicates.

The third factor influencing decomposition temperature is the ability of the residual structure to transform. This is possible because the accommodation of oxygen generally requires the residual structure to change the co-ordination number. This is possible only at a certain temperature. In other cases, dissociation is accompanied by simultaneous structural decomposition or rearrangement.

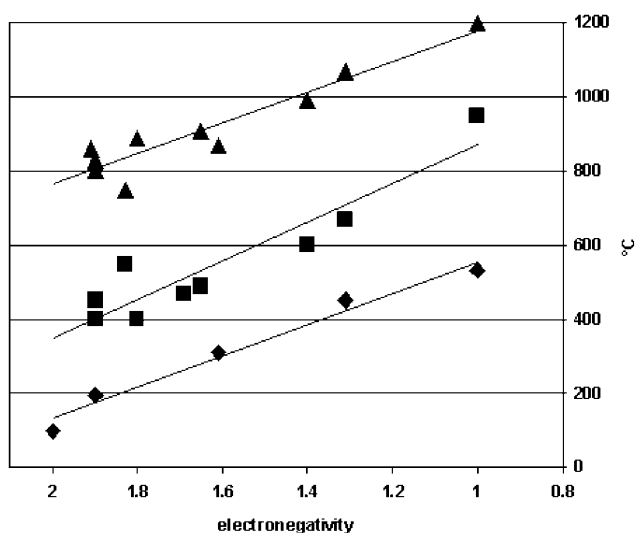


Figure 49. Decomposition temperature versus electronegativity (hydroxides ■, carbonates ♦, sulphates ▲)

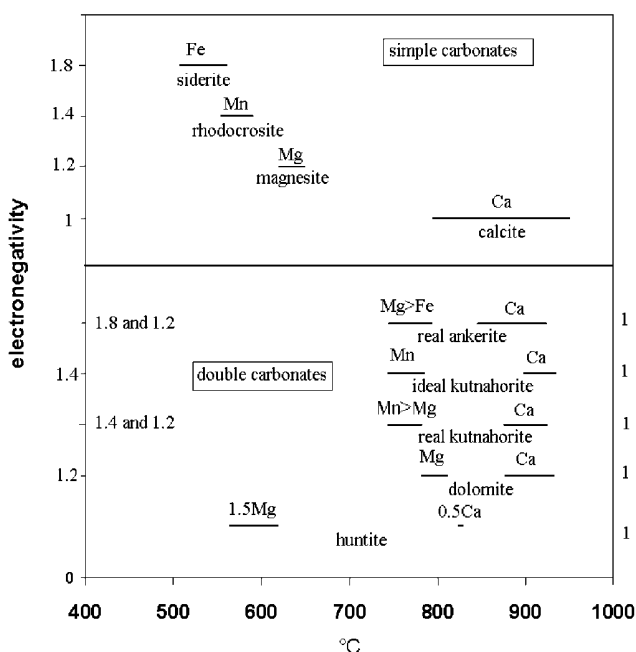


Figure 50. Comparison of the decomposition temperature of single and double carbonates (ideal ankerite is unknown in the nature)

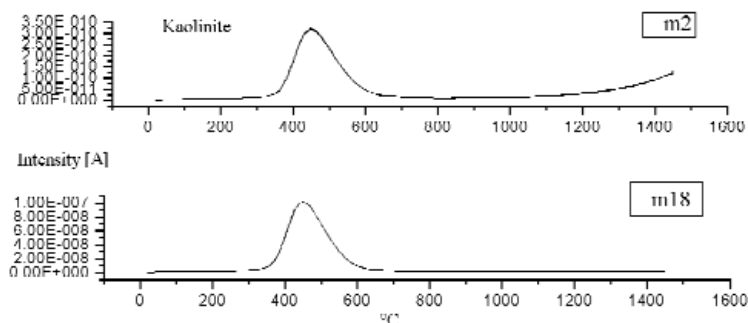


Figure 51. H<sub>2</sub>- and H<sub>2</sub>O-release from standard kaolinite KGa-1, Georgia, USA

It is a noteworthy phenomenon that the dissociation of the minerals with molecular water takes places at a temperature lower than in the case of similar water-free structures (hydromica, phosphates with water content etc.).

Dissociation processes are essentially of isothermal character (see portlandite, Figure 52, calcite Figure 53, and chalcantite Figure 54a, b).

The more complicated feature of the lattice structure is expressed not only by the shifting of the reaction to higher temperatures, but also by the

**Table 17.** Temperature of decomposition of hydroxide in different types of structures depending on the electronegativity

Cation	Electro- negativity	Dehydroxylation															
		°C	hydroxides	°C	oxid- hydroxides	°C	1:1 phyllosilicates	°C	smeectites	°C	primary chlorites	°C	clay micas	°C	micas	°C	pyrophyllite- talc series
B	2	160	sussolite														
Fe(3)	1,9	195	hercynite	370	goethite			490	nontronite								
Fe(2)	1,8					590	Fe-serpentine (greenalite)			560	thuringite, chamosite						
Ni	1,8					620	Ni(Mg)- serpentine (falcondoite- garnierite)										
Al	1,5	310	gibbsite	560	boehmite	590	kaolinite	590	heidelite	520	sudowite	570	illite	840	muscovite	740	pyrophyllite
Mn(3)	1,5			370	manganite												
Al,Mg								690	montmorillonite								
Mg	1,2	450	brucite			720	Mg serpentines	850	saponite	820	Mg- chlorites	860	lepidite	1230	phlogopite	970	talc
Ca	1	530	portlandite														

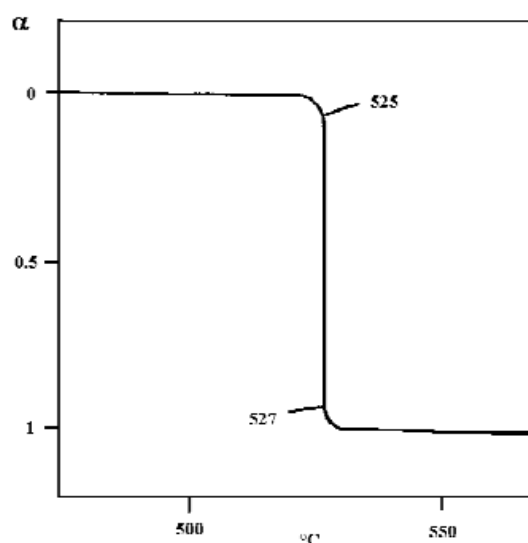


**Figure 52.** Q-TG curve of portlandite

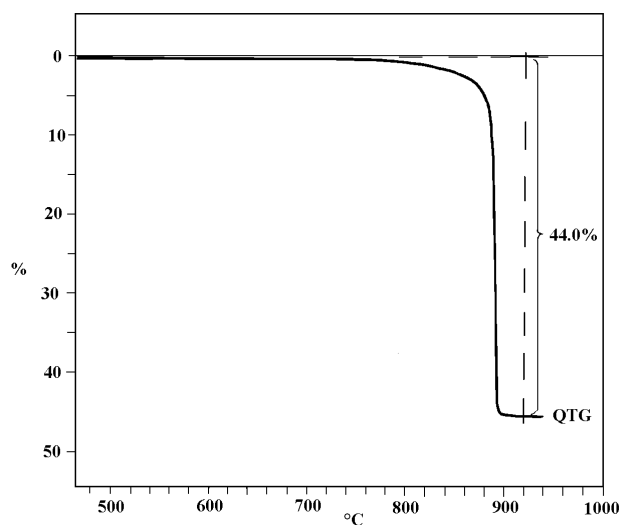


**Figure 53.** Q-TG curve of calcite

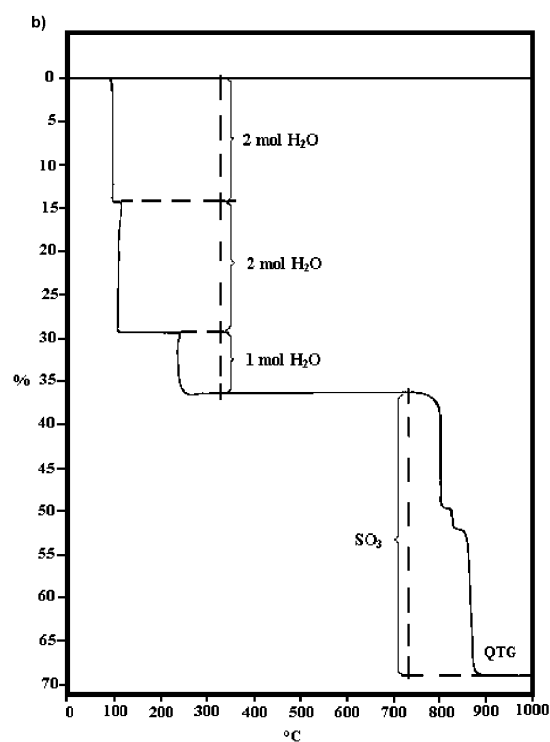
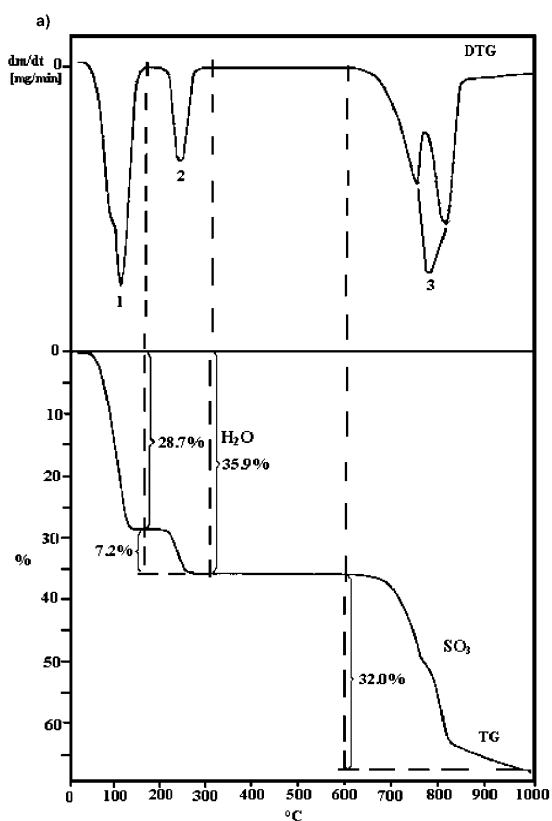


**Figure 54.** TG and DTG curve of chalcantite under dynamic heating (a), TG curve of chalcantite under quasi-static circumstances (b)

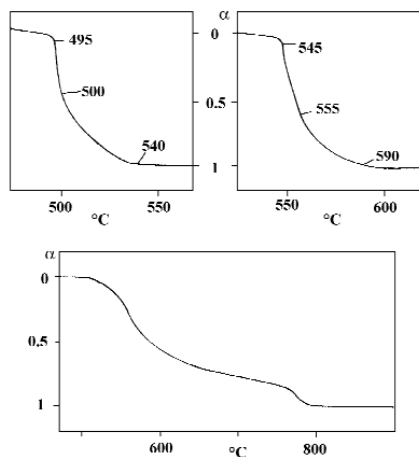


**Figure 55.** Q-TG curves of dehydroxylation processes of boehmite, kaolinite and pyrophyllite

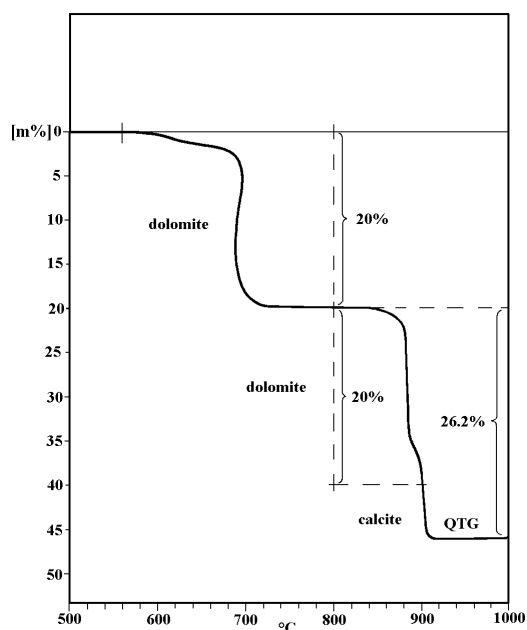


**Figure 57.** TG curve of mixture of dolomite and calcite under quasi-static circumstances

fact that the process of the reaction will gradually shift away from the zero-order, isothermal character (see boehmite, kaolinite, pyrophyllite, Figure 55, or dolomite Figure 56, 57)

\*\*\*

References for thermal dissociation: 129, 321, 323, 350, 471, 513, 688, 689, 690, 841, 920, 1006, 1009, 1071, 1072, 1081, 1092, 1101, 1112

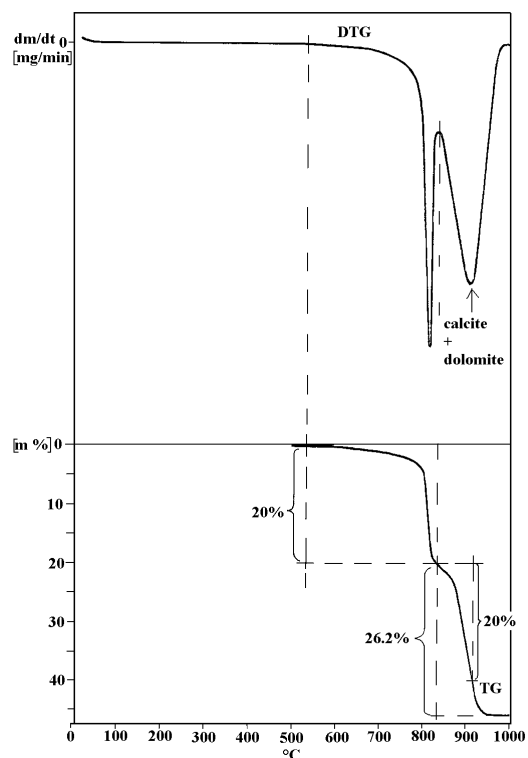


**Figure 56.** TG and DTG curve of mixture of calcite and dolomite

### Other thermal reactions with mass change (sublimation, oxidation, reduction)

From the last column of Table 10 may be seen, that beside the main dehydration and decomposition reactions there are some reactions which also may cause mass change. Some characteristic examples are summarised in Table 18 and 19.

Oxidation occurs in the organic material or coal apart from minerals in the geological samples.

**Table 18.** Characteristic evaporation and sublimation temperature of minerals

Mineral	Temperature °C
Sulphur	≈444
Cinnabar	320-460
Stibnite	≈500

**Table 19.** Characteristic temperatures of the oxidation and the reduction of minerals

Reaction type	Minerals	Temperature range °C	Note
Oxidation (exothermic)	sulphur	280-380	
	graphite	900-1000	
	sulphides	250-850	(see later in detail)
	magnetite	300-450	surface
	minerals containing FeSO <sub>4</sub>	500-1000	bulk
	siderite	475-760	
	rhodochrosite	655-870	to Mn <sub>2</sub> O <sub>3</sub>
	ankerite	775-820	
	vivianite	550-630	
Reduction (endothermic)	pyrolusite	625-725	MnO → Mn <sub>2</sub> O <sub>3</sub>
	pyrolusite, rhodochrosite	950-1050	Mn <sub>2</sub> O <sub>3</sub> → Mn <sub>3</sub> O <sub>4</sub>
	sulphides, carbonates, sulphates bearing CuO	950-1050	2CuO → Cu <sub>2</sub> O

## Other thermal reactions without mass change

### Solid-phase structural decomposition

In this special case of decomposition reactions the structure falls apart, but all products of the decomposition remain as solid phases in the sample. Since in this case no mass loss of the sample is detected, these reactions are not suitable for

**Table 20.** Types of solid-phase structural decomposition and crystallization of new phases

Solid-phase structural decomposition (endothermic)	Crystallization of new phases (exothermic)
1. Reaction of alkali and alkaline earth sulphates in Table 70	2. Reactions of alunite-type minerals: see Table 70
3. Structure decomposition of sulphides: e.g. chalcopyrite: at 330–350 °C	
4. Endothermic exothermic inversion of phyllosilicates Decomposition of the structure directly before the exothermic reaction (amorphous state) e.g. kaolinite chlorites Mg serpentines hydromicas smectites etc.	Crystallization of new phases (e.g. cristobalite, mullite, olivine, spinel, enstatite etc.) from the amorphous phases. 950–1000 °C (mullite) 830–900 °C (olivine, spinel) 800–840 °C (forsterite) >900 °C (spinel) <900 °C 5. Transformation of amorphous minerals into crystalline phases e.g. hematogel >800 °C allophane ≈1000 °C
	6. Formation of new phases after the dehydration of zeolites (feldspars, feldspathoids, wairakite, quartz etc.) e.g.: chabasite → anortite (750–900 °C)
	7. Crystallization of $AlPO_4$ , $FePO_4$ phases during the heating of phosphates e.g. – lazulite: 905 °C ( $AlPO_4$ ) – diadochite: 610–620 °C ( $FePO_4$ )
	8. Others: e.g. – Crystallization of $NaAlO_2$ from dawsonite at 810 °C – Formation of willemite from hemimorphite at 850–970 °C – Formation of copper-oxide at 660–730 and quartz and cristobalite at 930–970 °C form chrysocolla

quantitative determination. The most frequent solid-phase structural decomposition and crystallization of new phases during the heating of minerals are given in Table 20 as examples.

### Polymorphic transition

The changes of energy due to phase transition of minerals are much smaller than that of dehydration or decomposition reactions.

**Table 21.** Characteristic temperatures of polymorphic transition of minerals

Mineral class	Mineral	Temperature °C	Transition	Mineral class	Mineral
Native elements	sulphur	95	orthorhombic ( $\alpha$ )	→	monoclinic ( $\beta$ )
Sulphides	chalcocite	103	orthorhombic ( $\alpha$ )	→	hexagonal ( $\beta$ )
		348	hexagonal	→	cubic
	bornite	212	$\alpha$	→	$\beta$
		267	$\beta$	→	$\gamma$
	chalcopyrite	557	$\alpha$	→	$\beta$
		657	$\beta$	→	$\gamma$
	pyrrhotite	140	hexagonal	→	orthorhombic
		350–370			
	acanthite	179	monoclinic	→	cubic (argentite)
	argentite	175	isometric		
	millerite	395	trigonal	→	hexagonal?
	covellite	370			
		507	hexagonal		
	marcasite	530	orthorhombic		cubic (pyrite)
	herzenbergite	602	$\alpha$	→	$\beta$
Oxides					
Silica minerals	tridimite	117	$\alpha$	→	$\beta$
	cristobalite	250	$\alpha$	→	$\beta$
	quartz	571	$\alpha$	→	$\beta$
Others	hematite	677	$\alpha$	→	$\beta$
	magnetite	575	$\alpha$	→	$\beta$
	pyrolusite	690			
	hausmannite	750	$\alpha$	→	$\beta$

**Table 21.** Continuation

Mineral class	Mineral	Temperature °C	Transition	Mineral class	Mineral
Silicates	leucite	682	tetragonal	→	cubic
Carbonates	trona	170			
	soda	355			
		485			
	dawsonite	436			
	aragonite	450	orthorhombic	→	trigonal
	valerite	470		→	trigonal
	witherite	806	orthorhombic	→	tetragonal
	alstonite	900			
	norsethite	810-813			
		980-982			
Sulphates	strontianite	924	orthorhombic	→	hexagonal
	thenardite	177	orthorhombic(V)	→	orthorhombic (III)
		241	orthorhombic (III)	→	hexagonal (I)
		290	?		
	mirabilite	240			
	gypsum	320		→	anhydrite
	kainite	425			
	glaserite	437			
	arcandite	555-585	orthorhombic (α)		hexagonal (β)
	syngenite, leonite, picromerite	580			
	polyhalite	640			
	anglesite	865	orthorhombic	→	monoclinic
Phosphates	luzulite	489	orthorhombic	→	cubic
Nitrates	niter	128	orthorhombic	→	trigonal
	nitratine	276	α	→	β
Halides	cryolite	573	monocline		cubic

### Melting

Melting is such a physical process, when the substance changes from a solid to liquid state and remains in the crucible. This temperature may occur at broad interval (Table 22).

**Table 22.** Characteristic melting points of minerals

Mineral class	Mineral	Melting point (°C)
Sulphates	mirabilite	32
	epsomite	52, 97
	melanterite	60, 98
	morenosite	88
	chalcantite	95
	bloedite, loweite	668, 704
	leonite, picromerite	738, 842
	schoenite	750
	vanthoffite	800
	syngenite	875
	thenardite	882
	mirabilite	884
	polyhalite	890
	glaserite	940
	glaucoberite	944
	langbeinite	945
Native elements	sulphur	115.36
	silver	961

**Table 22.** Continuation

Mineral class	Mineral	Melting point (°C)
Nitrates	nitratine	308
	niter	337
Sulphides	millerite	790
	stibnite	565
	tetradymite	636
	villmannite	787
	argentite	788
	herzenbergite	880
Minerals with PbO content	massicotite	897
	cerussite	897
Halides	bischofite	118
	carnallite	160-165, 425
	chloromagnesite	700
	sylvite	770
	halite	801
Carbonates	cerussite	897
	natrite	820
	trona	800-900
	kalinite	900

### Curie point

Curie point is the temperature at which a ferromagnetic (or ferro-magnetic) material becomes paramagnetic on heating. The effect is reversible.

There are several methods to determine Curie point:

— By thermomagnetic methods (e.g. CHAKLADER, BLAIR 1970).

In the case of DTA techniques a weak endothermic effect of the substances near the Curie point (Figure 23) is utilized.

— By DTG: the furnace of the Derivatograph produces an alternating magnetic field inside the furnace. Field intensity and the magnetic gradient are sufficient to produce magnetic force acting on a ferromagnetic sample. The force is recorded as an apparent weight increase of the sample, immediately after the furnace is switched on. When temperature increase up to the TG temperature (Curie point) of the sample the force disappears and the TG curve shows a rapid weight decrease due to the disappearance of the interaction between the sample and the magnetic field generated by the heat current (MOSKALEWICZ 1975).

**Table 23.** Curie point of minerals

Mineral	Curie-temperature (Θ) °C ferromagnetism/paramagnetism	Note
Pyrrhotite	348 370	
Magnetite	450 590	depending on Cr <sub>2</sub> O <sub>3</sub> , TiO <sub>2</sub> , MgO etc. substitution
Maghemite	640	
Hematite	645–675	
Titanohematite	600–660	

### Solid phase reaction

Sometimes solid phase reactions may occurs between the different components of the sample (for example aluminite and calcite (FÖLDVÁRI, FARKAS 1985) Figure 58, 59, iron sulphate and alkali metal carbonate (SWAMY, PRASAD 1982) or calcite and pyrite (LANGIER-KUŹNIAROWA 1969, SELMECZI 1970, PAULIK, F. et al. 1989).

Reactions of the sample (Figure 58):

- between 30–660 °C: escape of H<sub>2</sub>O and OH of aluminite (36%),
- between 770–950 °C: loss of SO<sub>3</sub> (17.8%).

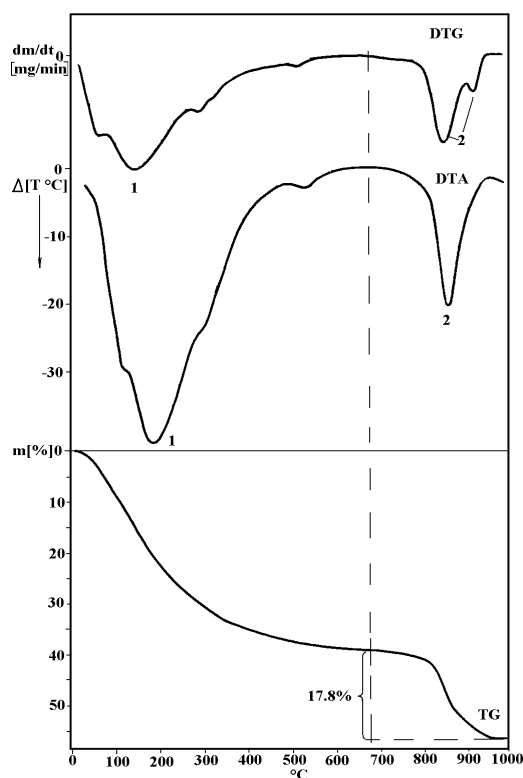


**Figure 58.** Aluminite Borehole Csordakút-421, 38.2–38.3 m (Hungary)

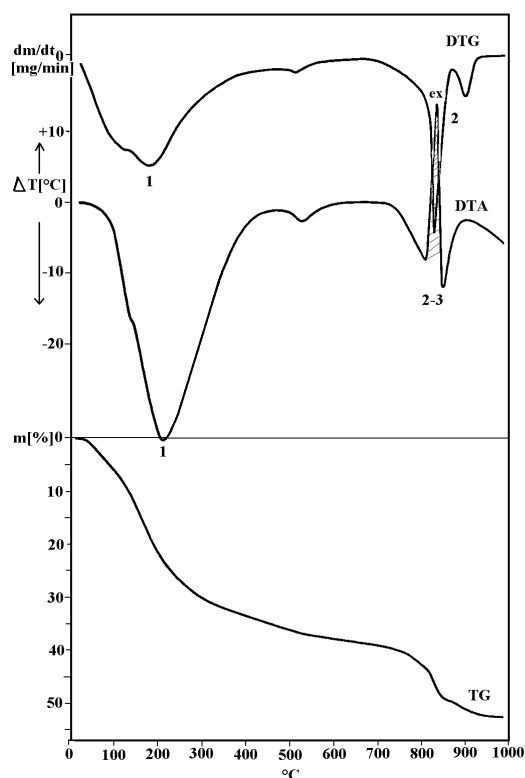
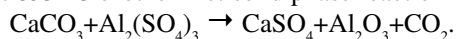


**Figure 59.** Calcite impurities in an aluminite sample Borehole Csordakút-421, 38.8–38.9 m (Hungary)

Reactions of the sample (Figure 59):

- between 30–660 °C: escape of H<sub>2</sub>O and OH of aluminite (38%),
- between 770–900 °C: loss of SO<sub>3</sub> from one part of aluminite (only 14%),
- at 835 °C exothermic: solid phase reaction between aluminium sulphate and calcite



CaSO<sub>4</sub> is decomposed only at temperatures higher than 1000 °C.

Similar reaction product of pyrite is  $\text{Fe}_2(\text{SO}_4)_3 + 3\text{CaCO}_3 \rightarrow 3\text{CaSO}_4 + \text{Fe}_2\text{O}_3 + 3\text{CO}_2$ .

The CaSO<sub>4</sub> decomposes only above 1000 °C.

\*\*\*

References for other thermal reactions: 170, 276, 329, 652, 763, 839, 908, 980, 1048

## **THERMOGRAVIMETRIC CURVES AND THEIR INTERPRETATION BY STOICHIOMETRIC PROCESSES OF MINERALS AND MATERIALS**

In this chapter a total of 148 figures show thermoanalytical curves up to 1000 °C for 114 minerals investigated by the author in the atlas encountered in geological routine work and having specific thermal reactions. Thermal processes are interpreted by thermoanalytical reaction equations or by the description of the reaction. For thermal reactions accompanied by mass changes a method for quantitative determination is also presented. All the presented samples were controlled by X-ray diffraction methods and many of the samples were analysed in the chemical composition point of view.

Most of the diagram selected from the 29 000 derivatograms made by the old type of Derivatograph and 6000 derivatograms made by Derivatograph-c, a computerised type (PAULIK, J. et al. 1986, 1987). Diagrams from the literature were used only in some cases.

The following additional informations may be reported:

The reference substance is  $\text{Al}_2\text{O}_3$ .

The sample holder is generally open and made of sintercorund. In the case of quasi-static investigation we use labyrinth crucible made from platinum.

The temperature of the sample and the difference between the temperature of the sample and the reference material are measured in the conventional way with two counter-connected PtRh-Pt thermoelements.

Data acquisition and manipulation by computers:

15 bit A/D conversion

signal sampled 0,1 sec. 900 point/programmed measuring time are averaged

References: 849, 850

## 1 Native elements

## 1. NATIVE ELEMENTS

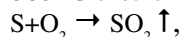
## 1.1. Sulphur: S

Thermal reactions:

$\approx 95^\circ\text{C}$  endothermic: transition: orthorhombic ( $\alpha$ )  $\rightarrow$  monoclinic ( $\beta$ ) (heat of transition: 36 kJ/mol),

$\approx 115^\circ\text{C}$  endothermic: melting,

$280\text{--}380^\circ\text{C}$  exothermic, mass loss: oxidation:



$\approx 445^\circ\text{C}$  endothermic, mass loss: sublimation  $\text{S} \uparrow$ .

Stoichiometric factor based on the mass loss of the 3<sup>rd</sup> and 4<sup>th</sup> reactions: 1.

Sample: Budajenő, borehole Bő-2: 268.85–268.87 m (Hungary)

Sample mass: 1000 mg

Heating rate:  $17^\circ\text{Cmin}^{-1}$

Mass loss during the 3<sup>rd</sup> and 4<sup>th</sup> reaction: 32%

Sulphur content of the sample: 32%

References: 201, 513, 603, 981

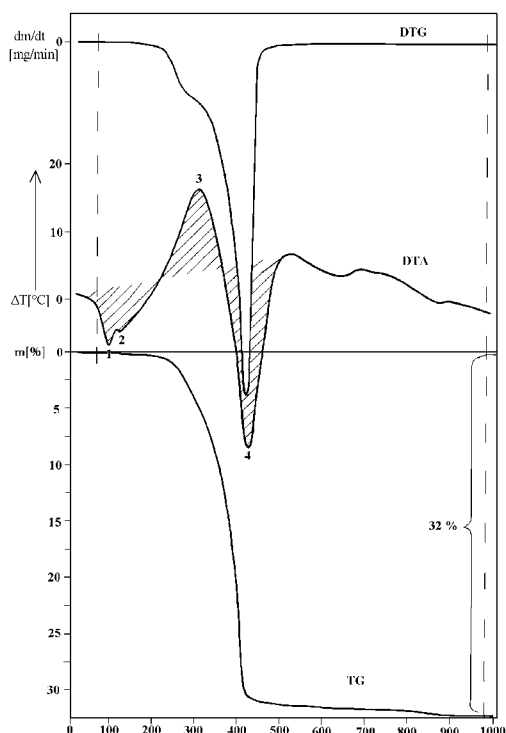


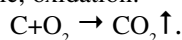
Figure 1.1. Thermoanalytical curves of sulphur

## 1.2. Graphite C

## 1.2.1. Analysis in air

Thermal reaction:

between  $600\text{--}1000^\circ\text{C}$  (depending on the condition of analysis) exothermic, oxidation:



Stoichiometric factor based on the reaction: 1.

Sample: Graphite electrode

Sample mass: 100 mg

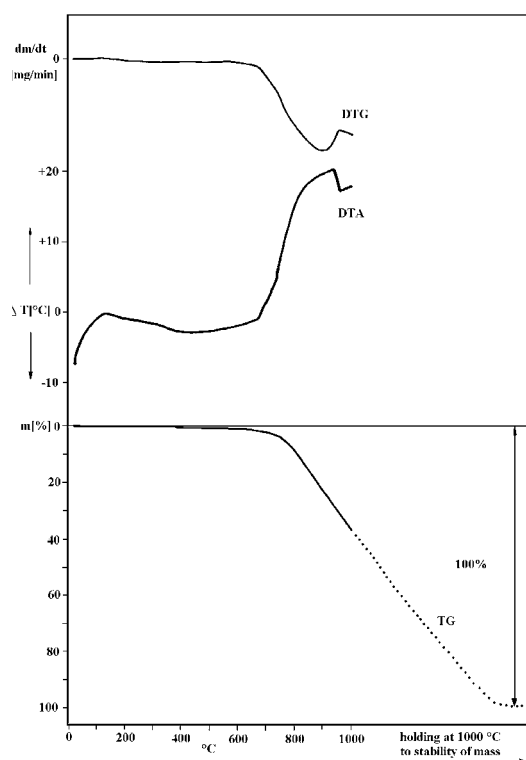
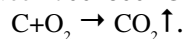


Figure 1.2.1. Graphite oxidation in air

### 1.2.2. Analysis in oxygen

Thermal reaction:

Between 700–800 °C exothermic, oxidation:



Sample: Graphite electrode

Sample mass: 20 mg

Diluted by 980 mg  $\text{Al}_2\text{O}_3$

Heating rate: 10 °C/min

Atmosphere:  $\text{O}_2$  (20 l/h)

Titration: pH = 9.3

Absorbing solution: 0.1 m NaOH

Mass loss during the reaction: 100%

Measured  $\text{CO}_2$  determined by titration related to sample mass 360.5% = 98% C content

References: 525, 820, 1185

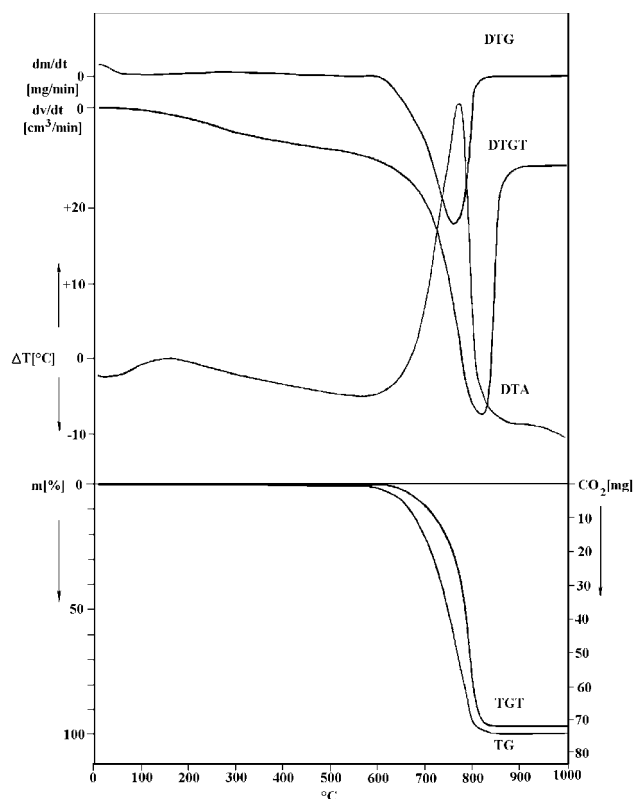


Figure 1.2.2. Graphite oxidation in oxygen (DTA, TG, DTG, TGT and DDTG curves)

## 2. SULPHIDES

The investigation of sulphide minerals is much more difficult than that of other minerals, because they are very strongly oxidative and their oxidation behaviour is complicated.

Atmosphere: air or  $\text{O}_2$ :

The characteristic mean reaction is exothermic oxidation. These reactions are very complex. Their categories:

- Complete oxidation of the original compound.
- Incomplete oxidation with the formation of intermediate sulphates and oxysulphates.
- Dissociation to form a vapour phase that is simultaneously oxidized.
- Selective and sequential oxidation of members of a cation complex.
- Selective and sequential oxidation of members of an anion complex.

Some examples for the selective oxidation of sulphides with different cations or anions:

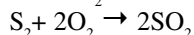
1. Tetrahedrite:  $\text{Cu}_3\text{SbS}_{3-4}$ :

— at lower temperature:  $\text{Sb}_2\text{S}_3 \rightarrow \text{Sb}_2\text{O}_3$ ,

— at higher temperature:  $\text{CuS} \rightarrow \text{CuSO}_4$ .

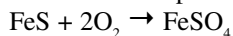
2. Chalcopyrite:  $\text{CuFeS}_2$ :

— 330–350 °C: solid-phase structural decomposition:

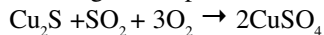


— 350–600 °C:

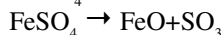
— at lower temperature: oxidation of iron:



— at higher temperature: oxidation of copper:



— at about 750 °C: decomposition of intermediate sulphate products:



after this :  $\text{FeO} \rightarrow \text{Fe}_2\text{O}_3$

## 2 Sulphides

3. Galena: PbS with Se substitution:

— oxidation of PbSe (clausthalite) at 660 °C

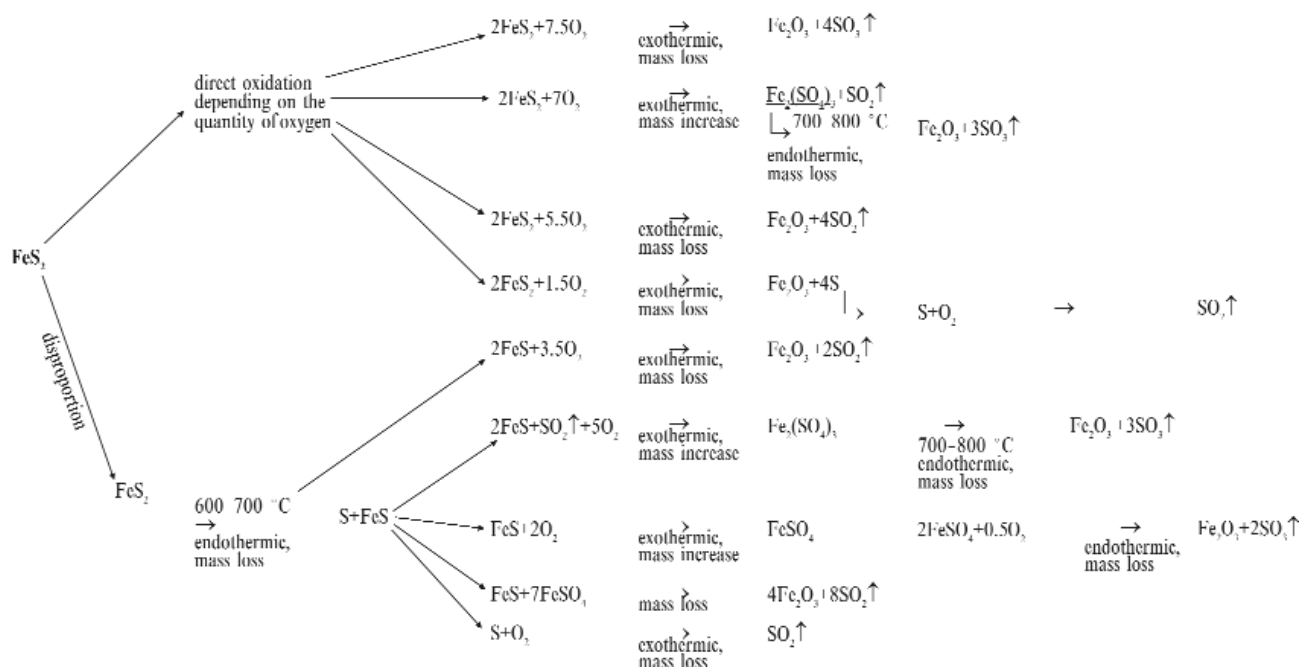
— oxidation of galena: at 800 °C.

**Data** in the literature related to the temperature ranges of sulphide oxidation in air **are** largely **inconsistent** (Table T2a). This is explained by the depending of the process of oxidation on several different factors (experimental variables such as **quantity of sulphides, oxygen concentration, particle size, shape and material of crucible, heating rate** etc.) that can influence the number and intensity of the peaks and the reaction can be different and very complex. (See scheme of oxidation of pyrite Table T2b). According to KOPP, KERR (1958a), peak temperatures are found to decrease by about 3 °C for each °C per minute the heating rate is lowered. Peak temperatures also decrease with diminution in grain size, resulting in the increased surface area available for oxidation. If the amount of sample is reduced, peak temperature will also decrease.

**Table T2a.** Oxidation of the most common simple sulphide minerals in order of temperature (°C)

Element	Mineral	°C
Hg	cinnabar	160-450
As	orpiment	220-580
Mn	alabandite	300-350
Fe	pyrite, pyrrhotite, marcasite	350-600
Sb	stibnite	
Cu	chalcocite, covellite	520-720
Bi	bismuthinite	
Mo	molybdenite	550-600
Ag	argentite	650-750
Cd	greenockite	620-800
Ni	millerite	610-800
Zn	sphalerite	800-900
Pb	galena	800-850

**Table T2b.** Principal modes of oxidation of pyrite



The temperature of oxidation reaction is more characteristic when oxidizing agents (CuO, MnO<sub>2</sub>, V<sub>2</sub>O<sub>5</sub> etc.) are used. Further reactions of sulphides are summarized in Table T2c.

The elimination of the oxidation peak is possible in inert atmosphere, the reaction is the thermal dissociation e.g.:

— pyrite: at 600–700 °C:  $\text{FeS}_2 \rightarrow \text{S} + \text{FeS}$  (stoichiometric factor of the reaction: 3,75)

— chalcopyrite: at 330–350 °C:  $4\text{CuFeS}_2 \rightarrow 4\text{FeS} + 2\text{Cu}_2\text{S} + \text{S}_2$ ;

— covellite: at 400–550 °C:  $2\text{CuS} \rightarrow \text{Cu}_2\text{S} + 0.5\text{S}_2$ ,

or at 310–338 °C:  $1.84\text{CuS} \rightarrow \text{Cu}_{1.84}\text{S}$  (digenite) + 0.84S;

— tetradymite: at 560–590 °C:  $\text{Bi}_2\text{Te}_2\text{S}_3$ ;

— arsenopyrite: at 670–740 °C:  $\text{FeAsS} \rightarrow \text{FeAs}_2$  (loellingite) +  $\text{Fe}_{1-x}\text{S} + \text{As}_4\text{S}_4 + \text{As}_4$ ;

— ullmannite: at 740 °C:  $\text{NiSbS}$ ;

— gersdorffite: at 800–860 °C:  $(\text{NiFe})\text{AsS} \rightarrow \text{NiAs}$  (niccolite) + pentlandite;

— cobaltite: at 885–905 °C:  $(\text{Co,Fe})\text{AsS} \rightarrow \text{CoS}_2$  (cattierite) +  $\text{S}_2 + \text{Fe}_{1-x}\text{S} + \text{As}_4\text{S}_4 + \text{As}_4$ ;

— pentlandite: at 610 °C:  $(\text{Fe,Ni})_9\text{S}_8 \rightarrow \text{Fe,Ni}_{1-x}\text{S} + (\text{Fe,Ni})_{3-x}\text{S}_2$  (heazlewoodite),

at 845 °C:  $(\text{Fe,Ni})_{3-x}\text{S}_2 \rightarrow (\text{Fe,Ni})_{1+x}\text{S} + \text{S}_2$ .

Decomposition of iron sulphates at 600–750 °C.

Decomposition of copper sulphates at about 780 °C.

Decomposition of cobalt sulphates at about 870 °C.

**Table T2c.** Further reactions of sulphides

Reaction	Mineral	Formula	Temperature (°C)	Polimictic transition		
Melting	millerite	NiS	790			
	stibnite	Sb <sub>2</sub> S <sub>3</sub>	565			
	chalcocite	Cu <sub>2</sub> SbS <sub>2</sub>	570			
	tetradymite	Bi <sub>2</sub> Te <sub>2</sub> S	636			
	stromeyerite	AgCuS	665			
	tennantite	(Cu,Fe) <sub>15</sub> As <sub>2</sub> S <sub>11</sub>	710–735			
	ullmannite	NiSbS	787			
	argentite	Ag <sub>2</sub> S	788 960			
	shandite	Pb <sub>2</sub> Ni <sub>2</sub> S <sub>2</sub>	790			
	pentlandite	(Fe,Ni) <sub>9</sub> S <sub>8</sub>	830			
	teallite	PbSnS <sub>3</sub>	870			
	herzenbergite	SnS	880			
	vaesite	NiS <sub>2</sub>	993			
Sublimation	cinnabar	HgS	320 460			
	stibnite	Sb <sub>2</sub> S <sub>3</sub>	≈500			
Curie-point	pentlandite	(Fe,Ni) <sub>9</sub> S <sub>8</sub>	220			
	pyrrhotite	Fe <sub>(1-x)}</sub> S (x = 0–0.17)	348–370			
Phase transition	digenite	Cu <sub>2</sub> S <sub>1</sub>	74 90	pseudo isometric	→	isometric
	stromeyerite	AgCuS	82 94	orthorhombic	→	hexagonal
	djurleite	Cu <sub>21</sub> S <sub>16</sub>	93	monoclinic		
	mckinstyrite	(Ag,Cu) <sub>2</sub> S	94–97	orthorhombic		
	jalpaite	Ag <sub>2</sub> CuS <sub>2</sub>	112–119	tetragonal	→	isometric
	bourbonite	PbCuSbS <sub>1</sub>	137			
	pyrrhotite	Fe <sub>(1-x)}</sub> S (x=0 0.17)	149	hexagonal	>	orthorhombic
	argentite	Ag <sub>2</sub> S	173			
	pyrrhotite	Fe <sub>(1-x)}</sub> S (x=0 0.17)	200 240	monoclinic		
	chalcocite	Cu <sub>2</sub> S	100–120	orthorhombic (α)	→	hexagonal (β)
			348	hexagonal	→	digenite
	acanthite	Ag <sub>2</sub> S	176	monoclinic	→	cubic (argentite)
	bornite	Cu <sub>3</sub> FeS <sub>4</sub>	212 228	pseudoisometric (α)	>	isometric (β)
			267	β	>	γ
	realgar	AsS	265	α	→	β
	stephanite	Ag <sub>4</sub> SbS <sub>4</sub>	270			
	tennantite	(Cu,Fe) <sub>15</sub> As <sub>2</sub> S <sub>11</sub>	319			
	cinnabar	HgS	344			metacinnabar
	chalcopyrite	CuFeS <sub>2</sub>	557	α	→	β
			657	β	→	γ
	millerite	NiS	395	trigonal-hexagonal α	→	β
	chalcocite	Cu <sub>2</sub> SbS <sub>2</sub>	500	orthorhombic		
	covellite	CuS	507	hexagonal		
	marcasite	FeS <sub>2</sub>	530	orthorhombic	>	isometric (pyrite)
	shandite	Pb <sub>2</sub> Ni <sub>2</sub> S <sub>2</sub>	546	trigonal hexagonal		
	rammelsbergite	NiAs <sub>2</sub>	560		→	pararammelsbergite
	herzenbergite	SnS	602	α	→	β
	pentlandite	(Fe,Ni) <sub>9</sub> S <sub>8</sub>	610 620	isometric	→	isometric (vaesite)
	teallite	PbSnS <sub>3</sub>	721	orthorhombic		
	sphalerite	ZnS	1020		>	wurtzite
Reduction	sulphides, bearing CuO		950–1050			

1 Both in oxygen and in inert atmosphere.

**Notice:** The reaction products (S, SO<sub>2</sub>, SeO etc.) are generally aggressive, and they combine with metals (thermocouple, crucible, furnace etc.) very quickly.

## 2 Sulphides

## Proposition:

- It is necessary to work in a sample holder made of ceramic material.
- It may be sufficient to mix the substance carefully with inert material (twice the amount of sulphides).
- In any case, the proposed standard conditions of analysis must be changed if chalcogenides or sulphur are to be investigated

References: 87, 106, 221, 238, 559, 605, 889, 1011

2.1. Pyrite  $\text{FeS}_2$ 

The reactions of the most frequent sulphide mineral, pyrite are the combination of oxidation, disproportion and thermal dissociation. These reactions overlap each other partly or completely (Figure 2.1.1).

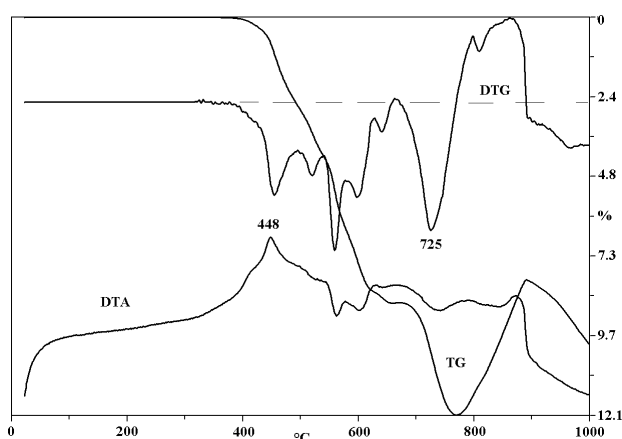
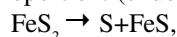


Figure 2.1.1 DTA, TG and DTG curves of the complex reactions of a sample with relatively high pyrite content

Simplified reactions of pyrite: between 350–700 °C overlapped

1. oxidation, depending on the oxygen quantity available with end-products of  $\text{Fe}_3\text{O}_4$ ,  $\text{Fe}_2\text{O}_3$ ,  $\text{Fe}_2(\text{SO}_4)_3$ ,  $\text{SO}_3$ ,  $\text{SO}_2$  and S (exothermic),

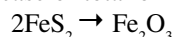
2. disproportion: (endothermic)



3. oxidation of FeS and S to  $\text{Fe}_2\text{O}_3$  (exothermic),

4. dissociation of iron sulphate to  $\text{Fe}_2\text{O}_3$  and  $\text{SO}_3$  (endothermic),

In the case of total oxidation, the whole process:



Stoichiometric factor for the whole reaction: 3.

Sample: pyritic breccia, Bükkszentkereszt, borehole Bszk-65 205–227 m, Hungary

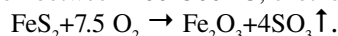
Sample mass: 114 mg

Heating rate: 10 °C/min

Other thermally active minerals in the sample: dolomite, muscovite.

When the investigation is carried out in **oxygen** or the sample has only a low pyrite content, the reaction of oxidation will be simple and complete (Figure 2.1.2).

Reaction between 400–500 °C, exothermic:



Stoichiometric factor based on the mass loss: 3.

Sample: Lovasberény, borehole Lbt-1: 104.3 m, Hungary

Sample mass: 500 mg

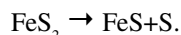
Heating rate: 10 °C/min

Mass loss during the reaction: 1.4%

Pyrite content of the sample based on the mass loss: 4%

In **nitrogen** only the reaction of disproportion can be estimated (Figure 2.1.3).

Reaction between 600–700 °C, endothermic:



Stoichiometric factor based on the mass loss: 3.75.

Sample: Pázmánd, borehole Pt-2: 86,6–90,3 m, Hungary

Sample mass: 1000 mg

Heating rate: 10 °C/min

Mass loss during the reaction: 3.6%

Pyrite content of the sample based on the mass loss: 13%

Other thermally active minerals in the sample: illite, illite-montmorillonite mixed layer, kaolinite, quartz

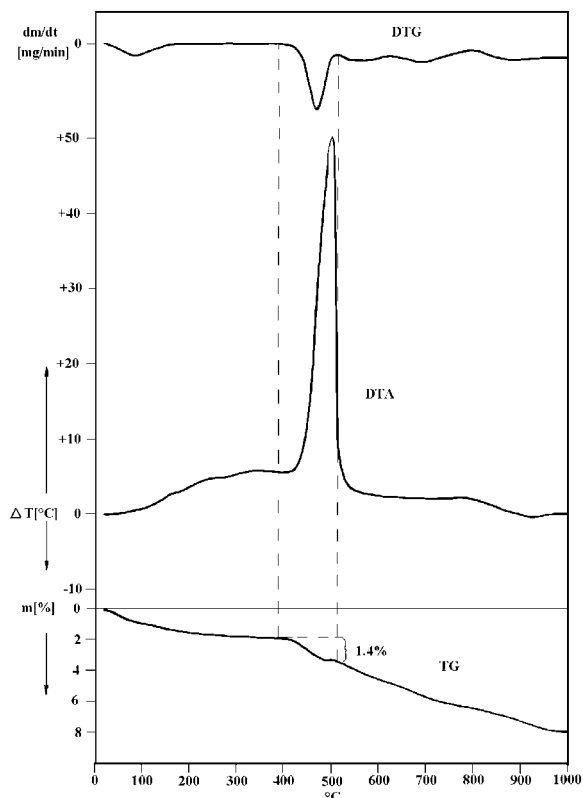
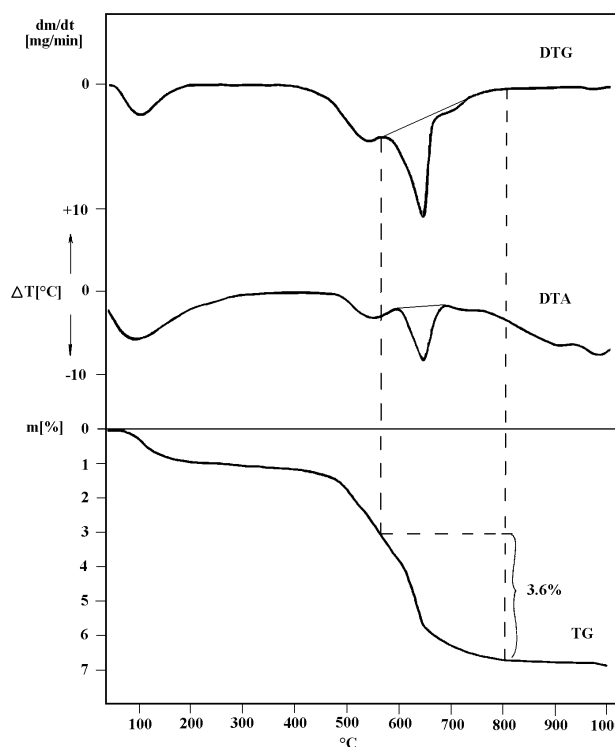


Figure 2.1.2. DTA, TG and DTG curves of the oxidation of pyrite in oxygen

According to HILLER, PROBSTHAIN (1956a), in  $N_2$  pyrite did not dissociate into FeS but rather into pyrrhotite ( $Fe_7S_8$ ).

Under the same conditions, the oxidation peak temperature of marcasite is around 80 °C lower than that of pyrite.

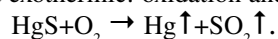
References: 32, 87, 106, 184, 244, 247, 248, 249, 252, 261, 485, 499, 501, 513, 534, 535, 536, 540, 559, 561, 569, 603, 605, 663, 722, 730, 759, 771, 829, 830, 834, 839, 857, 990, 1075, 1081, 1091, 1189



**Figure 2.1.3.** DTA, TG and DTG curves of the disproportion of pyrite in nitrogen

## 2.2 Cinnabar HgS

Reaction of the mineral between 310–500 °C, endothermic and exothermic: oxidation and sublimation:



Stoichiometric factor of the whole process: 1.

Sample: Locality unknown

Sample mass: 600 mg

Heating rate: 17 °C/min

Mass loss during the reaction: 18.3%

Cinnabar content of the sample based on the mass loss: 18%

Other thermally active minerals in the sample: dickite

In inert atmosphere the reactions of cinnabar are at 345 °C and 595 °C. (BERG, SHLYAPKINA 1975)

References: 45, 47, 87, 513, 981, 1081

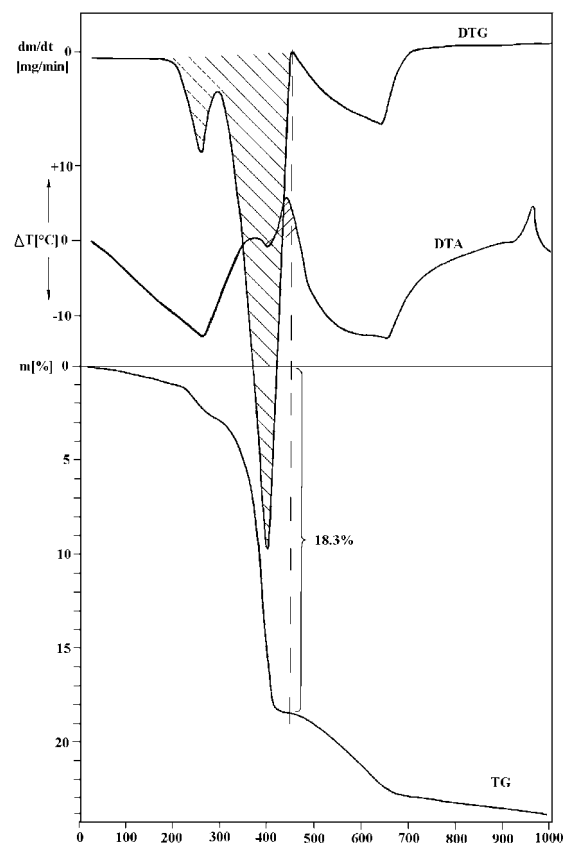


**Figure 2.2.** Oxidation and sublimation of cinnabar

## 2 Sulphides

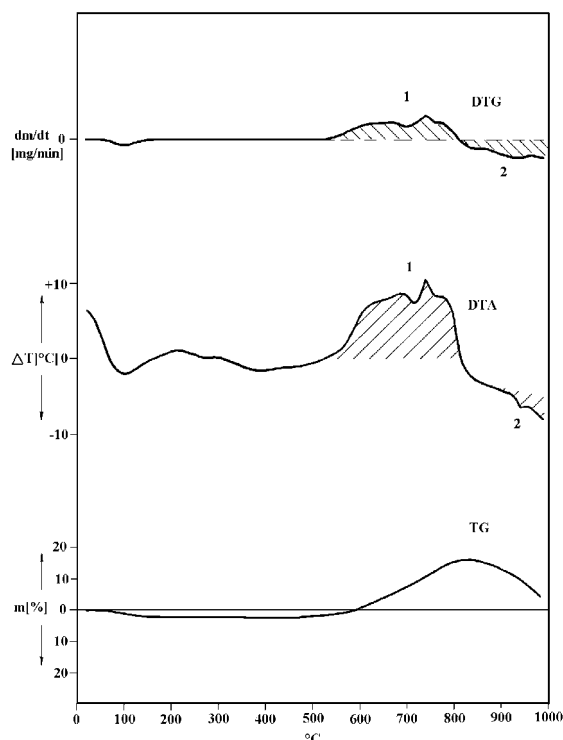
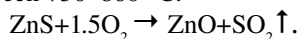


Figure 2.3. Thermoanalytical curves of galena

## 2.4. Sphalerite ZnS

Reaction:

between 750–860 °C:



Stoichiometric factor of the reaction: 6.1.

Sample: Locality: unknown

Sample mass: 100 mg

 Diluted by: 600 mg  $\text{Al}_2\text{O}_3$ 

Heating rate: 10 °C/min

A shift of peak temperatures may be observed with the variation in the amount of iron in the lattice. Peak temperatures decreased from 820 °C for low iron sphalerite (0.1% Fe) to 767 °C for sphalerite with 13% iron content. The temperature of the oxidation is depends also on the grain size, on the heating rate, on the amount of sample.

References: 43, 46, 87, 106, 513, 553, 603, 663, 722, 730, 759, 887, 904, 972, 1081, 1091

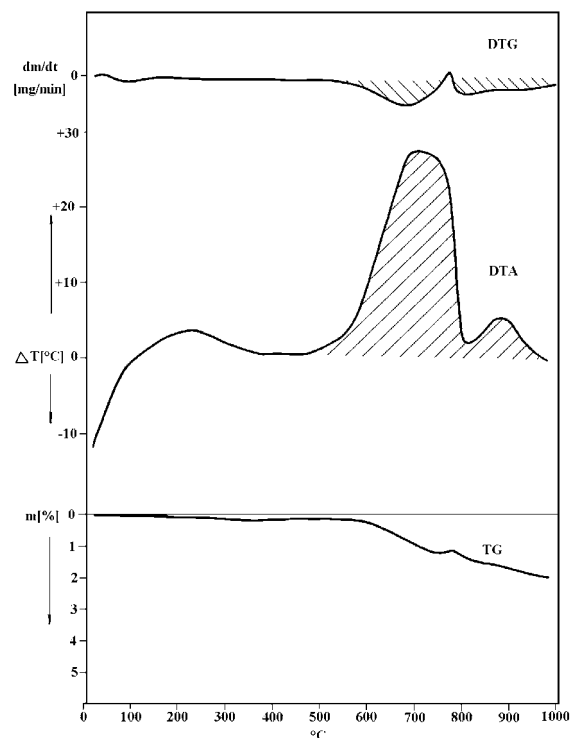


Figure 2.4. Thermoanalytical curves of sphalerite

## 2.3. Galena PbS

Reactions:

 1. Between 600–820 °C: exothermic: oxidation with different internal products of  $\text{PbO}$ ,  $\text{PbSO}_4$ , and  $\text{PbO} \cdot \text{PbSO}_4$ .

 2. Between 850–1100 °C: thermal decomposition, endothermic:  $\text{PbSO}_4 \rightarrow \text{PbO} + \text{SO}_3 \uparrow$ .

Sample: Locality: Borneo

Sample mass: 100 mg

 Diluted by: 900 mg  $\text{Al}_2\text{O}_3$ 

Heating rate: 10 °C/min

References: 1, 3, 87, 253, 254, 513, 663, 722, 730, 936, 1081, 1091

## 2.5. Other chalcogenide minerals

Reference: 6: hauerite, 20: chalcopyrite, 31: pyrrhotite, 32: pyrrhotine, arsenopyrite, löllingite, millerite, nickeline, gersdorffite, linnaeite, cobaltite, scutterudite, 44: chalcopyrite, 48: tetrahedrite, 66: chalcocite, jamesonite, tetradyte, eucairite, 87: sulphide minerals in air and in inert atmosphere: realgar, orpiment, covellite, boulangerite, frankeite, antimonite, chalcopyrite, molybdenite, tennantite, bornite, troilite, pyrrhotine, pentlandite, marcasite, arsenopyrite, chalcocite, cobaltite, 106: molybdenite, tungstenite, guanajuatite, bismuthinite, matildite, miargyrite, pyrrargyrite, proustite, naumannite, argentite, realgar, arsenopyrite, ferroselite, pyrrhotine, chalcopyrite, tennantite, tetrahedrite, stannite, klockmannite, cov-

ellite, chalcocite, 240: pyrrhotites, 241: violarite, 242: nickel sulphide, 243: pentlandite, 244: violarite, pyrrhotite, pentlandite 245: covellite 246: covellite, 250: chalcocite, 251: chalcocite, 341: argentite, 385: bornite, 438: Hg-tetradrite, tennantite, 485: marcasite, hauerite, chalcopyrite, cobaltite, arsenopyrite, covellite, troilite-pyrrhotine, chalcocite, bornite and synthetic sulphides and selenides in  $N_2$ , 486: copper sulfides, 500: arsenopyrite, auriferous sulfide and arsenides, 513: orpiment, realgar, covellite, löllingite, stibnite, chalcopyrite, bornite, chalcocite, cubanite, molybdenite, nickeline, pentlandite, pyrrhotine, arsenopyrite, bismuthinite, stannite, greenockite, 516: sarabauite, 553: alabandite, 559: troilite, hexagonal and monoclinic pyrrhotine, 603: arsenopyrite, chalcopyrite, 632: smythite, greigite, 641: valleriite, 643: troilite, 663: marcasite, chalcopyrite, tennantite, tetradrite, bornite, covellite, chalcocite, 722: pyrrhotine, löllingite, arsenopyrite, covellite, chalcocite, chalcopyrite, bornite, millerite, niccolite, gersdorffite, siegenite, scutterudite, carrollite, argentite, proustite, cobaltite, 730: chalcocite, marcasite, chalcopyrite), 743: chalcocite, covellite, 796: tetradrite, 808: enargite, 887: wurtzite, 912: copper sulfides, 936, 972: wurtzite, 1006: marcasite, pyrrhotite, arsenopyrite, chalcocite, chalcopyrite, bornite, germanite, bournonite, tennantite, wurtzite, proustite, stephanite, acanthite, molybdenite, 1011: chalcocite, digenite, stromeyerite, jalpaite, acanthite, 1035: copper sulfides, 1044: pentlandite, 1067: tetradrite, 1080: chalcopyrite, 1081: chalcocite, covellite, marcasite, pyrrhotine, chalcopyrite, 1091: iron and copper sulfides in air and in  $N_2$ : marcasite, chalcocite, chalcopyrite, bornite, tetradrite, arsenopyrite, stibnite, 1162: skutterudite

### 3. OXIDES

A restricted number of oxides are subject to thermoanalytical investigation.

#### 3.1. Silica minerals

The various kind of silica minerals (polymorphs) have different thermal properties (Table T3.1).

**Table T3.1.** Thermal reactions of silica minerals

Mineral	Temperature (°C)	Modification I		Modification II	Heat of transition (kJ/mol)*
<i>Polymorphic transition</i>					
Tridimite	117	$\alpha$	$\leftrightarrow$	$\beta_1$	0.08
	163	$\beta_1$	$< >$	$\beta_2$	
Cristobalite	180-270	$\alpha$	$\leftrightarrow$	$\beta$	0.79
Quartz	573	$\alpha$	$\leftrightarrow$	$\beta$	0.75
	870	$\beta$	$< >$	tridimite	
<i>Dehydration</i>					
Opal	100-200				

\*Data from MEYER (1968).

The processes are reversible with some hysteresis.

##### 3.1.1. Quartz $SiO_2$

The endothermic reaction at 573 °C corresponds to the structural transition of trigonal ( $\alpha$ )  $\rightarrow$  hexagonal ( $\beta$ ). As the inversion is a reversible process it is possible to detect the quartz peak, even if there are some other minerals, the peak of which appears in the same range of temperature and overlaps the small quartz peak. As the disturbing peaks are generally the results of irreversible processes, they do not appear on the cooling curve or in the case of second heating, thus this thermogram shows only the quartz exothermic peak. This represents a general method for measuring quartz in the presence of thermally interfering mineral species.

Sample: NBS ICTA Standard Reference Material 759

Sample mass: 1000 mg

Heating rate: 17 °C/min

Since no mass change occurred during the reaction, quantitative estimation is only possible on the basis of the intensity or the area of the small DTA peak.

Generally the temperature of the inversion is within a narrow temperature range, therefore the use of quartz as a temperature calibration standard in DTA was suggested (FAUST 1948, MCADIE et al. 1972). In spite of these, Tuttle found that

## 3 Oxides

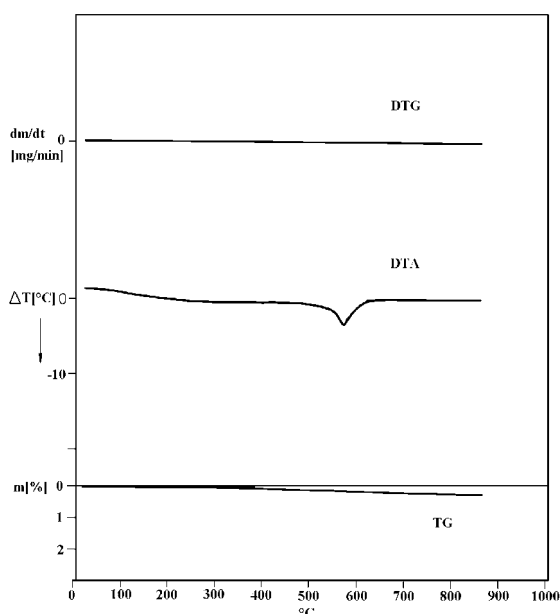


Figure 3.1.1. Thermoanalytical curves of quartz

the inversion temperature varied inversely with the temperature of formation and therefore it may become a useful geologic thermometer. SMYKATZ-KLOSS (1969, 1970, 1971, 1972) found also that certain quartzes gave DTA peak with variation in shape and temperature depending on the origin or genesis. Physical defects, chemical impurities, particle size, mechanical activation may also influence the shape and temperature of the transformation effects (DUBRAWSKI 1987, LISK et al. 1991, STOCH 1991). The paper of SMYKATZ-KLOSS, KLINKE (1997) reviews studies on the possible applications of the high-low quartz inversion in petrology.

References: 51, 211, 227, 232, 297, 318, 668, 672, 727, 757, 758, 957, 1013, 1028, 1031

3.1.2. Opal  $\text{SiO}_2 \cdot n\text{H}_2\text{O}$ 

Opal is a hydrated form of silica.

Reaction of the mineral between 40–600 °C, endothermic:



Opal contains a variable amount of water from less than 1% up to more than 20% (opal-AG=hyalite contains about 3%, opal-AN 5–10%, earthy types, such as diatomite about 20%). The temperature of water escape changes according to the water content. Total water content can be separated to contents of “molecular water” and “silanol-group water (Si-OH)” (see Water in amorphous phases in Chapter 3.3). Interpretation of geyserite suggests that the “wet” opal (average 12–13 wt%  $\text{H}_2\text{O} + \text{OH}$ ) forms as a result of rapid precipitation whereas the “dry” opal (average 5–6 wt% ( $\text{H}_2\text{O} + \text{OH}$ )) forms as a result of slower precipitation.

Sample: Erdőbénye, Hungary

Sample mass: 1000 mg

Heating rate: 17 °C/min

References: 105, 141, 319, 416, 531, 532, 533, 646, 737, 1139

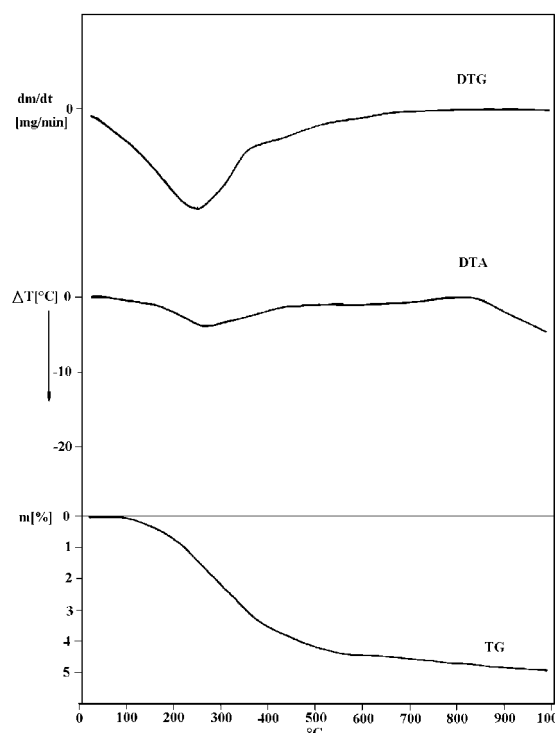


Figure 3.1.2. Thermoanalytical curves of opal

## 3.1.3. Other silica minerals

References: 164, 208, 415: tridimite, 777: cristobalite, 798: tridimite, 979: cristobalite, 984: tridimite, 1026: cristobalite

## 3.2. Iron oxides

### 3.2.1. Magnetite $\text{Fe}_3\text{O}_4$

Thermal reactions:

between 275–450 °C exothermic, oxidation of the surface,

between 480–1000 °C exothermic, oxidation of the bulk

$2\text{Fe}_3\text{O}_4 \rightarrow 3\text{Fe}_2\text{O}_3$  (weight increasing in the case of total oxidation: 3.5%).

About 580 °C endothermic, Curie-point (loses its ferromagnetism), temperature dependences on chemical composition. Substitution in natural magnetites lowers the Curie-temperature.

Sample: Krivoj Rog, Russia

Sample mass: 200 mg

Heating rate: 10 °C/min

By measuring the Curie-point during two heatings following each other it may become possible to determine whether the Ti content in a sample is titanomagnetite or separate ilmenite/rutile. The originally separate Ti-phase during heating up to 1000 °C homogenises with the magnetite. At the second heating in this case the Curie point is at a lower temperature (VINCENT et al. 1957, SMYKATZ-KLOSS 1974a).

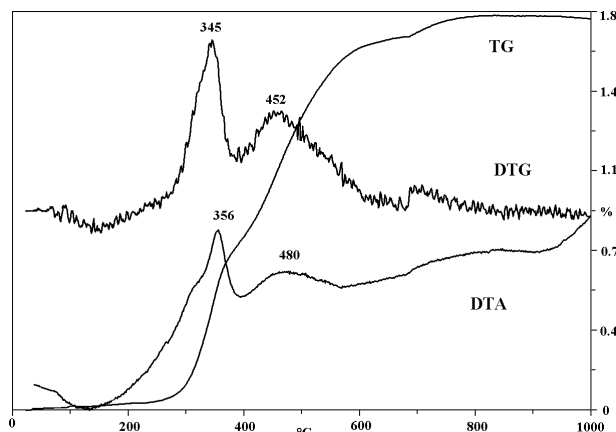


Figure 3.2.1. Oxidation reaction of magnetite

References: 168, 268, 272, 397, 662, 763, 921, 946, 947, 948, 960, 1006, 1107, 1180,

### 3.2.2. Hematite $\text{Fe}_2\text{O}_3$

On the DTA curve of hematite only a small endothermic peak appears at about 675–680 °C, which is the Curie-point of the mineral.

**Hematite-like materials:** cannot be related to pure stoichiometric hematite.

Minerals described in the literature “hydrohematite” originally considered as hydrated hematite,  $\text{Fe}_2\text{O}_3 \cdot n\text{H}_2\text{O}$  identical with hematite but of fine particle size and contains variable amounts of incorporated molecular water or with ordered incorporation of hydroxyl groups in the hematite lattice, which evolves at low temperature or over a wide temperature range and cation vacancies. Hydrohematite is an intermediate phase during the transformation of goethite or protohematite to hematite with nonstoichiometric composition.

The “hematogelite” (an amorphous iron-oxide or iron-hydroxide that transforms from amorphous into crystalline phase at about 800 °C) is probably the synonym for ferrihydrite.

References: 205, 813, 1039, 1170, 1171

### 3.2.3. “Ferrihydrite” $\text{Fe}^{3+}_{4-5}(\text{OH}, \text{O})_{12} (2.5\text{Fe}_2\text{O}_3 \cdot 4.5\text{H}_2\text{O} \text{ or } \text{Fe}_5\text{HO}_8 \cdot 4\text{H}_2\text{O})$

Ferrihydrite is a hydrous oxide of iron of short-range order. It is also known as “amorphous ferric oxide”, “hydrous ferric oxide”, “amorphous iron oxide” or “ferric hydroxide” and it means a poorly crystalline Fe oxide and may be a precursor in the formation of soil hematite.

This defect variation of hematite gives only some broad X-ray reflections named by CHUKHROV et al. (1971) as ferrihydrite. Formula according to the denominators is  $5\text{Fe}_2\text{O}_3 \cdot 9\text{H}_2\text{O}$ , however, a wide range of chemical composition and formula can be found in the literature:

$5\text{Fe}_2\text{O}_3 \cdot 9\text{H}_2\text{O}$ : CHUKHROV et al. 1973

$\text{Fe}_5\text{HO}_8 \cdot 4\text{H}_2\text{O}$ : TOWE, BRADLEY 1967

$\text{Fe}_2\text{O}_3 \cdot 2\text{FeOOH} \cdot 2.6\text{H}_2\text{O}$ : RUSSEL 1979

$\text{Fe}_{4.63}\text{O}_{3.15}(\text{OH})_{7.59} \cdot 1.26\text{H}_2\text{O}$ : EGGLETON, FITZPATRICK 1988

$\text{Fe}_{4.03}\text{O}_{1.58}(\text{OH})_9 \cdot 1.42\text{H}_2\text{O}$ : EGGLETON, FITZPATRICK 1988

$\text{Fe}_2\text{O}_3(n\text{OH}, \text{H}_2\text{O})$ : BOYD et al 1993

$\text{FeOOH} \cdot 0.4\text{H}_2\text{O}$ : ZHAO et al. 1994

## 3 Oxides

$\text{Fe}(\text{OH})_3$ : BALL, NORDSTROM 1991, RUNKEL, BENCALA 1995

$\text{Fe}_3\text{O}_7(\text{OH}) \cdot 4\text{H}_2\text{O}$ : BROOKS et al. 1998

$\text{Fe}(\text{OH})_3 \cdot n\text{H}_2\text{O}$ : GRAY 2000

Designations such as “2-line-ferrihydrite”, “6-line ferrihydrite” etc. refer to the number of peaks in the X-ray diffraction (XRD) patterns of ferrihydrite, but only 6-line ferrihydrite (6LFh) meet the strict definition of “ferrihydrite”.

Natural ferrihydrite is difficult to isolate and characterize, partly because grain size is very small, and many studies of ferrihydrites use synthetic analogues. Ferrihydrite as defined by the IMA (International Mineralogical Association) has five broad diffraction reflections (FLEISHER et al. 1975). The structural model was derived from the data of X-ray and electron-diffraction of synthetic samples, of weathering crust of basalt and the natural ferrihydrite published by CHUKHROV et al. 1973. The natural ferrihydrite is generally a poorly ordered Fe-oxide form only two broad reflections at 2.5 and 1.5 Å (2-line-ferrihydrite or protoferrihydrite).

Materials with seven to two diffraction maxima are a sequence of decreasing degree of order in a single mineral species (FARMER 1992). Protoferrihydrite is the precursor of ferrihydrite.

The structure of ferrihydrite is not yet fully understood and there are different interpretations of the coordination environment of Fe in ferrihydrite by various investigators.

The structure of ferrihydrite accepted by the IMA is a hematite-like structure with  $\text{FeO}_6$  octahedra except that it is highly disordered and hydrated. The disorder of the structure is manifested by that some O are replaced by  $\text{H}_2\text{O}$  and/or OH and by the presence of vacant Fe sites in the  $\text{FeO}_6$  octahedra. According to the structure model of EGGLETON, FITZPATRICK (1988), the coordination of the third of  $\text{Fe}^{3+}$  is tetrahedral. It would be later refused by the investigation of MANCEAU et al. (1992).

Based on the investigations of DRITS et al. (1993), ferrihydrite consists of the mixture of 3 structural components: “defect-free” ferrihydrite with random occupancy of 50% of the octahedral sites by Fe, “defective” ferrihydrite consisting of a random organization of fragments and a high degree of cation ordering, and ultradispersic hematite.

According to the most recent investigations of MANCEAU, GATES (1995), in contrast to bulk Fe atoms, which are bonded to O and OH ligands, surface Fe atoms are also coordinated octahedrally to  $\text{H}_2\text{O}$  ligands forming the first hydration shell  $[(\text{H}_2\text{O})\text{I}]$ . In the wet state, external water molecules of the second hydration shell  $[(\text{H}_2\text{O})\text{II}]$  are singly H-bonded to  $(\text{H}_2\text{O})\text{I}$ , while they are doubly coordinated in the dry state (Figure 3.2.3a). Accordingly, wet ferrihydrite contains twice as many sorbed water molecules as dry ferrihydrite, and the structural difference due to the second hydration shell accounts quantitatively for the 15% increase of ferrihydrite weight experimentally measured in moist atmosphere. However, on the basis of the IR investigations of CHUKHROV et al. (1973), SCHWERTMANN, FISCHER (1973) there is no measurable signal of stretching and bending vibration of Fe-OH-groups.

Most of the data regarding the thermal character of “ferrihydrite” refer to synthetic preparations (Table T3.2.3). For the DTA of freshly prepared ferric oxide gels MACKENZIE, BERGGREN (1970) gives the following characterisation: it shows a large low-temperature endothermic peak (due to the sorbed moisture) followed by a strong sharp exothermic peak between 200–400 °C, the temperature and shape of which depends on the pH of the suspension and the temperature of the precipitation. (Increase of the final pH of the suspension and the temperature of the precipitation leads to a marked broadening and to an increase of the temperature of the exothermic peak.)

In oxygen the exothermic peak becomes sharper. The peak could be interpreted as it represented the crystallization of amorphous material into hematite of fine particle size after molecular water had escaped from the structure. Others in the case of the natural sample explain the exothermic reaction with the presence of organic matter, because its formation preferred in the presence of large concentration of organic matter (e.g. SCHWERTMANN, FISCHER 1973), and the exothermic peak disappears in nitrogen. The mass loss after  $\text{H}_2\text{O}_2$  decreases.

Water content is variable (13–23%). This value from the stoichiometric formula is about 17%. Water content based on the chemical analysis of ferrihydrite precipitated from cold water is between 22% and 32%, and from hot water it is 10–38% CHUKHROV et al. (1973). According to SCHWERTMANN, FISCHER (1973), adsorptive water is in the range of 15–20%. In the publication of SINGH et al. (1999) water escape is about 10%, 17–23% and 26.3% at up to 160 °C, 500 °C and 1000 °C respectively. According to WELLS, CHILDS (1988), the water content of ferrihydrite and allophane is about 25%.

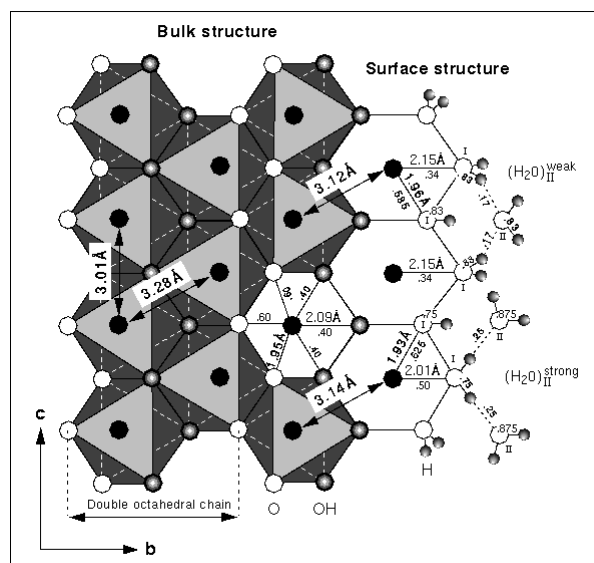


**Figure 3.2.3a.** Surface structural model for ferrihydrite. (MANCEAU, GATES 1995)

**Table T3.2.3.** DTA reaction of synthetic iron oxide gels

Endothermic		Exothermic		pH	References
°C					
190			490	10	CHUKHROV 1955: Card A 4097. In: MACKENZIE: Scifax Differential Thermal Data Index 1962
175		275		5	CHUKHROV 1955: Card A 4095. In: MACKENZIE: Scifax Differential Thermal Data Index 1962
	220	315			SHURYGINA 1958: Card A 4097. In: MACKENZIE: Scifax Differential Thermal Data Index 1962
100	230		345		SHURYGINA 1958: Card A 4098. In: MACKENZIE: Scifax Differential Thermal Data Index 1962
175			400		GHEITH 1952
180			380		RAMACHANDRAN, BHATTACHARYYA 1954: Card A 4096. In: MACKENZIE: Scifax Differential Thermal Data Index 1962
130		270		5	MACKENZIE 1957 p. 299.
130			370	10	
	240		360		SCHLEIFER et al. 1957.

According to our own investigations the thermogravimetric curves of ferrihydrites can be divided into three groups:

- One large asymmetric dehydration peak with average peak temperature at 95 °C.
- Three different dehydration steps with average peak temperatures at 99, 185 and 274 °C.
- Two dehydration steps with average peak temperatures at 90 and 266 °C. (Figure 3.2.3b).

These groups may be represented by the sequence of decreasing degree of order of ferrihydrite.

The two low temperature reactions can correspond to (H<sub>2</sub>O)II and (H<sub>2</sub>O)I in the model of MANCEAU, GATES (1995), the third one corresponds probably to the bulk composition of 5Fe<sub>2</sub>O<sub>3</sub>·9 H<sub>2</sub>O (about 17% mass loss), a goethite-like dehydroxylation but with lower temperatures at 50–75 °C. Mass loss in the same temperature range derives from organic matter.

The accompanying exothermic peak between 200 °C and 400 °C is the development of α-Fe<sub>2</sub>O<sub>3</sub> from “protohematite” and also could be a signal for organic materials.

Sample: Spring precipitation

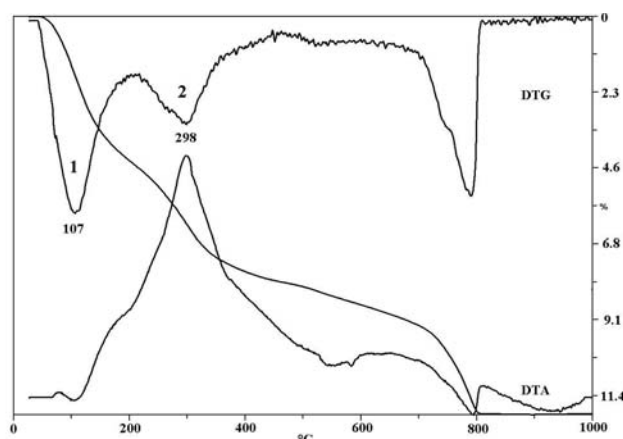
Sample mass: 98.7 mg

Heating rate: 10 °C/min

Mass loss during the first reaction: 4.3%

Mass loss during the second reaction: 3.3%

Other thermally active minerals in the sample: carbonate, quartz, clay mineral

**Figure 3.2.3b.** Derivatogram of ferrihydrite

References: 57, 111, 134, 151, 152, 153, 175, 178, 179, 223, 269, 294, 315, 397, 420, 520, 566, 636, 688, 689, 693, 710, 711, 723, 751, 868, 885, 932, 933, 955, 975, 976, 997, 1084, 1145, 1183, 1187

## 3 Oxides

## 3.3. Manganese oxides

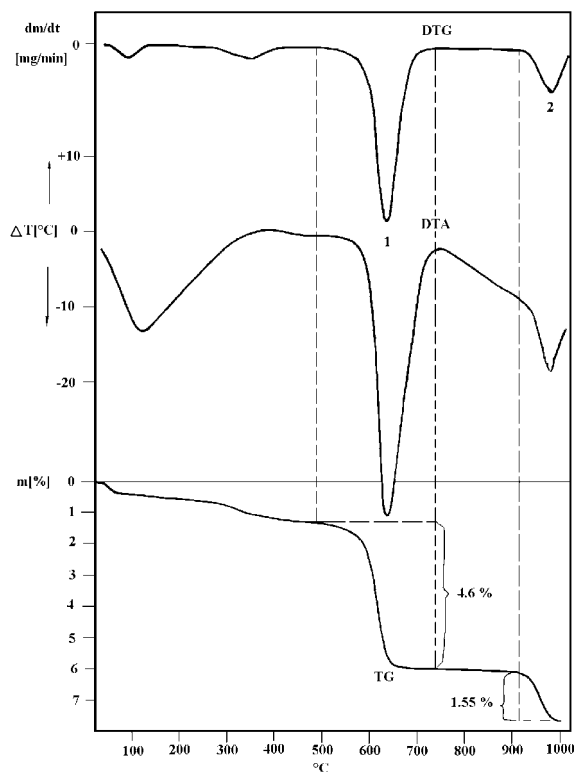
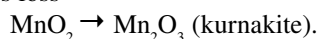
3.3.1. Pyrolusite  $\text{MnO}_2$ 

Figure 3.3.1. Derivatogram of pyrolusite

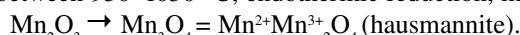
Thermal reactions of manganese of pyrolusite:

between 625–725 °C, endothermic reduction ( $\text{Mn}^{4+} \rightarrow \text{Mn}^{3+}$ ), mass loss



Stoichiometric factor of the reaction: 10.8.

between 950–1050 °C, endothermic reduction, mass loss



Stoichiometric factor of the reaction calculated for the mineral: 32.6.

Sample: Elgersburg, Germany

Sample mass: 500 mg

Heating rate: 17 °C/min

Mass loss during the first reaction: 4.6%

Mass loss during the second reaction: 1.55%

Pyrolusite content of the sample based on the first reaction: 50%

Pyrolusite content of the sample based on the second reaction: 51%

Ramsdellite ( $\text{MnO}_2$ ) gives a curve identical with pyrolusite except for a small exothermic peak at 360–500 °C corresponding to the ramsdellite  $\rightarrow$  pyrolusite conversion KULP, PERFETTI (1950).

References: 7, 96, 276, 341, 343, 344, 412, 418, 419, 513, 524, 553, 635, 670, 1073, 1081

## 3.3.2. Other manganese oxides

Wad is a generic name for the earthy manganese oxides/hydroxides, often containing significant amounts of hydroxides/oxides of other metals (iron, barium, etc.). There is the hydrovariation of hausmannite, manganite, manganosite, pyrolusite, braunite, other manganese oxides or their mixture (Table T3.3.2).

About the hydrated manganese-oxide may be found much less literature data than about “ferrihydrite”. The characterization of many hydrous manganese oxides is difficult and frequently incomplete because of their poor crystallinity. The hydrated manganese-oxide has also a structure of two-line  $\text{Mn}^{4+}$  hydrous gels ( $\beta\text{-MnO}_2$ ) (MANCEAU et al 1992).

Table T3.3.2. Thermal reactions of other manganese oxides

Mineral	Formula	Temperature and reaction type		625–725 reduction	950–1000 reduction
Manganosite	$\text{MnO}$		350 °C oxidation $\text{Mn}^{2+}$ to $\text{Mn}^{4+}$	$\text{MnO}_2 \rightarrow \text{Mn}_2\text{O}_3$	$\text{Mn}_2\text{O}_3 \rightarrow \text{Mn}_3\text{O}_4$
Nsutite	$(\text{Mn}_x)(\text{Mn}_{1-x})(\text{OH})_2$ where $x=0.06-0.07$	787 dehydration?		$\text{MnO}_2 \rightarrow \text{Mn}_2\text{O}_3$	$\text{Mn}_2\text{O}_3 \rightarrow \text{Mn}_3\text{O}_4$
Hausmannite	$\text{Mn}^{2+}\text{Mn}^{3+}_2\text{O}_4$		890–1000 °C		
Braunite	$\text{Mn}^{2+}\text{Mn}^{3+}_2\text{SiO}_5$				
Psilomelane (romanechite)	$\text{Ba}(\text{II},\text{O})\text{Mn}^{3+}_2\text{O}_{10}$	dehydration			$\text{Mn}_2\text{O}_3 \rightarrow \text{Mn}_3\text{O}_4$
Cryptomelane	$\text{K}(\text{Mn}^{2+},\text{Mn}^{3+})_8\text{O}_{16}$		600 °C $\rightarrow \text{Mn}_2\text{O}_3$	$\text{MnO}_2 \rightarrow \text{Mn}_2\text{O}_3$	$\text{Mn}_2\text{O}_3 \rightarrow \text{Mn}_3\text{O}_4$
Todorokite	$(\text{Na},\text{Ca},\text{K})(\text{Mn}^{2+},\text{Mn}^{3+})_8\text{O}_{16} \cdot 3-4.5(\text{H}_2\text{O})$	105 dehydration	330 dehydration	$\text{MnO}_2 > \text{Mn}_2\text{O}_3$	$\text{Mn}_2\text{O}_3 > \text{Mn}_3\text{O}_4$
Bixbyite	$(\text{Mn}^{2+},\text{Fe}^{2+})_2\text{O}_3$				
Birnessite	$(\text{Na},\text{Ca},\text{K})(\text{Mn}^{4+},\text{Mn}^{3+})_2\text{O}_{10} \cdot 1.5(\text{H}_2\text{O})$	dehydration		$\text{MnO}_2 \rightarrow \text{Mn}_2\text{O}_3$	$\text{Mn}_2\text{O}_3 \rightarrow \text{Mn}_3\text{O}_4$
Rancieite	$(\text{Ca},\text{Mn})_2\text{Mn}_2\text{O}_5 \cdot 3(\text{H}_2\text{O})$	dehydration	150–300 dehydration	$\text{MnO}_2 \rightarrow \text{Mn}_2\text{O}_3$	$\text{Mn}_2\text{O}_3 \rightarrow \text{Mn}_3\text{O}_4$
Vernadite	$\text{Mn}^{2+},\text{Fe}^{2+},\text{Ca},\text{Na})(\text{O},\text{OH})_2 \cdot n(\text{H}_2\text{O})$	100 dehydration		$\text{MnO}_2 > \text{Mn}_2\text{O}_3$	$\text{Mn}_2\text{O}_3 > \text{Mn}_3\text{O}_4$
Coronadite	$\text{Pb}(\text{Mn}^{2+},\text{Mn}^{3+})_2\text{O}_{10}$			$\text{MnO}_2 > \text{Mn}_2\text{O}_3$	$\text{Mn}_2\text{O}_3 > \text{Mn}_3\text{O}_4$
Buserite	$\text{Na}_2\text{Mn}_2\text{O}_5 \cdot 2\text{H}_2\text{O}$	100 dehydration (2/3 $\text{H}_2\text{O}$ )	700 dehydration		
Takamchite	$(\text{Mn}^{2+},\text{Ca})\text{Mn}_2\text{O}_5 \cdot (\text{H}_2\text{O})$	dehydration			
Chalcophamite	$\text{ZnMn}_2\text{O}_5 \cdot 3\text{H}_2\text{O}$	dehydration			

References: 7: hausmannite, psilomelane, braunite 62: rancieite, 96: coronadite, romanechite, todorokite, 231: busserite, todorokite, vernadite, birnessite, 296: cryptomelane, 313: psilomelane, 343:  $\text{Mn}_2\text{O}_3$ ,  $\text{Mn}_3\text{O}_4$ , 344: hausmannite, braunite, psilomelane 353: hausmannite, 401: hausmannite, 402: romanechite 408, 409: birnessite, 412, 418:  $\text{MnO}_2$ ,  $\text{Mn}_2\text{O}_3$ ,  $\text{Mn}_3\text{O}_4$ , 419: psilomelane, wad, 513: braunite, vernadite, hausmannite, cryptomelane, coronadite, todorokite, psilomelane = wad, rancieite, zincdibraunite, 553: psilomelane, hollandite, hausmannite, wad, 630: cryptomelane 635: psilomelane, hausmannite, braunite 669, 670: todorokite, 693, 711, 754, 864: romanéchite, cryptomelane, coronadite, hollandite, 752: wad, 881: todorokite 1032: todorokite, 1081: manganosite, braunite, hausmannite, 1192 nsutite

### 3.4. Other oxides

Reference: 406: hydrated aluminium oxide

## 4. HYDROXIDES

### 4.1. Simple hydroxides

**Table T4.1.** Dehydroxylation process of simple hydroxide minerals

Mineral name	Formula	Temperature of dehydroxylation (°C)	Stoichiometric factor
Sassolite	$2\text{B}(\text{OH})_3$	155–190	2.26
Bernalite	$\text{Fe}(\text{OH})_3$	190–200	3.95
Pyrochroite	$\text{Mn}(\text{OH})_2$	210	4.94
Gibbsite	$2\text{Al}(\text{OH})_3$	300–340	2.89
Brucite	$\text{Mg}(\text{OH})_2$	350–450	3.24
Portlandite	$\text{Ca}(\text{OH})_2$	480–620	4.12

#### 4.1.1. Gibbsite $\text{Al}(\text{OH})_3$

Reaction of natural gibbsite:  
at 280–340 °C: dehydroxylation  
 $\text{Al}(\text{OH})_3 \rightarrow \text{Al}_2\text{O}_3 + \text{H}_2\text{O}$   
Stoichiometric factor of the reaction: 2.89.

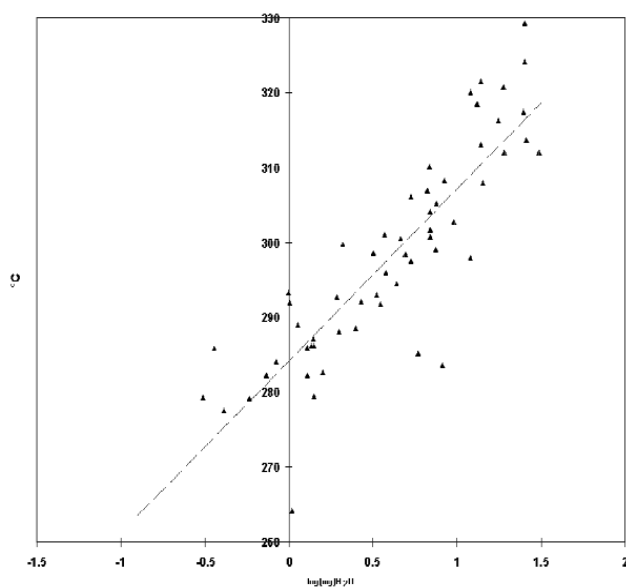


**Figure 4.1.1b.** PA curve of natural gibbsite

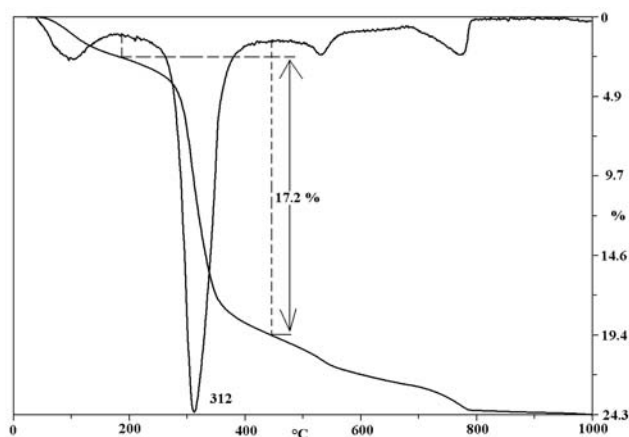


**Figure 4.1.1a.** Thermogravimetric curves of natural gibbsite

Sample: Ziar, Slovakia

Sample mass: 179.7 mg

Heating rate: 10 °C/min

Mass loss during the reaction: 17.2%.

Gibbsite content of the sample based on the reaction: 49.6% (Figure 4.1.1a, b).

Other thermally active minerals in the sample: kaolin-ite(15%), calcite (4%), boehmite (3%).

## 4 Hydroxides

Decomposition mainly of artificial gibbsite (bayerite) consists of three partial reactions:

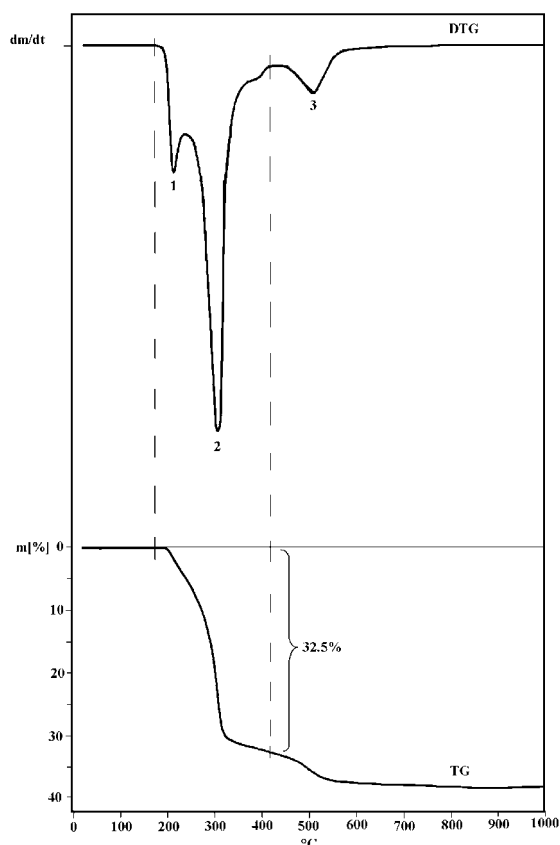
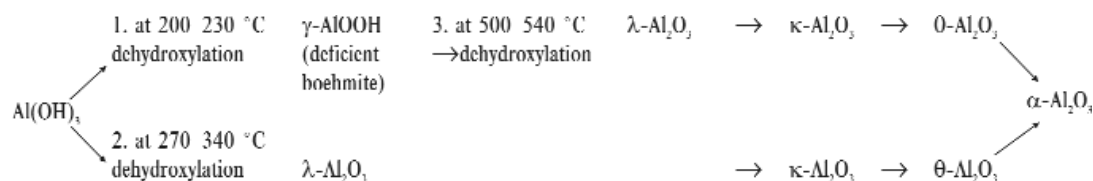


Figure 4.1.1c. Thermogravimetric curves of artificial gibbsite

Empirical factor based on the mass loss during the first two reactions: 3.15

Sample: artificial gibbsite

Sample mass: 1000 mg

Heating rate: 17 °C/min

Mass loss during the first two reactions: 32.5%

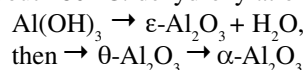
Partially overlapping peaks of gibbsite and goethite in bauxite may be resolved (Figure 4.1.1c).

References: 19, 53, 125, 204, 287, 537, 553, 579, 608, 686, 688, 694, 702, 714, 732, 733, 784, 794, 795, 821, 823, 827, 833, 836, 862, 878, 918, 949, 950, 953, 954 1068

#### 4.1.2. Nordstrandite $\text{Al(OH)}_3$

Thermal reactions of nordstrandite are very similar to that of natural gibbsite:

at about 280 °C: dehydroxylation



Sample: Aggtelek, Hungary

Sample mass: 111.9 mg

Heating rate: 10 °C/min

Mass loss during the dehydroxylation: 10.8%

Nordstrandite content of the sample based on the reaction: 31%.

Other thermally active minerals in the sample: kaolinite, bassanite, boehmite, dolomite, amorphous.

References: 513, 953, 954

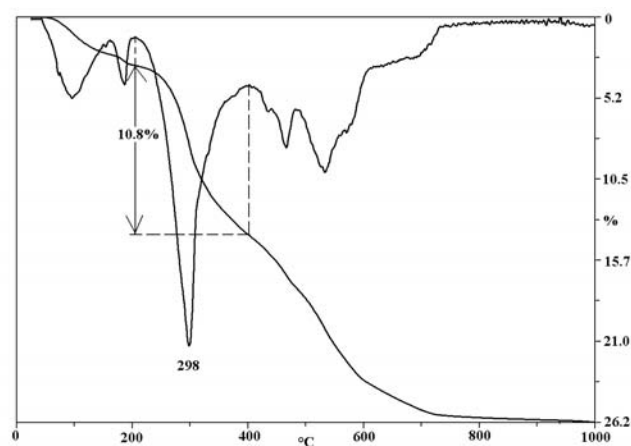
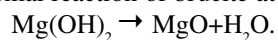


Figure 4.1.2. Thermogravimetric curves of a sample containing nordstrandite

### 4.1.3. Brucite $\text{Mg}(\text{OH})_2$

Thermal reaction of brucite at 350–450 °C:



Stoichiometric factor of the reaction: 3.24.

Sample locality: Polgárdi, Hungary

Sample mass: 1000 mg

Heating rate: 17 °C/min

Mass loss during the dehydroxylation: 6.8%

Brucite content of the sample based on the reaction: 22%

Other thermally active minerals in the sample: calcite

References: 58, 102, 173, 295, 389, 394, 498, 553, 563, 572, 656, 679, 841, 1081

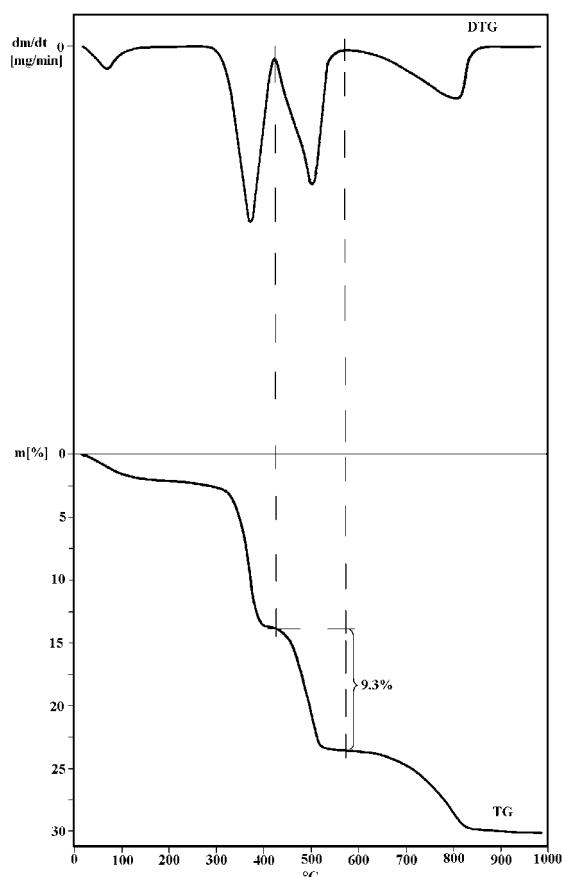


Figure 4.1.4. Thermogravimetric curves of a sample containing portlandite

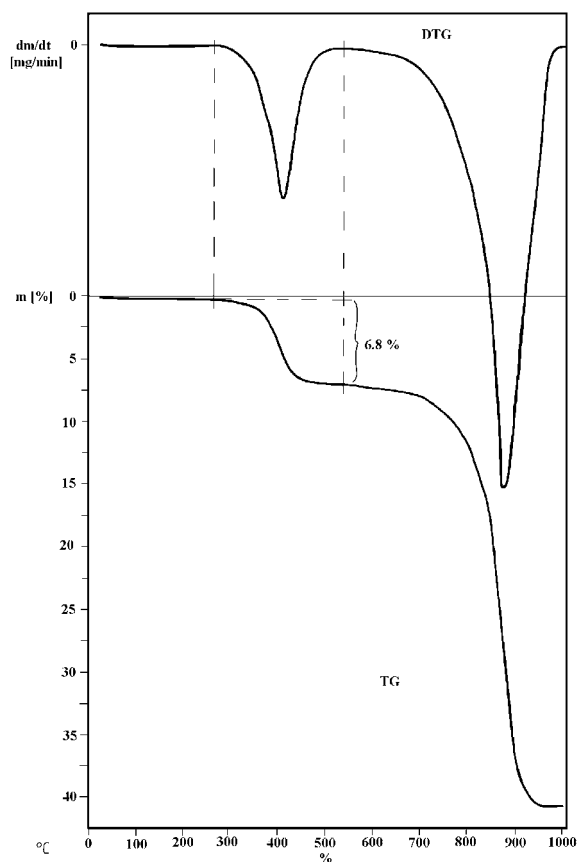
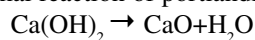


Figure 4.1.3. Thermogravimetric curves of a sample containing brucite

### 4.1.4. Portlandite $\text{Ca}(\text{OH})_2$

Thermal reaction of portlandite at 480–620 °C:



Stoichiometric factor of the reaction: 4.12.

Sample locality: Mosso, Burundi

Sample mass: 1000 mg

Heating rate: 10 °C/min

Mass loss during the dehydroxylation: 9.3%

Portlandite content of the sample based on the reaction: 38%

Other thermally active minerals in the sample: brucite, calcite

Reference: 841

### 4.1.5. Other simple hydroxides

References: 95: bernalite, 513: sassolite, 730: sassolite, 782: bernalite

## 4 Hydroxides

## 4.2. Oxides containing hydroxyl (oxyde-hydroxides)

The main thermal reaction of the minerals containing both oxygen and hydroxyl anions is the dehydroxylation (Table T4.2.).

**Table T4.2.** Dehydroxylation of oxyhydroxide minerals

Mineral name	Polymorphic transition			Temperature of dehydroxylation (°C)	Stoichiometric factor
Lepidocrocite	$\gamma$ FeOOH	>	$\gamma$ Fe <sub>2</sub> O <sub>3</sub>	300–370	9.9
Goethite	$\alpha$ FeOOH	>	$\alpha$ Fe <sub>2</sub> O <sub>3</sub>	330–420	9.9
Manganite	$\gamma$ -MnOOH	→	Mn <sub>2</sub> O <sub>3</sub>	350–400	9.8
Boehmite	$\gamma$ -AlOOH	→	$\gamma$ -Al <sub>2</sub> O <sub>3</sub>	550–600	6.6
Diaspore	$\alpha$ -AlOOH	→	$\alpha$ -Al <sub>2</sub> O <sub>3</sub>	500–600	6.6

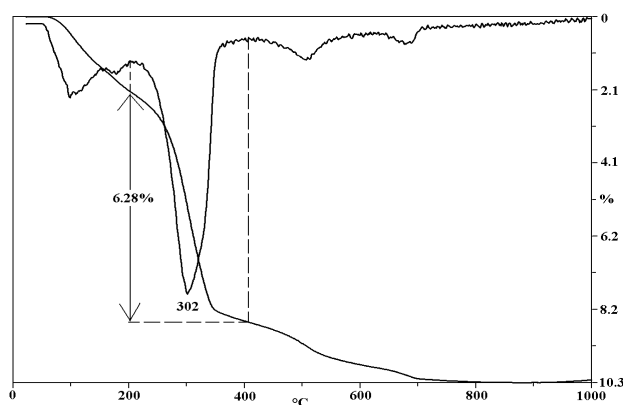


**Figure 4.2.1a.** Thermogravimetric curves of a sample containing goethite

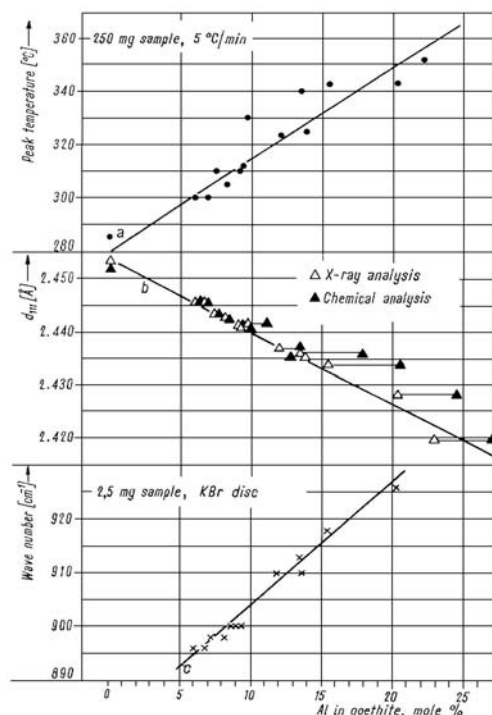
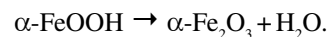


**Figure 4.2.1b.** Temperature of dehydration peak, the shift of  $d_{III}$  X-ray reflection and the wave number of the deformation band around 900  $\text{cm}^{-1}$  as function of the aluminium content of goethite (after JÓNÁS, SOLYMÁR 1970b)

4.2.1. Goethite  $\alpha$ -FeOOH

Reaction of the mineral at 290–330 °C dehydroxylation:



Stoichiometric factor of the reaction: 9.9.

Sample: limonite nodule, Zirc, Hungary

Sample mass: 142.1 mg

Heating rate: 10 °C/min

Mass loss during the dehydroxylation: 6.28%

Goethite content of the sample based on the reaction: 62% (Figure 4.2.1a).

Other thermally active minerals in the sample: montmorillonite, illite, calcite

Natural goethite first of all in bauxite often contains appreciable quantities of aluminum ion substituting Fe. Other cations such as Cr, Ge, Ni, Co and Mn may also substitute Fe in natural goethite.

This substitution may affect the dehydroxylation temperature. The main peak for the dehydroxylation of Mn-bearing goethite is identified at about 30 °C higher as in the case of pure goethite (Figure 4.2.1b) (The XRD pattern for manganese goethite shows broadened  $hkl$  reflections that have approximately the same  $d$  values as those of goethite

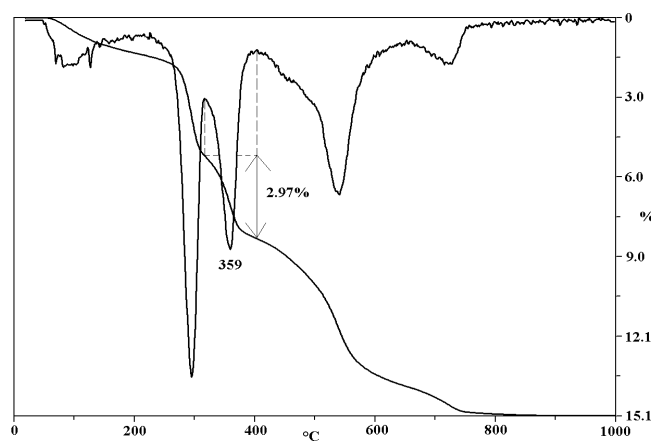


**Figure 4.2.1c.** Thermogravimetric curves of a sample containing aluminogoeite

(MANCEAU et al 1992, WELLS et al. 1992).) The same trend in the temperature shifting of dehydroxylation is observed for Al-substituted goethites with aluminium concentrations up to 25 mol% (Figure 4.2.1b — JÓNÁS, SOLYMÁR 1970a, b).

Sample: bauxite, Koldusszállás, Hungary

Sample mass: 118.7 mg

Heating rate: 10 °C/min

Mass loss during the dehydroxylation: 2.97%

Alumo-goethite content of the sample based on the reaction: 19–29%\*

Other thermally active minerals in the sample: gibbsite, kaolinite, diaspor, calcite.

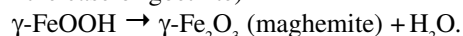
\*Stoichiometric factor varies between 6.6 (pure boehmite) and 9.9 (pure goethite) (Figure 4.2.1c).

References: 17, 210, 309, 368, 410, 430, 528, 529, 553, 557, 558, 583, 636, 699, 711, 751, 782, 927, 928, 974, 996, 1116, 1018, 1142, 1144, 1172

## 4.2.2 Lepidocrocite $\gamma$ -FeOOH

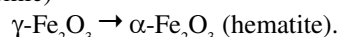
Reactions of the mineral:

1. Dehydroxylation (the reaction is at a somewhat (about 10–40 °C) lower temperature and the peak is much narrower than in the case of goethite)



Stoichiometric factor of the reaction: 9.9.

2. After dehydroxylation over 400 °C, recrystallization (exothermic)



Sample: Beremend, Hungary

Sample mass: 165.8 mg

Heating rate: 10 °C/min

Mass loss during the dehydroxylation: 0.74%

Lepidocrocite content of the sample based on the reaction: 7%.

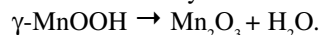
Other thermally active minerals in the sample: montmorillonite, kaolinite, calcite, amorphous ferric hydroxide.

References: 41, 212, 636, 751, 782, 1038, 1081, 1172

## 4.2.3 Manganite $\gamma$ -MnOOH

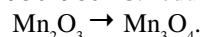
Reactions of the mineral:

1. at 350–400 °C: dehydroxylation



Stoichiometric factor of the reaction: 9.8.

2. at 950–980 °C: reduction:



Stoichiometric factor of the reaction calculated for the mineral: 30.3.

Sample: Eplény, Hungary

Sample mass: 1000 mg

Heating rate: 17 °C/min

Mass loss during the dehydroxylation: 5.6%

Manganite content of the sample based on the reaction: 55%.

Other thermally active minerals in the sample: pyrolusite.

Reaction 2 belongs to both manganite and pyrolusite.

References: 7, 96, 231, 412, 419, 635, 665, 761

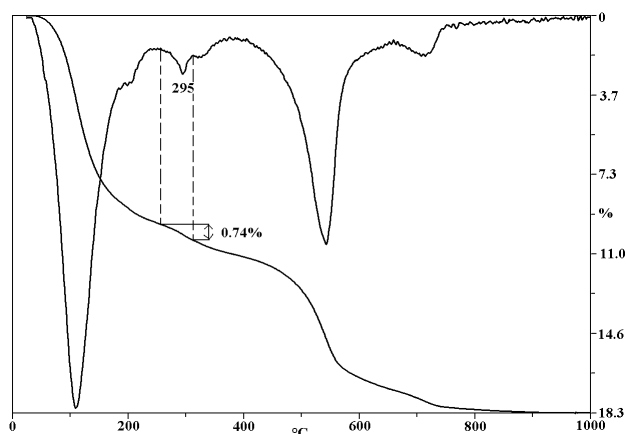


Figure 4.2.2. Thermogravimetric curves of a sample containing lepidocrocite

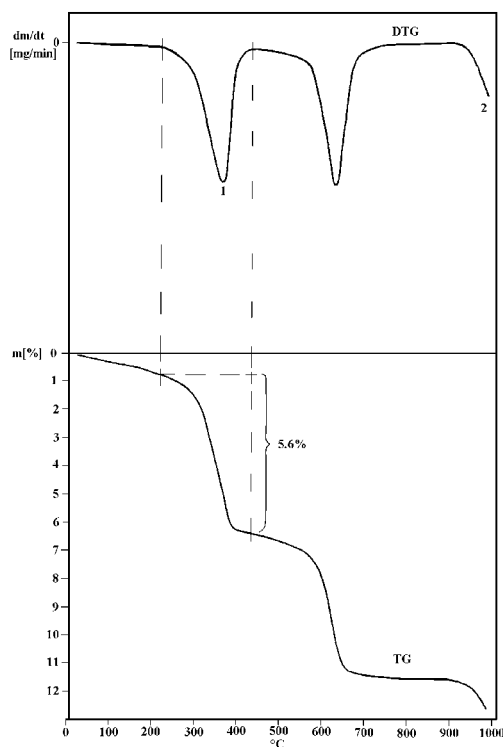
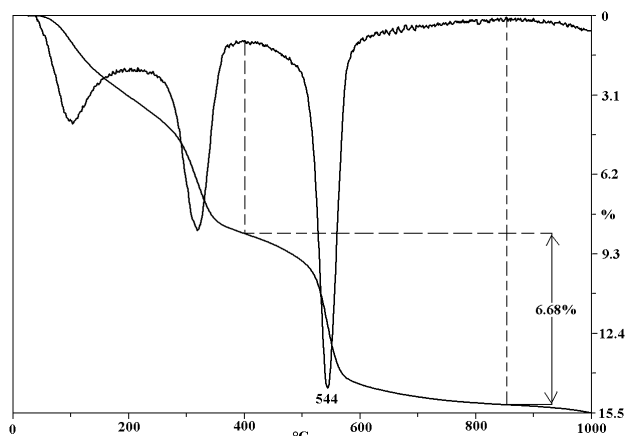


Figure 4.2.3. Thermogravimetric curves of a sample containing manganite

## 4 Hydroxides



**Figure 4.2.4.** Thermogravimetric curves of a sample containing boehmite

References: 133, 336, 363, 508, 553, 579, 953, 954

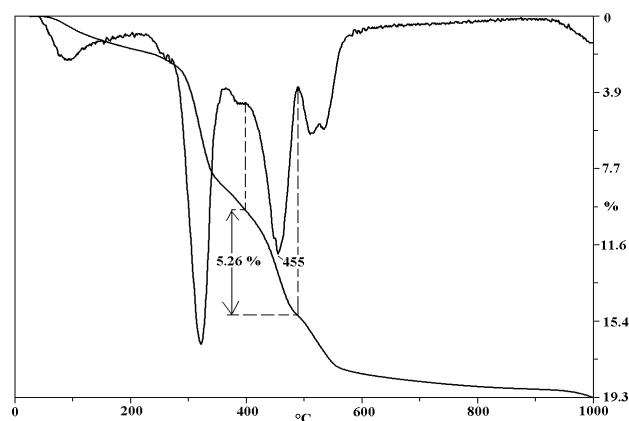


**Figure 4.2.5a.** Thermogravimetric curves of a sample containing diaspor

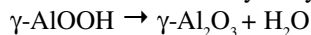
Two varieties of diaspor (well- and badly crystallized) can be distinguished by thermal analysis or by infrared spectroscopy. On X-ray diffraction diagrams the two varieties give homologous lines (GOUT, JAUBERTHE 1976).

References: 133, 364, 414, 427, 428, 553, 579, 953

#### 4.2.4. Boehmite $\gamma$ -AlOOH

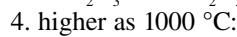
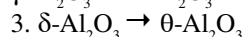
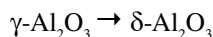
Detailed reactions of boehmite:

1. at 500–600 °C: dehydroxylation:



Stoichiometric factor of the reaction: 6.6.

2. at 850–930 °C: exothermic



Sample: Pružina, Slovakia

Sample mass: 213.9 mg

Heating rate: 10 °C/min

Mass loss during the dehydroxylation: 6.68%

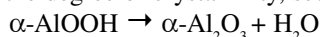
Boehmite content of the sample based on the reaction: 44%.

Other thermally active minerals in the sample: goethite.

#### 4.2.5. Diaspor $\alpha$ -AlOOH

Thermal reaction of dispor:

at 450–600 °C: dehydroxylation: (temperature depends on the degree of crystallinity, see Figure 4.2.5b)



Stoichiometric factor of the reaction: 6.6.

Sample: Szőc, Hungary

Sample mass: 206.9 mg

Heating rate: 10 °C/min

Mass loss during the dehydroxylation: 5.26%

Diaspor content of the sample based on the reaction: 35%

Other thermally active minerals in the sample: gibbsite, boehmite, Al-goethite, kaolinite

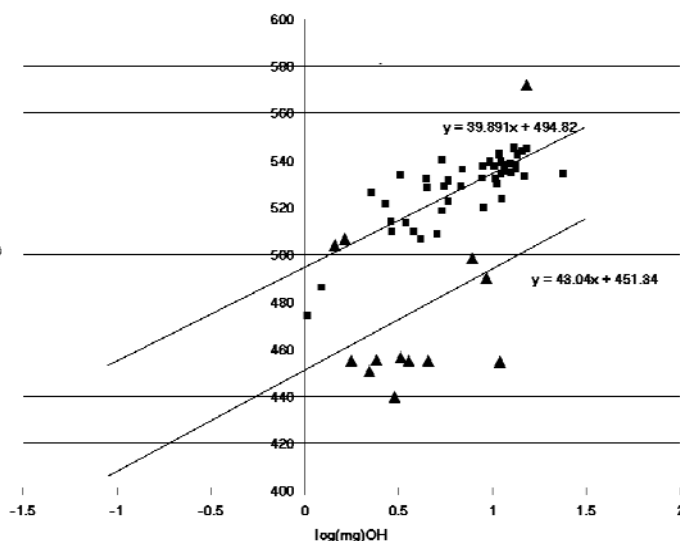


**Figure 4.2.5b.** PA curves of Hungarian diaspor and boehmite minerals from bauxite  
(■ = boehmite, ▲ = diaspor)

## 4 Hydroxides

4.2.6. Alumogel  $\text{AlOOH} \cdot n\text{H}_2\text{O}$ 

It is an amorphous aluminum hydroxide that is a constituent of bauxite

Thermal reactions:

1. 100–150 °C: dehydration  $\rightarrow$  amorphous aluminum hydroxide,
2. 400–500 °C: dehydroxylation (broad)  $\rightarrow$  amorphous  $\text{Al}_2\text{O}_3$ ,  
 $\rightarrow \gamma\text{-(and/or } \kappa\text{)-Al}_2\text{O}_3 \rightarrow \theta\text{-Al}_2\text{O}_3 \rightarrow \alpha\text{-Al}_2\text{O}_3$ .

Reference: 956

## 4.3. Hydroxide containing multiple cations

4.3.1. Lithiophorite  $(\text{Al,Li})(\text{OH})_2 \cdot \text{MnO}_2$ 

Thermal reaction of the mineral between 430–500

°C: escape of OH and structural decomposition.

Stoichiometric factor of the reaction: 7.1–8.2.

Sample: Eplény, borehole 35, Hungary

Sample mass: 1000 mg

Heating rate: 17 °C/min

Mass loss during the dehydroxylation: 1.8%

Lithiophorite content of the sample based on the reaction: 12–15%

Other thermally active minerals in the sample: gibbsite, boehmite, calcite

References: 314, 402, 1165

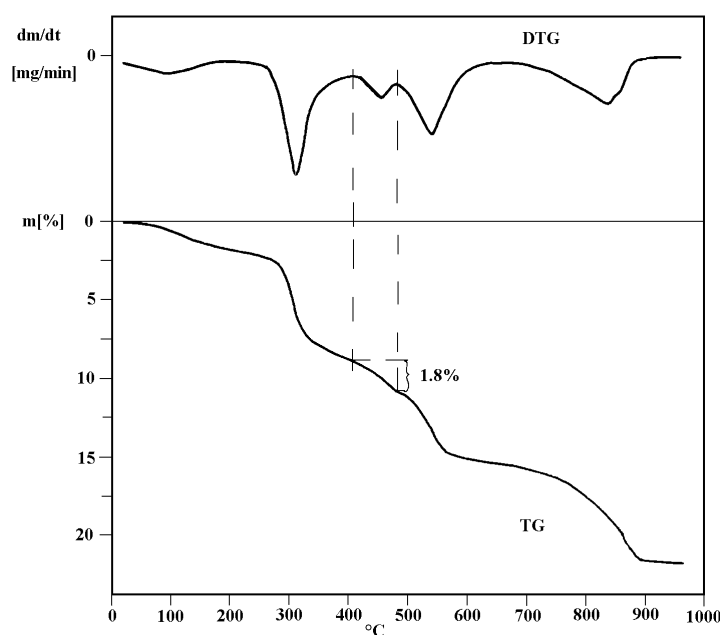


Figure 4.3.1. Thermogravimetric curves of a sample containing lithiophorite

## 4.4. Other hydroxides

References: 176: feroxyhyte, 513: elisavetite = asbolane, 567: manganates, 782: acaganeite

## 4.5. References for bauxite

61, 322, 515, 560, 561, 565, 608, 612, 654, 736, 813, 1018, 1179, 1188

## 5. SILICATES

Phyllosilicates are investigated by thermal analysis most frequently among silicate minerals.

### 5.1. Phyllosilicates

Phyllosilicates are the most intensively investigated category of the silicates by thermal analysis.

Classification of the main groups is based on the condensation of tetrahedra and octahedra sheets. Further subdivisions can be made on the basis of the nature of octahedral sheets:

— Dioctahedral sub-groups: two out of three octahedral positions are filled by trivalent ions, such as  $\text{Al}^{3+}$  (gibbsite-like sheets)

— Trioctahedral sub-groups: all the three octahedral positions filled with divalent ions, such as  $\text{Mg}^{2+}$  (brucite-like sheets)

The next step of subdivision to species can be based either on chemical (the nature of the ions in octahedral positions) or on structural (manner of superposition of the layers) features.

Many isomorphous substitutions can occur in these minerals and this frequently leads to an excess negative charge which may be satisfied by other substitutions within the lattice, or usually, by cations or water external to the layer.

The main thermic reactions are:

— dehydration (information on interlayer space and on the order of the structure),

— dehydroxylation (information on the octahedric layer).

#### 5.1.1. The 1:1 layer type clay minerals

Structure of these minerals consists of one octahedral joined to one tetrahedral sheet.

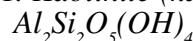
**Table T5.1.1.** Thermoanalytical data of 1:1 layer type clay minerals

Group	Subgroup	Type of species	Species	Dehydration	Dehydroxylation	Phase transition
					(°C)	
Kaolinite-serpentine	dioctahedric: <b>kaolinite</b>	structural	kaolinite	-	530-590	990-1000
			fireclay	H <sub>2</sub> O<OH	500 560	940 980
			halloysite	H <sub>2</sub> O=OH		
			dickite	-	600-670	995-1010
	trioctahedric: <b>serpentine</b>	chemical	l'e serpentine (cronstedtite)	at the "hydro" variations	400 650	640 650
			Ni-serpentine (falcondoite)		500-750	800-830
		structural	Mg-serpentine		640-730	800-840
chrysotile antigorite	780-820		800-840			

Reference: 323

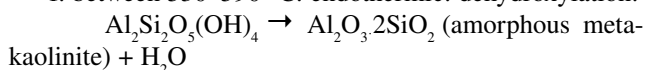
#### 5.1.1.1. Kaolinite subgroup

##### 5.1.1.1.1. Kaolinite (kaolinite- $T_c$ )



Reactions:

1. between 530–590 °C: endothermic: dehydroxylation:



Stoichiometric factor of the reaction: 7.17.

2. between 900–1000 °C: exothermic: transformation into crystalline phases

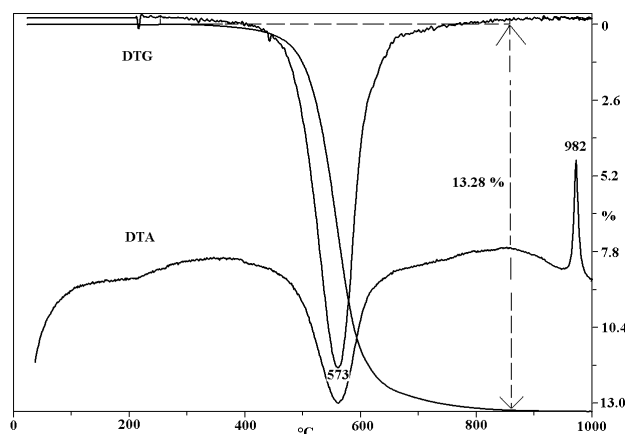
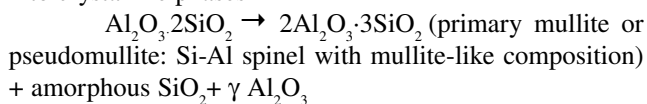


**Figure 5.1.1.1.1a.** Thermoanalytical curves of kaolinite

Sample: Georgia (International Standard, Clay Minerals Society)

Sample mass: 130 mg

Heating rate: 10 °C/min

Mass loss during the dehydroxylation: 13.28%

Kaolinite content of the sample based on the reaction: 95%

Based on the temperature and empirical quantities describing the shape of thermoanalytical peaks as well as on the estimated kinetic constants it is possible to determine the polytype modification and the crystallinity stage of kaolinite also by thermal analysis. Observation of fine changes in certain parameters can be useful for genetic interpretation. Many of the authors have published different classifications of kaolinite types based on temperature, symmetry, width, intensity ratios of thermal peak (Table T5.1.1.1.a, b; Figure 5.1.1.1.b).

**Table T5.1.1.1.a.** Characterisation of kaolinite types based on different DTA parameters

Mineral name	Peak temperature of dehydroxylation	Slope ratio of the dehydroxylation peak		Peak temperature of the exothermic peak	Activation energy of dehydroxylation (from isothermal weight loss)	Reaction order (from DTA)
	MACKENZIE (1957)	BRAMAO et al. (1952)	ROBERTSON et al. (1954)	SMYKATZ, KLOSS (1974)	MURRAY, WHITE (1949)	KISSINGER (1957)
					in Kcal/mol (in kJ/mol)	
Dickite	680				48 (199)	
Nacrite	660					
Kaolinite	580	0.78 1.5	0.8 1	980 1005	38 40 (159 167)	1.06
Fireclay		1.5-2.4	1.2-1.4	940	22-30 (92-126)	
Halloysite	560	2.5 3.8	1.8		34 37 (142 155)	0.5 0.7

These data reflect that dehydroxylation in effect is a two-stage process. The first step is the removal of the OH-groups from the external surface; the second step is the removal of internal OH-groups. With the change of the stacking of the layers at different orders or polytypes, the process of the removal of OH is different.

The 980 °C exothermic peak is affected by impurities. Ferric oxide on particle surfaces broadens and reduces the size of the peak markedly.

The SMYKATZ-KLOSS (1974) use another nomenclature (Table T5.1.1.1.b).

The author introduced different new parameters that may be possible to measure from the thermogravimetric data (FÖLDVÁRI, KOVÁCS-PÁLFFY 1993, FÖLDVÁRI, GERMÁN-HEINS 1994, FÖLDVÁRI 1997). These are the followings:

- corrected peak temperature or temperature deviation from the comparative standard (Figure 5.1.1.1.c),
- calculation of the activation energy based on dynamic TG (ARNOLD et al. 1987),

**Table T5.1.1.1.b.**

SMYKATZ, KLOSS (1974)	Peak temperature of dehydroxylation (°C)
Extremely disordered	<530
Strongly disordered	530-555
Slightly disordered	555-575
Well ordered	>575

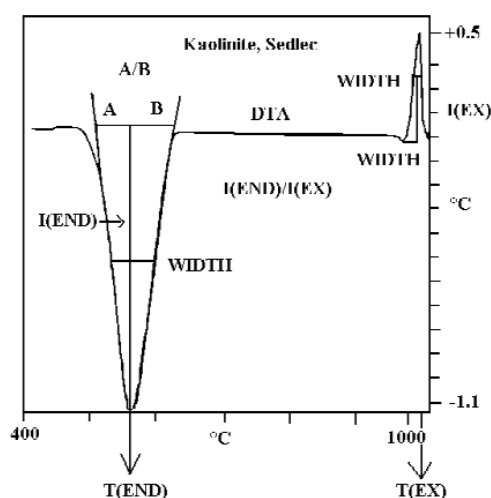


**Figure 5.1.1.1.b.** Thermoanalytical parameters used for the determination of the crystallinity of kaolinite from the DTA curve

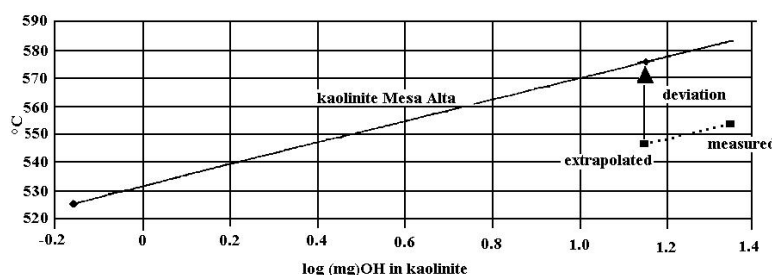


**Figure 5.1.1.1.c.** Indirect parameters for the characterisation of kaolinite

Corrected (extrapolated) temperature=peak temperature of 13.95 mg OH in 100 mg kaolinite, deviation = peak temperature difference between 100 mg the well-ordered kaolinite from Mesa Alta and kaolinite examined

## 5 Silicates

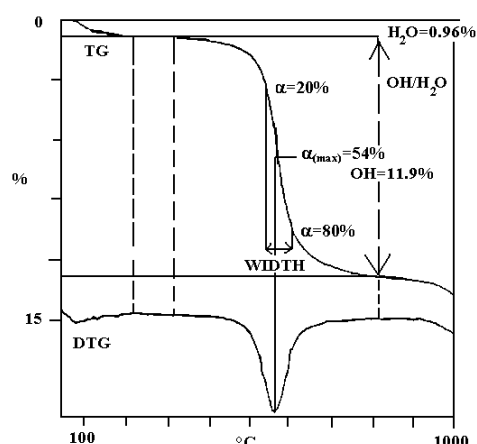


**Figure 5.1.1.1d.** Thermoanalytical parameters used for the determination of the crystallinity of the kaolinite from the DTG curve

- symmetry characterised by  $\alpha_{(max)}$  = percentage of decomposed part at the maximum rate of the reaction,
- width of the dehydroxylation peak  $T(0.8-0.2)$ ,
- proportion of  $OH/H_2O$ .

The use of corrected temperature data is more characteristic and comparable. An extrapolation from the measured peak temperature and from the mass change during the decomposition process (measured by TG) to a standard quantity (e.g. 100 mg kaolinite=13.95 mg OH in kaolinite) of the decomposed product makes our data comparable.

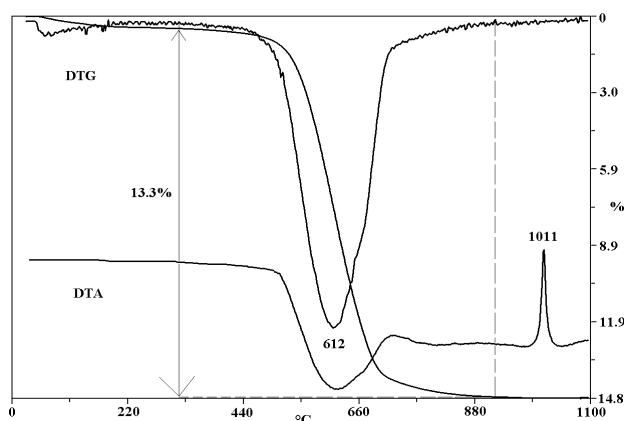


**Figure 5.1.1.2.** Thermoanalytical curves of dickite

#### 5.1.1.1.2. Dickite (kaolinite-2M) $Al_2Si_2O_5(OH)_4$

Reactions:

1. between 600 and 670 °C: endothermic: dehydroxylation:  
 $Al_2Si_2O_5(OH)_4 \rightarrow Al_2O_3 \cdot 2SiO_2$  ( amorphous metadickite)+ $H_2O$

Stoichiometric factor of the reaction: 7.17.

2. between 990 and 1020 °C: exothermic: transformation into crystalline phases



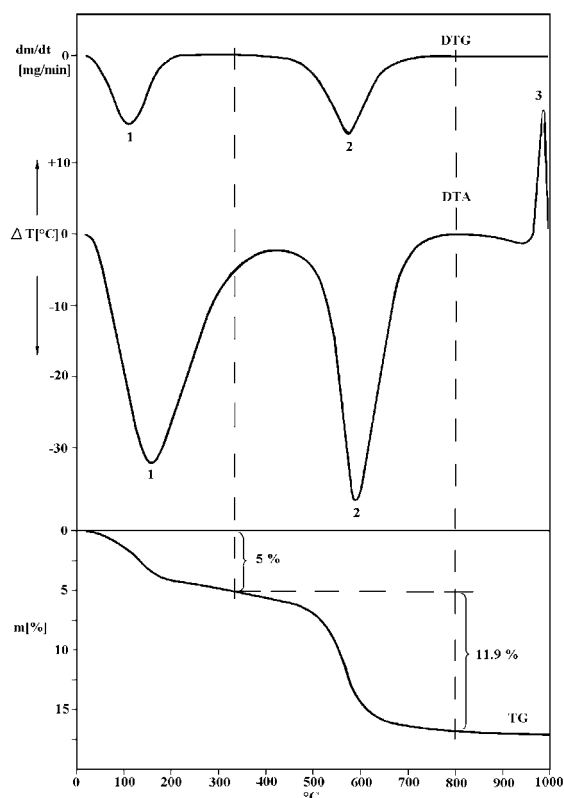
Sample: Borehole Sáropatak-65 10.2 m, Hungary

Sample mass: 118.9 mg

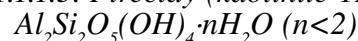
Heating rate: 10 °C/min

Mass loss during the dehydroxylation: 13.31%

Dickite content of the sample based on the reaction: 95%

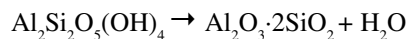


#### 5.1.1.1.3. Fireclay (kaolinite-1M<sub>d</sub>)



Reactions

1. between 40 and 200 °C: evolution of adsorbed water:  
 $Al_2Si_2O_5(OH)_4 \cdot nH_2O \rightarrow Al_2Si_2O_5(OH)_4 + nH_2O$
2. between 530 and 590 °C: endothermic: dehydroxylation:



Stoichiometric factor of the reaction: 7.17

3. between 900 and 1000 °C: exothermic: transformation into crystalline phases

$Al_2O_3 \cdot 2SiO_2 \rightarrow 2Al_2O_3 \cdot 3SiO_2$  (primary mullite or pseudomullite: Si-Al spinel with mullite-like composition) + amorphous  $SiO_2 + \gamma Al_2O_3$ .

Sample: Germany

Sample mass: 1000 mg

Heating rate: 17 °C/min

Mass loss during dehydration: 5.0%

Mass loss during dehydroxylation: 11.9%

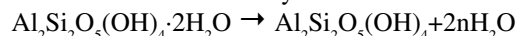
Fireclay content of the sample based on the reaction:  
 $(11.9 \cdot 7.17) + 5 = 90\%$

**Figure 5.1.1.3.** Thermoanalytical curves of fireclay

5.1.1.1.4. Halloysite  $Al_2Si_2O_5(OH)_4 \cdot 2H_2O$ 

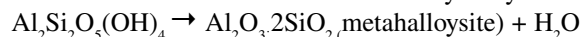
## Reactions

1. between 40 and 200 °C: dehydration:



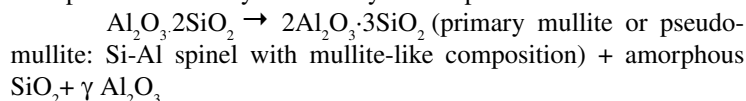
Stoichiometric factor of the reaction: 8.2.

2. between 530 and 590 °C: endothermic: dehydroxylation:



Stoichiometric factor of the reaction: 8.2.

3. between 900 and 1000 °C: exothermic: transformation from amorphous metahalloysite into crystalline phases



Sample: Aranybányabérc, Mátra Mountains, Hungary

Sample mass: 900 mg

Heating rate: 10 °C/min

Mass loss during dehydration: 11.8%

Mass loss during dehydroxylation: 11.8%

Halloysite content of the sample based on both reactions: 97%

Metahalloysite curve is the same with the difference that the sorbed water peak is absent.

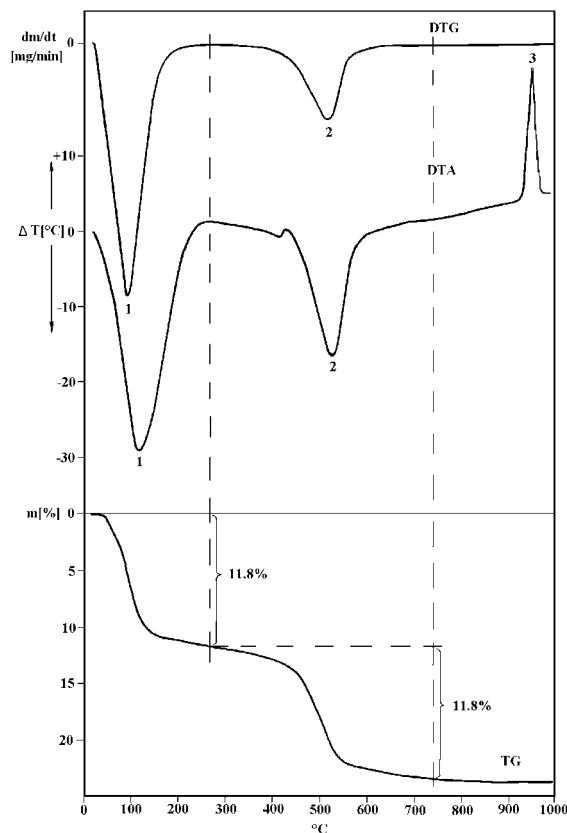


Figure 5.1.1.1.4. Thermoanalytical curves of halloysite

5.1.1.1.5. Allophane non-crystalline  
 $mAl_2O_3 \cdot nSiO_2 \cdot pH_2O$  or  $Al_2O_3 \cdot (SiO_2)_{1.3-2} \cdot (H_2O)_{2.5-3}$ 

## Reactions

1. at 100–200 °C: endothermic: dehydration of the colloidal aluminosilicate, the process is continuous up to much higher temperatures.
2. exothermic peak at 950–1000 °C: formation of spinel.

Sample: Venezuela

Sample mass: 104.4 mg

Heating rate: 10 °C/min

Temperature of the exothermic peak decreases with increasing Fe-content of allophane.

Thermoanalytical curves of hisingerite  $[Fe_2^{3+}Si_2O_5(OH)_4 \cdot 2H_2O]$  which is an iron containing member of the allophane group are similar to the curves of allophane, however, the exothermic reaction is at a slightly lower temperature (850–900 °C).

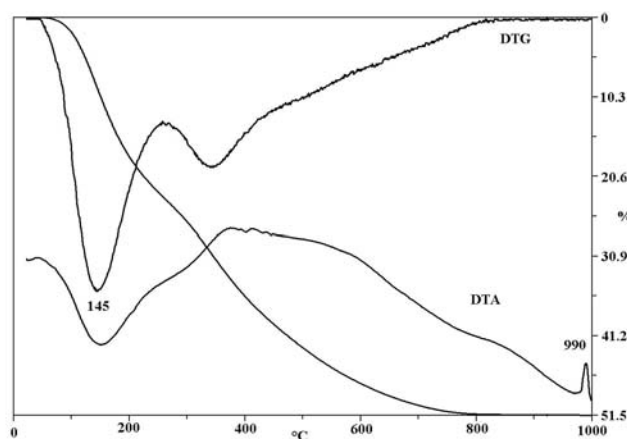


Figure 5.1.1.1.5. Thermoanalytical curves of an allophane containing sample

\*\*\*

References for kaolinite subgroup: 19, 28, 76, 80, 109, 128, 129, 145, 150, 155, 156, 169, 170, 214, 322, 324, 331, 346, 362, 367, 387, 393, 403, 423, 451, 464, 467, 471, 479, 492, 494, 495, 527, 553, 563, 572, 575, 595, 619, 625, 626, 645, 659, 674, 675, 694, 697, 700, 701, 735, 747, 770, 907, 929, 951, 987, 1007, 1008, 1027, 1029, 1030, 1041, 1108, 1142, 1153, 1182

## 5 Silicates

5.1.1.2. *Serpentine subgroup*

The main thermal reactions of serpentines are similar to that of kaolinites, namely a dehydroxylation and an exothermic phase transition. However, in the case of serpentines there is no intermediate phase or by comparison with kaolinite dehydroxylate, amorphous phase exists over a very short temperature range. The decomposition of chrysotile is more complex than understood previously.

Temperature of the reactions depends on the cation type in the octahedral layer (see Table T5.1) and on the polymorph modification. Sometimes there is a small low-temperature endothermic peak due to the adsorbed moisture of the hydro-variety. Serpentine readily adsorbs water on its highly hydrophobic surface.

The thermally best interpreted serpentine minerals are antigorite, chrysotile and lizardite. There are some contradictions in the literature data for the main Mg-serpentine types (Table T5.1.1.2a, b).

**Table T5.1.1.2a.** Characteristic peak temperatures of Mg-serpentines based on different references

References	Endothermic (°C)			Exothermic (°C)	
	lizardite	chrysotile	antigorite	chrysotile	antigorite
NAGY, FAUST (1956)	Inflexion at the low temperature side of the chrysotile peak	670-710	800	805-825	870
VENIALE (1962)		680-700	780-800	800-810	820-840
WEBER, GRIER (1965)	635	665	700		
NAUMANN, DRESHER (1966)		700		800	
BASTA et al. (1969)	650-685	690-730	780-820	770-835	810-855
IVANOVA (1974)		750	800	790-820	overlapped
SMYKATZ-KLOSS (1974)		775	720	820	835
MARTIN (1977)				810	
MACKENZIE, CAILLÈRE (1979)		699		809	
PEREZ-RODRÍGUEZ et al. (2005)			748		816

**Table T5.1.1.2b.** Temperature interval data of Mg-serpentines

References	ΔEX-EN (°C)		α-Value (°C)	
	chrysotile	antigorite	chrysotile	antigorite
BASTA et al. (1969)	73-100	30-35		
SMYKATZ-KLOSS (1974)			48	113

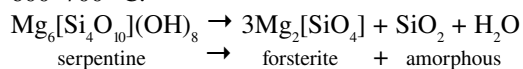
Proposed other DTA characteristics for the serpentine types ΔEX-EN = α-Value = the temperature interval between the decomposition peak and the exothermic peak.

Further problems are the nature of the dehydroxylate influences the further course of the reaction sequence.

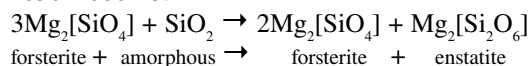
The exothermic peak at the Mg-serpentines is related first of all to the formation of forsterite.

Interpretation of reactions according to GRUNER (1948) and BRINDLEY, ZUSSMANN (1957):

600–700 °C:

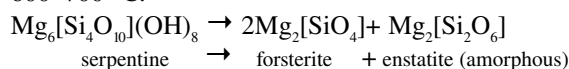


1050–1080 °C:

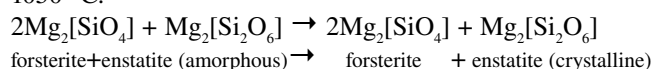


Interpretation of reactions according to KOLTERMANN, RASCH (1964):

600–700 °C:



1050 °C:



According to the concept of the following authors, a subsequent separation plays role during the transition as shown by Figure 5.1.1.2a.

The concept of MACKENZIE, MEINHOLD (1994) in Figure 5.1.1.2b explains the doublestage dehydroxylation that may be seen on the TG and DTG curves of numerous diagrams (e.g. 5.1.1.2c, 5.1.1.2d, 5.1.1.2e)

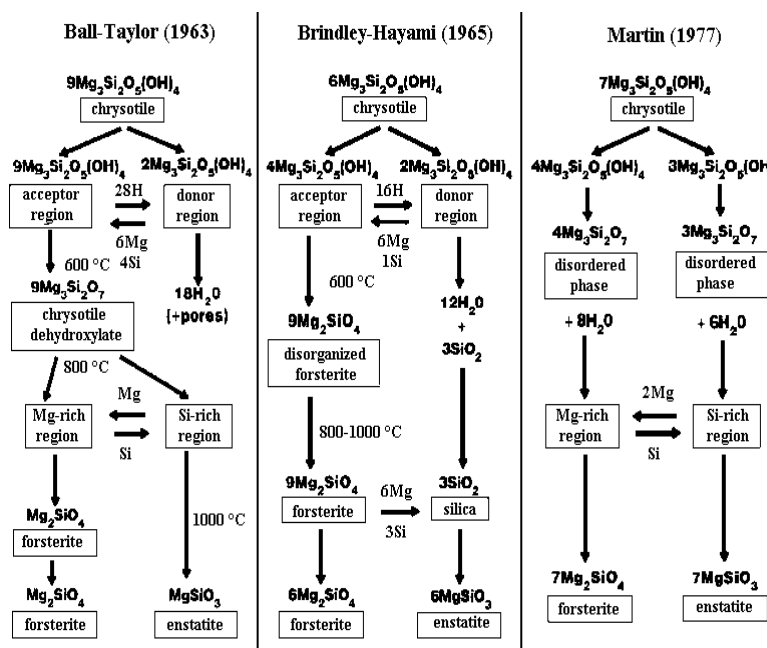


Figure 5.1.1.2a. Thermal reaction schemes of reaction sequences of Mg-chrysotile. According to BALL, TAYLOR (1963), BRINDLEY, HAYAMI (1965), and MARTIN (1977). Summarized by MACKENZIE, MEINHOLD (1994)

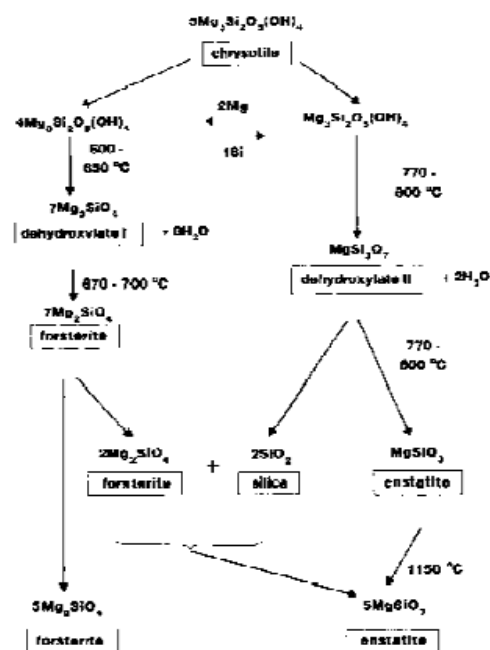
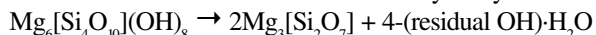


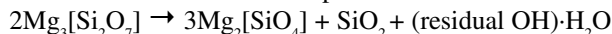
Figure 5.1.1.2b. Schematic representation of proposed chrysotile reaction sequences according to MACKENZIE, MEINHOLD (1994)

The simplified reactions of Mg-serpentines for quantitative evaluation

1. between 640 and 820 °C: endothermic: dehydroxylation and



2. between 800 and 840 °C: exothermic: structural decomposition, formation of forsterite and escape of residual OH



Stoichiometric factor of the whole dehydroxylation: 7.7.

Sample (Figure 5.1.1.2c): Tornakápolna, borehole Tk-3 371.5 m, Hungary

Sample mass: 1000 mg

Heating rate: 17 °C/min

Mass loss during dehydroxylation: 11.8%

Serpentine content of the sample based on the reactions: 90%

Sample (Figure 5.1.1.2d): Italy

Sample mass: 1000 mg

Heating rate: 10 °C/min

Mass loss during dehydroxylation: 11.2%

Serpentine content of the sample based on the reactions: 86%

“Hydroantigorite” was described as a new mineral species by ERDÉLYI et al. (1962) from a serpentine xenolith found in a quarry at Csódi Hill near Dunabogdány, Hungary. It was defined as monoclinic serpentine that is characterised by an OH for O substitution in the tetrahedral layer. Standard reference works (e.g. STRUNZ, TENNYSON 1982, CLARK 1993) regard “hydroantigorite” as antigorite with some OH excess.

Topotype specimens corresponding to the original description given by ERDÉLYI et al. (1962) were examined by optical, XRPD, thermal (Figure 5.1.1.2e) and IR methods and data were reinterpreted (PAPP et al. 1999). Despite its name “hydroantigorite”

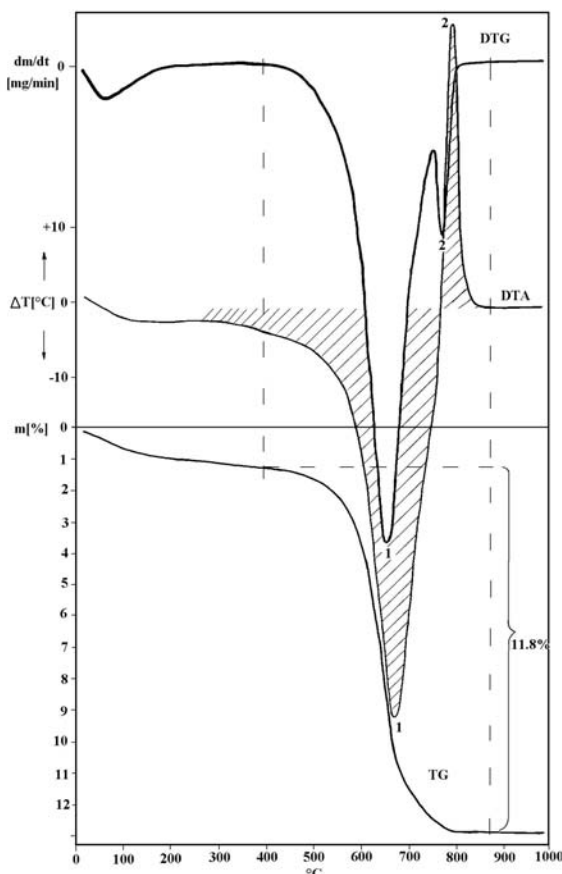


Figure 5.1.1.2c. Thermoanalytical curves of chrysotile

## 5 Silicates

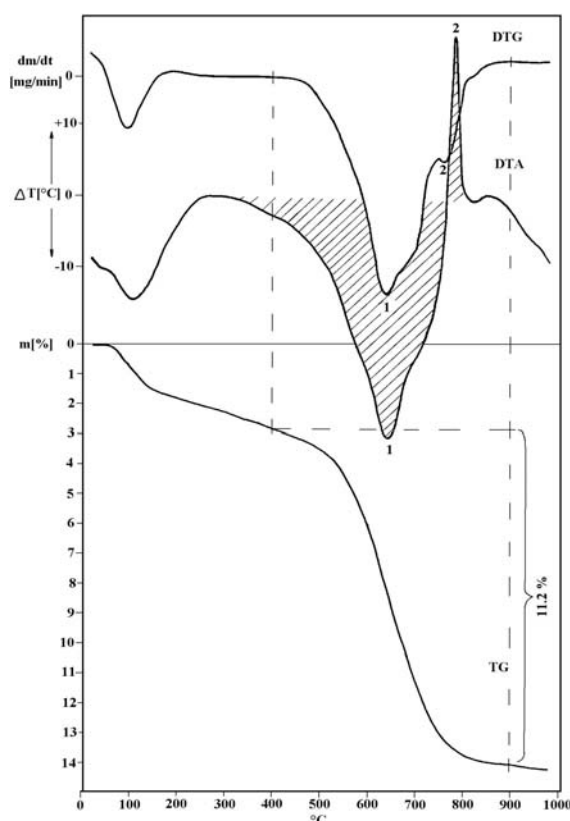


Figure 5.1.1.2d. Thermogravimetric curves of lizardite

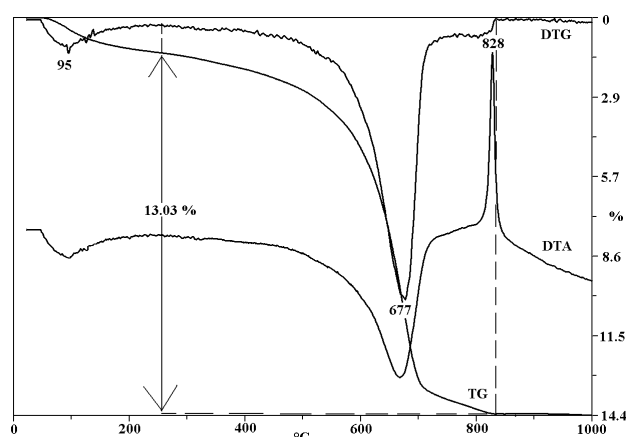


Figure 5.1.1.2e. Thermogravimetric curves of "hydroantigorite"

proved to be unrelated to antigorite, the dominant component of the samples was found to be orthochrysotile and some polygonal serpentine, poorly formed serpentine (deweyite), and very few lizardite. No direct evidence was found for the supposed OH for O substitution.

Sample (Figure 5.1.1.2e): Dunabogdány, Csódi Hill, Visegrád Mts, Hungary

Sample mass: 107.4 mg

Heating rate: 10 °C/min

Mass loss during dehydroxylation: 13.03%

Serpentine content of the sample based on the reactions: 100%

In the case of iron serpentine (berthierine, greenalite, cronstedtite etc.) there is the oxidation of iron as additive reaction. The internal oxidation of  $\text{Fe}^{2+}$  to  $\text{Fe}^{3+}$  occurs before or simultaneously with the dehydroxylation. During the low-temperature oxidation of octahedral  $\text{Fe}^{2+}$ , tetrahedral  $\text{Fe}^{3+}$  also moves into vacant octahedral sites. At higher temperatures, dehydroxylation continues in the immediate formation of iron and silicon that transform subsequently into crystalline hematite, olivine and cristobalite, while the more aluminous sample forms  $\text{FeAlO}_3$  and mullite as well (MACKENZIE, BEREZOWSKI 1981, 1984; MACKENZIE, MCGAVIN 1994).

Conclusion of the experiments: In the teeth of multiple information the confident identification of the member of serpentine by both thermal and XRD analyses (WICKS 2000) is limited.

\*\*\*

References for serpentine subgroup: 5, 59, 70, 126, 127, 130, 132, 148, 158, 180, 188, 286, 303, 482, 513, 553, 564, 594, 676, 677, 678, 681, 694, 708, 714, 717, 775, 783, 811, 861, 866, 890, 925, 956, 981, 1071, 1102, 1103, 1140, 1154

## 5.1.2. 2:1 layer type clay minerals

Table T5.1.2. Thermogravimetric data of the main 2:1 layer type clay minerals

Group	Subgroup	Type of species	Species	Dehydration	Dehydroxylation	Phase transition
Pyrophyllite-talc	dioctahedric: pyrophyllite	Al			650 850 °C	
	trioctahedric: minnesotaite talc	$\text{Fe}^{2+}$ , Mg Mg			≈600 °C 850 1000 °C	
Smectite	dioctahedric	chemical: Cr Fe Al $\text{Al}_{1.67}\text{Mg}_{0.33}$	volkonskoite nontronite beidellite montmorillonite	+	390 470 °C 400 500 °C 550–600 °C ≈700 °C	<900 °C
	trioctahedric	Zn Mg, Li Mg	sauconite hectorite saponite	+	680 750 °C 850–900 °C 850 900 °C	<900 °C

**Table T5.1.2.** Continuation

Group	Subgroup	Type of species	Species	Dehydration	Dehydroxylation	Phase transition
Mica	dioctahedric		muscovite paragonite		820-920 °C 800-850 °C	
	di-trioctahedric	chemical: Li,Al	lepidolite		≈900 °C 900-950 °C	
		Li,Fe,Al	zinwaldite			
	trioctahedric	chemical: Mg,Fe,Mn Mg	biotite phlogopite		1080-1180 °C 1180-1280 °C	
Hydromica	dioctahedric	Al	illite	+	≈550 °C	>900 °C
	di-trioctahedric	Fe <sup>3+</sup> ,Al,Fe <sup>2+</sup> ,Mg	glauconite, celadonite	+	≈550 °C	>900 °C
	trioctahedric	Mg	„ledikite“ parasepiolite	+	≈860 °C	>900 °C

The structure of these minerals is composed of two tetrahedral sheets with the octahedral sheet in between.

Typical dehydroxylation reactions of 2:1 type phyllosilicates are summarized in Table T5.1.2

During the dehydroxylation of dioctahedric phyllosilicates cations often migrate and change the *cis*- and *trans*-octahedra and have (partly?) 5-fold coordination. Al and Mg cations have a greater ability to migrate. (BROWN et al. 1987, CUADROS, ALTANER 1998, EMMERICH, KAHR 2000, 2001, MULLER et al. 2000a, b, SAIZ-DÍAZ et al. 2005)

References: 140, 200, 274, 275, 323, 433, 764, 765, 937, 1008, 1009

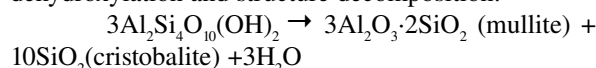
### 5.1.2.1. Pyrophyllite-Talc group

Since these minerals have no substitution in their layers, their structure consist only of the octahedral and tetrahedral layers without any interlayer cation and molecular water.

The typical thermal reaction is the dehydroxylation of the octahedral layer. The temperature of this reaction depends first of all on the cation in the octahedra.

#### 5.1.2.1.1. Pyrophyllite: $Al_2Si_4O_{10}(OH)_2$

Reaction of the mineral between 650 and 850 °C: dehydroxylation and structure decomposition:



The dehydroxylation of pyrophyllite may be a two-stage process.

Stoichiometric factor of the reaction: 20.

According to some of the authors an exothermic peak detected at 1000–1050 °C in DTA curves signals the transformation of pentahedral coordination of Al into mullite.

Sample: Berezovsk, Russia

Sample mass: 280 mg

Heating rate: 17 °C/min

Mass loss during dehydroxylation: 5.0%

Pyrophyllite content of the sample based on the reactions: 100%

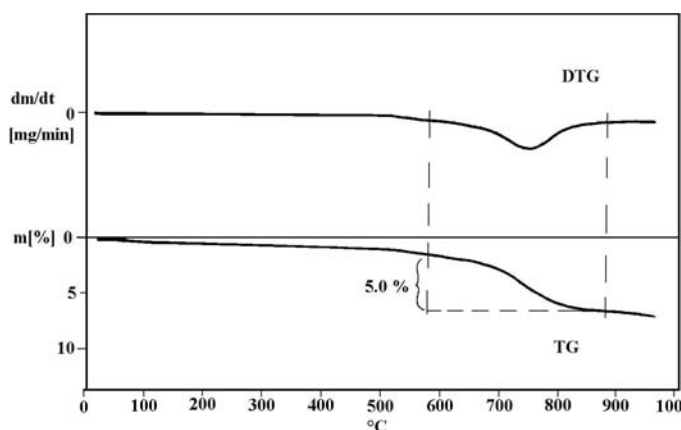


**Figure 5.1.2.1.1.** Thermogravimetric curves of pyrophyllite

## 5 Silicates

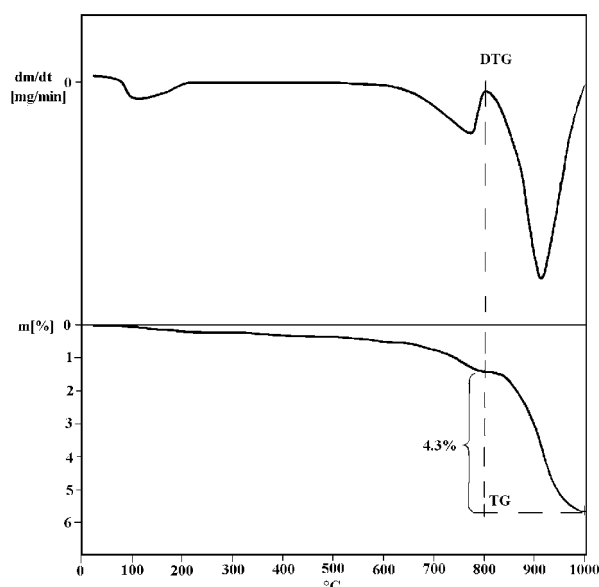
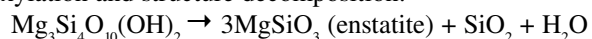


Figure 5.1.2.1.2. Thermogravimetric curves of a talc containing sample

### 5.1.2.1.2 Talc $Mg_3Si_4O_{10}(OH)_2$

The reaction of the mineral between 850 and 1000°C: dehydroxylation and structure decomposition:



Stoichiometric factor of the reaction: 21.05.

Sample: Szögliget, Hungary

Sample mass: 1000 mg

Heating rate: 17 °C/min

Mass loss during dehydroxylation: 4.3%

Talc content of the sample based on the reactions: 90%

Other thermally active mineral in the sample: calcite

\*\*\*

References for pyrophyllite-talc group : 14, 21, 115, 341, 427, 428, 448, 478, 513, 553, 623, 680, 682, 694, 714, 745, 778, 859, 874, 941, 942, 943, 944, 945, 956, 963, 967, 970, 981, 1071, 1118, 1119, 1151

### 5.1.2.2. Smectite group

Typical dehydroxylation reactions of the minerals in the smectite group are shown in Table 17 and 36. The features of dehydration are discussed in detail in the Chapter of “Water in Minerals. Dehydration: Adsorbed water: Interlayer waters bound by phyllosilicates”. Further we follow the point of view that dehydroxylation depends on the octahedral cation and the structure.

#### 5.1.2.2.1. Montmorillonite (Na,Ca)<sub>0.3</sub>(Al,Mg)<sub>2</sub>Si<sub>4</sub>O<sub>10</sub>(OH)<sub>2</sub>·n(H<sub>2</sub>O)

##### 5.1.2.2.1.1. Ca-montmorillonite

The reaction of Ca-montmorillonite:

1. between 100 and 200 °C: endothermic dehydration (loss of sorbed moisture and interlayer free water). On the high temperature side of the peak an inflexion signals the escape of the water bounded to interlayer cation.

Stoichiometric factor of the reaction for air-dried sample (n≈7): about 6.8 (because of the two water layers in the interlayer space).

2. about 700 °C: endothermic: dehydroxylation and formation of an amorphous meta-montmorillonite phase.

Stoichiometric factor of the reaction: about 24.

3. between 850 and 1000 °C endothermic-exothermic peak system: solid phase structural decomposition and crystallization of cordierite, mullite, Mg-spinel, quartz, cristobalite.

Due to the uncertainty of the water content of montmorillonite a control method is required for the calculation based on the quantity of OH in the molecular-waterfree structure (4.9%). The calculated montmorillonite content in this case: stoichiometric factor based on the mass loss during the second reaction related to interlayer-waterfree structure: 20.4 (+ the interlayer-water content in absolute value).

Sample (Figure 5.1.2.2.1a): Buru, Romania

Sample mass: 158.1 mg

Heating rate: 10 °C/min

Mass loss during dehydration: 7.6%

Mass loss during dehydroxylation: 2.6%

Montmorillonite content of the sample based on the first reaction: 52%

Montmorillonite content of the sample based on the second reaction: 62%

Montmorillonite content of the sample based on the waterfree calculation: 61%

Another excellent control method for the quantitative determination of montmorillonite and other swelling clay minerals was introduced by FIEDLER, WAGNER (1967). The method is based on the measurement of intercalated ethylenglycole content that correlates to the montmorillonite content of the sample (Figure 5.1.2.2.1b and c)

Sample: Végardó, borehole III. 50.98–52.93 m, Hungary

Sample mass: 1000 mg

Heating rate: 17 °C/min

Mass loss during dehydration: 15.3%

Mass loss during dehydroxylation: 3.25%

Montmorillonite content of the sample based on the first reaction: 100%

Montmorillonite content of the sample based on the second reaction: 77%

Montmorillonite content of the sample based on the waterfree calculation: 81%

Other thermally active mineral in the sample: pyrite

The same sample with ethylenglycole treatment:

For the quantitative determination 1 mg ethylenglycole is built in 10.7 mg montmorillonite relation used.

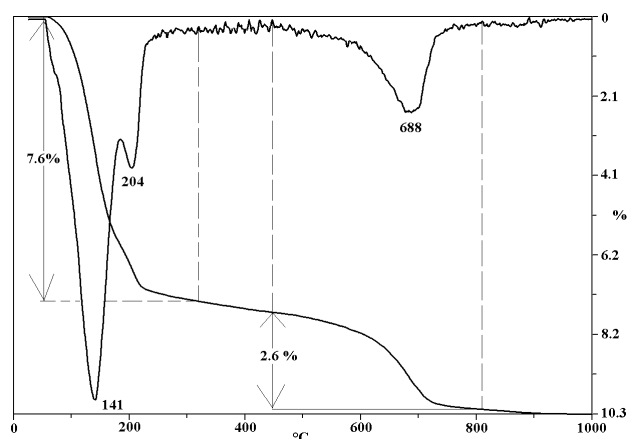


Figure 5.1.2.2.1.a. Typical thermogravimetric curves of primary Ca-montmorillonite

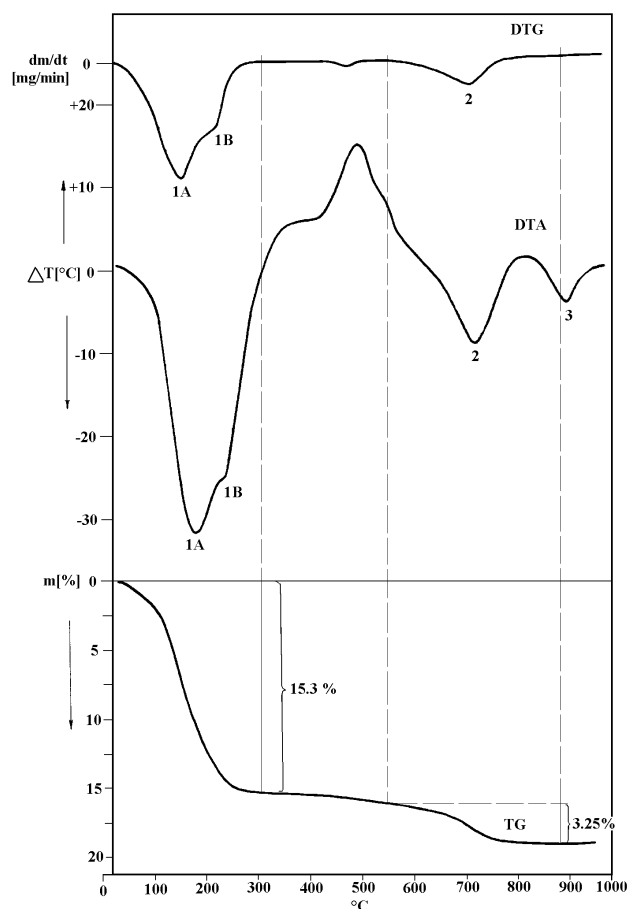


Figure 5.1.2.2.1.b. Derivatogram of sample containing montmorillonite

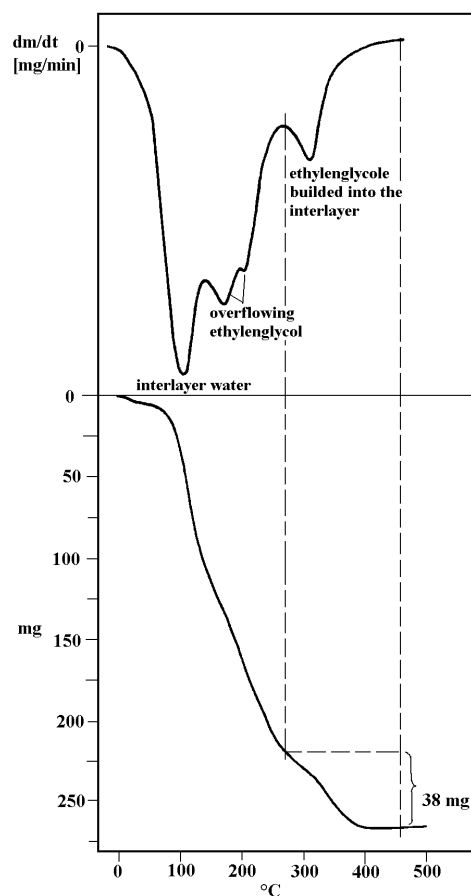


Figure 5.1.2.2.1.c. Quantitative determination using ethylenglycole

## 5 Silicates

Sample: Végardó, borehole III. 50.98–52.93 m, Hungary

Sample mass: 500 mg

Ethylenglycole: 120 mg

Heating rate: 10 °C/min

Mass loss during the third reaction (ethylenglycole built into the montmorillonite: 38 mg

Montmorillonite content based on the measured ethylenglycole content: 81%

The above base reactions are modified depending on the composition, substitution and history of montmorillonite.

## 5.1.2.2.1.2. Na-montmorillonite

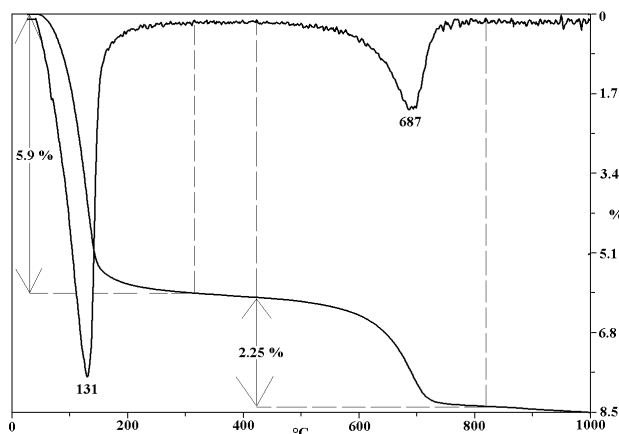


**Figure 5.1.2.2.1.2.** Typical thermogravimetric curves of primary Na-montmorillonite

The reaction of Na-montmorillonite:

1. between 100 and 200 °C: endothermic: dehydration

Stoichiometric factor of the reaction for air-dried sample ( $n \approx 3.5$ ): about 13 (because of the one water layer in the inter-layer space).

2. about 700 °C: endothermic: dehydroxylation

Stoichiometric factor of the reaction: about 22.7.

3. between 850 and 1000 °C: endothermic-exothermic peak system: structural decomposition and crystallization of cordierite, mullite, Mg-spinel, quartz, cristobalite.

Stoichiometric factor based on the mass loss during the 2. reaction related to interlayer-waterfree structure: 20.8 (+ the interlayer-water content in absolute value).

Sample: Valea Chioarului, Romania

Sample mass: 135.7 mg

Heating rate: 10 °C/min

Mass loss during dehydration: 5.94%

Mass loss during dehydroxylation: 2.25%

Montmorillonite content of the sample based on the first reaction: 77%

Montmorillonite content of the sample based on the second reaction: 51%

Montmorillonite content of the sample based on the waterfree calculation: 53%

## 5.1.2.2.1.3. “Abnormal montmorillonites”

In numerous cases the dehydroxylation of montmorillonite is a double step reaction. The structural irregularity may be responsible for the double dehydroxylation peaks (“abnormal montmorillonite”). The “abnormal montmorillonite” gives either two endothermic peaks at about 550 and 650 °C (Figure 5.1.2.2e), or a single peak at about 550 °C (Figure 5.1.2.2f). This could be related to the different composition of the octahedral cation. Montmorillonites with different dehydroxylation character but similar chemical composition are frequent. The dehydroxylation behaviour of dioctahedral smectites varies with their origin and is related to the distribution of the cation and vacancies in the octahedral sheet and their cis- and trans-

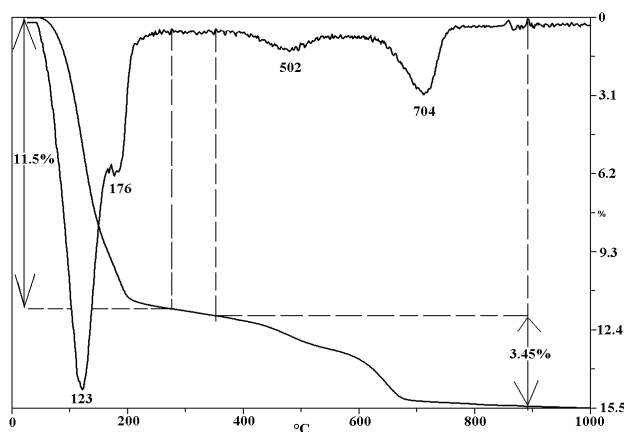


**Figure 5.1.2.2.1.3a.** Thermogravimetric curves of an “abnormal montmorillonite” with double dehydroxylation

vacant configuration. The hydroxyl configuration around the two types of octahedral sites [cis (M2) and trans (M1)] is different. The cis-vacant configuration in montmorillonite is more stable. The trans-vacant variety of montmorillonite is characterised by dehydroxylation temperatures lower (150–200 °C) than that of the cis-vacant one (CUADROS, ALTANER 1998, EMMERICH, KAHR 2001). Their transformation is possible in various geological environments. An important reason of the double or low temperature dehydroxylation may be a secondary geological process (e.g. weathering). The degraded montmorillonite is more widespread in the nature than the “normal” variant.

Sample (Figure 5.1.2.2.1.3a): Lastovce, Slovakia

Sample mass: 108.3 mg

Heating rate: 10 °C/min

Mass loss during dehydration: 11.5%

Mass loss during dehydroxylation: 3.45%

Montmorillonite content of the sample based on the first reaction: 78%

Montmorillonite content of the sample based on the second reaction: 82%

Montmorillonite content of the sample based on the waterfree calculation: 82%

Sample (Figure 5.1.2.2.3b): Tállya, Hungary

Sample mass: 112 mg

Heating rate: 10 °C/min

Mass loss during dehydration: 12.75%

Mass loss during dehydroxylation: 3.95%

Montmorillonite content of the sample based on the first reaction: 87%

Montmorillonite content of the sample based on the second reaction: 93%

Montmorillonite content of the sample based on the waterfree calculation: 92%

Other thermally active mineral in the sample: goethite

The high temperature endothermic-exothermic peak system reflects also the composition of the smectite. The shape and magnitude of this peak system are affected by the substitution taking place in the lattice. The magnitude is intensive in the case of montmorillonite with high Mg content, and decreases or absent in the case of high Al or iron content. They are divided into two different types, namely Cheto- and Wyoming-types. Regarding the Wyoming-type, the third endothermic peak is followed immediately by the exothermic peak (Figure 5.1.2.2.1.3c). In the case of the Cheto-type, the intense endothermic reaction is followed after an interval of 50–150 °C by a sharp exothermic peak (Figure 5.1.2.2.1.3d) that can be correlated with the appearance of quartz.

Substitution	Wyoming-type	Cheto-type
Si → Al	5–15%	5%
Al → Mg	5–10%	25–35%
Al → Fe	5–15%	5%

Sample (Figure 5.1.2.2.1.3c): Ond borehole 318.8– 318.9 m, Hungary

Sample mass: 800 mg

Heating rate: 17 °C/min

Other thermally active mineral in the sample: pyrite

Sample (Figure 5.1.2.2.1.3d): Hetvehely, Mecsek Mts, Hungary

Sample mass: 1000 mg

Heating rate: 10 °C/min

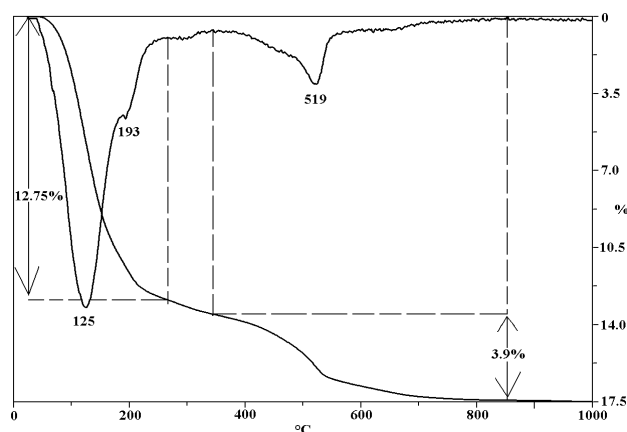


Figure 5.1.2.2.1.3.b. Thermogravimetric curves of an "abnormal montmorillonite" with a low temperature dehydroxylation

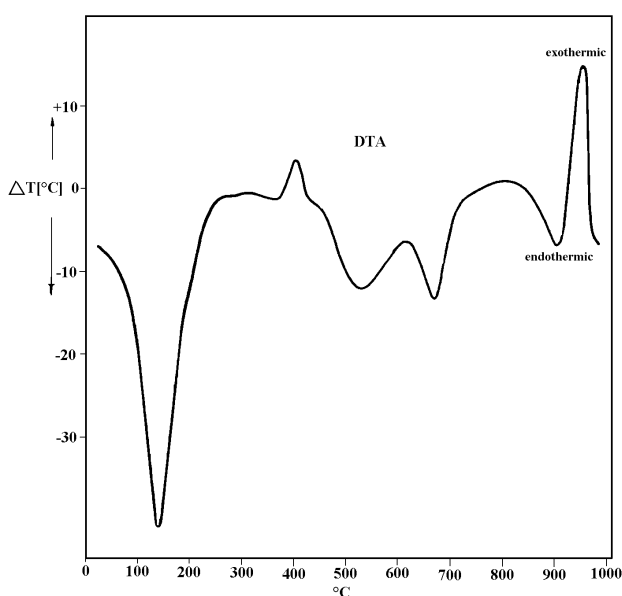


Figure 5.1.2.2.1.3c. DTA curve of a Wyoming-type montmorillonite

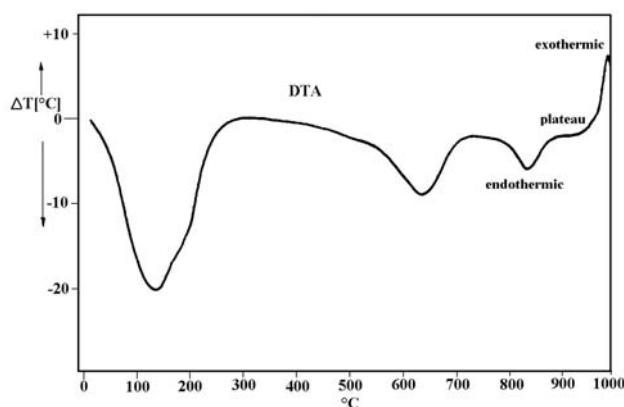


Figure 5.1.2.2.1.3d. DTA curve of a Cheto-type montmorillonite

## 5 Silicates

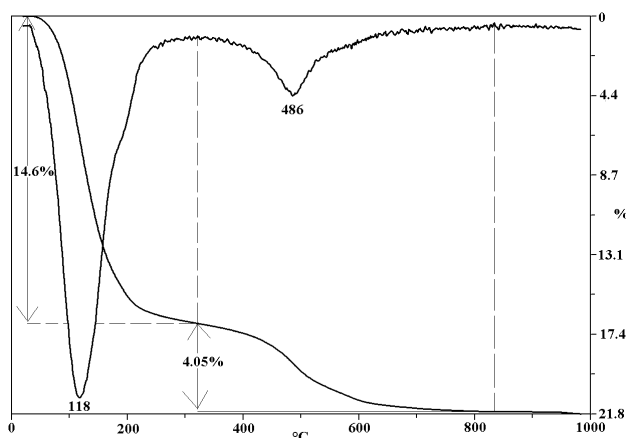


Figure 5.1.2.2.2. Thermogravimetric curves of iron beidellite

Mass loss during dehydroxylation: 4.05%

Beidellite content of the sample based on the first reaction: 99%

Beidellite content of the sample based on the second reaction: 96%

Beidellite content of the sample based on the waterfree calculation: 97%

### 5.1.2.2.2. Beidellite

$$(Na,Ca)_{0.5}Al_2(Si_{3.5}Al_{0.5})O_{10}(OH)_2 \cdot n(H_2O)$$

The reaction of beidellite:

1. between 100 and 200 °C: endothermic dehydration:

Stoichiometric factor of the reaction for air-dried sample ( $n \approx 7$ ): about 5.8.

2. about 500–600 °C: endothermic: dehydroxylation

Stoichiometric factor of the reaction: about 20.4.

3. between 850 and 1000 °C: endothermic-exothermic peak system: structural decomposition and crystallization of new phases (spinel, quartz, cristobalite).

Sample: Egyházaskesző, Hungary, basaltbentonite

Sample mass: 114.7 mg

Heating rate: 10 °C/min

Mass loss during dehydration: 14.65%

### 5.1.2.2.3. Nontronite $(Na,Ca)_{0.3}Fe^{3+}_2(Si,Al)_4O_{10}(OH)_2 \cdot n(H_2O)$

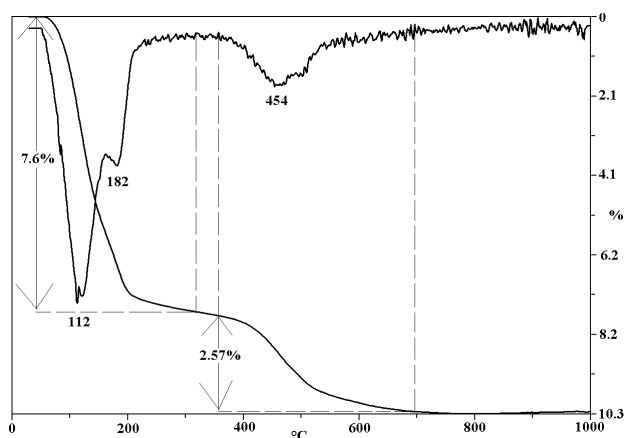


Figure 5.1.2.2.3. Thermogravimetric curves of nontronite

The reaction of nontronite:

1. Between 100 and 200 °C: endothermic dehydration:

Stoichiometric factor of the reaction for air-dried sample ( $n \approx 7$ ): about 7.75.

2. About 400–500 °C: endothermic: dehydroxylation.

Stoichiometric factor of the reaction: about 27.

3. Between 850 and 1000 °C: endothermic-exothermic peak system: structural decomposition and crystallization of new phases (hematite, spinel, quartz, cristobalite).

Sample: Sajóbábony, Hungary

Sample mass: 81.6 mg

Heating rate: 10 °C/min

Mass loss during dehydration: 7.58%

Mass loss during dehydroxylation: 2.57%

Nontronite content of the sample based on the first reaction: 59%

Nontronite content of the sample based on the second reaction: 69%

Nontronite content of the sample based on the waterfree calculation: 69%

### 5.1.2.2.4. Saponite

$$(Na,Ca)_{0.3}(Mg,Fe^{2+})_3(Si,Al)_4O_{10}(OH)_2 \cdot 4(H_2O)$$

1. Between 100 and 200 °C: endothermic: dehydration:

Stoichiometric factor of the reaction for air-dried sample ( $n \approx 7$ ): about 7.75.

2. Between 800 and 850 °C: endothermic: dehydroxylation:

Stoichiometric factor of the reaction: about 27.

Simultaneous crystallization of enstatite, later cristobalite and clinoenstatite.

Sample: synthesized, JCSS-3501 Reference Material, Japan Calibration Service System

Sample mass: 130.4 mg

Heating rate: 10 °C/min

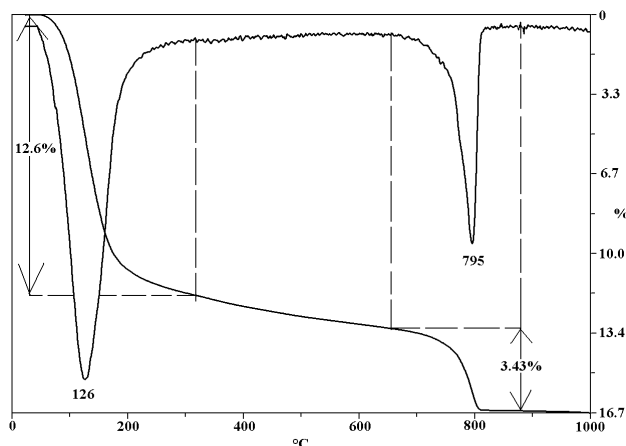


Figure 5.1.2.2.4a. Thermogravimetric curves of saponite

Mass loss during dehydration: 12.6%  
 Mass loss during dehydroxylation: 3.43%  
 Saponite content of the sample based on the first reaction: 86%  
 Saponite content of the sample based on the second reaction: 92%  
 Saponite content of the sample based on the waterfree calculation: 98%

Sample: Prága Hill, Bazsi, Hungary

Sample mass: 125.9 mg

Heating rate: 10 °C/min

Mass loss during dehydration: 8.85%

Mass loss during dehydroxylation: 3.96%

Saponite content of the sample based on the second reaction: 94%

Saponite content of the sample based on the waterfree calculation: 90%

\*\*\*

References for smectite group : 52, 54, 65, 68, 115, 140, 146, 147, 192, 200, 259, 260, 263, 274, 275, 291, 299, 301, 302, 304, 305, 310, 365, 400, 421, 423, 426, 434, 437, 490, 563, 590, 611, 615, 631, 634, 657, 687, 694, 709, 714, 740, 741, 749, 772, 882, 892, 897, 959, 966, 968, 971, 1040, 1085, 1103, 1141, 1158, 1164

### 5.1.2.3. Vermiculite group $(Mg, Fe^{2+}, Al)_3(Al, Si)_4O_{10}(OH)_2 \cdot n(H_2O)$

In natural vermiculite the exchangeable cation is Mg, or perhaps Ca. In natural vermiculite, the silicate layers are separated by double sheets of water molecules carrying exchangeable cations. The dehydration reaction is three steps process: the first peak representing the water adsorbed on the surface, the second one the water adsorbed between the layers and third between 250–300 °C the escape the water bound to the exchangeable cation respectively. The dehydroxylation process takes place in the 450–850 °C range. The rate of this reaction is very slow, therefore often it cannot be observed as a distinct peak. The wide variations of the composition of the vermiculites yield many differences in the dehydroxylation. The product of dehydroxylation is a biopyrrobole (SUQUET et al. 1984). The dehydroxylation is followed by an endothermic-exothermic peak system at about 800–900 °C. Here the structure is destructed and the exothermic peak corresponds to the crystallization of enstatite. With the variation of the iron-content the oxidation of ferrous to ferric iron may be observed. Hydrobiotite is an interstratification of vermiculite and biotite, however, thermoanalytical curves show only the vermiculite component.

Sample (Figure 5.1.2.3): Transvaal, South Africa

Sample mass: 115.2 mg

Heating rate: 10 °C/min

Mass loss during dehydration: 9.24%

References: 67, 68, 69, 345, 542, 713, 860, 914, 1045, 1081, 1115

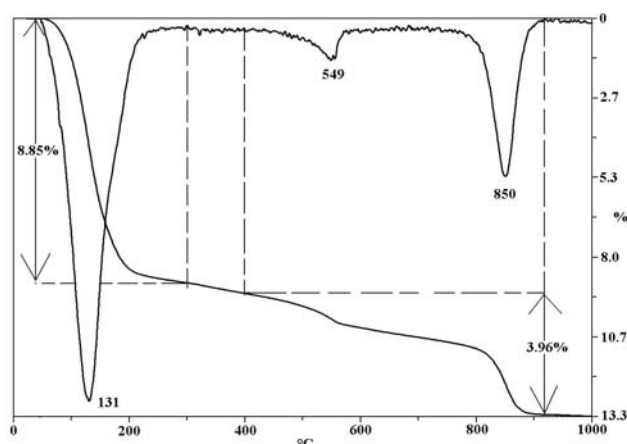


Figure 5.1.2.2.4b. Thermogravimetric curves of iron-saponite

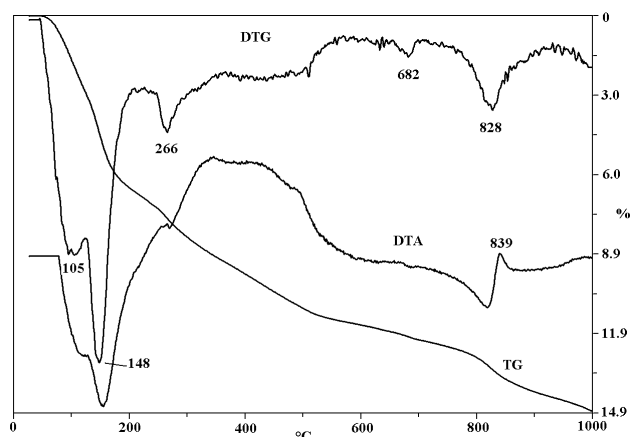


Figure 5.1.2.3. Thermoanalytical curves of vermiculite

## 5 Silicates

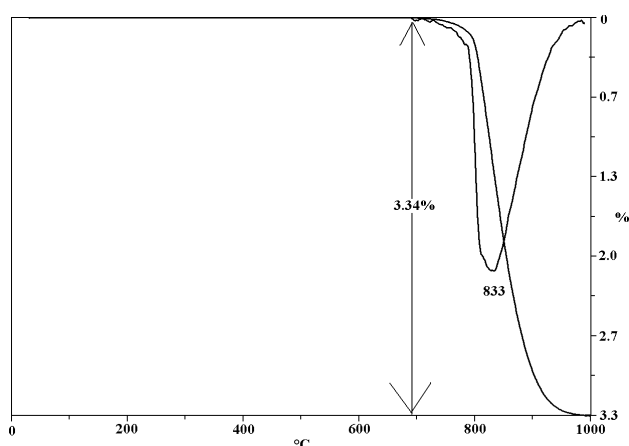


Figure 5.1.2.4.1a. Unpulverised sample containing muscovite

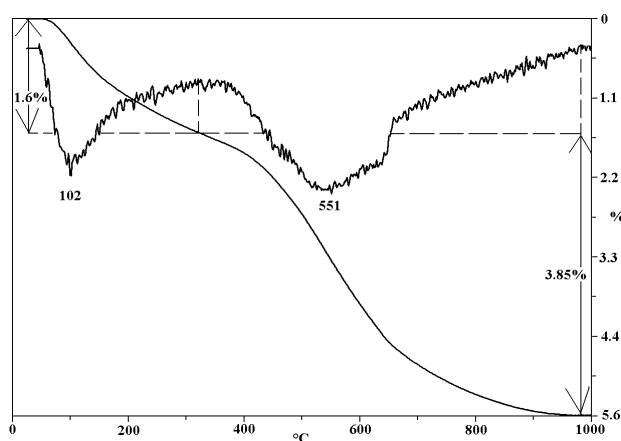


Figure 5.1.2.4.1b. Effects of dry grinding on muscovite

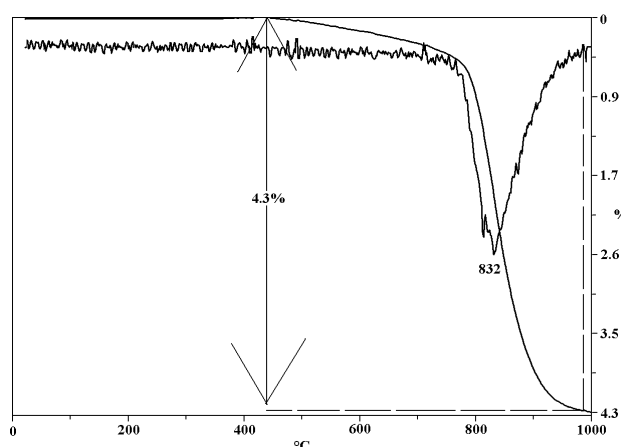
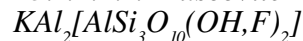


Figure 5.1.2.4.1c. Thermogravimetric curves of same muscovite pulverised under methanol

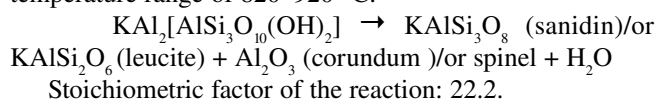
## 5.1.2.4. Mica group

Muscovite is the most common dioctahedral mica.

## 5.1.2.4.1. Muscovite



Muscovite has a simple dehydroxylation reaction in the temperature range of 820–920 °C.



Stoichiometric factor of the reaction: 22.2.

1100–1200 ° recrystallization to cristoballite, and mullite

Sample (Figure 5.1.2.4a): Piciorul Popii, Romania

Sample mass: 176.2 mg

Heating rate: 10 °C/min

Mass loss during dehydroxylation up to 1000 °C: 3.34%

Muscovite content of the sample based on dehydroxylation up to 1000 °C: 74%

The structure of muscovite is very sensitive for powering. The mechanical activation of grinding results in the rearrangement and the activation of Al-OH bond (dehydroxylation at lower temperature) and migration of hydroxyls (protons) occurs (thermal diffusion, prototropic rearrangement) from the inner part of the mineral to the surface and molecularly-bound water is formed. The increased specific surface and the broken edges make the adsorption of atmospheric water also possible (Figure 5.1.2.4.1b).

Sample (Figure 5.1.2.4b): Piciorul Popii, Romania

Sample mass: 147.9 mg

Heating rate: 10 °C/min

Mass loss during dehydroxylation: 1.6%

Mass loss during dehydroxylation up to 1000 °C: 3.85%

Muscovite content of the sample based on dehydroxylation up to 1000 °C: 84%

In the case of grinding under methanol the crystalline structure is preserved.

Sample (Figure 5.1.2.4c): Piciorul Popii, Romania

Sample mass: 64 mg

Heating rate: 10 °C/min

Mass loss during dehydroxylation up to 1000 °C: 4.3%

Muscovite content of the sample based on dehydroxylation up to 1000 °C: 95%

Thermal curves of paragonite are similar to that of muscovite (the cation in the octahedral sheet is the same).

5.1.2.4.2. Biotite  $K(Mg,Fe^{2+})_3[AlSi_3O_{10}](OH,F)_2$ 

As it is shown in Table 17 and Table T5.1.2 the trioctahedral micas have no thermal reaction below 1000 °C (Figure 5.1.2.4.2a). Biotites sometimes show an exothermic effect between 400 and 600 °C, due to the oxidation of bivalent iron. The most common alteration product of biotite is chlorite. The initial chlorite interlayering may be estimated in the thermal curves at about 500 °C (Figure 5.1.2.4.2b). It is below the sensitivity of the X-ray diffraction. The other variation of biotite (phlogopite) → hydrobiotite → vermiculite weathering is mentioned later.

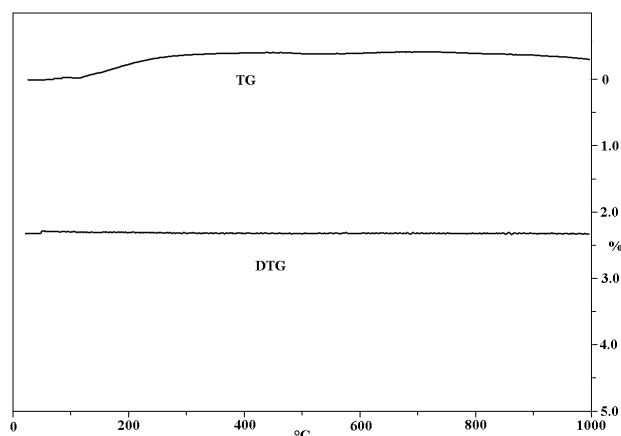


Figure 5.1.2.4.2a. Thermogravimetric curves of fresh biotite

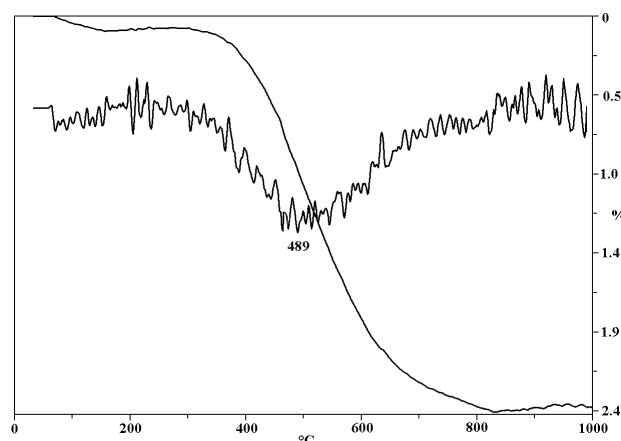


Figure 5.1.2.4.2b. Signal of the initial chloritization of a biotite separate

Sample (Figure 5.1.2.4.2a): Separated from rhyolithe, Greece

Sample mass: 73.3 mg

Heating rate: 10 °C/min

Sample (Figure 5.1.2.4.2b): Separated from rhyolithe tuff, Kisterenye, Hungary

Sample mass: 40,2 mg

Heating rate: 10 °C/min

Mass loss during dehydroxylation up to 1000 °C: 2.34%

The oxidation of iron in the temperature range of 500–600 °C and dehydroxylation as well as decomposition of phlogopite in the temperature range of 900–1200 °C. The high temperature phases are spinel, leucite, mullite.

\*\*\*

References for mica group: 6: biotite, 68: muscovite, paragonite, 119, 174: biotite, 340, 431: muscovite, 442, 502: biotite, 513: muscovite, phlogopite, biotite, lepidolite, zinnwaldite, 523: biotite, 541, 623, 652: muscovite, biotite, lepidolite, zinnwaldite, phlogopite, 652, 683: muscovite, 695, 696: muscovite, 714: muscovite, zinnwaldite, lepidolite, biotite, 799: lepidolite, 905, 968: 969: muscovite, phlogopite, lepidolite, zinnwaldite, 973, 999: biotite, 1015: biotite, 1081: muscovite, margarite, biotite 1093: phlogopite, 1101: muscovite, biotite, phlogopite, 1163: biotite

### 5.1.2.5. Hydromica (clay-mica, interlayer-deficient mica) group

Hydromicas have lower K than true micas that are replaced by water or oxonium.

Table T5.1.2.5. Composition of the members of the muscovite-illite series

	K <sub>2</sub> O+Na <sub>2</sub> O %	H <sub>2</sub> O or H <sub>3</sub> O <sup>+</sup> mole
Muscovite (ideal)	11.8	-
Muscovite	>9	
Hydromuscovite	8–9	0.4–0.6
Illite	6–8	0.6–1.0

#### 5.1.2.5.1. Illite $K_{0.65}[Al,Mg,Fe]_2Al_{0.65}Si_{3.35}O_{10}(OH)_2 \cdot H_2O$ or $(K,H_3O)Al_2(Si_3Al)O_{10}(H_2O,OH)_2$

Thermal reaction of the mineral:

Between 100 and 200 °C: endothermic escape of adsorbed and interlayer water (see chapter of “Water in Minerals. Dehydration: Adsorbed water: Interlayer waters bound by phyllosilicates”). The quantity of the water content is about 4% (1 mole).

Stoichiometric factor of the reaction: about 25.

About 550 °C: endothermic: dehydroxylation

Stoichiometric factor of the reaction: 23.3.

## 5 Silicates

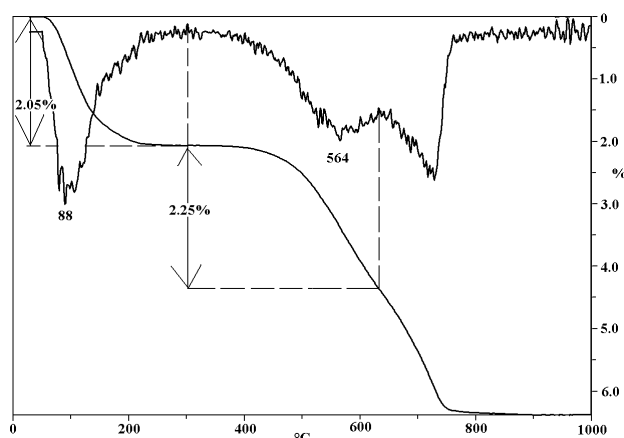


Figure 5.1.2.5.1. Thermogravimetric curves of illite containing sample

At ca. 900 °C: endothermic-exothermic peak system: destruction of the lattice and formation of spinel.

Sample: Bátaapáti, borehohe Üh–22 182.6 m, Hungary, fissure filling in granite

Sample mass: 84 mg

Heating rate: 10 °C/min

Mass loss during dehydration: 2.05%

Mass loss during dehydroxylation: 2.25%

Illite content of the sample based on dehydration: 51%

Illite content of the sample based on dehydroxylation: 52%

Other thermally active mineral in the sample: calcite

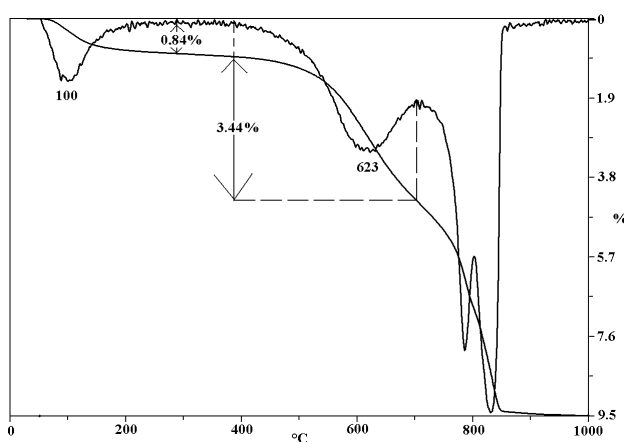


Figure 5.1.2.5.2. Thermogravimetric curves of a hydromuscovite containing sample

5.1.2.5.2. Hydromuscovite (*sericite*)

In hydromuscovite the K content is intermediate between that of muscovite and illite. The same regards to the temperature of the dehydroxylation (about 620–650 °C).

Sample: Boda, borehohe Delta–8 117–117.5 m, Hungary, permian siltstone

Sample mass: 222.7 mg

Heating rate: 10 °C/min

Mass loss during dehydration: 0.84%

Mass loss during dehydroxylation: 3.44%

Illite content of the sample based on dehydroxylation: 79%

Other thermally active mineral in the sample: dolomite

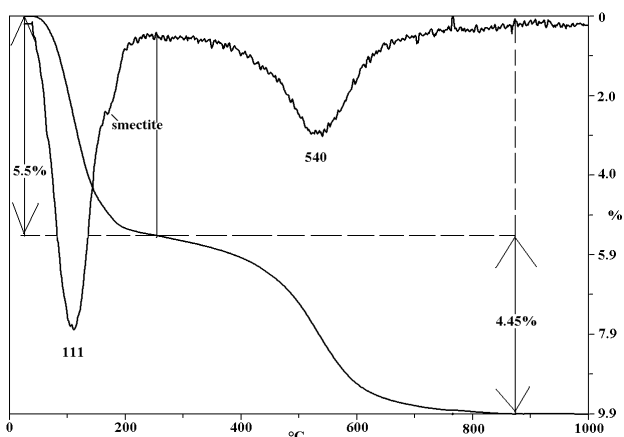
5.1.2.5.3. Glauconite  $(K,Na)(Fe^{3+},Al,Mg)_2(Si,Al)_4O_{10}(OH)_2 \cdot H_2O$ 

Figure 5.1.2.5.3. Thermogravimetric curves of a glauconite separate

The thermoanalytical data of glauconite are very similar to illite. The differences between the composition of the octahedral layers are compensated, because iron reduces, Mg increases the dehydroxylation temperature. The dehydroxylation of celadonite appears somewhere higher, than of glauconite.

Glauconite in most cases is interstratified with some smectite. Glauconite in sensu stricto has less than 10% expandable layer and its  $K_2O$  content is >7%.

Sample: Tihau, Romania, from miocene aleurolite

Sample mass: 119.5 mg

Heating rate: 10 °C/min

Mass loss during dehydration: 5.5%

Mass loss during dehydroxylation: 4.45%

Glauconite content of the sample: 100% with about 10–15% smectite interlayering

In the case of true trioctahedral illite dehydroxylation appears at much higher temperature, ca. 860 °C.

\*\*\*

References for hydromica group: 26, 68: glauconite, celadonite, 115, 137, 222, 224, 262, 327, 328: glauconite, 423, 424, 425, 503, 510, 553: illite, glauconite, 563, 587, 598, 623, 628, 684, 694, 731, 764: glauconite, celadonite, 765: illite, glauconite, celadonite, 769: Fe-rich illite, 964, 968, 1066, 1076

### 5.1.2.6. Chlorite group (2:1 layer with interlayer hydroxide sheet / or 2:1:1 / or 2:2 layer type)

Structure of the minerals in the chlorite group consist an octahedral hydroxide layer as an interlayer between the mica layers. Numerous substitutions are possible also in tetrahedral as well as in the octahedral and in the interlayer. Both octahedral and interlayer may be di- or trioctahedral. According to the AIPEA Nomenclature (GUGGENHEIM et al. 2006) *dioctahedral chlorite* is dioctahedral in both the 2: 1 layer and the interlayer hydroxide sheet. An example is *donbassite*. *Trioctahedral chlorite* is trioctahedral in both octahedral sheets. Recommended species names are *clinochlore* for Mg-dominant [end member =  $(\text{Mg}_5\text{Al})(\text{Si}_3\text{Al})\text{O}_{10}(\text{OH})_8$ ], *chamosite* for  $\text{Fe}^{2+}$ -dominant [end member =  $(\text{Fe}_5^{2+}\text{Al})(\text{Si}_3\text{Al})\text{O}_{10}(\text{OH})_8$ ], *nimite* for Ni-dominant [end member =  $(\text{Ni}_5\text{Al})(\text{Si}_3\text{Al})\text{O}_{10}(\text{OH})_8$ ], and *pennantite* for  $\text{Mn}^{2+}$ -dominant [end member =  $(\text{Mn}_5^{2+}\text{Al})(\text{Si}_3\text{Al})\text{O}_{10}(\text{OH})_8$ ]. A *di-, trioctahedral chlorite* is dioctahedral in the 2: 1 layer but trioctahedral in the interlayer sheet. *Cookeite* and *sudoite* are examples, with cookeite being Li-rich and sudoite Li-poor. The only known example of a structure with trioctahedral 2:1 layers but dioctahedral interlayers is *franklinfurnaceite*, which is an intermediate between a chlorite and a brittle mica.

Variation in composition leads to variation in thermal processes. Corresponding to the two different layers having hydroxyl, the dehydroxylation of these minerals takes places generally in two steps. The first step between 470 and 650 °C is related to the dehydroxylation of the interlayer hydroxide. The second step is due to the dehydroxylation of the mica layer. The number of hydroxyls belonging to the hydroxide sheet is three times more than in the mica layer. Further characteristic reaction after the dehydroxylation

**Table T5.1.2.6.** Thermoanalytical data of the main 2:1:1 layer type phyllosilicates

Layer type	Species	Dehydroxylation of the 2:1 layer	Phase transition
2:1:1	Al-chlorite (sudoite, cookeite)	500–530 °C	≈900 °C
	Fe <sup>2+</sup> -chlorite (chamosite, thuringite*, delessite*)	520–580 °C	
	Fe-Mg-chlorite (Mg:Fe=1:1, aphrosiderite*, pseudothuringite*)	720–730 °C	≈830 °C
	Mg-Fe-chlorite (ripidolite*, prochlorite*)	770–790 °C	
	Cr-chlorite (Cr in tetrahedral cotsubeite*)	≈800 °C	
	Mg-Fe-chlorite (Mg:Fe=3:2–5:1 pennine*)	810–835 °C	850–870 °C
	Cr-chlorite (Cr in octahedral kaemmererite*)	≈860 °C	
	Mg-Fe-chlorite (Mg:Fe=15:1–30:1 clinochlore, leuchtenbergite*)	835–865 °C	≈880 °C

\*discredited names.

is an exothermic peak that represents the chlorite recrystallizing into new minerals (olivine, spinel, enstatite etc.). The “a-value” (=temperature interval between the second dehydroxylation and the following exothermic peak) has been introduced by SMYKATZ-KLOSS (1974). The “a-value” correlates with the Mg content (the larger the MgO content is, the larger the a-value will be).

From the Table T5.1.2.6. it can be seen that the two dehydroxylation steps at the Al- and iron chlorite are overlapped. Data in the table are characteristic for primary chlorites.

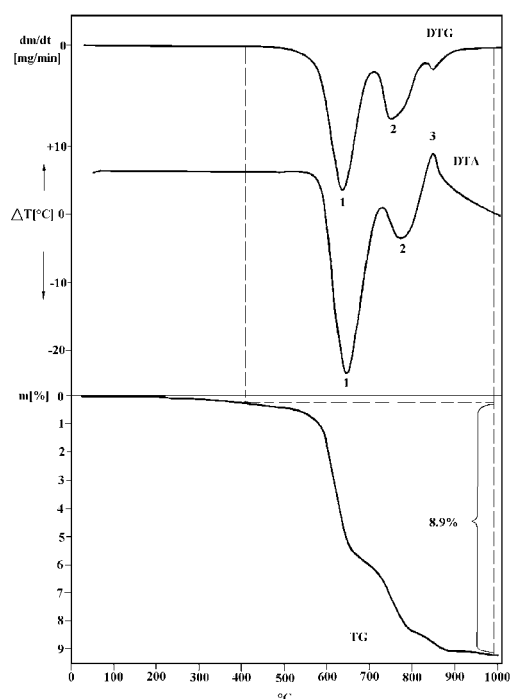


**Figure 5.1.2.6a.** Typical thermoanalytic curves of primary chlorite

Stoichiometric factor based on the mass during the reactions depends on the substitution: 7.5 (Mg) – 10.5 (Fe) for end members.

Sample (Figure 5.1.2.6a): Bălan, Romania

Sample mass: 1000 mg

Heating rate: 17 °C/min

Mass loss during dehydroxylation: 8.9%

Chlorite content of the sample based on the mass loss: 68–92%

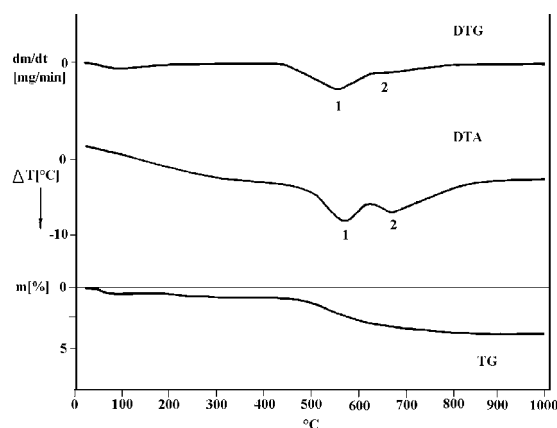


**Figure 5.1.2.6b.** Typical thermoanalytic curves of sedimentary chlorite

## 5 Silicates

Temperature of the dehydroxylation of sedimentary chlorites due to the large degree of structural disorder appears at 100–150 °C lower and less pronounced. The exothermic peak cannot be observed in the disordered chlorite.

Sample (Figure 5.1.2.6b): Felsőtárkány, Bükk Mts, Hungary

Sample mass: 1000 mg

Heating rate: 17 °C/min

\*\*\*

References for interstratified clay minerals: 37, 93, 115, 123, 124, 131, 148, 198, 266, 301, 391, 435, 447, 513, 578, 607, 613, 615, 642, 803, 871, 888, 896, 931, 935, 961, 965, 981, 1001, 1006, 1009, 1010, **1043**, 1081, 1087, 1103, 1152, 1159

### 5.1.2.7. Interstratified or mixed-layer minerals

In these clay minerals two different types alternate in the same crystallite. Thermal analysis alone cannot be used for estimating an interstratified structure. Thermal curves are sometimes similar to those of the mixture of components.

#### 5.1.2.7.1. Regularly interstratified minerals

##### 5.1.2.7.1.1. Rectorite

(1:1 interstratification of dioctahedral paragonite-smectite)  $(\text{Na}, \text{Ca})\text{Al}_4(\text{Si}, \text{Al})_8\text{O}_{20}(\text{OH})_4 \cdot 2\text{H}_2\text{O}$

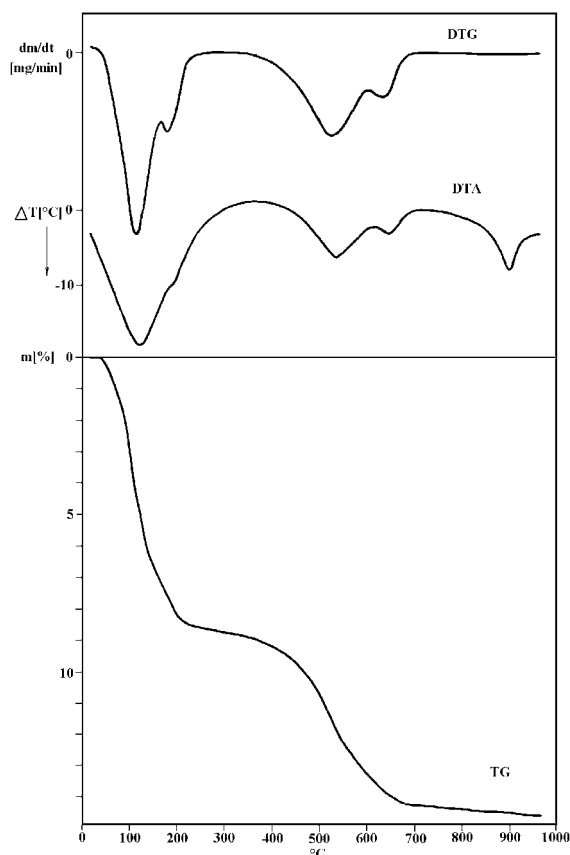


Figure 5.1.2.7.1.1. Thermoanalytic curves of K-rectorite (alleverdite)

Sample: Mád, Király Hill, Hungary

Sample mass: 1000 mg

Heating rate: 10 °C/min

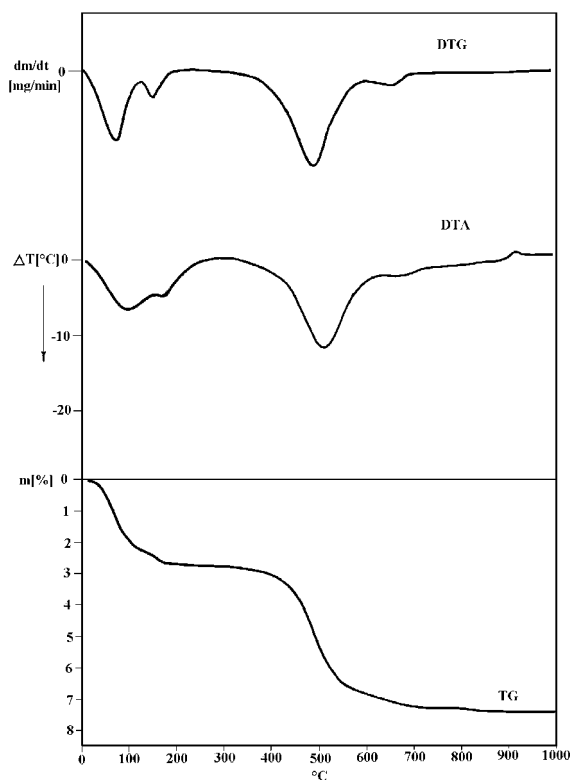


Figure 5.1.2.7.1.2. Thermoanalytic curves of tosudite

##### 5.1.2.7.1.2. Tosudite (1:1 interstratification of dioctahedral chlorite-smectite)

Sample: Sukoró, borehole St-1 92.98 m, Hungary

Sample mass: 1000 mg

Heating rate: 10 °C/min

## 5.1.2.7.2 Randomly interstratified minerals

## 5.1.2.7.2.1. Illite-montmorillonite

Sample (Figure 5.1.2.7.2.1): Füžerradvány, Hungary

Sample mass: 900 mg

Heating rate: 10 °C/min

Literature related to the type of the I/S mixed layer from Füžerradvány is abundant (e.g. NEMECZ, VARJÚ 1970, SRODON 1984, SZEGEDI 1988, VEBLEN et al. 1990, SRODON et al. 1992). These investigations suggest a I/S mixed layer mineral with a composition of 10–27% smectite layers (XRD results) respectively 21–32% (HRTEM or TEM results). The mineral that was called “sarospatakite” or “sarospatite”, recently became a popular standard material called “Zempleni” illite.

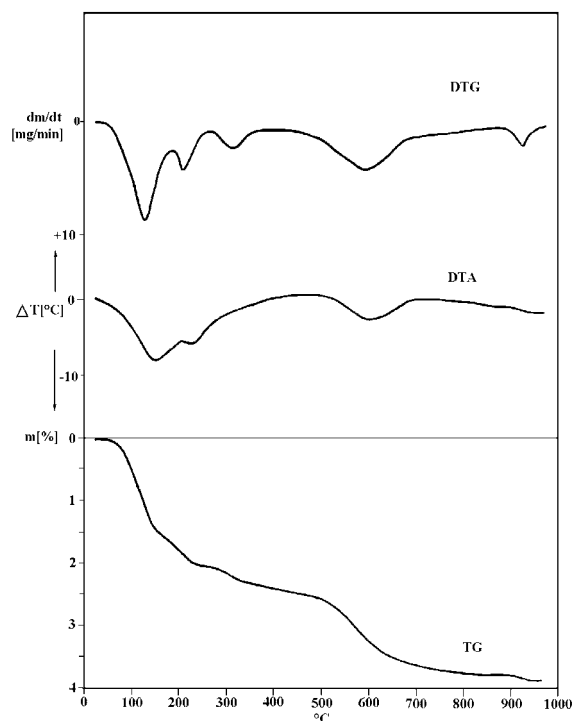


**Figure 5.1.2.7.2.2.** Thermogravimetric curves of interstratified chlorite-vermiculite

## 5.1.2.7.2.2 Chlorite-vermiculite

Sample (Figure 5.1.2.7.2.2): Mecsek Mountains, Hungary

Sample mass: 1000 mg

Heating rate: 17 °C/min

## 5.1.2.7.2.3 Talc-saponite

Sample (Figure 5.1.2.7.2.3): Szabadsbattyán, Hungary

Sample mass: 1000 mg

Heating rate: 10 °C/min

Other thermally active mineral in the sample: quartz

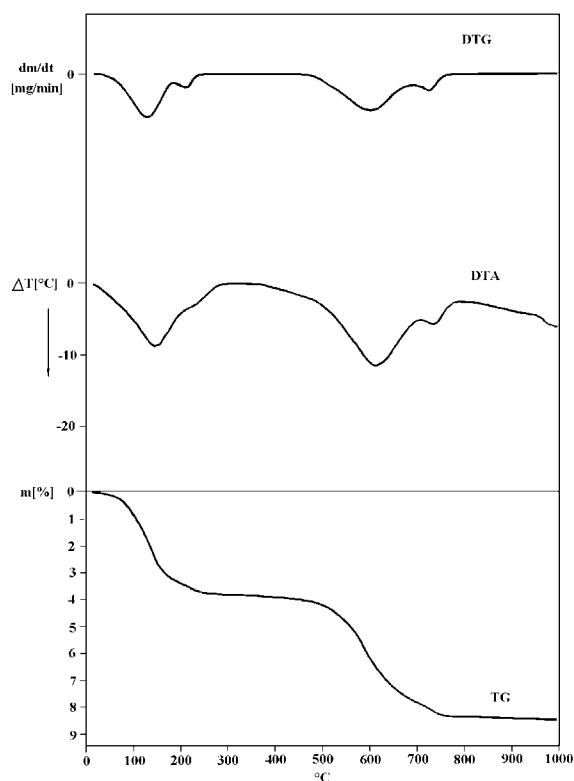


**Figure 5.1.2.7.2.1.** Thermogravimetric curves of interstratified illite/montmorillonite

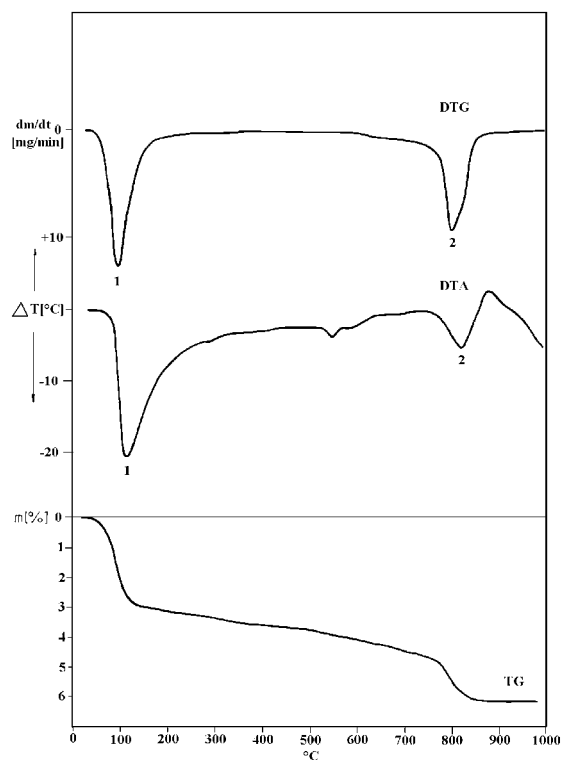


**Figure 5.1.2.7.2.3.** Thermogravimetric curves of interstratified talc-saponite

## 5 Silicates

References for pseudo-layer silicates: 13: talc-saponite, 56, 81: K-rich rectorite, 113: rectorite, 114, 115: sáropatite=illite from Füžérradvány, 116: chlorite-vermiculite, 138: rectorite = allevardite, 183, 185, 224, 290: biotite-chlorite, 435, 483, 571: illite from Füžérradvány, 577: rectorite, 585, 586, 666, 667, 786: sáropatakite, 787: allevardite, 866, 952, 962, 988, 1001: chlorite-montmorillonite, 1020, 1021, 1042, 1053: illite from Füžérradvány, 1065: kaolinite-smectite, 1100, 1103: saponite-swelling chlorite, 1104: talc-saponite, 1105, 1106: illite from Füžérradvány 1159: Nickel containing regularly interstratified chlorite-saponite, 1163

## 5.1.2.8. Pseudo-layer silicates

Palygorskite and sepiolite are naturally occurring fibrous clay minerals. The discontinuous nature of the octahedral sheet allows for the formation of channel-like nanopores that are filled completely by zeolitic water at room temperature.

5.1.2.8.1. Palygorskite  $(Mg,Al,Fe)_2Si_4O_{10}(OH) \cdot 4H_2O$ 

The mineral belongs to clay minerals, but its structure is very different from that of other clay minerals: essentially layer-like, it consists of duplicate pyroxene chains with alternating connections.

The water molecules in the palygorskite structure can be found in different positions (see Figure 45):

- connected to the terminal ion (mainly Mg) of the repeatedly broken octahedral-sheet (structural water, bound water, coordination water),
- placed in the chanells in the structure (zeolitic or free water), exchangeable to different ions,
- sometimes bound to the external surface (adsorbed water).

**Table T5.1.2.8.1.** Dehydration temperature of water evaluated from palygorskite on the basis of published data

Reactions	°C	Explanation	Water amount %				
			1	2	3	4	5
1	180 (2) <210 (4) 50–200 (5)	Free water (adsorbed water and zeolitic water)	8.5	9.0	7.5	8.0	10
2	280 (2) 210–350 (4) 200–300 (5)	Bound water I	2.1	2.0	3.0	4.1	2–4
3–4	350–600 (2) often double peaks 350–580 (4) 400–600 (5)	Bound water II	6.4	6.0	8.5	5.2	6
5	about 800 580–800 (4) 800–900 (5)	OH	2.0	2.0		2.1	2
Total:			19.0	19.0	19.0	19.4	20–22

After the temperature data and also in the column of the water content, the numbers refer to: (1) BRADLEY 1940, (2) MARTIN VIVALDI, FENOLL HACH-ALI 1970, (3) KULBICKI, GRIM 1959, (4) HAYASHI et al. 1969, (5) IVANOVA et al. 1974.

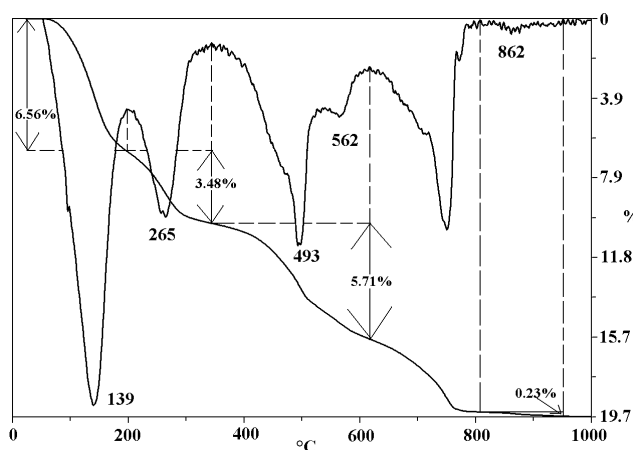


**Figure 5.1.2.8.1.** Thermogravimetric curves of a palygorskite-bearing sample

According to the theoretical calculations, the total water found in palygorskite, with the water originated from the OH-groups, is 19.6%. Higher values could be measured because of the adsorbed water (Table T5.1.2.8.1).

Sample: Bátaapáti, borehole Üh-36 147.5 m, Hungary, fissure filling in granite.

Sample mass: 147.5 mg

Heating rate: 10 °C/min

Mass loss during the first dehydration: 6.56%

Mass loss during the second dehydration: 3.48%

Mass loss during the third step: 5.71%

Mass loss during the last dehydroxylation: 0.23%

Palygorskite content of the sample based on the total water content: about 85%

Other thermally active minerals in the sample: calcite, chlorite

### 5.1.2.8.2. Sepiolite $Mg_4Si_6O_{15}(OH)_2 \cdot 6(H_2O)$

Water in the structure of sepiolite is very similar to that in palygorskite. The first endothermic peak of sepiolite appears at cca. 150 °C, representing the escape of free water, both from external surfaces and from within the channels. This is followed by one or two smaller endothermic peaks at 350–450 °C and at about 600 °C representing the bound water. According to KIYOHRO, OTSUKA (1989), the two-step dehydration of bound water is caused by the following two factors: (1) the difference in the activation energy of dehydration between the water in the unfolded open channel and that in the folded one, and (2) the change in the rate determining process from the water separation process to the water diffusion one.

A further endothermic peak appearing at 750 °C representing the escape of OH and the total destruction of the lattice, this one is immediately followed, over 800 °C, by a sharp exothermic peak representing the heat released at the formation of a new crystal phase (enstatite, cristobalite, olivine, spinel, cordierite). The theoretical water content is 19.5%. The measured data of different authors are presented in Table T5.1.2.8.2.

**Table T5.1.2.8.2.** Steps of the water escape from sepiolite based on published data

Explanation	Theoretical	Water amount %							
		1	2	3	4	5	6	7	8
Free water	4 moles=11.12%	8.2	10.9	7.1	10.2	10	10 12	6.7	11
Bound water	2 moles=2.78%	5.4	5.4	6.8	3.1	2	3-5	4.2	3.3
	2 moles=2.78%			2.6	2.2	4		4.2	2.3
Hydroxyl	2 moles=2.78%	5.4	2.7	2.5	3.1	3	3	4.2	2.1
Total:	19.3%	19.0	19.0	19.0	18.6	19	16-20	19.3	18.7

Numbers refer to: (1) NAGY, BRADLEY 1955, (2) BRAUNER, PREISINGER 1956 (3) KULBICKI, GRIM 1959, (4) MARTIN VIVALDI, CANO RUIZ 1956, (5) FENOLL HACH-ALI 1970, (6) IVANOVA et al. 1974, (7) KALMÁR et al. 1997, (8) FROST, DING 2003.

Sample: Măgureni Hill, Preluca Mts, Romania  
 Sample mass: 103.5 mg  
 Heating rate: 10 °C/min  
 Sepiolite content of the sample based on the total water content: about 100%

References: 8, 88, 112, 115, 120, 149, 265, 307, 355, 411, 449, 487, 513, 530, 545, 573, 614, 629, 631, 632, 634, 694, 719, 720, 742, 767, 773, 774, 898, 920, 930, 981, 983, 993, 994, 1181,

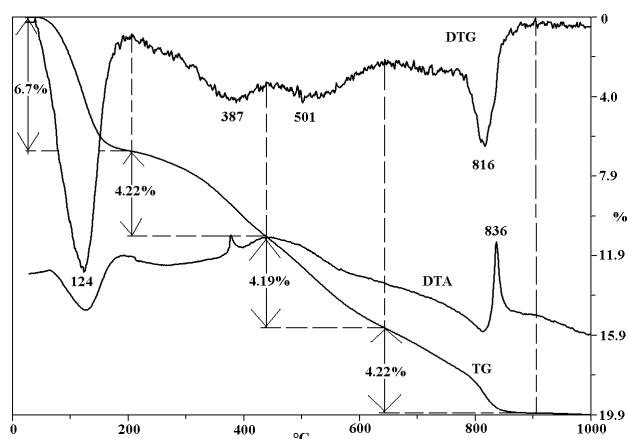


**Figure 5.1.2.8.2.** Thermoanalytic curves of sepiolite

### 5.1.2.9. Phyllosilicate two-dimensional infinite sheets with other than six-membered rings

#### 5.1.2.9.1. Apophyllite $KCa_4(Si_4O_{10})_2(F,OH) \cdot 8(H_2O)$

Reaction of the mineral:

1. Between 300 and 350 °C: endothermic: loss of 4 molecules water.

Stoichiometric factor of the reaction: about 12.6.

2. Between 400 and 450 °C: endothermic: loss of 4 molecules water (and structural OH).

Stoichiometric factor of the reaction: about 11.2.

Dehydration reactions depend on the fluorine content. The product is a non-diffracting amorphous phase.

Sample: Recsk, Hungary

Sample mass: 500 mg

Heating rate: 10 °C/min

Mass loss during the first reaction: 7.8%

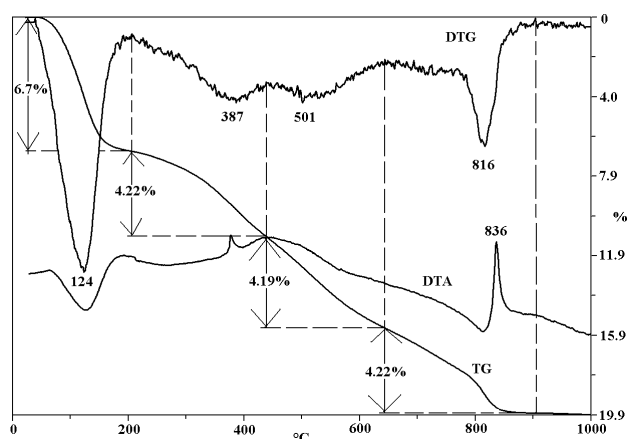


**Figure 5.1.2.9.1.** Thermoanalytic curves of apophyllite

## 5 Silicates

Mass loss during the second reaction first reaction: 8.9%

Apophyllite content of the sample based on the first reaction: 98%

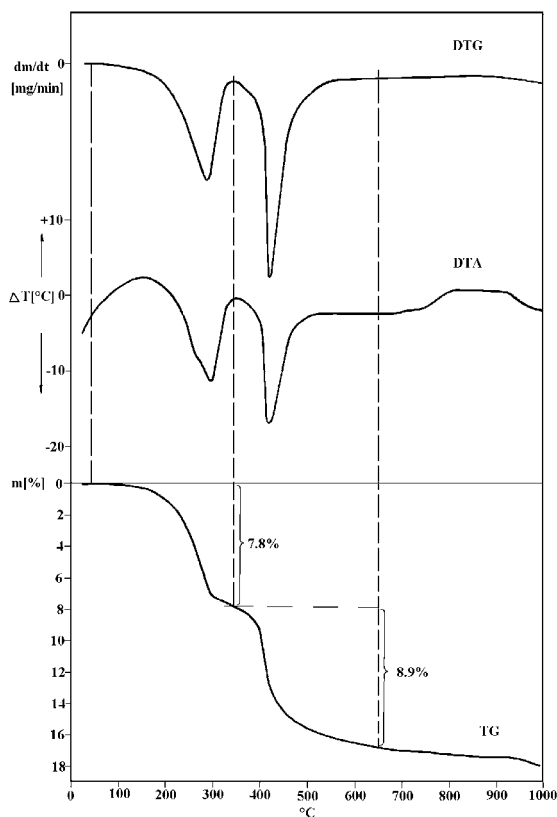


Figure 5.1.2.9.2. Thermogravimetric curves of prehnite

#### 5.1.2.9.2 Prehnite $\text{Ca}_2\text{Al}_2\text{Si}_3\text{O}_{10}(\text{OH})_2$

Reactions of the mineral:

1. Between 730 and 870 °C: double endothermic: dehydroxylation.

Stoichiometric factor of the reaction: about 23.

2. Between 900 and 1000 °C: exothermic: crystallisation of new phases (anortite, wollastonite, cristobalite), and in the case of iron substitution  $\text{Fe}_2\text{O}_3$

Sample: Szarvaskő, Hungary

Sample mass: 1000 mg

Heating rate: 10 °C/min

Mass loss during dehydroxylation: 3.7%

Prehnite content of the sample based on the reaction: 85%

Other thermally active minerals in the sample: quartz

#### 5.1.2.9.3 Tobermorite $\text{Ca}_5(\text{OH})_2\text{Si}_6\text{O}_{16} \cdot 4\text{H}_2\text{O}$

This calcium silicate hydrate occurs in both nature and hydration products of Portland cements. Possible natural occurrences are the hydrothermal alteration products of calcium carbonate rocks, due to contact metamorphism and metasomatism or in filling vesicles and cavities in basaltic rocks. The freshly precipitated tobermorite is X-ray amorphous. The crystalline variety is a layer-structure silicate with a basal spacing 11.3 Å. Its structure is transitional between phyllosilicates and inosilicates. The water bound is zeolitic-like.

Reaction of the mineral:

1. 250–300 °C: endothermic: loss of water (the reaction continues over a wide temperature range)

Stoichiometric factor of the reaction: 8.1.

2. 800–850 °C: sharp exothermic peak representing the recrystallization of an amorphous dehydrated material into wollastonite. The character of the exothermic peak depends on the crystallinity of the tobermorite. It is weak or absent in natural samples.

Sample: Prága Hill, Bazsi, Hungary, in cavities of basalt

Sample mass: 23.0 mg

Heating rate: 10 °C/min

Mass loss during the endothermic reaction: 10.83%

Tobermorite content of the sample based on the mass loss: ≈88%

Other thermally active minerals in the sample: fibroferite, pyrite

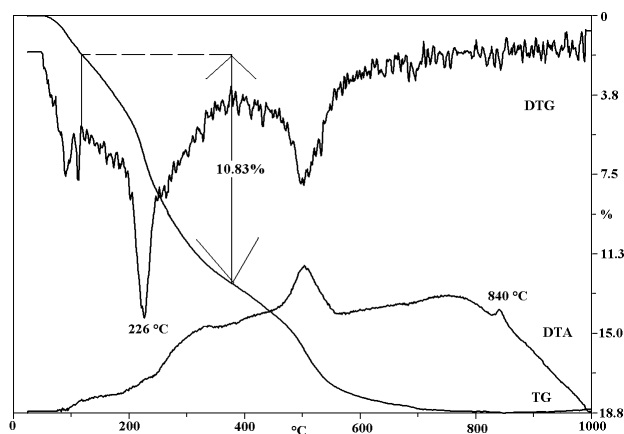


Figure 5.1.2.9.3. Thermogravimetric curves of tobermorite

References for phyllosilicate two-dimensional infinite sheets: 288: apophyllite, prehnite, 405, 513: apophyllite, prehnite, pumpellyite, 706, 734: riversideite, tobermorite, plombierite, 753: natroapophyllite, 785, 866: prehnite, 890: prehnite, 1015: apophyllite, 1081: prehnite, 1168: fluorapophyllite,

## 5.2. Nesosilicates

The structure of silicates is generally stable and they have reactions only above 1000 °C. The most important reaction below 1000 °C is dehydroxylation and in the some cases dehydration (Table T5.2).

**Table T5.2.** Dehydroxylation temperature of some mesosilicates

Mineral	Formula	Dehydroxylation
Topaz	$\text{Al}_2(\text{OH},\text{F})_2\text{SiO}_4$	$\approx 950\text{ }^\circ\text{C}$
Zoizite, epidote	$\text{Ca}_2\text{Al}_2(\text{O}\cdot\text{OH}\cdot\text{SiO}_4\cdot\text{Si}_2\text{O}_7)$ and $\text{Ca}_2(\text{Al},\text{Fe})\text{Al}_2(\text{O}\cdot\text{OH}\cdot\text{SiO}_4\cdot\text{Si}_2\text{O}_7)$	$\approx 1000\text{ }^\circ\text{C}$
Zunyite	$\text{Al}_{12}[\text{AlO}_4(\text{OH},\text{F})_2]_{18}(\text{ClSi}_2\text{O}_7)_6$	$750\text{--}850\text{ }^\circ\text{C}$
Vesuvianite	$\text{Ca}_{10}(\text{Mg},\text{Fe})_2\text{Al}_4[(\text{OH},\text{F})_4]_4(\text{SiO}_4)_5(\text{Si}_2\text{O}_7)_2$	$>900\text{ }^\circ\text{C}$

### 5.2.1. Topaz $\text{Al}_2\text{SiO}_4(\text{F},\text{OH})_2$

Reaction of the mineral above 950 °C: endothermic: escape of OH and F

Products of dehydroxylation are mullite  $[(\text{Al}_2\text{O}_3)_{3-4}(\text{SiO}_2)_2]$  and silica.

Stoichiometric factor of the reaction: 10–6.5 (increasing F content results in decreasing stoichiometric factor).

Sample: Pázmánd, borehole Pd-2 145.3–146.9 m, Hungary

Sample mass: 1000 mg

Heating rate: 17 °C/min

Other thermally active minerals in the sample: pyrite, kaolinite

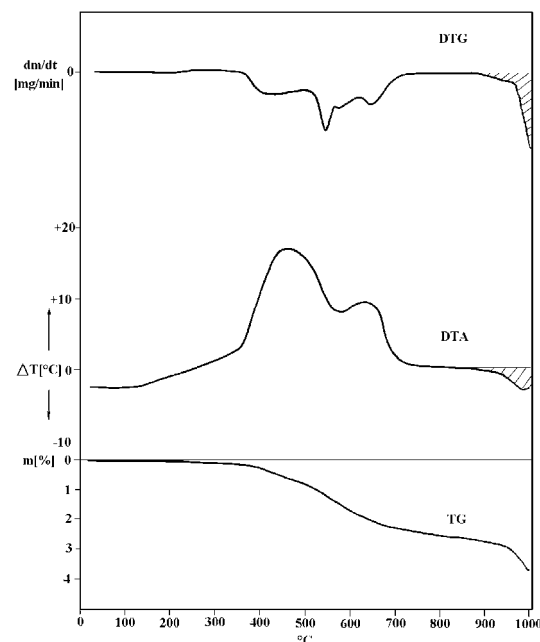


**Figure 5.2.1.** Thermoanalytic curves of a topaz-bearing sample

### 5.2.2 Epidote $\text{Ca}_2(\text{Fe}+\text{Al})\text{Al}_2(\text{SiO}_4)(\text{Si}_2\text{O}_7)\text{O}(\text{OH})$

Reaction of the mineral between 900 and 1000 °C: endothermic dehydroxylation. The temperature of dehydroxylation depends on their iron content.

Stoichiometric factor of the mineral based on the mass loss during dehydroxylation with increasing Fe substitution: changes from 54 to 50.

Sample: Bátaapáti, borehole Üh-22 406.3 m, Hungary, fissure filling in granite

Sample mass: 163.2 mg

Heating rate: 10 °C/min

Mass loss during dehydroxylation: >1.15%

Epidote content of the sample based on dehydroxylation: >58%

Other thermally active mineral in the sample: chlorite

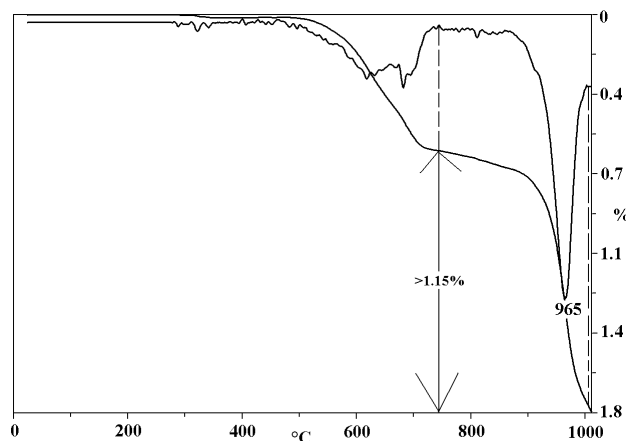


**Figure 5.2.2.** Thermogravimetric curves of an epidote-bearing sample

## 5 Silicates

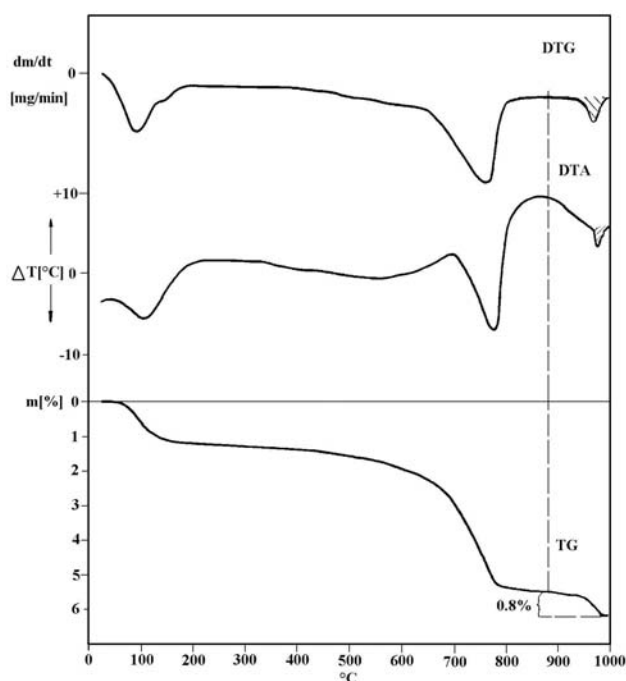


Figure 5.2.3. Thermoanalytic curves of a vesuvianite-bearing sample

**5.2.3. Vesuvianite**


Reaction of the mineral above 900 °C: endothermic: escape of OH and F.

Stoichiometric factor of the mineral changes depending on composition: between 18 and 41.

Sample: Szabadbattyán, Hungary

Sample mass: 1000 mg

Heating rate: 0.8%

Other thermally active minerals in the sample: montmorillonite, calcite

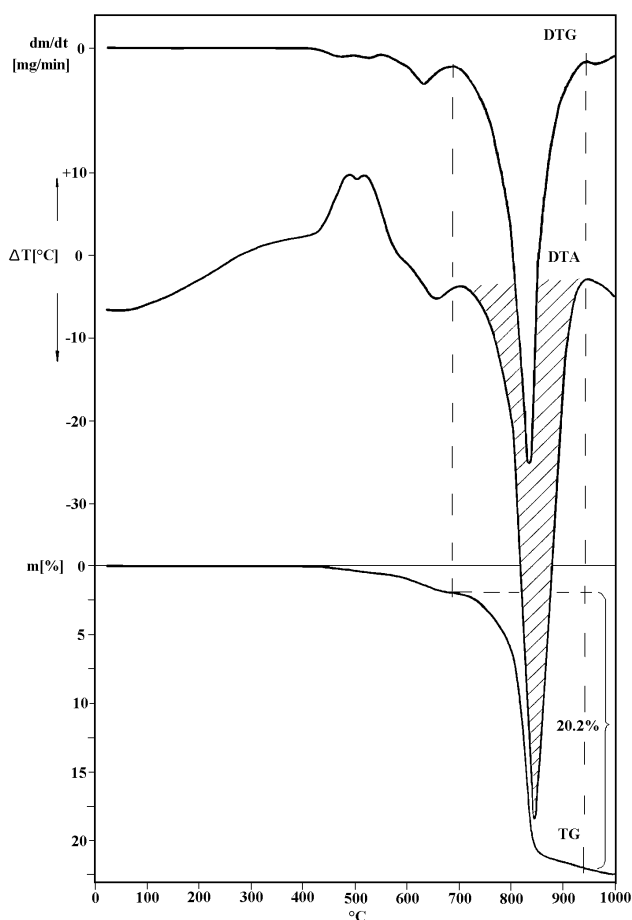


Figure 5.2.4. Thermoanalytic curves of a zunyite-bearing sample

**5.2.4 Zunyite  $\text{Al}_{13}\text{Si}_5\text{O}_{20}(\text{OH,F})_{18}\text{Cl}$** 

Reaction of the mineral between 700 and 900 °C endothermic: escape of OH, F and Cl.

Stoichiometric factor of the mineral changes depending on the OH:F proportion: 3.15–5.84.

Based on the chemical analysis, the OH:F:Cl ratio in this sample is 10:8:1 (KONTA, MRAZ 1961). Dillnite is a variation of zunyite with higher fluorine content.

Sample: Banská Bela, Czech Republic

Sample mass: 1000 mg

Heating rate: 17 °C/min

Mass loss during the reaction: 20.2%

Zunyite content of the sample based on the reaction: 85%

Other thermally active mineral in the sample: pyrite

### 5.2.5 Katoite $\text{Ca}_3\text{Al}_2(\text{SiO}_4)_3 \cdot \text{Ca}_3\text{Al}_2(\text{OH})_{12}$

OH-bearing garnet is the hydrogrossular [hibschite:  $(\text{Ca}_3\text{Al}_2(\text{SiO}_4)_{3-x}(\text{OH})_{4x})$   $x=0-3$ ] where OH-groups substitute  $(\text{SiO}_4)$ -tetrahedra. The OH content of grossular crystals can be as high as to 13% (ROSSMAN, AINES 1991).

A Si-free hydrogarnet, the tricalcium aluminate hexahydrate (the end-member of katoite  $[\text{Ca}_3\text{Al}_2(\text{SiO}_4)_3 - \text{Ca}_3\text{Al}_2(\text{OH})_{12}]$  series) also has the name hydrogrossular, as a cement material that is not a silica mineral in sensu stricto.

Sample: Cement-milk

Sample mass: 118.6 mg

Heating rate: 10 °C/min

Mass loss during the reaction: 17.0%

A water bearing mineral from this group represents bakerite. The dehydroxylation of this mineral takes place at a lower temperature (around 590 °C) than in the case of minerals without water content in this group.

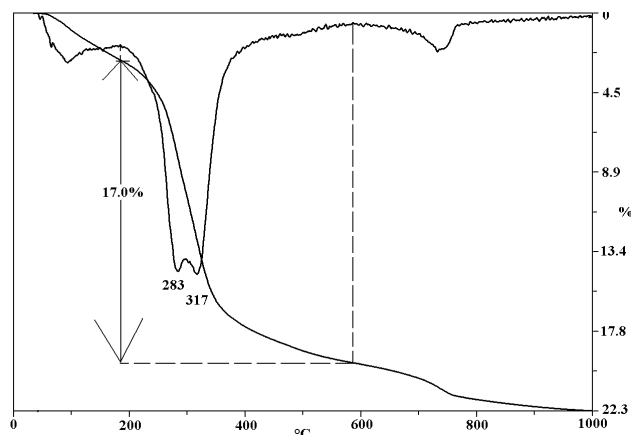


Figure 5.2.5. Thermogravimetric curves of katoite

\*\*\*

References for nesosilicates: 2, 75: bakerite, 159: strontian piemontite, 441: topaz, 452: chromian hydrogrossular, 502: epidote, 513: vesuvianite, epidote, zoizite, hydrogrossular, 521: allanite and gadolinite, 553: allanite, braunite, 597: zunyite, 599: zunyite, 865: vesuvianite, 866: epidote, vesuvianite, 916: grossular-hydrogrossular, 1081: epidote, zoizite, 1184: vesuvianite

## 5.3. Sorosilicates (and cyclosilicates)

### 5.3.1. Hemimorphite $\text{Zn}_4((\text{Si}_2\text{O}_7(\text{OH})_2 \cdot \text{H}_2\text{O})$

Reactions of the mineral:

1. At about 390–660 °C: endothermic: continuously dehydration

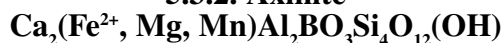
Stoichiometric factor of the reaction: 26.8.

2. 660–740 °C: endothermic: dehydroxylation

Stoichiometric factor of the reaction: 26.8.

3. 850–970 °C: exothermic: forming of willemite ( $\beta\text{-Zn}_2\text{SiO}_4$ )

### 5.3.2. Axinite



Reaction of the mineral at ca. 900 °C: endothermic: dehydroxylation

Stoichiometric factor of the reaction: about 63.

Decomposition products are anorthite, rankinite and a small amount of other, partly amorphous phases.

Sample: Lillafüred, Hungary

Sample mass: 101.4 mg

Heating rate: 10 °C/min

Mass loss during dehydroxylation: 0.8%

Axinite content of the sample based on the reaction:  $\approx 50\%$

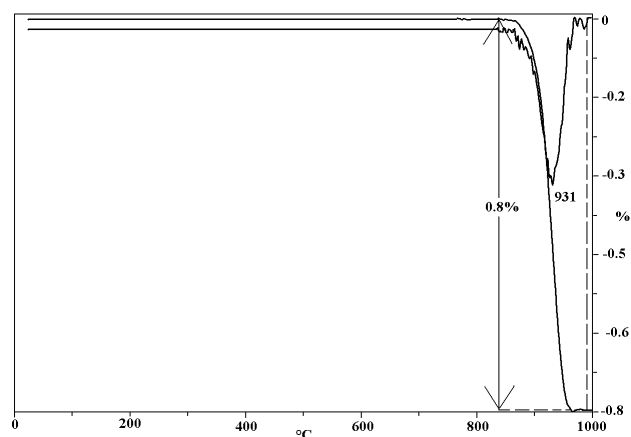
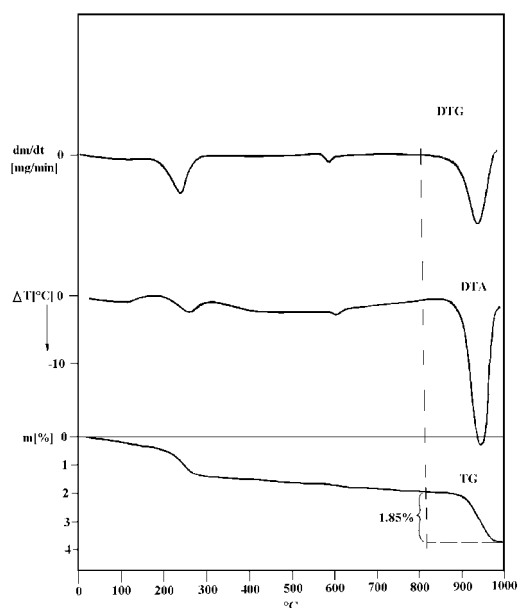


Figure 5.3.2. Thermogravimetric curves of ferroaxinite

## 5 Silicates



**Figure 5.3.3.** Thermoanalytical curves of a tourmaline (dravite)-bearing sample

### 5.3.3. Tourmaline



Reaction of the mineral at about 950 °C: dehydroxylation and escape of F and  $\text{B}_2\text{O}_3$ , and at the same time melting.

Stoichiometric factor of the reaction: 6.4–6.8.

Sample (Figure 5.3.3): Nadap, borehole Nt-2 12.3 m, Hungary

Sample mass: 1000 mg

Heating rate: 17 °C/min

Mass loss during the reaction: 1.85%

Tourmaline content of the sample based on the reaction: about 12%

Other thermally active minerals in the sample: goethite and undetermined

\*\*\*

References for sorosilicates: 157: tourmaline, 177: chrysocolla, 190: hemimorphite, 299: hemimorphite, 341: tourmaline, 396: cordierite, 513: chrysocolla, diopside, axinite, tourmaline, 553: tourmaline, hemimorphite, chrysocolla, 639: tourmaline, 924, 981: tourmaline, 1006: tourmaline, chrysocolla, 1015: cordierite, 1049: ferro-axinite, 1071: hemimorphite, 1081: diopside, 1111: axinite

## 5.4. Inosilicates

### 5.4.1 Amphiboles



An endothermic peak represents dehydroxylation at higher than 850 °C, at the same time transformation to meta-phase or depending on the composition to other phases (e.g. pyroxene, cristobalite, plagioclase, hematite etc.). The temperature at which dehydroxylation occurs is largely dependent on the type of the cation that occupies the  $\text{M}_3$  and  $\text{M}_1$  sites. The dehydroxylation temperature of amphiboles increases with increasing content of magnesium (>980 °C). In oxidizing atmosphere the iron-bearing amphiboles give an exothermic peak between 400 and 800 °C representing the oxidation of  $\text{Fe}^{2+}$ .

### 5.4.2 Charoite $\text{K}_5\text{Ca}_8(\text{Si}_6\text{O}_{15})_2(\text{Si}_2\text{O}_7)\text{Si}_4\text{O}_9(\text{OH}, \text{F}) \cdot 3(\text{H}_2\text{O})$

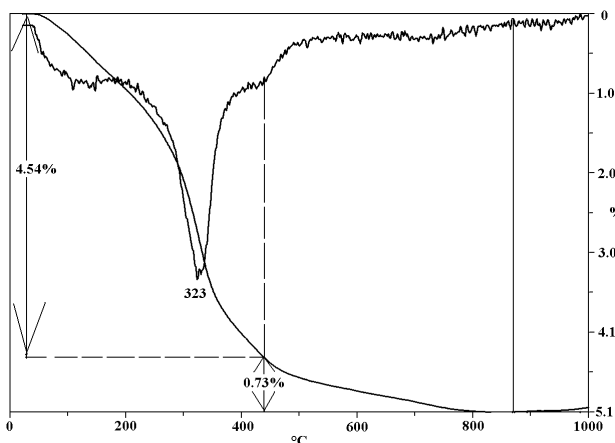


**Figure 5.4.2.** Thermogravimetric curves of charoite

Reactions of the mineral:

1. Dehydration: peak maximum at 323 °C.
2. Dehydroxylation.

Sample: Russia

Sample mass: 200 mg

Heating rate: 10 °C/min

Mass loss during the reactions: 5.1%

Charoite content of the sample based on the total mass loss: 100%

References for inosilicates: 7 rhodonite, 351, 405, 488: crocidolite, 489: amosite, 502: hornblende, 553 glaucophane, hillebrandite, 610: tremolite, nephrite, actinolite, pargasite, arfvedsonite, 694: crocidolite, 866: actinolite, 875: ferrian sodium-amphibole, 981: hornblende, 1015: hornblende, charoite, 1081: amphibole, pectolite, 1166: amphibole, 1167: tremolite, richterite, glaucophane, antophyllite

## 5.5. Tectosilicates

### 5.5.1. Zeolites

The main thermoanalytical reactions of the zeolites are dehydration and phase transitions. Water in the zeolite structure may be “zeolitic water” in the channels of the structure and structurally bound water. Water molecules have water–water, water–framework and water–extra-framework cations interactions. The zeolitic water according to the classic sense, means that water moves free in the structure, without any well defined position or cation. Its distribution is random. One of its types is water around the cations, in coordination with it, water forms a hydrate shell around it. The escape of weakly bounded water is at low temperature, gradually, generally as a broad reaction. Crystalline water occurring in a definite position and bounded to the structure by hydrogen bridge escapes by one or several well defined, sharp reactions at higher temperatures. The nature of the internal space depends on the system of the interconnecting channels (see chapter “Zeolitic water”).

The thermal data for certain zeolites are not always the same in the literature (see later Tables T5.5.1.1.1–T5.5.1.6.4).

#### 5.5.1.1. Zeolites with chains of 4-membered rings, $Al_2Si_2O_{10}$

Water in the zeolites of this group is found in 3-dimensional large channels

##### 5.5.1.1.1. Natrolite $Na_2[Al_2Si_3O_{10}]\cdot 2H_2O$

Crosslinked two-dimensional chains. Al and Si atoms are ordered. Location of  $H_2O$  molecules in channels coordinated to oxygen in framework and sodium ions. Free apertures:  $2.6 \times 3.9$  and  $2.5 \times 4.1$  Å.

Data of the reaction of the mineral based on different publications are summarized in Table T5.5.1.1.1. Major differences between the temperatures of dehydration can be explained by the possible disorder structure and by Ca and K substitutions in channels (tetranatrolite).

**Table T5.5.1.1.1.** Thermoanalytical data of natrolite

References	Temperature of dehydration (°C)			Temperature and products of transformations (°C)		
	200–300	300–400	400–500			
KOIZUMI (1953)	210		<b>405</b>			
PENG (1955)			455	564 metanatlrolite	910 940 amorphous	1010 nepheline
PÉCSI (1962)		300–350	<b>400</b>	565 metanatlrolite	910	1010 nepheline
PÉCSI-DONÁTH (1965)				480 metanatlrolite	560 carnegieite + nepheline + $SiO_2$	680 nepheline
PANES et al. (1967)			<b>400–425</b>			
PÉCSI DONÁTH (1968)						1000 albite+nepheline
BATIASVILI (1972)			<b>440–450</b>		900–1000 amorphous	1000–1100 nepheline
RIEUDWIK (1972)		<b>350</b>		at 785 amorphous	900 carnegieite	970 nepheline + amorphous $SiO_2$
BRICK (1973)		<b>350</b>		565 new structure	785 amorphous	970–1010 nepheline
SMYKATZ KLOSS (1974)		<b>350–370</b>				
IVANOVA et al. (1974)		<b>300–420</b>		500 600 metanatlrolite	900 1000 amorphous	1000 1100 nepheline and quartz (?)
JINYING, SHAOYING (1984)		<b>388</b>		540		
GOTTARDI, GALLI (1985)		<b>330</b>		285 metanatlrolite	510 ?metanatlrolite	775 amorphous
ULLRICH et al. (1987)	255	380	<b>425–480</b>	400–540 metanatlrolite	785 amorphous	950–1020 nepheline, carnegieite
PIHADKE, APTE (1997) German natrolite		<b>360</b>				970–980
PIHADKE, APTE (1997) Indian natrolite		300–310	<b>405–410,</b> 455–460, 470	560–570		980–995
Mass loss		2%	6.8%+1%			

Mean peaks in bold.

## 5 Silicates

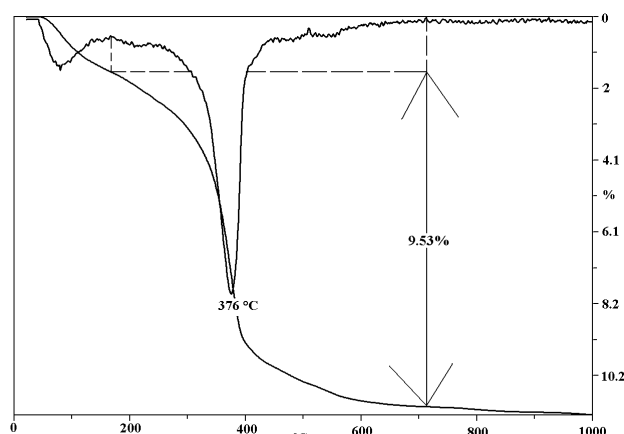
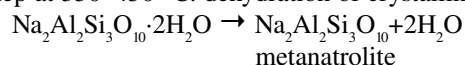


Figure 5.5.1.1.1. Thermogravimetric curves of natrolite

The dehydration of natrolite takes place in one sharp well-defined step at 350–450 °C: dehydration of crystalline water.



Stoichiometric factor of the reaction: 10.5.

In dehydrated zeolites  $\alpha$ -metanatrrolite  $\rightleftharpoons$   $\beta$ -metanatrrolite transformation.

Heating of fibrous zeolites above 500–700 °C causes their amorphization.

Sample: Prága Hill, Bazsi, Hungary

Sample mass: 90.1 mg

Heating rate: 10 °C/min

Mass loss during the reactions: 9.53%

Natrolite content of the sample based on the total mass loss:  $\approx 100\%$

### 5.5.1.1.2. Gonnardite (tetranatrrolite) $(\text{Na}, \text{Ca})_{6-8}[\text{Al}, \text{Si}]_{20}\text{O}_{40} \cdot 12\text{H}_2\text{O}$

The structure is similar to that of natrolite, but with Si, Al disordered. Location of  $\text{H}_2\text{O}$  molecules: 1/3 of the water is zeolitic, 2/3 is probably bound to cation in channels. Water content is between 14–16%.

Reactions of the mineral based on publications are summarized in Table T5.5.1.1.2.

Table T5.5.1.1.2. Thermoanalytical data of gonnardite

References	Temperature of dehydration (°C)						Temperature and products of transformations (°C)		
	0–100	100–200	200–300	300–400	400–500	500–800			
DONATI, SIMÓ (1966)		140	250	380			250 350 amorphous		950 nepheline
REEUWIK (1972)	75		220		420, 450				
	1.5 moles		1.5 moles		2.5 moles + 0.5 mole	remaining water	300 metaphase	460 collapse of structure	900 plagioclase + nepheline
IVANOVA et al. (1974)			200 300	320 450		500 600			1000 amorphous
GOTTARDI, GALLI (1985)	50	130	200	330	420		above 300 lattice destroyed		

### 5.5.1.1.3. Mesolite $\text{Na}_2\text{Ca}_2[\text{Al}_6\text{Si}_9\text{O}_{30}] \cdot 8\text{H}_2\text{O}$

Channel system and free apertures are the same as in the case of natrolite. Free apertures:  $2.6 \times 3.9 \text{ \AA}$ .

Reactions of the mineral based on publications are summarized in Table T5.5.1.1.3.

Table T5.5.1.1.3. Thermoanalytical data of mesolite

References	Temperature of dehydration (°C)						Temperature and products of transformations (°C)			
	200 300	300 400	400 500	500 600	700 800					
KOIZUMI (1953)	266 (300)		418							
	2.5 moles									
PENG (1955)		310–(325) double	440			490 structural breakdown		1040 plagioclase		
PÉCSI (1962)		2 + 2 moles 300	4 moles 410 440							
PÉCSI-DONÁTH (1968)								1000 bytownite		
BATIASVILI (1972)		310–340 double	440–450	530		560 amorphous		1100 labradorite		
		4 moles	2 moles	2 moles						
REEUWIK (1972)	255, 275 double	380–410 double				540 collapse of the structure	910 plagioclase	975 plagioclase + nepheline + amorphous SiO <sub>2</sub>		
	4 moles	$\approx 2.5$ moles	remaining water							

**Table T5.5.1.1.3.** Continuation

References	Temperature of dehydration (°C)					Temperature and products of transformations (°C)			
	200-300	300-400	400-500	500-600	700-800				
BRICK (1973)	225 (double)	380				440-490 structure decomposing	910 feldspar	1040	
IVANOVA et al. (1974)	200-380		380-500			600-650 amorphous	1000 melting	1020 nepheline	1100 plagioclase
	4 moles		remaining water						
GOTTARDI, GALLI (1985)						320 amorphous			
PIADKE, APTE (1997)	240 260	270 325	420 470	480 515					

#### 5.5.1.1.4. Thomsonite $\text{NaCa}_2[\text{Al}_5\text{Si}_5\text{O}_{20}]\cdot 6\text{H}_2\text{O}$

Chains occur as natrolite structure type but they are crosslinked in a different way. Location of  $\text{H}_2\text{O}$  molecules is in zigzag chains in the channels. Free apertures:  $2.6 \times 3.9 \text{ \AA}$ . Theoretical water content: 13.4%.

**Table T5.5.1.1.4.** Thermoanalytical data of thomsonite

References	Temperature of dehydration (°C)							Temperature and products of transformations (°C)		
	0-100	100-200	200-300	300-400	400-500	500-600	600-700			
KOIZUMI (1953)	75			358	428	523				
PÉCSI (1962)	100			350-360	420-430, 460-520	520-550		360 metathomsonite	930-960	
PÉCSI (1968)			250		420, 460	510, 560		460 amorphous	1010 anorthite + nepheline	
			3 moles	2 moles (crystal water)		1 mole				
BATTASVILI (1972)			120-300	310-470	470-520	550		700 amorphous	980 anorthite	
			1.5 moles	2 moles	0.5 mole	2 moles				
RELUWIJK (1972)			200	325-350 double				350-440 metaphases	520 collapse of the structure	900 plagioclase + nepheline
			3 moles	3 moles	remaining water					
BRICK (1973)		175		325	400, 440	520		520 structure collapse		
SMYKATZ, KLOSS (1974)			208	371	425-449 and 477	544		889		
IVANOVA et al. (1974)			180-270	300-400		500-600		600 amorphous	1000 anorthite + nepheline	
			2 moles	2 moles	remaining water					
DONÁTH (1974)				340	420, 440	560		400 microcrystalline	1000 total collapse of the lattice	
ULLRICH et al. (1987)			230-265		410-420, 440-460	520-560		980-1000 feldspar + nepheline		
YAMAZAKI et al. (1993)		167-184		323-332, 371-395	(410)	503-521				
		about 1/3 of water		about 1/3+1/3 of water		dehydroxyl- ation				

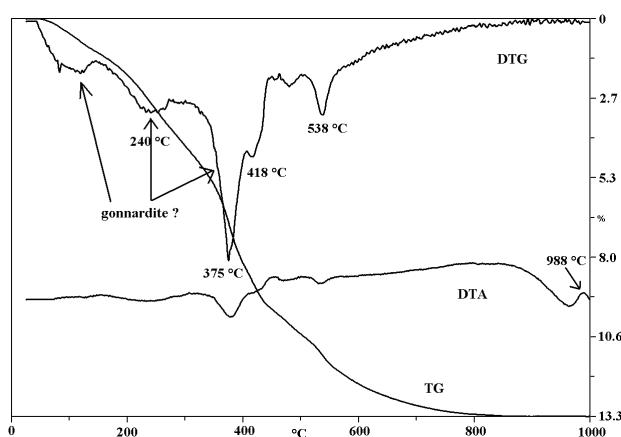
Reactions of the mineral based on publications are summarized in Table T5.5.1.1.4.

According to GOTTARDI, GALLI (1985), the last broad peak between 500 and 700 °C could be explained by the loss of hydroxyls formed by the reaction of the framework with water at lower temperature.

Sample: Prága Hill, Bazsi, Hungary

Sample mass: 134.7 mg

Heating rate: 10 °C/min

**Figure 5.5.1.1.4.** Thermoanalytic curves of a thomsonite-bearing sample with gonnardite? impurities

## 5 Silicates

5.5.1.1.5. *Scolecite*  $\text{Ca}[\text{Al}_2\text{Si}_3\text{O}_{10}]\cdot 3\text{H}_2\text{O}$ 

The structure is similar to that of natrolite, with a well-ordered Si, Al framework, Ca instead of Na, and an extra molecule of  $\text{H}_2\text{O}$ . Free apertures:  $2.6 \times 3.9 \text{ \AA}$ . Location of  $\text{H}_2\text{O}$  molecules: (1) occupy a vacant cation position, (2) are the same as in natrolite. Hydrogen bonding is between the water molecules and the network, and also with the extra-framework cation. Theoretical water content is 13.78%.

Reactions of the mineral based on publications are summarized in Table T5.5.1.1.5.

Table T5.5.1.1.5. Thermoanalytical data of scolecite

References	Temperature of dehydration (°C)								Temperature and products of transformations (°C)		
	100 200	200 300	300 400	400 500	500 600	600 700	700 800	800 900			
KOIZUMI (1953)		<b>215, 275 double</b>		460, 530 double							
PENG (1955)	170		310	470, 500					320 metascolecite	525 560 structural disintegration	1050 amorphous
			1 mole	2 moles							
PÉCSI (1962)		290	310	460, 490	540						
PÉCSI (1966)		200–220		470	490–570, 540–560	690		840	350 amorphous	1000 anorthite	
PANES et al. (1967)		280		500	560		790				
BATTASVILI (1972)		140 400		400 545	570				400 metascolecite	900 amorphous	1100 anorthite
		1 mole		1 mole	1 mole						
BRECK (1973)		225		410					490 structure decompose		910 feldspar
SMYKATZ KLOSS (1974)		268		<b>465</b>	550	645					
GOTTARDI, GALLI (1985)		240		420					420 amorphous		
		1 mole		2 moles							
ULLRICH et al. (1987)		250–350		<b>450–460, 480–500</b>	540–580				860 structural collapse	1000 anorthite and glass	
PHANKE, APPEL (1997)		230–300		405, 440–445, 490	575–580						

Mean peaks in bold.

5.5.1.1.6. *Edingtonite*  $\text{Ba}[\text{Al}_2\text{Si}_3\text{O}_{10}]\cdot 4\text{H}_2\text{O}$ 

The structure is similar to that of natrolite, but with a distinctive crosslinking of the chains. Free apertures:  $3.5 \times 3.9 \text{ \AA}$ . Three types of water are in the structure. Theoretical water content is 14.2%.

Reactions of the mineral based on publications are summarized in Table T5.5.1.1.6.

Table T5.5.1.1.6. Thermoanalytical data of edingtonite

References	Temperature of dehydration (°C)				Temperature and products of transformations (°C)	
	100 200	200 300	300 400	400 500		
PÉCSI (1962)	190		360	480	530 decompose of lattice	980?
REUWIK (1972)	160	270		450	500 celsian + unidentified phase	

Table T5.5.1.2.1. Thermoanalytical data of analcime

References	Temperature of dehydration (°C)		
	200–300	300–400	400–500
KOIZUMI (1953)		300 390	
PANES et al. (1967)			440
BRECK (1973)		200 400	
IVANOVA et al. (1974)			430
GOTTARDI, GALLI (1985)		350	
GIAMPAOLO, LOMBARDI (1994) II-type (hydrothermal) X-type (from leucite)	235 320	350–370	
KIM, KIRKPATRICK (1998) hydrothermal diagenetic	330	390	

5.5.1.2. *Zeolites with chains of single connected 4-membered rings*

In this group  $\text{H}_2\text{O}$  is accommodated in non-intersecting channels.

5.5.1.2.1. *Analcime*  $\text{Na}[\text{AlSi}_2\text{O}_6]\cdot \text{H}_2\text{O}$ 

One-dimensional channel system. Kinetic diameter:  $2.6 \text{ \AA}$ .

Reactions of the mineral based on publications are summarized in Table T5.5.1.2.1.

Reaction of the mineral at 250–400 °C: endothermic: dehydration, as a one step process.

Stoichiometric factor of the reaction: 12.2.

Sample: Csódi Hill, Dunabogdány, Hungary

Sample mass: 79.1 mg

Heating rate: 10 °C/min

Mass loss during the reaction: 8.18%

Analcime content of the sample based on the reaction:  
100%

Regarding the genetic condition, analcimes divided into five groups (primary igneous P-type, by cation exchanged from leucite X-type, hydrothermal H-type, sedimentary S-type and metamorphic M-type. H-type and X-type analcimes have very similar XRD patterns but different thermal behaviours. Dehydration of the H-type analcime takes place between 350 and 370 °C, whereas the X-type yields a wide peak between 235 and 320 °C (GIAMPAOLO, LOMBARDI 1994).

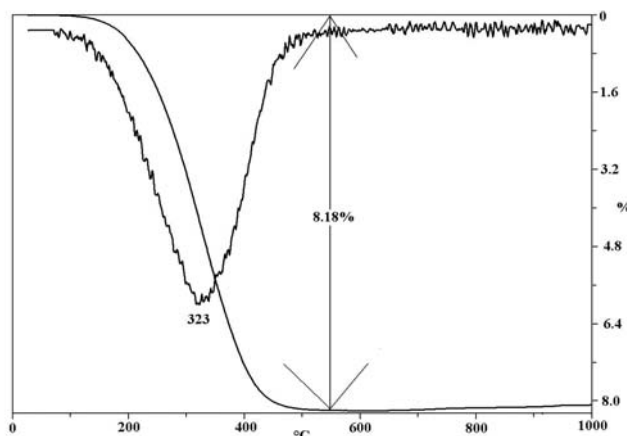


Figure 5.5.1.2.1. Thermogravimetric curves of analcime

#### 5.5.1.2.2 Laumontite $\text{Ca}[\text{Al}_2\text{Si}_4\text{O}_{12}]\cdot 4\text{--}4.5\text{H}_2\text{O}$ (fully hydrated laumontite)

„Leonhardite” a partially dehydrated laumontite, with 3–3.5 moles of  $\text{H}_2\text{O}$ , is formed reversibly by the dehydration of laumontite near room temperature in air. Equilibrium between laumontite and leonhardite occurs at 70 to 80% relative humidity. NEUHOFF, BIRD (2001) suggests that laumontite forms as ‘leonhardite’ during metamorphism and diagenesis. Water in laumontite is largely crystal-water.

The mineral has one-dimensional channel system. Free apertures:  $4.6 \times 6.3 \text{ \AA}$ .

Reactions of the mineral based on publications are summarized in Table T5.5.1.2.2.

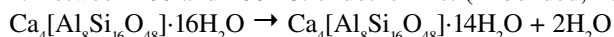
Theoretic water content: 15.3%. Stoichiometric factor of the reaction based on water content: 5.9–7.3.

Table T5.5.1.2.2. Thermoanalytical data of laumontite

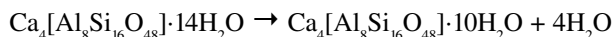
References	Temperature of dehydration (°C)								Temperature and products of transformations (°C)
	0–100	100–200	200–300	300–400	400–500	500–600	600–700	800–900	
SAKURAI, HAYASHI (1952)		85 125 double	270		470				
KOIZUMI (1953)	71		267		431, 467				
PÉCSI (1962)		140	270		460, 490				oligoclas
BATIASVILI (1972)		170		310	490		700		910 anortite + quartz
		2/3 moles		4/3 moles	2 moles		2 moles (OH)		
SMYKALZ-KLOSS (1974)			215	357	493	557			870 ?
GOTTARDI, GALLI (1985)	100		240		400				
	1 mole		5/3 moles		5/3 moles				
ULLRICH et al. (1988b)		80 140	270 350		420 460, 480–500	550		850	980 glass, feldspar

Reaction of the mineral: stepwise dehydration:

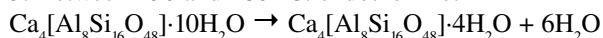
1. Between 100 and 200 °C: endothermic: (H-bonded, not bonded to the Ca cations)



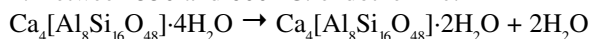
2. Between 250 and 300 °C: endothermic:



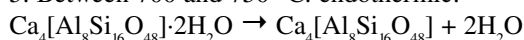
3. Between 430 and 480 °C: endothermic:



4. Between 550 and 600 °C: endothermic:

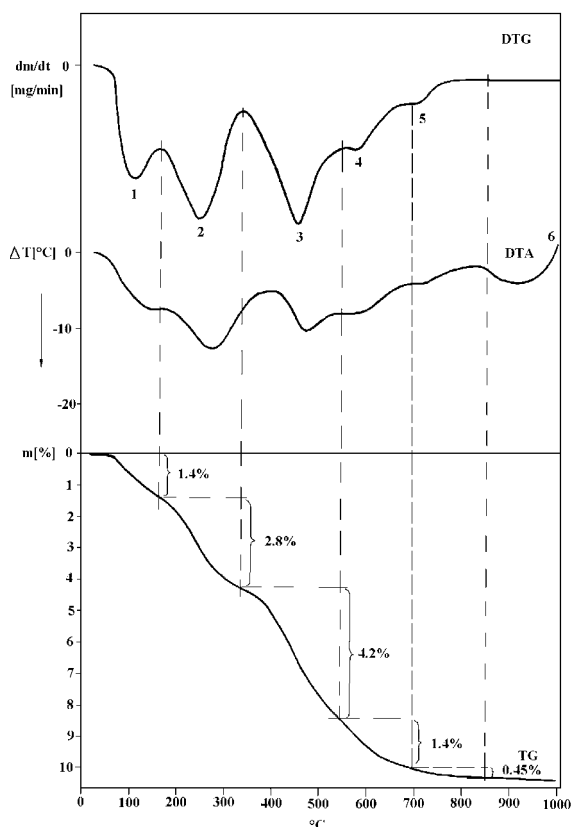


5. Between 700 and 750 °C: endothermic:



6. 900–1000 °C: exothermic: transformation to new phase.

## 5 Silicates

**Figure 5.5.1.2.2.** Thermoanalytical curves of laumontite (leonhardtite?)

Sample: Kápolnásnyék, borehole Kny-2 736.1–736.7 m, Hungary

Sample mass: 1000 mg

Heating rate: 17 °C/min

Mass loss during the reactions: 9.8%

Laumontite content of the sample based on the reactions: 72%

### 5.5.1.3. Zeolites with chains of double-connected 4-membered rings

#### 5.5.1.3.1. Gismondine $\text{Ca}[\text{Al}_2\text{Si}_2\text{O}_8] \cdot 4.4\text{--}4.5\text{H}_2\text{O}$

The  $\text{H}_2\text{O}$  molecules are connected to the Ca in the intersecting three-dimensional channel system with  $3.1 \times 4.4$  and  $2.8 \times 4.9$  Å free apertures. This mineral contains zeolitic water mainly.  $\text{H}_2\text{O}$  content varies between 22 and 22.55%.

Reactions of the mineral based on publications are summarized in Table T5.5.1.3.1.

**Table T5.5.1.3.1.** Thermoanalytical data of gismondine

References	Temperature of dehydration (°C)					Temperature and products of transformations (°C)
	0 100	100 200	200 300	300 400	800 900	
PÉCSI (1962)		170	240, 290	340	820 ?	
PÉCSI (1968)						1000 anorthite
REEUWIJK (1971)	0–73 73–88 88–115	115–208	208–290			After 5 intermediate phases 375 anorthite
	≈0.5, 0.75, 0.5 moles	≈1.5 moles	≈0.5 mole			
BRÜCK (1973)		140, 160, 190	270			Metastable phases, 375 feldspar
SMYKATZ-KLOSS (1974)			201	326		

#### 5.5.1.3.2 Phillipsite $(\text{K}, \text{Na}, \text{Ca})_4[(\text{Si}, \text{Al})_{16}\text{O}_{32}] \cdot 12\text{H}_2\text{O}$

The  $\text{H}_2\text{O}$  molecules are connected to the cations in the three-dimensional intersecting channels with  $4.2 \times 4.4$ ,  $2.8 \times 4.8$  and  $3.3$  Å free apertures.

Reactions of the mineral based on publications are summarized in Table T5.5.1.3.2.

**Table T5.5.1.3.2.** Thermoanalytical data of phillipsite

References	Temperature of dehydration (°C)				Temperature and products of transformations (°C)	
	0 100	100 200	200 300	300 400		
HOSS, ROY (1960)					245 metaphillipsite	345 feldspar
KOIZUMI (1960)					260 wairakiite	
DONÁTH, SIMÓ (1966)			250 double	360		1000 anorthite
PÉCSI (1968)						1000 nepheline
BRECK (1973)		100	200	300	160–200 new structure	
GOTTARDI, GALLI (1985)	70	120, 140, 180	(250, 280 shoulders)	320	400 destroyed	

The stepwise dehydration of the mineral based on own measurement:

1. Between 200 and 300 °C: endothermic (with an inflexion on the low temperature side): loss of about 8 moles of zeolitic and crystalline water.

2. Between 300 and 400 °C: endothermic double peak: loss of about 4 moles of crystalline water.

Theoretical water content of the mineral is about 16.5%.

Sample: Prága Hill, Bazsi, Hungary

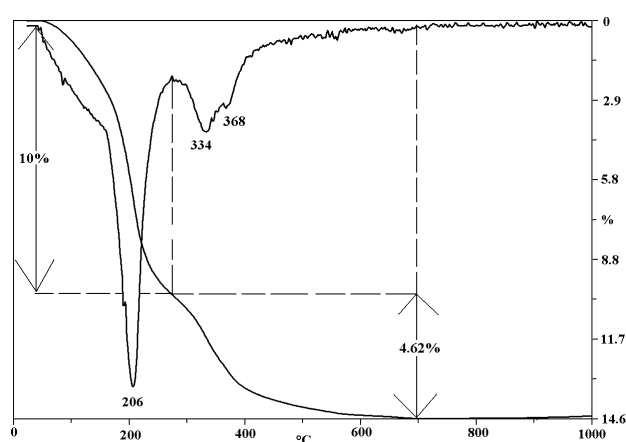
Sample mass: 105.3 mg

Heating rate: 10 °C/min

Mass loss during the reactions: 14.62%

Phillipsite content of the sample based on water content:

≈89%

**Figure 5.5.1.3.2.** Thermogravimetric curves of phillipsite

#### 5.5.1.3.3. Harmotome $Ba_2(Ca_{0.5}Na)[Al_6Si_{10}O_{32}]\cdot 12H_2O$

Channel system is three-dimensional with the same free apertures as phillipsite. The water is partly zeolitic type. Location of  $H_2O$  molecules is coordinated to the Ba ion. Dehydration is stepwise. Theoretical water content is 14.5–15.5%.

Reactions of the mineral based on publications are summarized in Table T5.5.1.3.3.

**Table T5.5.1.3.3.** Thermoanalytical data of harmotome

References	Temperature of dehydration (°C)			Temperature and products of transformations (°C)	
	100–200	200–300	300–400		
PÉCSI (1962)					>600 double structure decomposition and transformation
BRECK (1973)	170 190			250 new structure	700 celsian formation
IVANOVA et al. (1974)	200		350	750	
GOTTARDI, GALLI (1985)	120	230	320		750 new phase

#### 5.5.1.4. Zeolites with chains of 5-membered rings

##### 5.5.1.4.1 Mordenite $(Na,Ca,K)_6[AlSi_5O_{12}]_8\cdot 28H_2O$

Two-dimensional channel system with  $6.7\times 7.0$  and  $2.9\times 5.7$  Å free apertures.

Contains zeolitic water mainly in classic sense. Water content: between 12–14.5%

Reactions of the mineral based on publications are summarized in Table T5.5.1.4.1.

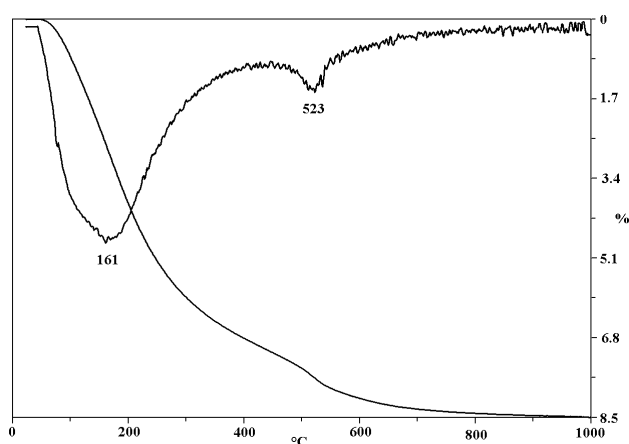
The dehydration occurs in one broad step up to 700 °C with the peak maximum at about 150 °C and another little peak at about 550 °C. In some cases the interpretation of the latter corresponds to dehydroxylation.

## 5 Silicates

**Table T5.5.1.4.1.** Thermoanalytical data of mordenite

References	Temperature of dehydration (°C)						Temperature and products of transformations (°C)
	0 100	100 200	200 300	300 400	400 500	500 600	
SAKURAI, HAYASHI (1952)		<b>110–170–240</b>					
KOIZUMI (1953)		<b>90–170</b>					
PÉCSI (1963)		+		540		780	
NASEDKIN, NASEDKINA (1967)		<b>150</b>					
BATIASVILI (1972)			<b>220</b>			700–800	
BRECK (1973)		<b>25–300</b>					
IVANOVA et al. (1974)		<b>200</b>					1000–1200 new phase
GOTTARDI, GALLI (1985)	60	<b>160</b>					
ULLRICH et al. (1988)			<b>190–240</b>		600–620		1000 glass-phase and feldspar in trace

Mean peaks in bold.



Sample: Mád, Hungary  
 Sample mass: 163.6 mg  
 Heating rate: 10 °C/min  
 Mass loss during the reactions: 8.5%  
 Mordenite content of the sample based on water content: 60–70%

**Figure 5.5.1.4.1.** Thermogravimetric curves of mordenite

### 5.5.1.5 Zeolites with sheets of 4–4–1–1 structural units

#### 5.5.1.5.1. Heulandite $(Ca,Na,K,Sr)_9[(Si,Al)_{36}O_{72}] \cdot nH_2O$ ( $n=22–26$ )

Two-dimensional channel system of three relatively open channels with  $4.0 \times 5.5$ ,  $4.4 \times 7.2$ ,  $4.1 \times 4.7$  Å free apertures. Contains zeolitic water mainly. Dehydration during a broad thermal reaction with a sharp peak at about 300 °C in addition to zeolitic water, because some of the water molecules are closer to calcium than others weakly held water molecules. Water content is between 13–17%.

Reactions of the mineral based on publications are summarized in Table T.5.5.1.5.1.

**Table T5.5.1.5.1.** Thermoanalytical data of heulandite

References	Temperature of dehydration (°C)						Temperature and products of transformations (°C)		
	0 100	100 200	200 300	300 400	400 500	500 600			
KOIZUMI (1953)		<b>120, 170</b>		<b>341</b>					
MUMPTON (1960)			230	<b>345</b>			≈230 heulandite B	350 amorphous	
PÉCSI (1962)		191		340, 360					
PÉCSI (1966)			220		420	520	300 wairakite and SiO <sub>2</sub>		
PANES et al. (1967)			200–220	340–360	410		about 500		
MERKLE, SLAGHTER (1968)			215	<b>372</b>			215 heulandite B	372 amorphous	
PÉCSI DONÁTH (1968)									1000 bytownite
BATIASVILI (1972)			240	<b>400</b>				460 amorphous	1000 bytownite
ALLJETH (1972)							215 phase I	≈400 phase B	450 complete destruction

**Table T5.5.1.5.1.** Continuation

References	Temperature of dehydration (°C)						Temperature and products of transformations (°C)		
	0-100	100-200	200-300	300-400	400-500	500-600			
BRECK (1973)		25-300		300			215 heulandite B	>360 structure collapse	
IVANOVA et al. (1974)		<b>230</b>			350-540				
SMYKATZ KLOSS (1974)	97	<b>176</b>			470		392	787	887
GOTTARDE, GALLI (1985)		<b>50-200</b>	<b>280</b>	up to 900					
		11 moles	8 moles	5 moles					
ULLRICH et al. (1988)			200-265	<b>340-400</b>				480	1000 glass phase and feldspar trace

Mean peaks in bold.

		(020) spacing Å
Heulandite A	Initial phase	8.97-9.05
Heulandite I	Intermediate	
	collapsed phase	8.73-8.87
Heulandite B	Collapsed phase	8.30-8.35

### 5.5.1.5.2. Clinoptilolite $(K,Na,Ca)_6[(Si,Al)_{36}O_{72}] \cdot nH_2O$ ( $n=20-24$ )

Clinoptilolite is defined as the series with the similar framework as heulandite, but the ratio of Si:Al is >4.0 (silica rich heulandite). X-ray patterns are not suitable for separating clinoptilolite and heulandite. Kinetic diameter: 3.5 Å. Water content of clinoptilolite: 13-16%.

The high silica content can be correlated to increased thermal stability and the appearance of intermediate phases. Thermal stability has been used by some investigators to distinguish clinoptilolite from heulandite (heulandite is amorphous above 400 °C, while the clinoptilolite structure is stable up to 750 °C), but it seems to be also an unclear criterion because there are intermediate properties. The different Si/Al ratio and the extra-framework cation composition play a role in the thermal behavior of clinoptilolite or heulandite.

**Table T5.5.1.5.2.** Thermoanalytical data of clinoptilolite

References	Temperature of dehydration (°C)		Temperature and products of transformations (°C)	
	100-200	200-300		
BRECK (1973)	125-300			
ULLRICH et al. (1987)	125	<b>165-250</b>	380-490	1000 glass phase, traces of feldspar and cristobalite

Mean peaks in bold.

Reactions of the mineral based on publications are summarized in Table T5.5.1.5.2.

Reaction of clinoptilolite:

1. between 30 and 900 °C: endothermic: broad dehydration with a peak maximum at about 100 °C.

Stoichiometric factor based on the dehydration: 6.3-7.5.

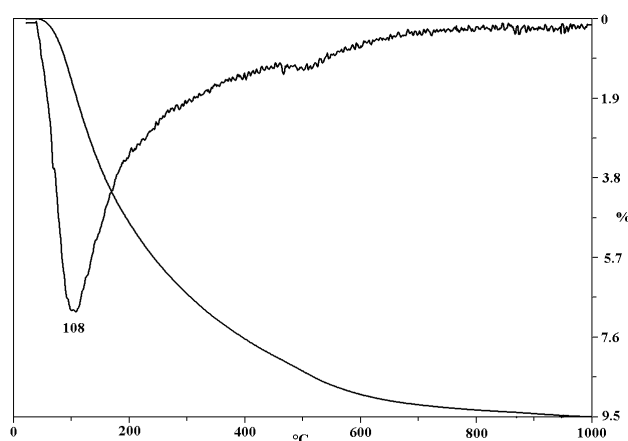
Sample: Mád, Hungary

Sample mass: 155.5 mg

Heating rate: 10 °C/min

Mass loss during the reactions: 9.54%

Clinoptilolite content of the sample based on water content: 61-72%

**Figure 5.5.1.5.2.** Thermogravimetric curves of clinoptilolite

## 5 Silicates

5.5.1.5.3. *Stilbite*  $(Na, Ca)_9[Al(Si, Al)_{36}O_{72}] \cdot 27-30 H_2O$ 

Two-dimensional channel system with  $4.1 \times 6.2$  and  $2.7 \times 5.7 \text{ \AA}$  free apertures is in the structure. It consists of both zeolitic and crystal-water, water molecules are coordinated with  $Ca^{2+}$  or  $Na^+$  ions. The water content is about 17–19%.

Reactions of the mineral based on publications are summarized in Table T5.5.1.5.3.

**Table T5.5.1.5.3.** Thermoanalytical data of stilbite

References	Temperature of dehydration (°C)						Temperature and products of transformations (°C)	
	100–200	200–300	300–400	400–500	700–800	800–900		
KOIZUMI (1953)	100, <b>191</b>	261						
PÉCSI (1962)		230, 290					870 anorthite, bywtonite	870 anorthite, bywtonite
BATIASVILI (1972)		<b>250</b>					470–550	
BRECK (1973)	191	262					500	
NASEDKINA–NASEDKIN (1967)		210			740		450 490	
SMYKATZ KLOSS (1974)	100	<b>200–204, 276–288</b>				850	481 510	
IVANOVA et al. (1974)		<b>200–230</b>					470–550	
GOTTARDI, GALLI (1985)	(70)	<b>175</b> 15 moles	250 13 moles	500 1.5 moles probably hydroxyl				
ULLRICH et al. (1988)	100–140	<b>200–280</b>	280–320				445–500	960 glass phase, traces of feldspar and cristobalite

Mean peaks in bold.

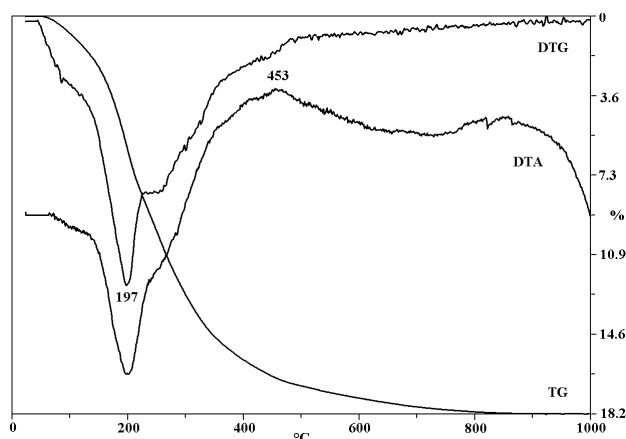


**Figure 5.5.1.5.3.** Thermoanalytical curves of stilbite

Reactions of stilbite:

1. between 50 and 470 °C: endothermic: dehydration (with two maximum at about 200 and 330 °C):  
Loss of the major part of the water content.
2. between 450 and 510 °C: exothermic: phase transition and loss of the rest of the water

Stoichiometric factor based on the whole water content: 5.4–5.9.

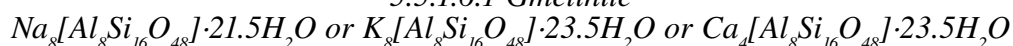
Sample: Csódi Hill, Dunabogdány, Hungary

Sample mass: 99.3 mg

Heating rate: 10 °C/min

Mass loss during dehydration: 18.22 %

Stilbite content of the sample based on the dehydration: 98–100%

5.5.1.6. *Zeolites with cages and double cages of 4-, 6- and 8-membered rings*5.5.1.6.1 *Gmelinite*

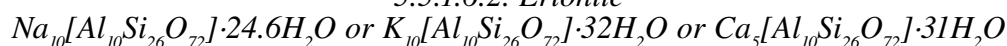
The mineral has a three-dimensional channel system with a 7 and  $3.6 \times 3.9 \text{ \AA}$  free apertures. Largely contains zeolitic water. Water content is about 19–20%.

Reactions of the mineral based on publications are summarized in Table T5.5.1.6.1.

**Table T5.5.1.6.1.** Thermoanalytical data of gmelinite

References	Temperature of dehydration (°C)			Temperature and products of transformations (°C)	
	100 200	200 300	300 400		
PÉCSI (1962)		1	340, 370	340 change in the lattice	
PÉCSI (1966)		240	<b>340</b> , 380	340 change in the lattice	1000 oligoclas
BRECK (1973)				>300 structure change	
GOTTARDI, GALLI (1985)	100 (shoulder), 175		300		

Mean peaks in bold.

**5.5.1.6.2. Erionite**

The mineral has a three-dimensional channel system with a 3.6×5.2 Å free apertures.

Reactions of the mineral based on publications are summarized in Table T5.5.1.6.2.

**Table T5.5.1.6.2.** Thermoanalytical data of erionite

References	Temperature of dehydration (°C)			Temperature and products of transformations (°C)
	100 200	200 300	300 400	
BATIASVILI (1972)			360	920 amorphous
BRECK (1973)	50 400			920
GOTTARDI, GALLI (1985) hydrothermal sedimentary	100, 140, 170	250 (shoulder)		
	25–300			

**5.5.1.6.3. Chabasite**( $Ca_{0.5}, Na, K$ ) $_4[Al_4Si_8O_{24}]\cdot 12H_2O$ 

The mineral has a three-dimensional channel system with a 3.7×4.2 and 2.6 Å free apertures. Largely contains zeolitic water. Theoretical water content: 18–23%.

Reactions of the mineral based on publications are summarized in Table T5.5.1.6.3.

**Table T5.5.1.6.3.** Thermoanalytical data of chabasite

References	Temperature of dehydration (°C)						Temperature and products of transformations (°C)
	0 100	100 200	200 300	300 400	400 500	500 600	
KOIZUMI (1953)		95–160–240					
PÉCSI (1962)			220				870 anorthite, bytownite
SOKOLOVA (1967)			270–280				860–870
PANES et al. (1967)			200	400			860
PASSAGLIA (1970)		100–170	210–225				820–875 exothermic destruction of the framework
BATIASVILI (1972)			230				750–850 structural transformation
BRECK (1973)		25 300					900
IVANOVA et al. (1974)			220				750–850 amorphous
SMYKATZ, KLOSS (1974)		108 120, 172–183		312 350	495	520	650 700, 882 886
GOTTARDI, GALLI (1985) Na-chabasite Ca-chabasite Sr-Al-chabasite	80	170	250 220, 280				
		100, 150					
		160					
		(shoulder), 200					
ULLRICH et al. (1987)		150	200 255				690, 750–975 glass phase with anorthite trace

## 5 Silicates

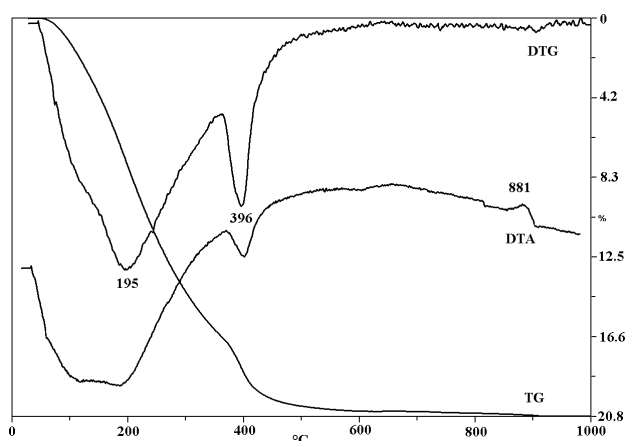


Figure 5.5.1.6.3. Thermoanalytical curves of chabasite

Thermal reaction of chabasite:

1. The dehydration of chabasite is characterised by a double endothermic peak at 200 and 350 °C up to 900 °C.
2. The exothermic peak at 800–900 °C is the result of the destruction of the framework.

Stoichiometric factor based on the whole water content: 4.3–5.6.

Sample: Csódi Hill, Dunabogdány, Hungary

Sample mass: 114.3 mg

Heating rate: 10 °C/min

Mass loss during dehydration: 20.76%

Chabasite content of the sample based on dehydration: 89–100%

The thermal curves are influenced by the dominant cation present in the chabasite.

#### 5.5.1.6.4. Faujasite $(Na, Ca, Mg)_2[(Si, Al)_{12}O_{24}] \cdot nH_2O$ ( $n \approx 16$ )

The mineral has a three-dimensional channel system with a 7.4 and 2.2 Å free aperture.

Theoretical water content about: 25–27.5%.

Reactions of the mineral based on publications are summarized in Table T5.5.1.6.4.

Table T5.5.1.6.4. Thermoanalytical data of faujasite

References	Temperature of dehydration (°C)		Temperature and products of transformations (°C)
	100 200	200 300	
BRECK (1973)		50–400	770–795
GOTTARDI, GALLI (1985)	175	300	
ÜLLRICH et al. (1987)		190–250	900–980

#### 5.5.1.7. Thermoanalytical data of other zeolites

Thermoanalytical data of other zeolites are based on data of GOTTARDI, GALLI (1985) are summarized in Table T5.5.1.7.

Table T5.5.1.7. Thermoanalytical data of other zeolites

Mineral	Temperature of dehydration (°C)								Temperature and products of transformations (°C)
	0 100	100 200	200 300	300 400	400 500	500 600	600 700	800 900	
Wairakite				360		500			
Yugawaralite	70–100		200–300		450				
	2 moles		2 moles		4 moles				
Roggianite	113							874	910 exotherm
	loss of zeolitic water							loss of hydroxyl	recrystallization
Garronite	60	170		320					
Amicite	60	140		320					
Gobhinsite	80 (shoulder)	150	200 400 continuous						
Wellsite		120	230	350					
Merlionite		5 peaks between 25 and 450							
Paulingite		100	200	380					
Levyne	70	180 (shoulder)		300					
Offretite		125, 195							
Dachiardite	100	200 (shoulder)							
Epistilbite	100		250	300, 345					
Ferrierite	80	≈160 (shoulder)	240				680		
Bikitaile			260						750 spodumen and eneryptite
Stellerite	70	175	25				680 probably hydroxyl		
Barrerite	50	150	200				500–900 probably hydroxyl		
Brewsterite	50 (shoulder)	190	260	380					
Cowlesite	100 (shoulder)	150		300					

References for zeolites: 11: brewsterite, 9: amicitite, 10: heulandite, 12: heulandite, clinoptilolite, 29: mesolite, 30: yugawaralite, 71: natrolite, mesolite, scolecite, thomsonite, heulandite, desmiste (stilbite), leonhardite (laumontite), mordenite, chabasite, erionite, 79: natrolite, edingtonite, 104: heulandite group minerals, 108: chiavennite 121, 122: heulandite, clinoptilolite, 144: analcime, heulandite, 165: stilbite, 189, 196: analcime, 197, 218, 219: phillipsite, gonnardite, 220: heulandite, 255: chabasite, phillipsite, 308: bikitaite, 311: heulandite-stilbite group, 317: phillipsite, 351: laumontite, 352: laumontite, 392: rhodesite, mountainite, 398: analcime, 413, 443: stilbite, 496: phillipsite, gismondine, harmotome, chabasite, gmelinite 512: partheite, 513: natrolite, mesolite, thomsonite, gonnardite, scolecite, mordenite, heulandite, desmiste (stilbite), chabasite, 526: natrolite, mesolite, scolecite, 538: stilbite, 539: scolecite, 549: heulandite type minerals, 568: analcime, 582: clinoptilolite, 584: bikitaite, 591: natrolite, scolecite, mordenite, laumontite, analcime, thomsonite, mesolite, heulandite, 592: clinoptilolite, scolecite, phillipsite, laumontite, heulandite, epistilbite, 601: natrolite-group, 644: clinoptilolite, 660: paulingite, 721: clinoptilolite, heulandite, 738: heulandite, 750: desmine, 768: clinoptilolite, 780: mordenite, 789: laumontite, 805: natrolite, 810: natrolite, scolecite, chabasite, heulandite, desmiste (stilbite), heulandite, laumontite, thomsonite, mesolite 814: roggianite, 815: chabasite, 816, 817: levyne, erionite, 818: phillipsite 852: analcime, natrolite, mesolite, thomsonite, scolecite, edingtonite, gismondine, laumontite, mordenite, heulandite, stilbite, epidesmine, epistilbite, phillipsite, harmotome, gmelinite, chabasite, levynee, faujasite, 853: chabasite, desmiste (stilbite), natrolite, 854: heulandite, scolecite, 855: thomsonite, analcime, chabasite, natrolite, gmelinite, scolecite, mesolite, phillipsite, harmotome, gismondine, mordenite, clinoptilolite, laumontite, brewsterite, stilbite, 858: natrolite, scolecite, mesolite, 870: natrolite, scolecite, mesolite, 900: gismondite, 901: natrolite, mesolite, scolecite, thomsonite, gonnardite, edingtonite, 934: phillipsite, 938: yugawaralite, 939, 981: chabasite, 991, 1006: natrolite, scolecite, thomsonite, laumontite, heulandite, stilbite, gismondite, chabasite, 1019: chabasite, 1024: laumontite, 1037, 1096: natrolite, thomsonite, scolecite, 1097: heulandite, stilbite, clinoptilolite, 1098: mordenite, laumontite, chabasite, faujasite, 1174: thomsonite, 1175: fibrous zeolites

### 5.5.2. Other tectosilicates

The H<sub>2</sub>O content of nepheline varies from 0.05 to 0.39 wt% and it is mainly located in vacancies in the alkali site.

In the case of ammonioleucite the TG curve indicates only one stage of weight loss between 415 and 550 °C. This weight loss is attributed to the decomposition of the ammonium ion to NH<sub>3</sub> + 1/2H<sub>2</sub>O.

References: 42: nepheline, 102: hyalophane, buddingtonite, 493: ammonioleucite, 510: buddingtonite

## 6. CARBONATES

The general reaction of carbonates is the following: MeCO<sub>3</sub> → MeO + CO<sub>2</sub>

### 6.1. Water free simple carbonates

The most important reaction of simple carbonate point of view of thermogravimetry is the thermal decomposition (Table T6.1a). Other reactions mainly may be shown only on DTA curves (Table T6.1b).

**Table T6.1a.** The most important reactions of simple carbonate minerals

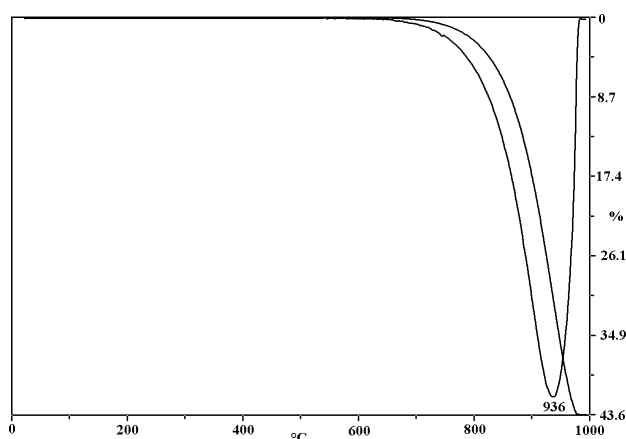
Mineral	Formula	Thermal dissociation °C	Stoichiometric factor	Notice
Siderite	FeCO <sub>3</sub>	540-555	2.63	in nitrogen
Otavite	CdCO <sub>3</sub>	440-450	3.92	
Cerussite	PbCO <sub>3</sub>	407-427	6.07	
Smithsonite	ZnCO <sub>3</sub>	470-590	2.84	
Rhodochrosite	MnCO <sub>3</sub>	515-680	2.61	in nitrogen
Magnesite	MgCO <sub>3</sub>	625-643	1.92	
Calcite	CaCO <sub>3</sub>	895	2.27	
Aragonite	CaCO <sub>3</sub>	895	2.27	
Strontianite	SrCO <sub>3</sub>	1142-1151	3.36	
Natrite	Na <sub>2</sub> CO <sub>3</sub>	900-1200	2.41	
Witherite	BaCO <sub>3</sub>	1195	4.48	

## 6 Carbonates

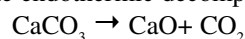
**Table T6.1b.** Further reactions of simple carbonates

Reaction	Mineral	Temperature (°C)	Polymorphic transition		
Melting	cerussite	897			
	natrite	820			
	trona	800 900			
	kalicinite	900			
Phase transition	witherite	806	orthorhombic	→	tetragonal
	strontianite	924	orthorhombic	→	hexagonal
	aragonite	450	orthorhombic	→	trigonal
Oxidation	siderite	475–760			
	rhodochrosite	655–870	to $\text{Mn}_2\text{O}_3$		
Reduction	rhodochrosite	950 1050	$\text{Mn}_2\text{O}_3$ ? $\text{Mn}_3\text{O}_4$		

Temperature of decomposition depends on the quantity of the mineral, on substitution and on crystallinity. The slope of the PA curve is very steep. Temperature shifts when the amount of calcite changes by an order of magnitude in the case of calcite is about 100 °C.

6.1.1. Calcite  $\text{CaCO}_3$ **Figure 6.1.1a.** Thermogravimetric curves of calcite

The endothermic decomposition reaction:



Stoichiometric factor of the reaction: 2.27.

Sample (Figure 6.1.1a): Vöröshíd, Gerecse Hill, Hungary

Sample mass: 193.9 mg

Heating rate: 10 °C/min

Mass loss during dissociation: 43.56%

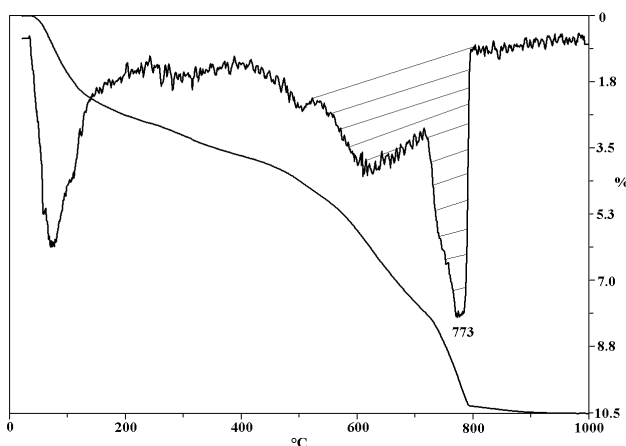
Calcite content of the sample based on dehydration: 99%

The temperature of calcite with lower crystallinity is lower by about 20–50 °C than that of the well crystallized variation. Another indicator of the thermal decomposition process of the calcite structure disintegrated by the weathering process is that the normal single-step reaction will gradually turn into a double-stage reaction (see Figure 6.1.1b).

Sample (Figure 6.1.1b): Udvari, borehole Ud-2a 10.8–11.0 m, Hungary

Sample mass: 83.1 mg

Heating rate: 10 °C/min

**Figure 6.1.1b.** Thermogravimetric curves of a strongly weathered calcite

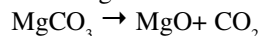
This sample was taken from a palaeosoil horizon in a Quarternary loess section. The soil formation in this environment is characterized by the dissolution and gradual leaching of  $\text{CaCO}_3$  from the loess and the carbonate has very distinct structural disorders.

Substitution in a calcite type lattice is limited. The iron-, magnesium- and manganocalcite have a very similar thermoanalytical curve to that of calcite, however, during heating the manganocalcite sample becomes black.

Aragonite changes into calcite at about 455 °C. The TG curves showed that in a number of cases the solid solution structure contained occluded water that was released during the transformation. (see chapter Water bound in solid solution and Figure 39). The decomposition is the same as that of calcite.

### 6.1.2. Magnesite $\text{MgCO}_3$

The endothermic decomposition takes place at 620–650 °C with the following reaction:



Stoichiometric factor of the reaction: 1.92.

Decomposition temperatures decrease markedly with increasing Fe substitution.

Sample: Hnusta, Slovakia

Sample mass: 900 mg

Heating rate: 10 °C/min

Mass loss during dissociation: 49.2%

Magnesite content of the sample based on decomposition: 95%

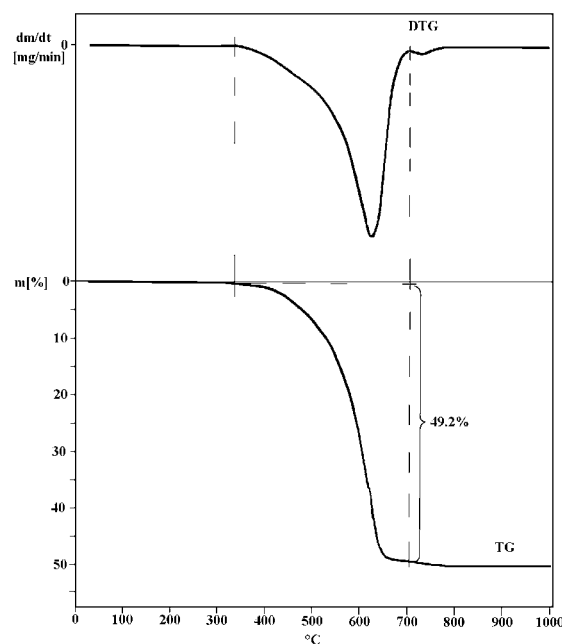
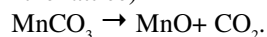


Figure 6.1.2. Thermogravimetric curves of magnesite

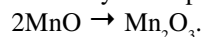
### 6.1.3 Rhodochrosite $\text{MnCO}_3$

Reactions of the mineral:

1. endothermic decomposition reaction at 515–680 °C: (temperature at which decarbonation occurs is raised by the presence of Ca and Mg while lowered if iron substitutes manganese in the lattice)



2. immediately overlaps the oxidation:



stoichiometric factor for reactions 1 and 2 in the case of complete oxidation: 3.23

3. at about 900 °C: endothermic reduction:



Sample: Úrkút, Hungary

Sample mass: 112.5 mg

Heating rate: 10 °C/min

Mass loss during reactions 1 and 2: 10.5%

Rhodochrosite content of the sample based on these reactions: 34%

Other thermally active minerals in the sample: goethite with Mn content, celadonite, kutnahorite

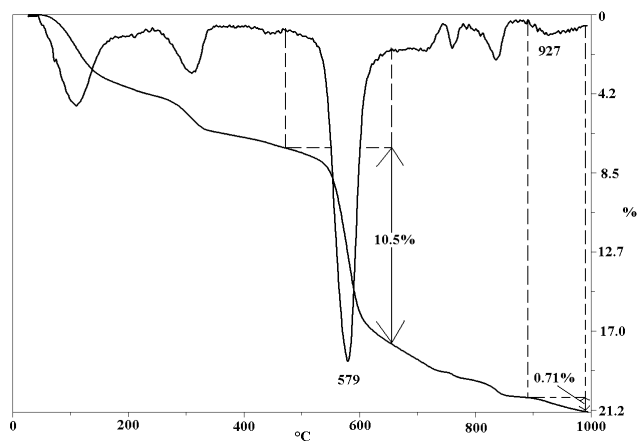
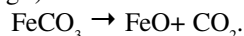


Figure 6.1.3. Thermogravimetric curves of rhodochrosite

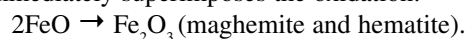
### 6.1.4. Siderite $\text{FeCO}_3$

Reactions of the mineral:

1. endothermic decomposition reaction at 500–550 °C: (decomposition temperature is dependent on substitution of  $\text{Mn}^{2+}$ ,  $\text{Mg}^{2+}$ )



2. immediately superimposes the oxidation:



## 6 Carbonates

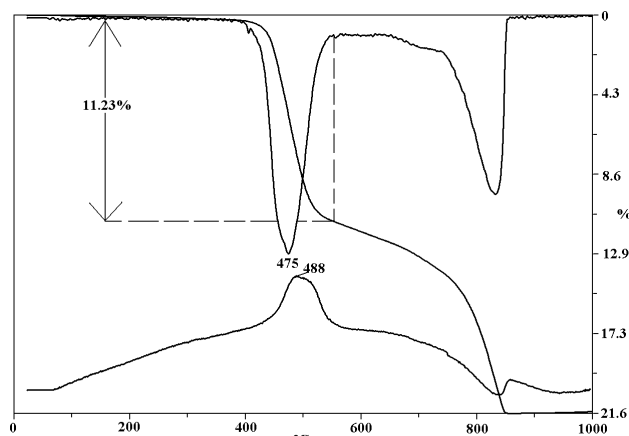


Figure 6.1.4a. Thermoanalytical curves of siderite

The endothermic and exothermic peaks are often overlapped and — especially in the case of small quantity of the mineral — compensated by each other. In this case no reaction can be seen in the DTA curve, but a well defined reaction occurs in the DTG curve (Figure 6.1.4.b).

Endothermic: 82.8 kJoule/mole, mass loss 18%.

Exothermic: 138.0 kJoule/mole, mass increasing: 6.9%.

Sample: Smolnik, Slovakia

Sample mass a): 200 mg

Sample mass b): 100 mg

Sample mass c): 50 mg

Sample mass d): 10mg

All samples are complemented to 1000 mg with  $\text{Al}_2\text{O}_3$

Mass loss during the reactions a): 6.0%

Mass loss during the reactions b): 3.0%

Mass loss during the reactions c): 1.5%

Mass loss during the reactions d): 0.35%

Siderite content of the original sample based on these reactions a): 97%

Siderite content of the original sample based on these reactions b): 97 %

Siderite content of the original sample based on these reactions c): 97%

Siderite content of the original sample based on these reactions d): more than 100%

Stoichiometric factor for reactions 1 and 2 in the case of complete oxidation: 3.22.

Higher content of Mg in siderite shifts the maximum of this reaction towards higher temperatures (breunnerite, pistomesite).

Sample: Chile

Sample mass: 113.0 mg

Heating rate: 10 °C/min

Mass loss during reactions 1 and 2: 11.23%

Siderite content of the sample based on these reactions: 36%

Other thermally active minerals in the sample: calcite

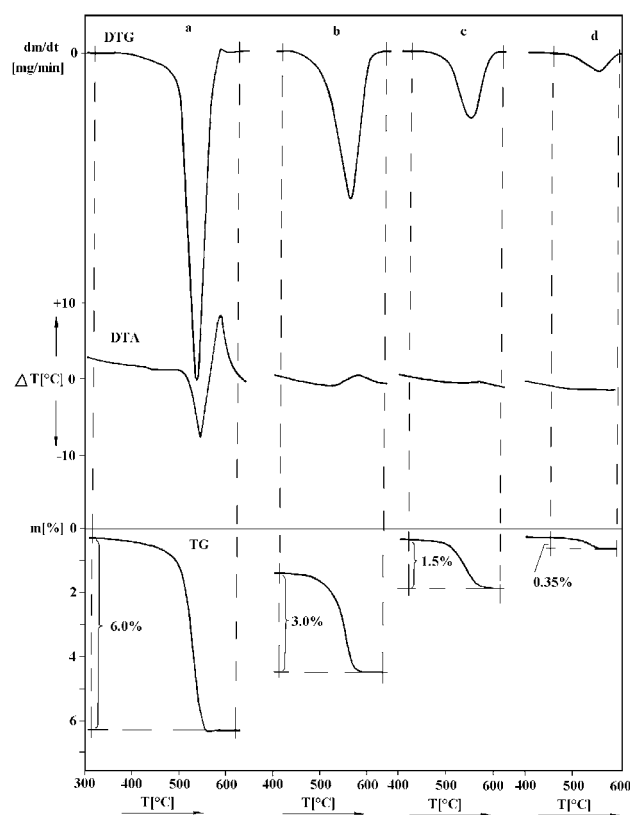


Figure 6.1.4b. Superposition of the endothermic and exothermic reactions on the DTA curve of siderite

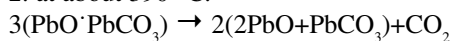
6.1.5. Cerussite  $\text{PbCO}_3$ 

Decomposition of cerussite is a complex process with intermediate phases.

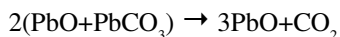
1. at about 300 °C:



2. at about 390 °C:



3. at about 430–510 °C



reactions 2 and 3 are overlapped

intermediate phases:  $6\text{PbO} + \text{O}_2 \rightarrow 2\text{Pb}_3\text{O}_4$  and later  $2\text{Pb}_3\text{O}_4 \rightarrow 6\text{PbO} + \text{O}_2$

4. at about 860–880 °C: melting of PbO

Sample: unknown  
 Sample mass: 69.3 mg  
 Heating rate: 10 °C/min  
 Mass loss during decomposition: 15.09%  
 Cerussite content of the sample based on these reactions: 92%  
 Other thermally active minerals in the sample: galena

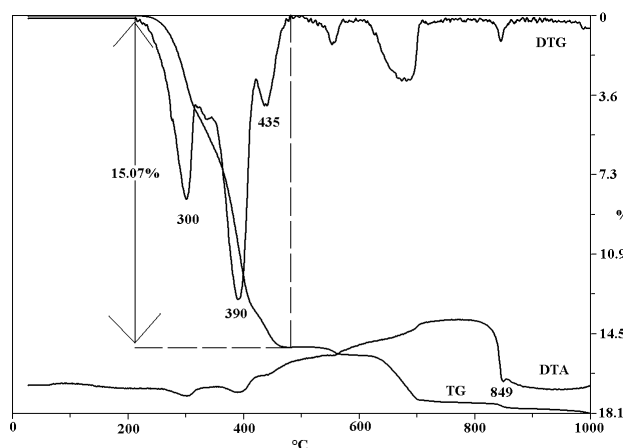


Figure 6.1.5. Thermoanalytical curves of cerussite

## 6.2. Water free double carbonates

Double carbonates according to the different bonding energy of different cations have two (or because of their real stoichiometry sometimes three) steps decomposition process (Table T.6.2.).

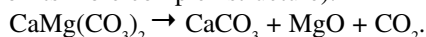
Table T6.2. The main reactions of double carbonate minerals

Mineral	Formula	Thermal dissociation (characteristic peak) °C	Thermal dissociation (second step) °C	Notice
Ankerite	$\text{FeCa}(\text{CO}_3)_2$	650–700	850–950	theoretical
Ankerite	$(\text{Mg} > \text{Fe}), \text{Ca}(\text{CO}_3)_2$	700–750	850–950	real
Kutnahorite	$\text{MnCa}(\text{CO}_3)_2$	660–730	850–950	theoretical
Kutnahorite	$(\text{Mn} > \text{Mg}), \text{Ca}(\text{CO}_3)_2$	700–800	850–950	real
Huntite	$\text{Mg}_{1.5}\text{Ca}_{0.5}(\text{CO}_3)_2$	600–650	850–950	
Dolomite	$\text{MgCa}(\text{CO}_3)_2$	750–800	850–950	

### 6.2.1. Dolomite $\text{MgCa}(\text{CO}_3)_2$

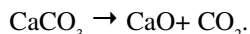
Reactions of the mineral:

1. At 750–800 °C: endothermic: (the first dolomite peak occurs at higher temperature than the magnesite reaction, because of its more complex structure):



Stoichiometric factor of the reaction: 4.2.

2. Between 840 and 950 °C: endothermic



Stoichiometric factor of the reaction: 4.2.

Sample: Gellért Hill, Budapest, Hungary

Sample mass: 267.9 mg

Heating rate: 10 °C/min

Mass loss during the first decomposition: 21.85%

Mass loss during the second decomposition: 23.22%

Dolomite content of the sample based on the first reaction: 92%

Other thermally active minerals in the sample: calcite (3%), clay mineral

In the case of a large sample mass well expressed double thermal effects of dolomite can be observed. For small samples both peaks of thermal decomposition of carbonate components occurred in very close or at almost identical temperatures.

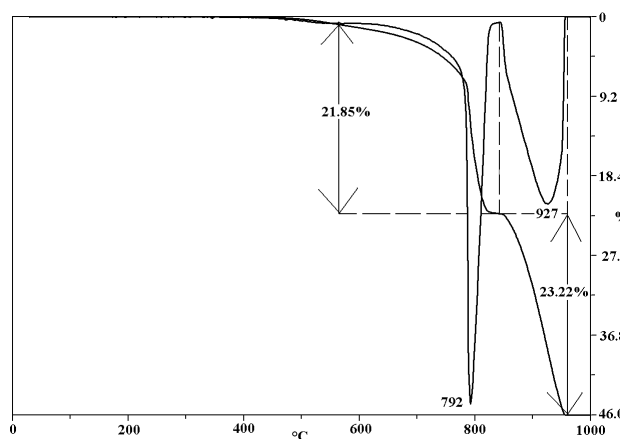


Figure 6.2.1a. Thermogravimetric curves of dolomite

## 6 Carbonates

In many cases the dissociation of dolomite produces certain irregularities.

The thermoanalytical curves indicate also the crystallinity stage of dolomite. Well crystalline dolomite has a double stage decomposition in the loess (Figure 6.2.1b) but the two step merge into one another by the process of solution during the soil formation in the palaeosoil (Figure 6.2.1c). The two samples have very similar carbonate composition according to other analytical methods (Table T6.2.1).

**Table 6.2.1.** Composition of carbonate in loess and palaeosoil analysed by different methods

Analytical method	4.8–5.0 m	(well crystallised)	31.3–31.5 m	(weathered)
	calcite	dolomite	calcite	dolomite
	%			
XRD	14	10	8	13
Calcimetry	10	12	9	8
DTG	15	11	22	
DDTG	15	11	13	9

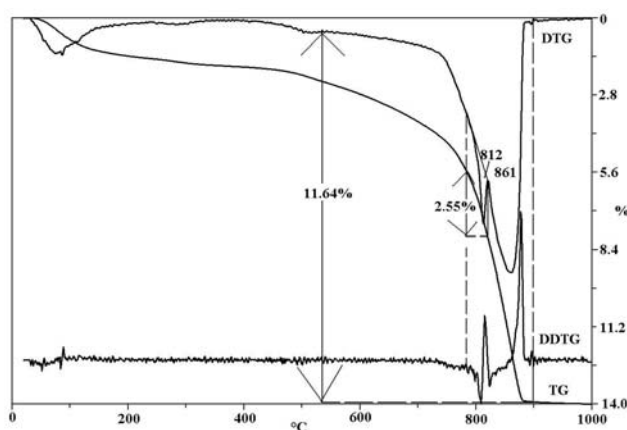


**Figure 6.2.1b.** Thermogravimetric curves of dolomite in loess

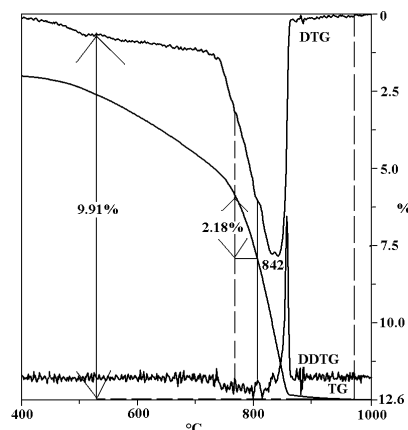


**Figure 6.2.1c.** Thermogravimetric curves of dolomite in palaeosoil

Sample (Figure 6.2.1b): Udvari, borehole Ud-2a 4.8–5.0 m, Hungary

Sample mass: 193.6 mg

Heating rate: 10 °C/min

Mass loss during the first decomposition based on the DDTG (the first decarbonation peak of dolomite sits on the peak of  $\text{CaCO}_3$  decomposition): 2.55%

Mass loss during the whole decomposition: 11.64%

Dolomite content of the sample based on the first reactions: 11%

Other thermally active minerals in the sample: calcite (15%), illite, montmorillonite, chlorite, gypsum

Sample (Figure 6.2.1c): Udvari, borehole Ud-2a 31.3–31.5 m, Hungary

Sample mass: 164.1 mg

Heating rate: 10 °C/min

Mass loss during the first decomposition based on the DDTG: 2.18%

Mass loss during the whole decomposition: 9.91%

Dolomite content of the sample based on the first reactions: 9%

Other thermally active minerals in the sample: calcite (13%), illite, montmorillonite, chlorite, kaolinite, goethite

Soluble salts lowered the first decomposition peak of dolomite (Figure 6.2.1d). As much as 0.1% of NaCl perceptibly decreased the temperature of this reaction. The curves are similar to that of the mixture of calcite and magnesite. Removal of the salts by washing with distilled water resulted in the usual appearance of dolomite peaks appeared.

Sample (Figure 6.2.1d): Egypt

Sample mass: 112.1 mg

Heating rate: 10 °C/min

Mass loss during the whole decomposition: 35.68%

Dolomite content of the sample based on the whole mass loss: 75%

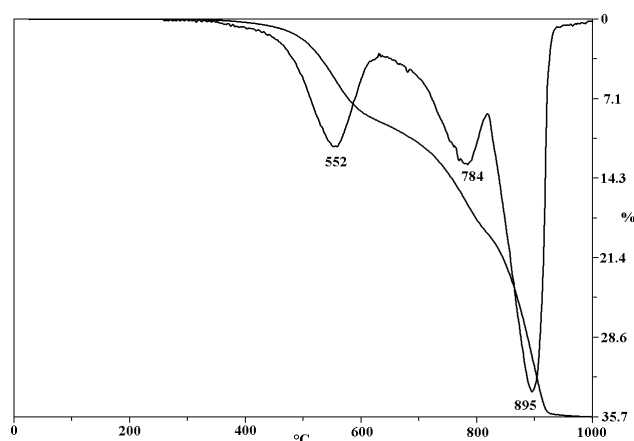


**Figure 6.2.1d.** Thermogravimetric curves of “protodolomite” (Mg-poor dolomite) bearing rock with halite content

Sample(Figure 6.2.1e): Egypt

Sample mass: 75.8 mg

Heating rate: 10 °C/min

Mass loss during the whole decomposition: 37.55%

Dolomite content of the sample based on the whole mass loss: 79%

In shallow lakes, as in bottom muds of Lake Balaton autochthonous disordered high magnesium calcite with up to 20 mol per cent  $\text{MgCO}_3$  [(014)-reflection  $2\theta=30.00^\circ$ ] and “protodolomite” [ $2\theta=30.6\text{--}30.85^\circ$ , mean composition of  $\text{Ca}_{1.05}\text{Mg}_{0.95}(\text{CO}_3)_2$ ] formed at low water levels during periods of high evaporation from solution with higher Mg/Ca ratios. The shape of thermal curves is very variable.

Sample(Figure 6.2.1f): Borehole Tó-19 0.5–0.6 m Lake Balaton, Hungary

Sample mass: 109.9 mg

Heating rate: 10 °C/min

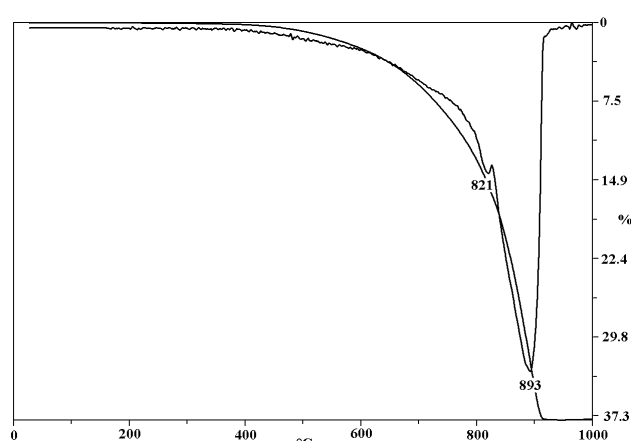


**Figure 6.2.1e.** Thermogravimetric curves of the previous sample after washing by distilled water

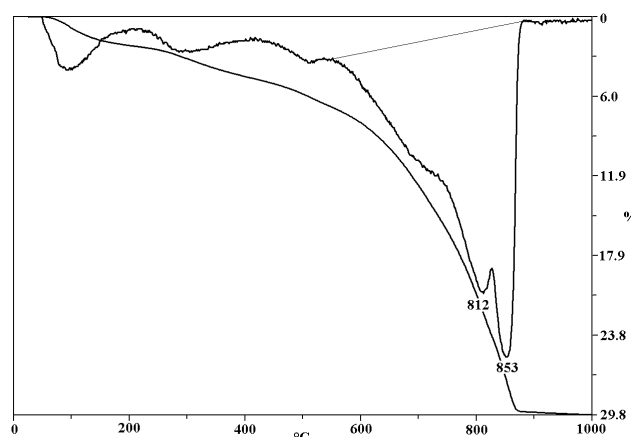


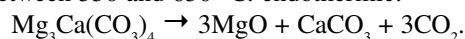
**Figure 6.2.1f.** Thermogravimetric curves of high magnesium calcite and Ca-dolomite (“protodolomite”)

## 6.2.2. Huntite $\text{Mg}_3\text{Ca}(\text{CO}_3)_4$

Due to the higher Mg ratio the decomposition of  $\text{MgCO}_3$  appears at a lower temperature than that of dolomite. The curves are similar to that of the mixture of calcite and magnesite.

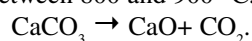
Reactions of the mineral:

1. Between 550 and 650 °C: endothermic:



Stoichiometric factor of the first reaction: 2.67.

2. Between 800 and 900 °C: endothermic:



Stoichiometric factor of the second reaction: 8.

Sample: Dorog, Hungary

Sample mass: 500 mg

Heating rate: 17 °C/min

Mass loss during the first decomposition: 27.4%

Huntite content of the sample based on the first reaction: 73%

Other thermally active minerals in the sample: calcite + aragonite (9%), clay mineral

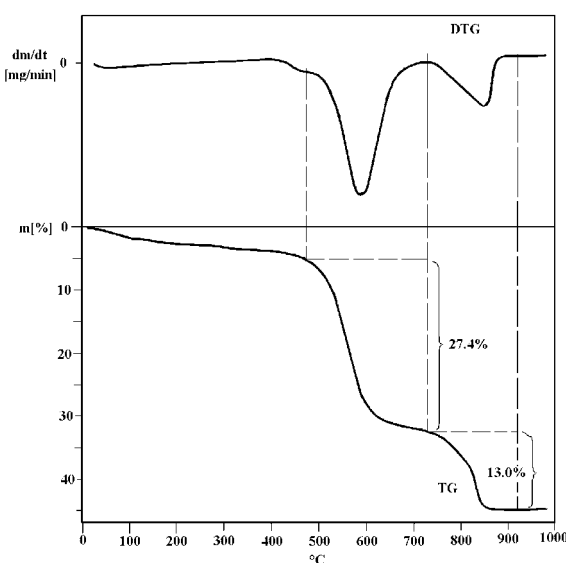


**Figure 6.2.2.** Thermogravimetric curves of huntite

## 6 Carbonates

### 6.2.3 Ankerite (real) (Mg>Fe), $\text{Ca}(\text{CO}_3)_2$

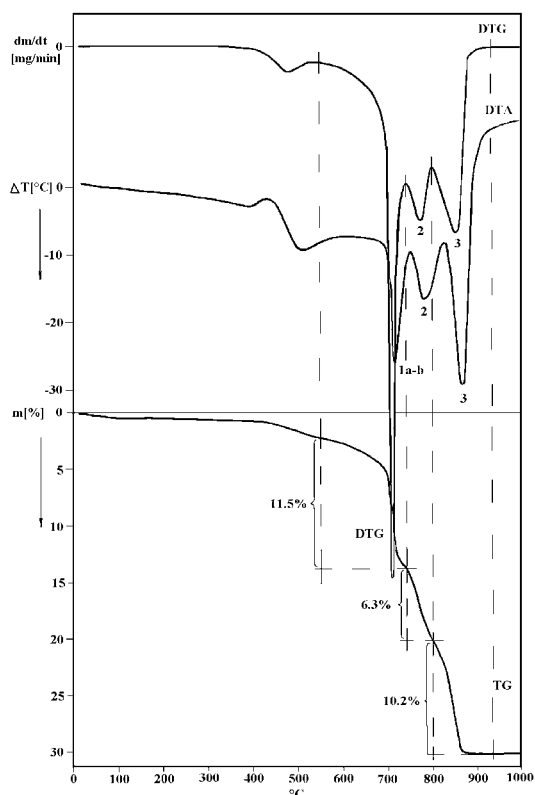


Figure 6.2.3. Thermoanalytical curves of real ankerite

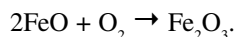
Reactions of the mineral:

1. Between 700 and 770 °C:

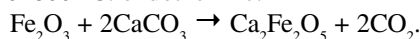
a) endothermic:



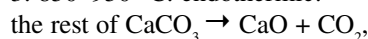
b) exothermic:



2. 750–800 °C: endothermic:



3. 850–950 °C: endothermic:



hence:  $(\text{CO}_2)_{\text{Ca}}$  = mass loss of reactions 2<sup>nd</sup>+3<sup>rd</sup>,

$(\text{CO}_2)_{\text{Fe}}$  = mass loss of reaction,

$(\text{CO}_2)_{\text{Mg}}$  = mass loss of reaction 1<sup>st</sup> —  $(0.82 \times \text{the mass loss of reaction 2}^{\text{nd}})$ ,

$\text{CO}_2$  content belongs to calcite:  $(\text{CO}_2)_{\text{Ca}} - (\text{CO}_2)_{\text{Fe}} - (\text{CO}_2)_{\text{Mg}}$ .

Sample: Sukoró, borehole St 1 55.6 56.4 m, Hungary (from carbonatite)	Belongs to "ankerite"	Belongs to calcite
Sample mass: 1000 mg		
Heating rate: 17 °C/min		
Mass loss during the first decomposition: 11.5 %	11.5 %	
Real $\text{CO}_2$ content of the first reaction:	$11.5 + (6.3 \times 0.18) = 12.6\%$	
Mass loss during the second decomposition: 6.3%	2.6 %	
Mass loss during the third decomposition: 10.2%	6.3 %	
$\Sigma$ Measured $\text{CO}_2$	12.6-second reaction)=6.3%	3.9%
Hence: CaO content of ankerite	24.1 %	
MgO content of ankerite	16.1%	
FeO content of ankerite	5.8%	
	10.3%	
The real $\text{CO}_2$ content of the mineral:	Total mass loss + ( $0.18 \times \text{the mass loss}$ of the reaction 2 <sup>nd</sup> )	$24.1 + 1.13 = 25.23\%$
Ankerite content of the sample		$\approx 57\%$
Cation composition of "ankerite"	$\text{Ca}_{1.5}\text{Mg}_{0.25}\text{Fe}_{0.25}$	
Calcite content of the sample		9%
Other thermal active minerals in the sample: Montmorillonite, illite, kaolinite, pyrite		

### 6.2.4 Ferrous dolomite

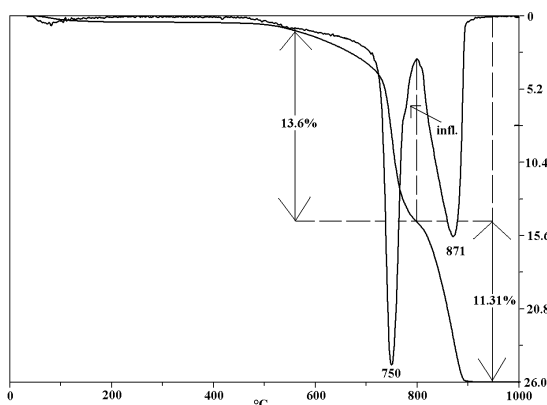


Figure 6.2.4a. Thermogravimetric curves of ferrous dolomite with higher iron content

In the case of higher iron content the first and the second or the second and third reactions are overlapped.

A further signal of iron content in the dolomite may be, when the mass loss at the first reaction is higher than that at the second reaction and/or the inflexion on the peak of decomposition.

Sample: Bátaapáti, borehole Űh-1 346 m, Hungary, fissure filling in granite

Sample mass: 175.6 mg

Heating rate: 10 °C/min

Mass loss during the first and second overlapped decomposition: 13.6%

Mass loss during the third decomposition: 11.31%

Other thermally active minerals in the sample: calcite, montmorillonite, illite, chlorite

Ferrous dolomite content and iron substitution may be calculated in the absence or known quantity of calcite.

The second derivate of the TG might show the overlapped first or second reaction.

In the case of low iron content the first and the second reaction can be separated and the third reaction overlapped.

Sample: Bataapáti, borehole Űh 1: 272.4 m, Hungary, fissure filling in granite	Belongs to ferrous dolomite	Belongs to calcite
Sample mass: 202.9 mg		
Heating rate: 10 °C/min		
Mass loss during the first decomposition: 14.16%	14.16%	
Real CO <sub>2</sub> content of the first reaction:	14.16+(3.88×0.18)= 14.86%	
Mass loss during the second decomposition: 3.88%	3.88	
Mass loss during the third decomposition: 18.39%	14.86 second reaction)=10.98%	3.9%
ΣMeasured CO <sub>2</sub>	36.08%	
Hence: CaO content of ankerite	22.91%	
MgO content of ankerite	13.03%	
FeO content of ankerite	6.32%	
Total mass loss		
The real CO <sub>2</sub> content of the mineral: (0.18 × the mass loss of the reaction 2 <sup>nd</sup> )	40.31%	
Ankerite content of the sample	=78%	
Cation composition of "ankerite" Ca <sub>0.18</sub> Mg <sub>0.10</sub> Fe <sub>0.11</sub>		
Calcite content of the sample		9%
Other thermally active minerals in the sample: montmorillonite, kaolinite		

Sample: Sopron, borehole S-89 150.1 m

Sample mass: 150.1 mg

Heating rate: 10 °C/min

Mass loss during the first and second decomposition: 12.56%

Mass loss during the third decomposition: 7.5%

Other thermally active minerals in the sample: siderite

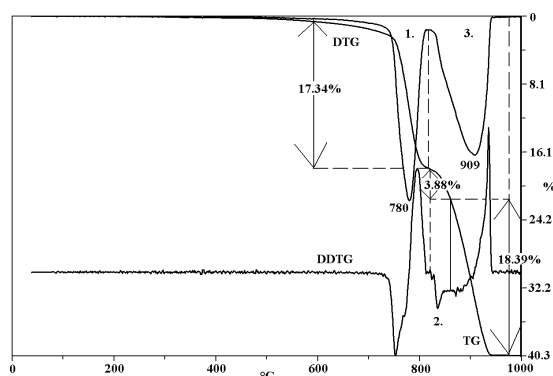


Figure 6.2.4b. Thermogravimetric curves of ferrous dolomite

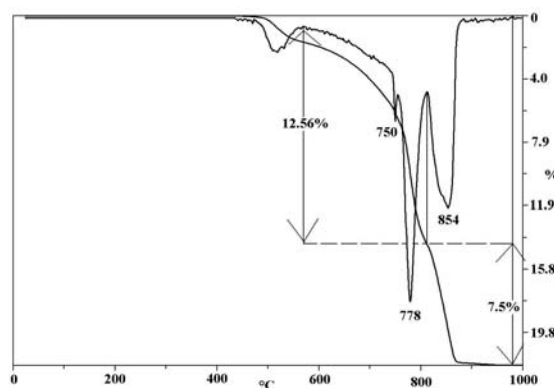


Figure 6.2.4c. Thermogravimetric curves of ferrous dolomite with low iron content

### 6.2.5. Kutnahorite (real) generally (Mn>Mg,Ca,Fe),Ca(CO<sub>3</sub>)<sub>2</sub>

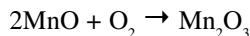
The thermal reactions of kutnahorite are similar to those of ankerite.

1. Between 700 and 770 °C:

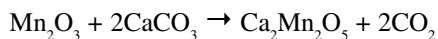
a) endothermic:



b) exothermic:



2. 750–800 °C: endothermic:



3. 850–950 °C: endothermic:



Hence: (CO<sub>2</sub>)<sub>Ca</sub> = mass loss of reaction 2<sup>nd</sup>+ 3<sup>rd</sup>

(CO<sub>2</sub>)<sub>Mn</sub> = mass loss of reaction 2<sup>nd</sup>

(CO<sub>2</sub>)<sub>Mg</sub> = mass loss of reaction 1<sup>st</sup> — (0.82× the mass loss of reaction 2<sup>nd</sup>)

CO<sub>2</sub> content belongs to calcite: (CO<sub>2</sub>)<sub>Ca</sub> - (CO<sub>2</sub>)<sub>Mn</sub> - (CO<sub>2</sub>)<sub>Mg</sub>

The colour of the sample after heating will be black.

Sample: Bataapáti, borehole Űh-22 159.7 m, Hungary, fissure filling in granite	Belongs to "kutnahorite"	Belongs to calcite
Sample mass: 235.6 mg		
Heating rate: 10 °C/min		
Mass loss during the first decomposition: 14.66%	14.66%	
Real CO <sub>2</sub> content of the first reaction:	14.66+(5.35×0.18)= 15.62%	

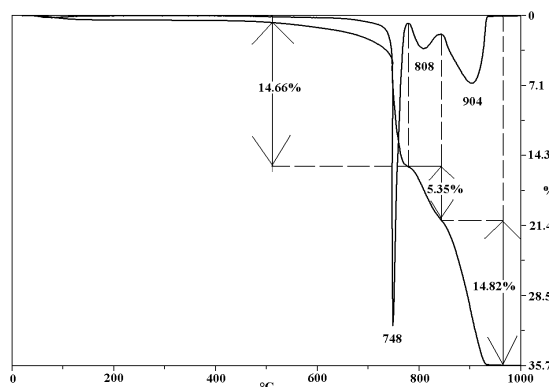


Figure 6.2.5. Thermogravimetric curves of kutnahorite

## 6 Carbonates

Mass loss during the second decomposition: 5.35%	5.35	
Mass loss during the third decomposition: 14.82%	15.62-second reaction) – 10.27%	5.52%
$\Sigma$ Measured $\text{CO}_2$	33.86%	
Hence: CaO content of "kutnahorite"	18.61%	
MgO content of "kutnahorite"	8.56%	
MnO content of "kutnahorite"	8.72%	
Total mass loss <sup>1</sup>		
The real $\text{CO}_2$ content of the mineral: $(0.18 \times \text{the mass loss of reaction 2.})$	40.31%	
"Kutnahorite" content of the sample	$\approx 65\%$	
Cation composition of "kutnahorite" $\text{Ca}_{0.5}\text{Mg}_{0.32}\text{Mn}_{0.18}$		
Calcite content of the sample		13%
Other thermally active minerals in the sample: illite, chlorite trace		

## 6.3. Waterfree carbonates without additional anions

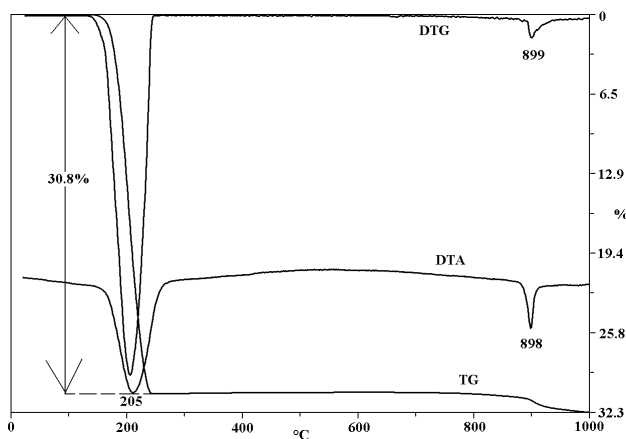
6.3.1. Kalicinite  $\text{KHCO}_3$ 

Figure 6.3.1. Thermoanalytical curves of kalicinite

Thermal reactions of the mineral:



Theoretical mass loss during the reaction: 30.88%

2. at about 900 °C: melting of  $\text{K}_2\text{CO}_3$  (thermal decomposition begins already in the solid phase)

Sample: unknown

Sample mass: 111.0 mg

Heating rate: 10 °C/min

Mass loss during the first decomposition: 30.8%

$\text{KHCO}_3$  content of the sample: 100%

6.3.2. Teschemacherite  $(\text{NH}_4)\text{HCO}_3$ 

Thermal reactions of the mineral:



Theoretical mass loss during the reaction: 100%

Sample: unknown

Sample mass: 201.2 mg

Heating rate: 10 °C/min

Mass loss during decomposition: 16.0%

$\text{NH}_4\text{HCO}_3$  content of the sample: 16.0%

Other thermally active minerals in the sample: calcite

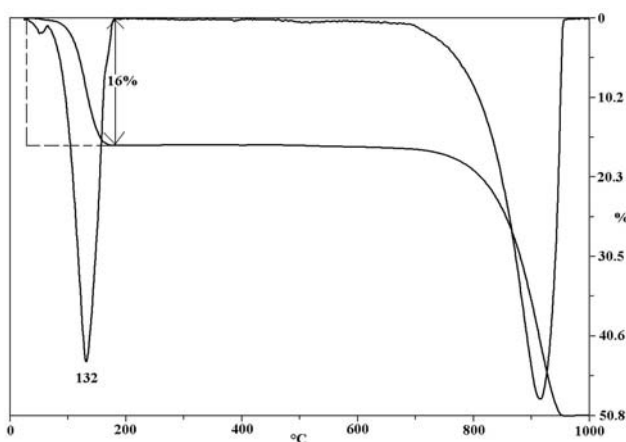
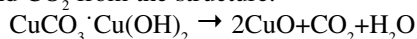


Figure 6.3.2. Thermogravimetric curves of teschemacherite

## 6.4. Waterfree carbonates with additional anions

### 6.4.1 Malachite $\text{Cu}_2(\text{OH})_2\text{CO}_3$

Thermal reaction of the mineral:  
at about 380 °C: endothermic; simultaneous loss of both OH  
water and  $\text{CO}_2$  from the structure:



mass loss during the reaction: 28.05%

Sample: unknown, Standard from the former Sovietunion 1978

Sample mass: 178.6 mg

Heating rate: 10 °C/min

Mass loss during the first decomposition: 27.59%

Malachite content of the sample: 98%

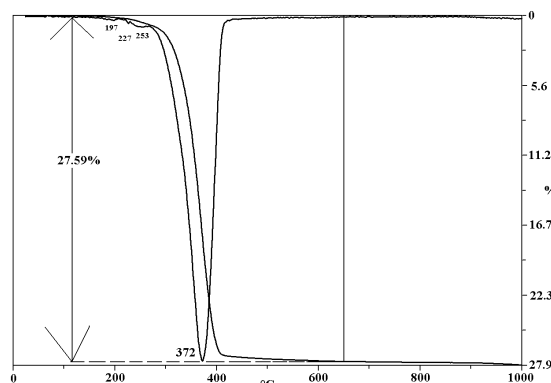


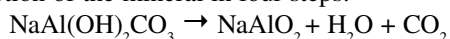
Figure 6.4.1. Thermogravimetric curves of malachite

### 6.4.2. Azurite $\text{Cu}_3((\text{OH})\text{CO}_3)_2$

Reaction of azurite is similar to that of malachite but due to the higher  $\text{CO}_3$  and OH proportion the reaction appears at about 30–50 °C higher temperature. Azurite decomposes under certain conditions (e.g. heated in helium carrier gas at 10 °Cmin<sup>-1</sup>) in two approximately equal steps (BROWN et al. 1984).

### 6.4.3 Dawsonite $\text{Na}_3\text{Al}(\text{CO}_3)_3 \cdot 2\text{Al}(\text{OH})_3$

Reaction of the mineral in four steps:



Stoichiometric factor of the whole mass loss: 2.32.

A small exothermic peak at 828 °C, crystallization of sodium aluminate.

Sample: unknown, Standard from the former Sovietunion 1978

Sample mass: 130.5 mg

Heating rate: 10 °C/min

The whole mass loss during decomposition: 33.35%

Dawsonite content of the sample: 77%

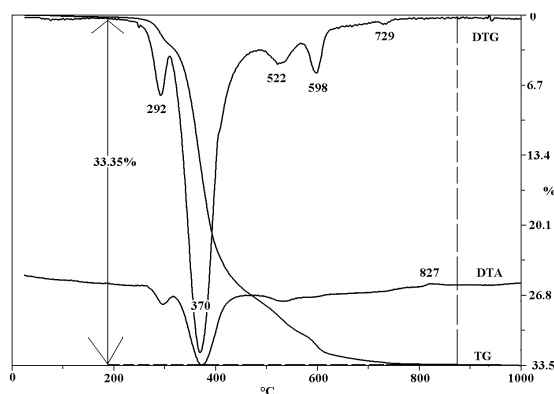


Figure 6.4.3. Thermoanalytical curves of dawsonite

## 6.5. Water-bearing carbonates

Thermal decomposition of hydrated and basic magnesium carbonates always occurs at lower temperatures than that of anhydrous carbonates.

### 6.5.1. Nesquehonite $\text{MgCO}_3 \cdot 3\text{H}_2\text{O}$ or $\text{Mg}(\text{HCO}_3)(\text{OH}) \cdot 2(\text{H}_2\text{O})$

Reactions and interpretation according to different authors are in Table T6.5.1.

Table T6.5.1. Thermal reactions of nesquehonite

References	Temperature interval (°C)				
	200 300	400 500	500 600	600 700	other reaction
BECK (1950)	210 235	425	535 585		510
	dehydration	dehydroxylation	decarbonation		crystallisation of MgO ?

## 6 Carbonates

**Table T6.5.1.** Continuation

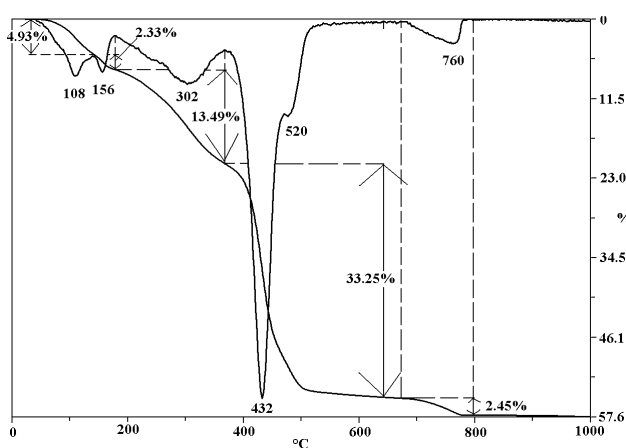
References	Temperature interval (°C)				
	200 300		200 300		200 300
ISVETKOV et al. (1964)	210 and 235	425	535 and 585		510
	2 moles of water	1 mole of water	decarbonation		
QUERALT et al. (1997) (IICMC)		455		630	
		loss of structural H <sub>2</sub> O		release of CO <sub>2</sub>	
LAUER et al. (2000)	262	462			
	dehydration	CO <sub>2</sub> evolution			

**6.5.2. Hydromagnesite  $3\text{MgCO}_3 \cdot \text{Mg}(\text{OH})_2 \cdot 3\text{H}_2\text{O}$** 

Reactions and interpretation according to different authors are in Table 6.5.2.

**Table 6.5.2.** Thermal reactions of hydromagnesite

References	Temperature interval (°C)					
	200 300	300 400	400 500	500 600	600 700	other reaction
BECK (1950)		375	440	565	600	510
		dehydration	dehydroxylation	decarbonation	decarbonation	crystallisation of MgO
LAUER et al. (2000)	296		426	548		511
	dehydration		dehydroxylation	dissociation		formation of well-crystalline magnesite
MONTOYA et al. (2001)		320	420	530		

**6.5.3. Dypingite  $\text{Mg}_5(\text{CO}_3)_4(\text{OH})_2 \cdot 5\text{H}_2\text{O}$** **Figure 6.5.1.** Thermogravimetric curves of dypingite

Reactions of the mineral:

1. Double endothermic peak at low temperature: loss of 2 moles water
2. Endothermic peak at about 300 °C: loss of 3 moles water and 2 moles OH
3. double peak at 430 and 520 °C: decarbonation
4. at about 760 °C: loss of the residual CO<sub>2</sub>

Water content of the mineral (molecular water + OH) = 22.26%, CO<sub>2</sub> content of the mineral is 36.25%.

Sample: Recsk, Hungary

Sample mass: 68.7 mg

Heating rate: 10 °C/min

Mass loss during the first reactions: 7.26%

Mass loss during the second reaction: 13.49%

Dypingite content of the sample based on water escape: 93%

Mass loss during the decarbonation reactions: 35.70%

Dypingite content of the sample based on CO<sub>2</sub> escape: 98%

The whole mass loss of the sample: 57.58%

Dypingite content of the sample based on the whole mass change: 98%

**6.5.4 Hydrotalcite  $\text{Mg}_6\text{Al}_2(\text{CO}_3)(\text{OH})_{16} \cdot 4(\text{H}_2\text{O})$** 

Reactions and interpretation according to different authors are in Table T6.5.4.

**Table T6.5.4.** Thermal reactions of hydrotalcite

References	Temperature interval (°C)					
	0-100	100-200	200-300	300-400	400-500	500-600
BECK (1950)			285		405	495
			dehydration		dehydroxylation of Al	dehydroxylation and decarbonation of Mg

**Table T6.5.4. Continuation**

References	Temperature interval (°C)					
	0-100	100-200	200-300	300-400	400-500	500-600
TSNETKOV et al. (1964)			150-300 dehydration			400-550 dehydration and decarbonation
ROSS, KODAMA (1967)			248, 267 H <sub>2</sub> O		447	
			250-280	300-400	Oil, CO, >400	
MACKENZIE et al. (1997)			loss of water	dehydration of Al	dehydration and decarbonation of Mg	
					400	
KLOPPROGGE, FROST (1999)	70 dehydration		222 decarbonation		400 dehydration	
HICKY et al. (2000)			3 major weight losses			
	dehydration		dehydration		decarbonation	
PARTHASARATHI BERA et al. (2000)	25-200 dehydration		225-300 dehydration and decarbonation			

## 6.6. Other carbonates

BECK (1950) published many data for rare carbonate minerals Table T.6.6.

**Table T6.6.** Thermal reaction of other carbonates according to data of BECK (1950)

Mineral	Formula	Endothermic	Exothermic	Reaction product
Breunnerite	(Mg,Fe)(CO) <sub>2</sub>	755		CO <sub>2</sub> , MgO
Pistolensite	(Fe,Mg)(CO) <sub>2</sub>	580	785 725	Fe <sub>2</sub> O <sub>3</sub> CO <sub>2</sub> , MgO Fe <sub>2</sub> O <sub>3</sub>
Nickolsomite	(Ca,Zn)CO <sub>2</sub>	500, 970		CO <sub>2</sub> , CO <sub>2</sub>
Nacholite	NaHCO <sub>3</sub>	205		H <sub>2</sub> O, CO <sub>2</sub> , NaCO <sub>3</sub>
Troms	NaHCO <sub>3</sub> ·Na <sub>2</sub> O·2H <sub>2</sub> O	170		H <sub>2</sub> O, CO <sub>2</sub> , Na <sub>2</sub> CO <sub>3</sub>
Gaylussite	CaCO <sub>3</sub> ·Na <sub>2</sub> O·5H <sub>2</sub> O	145, 175 210-235, 440		H <sub>2</sub> O H <sub>2</sub> O H <sub>2</sub> O, OH <sup>-</sup>
Lansfordite	MgCO <sub>3</sub> ·5H <sub>2</sub> O		510	MgO?
		555		CO <sub>2</sub>
Uramothallite	Ca <sub>11</sub> (CO <sub>3</sub> ) <sub>10</sub> H <sub>2</sub> O	110, 175, 475, 750, 890		?
Schröckingerite	NaCa <sub>2</sub> (UO <sub>2</sub> ) <sub>2</sub> (CO <sub>3</sub> ) <sub>2</sub> (SO <sub>4</sub> ) <sub>2</sub> ·10H <sub>2</sub> O	190, 385, 700	410	?
Bastnäsit (tysonite)	CeFCO <sub>3</sub>	620-625		CO <sub>2</sub> , F <sub>2</sub>
			650-655	CeF <sub>3</sub>
Kischymite	hydroxyl bastnäsit ?	580		CO <sub>2</sub> , F <sub>2</sub>
			650	CeF <sub>3</sub>
Parisit	2 CeFCO <sub>3</sub> ·CaCO <sub>3</sub>	660		CO <sub>2</sub> , F <sub>2</sub>
			720	CeF <sub>3</sub>
		280		H <sub>2</sub> O
Artinit	MgCO <sub>3</sub> ·Mg(OH) <sub>2</sub> ·2H <sub>2</sub> O	410 480		OH <sup>-</sup> CO <sub>2</sub>
			510	MgO
		540 345		CO <sub>2</sub> H <sub>2</sub> O
Hydrocerussit	2PbCO <sub>3</sub> ·Pb(OH) <sub>2</sub>	380-385 485-500		CO <sub>2</sub> CO <sub>2</sub>
Azurit	2CuCO <sub>3</sub> ·Cu(OH) <sub>2</sub>	430		H <sub>2</sub> O, CO <sub>2</sub>
Malachit	CuCO <sub>3</sub> ·Cu(OH) <sub>2</sub>	385		H <sub>2</sub> O, CO <sub>2</sub>
Hydrozincit	2ZnCO <sub>3</sub> ·3Zn(OH) <sub>2</sub>	310		H <sub>2</sub> O, CO <sub>2</sub>
Aurichalcit	2(Zn,Cu)CO <sub>3</sub> ·3(Zn,Cu)(OH) <sub>2</sub>	415		H <sub>2</sub> O, CO <sub>2</sub>
Bismutit	Bi <sub>2</sub> CO <sub>3</sub>	495-530 605-625 710-730		CO <sub>2</sub> inversion? simple cubic and Bi <sub>2</sub> O <sub>3</sub>
Beyerit	(Ca,Pb)Bi <sub>2</sub> (CO <sub>3</sub> ) <sub>2</sub> O <sub>2</sub>	570 675 725		CO <sub>2</sub> inversion? Bi <sub>2</sub> O <sub>3</sub>
Rutherfordine	11O <sub>2</sub> CO <sub>2</sub> ?	190		?
			715	?
Dundasit	Pb(AlO) <sub>2</sub> (CO <sub>3</sub> ) <sub>2</sub> ·4H <sub>2</sub> O	350		H <sub>2</sub> O, CO <sub>2</sub>
Dawsonit	Na <sub>2</sub> Al(CO <sub>3</sub> ) <sub>2</sub> ·2Al(OH) <sub>3</sub>	300 410	660	? H <sub>2</sub> O OH <sup>-</sup> , CO <sub>2</sub>

## 6 Carbonates

Table T6.6. Continuation

Mineral	Formula	Endothermic	Exothermic	Reaction product
Manasseite	$\text{MgCO}_3 \cdot 5\text{Mg}(\text{OH})_2 \cdot 2\text{Al}(\text{OH})_3 \cdot 4\text{H}_2\text{O}$	315		$\text{H}_2\text{O}$
		400		$\text{OH}$
		495		$\text{OH}, \text{CO}_2$
Pyroaurite and sjögrenite	$\text{MgCO}_3 \cdot 5\text{Mg}(\text{OH})_2 \cdot 2\text{Fe}(\text{OH})_3 \cdot 4\text{H}_2\text{O}$	270		$\text{H}_2\text{O}$
		350		$\text{OH}$
		455		$\text{OH}, \text{CO}_2$
Stichtite and barbertonite	$\text{MgCO}_3 \cdot 5\text{Mg}(\text{OH})_2 \cdot 2\text{Cr}(\text{OH})_3 \cdot 4\text{H}_2\text{O}$	275		$\text{H}_2\text{O}$
		455		$\text{OH}, \text{CO}_2$
Phosgenite	$\text{PbCO}_3 \cdot \text{PbCl}_2$	435		$\text{CO}_2$
Leadhillite	$2\text{PbCO}_3 \cdot 2\text{Pb}(\text{OH})_2 \cdot \text{PbSO}_4$	345		$\text{H}_2\text{O}, \text{CO}_2$
		485		$\text{CO}_2$

\*\*\*

References for carbonates: 7: rhodochrosite, 40: vaterite, 60: dolomite, 72: aragonite, 77: dundasite, 78: nahcolite, trona, calcite, magnesite, ferroan magnesite (breunnerite), rhodochrosite, magnesian siderite (pistomesite), siderite, smithsonite, dolomite, ferroan dolomite, aragonite, zincian aragonite (nickolsonite), alstonite, cerussite, gaylussite, nesquehonite, lansfordite, uranothallite, schroedingerite, bastnäsité, tysonite, kischtymite, parasite, hydromagnesite, artinite, hydrocerussite, azurite, malachite, hydrozincite, aurichalcite, bismutite, beyerite, rutherfordite, dundasite, dawsonite, hydrotalcite, manasseite, pyroaurite, sjögrenite, stichtite, barbertonite, phosgenite, leadhillite, 82: hydrotalcite, 90: dolomite, 117: dolomite, 139: malachite, azurite, 161: Ca-Mg carbonates, 171: carletonite, 172, 186: huntite, 187: huntite, 194: manganese carbonate, 195: siderite, 199: protodolomite, 202: calcite, aragonite, magnesite, dolomite, witherite, cerussite, siderite, 203, 207: dolomite, 217: dolomite, limestone 228, 229: siderite-magnesite, 230: strontium-bearing aragonite, 233: dolomite-ankerite mineral series, 234: dolomite-ferroan dolomite-ankerite series 235: scarbroite, 276: siderite, 284: dolomite, 285: dolomite, 298: aragonite, calcite, 299: smithsonite, 300: huntite, 316: hydrocerussite and plumbonacrite, 321, 332, 336: water in aragonite, 342: dolomite, 343: rhodochrosite, 344: rhodochrosite, 347: siderite, 349: siderite, 354: kutnahorite, 366: azurite, malachite, 356: hydrotalcite, reevesite, pyroaurite, 357: iowaite, 369: hydrotalcites of Mg and Zn, 377: Zn-takovite, 370: hydrotalcites, carrboydite, hydrohonessite, 390: siderite, 407, 417: low-iron dolomite, 422: adamsite, 445: dolomite, 484: magnesium-aluminium hydrotalcite, 491: lansfordite, sjögrenite, 511: 516: ferromanganoan dolomite, 517: magnesian kutnahorite, 548: zinc carbonate hydroxide, 553: hydrozincite, calcite, aragonite, magnesite, rhodochrosite, siderite, cerussite, azurite, whiterite, strontianite, 561: siderite, 562: siderite, 563: smithsonite, siderite, rhodochrosite, magnesite, dolomite, calcite, 572: magnesite, calcite, 576, 588: malachite, hydrozincite, 593: dolomite, 596: 609: calcite, aragonite, strontianite, 614: dolomite, iron dolomite, ankerite, 617: dolomite, 618: dolomite, 638: calcite, siderite, magnesite, dolomite-ankerite, 637: rhodochrosite, 640, 651: rhodochrosite, 655: hydromagnesite, nesquehonite, 685: hydrotalcite, 694: magnesite, calcite 707: dolomite, 712: basic copper carbonate, 714: magnesite, siderite, strontianite, witherite, rhodochrosite, smithsonite, 718, 729: dolomite, 734: dolomite, 746: dolomite-ferroan dolomite-ankerite series, 748, 755: dolomite, 756: dolomite, 759: dolomite, malachite, calcite+graphite, 760: caledonite, 1095: surite, 766: protodolomite, 790: eardleyerite, 804: dolomite group, 807: huntite, 812: zemkorite, 819: aragonite, 831: calcite, magnesite, dolomite, 827: calcite, 845, 848, 886, 893: hydrous Ca-bearing magnesium carbonate, 899: amorphous calcium carbonate, 913: manasseite and hydrotalcite, 922: siderite, 940: dolomite, 978:  $\text{MnCO}_3$ , 981: malachite, ankerite, 985: magnesite, dolomite, 986: huntite, 992: calcite, 998: dolomite, 1000, 1001, 1006: nahcolite, cerussite, Mn-calcite, smithsonite, siderite, huntite, magnesite, breunnerite, ankerite, dolomite, plumbocalcite, calcite, strontianite, norsethite, witherite, tarnowitzite, aragonite, malachite, azurite, hydrozincite, aurichalcite, bastnäsité, parisite, phosgenite, nesquehonite, soda, trona, pirssonite, gaylussite, hydromagnesite, artinite, brugnatellite, zaraitite, hydrotalcite, schrockingerite, voglite, 1009: nahcolite, cerussite, smithsonite, siderite, huntite, magnesite, breunnerite, ankerite, dolomite, plumbocalcite, calcite, strontianite, norsethite, witherite, trona, pirssonite, gaylussite, zaraitite, 1010: Mg-bearing carbonates, 1019: alumohydrocalcite, 1022, 1081: aragonite, magnesite, witherite, strontianite, siderite, rhodochrosite, smithsonite, cerussite, dolomite, manganocalcite, baritocalcite, manganosiderite (oligonite), monheimite, huntite, ankerite, manganodolomite, malachite, azurite, hydrocerussite, hydrozinkite, artinite, hydromagnesite, 1088: magnesian kutnahorite, 1092: azurite, alstonite, alumohydrocalcite, ankerite, ancylite, aragonite, artinite, aurichalcite, barbertonite, barytocalcite, bastnäsité, berbankite, beyerite, brugnatellite, witherite, wiartite, gaylussite, hydrocalcite, vaterite, hydromagnesite, hydrocerussite, hydrozincite, dawsonite, dundasite, dolomite, kalicinite, calcite, cancrinite, lithiumcarbonate, carbocernaite, cobaltocalcite (spherocobaltite), cordilyte, kutnahorite, lansfordite, leadhillite, magnesite, malachite, manasseite, manganocalcite, monheimite, nacholite, nesquehonite, oligonite, otavite, parisite, pyroaurite, pistomesite, podolite, rutherfordine, rhodochrosite, rosasite, siderite, synhyssite, scarbroite, scawtite, smithsonite, soda, stichtite, strontianite, thaumasite, teschemacherite, thermonatrite, trona, uranothallite, phosgenite, huntite, cerussite, sjögrenite, schrockingerite, 1114: grimselite, 1120: siderite, 1121: calcite, dolomite, 1122, 1123, 1124: magnesite, 1126, 1127, 1131: cerussite, 1133: siderite, magnesite, 1135, 1136: magnesite, dolomite, calcite, siderite, 1137: 1138: dolomite, ferroan dolomite, ankerite, 1155: dolomite, calcite, magnesite, 1156: dolomite, 1160: calcium carbonate, 1161, 1186: rhodochrosite

## 7. SULPHATES

The characteristic thermal reactions of sulphate minerals are summarized in Table T7a and b.

**Table T7a.** The main reactions of the most frequent simple sulphate minerals

Mineral	Formula	Dehydration (frequently in several steps)	The last step of dehydration	Water content (%)	Decomposition °C	SO <sub>3</sub> content (%)
<b>Ammonium</b>						
Muscagnite	(NH <sub>4</sub> ) <sub>2</sub> SO <sub>4</sub>			(13.6)	520-555	60.1
<b>Copper</b>						
Chalcantite	CuSO <sub>4</sub> ·5H <sub>2</sub> O	+	280	36		32
<b>Iron</b>						
Melanterite	FeSO <sub>4</sub> ·7H <sub>2</sub> O	+	300	45.8	650-750	29.2
Siderotile	FeSO <sub>4</sub> ·5H <sub>2</sub> O	+	300	36.7		33
Rozenite	FeSO <sub>4</sub> ·4H <sub>2</sub> O	+	300	33	650-750	36.3
Szomolnokite	FeSO <sub>4</sub> ·H <sub>2</sub> O		300	10.3	650 750	46.7
<b>Nickel</b>						
Morenosite	NiSO <sub>4</sub> ·7H <sub>2</sub> O	+	360 390	44.4	780 840	28.5
<b>Lead</b>						
Anglesite	PbSO <sub>4</sub>				880 900	26.4
<b>Aluminium</b>						
Alunogen	Al <sub>2</sub> (SO <sub>4</sub> ) <sub>3</sub> ·18H <sub>2</sub> O	+	320	50	750-950	35.1
Meta-alunogen	Al <sub>2</sub> (SO <sub>4</sub> ) <sub>3</sub> ·13.5H <sub>2</sub> O	+	300	41.5	750-950	41
Aluminium sulphate hydrate	Al <sub>2</sub> (SO <sub>4</sub> ) <sub>3</sub> ·12H <sub>2</sub> O	+	300	38.7	750-950	43
Hydrobasaluminite	Al <sub>2</sub> (OH) <sub>10</sub> SO <sub>4</sub> ·36H <sub>2</sub> O	+	300	72.3	750 950	7.6
Aluminite	Al <sub>2</sub> (OH) <sub>8</sub> SO <sub>4</sub> ·8H <sub>2</sub> O	+	300	46.8	750-950	23.4
Meta-aluminite	Al <sub>2</sub> (OH) <sub>6</sub> SO <sub>4</sub> ·5H <sub>2</sub> O	+	300	41.5	750 950	41
I'elsőbányaite	Al <sub>2</sub> (OH) <sub>10</sub> SO <sub>4</sub> ·5H <sub>2</sub> O	+	300	37.3	750-950	16.5
Basaluminite	Al <sub>2</sub> (OH) <sub>10</sub> SO <sub>4</sub> ·4 5H <sub>2</sub> O	+	300	34.2	750 950	17
Metabasaluminite	Al <sub>2</sub> (OH) <sub>10</sub> SO <sub>4</sub>		300	24	750-950	21
<b>Manganese</b>						
Mallardite	MnSO <sub>4</sub> ·7H <sub>2</sub> O	+	260-300	44.5	≈1000	29
<b>Magnesium</b>						
Epsomite	MgSO <sub>4</sub> ·7H <sub>2</sub> O	+	340	51.1	≈1000	32.3
Hexahydrate	MgSO <sub>4</sub> ·6H <sub>2</sub> O	+	340	46.4	≈1000	34.5
Pentahydrate	MgSO <sub>4</sub> ·5H <sub>2</sub> O	+	340	43	≈1000	36.1
Starkeyite	MgSO <sub>4</sub> ·4H <sub>2</sub> O	+	340	37.4	≈1000	41.6
Sanderite	MgSO <sub>4</sub> ·2H <sub>2</sub> O	+	340	23	≈1000	51.2
Kieserite	MgSO <sub>4</sub> ·H <sub>2</sub> O		340	13	≈1000	57.6
<b>Calcium</b>						
Gypsum	CaSO <sub>4</sub> ·2H <sub>2</sub> O	+		20.9	>1000	
Anhydrite	CaSO <sub>4</sub>				>1000	

**Table T7b.** Further reactions of sulphates

Reaction	Notice	Temperature (°C)
Melting:	see Table 22	
Phase transition	see Table 21	
Dehydroxylation	alunite, jarosite, aluminite etc.	
Oxidation	minerals containing FeSO <sub>4</sub>	430 450
Reduction	sulphates, bearing CuO	950 1050
<b>Solid-phase structural decomposition (endothermic)</b>		
1. Reaction of alkaline sulphates and alkaline earth sulphates e.g. dehydrated syngenite at 430 °C: $2\text{K}_2\text{SO}_4 \cdot \text{CaSO}_4 \rightarrow 2\text{K}_2\text{SO}_4 + \text{CaSO}_4 \cdot 2\text{CaSO}_4$ similar reactions between 400 650 °C: bloedite, loweite, vanthoffite, glaserite, glauberite, langbeinite, görgöyite etc.		
2. Reactions of alunite-type minerals: e.g. alunite 700 790 °C $\text{K}_2\text{SO}_4 \cdot \text{Al}_2(\text{SO}_4)_3 \rightarrow \text{K}_2\text{SO}_4 + \text{Al}_2(\text{SO}_4)_3$ similar reactions: aluminite etc.		

## 7 Sulphates

## 7.1. Waterfree sulphates

7.1.1. Mascagnite  $(\text{NH}_4)_2\text{SO}_4$ 

The mineral has different, partly overlapped decomposition process during the heating. Data found in the literature are in the Table T7.1.1.

Reactions of the mineral

1. deammoniation:



theoretical mass loss during the reaction: 12.9%

2. sulphate decomposition:

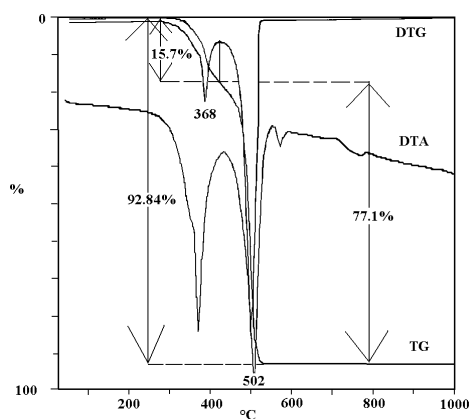


Figure 7.1.1. Thermogravimetric curves of a mascagnite bearing sample

Table T7.1.1. Reaction of mascagnite according to the literature

References	Temperature of reaction (°C)					
COCCO 1952	180	400	425	455	590	790
ISVETKOV, VALYASHKINA 1955		350	410		555	
		deammoniation			dissociation of sulphate	

Sample: artificial

Sample mass: 132.15 mg

Heating rate: 10 °C/min

Mass loss during the first reactions: 15.7%

Mass loss during the second reaction: 77.1%

Mascagnite content of the sample: 93%

Some impurities

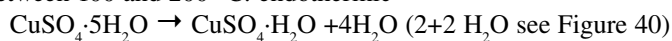
## 7.2. Water-bearing sulphates with mono cation

For the features of the water content of sulphates see in the chapter Crystal hydrates (constitutional water in water-bearing carbonate, sulphate, phosphate and salt minerals)

7.2.1. Chalcanthite  $\text{CuSO}_4 \cdot 5\text{H}_2\text{O}$ 

Reactions of the mineral:

1. Between 100 and 200 °C: endothermic



Stoichiometric factor of the first reaction: 3.46.

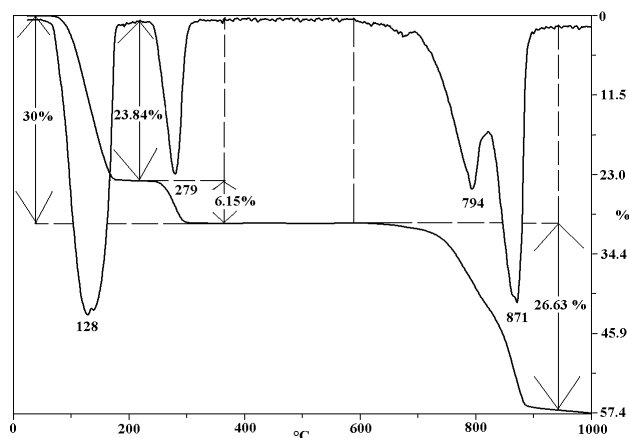
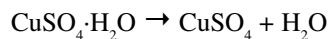


Figure 7.2.1. Thermogravimetric curves of chalcanthite

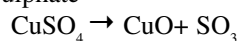
2. At about 250 °C: endothermic:



Stoichiometric factor of the second reaction: 13.87.

Stoichiometric factor for the whole water content: 2.77.

3. Between 700 and 850 °C: endothermic (double peak):  
loss of sulphate



Stoichiometric factor of the third reaction: 3.12.

Sample: Recsk, Hungary

Sample mass: 85.6 mg

Heating rate: 10 °C/min

Mass loss during the first reactions: 30.01%

Mass loss during the second reaction: 6.15%

Mass loss during the third reaction: 26.53%

Chalcanthite content of the sample based on the first reaction: 83%

Chalcanthite content of the sample based on the second reaction: 85%

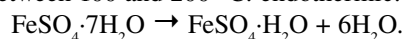
Chalcanthite content of the sample based on the whole water content: 83%

Chalcanthite content of the sample based on the third reaction: 83%

### 7.2.2. Melanterite $\text{FeSO}_4 \cdot 7\text{H}_2\text{O}$

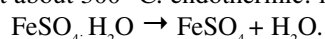
Reactions of the mineral:

1. Between 100 and 200 °C: endothermic:



Stoichiometric factor of the first reaction: 2.57.

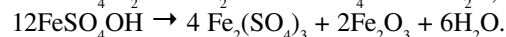
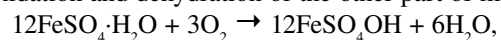
2. At about 300 °C: endothermic: loss of one part of monohydrate:



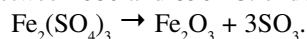
3. Between 400 and 600 °C: exothermic (endothermic)

a) oxidation:  $12\text{FeSO}_4 + 3\text{O}_2 \rightarrow 4\text{Fe}_2(\text{SO}_4)_3 + 2\text{Fe}_2\text{O}_3$ .

b) oxidation and dehydration of the other part of monohydrate:



4. Between 680 and 830 °C: endothermic: sulphate decomposition



Stoichiometric factor of the fourth reaction related to the mineral: 3.47.

Sample: Pázmánd, borehole Pd-2 156.9 m, Hungary (encrust on core)

Sample mass: 600 mg

Heating rate: 17 °C/min

Mass loss during the first reaction: 38.3%

Mass loss during the fourth reaction: 28.3%

Melanterite content of the sample based on the first reaction: 99%

Melanterite content of the sample based on the fourth reaction: 99%

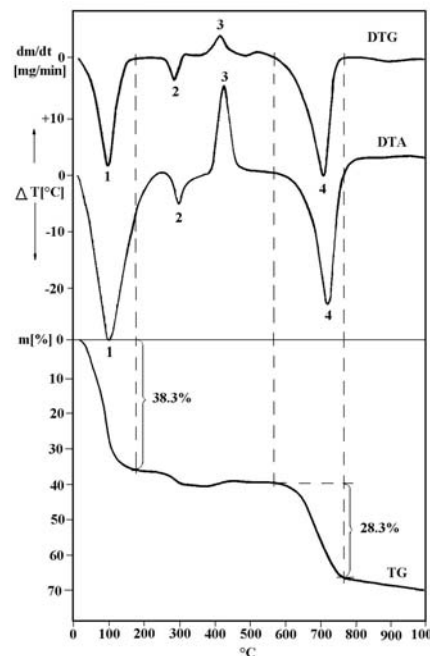
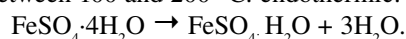


Figure 7.2.2. Thermoanalytical curves of melanterite

### 7.2.3. Rozenite $\text{FeSO}_4 \cdot 4\text{H}_2\text{O}$

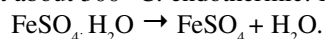
Reactions of the mineral:

1. Between 100 and 200 °C: endothermic:



Stoichiometric factor of the first reaction: 4.1.

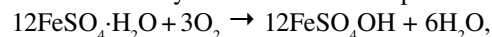
2. At about 300 °C: endothermic: loss of one part of monohydrate:



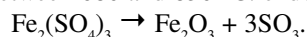
3. Between 400 and 600 °C: exothermic (endothermic)

a) oxidation:  $12\text{FeSO}_4 + 3\text{O}_2 \rightarrow 4\text{Fe}_2(\text{SO}_4)_3 + 2\text{Fe}_2\text{O}_3$ ,

b) oxidation and dehydration of the other part of monohydrate:



4. Between 680 and 830 °C: endothermic: desulphation



Stoichiometric factor of the fourth reaction related to the mineral: 2.8.

Sample: Gyék, borehole Gy-8 235.0–235.8 m, Hungary

Sample mass: 1000 mg

Heating rate: 17 °C/min

Mass loss during the first reaction: 19.0%

Mass loss during the fourth reaction: 27.4%

Rozenite content of the sample based on the first reaction: 78%

Rozenite content of the sample based on the fourth reaction: 77%

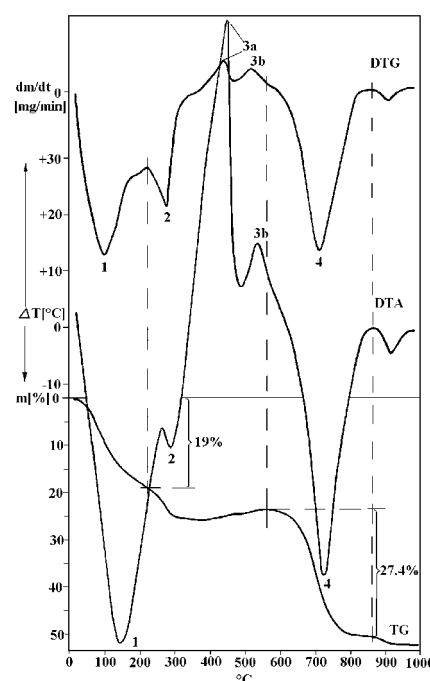


Figure 7.2.3. Thermoanalytical curves of rozenite

## 7 Sulphates

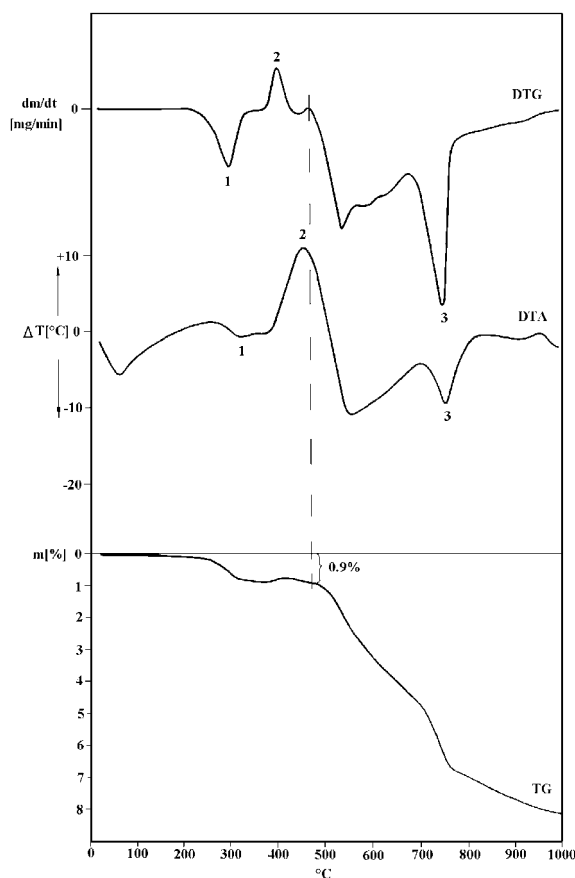
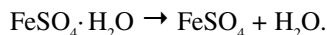


Figure 7.2.4. Thermoanalytical curves of szomolnokite bearing sample

 7.2.4. Szomolnokite  $\text{FeSO}_4 \cdot \text{H}_2\text{O}$ 

Reactions of the mineral:

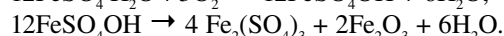
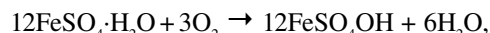
1. At about 300 °C: endothermic: loss of one part of monohydrate:



2. Between 400 and 600 °C: exothermic (endothermic):



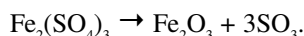
b) oxidation and dehydration of the other part of the monohydrate:



Balance of the mass change in the case of complete oxidation: loss of one molecule water and intake of 0.25  $\text{O}_2$  (real water content =  $1.8 \times$  measured mass loss).

Stoichiometric factor based on the real water content: 9.4.

3. Between 680 and 830 °C: endothermic: sulphate decomposition



Stoichiometric factor of the third reaction related to the mineral: 2.13.

Sample: Pázmánd, borehole Pd-3 105.0–106.5 m, Hungary

Sample mass: 1000 mg

Heating rate: 17 °C/min

Mass loss during the first and second reactions: 0.9%

Szolnokite content based on the mass loss: 19%

Other thermally active minerals in the sample: quartz, kaolinite, alunite, illite

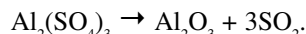
 7.2.5. Alunogen  $\text{Al}_2(\text{SO}_4)_3 \cdot 17\text{H}_2\text{O}$ 

Reactions of the mineral:

1. at about 150 °C: endothermic: loss of 13 moles water

2. at about 300 °C: endothermic: loss of 3.5 moles water

3. between 800 and 850 °C: sulphate decomposition



Sample: Červenica, Slovakia

Sample mass: 99.4 mg

Heating rate: 10 °C/min

Mass loss during the first reactions: 35.2%

Mass loss during the second reaction: 9.72%

Mass loss during the third reaction: 36.57%

Alunogen content of the sample based on the water content (calculated with 16.5 moles water): 97%

Alunogen content of the sample based on the third reaction (calculated with 16.5 moles water): 97%

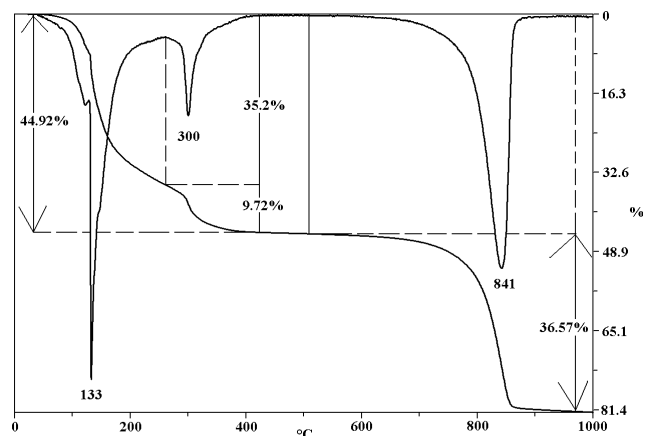


Figure 7.2.5. Thermogravimetric curves of alunogen

 7.2.6 Hexahydrate  $\text{MgSO}_4 \cdot 6\text{H}_2\text{O}$ 

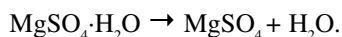
Reactions of the mineral:

1. Between 100 and 250 °C: endothermic in several steps: loss of five moles of water



Stoichiometric factor of the reaction: 2.54.

2. At about 350 °C: endothermic: loss of the last mole of water



Stoichiometric factor of the reaction: 12.7.

Stoichiometric factor of the whole water content: 2.11.

3. At about 1000°C: endothermic: sulphate decomposition:



Sample: artificial

Sample mass: 100.9 mg

Heating rate: 10 °C/min

Mass loss during the first reactions: 39.13%

Mass loss during the second reaction: 8.18%

Proportion of the two steps: 4.78

Hexahydrate content of the sample based on the first reaction: 99%

Hexahydrate content of the sample based on the second reaction: 104%

Hexahydrate content of the sample based on the whole water content: 99%

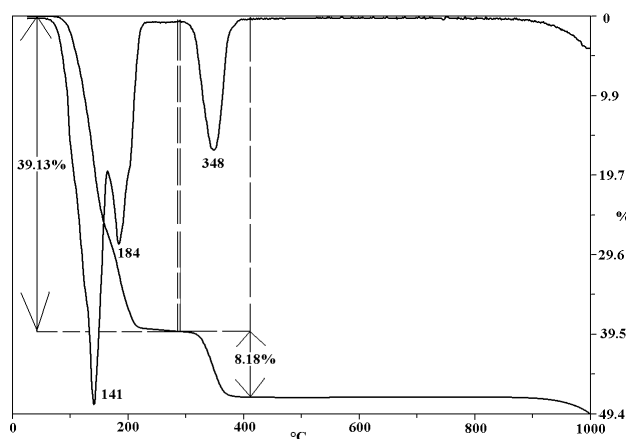
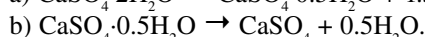


Figure 7.2.6. Thermogravimetric curves of hexahydrate

### 7.2.7. Gypsum $\text{CaSO}_4 \cdot 2\text{H}_2\text{O}$

Reaction of the mineral:

1. Between 150 and 250 °C: endothermic: dehydration in two steps (overlapped):



Stoichiometric factor of the whole water content: 4.78.

2. Decomposition of the mineral at about 1200 °C

Sample: soil sample from Hunyad, depth 60–80 cm, Hungary

Sample mass: 77.8 mg

Heating rate: 10 °C/min

Mass loss during the first reactions: 10.14%

Mass loss during the second reaction: 3.48%

Gypsum content of the sample based on the whole water content: 65%

Other thermally active minerals in the sample: calcite

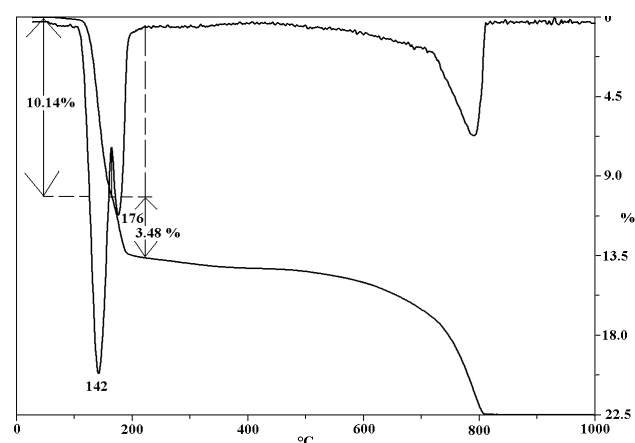


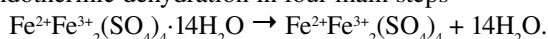
Figure 7.2.7. Thermogravimetric curves of a gypsum bearing sample

## 7.3. Water-bearing sulphates with several different cations

### 7.3.1. Römerite $\text{Fe}^{2+}\text{Fe}^{3+}_2(\text{SO}_4)_4 \cdot 14\text{H}_2\text{O}$

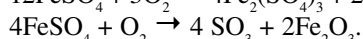
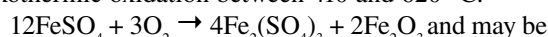
Reactions of the mineral:

1. Endothermic dehydration in four main steps

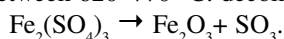


Stoichiometric factor based on the water content: 3.19.

2. Exothermic oxidation between 410 and 620 °C:



3. Between 620–770 °C: decomposition of  $\text{Fe}_2(\text{SO}_4)_3$



Stoichiometric factor based on the decomposition: 2.51.

Sample: Nagybörzsöny, Hungary

Sample mass: 100.8 mg

Heating rate: 10 °C/min

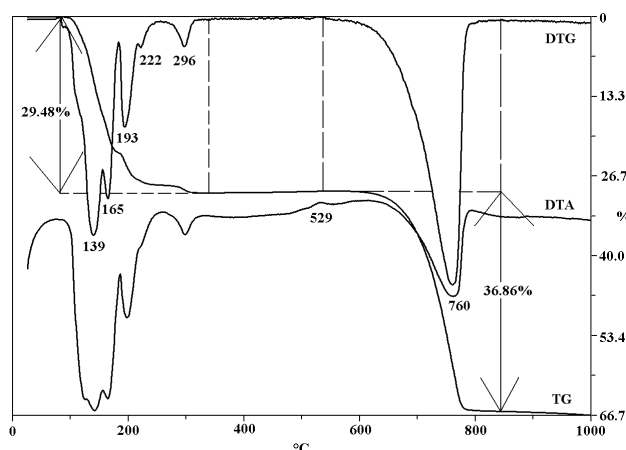


Figure 7.3.1. Thermoanalytical curves of römerite

## 7 Sulphates

Water content of the sample: 29.48%

Mass loss during decomposition: 36.86%

Römerite content of the sample based on the water content: 94%

Römerite content of the sample based on the sulphate decomposition: 93%

### 7.3.2. Voltaite $\text{K}_2\text{Fe}^{2+}_5\text{Fe}^{3+}_3\text{Al}(\text{SO}_4)_{12} \cdot 18(\text{H}_2\text{O})$

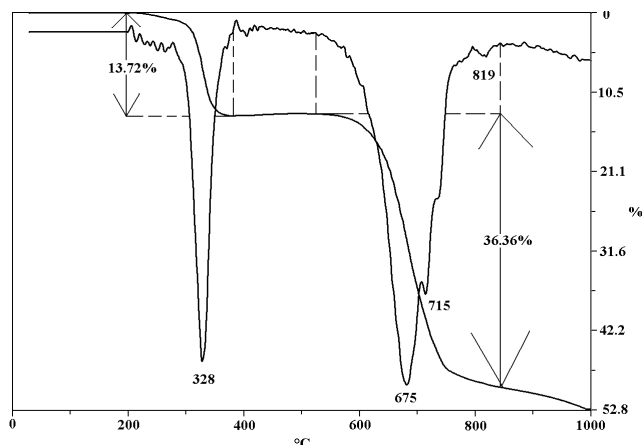


Figure 7.3.2. Thermogravimetric curves of voltaite

Theoretical reaction of the mineral:

1. 300–350 °C: endothermic: dehydration  
Stoichiometric factor of the water content: 6.26.
2. probably oxidation of the  $\text{FeSO}_4$  component
3. 650–750 °C: decomposition of the  $\text{Fe}_2(\text{SO}_4)_3$  component (originally 3 moles  $\text{SO}_3$ )
4. 650–750 °C: decomposition of the  $\text{FeSO}_4$  component (originally 5 moles  $\text{SO}_3$ )
5. 750–850 °C: decomposition of the  $\text{Al}_2(\text{SO}_4)_3$  component (3 moles  $\text{SO}_3$ )
6. higher than 1000 °C: decomposition of the  $\text{K}_2\text{SO}_4$  component (1 mole  $\text{SO}_3$ )  
Stoichiometric factor of 17 moles  $\text{SO}_3$ : 2.3.

Sample: Smolnik, Slovakia

Sample mass: 24.5 mg

Heating rate: 10 °C/min

Water content of the sample: 13.72%

Mass loss during decomposition: 36.36%

Voltaite content of the sample based on the water content: 86%

Voltaite content of the sample based on the sulphate decomposition: 84%

### 7.3.3. Halotrichite $\text{Fe}^{2+}\text{Al}_2(\text{SO}_4)_4 \cdot 22(\text{H}_2\text{O})$

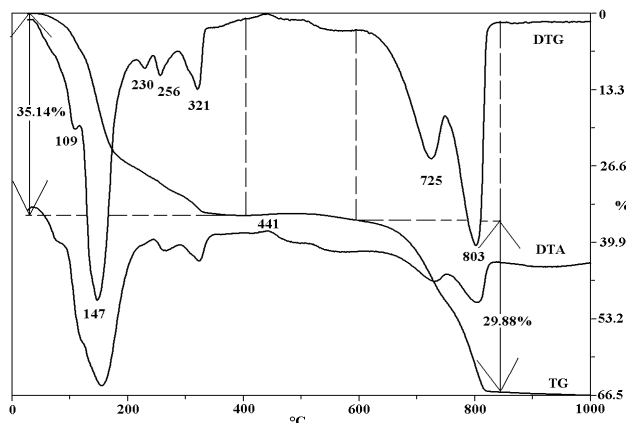


Figure 7.3.3. Thermoanalytical curves of halotrichite

Theoretical reactions of the mineral:

1. Between 50 and 350 °C: endothermic: dehydration in several steps  
Stoichiometric factor based on the water content: 2.25
2. At about 450 °C: exothermic: oxidation
3. Between 630 and 780 °C: endothermic: decomposition of iron sulphate (1 mole)
4. Between 800 and 820 °C: endothermic: decomposition of  $\text{Al}_2(\text{SO}_4)_3$  (3 moles)  
Stoichiometric factor based on the  $\text{SO}_3$  content: 2.78.

Sample: unknown

Sample mass: 169.7 mg

Heating rate: 10 °C/min

Water content of the sample: 35.14%

Mass loss during decomposition: 29.88%

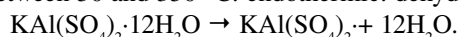
Halotrichite content of the sample based on the water content: 79%

Halotrichite content of the sample based on the sulfate decomposition: 83%

### 7.3.4. Potassium-alum $\text{KAl}(\text{SO}_4)_2 \cdot 12\text{H}_2\text{O}$

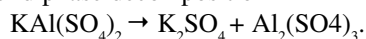
Reactions of the mineral:

1. Between 50 and 350 °C: endothermic: dehydration in several steps

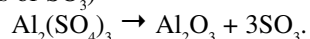


Stoichiometric factor based on the water content: 2.2.

2. Solid phase decomposition



3. Between 750 and 950 °C decomposition of  $\text{Al}_2(\text{SO}_4)_3$  (3 moles of  $\text{SO}_3$ )



Stoichiometric factor of the reaction: 3.95.

4. At about 1100 °C: endothermic: decomposition of  $\text{K}_2\text{SO}_4$ .

Sample: unknown

Sample mass: 174.0 mg

Heating rate: 10 °C/min

Water content of the sample: 45.17%

Mass loss during the  $\text{Al}_2(\text{SO}_4)_3$  decomposition: 24.08%

Potassium-alum content of the sample based on the water content: 99%

Potassium-alum content of the sample based on the sulphate decomposition: 95%

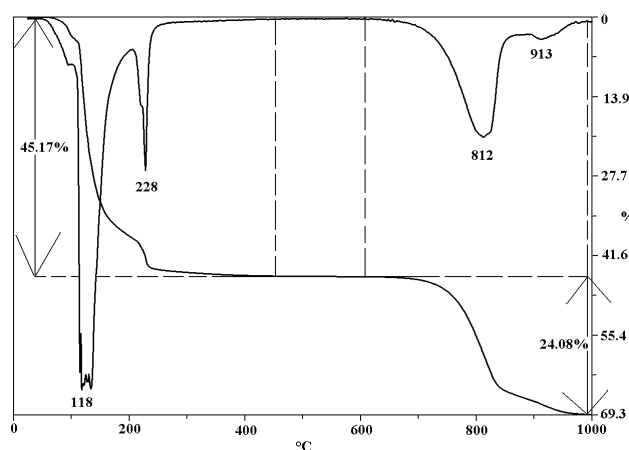
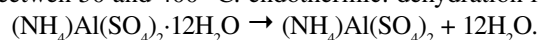


Figure 7.3.4. Thermogravimetric curves of potassium-alum

### 7.3.5 Tschermigite $(\text{NH}_4)\text{Al}(\text{SO}_4)_2 \cdot 12\text{H}_2\text{O}$

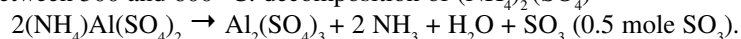
Reactions of the mineral:

1. Between 50 and 400 °C: endothermic: dehydration in several steps



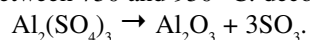
Stoichiometric factor based on the water content: 2.1.

2. Between 500 and 600 °C: decomposition of  $(\text{NH}_4)_2(\text{SO}_4)$



Stoichiometric factor based on the water content: 6.86

3. Between 750 and 950 °C: decomposition of  $\text{Al}_2(\text{SO}_4)_3$  (1.5 moles of  $\text{SO}_3$ )



Stoichiometric factor of the reaction: 3.77.

Sample: Komló, Hungary

Sample mass: 141.8 mg

Heating rate: 10 °C/min

Water content of the sample: 46.13%

Mass loss during the  $(\text{NH}_4)_2\text{SO}_4$  decomposition: 13.61%

Mass loss during the  $\text{Al}_2(\text{SO}_4)_3$  decomposition: 24.85%

Tschermigite content of the sample based on the water content: 97%

Tschermigite content of the sample based on  $(\text{NH}_4)_2\text{SO}_4$  decomposition: 93%

Tschermigite content of the sample based on the sulphate decomposition: 94%

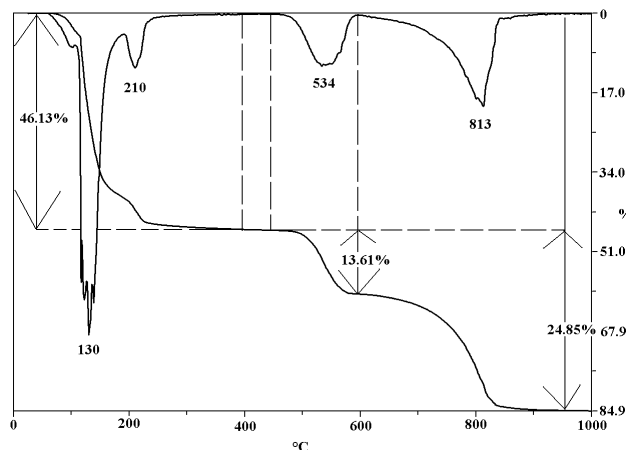


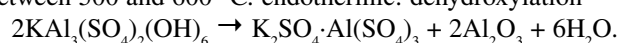
Figure 7.3.5. Thermogravimetric curves of tschermigite

## 7.4. Waterfree sulphates with additional anions

### 7.4.1. Alunite $\text{KAl}_3(\text{SO}_4)_2(\text{OH})_6$

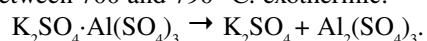
Reaction of the mineral:

1. Between 500 and 600 °C: endothermic: dehydroxylation

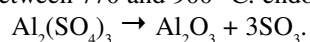


Stoichiometric factor of the reaction: 7.67.

2. Between 700 and 790 °C: exothermic:



3. Between 770 and 900 °C: endothermic: decomposition of  $\text{Al}_2(\text{SO}_4)_3$



## 7 Sulphates

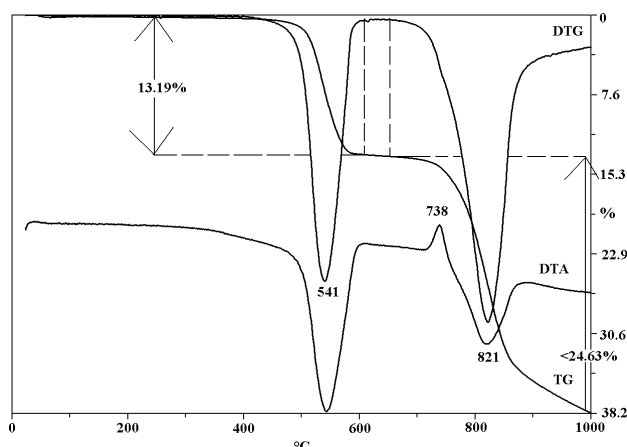


Figure 7.4.1. Thermoanalytical curves of alunite

Stoichiometric factor of the reaction: 3.45.

4. At about 1100 °C: endothermic: decomposition of  $K_2SO_4$  (this reaction in the presence of silica starts at lower temperature)

Sample: Sárszentmiklós, Hungary

Sample mass: 239.4 mg

Heating rate: 10 °C/min

Mass loss during dehydroxylation: 13.19%

Mass loss during the decomposition (3 moles of  $SO_3$ ): >24.63%

Alunite content of the sample based on the first reaction: 100%

Alunite content of the sample based on the sulphate decomposition: >85%

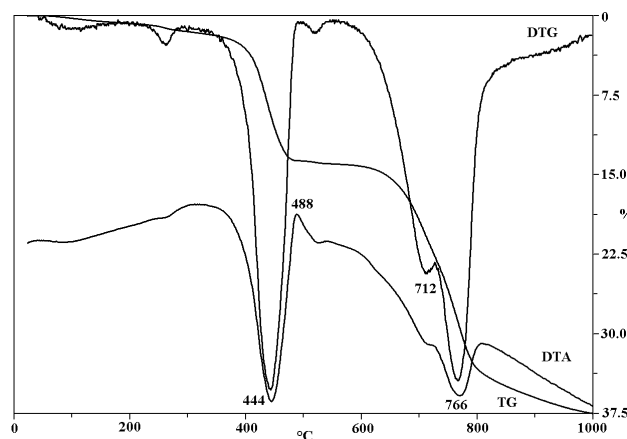
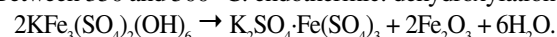


Figure 7.4.2. Thermoanalytical curves of a jarosite bearing sample

 7.4.2. Jarosite  $KFe_3(SO_4)_2(OH)_6$ 

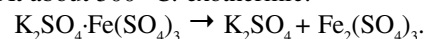
Reactions of the mineral:

1. Between 350 and 500 °C: endothermic: dehydroxylation

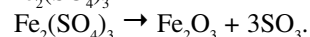


Stoichiometric factor of the reaction: 9.28.

2. At about 500 °C: exothermic:



3. Between 650 and 750 °C: endothermic: decomposition of  $Fe_2(SO_4)_3$



Stoichiometric factor of the reaction: 4.18.

4. At about 1100 °C: endothermic: decomposition of  $K_2SO_4$ .

Sample: Kazár, Hungary

Sample mass: 199.7 mg

Heating rate: 10 °C/min

Other thermally active minerals in the sample: goethite, kaolinite

## 7.5. Water-bearing sulphates with additional anions

 7.5.1. Aluminite  $Al_2(SO_4)(OH)_4 \cdot 7H_2O$ 

Reactions of the mineral:

1. Between 30 and 660 °C: endothermic: divided into two parts

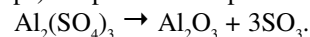
a) loss of 4 molecules of free crystal water

b) loss of 3 molecules of ligand water coordinated to the Al atoms and dehydroxylation

Stoichiometric factor of the reaction for 7+2 moles of  $H_2O$ : 2.12.

2. At about 850 °C: exothermic (overlapped by simultaneous endothermic): structural decomposition to  $Al_2O_3$  and  $Al_2(SO_4)_3$

3. Between 770 and 950 °C: endothermic (generally in two steps): sulphate decomposition



Stoichiometric factor of the reaction: 4.3.

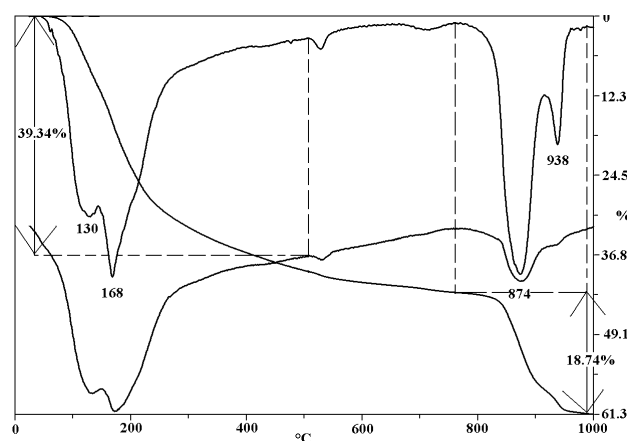


Figure 7.5.1. Thermoanalytical curves of an aluminite bearing sample

Sample: Csordakút, borehole 421 39.1–39.6 m, Hungary  
 Sample mass: 128.8 mg  
 Heating rate: 10 °C/min  
 Mass loss during dehydration and dehydroxylation: 39.34%  
 Mass loss during the  $\text{Al}_2(\text{SO}_4)_3$  decomposition: 18.74%  
 Aluminite content of the sample based on the whole water escape: 83%  
 Aluminite content of the sample based on the sulphate decomposition: 81%  
 Other thermally active mineral in the sample: boehmite

### 7.5.2 Fibroferrite $\text{Fe}^{3+}(\text{SO}_4)(\text{OH})\cdot 5\text{H}_2\text{O}$

Reactions of the mineral:

1. At 170 °C: endothermic dehydration:  
 $\text{Fe}^{3+}(\text{SO}_4)(\text{OH})\cdot 5\text{H}_2\text{O} \rightarrow \text{Fe}^{3+}(\text{SO}_4)(\text{OH})\cdot 2\text{H}_2\text{O} + 3\text{H}_2\text{O}$
2. At 230 °C: endothermic dehydration:  
 $\text{Fe}^{3+}(\text{SO}_4)(\text{OH})\cdot 2\text{H}_2\text{O} \rightarrow \text{Fe}^{3+}(\text{SO}_4)(\text{OH}) + 2\text{H}_2\text{O}$
3. At 530 °C: endothermic dehydroxylation:  
 $6\text{Fe}^{3+}(\text{SO}_4)(\text{OH}) \rightarrow 2\text{Fe}_2(\text{SO}_4)_3 + \text{Fe}_2\text{O}_3 + 3\text{H}_2\text{O}$
4. At 750 °C: endothermic sulphate decomposition:  
 $\text{Fe}_2(\text{SO}_4)_3 \rightarrow \text{Fe}_2\text{O}_3 + 3\text{SO}_3$

### 7.5.3. Copiapite $(\text{Fe}^{2+}, \text{Mg})(\text{Fe}^{3+}, \text{Al})_4(\text{SO}_4)_6(\text{OH})_2\cdot 20\text{H}_2\text{O}$

Reactions of the mineral:

1. Between 50 and 400 °C: endothermic dehydration in several steps:  
 $\text{Fe}^{2+}\text{Fe}^{3+}_4(\text{SO}_4)_6(\text{OH})_2\cdot 20\text{H}_2\text{O} \rightarrow \text{Fe}^{2+}\text{Fe}^{3+}_4(\text{SO}_4)_6(\text{OH})_2 + 20\text{H}_2\text{O}$
2. At about 400 °C: oxidation,
3. At about 540 °C: dehydroxylation.

Stoichiometric factor of the whole water escape: 3.3.

4. Between 740 and 780 °C: decomposition of iron sulphate.
5. Between 800 and 900 °C: decomposition of alumin-

im sulphate substitution.

6. At higher than 950 °C: decomposition of magnesium sulphate substitution.

Stoichiometric factor of the whole  $\text{SO}_3$  escape: 2.6.

Sample: Rudabánya, Hungary

Sample mass: 99.2 mg

Heating rate: 10 °C/min

Mass loss during dehydration and dehydroxylation:  
29.97%

Mass loss during sulphate decomposition: 38.3%

Copiapite content of the sample based on the whole water escape: 99%

Copiapite content of the sample based on the sulfate decomposition: 100%

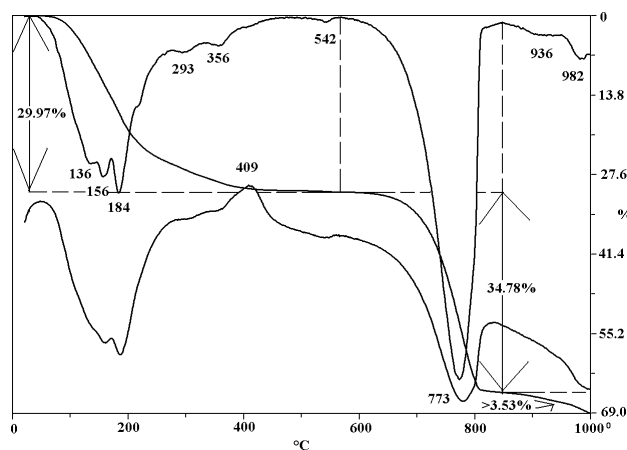


Figure 7.5.3 Thermoanalytical curves of copiapite

\*\*\*

References for sulphates: 16: ammonioalunite, 22: aluminium sulfate, aluminium potassium sulfate, aluminium ammonium sulfate and alunite 34: alunogen, copiapite, fibroferrite, slavikite 64: bassanite, metabasaluminite 63: aluminite, 73: alunite, 74: alunogen, 86, 136: rozenite, melanterite 135: pickeringite, 166, 181: hydrobasaluminite, basaluminite, 182: 215: konyaite, 225: fibroferrite, 277: chalcantite, 282: tschermigite, 283: magnesium sulphate hydrates 292: römerite, 293: aluminite, 378: jarosites, 381: alunites, 382: hydroniumjarosite, 384: ammoniojarosite, 379: argentojarosite, 380: plumbojarosite, 395: aluminite, 440: epsomite, 454: epsomite-kieserite, 455: schoenite, leonite, 456: epsomite, morenosite, goslarite, 457: kieserite, leonite, 458: astrachanite=bloedite, loweite, 459: kieserite, 460: polyhalite, kieserite, 461: kieserite, 462: gypsum, 463: epsomite, 467: anhydrite, gypsum, bassanite, glauberite, polyhalite, syngenite, glaserite, mirabilite,

## 7 Sulphates

## 8 Phosphates, arsenates, vanadates

thenardite, epsomite, kieserite, astrachanite (bloedite), loweite, vanthoffite, schoenite (picromerite), leonite, langbeinite, 510: alunite, jarosite, 513: barite, celestine, anhydrite, gypsum,  $K_2SO_4$ , thenardite, mirabilite, glauberite, polyhalite, astrachanite (bloedite), epsomite, alunogen, aluminite, melanterite, coquimbite, fibroferrite, pickeringite, halotrichite, römerite, botryogen, copiapite, goslarite,  $NiSO_4 \cdot 6H_2O$  (retgersite),  $CoSO_4 \cdot 4H_2O$  (cobaltkieserite),  $ZnSO_4 \cdot 16H_2O$ , alunite, loewigite, jarosite, plumbojarosite, bieberite, linarite, chalcantite, brochantite, cyanotrichite, 551: jarosites, 552: alunite, 553: celestite, gypsum, alunite, 563: alunite, jarosite, 633: alunite, jarosite, plumbojarosite, argentojarosite, 661: astrachanite (bloedite), gypsum, glaserite, glauberite, epsomite, kainite, langbeinite, loweite, leonite, mirabilite, polyhalite, syngenite, schoenite, thenardite, vanthoffite, 694: gypsum, 702: alunogen, 730: arcanite, thenardite, anglesite, bloedite, polyhalite, alunite, jarosite, 759: alunite, chalcantite, 806: plumbojarosite, 847: epsomite, 856: alunite, 872: gypsum, 873: alunite, 891: basic aluminium ammonium sulphate, 977: metasideronatrite, 1014: bassanite, 1017: jarosite 1033: hydrated iron sulphate, 1051: römerite, starkeyite, 1069: hydroniumjarosite, 1077: hydrobasaluminite and basaluminite, 1081: thenardite, mirabilite, arcanite, glaserite, gypsum, bassanite, anhydrite, epsomite, hexahydrate, kieserite, langbeinite, schoenite, leonite, polyhalite, astrachanite (bloedite), glauberite, chalcantite, melanterite, mallardite, morenosite, goslarite etc., 1089: fibroferrite, melanterite 1090: barite, celestine, anglesite, anhydrite, gypsum, mascagnite, thenardite, mirabilite, glauberite, astrachanite (bloedite), polyhalite, melanterite, pisanite, szomolnokite, epsomite, bieberite, morenosite, goslarite,  $MnSO_4 \cdot 5H_2O$  (jokukoite), chalcantite, alunite, loewigite, natroalunite, jarosite, natrojarosite, plumbojarosite, argentojarosite, ammoniojarosite, tschermigite, fibroferrite, aluminite, alunogen, römerite, halotrichite, 1169: ammonium and potassium alums, 1190: sideronatrite, melanterite

## 8. PHOSPHATES, ARSENATES, VANADATES

The existing structure of the phosphates persisted up to and above 1000 °C. In the course of the thermal analysis of phosphates processes of dehydration, dehydroxylation, dissociation of additional anions, oxidation, melting and inversion from one modification into another take place.

### 8.1. Hydrated phosphates

#### 8.1.1. Vivianite $Fe^{2+}_3(PO_4)_2 \cdot 8H_2O$

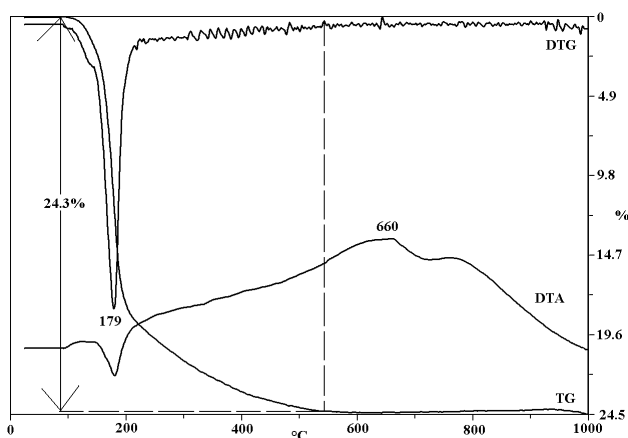


Figure 8.1.1. Thermoanalytical curves of vivianite

Reactions of the mineral:

1. Between 250 and 300 °C: endothermic: escape of crystal water (according to the literature sometimes in several steps)

Stoichiometric factor of the reaction: 3.48.

2. Above about 500 °C: oxidation

Sample: Egyházaskesző, Hungary

Sample mass: 13.8 mg

Heating rate: 10 °C/min

Mass loss during dehydration: 24.3%

Vivianite content of the sample based on the water escape: 85%

### 8.2. Anhydrous phosphates containing hydroxyl

#### 8.2.1. Lazulite $(Mg,Fe)Al_2(PO_4)_2(OH)_2$

Reactions of the mineral:

1. Between 700 and 800 °C: endothermic: dehydroxylation

Stoichiometric factor of the reaction: 16.8–18.5.

2. At about 900 °C: exothermic: crystallization of  $AlPO_4$  phase

## 8 Phosphates, arsenates, vanadates

Sample: unknown  
 Sample mass: 900 mg  
 Heating rate: 17 °C/min  
 Mass loss during dehydroxylation: 5.0%  
 Lazulite content of the sample based on the OH content: ≈90%

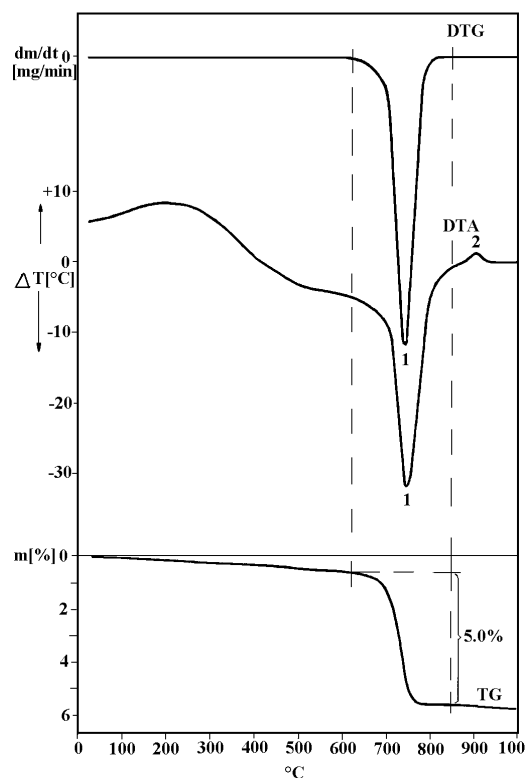


Figure 8.2.1. Thermoanalytical curves of lazulite

### 8.2.2. Gorceixite $\text{BaAl}_3(\text{PO}_4)(\text{PO}_3\text{OH})(\text{OH})_6$

Reactions of the mineral:

1. at about 420 °C: endothermic dehydroxylation (Al-OH?),
2. at about 520 °C: endothermic dehydroxylation [Ba(Ca, Sr)-OH?],
3. at 835 °C: endothermic decomposition of sulphate substitution as unfamiliar anion,
4. at 860 °C: exothermic crystallization of  $\text{AlPO}_4$  phase.

Sample: Borehole Szuhogy-6, Rudabánya Mts, Hungary

Sample mass: 900 mg

Heating rate: 10 °C/min

Mass loss during dehydroxylation: 7.4%

Gorceixite content of the sample based on the OH content: ≈60%

Other thermally active minerals in the sample: kaolinite, pyrite, calcite trace

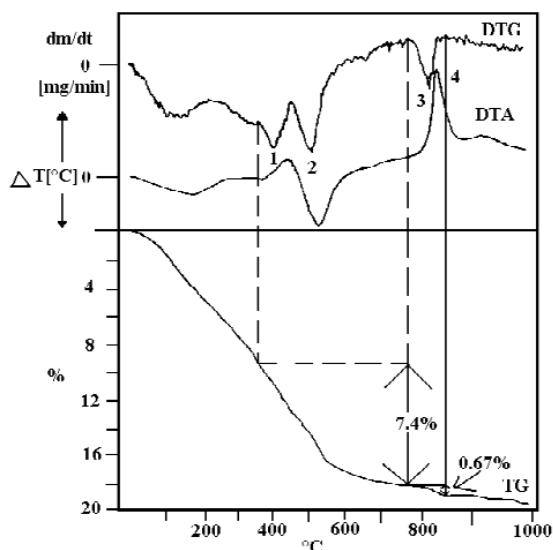


Figure 8.2.2. Thermoanalytical curves of gorceixite

## 8.3. Water-bearing phosphates with additional anions

### 8.3.1. Diadochite $\text{Fe}^{3+}_2(\text{PO}_4)(\text{SO}_4)(\text{OH})\cdot 6\text{H}_2\text{O}$

Reactions of the mineral:

1. Between 60 and 350 °C: endothermic: dehydration and probably dehydroxylation.

Stoichiometric factor of the reaction: 4.14.

## 8 Phosphates, arsenates, vanadates

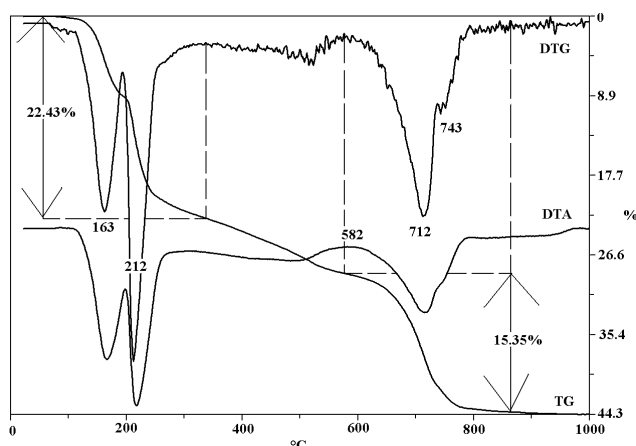


Figure 8.3.1. Thermoanalytical curves of diadochite

2. At about 600 °C: exothermic: crystallisation of  $\text{FePO}_4$  phase

3. Between 700 and 750 °C: endothermic: sulphate decomposition.

Stoichiometric factor of the reaction: 6.04.

Sample: Recsk, Sima Hill, Hungary

Sample mass: 101.2 mg

Heating rate: 10 °C/min

Mass loss during the first reactions: 22.43%

Mass loss during the third reaction: 15.35

Diadochite content of the sample based on the first reactions: 93%

Diadochite content of the sample based on the third reaction: 93%

## 8.4. Hydrated arsenates

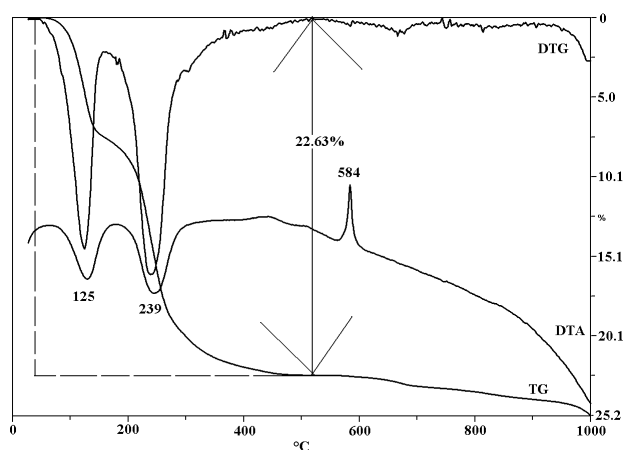
8.4.1. Kaňkite  $\text{Fe}^{3+}\text{AsO}_4 \cdot 3.5\text{H}_2\text{O}$ 

Figure 8.4.1. Thermoanalytical curves of kaňkite

Reactions of the mineral:

1. At 120–190 °C and 240–290 °C: endothermic: dehydration

Stoichiometric factor of the water content: 4.09.

2. At about 600 °C: exothermic: recrystallization of the waterfree phase?

3. In the higher temperature range: a slow decrease in weight loss caused by volatilization of As in varying amount.

Sample: Nagybörzsöny, Börzsöny Mts, Hungary

Sample mass: 81.7 mg

Heating rate: 10 °C/min

Mass loss during dehydration: 22.63%

Kaňkite content of the sample based on the dehydration: 93%

\*\*\*

References for phosphates, arsenates, vanadates: 4: sanjuanite, 27: variscite, metavariscite, strengite, barrandite, wavellite, taranakite, 84: brushite, struvite, 92: gorcexite arrojadite, brasilianite, hurlbutite, lazulite, lithiophyllite, metastrengite, moraesite, plumbogummite, scorzalite, svanbergite, vivianite, 98: crandallite, 99: crandallite, 110: destinezite, 128: crandallite, 162: kaňkite, 163: zykaite, 167: mounanaite, 191: crandallite, 236: brushite, 267: anapaite, 273: kingite, 306: florencite, 312: brushite, hydroxylapatite, taranakite 322: vivianite, 334: diadochite, destinezite, 374: peisleyite, 375: metazeunerite, 376: struvite, 371: vivianite, 372: erythrite, annabergite, hornesite, 383: kintoreite, 439: kemmlitzite, 446: schroderite, 465: newberyite, 467: brushite, newberyite, struvite, 506: bermanite, 513: berlinite, monetite, elite (pseudomalachite), libethenite, birûza (turquoise), lazulite, monacite, rabdophane, amblygonite, montebasite, augelite, crandallite, gorcexite, woodhouseite, svanbergite, carbonate-apatite (dahlite), destinesite, abucumalite (britholite), variscite, vivianite, wavellite, cefarovite, collinsite, evansite, luneburgite, kershenite (whitmoreite?), oxikersheinite, sampleite, arsenates: erythrite, annabergite, olivenite, scorodite, tyrolite, roselite, belovite, picropharmacolite, adamite, mimetesite (mimetite), 522: diadochite, 553: lithiophyllite, triphyllite, wavellite, dufrenite, wagnerite, 574: vivianite, 616: gorcexite, 664: gladiusite, 705: zepharovichite, wavellite, turquoise, variscite, bolivarite, lazulite, berlinite, amblygonite, vivianite, bobierrite, wardite, augelite, evansite, 715: vivianite, 730: wavellite, vivianite, 791: gorcexite, hinsdalite, 792: phosphorite, 793: kingite, 797: bukovskyite, 800: vashegyite, 801: vajdakite, 802: parascorodite, 883: gorcexite, 895: kaatialaite, 906: mansfieldite, 910: vivianite, metavivianite, baračite, ludlamite, vivianite/metavivianite admixtures 981: augelite, strengite, 1006: vivianite, annabergite, erythrite, struvite, haidingerite, amblygonite 1015: phosphates: bermanite, taranakite, torbernite, struvite, vivianite, autunite, paravauxite, sigolite, stewartite, strunzite, wavellite, kingite, newberyite, metatorbernite, phosphorite, anapaite, brushite, amblygonite, turquoise, augelite, metastrengite, variscite, strengite, arse-

nates: annabergite, erythrite, hornesite, tyrolite, lavendulaite, haidingerite, skorodite, adamite, olivenite, vanadates: steigerite, rusakovite, 1050: diadochite, 1052: kankite, 1054: gorceixite, 1070: calderonite, 1078: vivianite, 1081: wavellite, vivianite, ambligonite, apatite, augelite, autunite, berlinite, bosporite (santabarbaraite), bobierrite, evansite, 1083: apatites, 1086: scorodite, 1109: bassetite, 1117: bolivarite, 1191: variscite

## 9. BORATES

Thermal decomposition of borates is a complex mechanism. After BERG (1970) typical reactions of borates are dehydration, polymorphic transition, melting and solid phase transformation. The author has never investigated borate minerals so far, therefore here only some references are given.

References for borates: 24: ameghinite, 25: macallisterite, 26: teruggite, 86: boracite, calcium monoborate, calcium triborate, colemanite, hydroboracite, inderite, inyoite, kaliborite, magnesium triborate, magnesium triborate, pandermite, pinnoite, szájbelyite, ulexite, 89: tuzlaite, 289: iquiqueite, 444: borax, 453: ascharite, 476: boracite, 504: rivadavite, 505: ezcurrite, 661: hydroboracite, 730: sassolite, borax, colemanite, 1006: borax, kernite, colemanite, ulexite, 1028: colemanite, 1112: colemanite

## 10. HALIDES

Thermal analysis is not a usual method for detecting natural halogenides. In the thermal curves first of all inversion and melting can be observed. Water bearing salts show also complex dehydration, and HCl evolving reactions (for example bischofite, carnallite, tachyhydrite).

### 10.1. Halite NaCl

The reaction of the mineral: at 800 °C: endothermic: melting, then evaporation.

Sample mass (Figure 10.1a): 1000 mg

Heating rate: 10 °C/min

Melting temperatures are markedly dependent on the presence of impurities.

Sample (Figure 10.1b): Recsk, Hungary

Sample mass: 119.1mg

Heating rate: 10 °C/min

Other thermally active mineral in the sample: epsomite

The common occurrence of sylvine and halite also shifts the temperature of their melting to a lower value.

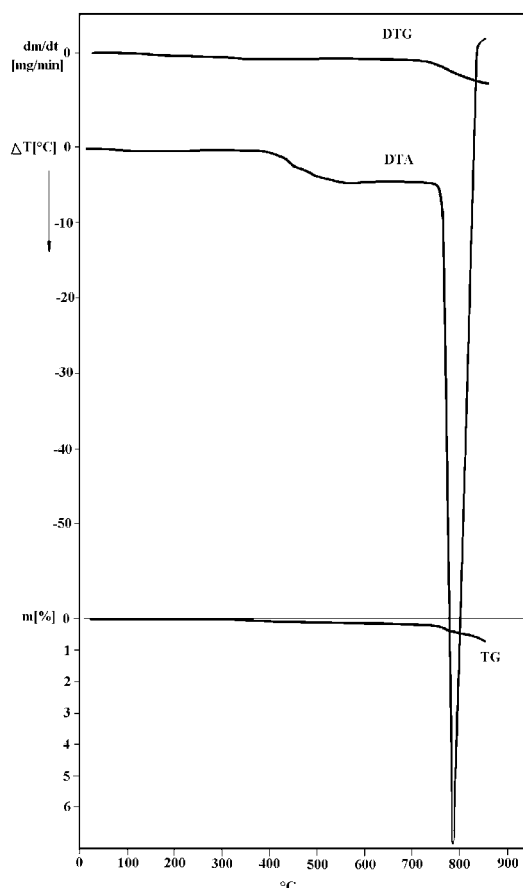


Figure 10.1a. Thermoanalytical curves of halite

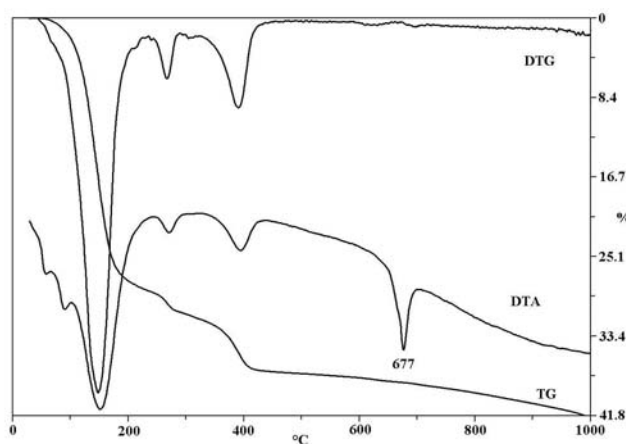


Figure 10.1b. Thermoanalytical curves of an admixture of epsomite and halite

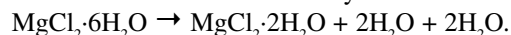
## 10 Halides

## 11 Organic minerals

10.2. Bischofite  $\text{MgCl}_2 \cdot 6\text{H}_2\text{O}$ 

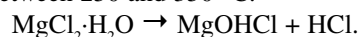
Reactions of the mineral:

1. At about 140 °C: endothermic: dehydration:



2.  $\text{MgCl}_2 \cdot 2\text{H}_2\text{O} \rightarrow \text{MgCl}_2 \cdot \text{H}_2\text{O} + \text{H}_2\text{O}.$

3. Between 250 and 350 °C:



4. At about 700 °C: melting.

\*\*\*

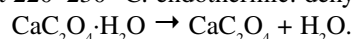
References for halides: 279: carnallite, 280: carnallite, 281: carnallite, bischofite, 469: halite, sylvite, 470: bischofite, 473: bischofite, 513: cryolite, halite, sylvite, bischofite, atacamite, 518: fluorite, 553: cryolite, fluorite, 589: iowaite, 647: carnallite, halite sylvite, 648: halite, sylvite, 661: bischofite, carnallite, kainite, 730: cryolite, carnallite, atacamite, paratacamite, 869: bischofite, 1081: halite, sylvite, bischofite, carnallite, tachyhydrite, kainite

## 11. ORGANIC MINERALS

11.1. Whewellite  $\text{Ca}(\text{C}_2\text{O}_4) \cdot \text{H}_2\text{O}$  (calcium oxalate monohydrate)

Reactions of the mineral:

1. At 220–230 °C: endothermic: dehydration of crystal water:



Stoichiometric factor of the reaction: 8.11.

2. At about 500 °C: combination of endothermic and exothermic: elimination and burning of CO

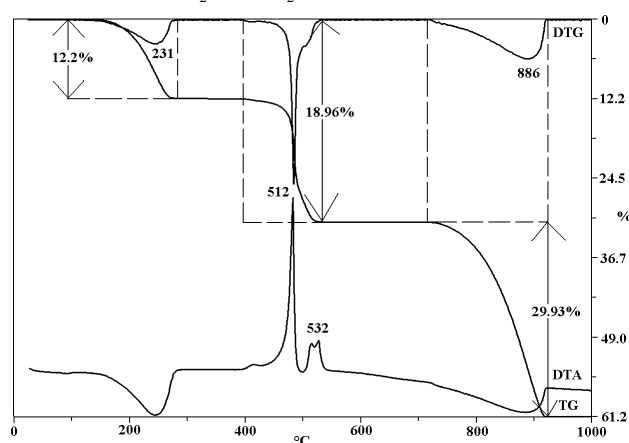
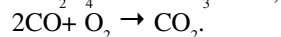
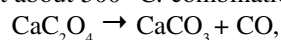
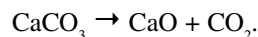


Figure 11.1. Thermoanalytical curves of whewellite

Stoichiometric factor of the reaction: 5.22.

3. At about 900 °C: endothermic:



Stoichiometric factor of the reaction: 3.31.

Sample mass: 100.0 mg

Heating rate: 10 °C/min

Mass loss during the first reaction: 12.2%

Mass loss during the second reaction: 18.96%

Mass loss during the third reaction: 29.93%

Whewellite content of the sample based on the first reaction: 99%

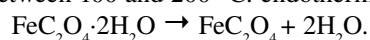
Whewellite content of the sample based on the second reaction: 99%

Whewellite content of the sample based on the third reaction: 99%

11.2. Humboldtine (oxalite)  $\text{Fe}^{2+}(\text{C}_2\text{O}_4) \cdot 2\text{H}_2\text{O}$ 

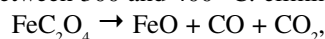
Reactions of the mineral:

1. Between 100 and 200 °C: endothermic: dehydration:

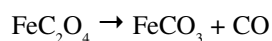


Stoichiometric factor of the reaction: 5.

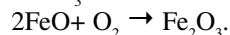
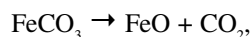
2. Between 300 and 400 °C: elimination of CO or  $\text{CO}_2$ :



or



and



Stoichiometric factor of the second reaction: 2.81.

Stoichiometric factor of the second reaction in inert atmosphere (without the last reaction of oxidation): 2.5.

Sample: Csordakút, Hungary

Sample mass: 5.8 mg

Heating rate: 10 °C/min

Mass loss during the first reaction: 17.41%

Mass loss during the second reaction: 31.38%

Humboldtine content of the sample based on the first reaction: 87%

Humboldtine content of the sample based on the second reaction: 88%

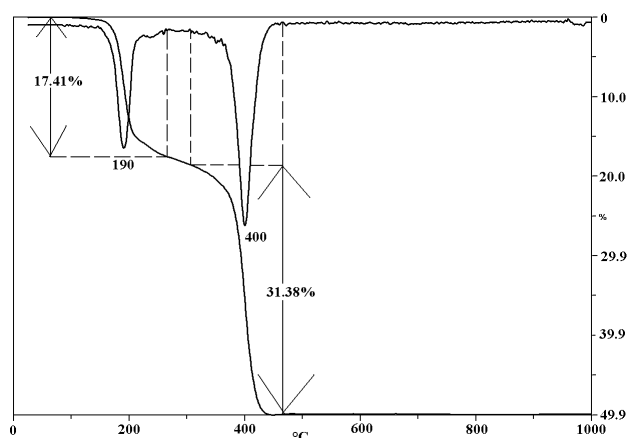


Figure 11.2. Thermoanalytical curves of humboldtine

\*\*\*

References for organic minerals: 33: lindbergite, 85: whewellite, 216: oxalates, 264: whewellite, caoxite, 373: moolooite, 358: weddelite, 359: humboldtine, 360: whewellite, 361: oxammite, 388: calciumoxalathydraten, 546: calcium oxalate, 580: weddelite, 1143: mellite, 1157: whewellite, weddelite

## 12. ORGANIC MATERIALS

Application of thermogravimetry gives various possibilities for the investigation of the natural organic matter, coal, oil shale, etc. The aspects of investigation may include the detection or quantitative determination of the organic matter content, the characterisation of the rank of coal or dispersed organic matter. Thermal reactions of organic material are generally complicated. The organic matter forms a continuous series according to the increasing degree of coalification.

### 12.1. Determination of the coalification of organic matter content of the sample

The burning of organic material causes a strong exothermic reaction frequently in a broad temperature range. There is a correlation between the temperature of exothermal effects during the combustion of the organic matter and the grade of coalification.

The area under the exothermic peak of oxidation is proportional to the heat of combustion and may be calibrated for example with the similar reaction of saccharose ( $\text{C}_{12}\text{H}_{22}\text{O}_{11}$ ), which produces 16.51 kJ/g heat during the burning.

### 12.2. Proximate (immediate) analysis of coal

As the degree of coalification (rank) increases, the carbon content increases and the amount of volatile decreases. These variations in thermal behaviour in accordance with a reduction in undersaturated bonds and functionalized groups, and an increase in the proportion of aromatized groups.

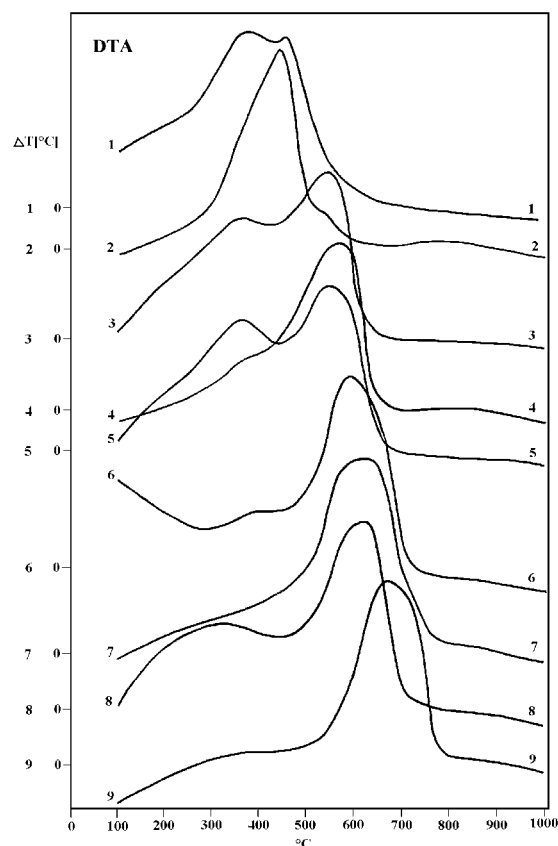


Figure 12.1. DTA curves of 20 mg coal sample diluted by 980 mg  $\text{Al}_2\text{O}_3$

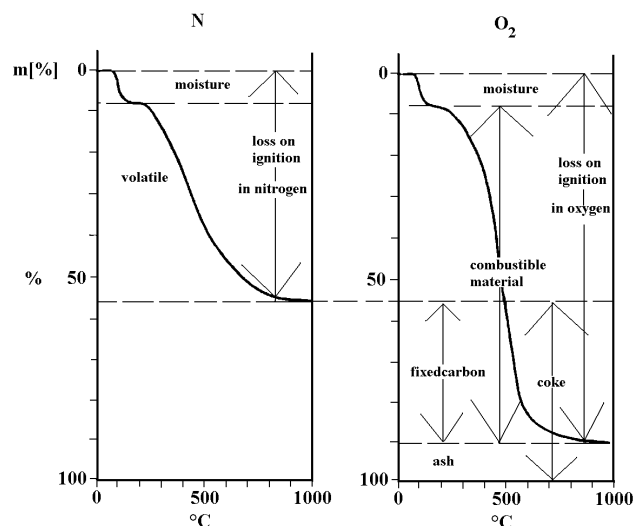
1 — brown coal, Tertiary, 2 — brown coal Jurassic, 3 — flame coal, Permian, 4 — gas coal Carboniferous, 5 — fat coal Carboniferous, 6 — coke coal, Jurassic, 7 — lean coal, Permian, 8 — semi-anthracite, Permian, 9 — anthracite, Carboniferous

## 12 Organic materials

## 13 Investigation of rocks

**Table T12.2.** Characterisation of coal by thermogravimetric analysis

Measurable parameters from the TG curve	Condition of the measurement	Result
Moisture	in N <sub>2</sub> or in O <sub>2</sub>	
Volatile	in N <sub>2</sub>	
Loss on ignition	in N <sub>2</sub>	Moisture + volatile matter
Loss on ignition	in O <sub>2</sub>	Moisture + combustible material
<b>Calculated values</b>		
Fixed carbon		combustible material - volatile
Ash		100 - loss on ignition in O <sub>2</sub>
Coke		fixed carbon - ash
<b>Characteristic values for the rank of coals</b>		
Volatile content of ash and moisture free sample		$\left( \frac{\text{volatile}}{\text{combustible material}} \right) * 100$
C <sub>org</sub> content	CO <sub>2</sub> content formed during burning of the combustible material (in O <sub>2</sub> ) and determined by titration	$C_{\text{org}} = \frac{CO_2}{3.67}$

**Figure 12.2.** Characterisation of coal by thermogravimetric analysis

For the characterisation of a coal sample a proximate analysis can be carried out by the combination of thermogravimetric curves measured in inert and oxygen atmosphere (determination of moisture, volatile matter, fixed carbon (by difference) and ash). (Table T12.2 and Figure 12.2).

\*\*\*

References for organic materials: 18, 55, 91, 100, 160, 257, 258, 261, 276, 320, 404, 513, 581, 602, 606, 714, 828, 902, 903, 958, 1113, 1125, 1128, 1130, 1132, 1133, 1134, 1135, 1146, 1147, 1148, 1149, 1150

## 13. INVESTIGATION OF ROCKS

## 13.1. Perlite

Acid volcanic glass is a frequently investigated rock type. The possible investigated features are water content and forms of water bonding. The typical thermoanalytical curves show a broad endothermic water escaping reaction (see Figure 13.1).

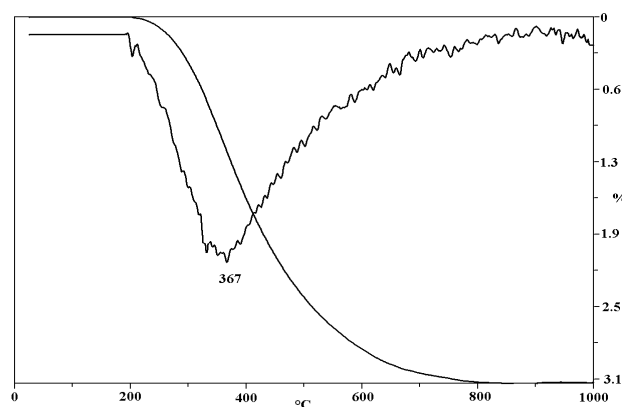
Sample (Figure 13.1): Pálháza, Hungary

Sample mass: 98.9 mg

Heating rate: 10 °C/min

Water content of the sample: 3.17%

PERLAKI, SZŐÖR (1973) could distinguish two major genetic types of perlites: 1. green perlites, richer in water content (>6%) and 2. grey (black) perlites, less rich in water (<6%). IVANOVA et al. (1974) based on the

**Figure 13.1.** Thermogravimetric curves of perlite

water content versus the proportion of water content  $H_2O < 480^\circ C$  /  $H_2O > 480^\circ C$  subdivided perlites into three groups.

References: 466, 507, 549, 658, 781, 863

## 13.2. Phase analysis

Thermogravimetric analysis is an important tool for qualitative or quantitative determination of the mineral component of rocks and soils.

As an example, bauxite is a typical rock suitable for phase analysis by thermogravimetry.

Sample: Szőc, Hungary

Sample mass: 201.4 mg

Heating rate:  $10^\circ C/min$

Table T13.2a. contents the calculation methods of the different minerals shown on the thermoanalytical curves (Figure 13.2). These results are compared with the results of other analytical methods in Table T13.2b.

**Table T13.2a.** Evaluation by the measured data

Peak temperature ( $^\circ C$ )	Identification	Mass loss (%)	Stoichiometric factor of the phase	Quantity of the phase (%)
83	adsorptive water	1.83		
322	gibbsite	9.31	2.89	27
384	alumo-goethite	0.6	9.9	6
461	diaspore	1.62	6.66	11
534	boehmite	2.2	6.66	15
549	kaolinite	1.63	7.17	12
678	calcite or sulphate ?	0.83		

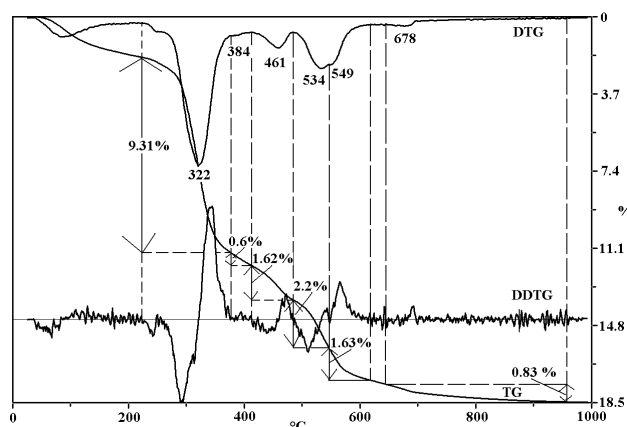


**Figure 13.2.** Quantitative evaluation of a bauxite sample

**Table T13.2b.** Comparison the results of different investigations

Mineral	XRD	TG	%	SiO <sub>2</sub>	TiO <sub>2</sub>	Al <sub>2</sub> O <sub>3</sub>	Fe <sub>2</sub> O <sub>3</sub>	FeO	CaO	MgO	Na <sub>2</sub> O	K <sub>2</sub> O	H <sub>2</sub> O	CO <sub>2</sub>	SO <sub>3</sub>	Total
Quartz			2	2												2.00
Kaolinite	14	12	12	5.59		4.74							1.68			12.00
Calcite		2?	2						1.12					0.88		2.00
Goethite	7	6	6				5.39						0.61			6.00
Hematite	18		20				20									20.00
Gibbsite	31	27	27			17.65							9.35			27.00
Boehmite	15	14	14			11.9							2.1			14.00
Diaspore	13	11	11			9.35							1.65			11.00
Anatase	1		2		2											2.00
Rutile	1		1		1											1.00
Water adsorption													1.83			97.00
<b>Total</b>		<b>70</b>	<b>97</b>	<b>7.59</b>	<b>3.00</b>	<b>43.63</b>	<b>25.39</b>	<b>0.00</b>	<b>1.12</b>	<b>0.00</b>	<b>0.00</b>	<b>0.00</b>	<b>17.22</b>	<b>0.88</b>	<b>0.00</b>	<b>98.83</b>
<b>Chemical analysis</b>				<b>8.26</b>	<b>3.2</b>	<b>42.1</b>	<b>25.7</b>	<b>0.18</b>	<b>1.2</b>	<b>0.54</b>	<b>0.26</b>	<b>0.03</b>	<b>18.1</b>	<b>0.02</b>	<b>0.66</b>	<b>100.25</b>
Deviation				0.67	0.20	-1.53	0.31	0.18	0.08	0.54	0.26	0.03	0.88	-0.86	0.66	
<b>From TG curve</b>													<b>17.44</b>	<b>0.83?</b>	<b>0.83?</b>	

References: 327, 338, 335, 560, 650, 759, 825, 830, 831, 839, 991

## 14 Special geological applications

## 14. SPECIAL GEOLOGICAL APPLICATIONS

A large number of publications in many fields of geology apply thermal methods for solving specific geoscientific problems. Traditionally, the major areas of application of thermal methods of analysis to minerals are: Assessment of raw material deposits, detailed characterization, classification and analysis. A relatively recent application of thermal techniques is in environmental studies. *Thermochimica Acta* 195 (1997) 1–183. is a complete issue of TA with papers from a symposium on environmental topics.

The references below give some examples.

1. There is a close analogy between **dehydration (dehydroxylation) and loss of argon** curves obtained by heating of muscovite. Structure disintegration, which may be seen from the thermogravimetric curve, introduces to the uncertainty in K/Ar age determination.

Reference: 119

2. A relatively recent application of thermal techniques is in **environmental studies**.

A review is presented of the applications of thermoanalytical techniques to problems encountered in the measurement and control of air pollution.

Reference: 726

3. **Investigations** have shown that **taxonomical difference** or genus (and possibly species) within the same biotop can be **determined by derivatographic measurement** of the total organic content and the bonding of organic material of **shell**. The fossilization coefficient determined from the thermogravimetric method is in close correlation with the time of burial of **tooth and bones of vertebrata**. Using this statement there is a possibility for **age determination**.

References: 519, 1055, 1056, 1057, 1058, 1060, 1061, 1062, 1063

4. **The inversion temperature of quartz as a petrologic tool**. The inversion temperature of quartz crystals from igneous rocks is higher than those from sedimentary rocks formed by processes of diagenesis or weathering.

References: 1002, 1003, 1004, 1005, 1013, 1094

5. Thermogravimetric examination of soils for soil mechanical and construction-geological application.

Reference: 1059

6. Determination of the degree of weathering of rocks.

The weathering of rocks means the destruction of primary minerals, mainly by the activity of water. This hydration of components results in the formation of hydroxides or clay minerals.

a) The peak area of dehydration and dehydroxylation effects in the DTA curve may **characterize the weathering of granitic rocks**.

Reference: 1009

b) **Weathering curve of loess sections** based on the measuring of molecular water and OH content of the samples (Figure 14.6b). This curve also indicates indirectly the **palaeoclimate** as soil development is a process of weathering of loess layers in the more humid, warmer climate of interglacials.

References: 209, 332, 716

7. Temperature of metasomatic rock alteration of andesitic magmatites.

In the Velence Mts heavily altered andesite volcanics belonging to silicate and sulphate series acidic and intermediar metasomatism were investigated with different temperatures. Temperature zones are assigned well by the molecular water content of clay minerals in the sample (Figure 14.7).

Reference: 206

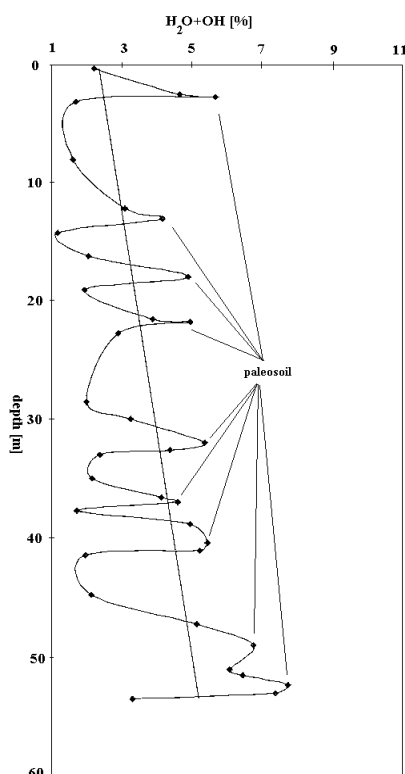


**Figure 14.6b.** Weathering (palaeoclimate) curve of a loess section in borehole Üvegkúta Úh-22 (Hungary), based on the molecular and hydroxide water content measured from TG curves

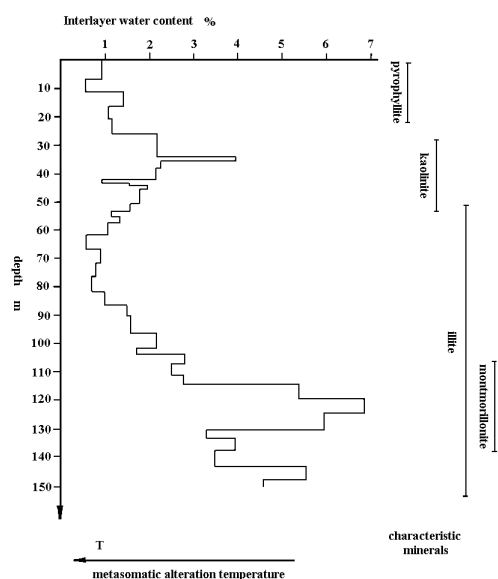


**Figure 14.7.** Relationship between the interlayer water content and the metasomatic alteration temperature in the Borehole Pázmánd-2, Hungary

#### 8. Kaolinite genetic and thermoanalytical parameters.

Based on measuring 362 different genetic kaolinite occurrences, the three best crystallinity parameters for the characterisation are summarized in Table T14.8. The temperature intervals of genetic types is shown on Figure 14.8a.

Figure 14.8b. presents that the order of structure increases during the diagenetic processes, and may reach the values of the kaolinite of hydrothermal genesis.

Interesting and new conclusions also from the temperature of the exothermic peak may be drawn (Figure 14.8c). For example diagenesis influences not only the temperature of dehydroxylation but that of exothermic reactions (see palaeosols from different ages) as well or the two different groups of data in the sandstone may indicate the different original genesis of the kaolinite content.

References: 324, 330, 331

#### 9. Degassing behavior of natural glasses and implications for their origin.

Degassing experiments showed that a remarkable difference existed between glasses from a range of geological environments. The gas release profiles of natural glasses can be divided into three groups: volcanic glasses, impact glasses and silica glasses and tectites. Gas release curves are suitable tools for the identification of vitreous samples of unknown origin.

Reference: 468

**Table T14.8.** Characteristic thermal parameters of crystallinity for kaolinite of different genesis

Genetic type	Geological effect	Number of samples	$T_{100\%}$ of dehydroxylation (°C)	Activation energy (joule/mol)	Temperature of the exothermic peak °C
					mean
High temperature hydrothermal	temperature	31	669	137	994
Low temperature hydrothermal	temperature	39	573	147	991
Paleosol (Devonian)	diagenesis	6	577	139	996
Palaeosol (Triassic)	diagenesis	5	565	134	968
Terrestrial sandstone		40	564	133	964
Low temperature weathering		69	564	133	959
Bauxite		114	560	130	961
Palaeosol (Pleistocene)		58	547	115	932

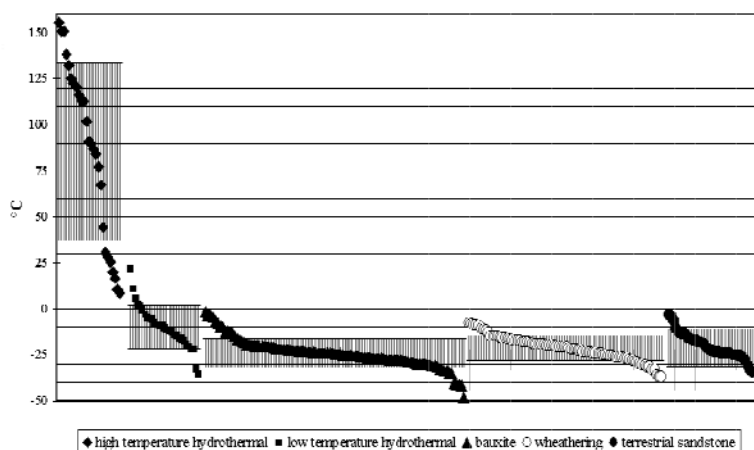


**Figure 14.8a.** Characteristic thermal decomposition temperature for kaolinite of different genesis compared to Mesa Alta kaolinite

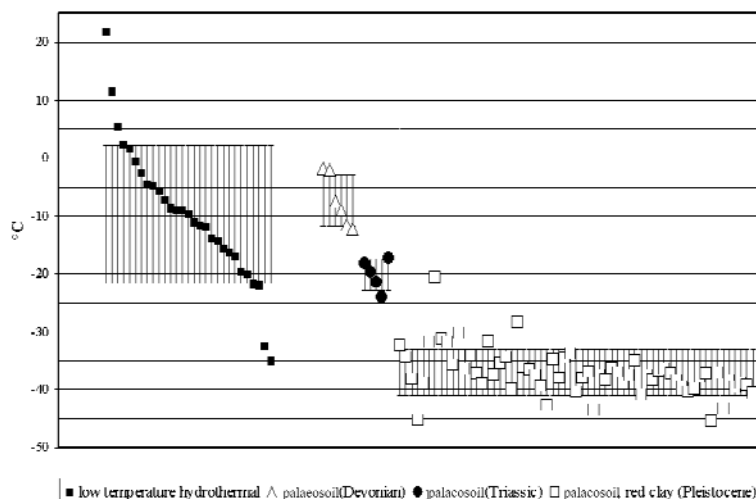


**Figure 14.8b.** Characteristic thermal parameters for kaolinite of different diagenetic stage compared to hydrothermal kaolinite

## 14 Special geological applications

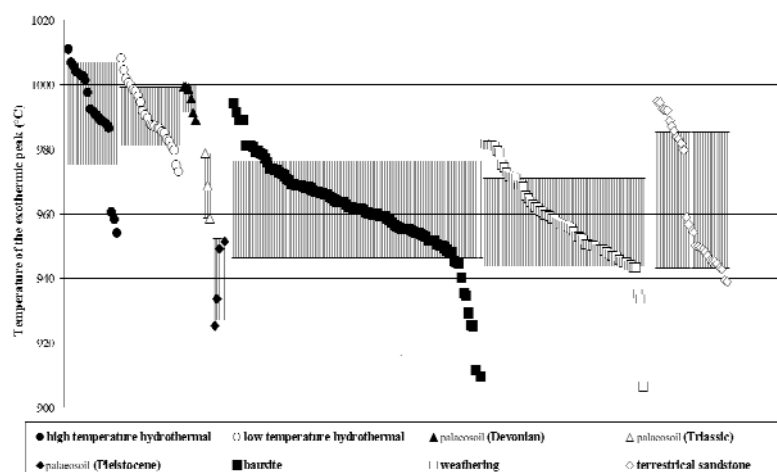


Figure 14.8c. Peak temperature of exothermic reaction for kaolinite of different genesis

in thermal behaviour correlate with a reduction in undersaturated bonds and functionalized groups, and an increase in the proportion of aromatized groups that characterize resin aging. Used judiciously, thermal behavior may indicate maturation histories and resin associations.

References: 513, 909, 911

## 12. Temperature of carbonate precipitation of lacustrine travertines.

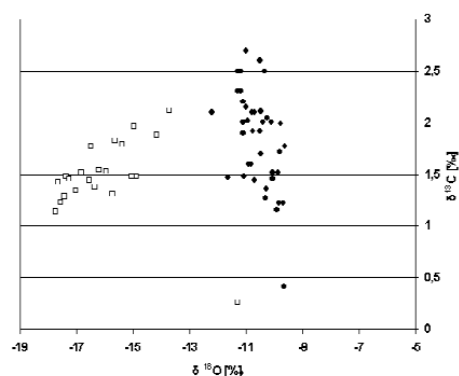


Figure 14.12a.  $\delta^{13}\text{C}$  and  $\delta^{18}\text{O}$  values

Buda-Várhegy travertine,  $\square$  Budakalász travertine

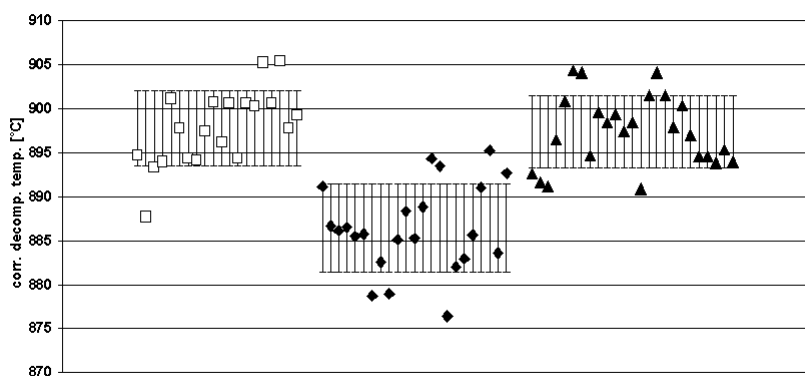


Figure 14.12b. Corrected decomposition temperature of travertine sample from different localities

$\square$  Buda-Várhegy travertine,  $\blacklozenge$  Budakalász travertine,  $\blacktriangle$  Szomód, Les Hill

TA data give comparable results with those of oxygen and carbon stable isotope composition (Figure 14.12a) and offer a new way to estimate the temperature of carbonate precipitation as may be seen on Figure 14.12b. in the case of travertine limestone from different localities.

Reference: 339

## 13. Rapid screening of soil properties

For mineral soils, different soil properties (organic C, total N, clay, and  $\text{CO}_3\text{-C}$ ) correlated closely with a specific temperature interval of weight losses.

Reference: 995

## 14. Other references of special geological applications: 239, 325, 649, 1012, 1129

## 10. Meteorites

References: 643, 1025

## 11. Thermal analytical study of fossil resins

Differential and thermogravimetric analyses of resins show a progressive change in their combustion profiles with increasing age. Differences between modern resins and Pleistocene Kauri gums are minimal. Diagenetic changes accompanying thermal maturation reveal a reduction in intensity of thermal responses below 200 °C and a progression in the temperature of the major thermal combustion event, from 350–450 °C in the younger resins, to 450–580 °C in the 40 000 000-year-old copals. These variations

## REFERENCES

1. ABDEL REHIM, A. M. 1991: Application of thermal analysis in mineral technology. — In: SMYKATZ-KLOSS W., WARNE S. ST. J. (eds): *Thermal Analysis in the Geosciences*. Series of Lecture Notes in Earth. Springer Verlag, pp. 188–222.
2. ABDEL REHIM, A. M. 1997: Application of thermal analysis to mineral synthesis. — *Journal of Thermal Analysis* 48 (1), pp. 177–202.
3. ABDEL REHIM, A. M. 2006: Thermal and XRD analysis of Egyptian galena. — *Journal of Thermal Analysis* 86 (2), pp. 393–401.
4. ABELEDO, DE M. E. J., ANGELELLI, V., BENYACAS, DE M. A. R., GORDILLO, C. 1968: Sanjuanite, a new hydrated basic sulfate-phosphate of aluminum. — *The American Mineralogist* 53 (1–2), pp. 1–8.
5. ABOU SEKKINA, M. M., GHONEIM, M. F., ALY, S. M., EL-KERSH, M. 1984: Application of thermal and X-ray analyses in the identification and quantitative estimation of some serpentines of South Hungarian Transdanubian and East Egyptian Precambrian rocks. — *Journal of Thermal Analysis* 29 (6), pp. 1309–1317.
6. AFANAS'EV, G. D. 1962: Osobennosti sjūd i polevih spatov važnye dlā geohronologii. — *Acta Geologica Hungarica* 6 (3–4), pp. 275–285.
7. AGIORGITIS, G. 1969: Über differential-thermoanalytische und infrarotspektroskopische Untersuchungen von Mangan-Mineralien. — *Tschermaks Mineralogische und Petrographische Mitteilungen* 13 (3–4), pp. 273–283.
8. AHLDRICH, J. L., SERNA, C. J., SERRATOSA, J. M. 1975: Structuralhydroxyls in sepiolites. — *Clays and Clay Minerals* 23 (2), pp. 119–124.
9. ALBERTI, A., VEZZALINI, G. 1979: The crystal structure of amicitite, a zeolite. — *Acta Crystallographica Section B* 35 (12), pp. 2866–2869.
10. ALBERTI, A., VEZZALINI, G. 1983: The thermal behaviour of heulandites: A structural study of the dehydration of Nadap heulandite. — *Tschermaks Mineralogische und Petrographische Mitteilungen* 31 (3), pp. 259–270.
11. ALBERTI, A., SACERDOTI, M., QUARTIERI, S., VEZZALINI, G. 1999: Heating-induced phase transformation in zeolite brewsterite: new 4- and 5-coordinated (Si,Al) sites. — *Physics and Chemistry of Minerals* 26 (3), pp. 181–186.
12. ALIETTI, A. 1972: Polymorphism and crystal-chemistry of heulandite and clinoptilolite. — *The American Mineralogist* 57 (9–10), pp. 1448–1462.
13. ALIETTI, A., MEJSNER, J. 1980: Structure of talc-saponite mixed-layer mineral. — *Clays and Clay Minerals* 28 (5), pp. 388–390.
14. ALONSO, M., GONZALEZ, A., DE SAJA MUNOZ, A., ESCALONA, J. A. 1991: Quality control of mineral impurities in industrial talcs by thermogravimetric analysis. — *Thermochimica Acta* 184 (1), pp. 125–130.
15. ALT, J. C., BACH, W. 2001: Data report: Low-grade hydrothermal alteration of uplifted lower oceanic crust, Hole 735B: mineralogy and isotope geochemistry. — In: NATLAND, J. H., DICK, H. J. B., MILLER, D. J., VON HERZEN, R. P. (eds): *Proceedings of the Ocean Drilling Program, Scientific Results*, 176. [Online]. [http://www-odp.tamu.edu/publications/176\\_SR/chap\\_01/chap\\_01.htm](http://www-odp.tamu.edu/publications/176_SR/chap_01/chap_01.htm)
16. ALTANER, S. P., FITZPATRICK, J. J., KROHN, M. D., BETHKE, PH. M., HAYDA, D. O., GOSS, J. A., BROWN, Z. A. 1988: Ammonium in aluminates. — *The American Mineralogist* 73 (1–2), pp. 145–152.
17. ALVAREZ, M., RUEDAAND, E. H., SILEO, E. E. 2006: Structural characterization and chemical reactivity of synthetic Mn-goethites and hematites. — *Chemical Geology* 231 (4), pp. 288–299.
18. AMARSKII, E. G., VYALOV, V. I. 1995: Thermal analysis of anthracites, meta-anthracites, and graphites. — *Fuel and Energy Abstracts* 36 (2), p. 404.
19. ANAND, R. R., GILKES, R. J. 1987: An application of thermogravimetry to quantitative studies of feldspar alteration in soils. — *Journal of Thermal Analysis* 32 (4), pp. 1163–1175.
20. ANEESUDDIN, M., CHAR, P. N., RAZA HUSSAI, N. M., SAXENA, E. R. 1983: Studies on thermal oxidation of chalcopyrite from Chitradurga, Karnataha State, India. — *Journal of Thermal Analysis* 26 (2), pp. 205–216.
21. ANTON, O. 1969: Study on thermal transformation of pyrophyllite. — *Revue Roumaine de Geologie, Geophysique et Geographie Serie de Geologie* 13 (1), pp. 29–38.
22. APTE, N. G., KIRAN, E., CHERNOSKY, J. V. 1988: Thermal decomposition of aluminium-bearing compounds. — *Journal of Thermal Analysis* 34 (4), 975–981.
23. ARAÚJO, J. H., SILVA, N. F. ACCHAR, W., GOMES, U. U. 2004: Thermal decomposition of illite. — *Materials Research* 7 (2), pp. 359–361.
24. ARISTARAIN, L. F., HURLBUT, C. S. JR 1967a: Ameghinite,  $\text{Na}_2\text{O} \cdot 3\text{B}_2\text{O}_3 \cdot 4\text{H}_2\text{O}$ , a new borate from Argentina. — *The American Mineralogist* 52 (7–8), pp. 935–945.
25. ARISTARAIN, L. F., HURLBUT, C. S. JR 1967b: Macallisterite,  $2\text{MgO} \cdot 6\text{B}_2\text{O}_3 \cdot 15\text{H}_2\text{O}$ , from Salta, Argentina. — *The American Mineralogist* 52 (11–12), pp. 1776–1784.
26. ARISTARAIN, L. F., HURLBUT, C. S. JR. 1968: Teruggite,  $4\text{CaO} \cdot \text{MgO} \cdot 6\text{B}_2\text{O}_3 \cdot \text{As}_2\text{O}_5 \cdot 18\text{H}_2\text{O}$ , a new mineral from Jujuy, Argentina. — *The American Mineralogist* 53 (11–12), pp. 1815–1827.
27. ARLIDGE, E. Z., FARMER, V. C., MITCHELL, W. A. 1963: Infra-red, X-ray and thermal analysis of some aluminium and ferric phosphates. — *Journal of Applied Chemistry* 13 (1), pp. 7–27.

28. ARNOLD, M., SOMOGYVÁRI, P., PAULIK, J., PAULIK, F. 1987: The Derivatograph-c. A microcomputer-controlled simultaneous TG, DTG, DTA, TD and EGA apparatus. II. A simple method of estimating kinetic parameters. — *Journal of Thermal Analysis* 32 (2), pp. 679–683.
29. ARTIOLI, G., SMITH, J. V., PLUTH, J. J. 1986: X-ray structure refinement of mesolite. — *Acta Crystallographica Section C* 42 (8), pp. 937–942.
30. ARTIOLI, G., STÜHL, K., CRUCIANI, G., GUALTIERI, A., HANSON, J. C. 2001: In situ dehydration of yugawaralite. — *The American Mineralogist* 86 (1–2), pp. 185–192.
31. ASAKI, Z., KONDO, Y. 1989: Oxidation kinetics of iron sulfide in the form of dense plate, pellet and single particle. — *Journal of Thermal Analysis* 35 (6), pp. 1751–1759.
32. ASENSIO, I., SABATIER, G. 1958: Analyse thermique différentielle de quelques minéraux sulfures et arsénies de fer, nickel et cobalts. — *Bulletin de la Société Française de Mineralogie et de Cristallographie* 81 (1–3), pp. 12–15.
33. ATENCIO, D., COUTINHO, J. M. V., GRAESER, S., MATIOLI, P. A., MENEZES FILHO, L. A. D. 2004: Lindbergite, a new Mn oxalate dihydrate from Boca Rica mine, Galiléa, Minas Gerais, Brazil, and other occurrences. — *The American Mineralogist* 89 (7), pp. 1087–1091.
34. AUGUST, C. 1991: The determination of hydrated sulphates in the weathered crystalline rocks by means of thermal analysis. — In: SMYKATZ-KLOSS W., WARNE S. St. J. (eds) 1991: *Thermal Analysis in the Geosciences: in Series of Lecture Notes in Earth*. Springer Verlag, pp. 102–114.
35. BABUSHKINA, M. S., LEPEKHINA, E. N., NIKITINA, L. P., OVCHINNIKOV, N. O., LOKHOV, K. I. 2000: Structural distortion of micas from lamproites: Evidence from Mössbauer and IR spectroscopy. — *Doklady Earth Sciences* 371A, pp. 797–801 (translated from Russian).
36. BABUSHKINA, M. S., NIKITINA, L. P., OVCHINNIKOV, N. O., SAVVA, E. V., LUKIANOVA, L. I., GENSHAFT, YU. S. 1997: Composition and real structures of phlogopites from Kostomuksha lamproites. — *Zapiski Vserossiyskogo Mineralogicheskogo Obshchestva* 2, pp. 71–84 (in Russian).
37. BAI, T. B., GUGGENHEIM, S., WANG, S. J., RANCOURT, D. G., VAN GROOS, A. F. K. 1993: Metastable phase relations in the chlorite-H<sub>2</sub>O system. — *The American Mineralogist* 78 (11–12), pp. 1208–1216.
38. BAILEY, S. W. 1982: Nomenclature for regular interstratifications. A report of the AIPEA Nomenclature Committee. — *Clay and Clay Minerals* 30 (1), pp. 76–78. and *Clay Minerals* 17 (2), pp. 243–248.
39. BAILEY, S. W. 1988: Chlorites: Structures and Crystal Chemistry. — In: BAILEY, S. W. (ed): *Hydrous Phyllosilicates*. — *Reviews in Mineralogy* 19, Mineralogical Society of America pp. 347–404.
40. BAITALOW, F., WOLF, G., SCHMIDT, H. G. 1998: Investigations of calcium carbonate phase transition I. Thermal activated vaterite-calcite transition. — *Journal of Thermal Analysis and Calorimetry* 52 (1), pp. 5–16.
41. BAKKER, P. M. A., GRAVE, E., VANDENBERGHE, R. E., BOWEN, L. H., POLLARD, R. J., PERSOONS, R. M. 1991: Mössbauer study of the thermal decomposition of lepidocrocite and characterization of the decomposition products. — *Physics and Chemistry of Minerals* 18 (2), pp. 131–143.
42. BALASSONE, G., BERAN, A., LUEGER-RING, K. 1995: Variable water content of nepheline from Somma-Vesuvio, Italy. — *Mineralogy and Petrology* 52 (1–2), pp. 75–83.
43. BALÁŽ, P., EBERT, I. 1992: Thermal decomposition of mechanically activated sphalerite. — *Thermochimica Acta* 180, pp. 117–123.
44. BALÁŽ P., TKÁČOVÁ K., AVVAKUMOV E. G. 1989: The effect of mechanical activation on the thermal decomposition of chalcopyrite. — *Journal of Thermal Analysis* 35 (5), pp. 1325–1330.
45. BALÁŽ, P., BRIANČIN, J., ŠEPELÁK, V., HOCMANOVÁ, I. 1992a: Dissociative sublimation of mechanically activated cinnabar. — *Thermochimica Acta* 196 (2), pp. 349–355.
46. BALÁŽ P., HUHN J., HEEGN H. 1992b: Differential thermal analysis of mechanically activated sphalerite. — *Thermochimica Acta* 194, pp. 189–195.
47. BALÁŽ P., POST E., BASTL Z. 1992c: Thermoanalytical study of mechanically activated cinnabar. — *Thermochimica Acta* 200, pp. 371–377.
48. BALÁŽ, P., BRIANČIN, J., TURČÁNOVÁ, L. 1995: Thermal decomposition of mechanically activated tetrahedrite. — *Thermochimica Acta* 249 (1–2), pp. 375–381.
49. BALCEROVIAK, W. 1988: The TG Base line. — *Journal of Thermal Analysis* 33 (1), pp. 211–215.
50. BALEK, V., KARABASCHEVA, N. A., GYÖRYOVÁ, K. 1993: Literature survey on thermal analysis reference materials. — *Journal of Thermal Analysis* 40 (3), pp. 1459–1463.
51. BALEK, V., FUSEK, J., KŘIŽ, J., MURAT, M. 1995: Differences in the thermal behaviour of natural quartz before and after mechanical grinding as observed by emanation thermal analysis. — *Thermochimica Acta* 262, pp. 209–214.
52. BALEK, V., MÁLEK, Z., YARIV, S., MATUSCHEK, G. 1999: Characterization of montmorillonite saturated with various cations. — *Journal of Thermal Analysis and Calorimetry* 56 (1), pp. 67–76.
53. BALEK, V., ŠUBRT, J., ROUQUEROL, J., LLEWELLYN, P., ZELENÁK, V., BOUNTSEWA, I. M., BECKMAN, I. N., GYÖRYOVÁ K. 2003: Emanation thermal analysis study of synthetic gibbsite: Evaluation of experimental ETA results by mathematical modelling. — *Journal of Thermal Analysis and Calorimetry* 71 (3), pp. 773–782.
54. BALEK, V., BENEŠ, M., MÁLEK, Z., MATUSCHEK, G., KETTRUP, A., YARIV, S. 2006: Emanation thermal analysis study of Na-montmorillonite and montmorillonite saturated with various cations. — *Journal of Thermal Analysis and Calorimetry* 83 (3), pp. 617–623.
55. BALEKA, V., MATUSCHEKB, G., KETTRUPB, A., SYKOROVÁ, I. 1995: Chemical, petrographic and thermoanalytical characterization of two Northbohemian low rank coals. — *Thermochimica Acta* 263, pp. 141–157.
56. BALL, D. F. 1968: Interstratified illitic clay in Ordovician ash from Conway, N. Wales. — *Clay Minerals* 7 (3), pp. 363–366.
57. BALL, J. W., NORDSTROM, D. K., 1991: User's manual for WATEQ4F, with revised thermodynamic data base and text cases for calculating speciation of major, trace, and redox elements in natural waters. — *U.S. Geological Survey Open-file report* 91–183, 189 p.
58. BALL, M. C., TAYLOR, H. F. W. 1961: The dehydration of brucite. — *Mineralogical Magazine* 32 (253), pp. 754–766.
59. BALL, M. C., TAYLOR, H. F. W. 1963: The dehydration of chrysotile in air and under hydrothermal conditions. — *Mineralogical Magazine* 33 (261), pp. 467–482.

60. BANDI, W. R., KRAPE, G. 1976: The effect of CO<sub>2</sub> pressure and alkali salt on the mechanism of decomposition of dolomite. — *Thermochimica Acta* 14 (1–2), pp. 221–243.
61. BÁRDOSSY, GY. 1970: Possibilities of the joint application of X-ray diffractometer and derivatograph to the quantitative phase analysis of bauxites and similar rocks. — *Acta Chimica Academiae Scientiarum Hungaricae Budapest* 63 (3), 267–277.
62. BÁRDOSSY, GY., BRINDLEY, G. W. 1978: Rancieite associated with a karstic bauxite deposit. — *The American Mineralogist* 63 (7–8), pp. 762–767.
63. BÁRDOSSY GY., SAJGÓ CS. 1968: Aluminit in Bauxitlagerstätten von Szőc, Ungarn. — *Acta Geologica Hungarica* 12 (1–4), pp. 3–10.
64. BÁRDOSSY, GY., DÓZSA, L., GECSE, É., KENYERES, J., SIKLÓS, L. 1979: Bassanite and metabasaluminit in Hungarian bauxites. — *Bulletin of the Hungarian Geological Society* 109 (1), pp. 111–119. (in Hungarian)
65. BARNA, ZS., FÖLDVÁRI, M. 1992: Basaltbentonites of W Hungary. — *Proceedings of the 12th Conference on Clay Mineralogy and Petrology Bratislava*, 8. p.
66. BARONE, V. L., BOTTO, I. L., SCHALAMUK, I. B. 2003: Thermal effects of minority chalcogenide minerals: dta-tg, ir spectroscopy and sem electron microscopy studies. — *Latin American Applied Research* 33 (1), pp. 1–6.
67. BARSHAD, I. 1948: Vermiculite and its relation to biotite as revealed by base exchange reaction, x-ray analyses, differential thermal curves and water content. — *The American Mineralogist* 3 (11–12), pp. 655–678.
68. BARSHAD, I. 1950: The effect of the interlayer cations on the expansion of the mica. Type of crystal lattice. — *The American Mineralogist* 35 (3–4), pp. 225–228.
69. BASSETT, W. A. 1958: Copper vermiculite from Northern Rhodesia. — *The American Mineralogist* 43 (11–12), pp. 1112–1133.
70. BASTA, E. Z., KADER, Z. A. 1969: The mineralogy of Egyptian serpentines and talc-carbonates. — *The Mineralogical Magazine* 37 (287), pp. 394–408.
71. BATIAŠVILI, T. V. 1972: *Termografičeskoe issledovanie ceolitov srednezocenovih vulkanogennih tols Gruzii*. — Mecniereba, Tbilisi, 80 p.
72. BAUMER, A., GANTEAUME, M., BERNAT, M. 1993: Variations de la teneur en eau des coraux lors de la transformation aragonite>calcite. Included water in corals for the transition aragonite>calcite. — *Thermochimica Acta* 221 (2), pp. 255–262.
73. BAYLISS, N. S., COWLEY, J. M., FARRANT, J. L., MILES, G. L. 1981: The thermal decomposition of synthetic and natural alunite: An investigation by X-ray diffraction, electron diffraction, and electron microscope methods. — *Australian Journal of Scientific Research* 1 (3), pp. 343–350.
74. BAYLISS, P. 1964: Some properties of alunogen from South Wales. — *The American Mineralogist* 49, 11–12, pp. 1763–1766.
75. BAYSAL, O., DÝLEKÖZ, E. 1975: A study of bakerite. — *Bulletin of the Mineral Research and Exploration Institute of Turkey* 84, pp. 90–96.
76. BEAUFORT, D., CASSAGNABERE, A., PETIT, S., LANSON, B., BERGER, G., LACHARPAGNE, J. C. JOHANSEN, H. 1998: Kaolinite-to-dickite reaction in sandstone reservoirs. — *Clay Minerals* 33 (2), pp. 297–316.
77. BEAUMONT, C., GUILLEMIN, C. 1960: La dundasite de Gonnese (Sardigne). — *Bulletin de la Société Française de Minéralogie et des Cristallographie* 83 (4–6), pp. 121–124.
78. BECK, C. W. 1950: DTA curves of carbonate minerals. — *The American Mineralogist* 35 (11–12), pp. 985–1013.
79. BELITSKY, I. A., FURSENKO, B. A., GABUDA, S. P., KHOLDEEV, O. V., SERYOTKIN, YU. V. 1992: Structural transformations in natrolite and edingtonite. — *Physics and Chemistry of Minerals* 18 (8), pp. 497–505.
80. BELLOTTO, M., GUALTIERI, A., ARTIOLI, G., CLARK, S. M. 1995: Kinetic study of the kaolinite-mullite reaction sequence. Part I: kaolinite dehydroxylation. — *Physics and Chemistry of Minerals* 22 (4), pp. 207–214.
81. BENINCASA, E., BRIGATTI, M. F., MEDICI, L., POPPI, L. 2001: K-rich rectorite from kaolinized micaschist of the Sesia-Lanzo Zone, Italy. — *Clay Minerals* 36 (3), pp. 421–433.
82. BERA, P., RAJAMATHI, M., HEGDE, M. S., VISHNU KAMATH, P. 2000: Thermal behaviour of hydroxides, hydroxysalts and hydrotalcites. — *Bulletin of Material Science, Indian Academy of Sciences* 23 (2), pp. 141–145.
83. BEREZ, I., BOHÁTKA, S., LANGER, G., SZÖÖR, GY. 1983: Quadrupole mass-spectrometer coupled to derivatograph. — *International Journal of Mass Spectrometry and Ion Processes* 47. (jan.), pp. 273–276.
84. BERÉNYI, M. 1974: Thermoanalyse. In: SCHNEIDER H. J. (ed.): *Technik der Harnsteinanalyse*. VEB G. Thieme Verlag, Leipzig, pp. 40–50.
85. BERÉNYI, M., LIPTAY, G. 1971: The use of thermal analysis in medical science with special reference to nephroliths. — *The Journal of Thermal Analysis* 3 (4), pp. 437–443.
86. BERG, L. G. 1970: Simple salts. — In: MACKENZIE R. C. (ed.): *Differential Thermal Analysis*. — Academic Press, London – New York, pp. 343–361.
87. BERG, L. G., SHLYAPKINA, E. N. 1975: Characteristic features of sulphide mineral DTA. — *Journal of Thermal Analysis* 8 (3), pp. 417–426.
88. BERGLUND, S. 1993: Reversible dehydration in syna sepiolite. — *Thermochimica Acta* 214 (1), pp. 59–66.
89. BERMANEC, V., URIČ, E., RAJIČ, M., KNIEWALD, G. 2003: Thermal stability and vibrational spectra of the sheet borate tuzlaite, NaCa[B<sub>5</sub>O<sub>8</sub>(OH)<sub>2</sub>]<sub>3</sub>·3H<sub>2</sub>O. — *The American Mineralogist* 88 (2–3), pp. 271–276.
90. BERUTO, D. T., VECCHIATTINI, R., GIORDANI, M., 2003: Solid products and rate-limiting step in the thermal half decomposition of natural dolomite in a CO<sub>2</sub> (g) atmosphere. — *Thermochimica Acta* 405 (2), pp. 183–194.
91. BHARGAVA, S., AWAJA, F., SUBASINGHE, N. D. 2005: Characterisation of some Australian oil shale using thermal, X-ray and IR techniques. — *Fuel* 84 (6), pp. 707–715.
92. BHASKARA RAO A. 1965: Note on the differential thermal analysis study of some rare Brazilian phosphate minerals. — *Mineralogical Magazine* 35. 270. pp. 427–428.
93. BILLAULT, V., BEAUFORT, D., PATRIER, P., PETIT, S. 2002: Crystal chemistry of Fe-sudoites from uranium deposits in the Athabasca Basin (Saskatchewan, Canada). — *Clays and Clay Minerals* 50 (1), pp. 70–81.
94. BILONIZHKA, P. 2001: Nature of inter-layered water in the hydromicas. — *VI Congress of the Ukrainian Mineralogical Society in: Mineralogical Collections* 51 (1), pp. 142–148.

95. BIRCH, W. D., PRING, A., RELLER, A., SCHMALLE, H. W. 1993: Bernalite,  $\text{Fe}(\text{OH})_3$ , a new mineral from Broken Hill, New South Wales: Description and structure. — *The American Mineralogist* 78 (7–8), pp. 827–834.
96. BISH, D. L., POST, J. E. 1989: Thermal behavior of complex, tunnel-structure manganese oxides. — *The American Mineralogist* 74 (1–2), pp. 177–186.
97. BLANC, R., ESCOUBES, M. 1975: Variations des propriétés d'adsorption d'eau de la montmorillonite-lithium en fonction du traitement thermique. — *Journal of Thermal Analysis* 7 (1) pp. 21–31.
98. BLANCHARD, F. N. 1971: Thermal analysis of crandallite. — *Quarterly Journal of the Florida Academy of Sciences* 34 (1), pp. 1–9.
99. BLANCHARD, F. N. 1972: Physical and chemical data for crandallite from Alachua County, Florida — *The American Mineralogist* 57 (3–4), pp. 473–484.
100. BLÜMAN, B. A., IVANOVA, B. P., KRASAVINA, T. N. 1969: Primenenie termičeskogo analiza dlâ opredeleniâ stepeni metamorfizma grafitosoderžasih mramorov nağor'â Sanğilen. — *Izvestiya Akademii Nauk, SSSR. Seriya Geologiya* 8, pp. 125–132.
101. BOHÁTKA, S., SZÖÖR, GY. 1987: Advances of a Quadrupole-Derivatograph Thermoanalytical instrument. — *Vacuum* 37 (1–2), pp. 187–188.
102. BOHÁTKA, S., SZÖÖR, GY., CZÉL, GY., BALÁZS, É. 2005: High temperature direct probe for MS and its use for thermal decomposition monitoring. — *Vacuum* 80 (1–3), pp. 247–252.
103. BÖHME, K., BOY, S., HEIDE, K., HÖLAND, W. 1978: Checking of mathematical calculation methods for determination of kinetic parameters from nonisothermal measurement by test functions. — *Thermochimica Acta* 23 (1), pp. 17–27.
104. BOLES, J. R. 1972: Composition, optical properties, cell dimensions, and thermal stability of some heulandite-group zeolites. — *The American Mineralogist* 57 (9–10), pp. 1463–1493.
105. BOLIS, V., FUBINI, B., COLUCCIA, S., MOSTACCI, E. 1985: Surface hydration of crystalline and amorphous silicas. — *Journal of Thermal Analysis* 30 (6), pp. 1283–1292.
106. BOLLIN, E. M. 1970: Chalcogenides. — In: MACKENZIE R. C. (ed.): *Differential Thermal Analysis*. — Academic Press, London – New York, pp. 193–234.
107. BOLLIN, E. M., KERR, P. F. 1961: Differential thermal pyrosynthesis. — *The American Mineralogist* 46 (7–8), pp. 823–858.
108. BONDI, M., GRIFFIN, W. L., MATTIOLI, V., MOTTANA, A. 1983: Chiavennite,  $\text{CaMnBe}_2\text{Si}_5\text{O}_{13}(\text{OH})_2 \cdot 2\text{H}_2\text{O}$ , a new mineral from Chiavenna (Italy). — *The American Mineralogist* 68 (5–6), pp. 623–637.
109. BOSAK, P., BELLA, P., CILEK, V., FORD, D. C., HERCMAN, H., KADLEC, J., OSBORNE, A., PRUNER, P. 2002: Orňhtiná aragonite cave (Slovakia): morphology, mineralogy and genesis. — *Geologica Carpathica* 53 (6), pp. 399–410.
110. BOUSKA, VL., LAZARENKO, E. K., MELNIK, J. M., SLANKÝ, E. 1960: Prispevek k poznani destinezitu. — *Acta Universitatis Carolinae Geologica, Prague*, 2, pp. 127–152.
111. BOYD, T., SCOTT, S. D., HEKINIAN, R. 1993: Trace element pattern in Fe-Si-Mn oxyhydroxydes at three hydrothermally active seafloor sites. — *Journal of the Society of Resource Geology Special Issue*, 17, pp. 83–95.
112. BRADLEY W. F. 1940: The structural scheme of attapulgite. — *The American Mineralogist* 25 (6), pp. 405–410.
113. BRADLEY W. F. 1950: Rectorite. — *The American Mineralogist* 35 (7–8), pp. 590–595.
114. BRADLEY W. F. 1953: Mixed-layer minerals. — *Analytical Chemistry* 25 (5), pp. 727–730.
115. BRADLEY W. F., GRIM R. E. 1951: High temperatures thermal effect of clay and related minerals. — *The American Mineralogist* 36 (3–4), pp. 182–201.
116. BRADLEY W. F., WEAVER C. E. 1966: A regularly interstratified chlorite-vermiculite clay mineral. — *The American Mineralogist* 41 (5–6), pp. 497–504.
117. BRADLEY W. F., BURST J. F., GRAF D. L. 1953: Crystal chemistry and differential thermal effects of dolomite. — *The American Mineralogist* 38 (3–4), pp. 207–217.
118. BRAMAO, L., CADY, J. G., HENDRICKS, S. B., SWERDLOW, M. 1952: Characterization of kaolin minerals. — *Soil Science* 73 (4), pp. 273–287.
119. BRANDT, S. B., VORONOVSKIY, S. N. 1967: Dehydration and diffusion of radiogenic argon in micas. — *International Geology Review* 9 (11), pp. 1504–1507.
120. BRAUNER, K., PREISINGER, A. 1956: Struktur und Entstehung des Sepioliths. Structure of Sepiolite. — *Tschermaks Mineralogische und Petrographische Mitteilungen* 6 (1–2), pp. 120–140.
121. BRECK, D. W. 1974: *Zeolite molecular sieves. Structure, chemistry and use*. — Wiley and Sons, New York – London – Sydney – Toronto. 771 p.
122. BREGER, I. A., CHANDLER, J. C., ZUBOVIC, P. 1970: An infrared study of water in heulandite and clinoptilolite. — *The American Mineralogist* 55 (5–6), pp. 825–840.
123. BRINDLEY, G. W. 1951: The crystal structure of some chamosite minerals. — *Mineralogical Magazine* 29 (212), pp. 502–525.
124. BRINDLEY, G. W., ALI, S. Z. 1950: X-ray study of thermal transformations in magnesian chlorites. — *Acta Crystallographica* 3 (1), pp. 25–30.
125. BRINDLEY, G. W., CHOE, J. O. 1961: Reaction series gibbsite → chi alumina → kappa alumina → corundum. — *The American Mineralogist* 46 (7–8), pp. 771–785.
126. BRINDLEY, G. W., HAYAMI, R. 1964: Kinetics and mechanism of dehydration and recrystallization of serpentine. Part I. — *Clay and Clay Minerals* 12 (1), pp. 35–47.
127. BRINDLEY, G. W., HAYAMI, R. 1965: Mechanism of formation of forsterite and enstatite from serpentine. — *Mineralogical Magazine* 35 (269), pp. 189–195.
128. BRINDLEY, G. W., PORTER, A. R. D. 1978: Occurrence of dickite in Jamaica-ordered and disordered varieties. — *The American Mineralogist* 63 (5–6), pp. 554–562.
129. BRINDLEY, G. W., SHARP, J. H., PATTERSON, J. H., NARAHARI, B. N. 1967: Kinetics and mechanism of dehydroxylation processes. I. Temperature and vapor pressure dependence of dehydroxylation of kaolinite. — *The American Mineralogist* 52 (1–2), pp. 201–211.
130. BRINDLEY, G., ZUSSMAN, J. 1957: A structural study of the thermal transformation of serpentine minerals to forsterite. — *The American Mineralogist* 42 (7–8), pp. 461–474.

131. BRINDLEY, G. W., YOELE, R. F. 1953: Ferrous chamosite and ferric chamosite. — *Mineralogical Magazine* 30 (220), pp. 57–70.
132. BRINDLEY, G. W., WAN, H. M. 1975: Compositions, structures, and thermal behavior of nickel containing minerals in the lizardite-nepouite series. — *The American Mineralogist* 60 (9–10), pp. 863–871.
133. BROERSMA, A., BRUYN, P. L., GEUS, J. W., STOL, R. J. 1978: Simultaneous DTA- and DTG-measurements on aluminium oxide monohydroxides. — *Journal of Thermal Analysis* 13 (2), pp. 341–355.
134. BROOKS, S. C., TAYLOR, D. L., JARDINE, P. M. 1998: Thermodynamic of bromide exchange on ferrihydrite: implications for bromide transport. — *Soil Science Society of America Journal* 62 (5), pp. 1275–1279.
135. BROUSSE, R., GUÉRIN, H. 1965: Découverte de pickéringite dans le Cantal. — *Bulletin de la Société Française de Minéralogie et des Cristallographie* 88 (4), pp. 704–705.
136. BROUSSE, R., GASSE-FOURNIER, G., LEBOUTEILLER, F. 1966: Cristaux de rozenite et de mélanterite dans la mine de diatomites de la Bade (Cantal). — *Bulletin de la Société Française de Minéralogie et des Cristallographie* 89 (3), pp. 348–352.
137. BROWN, G., NORRISH, K. 1952: Hydrous micas. — *Mineralogical Magazine* 29 (218), pp. 929–932.
138. BROWN, G., WEIR, A. H. 1965: The identity of rectorite and alleverdite. — In: ROSENQUIST, I. T., GRAFF-PETERSEN, P. (eds): *Proceedings of the International Clay Conference, Stockholm 1963*. Pergamon, Oxford 2, pp. 87–90.
139. BROWN, I. W. M., MACKENZIE, K. J. D., GAINSFORD, G. J. 1984: Thermal decomposition of the basic copper carbonates malachite and azurite. — *Thermochimica Acta* 75 (1–2), pp. 23–32.
140. BROWN, I. W. M., MACKENZIE, K. J. D., MEINHOLD, R. H. 1987: The thermal reactions of montmorillonite studied by high-resolution solid-state  $^{29}\text{Si}$  and  $^{27}\text{Al}$  NMR. — *Journal of Materials Science* 22 (9), pp. 3265–3275.
141. BROWN, L. D., RAY, A. S., THOMAS, P. S., GUERBOIS, J. P. 2002: Thermal characteristics of Australian sedimentary opals. — *Journal of Thermal Analysis and Calorimetry* 68 (1), pp. 31–36.
142. BROWN, M. E. (ed): 2001: *Introduction to thermal analysis. Techniques and application*. 2nd edition — Kluwer Academic Publisher 264 p.
143. BRYDON, J. E., KODAMA, H. 1966: The nature of aluminium hydroxide montmorillonite complexes. — *The American Mineralogist* 51 (5–6), pp. 875–889.
144. BULGARIU, D. 2002: The study of volcanic tuffs and natural zeolites by IR spectroscopy (I). Preliminary results. — *Analele Științifice ale Universității "Al. I. Cuza" Iași Geologie* 48, pp. 121–149.
145. CABRERA, J. G., EDDLESTON, M. 1983: Kinetics of dehydroxylation and evaluation of the crystallinity of kaolinite. — *Thermochimica Acta* 70 (1–3), pp. 237–247.
146. CAHOON, H. P. 1954: Saponite near Milford, Utah. — *The American Mineralogist* 39 (3–4), pp. 222–230.
147. CAILLÈRE, S., HÉNIN, S. 1951: Properties and identification of saponite (bowlingite). — *Clay Minerals Bulletin* 1 (5), pp. 138–144.
148. CAILLÈRE, S., HÉNIN, S. 1957a: The chlorite and serpentine minerals. — In: MACKENZIE, R.C. (ed.): *The differential thermal investigation of clays*. Mineralogical Society, London, pp. 207–230.
149. CAILLÈRE, S., HÉNIN, S. 1957b: The sepiolite and palygorskite minerals. — In: MACKENZIE, R.C. (ed.): *The differential thermal investigation of clays*. Mineralogical Society, London, pp. 231–247.
150. CAMPBELL, A. S., MITCHELL, B. D., BRACEWELL, J. M. 1968: Effects of particle size, pH and organic matter on the thermal analysis of allophane. — *Clay Minerals* 7 (4), pp. 451–454.
151. CAMPBELL, A. S., SCHWERTMANN, U., CAMPBELL, P. A. 1993: Thermal analysis of ferrihydrite. — *Proceedings of the 10th International Clay Conference, Adelaide, South Australia, Abstracts*, p. O-26.
152. CAMPBELL, A. S., SCHWERTMANN, U., CAMPBELL, P. A. 1997: Formation of cubic phases on heating ferrihydrite. — *Clay Minerals* 32 (4), pp. 615–622.
153. CAMPBELL, A. S., SCHWERTMANN, U., STANJEK, H., FRIEDL, J., KYEK, A., CAMPBELL, P. A. 2002: Si incorporation into hematite by heating Si-ferrihydrite. — *Langmuir* 18 (21), pp. 7804–7809.
154. CARLEER, R., REGGERS, G., RUYSEN, M., MULLENS, J. 1998: TG-MS analysis as tool for the evaluation of clay mixtures. — *Thermochimica Acta* 323 (1–2), pp. 169–178.
155. CARTHEW, A. R. 1955: Quantitative estimation of kaolinite by differential thermal analysis. — *The American Mineralogist* 40 (1–2), pp. 107–117.
156. CASES, J.-M., LIETARD, O., YVON, J., DELON, J.-F. 1982: Étude des propriétés cristallochimiques, morphologiques, superficielles de kaolinites désordonnées. — *Bulletin de Minéralogie* 105 (5), 439–455.
157. CASTAÑEDA, C., SIGRID, G., EECKHOUT, S. G., DA COSTA, G. M., BOTELHO, N. F., GRAVE DE, E. 2006: Effect of heat treatment on tourmaline from Brazil. — *Physics and Chemistry of Minerals* 33 (3), pp. 207–216.
158. CATTANEO, A., GUALTIERI, A. F., ARTIOLI, G. 2003: Kinetic study of the dehydroxylation of chrysotile asbestos with temperature by in situ XRPD. — *Physics and Chemistry of Minerals* 30 (3), pp. 177–183.
159. CATTI, M., FERRARIS, G., IVALDI, G. 1988: Thermal behaviour of the crystal structure of strontian piemontite. — *The American Mineralogist* 73 (11–12), pp. 1370–1376.
160. CEBULAK, S., GAWĘDA, A., LANGIER-KUŹNIAROWA, A. 1999: Oxyreactive thermal analysis of dispersed organic matter, kerogen and carbonization products A tool for investigation of the heated rock masses. — *Journal of Thermal Analysis and Calorimetry* 56 (2), pp. 917–924.
161. CEBULAK, S., LANGIER-KUŹNIAROWA, A., CZAPOWSKI, G., BZOWSKA, G. 2003: New aspects of the application for studies of Ca-Mg carbonate minerals exemplified by upper Permian rocks. — *Journal of Thermal Analysis and Calorimetry* 72 (1), pp. 405–411.
162. ČECH, F., JANSÁ, J., NOVÁK, F. 1976: Kaňkite,  $\text{FeAsO}_4 \cdot 3\text{H}_2\text{O}$ , a new mineral. — *Neues Jahrbuch für Mineralogie, Monatshefte* 9, pp. 426–436.
163. ČECH, F., JANSÁ, J., NOVÁK, F. 1978: Zýkaite,  $\text{Fe}^{3+}_4(\text{AsO}_4)_3(\text{SO}_4)(\text{OH}) \cdot 15\text{H}_2\text{O}$ , a new mineral. — *Neues Jahrbuch für Mineralogie, Monatshefte* 3, pp. 134–144.
164. CELLAI, D., CARPENTER, M. A., WRUCK, B., SALJE, E. K. H. 1994: Characterization of high-temperature phase transitions in single crystals of Steinbach tridymite. — *The American Mineralogist* 79 (7–8), 606–614.
165. ČERNÝ, P. 1965: Ionic substitutions in natural stilbite. — *Neues Jahrbuch für Mineralogie, Monatshefte* 7, pp. 198–208.

166. CESBORN, F. 1964: Contribution a la mineralogie des sulfates de fer hydrates. — *Bulletin de la Société Française de Minéralogie et des Cristallographie* 87 (2), pp. 125–143.
167. CESBORN, F., FRITSCHÉ, J. 1969: La mounanaïte, nouveau vanadate de fer et de plomb hydrate. — *Bulletin de la Société Française de Minéralogie et des Cristallographie* 92 (2), pp. 196–202.
168. CHAKLADER, A. C. D., BLAIR, G. R. 1970: Differential thermal study of FeO and Fe<sub>3</sub>O<sub>4</sub>. — *Journal of Thermal Analysis* 2 (2), pp. 165–179.
169. CHAKRAVORTY, A. K. 1993: Application of TMA and DTA for study of the crystallization behaviour of SiO<sub>2</sub> in the thermal transformation of kaolinite. — *Journal of Thermal Analysis* 39 (3), pp. 289–299.
170. CHAKRAVORTY, A. K. 2003: New data on thermal effects of kaolinite in the high temperature region. — *Journal of Thermal Analysis and Calorimetry* 71 (3), pp. 799–808.
171. CHAO, G. Y. 1971: Carletonite, KNa<sub>4</sub>Ca<sub>4</sub>Si<sub>8</sub>O<sub>18</sub>(CO<sub>3</sub>)<sub>4</sub>(F,OH)·H<sub>2</sub>O, a new mineral from, Mount St. Hilaire, Quebec. — *The American Mineralogist* 56 (11–12), pp. 1855–1866.
172. CHATTAMAJ, B. D., DUTTA, S. N., IYENGAR, M. S. 1973: Studies on thermal decomposition of calcium carbonate in the presence of alkali salts. — *Journal of Thermal Analysis* 5 (1), pp. 43–49.
173. CHEN, D. T. Y., FONG, P. H. 1977: Thermal analysis of magnesium hydroxide. — *Journal of Thermal Analysis* 12 (1), pp. 5–13.
174. CHEN, G. 1988: DTA character of biotite of different genetic types and their implications. — *Kexue Tongbao* 33 (13), pp. 1142–1143.
175. CHILDS, C. W. 1992: Ferrihydrite: A review of structure, properties and occurrence in relation to soils. — *Zeitschrift für Pflanzenernährung und Bodenkunde* 155 (5), pp. 441–448.
176. CHUKHROV, F. V., ZVYAGIN, B. B. 1976: Feroxyhyte, a new modification of FeOOH. — *Izvestiya Akademii Nauk, SSSR. Seriya Geologiya* 5, pp. 5–24.
177. CHUKHROV, F. V., ZVYAGIN, B. B., GORSKHOV, A. I., YERMILOVA, L. P., RUDNITSKAYA, E. S. 1968: O hrizokollah. — *Izvestiya Akademii Nauk SSSR, Seriya Geolicheskaya* 6, pp. 29–44.
178. CHUKROV, F. V., ZVYAGIN, B. B., GORSHKOV, A. I., YERMILOVA, L. P., RUDNITSKAYA, E. S. 1971: Faza Tau-Brëdli — produkt gipergenno izmeneniâ rud. — *Izvestiya Akademii Nauk, SSSR. Seriya Geologiya* 1, pp. 3–13.
179. CHUKROV, F. V., ZVYAGIN, B. B., GORSHKOV, A. I., YERMILOVA, L. P., BALASHOVA, V. V. 1973: O ferrigidrite. — *Izvestiya Akademii Nauk, SSSR. Seriya Geologiya* 4, pp. 23–33.
180. CLARK, A. M. 1993: *Hey's Mineral Index*. — Chapman and Hall, London, 852 p.
181. CLAYTON, T. 1980: Hydrobasaluminite and basaluminite from Chickerell, Dorset. — *Mineralogical Magazine* 43 (331), pp. 931–937.
182. COCCO, G. 1952: Differential thermal analysis of some sulphates. — *Periodico di Mineralogia* 21, pp. 103–141.
183. COLE, W. F., 1955: Interpretation of differential thermal analysis curves of mixed layer minerals of illite and montmorillonite. — *Nature* 175 (4452), pp. 384–385.
184. COLE, W. F., CROOK, D. N. 1966: A note on the examination of pyrite in conventional differential thermal analysis equipment. — *The American Mineralogist* 51 (3–4), pp. 499–502.
185. COLE, W. F., HOSKING, J. S. 1957: Clay mineral mixtures and interstratified minerals. — In: MACKENZIE, R. C. (ed.): *The differential thermal investigation of clays*. Mineralogical Society, London, pp. 248–274.
186. COLE, W. F., LANCUCKI, C. J. 1975: Huntite from Deer Park, Victoria, Australia. — *The American Mineralogist* 60 (11–12), pp. 1130–1131.
187. COLE, W. F., LANCUCKI, C. J. 1982: Huntite from Deer Park, Victoria, Australia: a correction. — *The American Mineralogist* 67 (11–12), p. 1290.
188. COMPAGNONI, R., FERRARIS, G., MELLINI, M. 1985: Carlostrunanite, a new asbestiform rock-forming silicate from Val Varaita, Italy. — *The American Mineralogist* 70 (7–8), pp. 767–772.
189. COOMBS, D. S., ALBERTI, A., ARMBRUSTER, T., ARTIOLI, G., COLELLA, C., GALLI, E., GRICE, J. D., LIEBAU, F., MANDARINO, J. A., MINATO, H., NICKEL, E. H., ELIO PASSAGLIA, E., PEACOR, D. R., QUARTIERI, S., RINALDI, R., ROSS, M., SHEPPARD, R. A., TILLMANN, E., VEZZALINI, G. 1998: Recommended nomenclature for zeolite minerals: report of the subcommittee on zeolites of the International Mineralogical Association, Commission on New Minerals and Mineral Names. — *Mineralogical Magazine* 62 (4), pp. 533–571.
190. COOPER, B. J., GIBBS, G. W. 1981: The effects of heating and dehydration on the crystal structure of hemimorphite up to 600 °C. — *Zeitschrift für Kristallographie* 156 (3–4), pp. 305–321.
191. COWGILL, U. M., HUTCHINSON, G. E., JOENSUU, O. 1963: An apparently triclinic dimorph of crandallite from a tropical swamp sediment in El Petén, Guatemala. — *The American Mineralogist* 48 (9–10), pp. 1144–1153.
192. COWKING, A. 1983: Structure and swelling of fibrous and granular saponitic clay from orrok quarry, Fife, Scotland. — *Clay Minerals* 18 (1), pp. 49–64.
193. CRĂCIUN, C. 1987: The study of some normal and abnormal montmorillonites by thermal analysis and infrared spectroscopy. — *Thermochimica Acta* 117, pp. 25–36.
194. CRIADO, J. M., GONZALEZ, F., GONZALEZ, M. 1982: Influence of the CO<sub>2</sub> pressure on the kinetics of thermal decomposition of manganese carbonate. — *Journal of Thermal Analysis* 24 (1), pp. 59–65.
195. CRIADO, J. M., GONZALEZ, M., MACIAS, M., 1988: Influence of grinding on both the stability and thermal decomposition mechanism of siderite. — *Thermochimica Acta* 135, pp. 219–223.
196. CRUCIANI, G., GUALTIERI, A. 1999: Dehydration dynamics of analcime by in situ synchrotron powder diffraction. — *The American Mineralogist* 84 (1–2), pp. 112–119.
197. CRUPI, V., LONGO, F., MAJOLINO, D., VENUT, V. 2006: Vibrational properties of water molecules adsorbed in different zeolitic frameworks. — *Journal of Physics: Condensed Matter* 18 (15), pp. 3563–3580.
198. CRUZ, M. D. R., REAL, L. M. 1995: Dehydroxylation of chlorites: an HTXRD, DTA-TG and IR study. — *Geologica Carpathica, Series Clays* 4 (2), p. 110.
199. CSERNY, T., FÖLDVÁRI, M., IKRÉNYI, K., NAGY BODOR, E., HAJÓS, M., SZUROMINÉ KORECZ, A., WOJNÁROVITS, L. 1991: Geological investigations of the lacustrine sediments of Lake Balaton based on the borehole Tó-24. — *Annual Report of the Geological Institute of Hungary of 1989*. pp. 178–239. (in Hungarian)

200. CUADROS, J., ALTANER, S. P. 1998: Compositional and structural features of the octahedral sheet in mixed-layer illite/smectite from bentonites. — *European Journal of Mineralogy* 10 (1), pp. 111–124.
201. CURRELL, B. R., WILLIAMS, A. J. 1974: Thermal analysis of elemental sulphur. — *Thermochimica Acta* 9 (3), pp. 255–259.
202. CUTHBERT, F. L., ROWLAND, R. A. 1947: Differential thermal analyses of some carbonate minerals. — *The American Mineralogist* 3–4, pp. 111–116.
203. DAGOUNAKI, C., CHRISSAFIS, K., KASSOLI-FOURNARAKI, A., TSIRAMBIDES, A., SIKALIDIS, C., PARASKEVOPOULOS, K. M. 2004: Thermal characterization of carbonate rocks, Kozani area, North-western Macedonia, Greece. — *Journal of Thermal Analysis and Calorimetry* 78 (1), pp. 295–306.
204. DANCHEVSKAYA, M. N., IVAKIN, YU. D., MARTYNOVA, L. F., ZUY, A. I., MURAVIEVA, G. P., LAZAREV, V. B. 1996: Investigation of thermal transformations in aluminium hydroxides subjected to mechanical treatment. — *Journal of Thermal Analysis* 46 (5), pp. 1215–1222.
205. DANG, M. Z., RANCOURT, D. G., DUTRIZAC, J. E., LAMARCHE, G., PROVENCHER, R. 1998: Interplay of surface conditions, particle size, stoichiometry, cell parameters, and magnetism in synthetic hematite-like materials. — *Hyperfine Interactions* 117 (1–4), pp. 271–319.
206. DARIDA-TICHY, M., HORVÁTH, I., FARKAS, L., FÖLDVÁRI, M. 1984: Rock alteration of andesitic magmatites on the Eastern Margin of the Velence Mts. — *Annual Report of the Geological Institute of Hungary of 1982.*, pp. 271–288. (in Hungarian)
207. DAVE, N. G., MASOOD, I. 1974: Estimation through catalyzation, thermogravimetric determination of dolomites. — *Proceedings of the fourth ICTA Budapest Thermal Analysis V.2.*, pp. 685–693.
208. DAWSON, J. B., WILBURN, F. W. 1970: Silica Minerals. — In: MACKENZIE, R. C. (ed.): *Differential Thermal Analysis*. — Academic Press, London – New York, pp. 477–495.
209. DEÁK, F., FÖLDVÁRI, M., MINDSZENTY, A. 2002: A new tool to detect exposure surfaces in shallow water carbonates depositional environments. — *Acta Geologica Hungarica* 45 (3), pp. 301–317.
210. DERIE, R., GHODSI, D. M., CALVO-ROCHE, C. 1976: DTA study of the dehydration of synthetic goethite  $\alpha$ -FeOOH. — *Journal of Thermal Analysis* 9 (3), pp. 435–440.
211. DEUTSCH, Y., SANDLER, A., YAACOV NATHAN, Y. 1989: The high-low inversion of quartz. — *Thermochimica Acta* 148 (4), pp. 467–472.
212. DINESEN, A. R., PEDERSEN, C. T., BENDER KOCH, C. 2001: The thermal conversion of lepidocrocite ( $\alpha$ -FeOOH) revisited. — *Journal of Thermal Analysis and Calorimetry* 64 (3), pp. 1303–1310.
213. DING, Z., FROST, R. L. 2004: Thermal study of copper adsorption on montmorillonites. — *Thermochimica Acta* 416 (1–2), pp. 11–16.
214. DION, P., ALCOVER, J. F., BERGAYA, F., ORTEGA, A., LLEWELLYN, P. L., ROUQUERO, L. F. 1998: Kinetic study by controlled-transformation rate thermal analysis of the dehydroxylation of kaolinite. — *Clay Minerals* 33 (2), pp. 269–276.
215. DOESBURG, VAN J. D. J., VERGOUWEN, L., VAN DER PLAS, L. 1982: Konyaite,  $\text{Na}_2\text{Mg}(\text{SO}_4)_2 \cdot 5\text{H}_2\text{O}$ , a new mineral from the Great Konya Basin, Turkey. — *The American Mineralogist* 67 (9–10), pp. 1035–1038.
216. DOLLIMORE, D. 1987: The thermal decomposition of oxalates, a review. — *Thermochimica Acta* 117, pp. 331–363.
217. DOLLIMORE, D., DUNN, J. G., LEE, Y. F., PENROD, B. M. 1994: The decrepitation of dolomite and limestone. — *Thermochimica Acta* 234 (1), pp. 125–131.
218. DONÁTH, É. 1974: Thermal analysis in the investigation of water bonds in natural zeolites. — *Thermal Analysis, Proceedings of the 4th ICTA-Conference, Budapest*, pp. 629–638.
219. DONÁTH, P. É., SIMÓ, B. 1966: Further studies into the relationship between lattice structure and water bond in phillipsite and gonnardite. — *Annales Universitatis Scientiarum Budapestinensis de Rolando Eötvös Nominatae Sectio Geologica* 9 (2), pp. 109–121. (in Russian)
220. DREBUSHCHAK, V. A. 1990: Thermogravimetric investigation of the phase transition in the zeolite heulandite at dehydration. — *Thermochimica Acta* 159, pp. 377–381.
221. DREBUSHCHAK, V. A., FEDOROVA, ZH. N., SINYAKOVA, E. F. 1997: Decay of  $(\text{Fe}_{1-x}\text{Ni}_x)_{0.96}\text{S}$  DSC investigation. — *Journal of Thermal Analysis and Calorimetry* 48 (4), pp. 727–734.
222. DRITS, V. A. 2003: Structural and chemical heterogeneity of layer silicates and clay minerals. — *Clay Minerals* 38 (4), pp. 403–432.
223. DRITS, V. A., SAKHAROV, B. A., SALYN, A. L., MANCEAU, A. 1993: Structural model for ferrihydrite. — *Clay Minerals* 28 (2), pp. 185–207.
224. DRITS, V. A., LINDGREEN, H., SALYN, A. L., YLAGAN, R., MCCARTY, D. K. 1998: Semiquantitative determination of trans-vacant and cis-vacant 2:1 layers in illites and illite-smectites by thermal analysis and X-ray diffraction. — *The American Mineralogist* 83 (11–12/1), pp. 1188–1198.
225. DUBANSKÝ, A. 1956: Příspěvky k poznání geochemie sekundárních sulfátů III. Sulfáty z Dubníku u Prešova. — *Chemické. Listy, Praha*, 50, pp. 1347–1361.
226. DUBBIN, W. E., GOH, T. B., OSCARSON, D. W., HAWTHORNE, F. C. 1994: Properties of hydroxy-Al and Cr interlayers in montmorillonite. — *Clays and Clay Minerals* 42 (3), pp. 331–336.
227. DUBRAWSKI, J. V. 1987: The effect of particle size on the determination of quartz by differential scanning calorimetry. — *Thermochimica Acta* 120, pp. 257–260.
228. DUBRAWSKI, J. V. 1991a: Differential scanning Calorimetry and its applications to mineralogy and the geosciences. — In: SMYKATZ-KLOSS W., WARNE S. ST. J. (eds): *Thermal Analysis in the Geosciences*. Series of Lecture Notes in Earth. Springer Verlag, pp. 16–59.
229. DUBRAWSKI J. V., 1991b: Thermal decomposition of some siderite-magnesite minerals using DSC. — *Journal of Thermal Analysis* 37 (6), pp. 1213–1221.
230. DUBRAWSKI, J. V., ENGLAND, B. M. 1993: Thermal transformations of some strontium-bearing-aragonites. — *Journal of Thermal Analysis* 39 (8–9), pp. 987–994.
231. DUBRAWSKI, J. V., OSTWALD, J. 1987: Thermal transformation of marine manganates. — *Neues Jahrbuch für Mineralogie, Monatshefte* 9, pp. 406–418.
232. DUBRAWSKI, S. V., WARNE, S. ST. J. 1986: The application of differential scanning calorimetry to mineralogical analysis. — *Thermochimica Acta* 107, pp. 51–59.

233. DUBRAWSKI, J. V., WARNE, S. ST. J. 1988a: Differential scanning calorimetry of the dolomite-ankerite mineral series in variable atmospheres. — *Thermochimica Acta* 135, pp. 225–230.
234. DUBRAWSKI, J. V., WARNE, S. ST. J. 1988b: Differential scanning calorimetry of the the minerals dolomite-ferroan dolomite-ankerite series in flowing carbon dioxide. — *Mineralogical Magazine* 52 (368), pp. 627–365. Part 5.
235. DUFFIN, W. J., GOODYEAR, J. 1960: A thermal and X-ray investigation of scarbroite. — *Mineralogical Magazine* 32 (248), pp. 353–362.
236. DUMITRAȘ, D. G., MARINCEA, ȘT., FRANSOLET, A. M. 2004: Brushite in the bat guano deposit from the “dry” Cioclovina Cave (Sureanu Mountains, Romania). — *Neues Jahrbuch für Mineralogie, Abhandlungen*, 180 (1), pp. 45–64.
237. DUNN, J. G. 1993: Recommendation for reporting thermal analysis data. — *Journal of Thermal Analysis* 40 (3), pp. 1431–1436.
238. DUNN, J. G. 1997: The oxidation of sulphide minerals. — *Thermochimica Acta* 300 (1–2), pp. 127–139.
239. DUNN, J. G. 1998: Applications of thermal methods of analysis to raw and processed minerals. — *Thermochimica Acta* 324 (1–2), pp. 59–66.
240. DUNN, J. G., CHAMBERLAIN, A. C. 1991: The effect of stoichiometry on the ignition behaviour of synthetic pyrrhotites. — *Journal of Thermal Analysis* 37 (6), pp. 1329–1346.
241. DUNN, J. G., HOWES, V. L. 1996: The oxidation of violarite. — *Thermochimica Acta* 282–283, pp. 305–316.
242. DUNN, J. G., KELLY, C. E. 1977: A TG/DTA/MS study of the oxidation of nickel sulphide. — *Journal of Thermal Analysis* 12 (1), pp. 43–52.
243. DUNN, J. G. KELLY, C. E. 1980: A TG/MS and DTA study of the oxidation of pentlandite. — *Journal of Thermal Analysis* 18 (1), pp. 147–154.
244. DUNN, J. G., MACKEY, L. C. 1991: The measurement of ignition temperatures and extents of reaction on iron and iron-nickel sulfides. — *Journal of Thermal Analysis* 37 (9), pp. 2143–2164.
245. DUNN, J. G., MUZENDA, C. 2001a: Quantitative analysis of phases formed during the oxidation of covellite (CuS) — *Journal of Thermal Analysis and Calorimetry* 64 (3), pp. 1241–1246.
246. DUNN, J. G., MUZENDA, C. 2001b: Thermal oxidation of covellite (CuS). — *Thermochimica Acta* 369 (1–2), pp. 117–123.
247. DUNN, J. G., DE, G. C., FERNANDEZ, P. G. 1988: The effect of experimental variables on the multiple peaking phenomenon observed during the oxidation of pyrite. — *Thermochimica Acta* 135, pp. 267–272.
248. DUNN, J. G., DE, G. C., O’CONNOR, B. H. 1989a: The effect of experimental variables on the mechanism of the oxidation of pyrite Part 1. Oxidation of particles less than 45  $\mu\text{m}$  in size. — *Thermochimica Acta* 145, pp. 115–130.
249. DUNN, J. G., DE, G. C., O’CONNOR, B. H. 1989b: The effect of experimental variables on the mechanism of the oxidation of pyrite Part 2. Oxidation of particles of size 90–125  $\mu\text{m}$ . — *Thermochimica Acta* 155, pp. 135–149.
250. DUNN, J. G., GINTING, A. R., O’CONNOR, B. H. 1994: A thermoanalytical study of the oxidation of chalcocite. — *Journal of Thermal Analysis* 41 (2–3), pp. 671–686.
251. DUNN, J. G., GINTING, A. R., O’CONNOR, B. H. 1997: Quantitative determination of phases present in oxidised chalcocite. — *Journal of Thermal Analysis* 50, (1–2), pp. 51–62.
252. DUNN, J. G., GONG, W., SHI, D. 1993: A Fourier transform infrared study of the oxidation of pyrite. The influences of experimental variables. — *Thermochimica Acta* 215, pp. 247–254.
253. DUNNE, J. A., KERR, P. F. 1960: An improved thermal head for the differential thermal analysis of corrosive materials. — *The American Mineralogist* 45 (7–8), pp. 881–883.
254. DUNNE, J. A., KERR, P. F. 1961: Differential thermal analysis of galena and clausthalite — *The American Mineralogist* 46 (1–2), pp. 1–11.
255. DYER, A. 1987: Thermal analysis of zeolites. — *Thermochimica Acta* 110, pp. 521–526.
256. EARLYEY, J. W., MILNE, I. H., MCVEAGH, W. J. 1953: Thermal, dehydration and X-ray studies on montmorillonite. — *The American Mineralogist* 38 (9–10), pp. 770–783.
257. EARNEST, C. M. 1982: Thermogravimetry of selected American and Australian oil shales in inert dynamic atmospheres. — *Thermochimica Acta* 58 (3), pp. 271–288.
258. EARNEST, C. M. 1983a: Comparative TG-DTG oxidative profiles of selected American and Australian oil shales. — *Thermochimica Acta* 60 (2), pp. 171–180.
259. EARNEST, C. M. 1983b: Thermal analysis of hectorite. Part I. Thermogravimetry. — *Thermochimica Acta* 63 (3), pp. 277–289.
260. EARNEST, C. M. 1983c: Thermal analysis of hectorite. Part II. Differential thermal analysis. — *Thermochimica Acta* 63 (3), pp. 291–306.
261. EARNEST, C. M. 1984: Descriptive oxidative profiles for pyrite in the low temperature ash component of coals by differential thermal analysis. — *Thermochimica Acta* 75 (1–2), pp. 219–232.
262. EARNEST, C. M. 1991a: Thermal analysis of selected illite and smectite clay minerals. Part I. Illite clay Specimens. — In: SMYKATZ-KLOSS W., WARNE S. ST. J. (eds): *Thermal Analysis in the Geosciences*. Series of Lecture Notes in Earth Sciences 38. — Springer Verlag, pp. 270–286.
263. EARNEST, C. M. 1991b: Thermal analysis of selected illite and smectite clay minerals. Part II. Smectite clay Minerals. In: SMYKATZ-KLOSS W., WARNE S. ST. J. (eds): *Thermal Analysis in the Geosciences*. Series of Lecture Notes in Earth 38. — Springer Verlag, pp. 288–312.
264. ECHIGO, T., KIMATA, M., KYONO, A., SHIMIZU, M., HATTA, T. 2005: Re-investigation of the crystal structure of whewellite  $[\text{Ca}(\text{C}_2\text{O}_4 \cdot \text{H}_2\text{O})]$  and the dehydration mechanism of caoxite  $[\text{Ca}(\text{C}_2\text{O}_4 \cdot 3\text{H}_2\text{O})]$ . — *Mineralogical Magazine* 69 (1), pp. 77–88.
265. ECHLE, W. 1967: Loughlinite, (Na-sepiolith) und Analcim in Neogen Sedimenten Anatoliens. — *Contributions to Mineralogy and Petrology* 14 (2), pp. 86–101.
266. ECKHARDT, F. J. 1958: Über Chlorite in Sedimenten. — *Geologisches Jahrbuch* 75, pp. 437–474.
267. ECKHOUT, S. G., VOCHTEN, R., BLATON, N. M. DE GRAVE, E., JANSSENS, J., DESSEYN, H. 1998: Thermal stability and dehydration of anapaite. — *Thermochimica Acta* 320, pp. 223–230.
268. EGGER, K. 1963: Zur Oxydation natürlicher Magnetite. — *Schweizerische Mineralogische und Petrographische Mitteilungen* 43 (2), pp. 493–497.

269. EGGLETON, R. A., FITZPATRICK, R. W. 1988: New data and a revised structural model for ferrihydrite. — *Clays and Clay Minerals* 36 (2), pp. 111–114.
270. EL-AKKAD, T. M., FLEX, N. S., GUINDY, N. M., EL-MASSRY, S. R., NASHED, S. 1982: Thermal analyses of mono- and divalent montmorillonite cationic derivatives. — *Thermochimica Acta* 59 (1), pp. 9–17.
271. EL-BARAWY, K. A., GIRGIS FELIX, N. S. 1986: Thermal treatment of some pure smectites. — *Thermochimica Acta* 98, pp. 181–189.
272. ELDER, T. 1965: Particle-size effect in oxidation of natural magnetite. — *Journal of Applied Physics* 36 (3), pp. 1012–1013.
273. ELSCHOLTZ, L., SELMECZINÉ ANTAL, P., SELMECZI, B. 1974: Ein Kingit-Vorkommen in Ungarn, das Derivatogramm von Kingit. — *Bulletin of the Hungarian Geological Society* 104 (3), pp. 328–335.
274. EMMERICH, K., KAHR, G. 2000: Umwandlung eines cis-vakanten in einen trans-vakanten Montmorillonit durch thermische Behandlung. — *Beiträge zur Jahrestagung DDTG 2000, Zürich* 7, pp. 67–69.
275. EMMERICH, K., KAHR, G. 2001: The cis- and trans-vacant variety of a montmorillonite: an attempt to create a model smectite. — *Applied clay science* 20 (3), pp. 119–127.
276. EMMERICH, K., SMYKATZ-KLOSS, W. 2002: Exothermic effects in soils during thermal analysis — *Clay Minerals* 37 (4), pp. 575–582.
277. EMMERICH, W. D., BAYREUTHER, K. 1975: Experiences with an EGA-DTA equipment. — *Thermal Analysis* 5 (3), *Proceedings of the fourth ICTA, Budapest, 1974*, pp. 1017–1021.
278. EMMERICH, W. D., KAISERSBERGER, E. 1979: Simultaneous TG-DTA Mass-spectrometry to 1550. — *Journal of Thermal Analysis* 17 (1), pp. 197–212.
279. EMONS, H. H. 1988: Mechanism and kinetics of formation and decomposition of carnallitic double salts. — *Journal of Thermal Analysis* 33 (1), pp. 113–120.
280. EMONS H. H., NAUMANN R., POHL T., FLAMMERSCHEIM H. J. 1984a: Die Anwendung der quantitativen DTA zur Bestimmung von Bischofit bei Anwesenheit von Carnallit. — *Freiberger Forschungshefte Reihe A*, 726, pp. 52–59.
281. EMONS, H. H., NAUMANN, R., POHL, T., VOIGT, H. 1984b: Vergleichende Untersuchungen des thermischen Verhaltens von Carnallit und Bischofit. — *Freiberger Forschungshefte Reihe A*, 726, pp. 40–51.
282. EMONS, H. H., NAUMANN, R., KOHNKE, K., HEIDE, K. 1989: Investigation on the thermal-behavior of  $\text{NH}_4\text{Al}(\text{SO}_4)_2 \cdot 12\text{H}_2\text{O}$ . — *Zeitschrift für Anorganische und Allgemeine Chemie* 577 (10), pp. 83–92.
283. EMONS, H. H., ZIEGENBALG, G., NAUMANN, R., PAULIK, F. 1990: Thermal decomposition of the magnesium sulphate hydrates under quasi-isothermal and quasi-isobaric conditions. — *Journal of Thermal Analysis* 36 (4), pp. 1265–1279.
284. ENGLER, PH., SANTANA, M. W., MITTLEMAN, M. L., BALAZS, D. 1988: Non-isothermal in situ XRD analysis of dolomite decomposition. — *The Rigaku Journal* 5 (2), pp. 3–8.
285. ENGLER, PH., SANTANA, M. W., MITTLEMAN, M. L., BALAZS, D., 1989: Non-isothermal, in situ XRD analysis of dolomite decomposition. — *Thermochimica Acta* 140, pp. 67–76.
286. ERDÉLYI, J., KOBLENCZ, V. N. VARGA, S. 1962: Neue strukturelle Regeln der Hydroglimmer. Hydroantigorit, ein neues Serpentin-Mineral und metakolloidaler Brucit vom Csódi-Berg bei Dunabogdány, Ungarn. — *Acta Geologica Hungarica* 6, pp. 65–93.
287. ERDEY, L., PAULIK, F. 1963: Derivatographische Untersuchung der Bauxite. Thermische Zersetzung des Hidrargillits. — *Acta Chimica Academiae Scientiarum Hungaricae, (Budapest)* 21 (2), pp. 1–24.
288. EREMEEV, V. V. 1967: Ceolity bassejna r. Tètèrè. — In: PETROV, V. P. (ed.) 1967: *Vodnye vulkaničeskie stekla i post vulkaničeskie mineraly*. Nauka, Moskow, pp. 119–150.
289. ERICKSEN, G. E., MROSE, M. E., MARINENKO, J. W., MCGEE, J. J. 1986: Mineralogical studies of the nitrate deposits of Chile. V. Iquiqueite,  $\text{Na}_4\text{K}_3\text{Mg}(\text{CrO}_4)_2\text{B}_{24}\text{O}_{39}(\text{OH}) \cdot 12\text{H}_2\text{O}$ , a new saline mineral. — *The American Mineralogist* 71 (5–6), pp. 830–836.
290. EROSHCHEV-SHAK, V. A. 1970: Mixed-layer biotite-chlorite formed in the course of local epigenesis in the weathering crust of a biotite gneiss. — *Sedimentology* 15 (1–2), pp. 115–121.
291. FAJNOR, V. Š., JESENÁK, K. 1996: Differential thermal analysis of montmorillonite. — *Journal of Thermal Analysis and Calorimetry* 46 (2), pp. 489–493.
292. FANFANI, L., NUNZI, A., ZANAZZI, P. F. 1970: The crystal structure of roemerite. — *The American Mineralogist* 55 (1–2), pp. 78–89.
293. FARKAS, L., KÜRTHY KOMLÓSI, J. 1981: Structural investigations on aluminite by x-ray and thermoanalytical methods. — *Annual Report of the Geological Institute of Hungary of 1979*, pp. 515–523. (in Hungarian)
294. FARMER, V. C. 1992: Possible confusion between so-called ferrihydrites and hisingerites. — *Clay Minerals* 27 (3), pp. 373–378.
295. FĂTU, D., ANGHEL, D., SEGAL, E. 1984: Thermal decomposition of a dolomitic limestone with brucite under quasi-isothermal conditions using a quasi-isobaric crucible and associated non-isothermal kinetic parameters. — *Thermochimica Acta* 76 (1–2), pp. 213–219.
296. FAULRING, G. M., ZWICKER, W. K., FORGENG, W. D. 1960: Thermal transformations and properties of cryptomelane. — *The American Mineralogist* 45 (9–10), pp. 946–959.
297. FAUST, G. T. 1948: Thermal analysis of quartz and its use in calibration in the thermal analysis studies. — *The American Mineralogist* 33 (5–6), pp. 337–345.
298. FAUST, G. T. 1950: Thermal analysis studies on carbonates (I): Aragonite and calcite. — *The American Mineralogist* 35 (3–4), pp. 207–222.
299. FAUST, G. T. 1951: Thermal analysis and X-ray studies of sauconite and some zinc minerals of the same paragenetic association. — *The American Mineralogist* 36 (11–12), pp. 795–822.
300. FAUST, G. T. 1953: Huntite,  $\text{Mg}_2\text{Ca}(\text{CO}_3)_4$ , a new mineral. — *The American Mineralogist* 38 (1–2), pp. 4–24.
301. FAUST, G. T. 1955: Thermal analysis and X-ray studies of griffithite. — *Journal of the Washington Academy of Science* 45 (3), pp. 66–70.
302. FAUST, G. T. 1957: A study of the montmorillonite variety galapektite. — *Journal of the Washington Academy of Science* 47 (5) pp. 143–147.
303. FAUST, G. T., FAHEY, J. J. 1962: The serpentine-group minerals. — *Geological Survey Professional Paper* 384–A 92 p.
304. FAUST, G. T., MURATA, K. J. 1953: Stevensite. Redefined as a member of montmorillonite group. — *The American Mineralogist* 38 (11–12) pp. 973–987.

305. FAUST, G. T., HATHAWAY, J. C., MILLOT, G. 1959: A restudy of stevensite and allied minerals. — *The American Mineralogist* 44 (3–4) pp. 342–370.
306. FAZEKAS, V., KÓSA, L., SELMECZI, B. 1975: Rare earth mineralization in the crystalline schists of the Sopron Mountains. — *Bulletin of the Hungarian Geological Society* 105 (3), pp. 297–306.
307. FENOL HACH-ALI, P. 1967: Thesis, University of Granada, Spain. — In: MARTIN VIVALDI, J. L., FENOLL HACH-ALI P. 1970: Palygorskite and sepiolite. — In: MACKENZIE, R. C. (ed.): *Differential Thermal Analysis*. — Academic Press. London – New York, pp. 553–573.
308. FERRO, O., QUARTIERI, S., VEZZALINI, G., CERIANI, CH., FOIS, E., GAMBA, A., CRUCIANI, G. 2004: Dehydration dynamics of bikitaite: Part I. In situ synchrotron powder X-ray diffraction study. — *The American Mineralogist* 49 (1), pp. 94–101.
309. FEY, M. B., DIXON, J. B. 1981: Synthesis and properties of poorly crystalline hydrated aluminous goethites. — *Clays and Clay Minerals* 29 (2), pp. 91–100.
310. FIEDLER, G., WAGNER, R. 1967: Untersuchungen zur quantitativen Bestimmung von Montmorillonit mit dem Derivatographen. — *Zeitschrift für Angewandte Geologie* 13 (5), pp. 262–266.
311. FILIZOVA, L., KIROV, G. N., BALKO, V. M. 1975: Thermal behaviour of the minerals of the heulandite and stilbite groups. — *Geochemistry Mineralogy and Petrology* 2, pp. 32–50.
312. FIORE, S., LAVIANO, R., 1991: Brushite, hydroxylapatite, and taranakite from Apulian caves (southern Italy): New mineralogical data. — *The American Mineralogist* 76 (9–10), pp. 1722–1727.
313. FLEISCHER, M. 1960: Studies of manganese oxide minerals III. Psilomelane. — *The American Mineralogist* 45 (1–2), pp. 176–187.
314. FLEISCHER, M., FAUST, G. T. 1963: Studies on manganese oxide minerals VII. Lithiophorite. — *Schweizerische Mineralogische und Petrographische Mitteilungen* 43 (1), pp. 197–216.
315. FLEISCHER, M., CHAO, G. Y., KATO, A. 1975: New mineral names: ferrihydrite. — *The American Mineralogist* 60 (5–6), pp. 485–486.
316. FLEMMING, N. J., LOPATA, V. J., SANIPELLI, B. L., TAYLOR, P. 1984: Thermal decomposition of basic lead carbonates: A comparison of hydrocerussite and plumbonacrite. — *Thermochimica Acta* 81, pp. 1–8.
317. FLÓRA, T. 1984: Beiträge zur Kinetik der Zeolith-dehydratation. — *Thermochimica Acta* 79, pp. 1–14.
318. FLÖRKE, O. W. 1961: Untersuchungen an feinkristallinem Quarz. — *Schweizerische Mineralogische und Petrographische Mitteilungen* 41 (2), pp. 311–327.
319. FLÖRKE, O. W., KOHLERHERBERTZ, B., LANGER, K., TÖNGES, I. 1982: Water in microcrystalline quartz of volcanic origin: Agates. — *Contributions to Mineralogy and Petrology* 80 (4), pp. 324–333.
320. FÖLDVÁRI, M. 1973: Derivatographic analysis of the organic content of metamorphic rocks in view of their rank of coalification. — *Annual Report of the Hungarian Geological Institute of 1971*, pp. 297–301. (in Hungarian).
321. FÖLDVÁRI, M. 1987: Gesichtspunkte bei dem Einsatz der Thermoanalyse als instrumentelle Methode zur Phasenanalyse von Gesteinen. — *Chemie der Erde – Geochemistry* 47 (1–2), pp. 19–30.
322. FÖLDVÁRI, M. 1990: New possibilities in phase analysis of rocks with derivatograph-c. — *Journal of Thermal Analysis* 36 (5), pp. 1707–1715.
323. FÖLDVÁRI, M. 1991: Measurement of different water species in minerals by means of thermal derivatography — In: SMYKATZ-KLOSS, W., WARNE, S. St. J. (eds): *Thermal Analysis in the Geosciences*. Series of Lecture Notes in Earth Sciences 38. — Springer Verlag, pp. 84–100.
324. FÖLDVÁRI, M. 1997: Kaolinite genetic and thermoanalytical parameters. — *Journal of Thermal Analysis* 48 (1), pp. 107–119.
325. FÖLDVÁRI, M. 1999: The use of corrected thermal decomposition temperature in the geological interpretation. — *Journal of Thermal Analysis and Calorimetry* 56 (2), pp. 909–916.
326. FÖLDVÁRI, M. 2000: Advanced possibilities of thermal analysis in the investigation of clay minerals. — *Acta Geologica Hungarica* 43 (4), pp. 447–461.
327. FÖLDVÁRI, M. 2005: Application of the fuzzy set theory for the quantitative phase analysis of rocks using thermal analysis applied to the Boda Siltstone Formation, Hungary — *Proceedings of International Symposium of Hungarian Researches, Computational Intelligence*. 2005. nov. 18–19. Budapest, pp. 144–150.
328. FÖLDVÁRI, M., BALOGH, K. 1984: Methodological analysis of K/Ar dating on sedimentary glauconites from Hungary. — *Annual Report of the Geological Institute of Hungary of 1982*, pp. 479–489. (in Hungarian)
329. FÖLDVÁRI, M., FARKAS, L. 1985: The joint use of instrument-based mineralogical phase-analytical methods. — *Annual Report of the Geological Institute of Hungary of 1983*, pp. 371–382. (in Hungarian)
330. FÖLDVÁRI, M., GERMÁN-HEINS, J. 1994: Thermal Analysis. — In: RETALLACK, G. J., GERMÁN-HEINS, J. (eds): Evidence from Paleosols for the geological antiquity of rain forest. *Science* 265 (5171), pp. 499–502.
331. FÖLDVÁRI, M., KOVÁCS-PÁLFFY, P. 1993: A critical study on crystallinity measurement of kaolinites — *Romanian Journal of Mineralogy* 76 (1), pp. 109–119.
332. FÖLDVÁRI, M., KOVÁCS-PÁLFFY, P. 2002: Mineralogical study of the Tengelic Formation and the loess complex of Tolna Hegyhát and Mórág Hills areas. — *Acta Geologica Hungarica* 45 (3), pp. 247–263.
333. FÖLDVÁRI, M., KOVÁCS-PÁLFFY, P. 2007: Thermoanalytical investigation of mono- and bivalent interlayer cations in montmorillonite. — *Annual Report of the Geological Institute of Hungary of 2005*, pp. 167–176.
334. FÖLDVÁRI, M., NAGY, B. 1985: Diadochite and destinezite from Mátraszentimre (N-Hungary). — *Bulletin of the Hungarian Geological Society* 115 (1–2), pp. 123–131. (in Hungarian)
335. FÖLDVÁRI, M., ROZS, M. 1991: A computer program for the quantitative thermoanalytical determination of clay mineral mixtures. — *Annual Report of the Geological Institute of Hungary of 1989*, pp. 567–571. (in Hungarian)
336. FÖLDVÁRI, M., PAULIK, F., PAULIK, J. 1988: Possibility of thermal analysis of different types of bonding of water in minerals. — *Journal of Thermal Analysis* 33 (1), pp. 121–132.
337. FÖLDVÁRI, M., KOVÁCS-PÁLFFY, P., NAGY, N. M., KÓNYA, J. 1998: The use of the second derivate of thermogravimetric curve for the investigation of exchanged interlayer cation in montmorillonite. — *Journal of Thermal Analysis and Calorimetry* 53 (2), pp. 547–558.

338. FÖLDVÁRI, M., BÁRDOSSY, GY., FODOR, J. 2001: Application of the fuzzy arithmetic to the quantitative phase analysis of rock samples by thermoanalytical methods, applied to the Boda Aleurolite Formation, Hungary. — *Bulletin of the Hungarian Geological Society* 132 (1), pp. 1–16.
339. FÖLDVÁRI, M., BERNER, ZS., STÜBEN, D. 2003a: Thermoanalytical study of Quarternary thermal lacustrine travertines in Hungary (Buda-Vár-hegy, Budakalász, Szomód-Leshegy). — *Acta Geologica Hungarica* 46 (2), pp. 193–202.
340. FÖLDVÁRI, M., KOVÁCS-PÁLFFY, P., PÉCSKAY, Z., HOMONNAY, Z. 2003b: Structural investigations of mica minerals with the object of suitability for K/Ar radiometric dating — *The 5th Symposium Baia Mare Branch of the Geological Society of Romania, Book of Abstract* p. 12.
341. FÖLDVÁRI-VOGL, M. 1958: The role of differential thermal analysis in mineralogy and geological prospecting. — *Acta Geologica Hungarica* 5 (1), pp. 3–102.
342. FÖLDVÁRI-VOGL, M., KOBLENCZ, V. 1955: Facteurs de la decomposition thermique des dolomies. — *Acta Geologica Hungarica* 3 (1–3), pp. 15–26.
343. FÖLDVÁRI-VOGL, M., KOBLENCZ, V. 1956: Differential thermal analysis of artificial manganese compounds. — *Acta Mineralogica et Petrographica, Universitatis Szegediensis* 9, pp. 7–14.
344. FÖLDVÁRI-VOGL, M., KOBLENCZ, V. 1957: Sur les possibilités de l'analyse thermique différentielle des minéraux de manganèse. — *Acta Geologica Hungarica* 4, pp. 85–94.
345. FOSTER, M. D. 1961: Interpretation of the composition of vermiculites and hydrobiotites. — *Clays and Clay Minerals* 10 (1), pp. 70–89.
346. FRANCO, F., PÉREZ-MAQUEDA, L. A., PÉREZ-RODRÍGUEZ, J. L. 2004: Influence of the particle-size reduction by ultrasound treatment on the dehydroxylation process of kaolinites. — *Journal of Thermal Analysis and Calorimetry* 78 (3), pp. 1043–1055.
347. FREDERICKSON, A. F. 1948: Differential thermal curve of siderite. — *The American Mineralogist* 33 (5–6), pp. 372–374.
348. FREEMAN, A. G. 1966: The dehydroxylation behaviour of amphiboles. — *Mineralogical Magazine* 35 (275), pp. 953–957.
349. FRENCH, B. M., ROSENBERG, P. E. 1965: Siderite ( $\text{FeCO}_3$ ): Thermal decomposition in equilibrium with graphite. — *Science* 147 (3663), pp. 1283–1284.
350. FREUND, F., GENTSCH, H. 1967:  $\text{H}_2$ -Abspaltung bei der Entwässerung von  $\text{Mg}(\text{OH})_2$ ,  $\text{Al}(\text{OH})_3$  und Kaoliniteinkristallen. — *Berichte der Deutschen Keramischen Gesellschaft* 44, pp. 51–58.
351. FRIDRIKSSON, TH., BISH, D. L., BIRD, D. K. 2003a: Hydrogen-bonded water in laumontite I: X-ray powder diffraction study of water site occupancy and structural changes in laumontite during room-temperature isothermal hydration/dehydration. — *The American Mineralogist* 88 (2–3), pp. 277–287.
352. FRIDRIKSSON, TH., CAREY, J. W., BISH, D. L., NEUHOFF, PH. S., BIRD, D. K. 2003b: Hydrogen-bonded water in laumontite II: Experimental determination of site-specific thermodynamic properties of hydration of the W1 and W5 sites. — *The American Mineralogist* 88 (7), 1060–1072.
353. FRITSCH, S., SARRIAS, J., ROUSSET, A., KULKARNI, G. U. 1998: Low-temperature oxidation of  $\text{Mn}_3\text{O}_4$  hausmannite. — *Materials Research Bulletin* 33 (8), pp. 1185–1194.
354. FRONDEL, C., BAVER, L. H. 1955: Kutnahorite, a Mn-dolomite. — *The American Mineralogist* 40 (7–8), pp. 748–760.
355. FROST, R. L., DING, Z. 2003: Controlled rate thermal analysis and differential scanning calorimetry of sepiolites and palygorskites. — *Thermochimica Acta* 397 (1–2), pp. 119–128.
356. FROST, R. L., ERICKSON, K. L. 2004a: Thermal decomposition of synthetic hydrotalcites reevesite and pyroaurite. — *Journal of Thermal Analysis and Calorimetry* 76 (1), pp. 217–225.
357. FROST, R. L., ERICKSON, K. L. 2004b: Thermal decomposition of natural iowaite. — *Journal of Thermal Analysis and Calorimetry* 78. 2. pp. 367–373.
358. FROST, R. L., WEIER, M. L. 2003: Thermal treatment of weddellite — a thermal analysis and Raman spectroscopic study. — *Thermochimica Acta* 406 (1–2), pp. 221–232.
359. FROST, R. L., WEIER, M. L. 2004a: Thermal decomposition of humboldtine: A high resolution thermogravimetric and hot stage Raman spectroscopic study. — *Journal of Thermal Analysis and Calorimetry* 75 (1), pp. 277–291.
360. FROST, R. L., WEIER, M. L. 2004b: Thermal treatment of whewellite — a thermal analysis and Raman spectroscopic study. — *Thermochimica Acta* 409 (1), pp. 79–85.
361. FROST, R. L., WEIER, M. L. 2004c: The 'cave' mineral oxammite: — a high resolution thermogravimetry and Raman spectroscopic study. — *Neues Jahrbuch für Mineralogie, Monatshefte* 1, pp. 27–48.
362. FROST, R. L., VASSALLO, A. M., VAN DER GAAST, S. J. 1995: The dehydroxylation of the kaolinite clay minerals. — *EUROCLAY'95 Clays and Clay Materials Sciences. Leuven 1995 aug. 20–24. Book of Abstracts*, pp. 40–41.
363. FROST, R. L., KLOPROGGE, J. T., RUSSELL, S. C., SZETU, J. 1999a: Dehydroxylation of aluminum (oxo)hydroxides using infrared emission spectroscopy. Part II: Boehmite. — *Applied Spectroscopy* 53 (5), pp. 572–582.
364. FROST, R. L., KLOPROGGE, J. T., RUSSELL, S. C., SZETU, J. 1999b: Dehydroxylation and the vibrational spectroscopy of aluminum (oxo)hydroxides using infrared emission spectroscopy. Part III: Diaspore. — *Applied Spectroscopy* 53 (7), pp. 829–835.
365. FROST, R. L., HUADA RUAN, D., KLOPROGGE, T. J., GATES, W. P. 2000: Dehydration and dehydroxylation of nontronites and ferruginous smectite. — *Thermochimica Acta* 346 (1–2), pp. 63–72.
366. FROST, R. L., DING, Z., KLOPROGGE, J. T., MARTENS, W. N. 2002a: Thermal stability of azurite and malachite in relation to the formation of mediaeval glass and glazes. — *Thermochimica Acta* 390 (1–2), pp. 133–144.
367. FROST, R. L., KRISTÓF, J., MAKÓ, E., DING, Z. 2002b: A DRIFT spectroscopic study of mechanochemically activated kaolinite. — *Spectrochimica Acta, Part A: Molecular and Biomolecular Spectroscopy* 58A (13), pp. 2849–2859.
368. FROST, R. L., DING, Z., RUAN, H. D. 2003a: Thermal analysis of goethite: Relevance to Australian indigenous art. — *Journal of Thermal Analysis and Calorimetry* 71 (3), pp. 783–797.
369. FROST, R. L., MARTENS, W., DING, Z., KLOPROGGE, J. T. 2003b: DSC and high-resolution TG of synthesized hydrotalcites of Mg and Zn. — *Journal of Thermal Analysis and Calorimetry* 71 (2), pp. 429–438.
370. FROST, R. L., WEIER, M. L., CLISSOLD, M. E., WILLIAMS, P. A., KLOPROGGE, J. T. 2003c: Thermal decomposition of the natural hydrotalcites carboydite and hydrohonessite. — *Thermochimica Acta* 407 (1–2), pp. 1–9.

371. FROST, R. L., WEIER, M. L., MARTENS, M., KLOPROGGE, J. TH., DING, Z. 2003d: Dehydration of synthetic and natural vivianite. — *Thermochimica Acta* 401 (2), pp. 121–130.
372. FROST, R. L., WEIER, M. L., MARTENS, M., KLOPROGGE, J. TH., DING, Z. 2003e: Thermal decomposition of the vivianite arsenates-implications for soil remediation. — *Thermochimica Acta* 403 (2), pp. 237–249.
373. FROST, R. L., ERICKSON, K., WEIER, M. 2004a: Thermal treatment of moolooite — a thermal analysis and Raman spectroscopic study. — *Journal of Thermal Analysis and Calorimetry* 77 (3), pp. 851–861.
374. FROST, R. L., MILLS, S. J., ERICKSON, K. L. 2004b: Thermal decomposition of peisleyite: a thermogravimetry and hot stage Raman spectroscopic study. — *Thermochimica Acta* 419 (1–2), pp. 109–114.
375. FROST, R. L., WEIER, M. L., ADEBAJO, M. O. 2004c: Thermal decomposition of metazeunerite—a high-resolution thermogravimetric and hot-stage Raman spectroscopic study. — *Thermochimica Acta* 419 (1–2), pp. 119–129.
376. FROST, R. L., WEIER, M. L., ERICKSON, K. L. 2004d: Thermal decomposition of struvite — implications for the decomposition of kidney stones. — *Journal of Thermal Analysis and Calorimetry* 76 (3), pp. 1025–1033.
377. FROST, R. L., MARTENS, W. N., ERICKSON, K. L. 2005a: Thermal decomposition of the hydrotalcite. Thermogravimetric analysis and hot stage Raman spectroscopic study. — *Journal of Thermal Analysis and Calorimetry* 82 (3), pp. 603–608.
378. FROST, R. L., WEIER, M. L., MARTENS, W. 2005b: Thermal decomposition of jarosites of potassium, sodium and lead. — *Journal of Thermal Analysis and Calorimetry* 82 (1), pp. 115–118.
379. FROST, R. L., WILLS, R., WEIER, M., MARTENS, W. 2005c: Thermal decomposition of synthetic argentojarosite — Implications for silver production in medieval times. — *Thermochimica Acta* 437 (1–2), pp. 30–33.
380. FROST, R. L., WILLS, R., WEIER, M., MUSUMECI, A., MARTENS, W. 2005d: Thermal decomposition of natural and synthetic plumbo-jarosites: Importance in ‘archeochemistry’. — *Thermochimica Acta* 432 (1), pp. 30–35.
381. FROST, R. L., WAIN, D. L., WILLS, R., MUSUMECI, A., MARTENS, W. 2006a: A Thermogravimetric study of the alunites of sodium, potassium and ammonium. — *Thermochimica Acta* 443 (1), pp. 56–61.
382. FROST, R. L., KLOPROGGE, J. T., WILLS, R., MARTENS, W. 2006b: Thermal decomposition of hydronium jarosite  $(\text{H}_3\text{O})\text{Fe}_3(\text{SO}_4)_2(\text{OH})_6$ . — *Journal of Thermal Analysis and Calorimetry* 83 (1), pp. 213–218.
383. FROST, R. L., WEIER, M. L., MARTENS, W., MILLS, S. 2006c: ThermoRaman spectroscopic study of kintoreite. — *Spectrochimica Acta* 63 (2), pp. 282–288.
384. FROST, R. L., WILLS, R., KLOPROGGE, J. T., MARTENS, W. N. 2006d: Thermal decomposition of ammonium jarosite  $(\text{NH}_4)\text{Fe}_3(\text{SO}_4)_2(\text{OH})_6$ . — *Journal of Thermal Analysis and Calorimetry* 84 (2), pp. 489–496.
385. FRUCH, A. J. JR 1950: Disorder in the mineral bornite. — *The American Mineralogist* 35 (3–4), pp. 185–192.
386. FUDALA, Á., HALÁSZ, J., KIRICSI, I. 1996: Thermogravimetric investigation solid-state ion-exchange procedure of  $\text{Cu}^{2+}$ ,  $\text{Co}^{2+}$ ,  $\text{Ni}^{2+}$  and  $\text{Fe}^{2+}$  ions into montmorillonite. — *Journal of Thermal Analysis* 47 (2), pp. 399–406.
387. GÁBOR, M., TÓTH, M., KRISTÓF, J., KOMÁROMY-HILLER, G. 1995: Thermal behaviour and decomposition of intercalated kaolinite. — *Clays and Clay Minerals* 43 (2), pp. 223–228.
388. GÁL, S., PAULIK, F., ERDEY, L., BAYER, J. 1963: Derivatographische Untersuchung von Calciumoxalathydraten. — *Periodica Polytechnica Chemical Engineering, Budapest*, 7 (3), pp. 215–222.
389. GALLAGHER, P. K. 1982: Applications of evolved gas analysis to the study of inorganic materials and processes. — *Journal of Thermal Analysis* 25 (1), pp. 7–20.
390. GALLAGHER, P. K., WARNE, S. ST. J. 1981: Thermomagnetometry and thermal decomposition of siderite. — *Thermochimica Acta* 43 (3), pp. 253–267.
391. GALLITELLI, P. 1954: Pennine from Boccassuolo. — *Tschermaks Schweizerische Mineralogische und Petrographische Mitteilungen* 4 (1–4), pp. 283–287.
392. GARD, J. A., TAYLOR, H. F. W., CHALMERS, R. A. 1957: An investigation of two new minerals: rhodesite and mountainite. — *Mineralogical Magazine* 31 (239), pp. 611–623.
393. GARN, P. D., ANTONY, G. D. 1969: Questionable kinetics of kaolin dehydroxylation. — *Journal of Thermal Analysis* 1, pp. 29–33.
394. GARN, P. D., KAWALEC, B., CHANG, J. C. 1978: Dehydration of brucite. — *Thermochimica Acta* 26 (1–3), pp. 375–381.
395. GEDEON, T. G. 1955: Aluminite (websterite) of Gánt, Hungary. — *Acta Geologica Hungarica* 3 (1–3), pp. 27–43.
396. GEIGER, C. A., RAHMOUN, N. S., HEIDE, K. 2001: Volatiles in cordierite. — *Berichte der Deutschen Mineralogischen Gesellschaft, Beihefte zum European Journal of Mineralogy* 13 (1), p. 60.
397. GEITH, M. A. 1952: Differential thermal analysis of certain iron oxides and oxide hydrates. — *American Journal of Science* 250 (9), pp. 677–695.
398. GIAMPAOLO, C., LOMBARDI, G. 1994: Thermal behaviour of analcimes from two different genetic environments. — *European Journal of Mineralogy* 6 (2), pp. 285–289.
399. GIESE, R. F., COSTANZO, P. M. 1986: Behavior of water on the surfaces of kaolin minerals. — In: GIESE, JR. R. F. 1989: Kaolin minerals: Structures and stabilities. — In: BAILEYS, S. W. (ed.): *Hydrous Phyllosilicates. Reviews in Mineralogy. Mineralogical Society of America* 19, pp. 29–66.
400. GIGGIS, B. S., FELIX, N. S., EL-BARAWY, K. A. 1987: Dehydroxylation of some pure smectites. — *Thermochimica Acta* 112 (2), pp. 265–274.
401. GILLOT, B., EL GUENDOUZI, M., LAARJ, M. 2001: Particle size effects on the oxidation–reduction behavior of  $\text{Mn}_3\text{O}_4$  hausmannite. — *Materials Chemistry and Physics* 70 (1), pp. 54–60.
402. GIOVANOLI, R. 1985: Layer structures and tunnel structures in manganates. — *Chemie der Erde* 44 (3), pp. 227–244.
403. GLASS, H. D. 1954a: High-temperature phases from kaolinite and halloysite. — *The American Mineralogist* 39 (3–4), pp. 193–207.
404. GLASS, H. D. 1954b: Investigation of rank in coal by differential thermal analysis. — *Economic Geology* 49 (3), pp. 294–309.
405. GLASSER, F. P. 1970: Other silicates. — In: MACKENZIE, R. C. (ed.): *Differential Thermal Analysis*. Academic Press, London – New York, pp. 575–608.
406. GLINKA, A., PACEWSKA, B., MICHAŁOWSKI, S. 1984: Investigation of thermal decomposition of hydrated aluminium oxide. — *Journal of Thermal Analysis* 29 (5), pp. 953–957.

407. GOKHALE, K. V. G. K., RAO, T. C. 1970: Studies on the thermal dissociation of some carbonate minerals. — *Journal of Thermal Analysis* 2 (1), pp. 83–85.
408. GOLDEN, D. C., DIXON, J. B., CHEN, C. C. 1986: Ion exchange, thermal transformations, and oxidizing properties of birnessite. — *Clays and Clay Minerals* 34 (5), pp. 511–520.
409. GOLDEN, D. C., CHEN, C. C., DIXON, J. B. 1987: Transformation of birnessite to buserite, todorokite, and manganite under mild hydrothermal treatment. — *Clays and Clay Minerals* 35 (4), pp. 271–280.
410. GOÑI-ELIZALDE, S., GARCÍA-CLAVEL, M. E. 1988: Thermal behavior in air of iron oxyhydroxides obtained from the method of homogeneous precipitation: Part I. Goethite samples of varying crystallinity. — *Thermochimica Acta* 124, pp. 359–369.
411. GONZÁLEZ, F., PESQUERA, C., BENITO, I. 1993: A study by thermal analysis of the reversible folding in palygorskite under vacuum thermal treatment. — *Thermochimica Acta* 223, pp. 83–91.
412. GONZÁLEZ, C., GUTIÉRREZ, J. I., GONZÁLEZ-VELASCO, J. R., CID, A., ARRANZ, A., ARRANZ, J. F. 1996: Transformations of manganese oxides under different thermal conditions. — *Journal of Thermal Analysis* 47 (1), pp. 93–102.
413. GOTTARDI, G., GALLI, E. 1985: Natural zeolites. In series: Minerals, Rocks and Inorganic Materials. Springer Verlag, Berlin–Heidelberg–Tokyo, 408 p.
414. GOUT, R., JAUBERTHIE, R. 1976: Two varieties of diasporite. — *Comptes rendus hebdomadaires des seances de l'academie des sciences* 282 (19), pp. 1697–1700.
415. GRAETSCH, H. 1998: Characterization of the high-temperature modifications of incommensurate tridymite L3-TO(MX-1) from 25 to 250 °C. — *The American Mineralogist* 83 (7–8), pp. 872–880.
416. GRAETSCH, H., FLÖRKE, O. W., MIEHE, G. 1985: The nature of water in chalcedony and opal-c from Brazilian agate geodes. — *Physics and Chemistry of Minerals* 12 (5), pp. 300–306.
417. GRAF, D. L. 1952: Preliminary report of the variation in differential thermal curves of low-iron dolomite. — *The American Mineralogist* 37 (1–2), pp. 1–27.
418. GRASSELLY, GY., KLIVÉNYI, E. 1956: Concerning the thermal properties of the manganese oxides of higher valencies. — *Acta Mineralogica et Petrographica, Universitatis Szegediensis* 9, pp. 15–32.
419. GRASSELLY GY., KLIVÉNYI E. 1957: Method for the determination of the mineral composition of sedimentary manganese oxide ores on the basis of their thermal properties. — *Acta Mineralogica et Petrographica, Universitatis Szegediensis* 10, pp. 33–46.
420. GRAY, D. J. 2000: Investigation of hydrogeochemical dispersion of gold and other elements in the Wollubar Palaeodrainage, Western Australia. — *Cooperative Research Centre for Landscape Environments and Mineral Exploration Open File Report* 33, 34 p.
421. GREENE-KELLY, R. 1957: The montmorillonite minerals (Smectites). — In: MACKENZIE, R. C. (ed.) 1957: *The differential thermal investigation of clays*. Mineralogical Society, London, pp. 140–164.
422. GRICE, J. D., GAULT, R. A., ROBERTS, A. C., COOPER, M. A. 2000: Adamsite-(y), a new sodium–yttrium carbonate mineral species from Mont Saint-Hilaire, Quebec. — *The Canadian Mineralogist* 38 (6), pp. 1457–1466.
423. GRIM, R. E. 1947: Differential thermal analysis curves of clay mineral mixtures. — *The American Mineralogist* 32 (9–10), pp. 493–501.
424. GRIM, R. E. 1948: Rehydration and dehydration of clay minerals. — *The American Mineralogist* 33 (1–2), pp. 50–59.
425. GRIM, R. E. 1953: *Clay mineralogy*. In: McGraw-Hill Series in Geology. — McGraw-Hill Publishing Company LTD. New York, London, Toronto 384 p.
426. GRIM, R. E., KULBICKI, G. 1961: Montmorillonite: high temperature reaction and classification. — *The American Mineralogist* 46 (11–12), pp. 1329–1369.
427. GRIM, R. E., ROWLAND, R. A. 1942: Differential thermal analysis of clay minerals and other hydrous materials. Part 1. — *The American Mineralogist* 27 (11), pp. 746–761.
428. GRIM, R. E., ROWLAND, R. A. 1942: Differential thermal analysis of clay minerals, and other hydrous materials. Part 2. — *The American Mineralogist* 27 (12), pp. 801–818.
429. GRUNER, J. W. 1948: Silicate structures. — *The American Mineralogist* 33 (11–12), pp. 679–691.
430. GUALTIERI, A. F., VENTURELLI, P. 1999: In situ study of the goethite-hematite phase transformation by real time synchrotron powder diffraction. — *The American Mineralogist* 84 (5–6), pp. 895–904.
431. GUGGENHEIM, S., CHANG, Y. H., KOSTER VAN GROOS, A. F. 1987: Muscovite dehydroxylation: High-temperature studies. — *The American Mineralogist* 72 (5–6), pp. 537–550.
432. GUGGENHEIM, S., KOSTER VAN GROOS, A. F. 1992a: High-pressure differential thermal analysis (HP-DTA). I. Dehydration reactions at elevated pressures in phyllosilicates. — *Journal of Thermal Analysis* 38 (7), pp. 1701–1728.
433. GUGGENHEIM, S., KOSTER VAN GROOS, A. F. 1992b: High-pressure differential thermal analysis (HP-DTA). II. Dehydroxylation reactions at elevated pressures in phyllosilicates. — *Journal of Thermal Analysis* 38 (11), pp. 2529–2548.
434. GUGGENHEIM, S., KOSTER VAN GROOS, A. F. 2001: Baseline studies of the clay minerals society source clays: Thermal Analysis. — *Clay and Clay Minerals* 40 (5), pp. 433–443.
435. GUGGENHEIM, S., ADAMS, J. M., BAIN, D. C., BERGAYA, F., BRIGATTI, M. F., DRITS, V. A., FORMOSO, M. L., GALÁN, E., KOGURE, T., STANJEK, H. 2006: Summary of recommendations of Nomenclature Committees relevant to clay mineralogy: report of the Association Internationale pour l'Étude des Argiles (AIPEA) Nomenclature Committee for 2006. — *Clays and Clay Minerals* 54 (6), pp. 761–772.
436. GUINDY, N. M., EL-AKKAD, T. M., FLEX, N. S., EL-MASSRY, S. R., NASHED, S. 1985: Thermal dehydration of mono- and di-valent montmorillonite cationic derivatives. — *Thermochimica Acta* 88 (2), pp. 369–378.
437. GÜVEN, N. 1988: Smectites. — In: BAYLEY, S. W. (ed.): *Hydrous Phyllosilicates*. — *Reviews in Mineralogy, Volume 19*. Mineralogical Society of America, pp. 497–560.
438. HAK, J. 1961: Chemicko-mineralogické stadium nekterých nerostu tetraedritova skupiny. — *Geologický Sborník* 12 (1), pp. 79–102.
439. HAK, J., JOHAN, Z., KVAČEK, M., LIEBSHER, W. 1969: Kemmlitzite, a new mineral of the woodhouseite group. — *Neues Jahrbuch für Mineralogie, Monatshefte* 5, pp. 201–211.
440. HAMAD, S. EL D. 1974: An experimental study of the salt hydrate  $\text{MgSO}_4 \cdot 7\text{H}_2\text{O}$ . — *Thermochimica Acta* 13 (4), pp. 409–418.

441. HAMPAR, M. S., ZUSSMAN, J. 1984: The thermal breakdown of topaz. — *Mineralogy and Petrology* 33 (4), pp. 235–252.
442. HANSEN, J. W. 1972: Zur Geologie, Petrographie und Geochemie der Bündnerschiefer-Serien zwischen Nufenenpass (Schweiz) und Cascata Toce (Italia). — *Schweizerische Mineralogische und Petrographische Mitteilungen* 52 (1), pp. 109–153.
443. HARADA, K., TOMITA, K. 1967: A sodian stilbite from Onigajo, Mié Prefecture, Japan, with some experimental studies concerning the conversion of stilbite to wairakite at low water vapor pressures. — *The American Mineralogist* 52 (9–10), pp. 1438–1450.
444. HARTUNG, E., HEIDE, K., NAUMANN, R., JOST, K. H., HILMER, W. 1983: Untersuchungen zur thermischen Zersetzung von Boraten. I. Untersuchungen an Borax ( $\text{Na}_2\text{B}_4\text{O}_7 \cdot 8\text{H}_2\text{O}$ ). — *Journal of Thermal Analysis* 26 (2), pp. 277–284.
445. HAUL, R. A. W., HEYSTEK, H. 1952: Differential thermal analysis of the dolomite decomposition — *The American Mineralogist* 37 (3–4), pp. 166–179.
446. HAUSEN, D. M. 1962: Schroderite, a new phosphovanadate mineral from Nevada. — *The American Mineralogist* 47 (5–6), pp. 637–648.
447. HAYASHI, H., OINUMA, K. 1964: Aluminian chlorite from Kmikita Mine, Japan. — *Clay Science (Society of Japan)* 2 (1), pp. 22–30.
448. HAYASHI, H., KOSHI, K., HADAMA, A., SAHABE, H. 1962: Structural change of pyrophyllite by grinding and its effect on toxicity of the cell. — *Clay Science (Society of Japan)* 1 (5), pp. 77–83.
449. HAYASHI, H., OTSUKA, R., IMAI, N. 1969: Infrared study of sepiolite and palygorskite. — *The American Mineralogist* 54 (11–12), pp. 1613–1624.
450. HE, H. P., GUO, J. G., XIE, X. D., PENG, J. L. 2001: Location and migration of cations in  $\text{Cu}^{2+}$ -adsorbed montmorillonite. — *Environment International* 26 (5–6), pp. 347–352.
451. HE, H., YUAN, P., GUO, J., ZHU, J., HU, C. 2005: The influence of random defect density on the thermal stability of kaolinites. — *Journal of the American Ceramic Society* 88 (4), pp. 1017–1019.
452. HEFLIK, W., ZABINSKI, W. 1969: A chromian hydrogrossular from Jordanow, Lower Silesia, Poland. — *Mineralogical Magazine* 37 (286), pp. 241–243.
453. HEIDE, K. 1962: Thermische Untersuchungen an Salzmineralien. I. Untersuchungen am Ascharit. — *Chemie der Erde* 22, pp. 180–221.
454. HEIDE, K. 1965a: Die Phasenanalyse bei dem thermischen Abbau der Krystallhydrate. — *Naturwissenschaften* 52 (8), pp. 183–184.
455. HEIDE, K. 1965b: Thermische Untersuchungen an Salzmineralien. II. Untersuchungen am Schoenit  $\text{K}_2\text{Mg}(\text{SO}_4) \cdot 6\text{H}_2\text{O}$  und Leonit  $\text{K}_2\text{Mg}(\text{SO}_4)_2 \cdot 4\text{H}_2\text{O}$ . — *Chemie der Erde* 24 (1), pp. 94–111.
456. HEIDE, K. 1965c: Thermische Untersuchungen an Salzmineralien III. Untersuchungen am Epsomit ( $\text{MgSO}_4 \cdot 7\text{H}_2\text{O}$ ) und den isotypen Verbindungen Morenosit ( $\text{NiSO}_4 \cdot 7\text{H}_2\text{O}$ ) und Goslarit ( $\text{ZnSO}_4 \cdot 7\text{H}_2\text{O}$ ). — *Chemie der Erde* 24 (3–4), pp. 279–302.
457. HEIDE, K. 1966a: Bestimmung der Aktivierungsenergie beim thermischen Abbau von Krystallhydraten aus thermogravimetrischen Daten. — *Naturwissenschaften* 53 (21), pp. 550–551.
458. HEIDE, K. 1966b: Thermische Untersuchungen an Salzmineralien IV. Untersuchungen am Astrakanit  $\text{Na}_2\text{Mg}(\text{SO}_4)_2 \cdot 4\text{H}_2\text{O}$  und Löweit  $4\text{Na}_2\text{SO}_4 \cdot 4\text{MgSO}_4 \cdot 9\text{H}_2\text{O}$ . — *Chemie der Erde* 25 (3), pp. 237–252.
459. HEIDE, K. 1967: Die Verwitterung des Kieserits. — *Chemie der Erde* 26 (2), pp. 133–139.
460. HEIDE, K. 1968: Zum Mechanismus der Umbildungsvorgänge in Salzgesteinen. — *Chemie der Erde* 27 (4), pp. 353–368.
461. HEIDE, K. 1969a: Zur Kristallchemie des Kieserits. — *Berichte der Deutschen Gesellschaft für Geologische Wissenschaften: Mineralogie und Lagerstättenforschung Reihe B*, 14 (2), pp. 97–105.
462. HEIDE, K. 1969b: Zur thermischen Zersetzung des Gipses  $\text{CaSO}_4 \cdot 2\text{H}_2\text{O}$ . — *Silikattechnik* 20 (7), pp. 232–234.
463. HEIDE, K. 1969c: Thermochemische und Kinetische Untersuchungen der endothermen Umbildungsreaktionen des Epsomits ( $\text{MgSO}_4 \cdot 7\text{H}_2\text{O}$ ). — *Journal of Thermal Analysis* 1 (2), pp. 183–194.
464. HEIDE, K. 1969d: Zur Kinetik der Kaolinitentwasserung. — *Zeitschrift für Geologische Wissenschaften* 14 (2), p. 191.
465. HEIDE, K. 1973: Chemische Zusammensetzung und Struktur der Harnsteine. — In: HINZSCH, E., SCHNEIDER, H. J. (eds): *Der Harnstein. Methoden der Harnsteinanalyse*. VEB Fischer-Verlag, Jena, pp. 157–181.
466. HEIDE, K. 1974: Untersuchung der Hochvakuumentgasung bei dynamischer Temperaturänderung bis 1200 °C von natürlichen Gläsern unterschiedlicher Genese. — *Chemie der Erde* 33 (2), pp. 195–214.
467. HEIDE, K. 1982: *Dynamische thermische Analysemethoden*. — VEB Deutscher Verlag für Grundstoffindustrie, Leipzig, p. 311.
468. HEIDE, K. 1991: The degassing behavior of natural glasses and implications for their origin. — *Journal of Thermal Analysis* 37 (7), pp. 1593–1603.
469. HEIDE, K., BRÜCKNER, U. 1967: Grundlagen zur Phasenanalyse von Salzgesteinen — *Chemie der Erde* 26 (4), pp. 235–255.
470. HEIDE, K., EICHORN, H. J. 1975: Die thermische Zersetzung des  $\text{MgCl}_2 \cdot 6\text{H}_2\text{O}$  unter dynamischen Bedingungen — Ein Beitrag zur kinetischen Analyse nichtisothermer Festkörperreaktionen. — *Journal of Thermal Analysis* 7 (2), pp. 397–409.
471. HEIDE, K., FÖLDVARI, M. 2006: High temperature mass spectrometric release studies of kaolinite decomposition ( $\text{Al}_2[\text{Si}_2\text{O}_5(\text{OH})_4]$ ). — *Thermochimica Acta* 446 (1–2), pp. 106–112.
472. HEIDE, K., KLUGE, G. 1983: Theorie und Analyse von Festkörperreaktionen unter nicht-isothermen Bedingungen. — *Zeitschrift für Chemie* 23 (5), pp. 167–174.
473. HEIDE, K., KÜHN, W. 1965: Bischofit im carnallitischen Strabfurthlager der stillgelegten Kaliwerke Aschersleben/Anhalt (Schachtanlage V.). — *Chemie der Erde* 24 (2), pp. 211–214.
474. HEIDE, K., SCHMIDT, C. M. 2005: Determination of volatiles in volcanic rocks and minerals with a directly coupled Evolved Gas Analyzing System (DEGAS) Part 1: Interpretation of degassing profiles (DEGAS-profiles) of minerals and rocks on the basis of melting experiments. — *Annals of Geophysics* 48 (4–5), pp. 719–729.
475. HEIDE, K., HANDEL, G., SCHNABEL, B. 1967: Zur Lage der Wassermoleküle im Kieserit  $\text{MgSO}_4 \cdot \text{H}_2\text{O}$ . — *Naturwissenschaften* 54 (3), pp. 69–70.
476. HEIDE, K., FRANKE, H., BRÜCKNER, H. P. 1980: Vorkommen und Eigenschaften von Boracit in den Zechsteinlagerstätten der DDR. — *Chemie der Erde* 39 (3), pp. 201–232.
477. HEIDE, K., GERTH, K., BÜCHEL, G., HARTMANN, E. 1997: EGA — A fingerprint characterization of minerals and rocks. — *Journal of Thermal Analysis* 48 (1), pp. 73–81.

478. HELLER, L., FARMER, V. C., MACKENZIE, R. C., MITCHEL, B. D., TAYLOR, H. F. W. 1962: The dehydroxylation of trimorphic dioctahedral clay minerals. — *Clay Minerals Bulletin* 5 (28), pp. 56–72.
479. HELLER-KALLAI, L., MACKENZIE, R. C. 1989: Interaction of kaolinite with calcite on heating. IV. Rehydrated and recarbonated samples. — *Thermochimica Acta* 148 (4), pp. 439–444.
480. HELLER-KALLAI, L., MOSSER, C. 1995: Migration of Cu ions in Cu montmorillonite heated with and without alkali halides. — *Clay and Clay Minerals* 43 (6), pp. 738–743.
481. HENSEN, E. J. M., TAMBACH, T. J., BLIEK, A., SMIT, B. 2001: Adsorption isotherms of water in Li-, Na-, and K-montmorillonite by molecular simulation. — *Journal of Chemical Physics* 115 (7), pp. 3322–3329.
482. HESS, H. H., DENG, G., SMITH, R. J. 1952: Antigorite from the vicinity of Caracas, Venezuela. — *The American Mineralogist* 37 (1–2), pp. 68–75.
483. HEYSTEK, H. 1954: A regular mixed-layer clay mineral. — *Mineralogical Magazine* 30 (225), pp. 400–408.
484. HICKEY, L., KLOPPROGGE, J. T., FROST, R. L. 2000: The effects of various hydrothermal treatments on magnesium-aluminium hydroxalcalites. — *Journal of Materials Science* 35 (17), 4347–4355.
485. HILLER, J. E., PROBSTHAIN, K. 1956a: Differentialthermoanalyse von Sulfidmineralen. — *Geologie* 5 (7), pp. 607–616.
486. HILLER, J. E., PROBSTHAIN, K. 1956b: Thermische und röntgenographische Untersuchungen am Kupferkies. — *Zeitschrift für Kristallographie* 108 (1–2), pp. 108–129.
487. HIRSIGER, W., MÜLLER-VONMOOS, M., WIEDEMANN, H. G. 1975: Thermal analysis of palygorskite. — *Thermochimica Acta* 13 (2), pp. 223–230.
488. HODGSON, A. A., FREEMAN, A. G., TAYLOR, H. F. W. 1965: The thermal decomposition of crocidolite from Koegas, South Africa. — *Mineralogical Magazine* 35 (269), pp. 5–30.
489. HODGSON, A. A., FREEMAN, A. G., TAYLOR, H. F. W. 1965: Thermal decomposition of amosite. — *Mineralogical Magazine* 35 (271), pp. 445–463.
490. HOFMANN, F., JÄGER, E. 1959: Saponit als Umwandlungsprodukt im basaltischen Tuff von Kareliefhof (Kanton Schaffhausen). — *Schweizerische Mineralogische und Petrographische Mitteilungen* 39 (1–2), pp. 115–124.
491. HÖLAND, W., HEIDE, K. 1976: Untersuchung des Einflusses der Analysenbedingungen auf die Zersetzung von  $4\text{MgCO}_3 \cdot \text{Mg}(\text{OH})_2 \cdot 4\text{H}_2\text{O}$  und die Bildung von Magnesit  $\text{MgCO}_3$ . — *Thermochimica Acta* 15 (3), pp. 287–294.
492. HOLDRIDGE, D. A., VAUGHAN, F. 1957: The kaolin minerals (Kandites). — In: MACKENZIE, R. C. (ed.) 1957: *The differential thermal investigation of clays*. Mineralogical Society, London. pp. 98–139.
493. HORI, H., NAGASHIMA, K., YAMADA, M., MIYAWAKI, R., MARUBASHI, T. 1986: Ammonioleucite, a new mineral from Tatarazawa, Fujioka, Japan. — *The American Mineralogist* 71 (7–8), pp. 1022–1027.
494. HORVÁTH, E., FROST, R. L., MAKÓ, É., KRISTÓF, J., CSEH, T. 2003: Thermal treatment of mechanochemically activated kaolinite. — *Thermochimica Acta* 404 (1–2), pp. 227–234.
495. HORVÁTH, I. 1985: Kinetics and compensation effect in kaolinite dehydroxylation. — *Thermochimica Acta* 85, pp. 193–198.
496. HOSS, H., ROY, R. 1960: Zeolite studies III. On natural phillipsite, gismondine, harmotome, chabasite and gmelinite. — *Beiträge zur Mineralogie und Petrographie* 7 (6), pp. 389–408.
497. HOWER, J., MOWATT, T. E. 1966: The mineralogy of illites and mixed-layer illite/montmorillonites. — *The American Mineralogist* 51 (5–6), pp. 825–854.
498. HRABE, Z., SVETÍK, Š. 1985: The influence of water vapour on decomposition of magnesite and brucite. — *Thermochimica Acta* 92, pp. 653–656.
499. HU, G., DAM-JOHANSEN, K., WEDEL, S., HANSEN, J. P. 2006: Decomposition and oxidation of pyrite. — *Progress in Energy and Combustion Science* 32 (3), pp. 295–314.
500. HU, Y., YU, Q., ZHOU, C., LI, G. 1997: Oxidative thermal analysis for arsenopyrite and gold-bearing concentrate. Second part of fundamental research for roasting of concentrates of auriferous sulfide and arsenides. — *Nonferrous Metals, Beijing (China)*, 49 (2), pp. 72–76.
501. HUANG, Q., FU, X. 1984: Mechanism of the formation of ferrous sulfide from pyrite. — *Acta Chimica Sinica* 42 (2), pp. 130–136.
502. HUNZIKER, J. C. 1966: Zur Geologie und Geochemie des Gebietes zwischen Valle Antigorio und Valle di Campo (Tessin). — *Schweizerische Mineralogische und Petrographische Mitteilungen* 46 (2), pp. 473–552.
503. HUNZIKER, J. C., FREY, M., CLAUSER, N., DALLMEYER, R. D., FRIEDRICHSEN, H., FLEHMIG, W., HOCHSTRASSER, K., ROGGWILER, P., SCHWANDER, H. 1986: The evolution of illite to muscovite: mineralogical and isotopic data from the Glarus Alps, Switzerland. — *Contributions to Mineralogy and Petrology* 92 (2), pp. 157–180.
504. HURLBUT, C. S. JR., ARISTARAIN, L. F. 1967: Rivadavite, a new borate from Argentina. — *The American Mineralogist* 52 (3–4), pp. 326–335.
505. HURLBUT, C. S. JR., ARISTARAIN, L. F. 1967: Ezcurrite, a restudy. — *The American Mineralogist* 52 (7–8), pp. 1048–1059.
506. HURLBUT, C. S. JR., ARISTARAIN, L. F. 1968: Bermanite and its occurrence in Cordoba, Argentina. — *The American Mineralogist* 53 (3–4), pp. 416–431.
507. ILKEY-PERLAKI, E., FÖLDVÁRI, M., IZVEKOV, V. 1996: TG-DTG, IR and NIR spectroscopic studies on water contents of some perlites in the Tokaj Mts., Hungary. — *Chemie der Erde – Geochemistry* 56 (4), pp. 355–363.
508. IMELIK, B., PETITJEAN, M., PRETTRE, M. 1953: Dehydration of crystalline boehmite. — *Comptes rendus Hebdomadaires des séances de l'Académie des sciences* 236 (12), pp. 1278–1280.
509. INCZEDY, J. (ed.) 1998: Compendium of Analytical Nomenclature International Union of Pure and Applied Chemistry. Nomenclature Books (3rd edition). — Blackwell Scientific Publications. 974 p.
510. INGLETHORPE, S., MORGAN, D. J. 1993: Detection of ammonium in geological materials by evolved gas analysis. — *Journal of Thermal Analysis* 40 (1), pp. 29–40.
511. IRIGARAY, J., OUDADESSE, H., FADL, H., SAUVAGE, T., THOMAS, G., VERNAY, A. 1993: Effet de la température sur la structure cristalline d'un biocorail. — *Journal of Thermal Analysis* 39 (1), pp. 3–14.
512. IVANOV, O. K., MOZZREHIN, Y. V. 1982: Partheite from gabbro and pegmatites of Denerhkina Kamnya, Urals; (first discovery in USSR). — *Zapiski Vsesoyuznogo Mineralogicheskogo Obshchestva* 111 (2), pp. 209–214.

513. IVANOVA, V. P., KASATOV, B. K., KRASAVINA, T. N., ROZINOVA, E. L. 1974: *Termičeskij analiz mineralov i gornyh porod.* — Nedra, Leningrad. 399 p.
514. IVEKOVIC, H., JANEKOVIC, A. 1973: Quantitative determination of the mineral composition of bauxite by the use of differential thermal analysis and organic solvents. — *Proceedings of the ICSOBA (International Committee for Study of Bauxites) Third International Congress Sept. 17–21. Nice*, pp. 345–353. (in French).
515. IVEKOVIC, H., JANEKOVIC, A. 1976: Total mineralogical analysis of bauxite. — *ICSOBA (International Committee for Study of Bauxites), Travaux, Zagreb*, 13, pp. 365–377.
516. IWAFUCHI, K. 1983: Thermal-decomposition of ferromanganooan dolomite. — *Thermochimica Acta* 66 (1–3), pp. 105–125.
517. IWAFUCHI, K., WATANABE, C., OTSUKA, R. 1983: Thermal decomposition of magnesian kutnahorite. — *Thermochimica Acta* 60 (3), pp. 361–381.
518. JÄGER, E., SCHILLING, S. 1956: Vorläufiger Bericht über DTA-Untersuchungen an Wölsendorfer Fluorit. — *Schweizerische Mineralogische Petrographische Mitteilungen* 36 (2), pp. 599–603.
519. JAKAB, G., BALÁZS, É., SZÖÖR, GY. 1984: Thermoanalytical investigation of the Unionidae shells with chemotaxonomical evaluation (Bivalvia) — *Soosiana* 12, pp. 43–48. (in Hungarian)
520. JAMBOR, J. L., DUTRIZAC, J. E. 1998: Occurrence and constitution of natural and synthetic Ferrihydrite, Widespread Iron Oxyhydroxide. — *Chemical Review* 98 (7), pp. 2549–2585.
521. JANECEK, J., EBY, R. K. 1993: Annealing of radiation damage in allanite and gadolinite. — *Physics and Chemistry of Minerals* 19 (6), pp. 343–356.
522. JARLOVSKY, J., CICEL, B. 1958: Vyskyt diadochitu v Banskej Belej. — *Geologické práce, Zpravy, Bratislava*, 13, pp. 97–104.
523. JEONG, G. Y., KIM, H. B. 2003: Mineralogy, chemistry, and formation of oxidized biotite in the weathering profile of granitic rocks. — *The American Mineralogist* 88 (2–3), pp. 352–364.
524. JEREZ, A., ALARIO, M. A. 1982: The reduction of pyrolusite in a hydrogen atmosphere. — *Thermochimica Acta* 58 (3), pp. 333–339.
525. JIANG, W., NADEAU, G., ZAGHIB, K., KINOSHITA, K. 2000: Thermal analysis of the oxidation of natural graphite — effect of particle size. — *Thermochimica Acta* 351 (1–2), pp. 85–93.
526. JOHNSON, G. K., FLOTOW, H. E., O'HARE, P. A. G., WISE, S. 1983: Thermodynamic studies of zeolites: natrolite, mesolite, scolecite. — *The American Mineralogist* 68 (11–12), pp. 1134–1145.
527. JOHNSON, S. L., GUGGENHEIM, S., KOSTER VAN GROOS, A. F. 1990: Thermal stability of halloysite by high-pressure differential thermal analysis. — *Clays and Clay Minerals* 38 (5), pp. 477–484.
528. JÓNÁS, K., SOLYMÁR, K. 1970a: Preparation, X-ray, derivatographic and infrared study of aluminium substituted goethite. — *Acta Chimica Academiae Scientiarum Hungaricae (Budapest)*, 66 (4), pp. 383–394.
529. JÓNÁS, K., SOLYMÁR, K. 1970b: The study of the isomorphous substitution by thermoanalytical method on synthetic alumo-goethite model. — *Proceedings of the III. Analytical Chemical Conference, Budapest*, pp. 393–399.
530. JONES, B. F., GALAN, E. 1988: Sepiolite and paygorskite. — In: BAYLEY, S. W. (ed): *Hydrous Phyllosilicates. Reviews in Mineralogy Volume 19. Mineralogical Society of America*, 631–674.
531. JONES, B., RENAUT, R. W. 2004: Water content of opal-A: implications for the origin of laminae in geyserite and sinter. — *Journal of Sedimentary Research* 74 (1), pp. 117–128.
532. JONES, J. B., SEGNET, E. R. 1971: The nature of opal I. nomenclature and constituent phases. — *Journal of the Geological Society Australia* 18 (1), pp. 57–68.
533. JONES, J. B., SEGNET, E. R., NICKSON, N. M. 1963: Differential thermal and x-ray analysis of opal. — *Nature* 198 (4886), p. 1191.
534. JØRGENSEN, F. R. A., MOYLE, F. J. 1982: Phases formed during the thermal analysis of pyrite in air. — *Journal of Thermal Analysis* 25 (2), pp. 473–485.
535. JØRGENSEN, F. R. A., MOYLE, F. J. 1984: Periodic thermal-instability during the differential thermal-analysis of pyrite. — *Journal of Thermal Analysis* 29 (1), pp. 13–17.
536. JØRGENSEN, F. R. A., MOYLE, F. J. 1986: Gas diffusion during the thermal analysis of pyrite. — *Journal of Thermal Analysis* 31 (1), pp. 145–156.
537. JØRGENSEN, S. S., BIRNIE, A. C., SMITH, B. F. L., MITCHELL, B. D. 1970: Assessment of gibbsitic material in soil clays by differential thermal analysis and alkali dissolution methods. — *Journal of Thermal Analysis* 2 (3), pp. 277–286.
538. JOSHI, M. S., MOHAN RAO, P., CHOUDHARI, A. L., KANITKAR, R. G. 1982: Thermal behaviour of natural stilbite crystals. — *Thermochimica Acta* 58 (1), pp. 79–86.
539. JOSHI, M. S., CHOUDHARI, A. L., RAO, P. M., KANITGAR, R. G. 1983: Dehydration behavior of scolecite crystals. — *Thermochimica Acta* 64 (1–2), pp. 39–45.
540. JOVANOVIĆ, DJ. 1989: Kinetics of thermal decomposition of pyrite in an inert atmosphere. — *Journal of Thermal Analysis* 35 (5), pp. 1483–1492.
541. JUHÁSZ, A. Z., OPOCZKY, L. 1990: Mechanical activation of minerals by grinding (pulverizing and morphology of particulates). — Ellis Horwood Limited Publ. Chichester, Akadémiai Kiadó, Budapest. 234 p.
542. JUSTO, A., PÉREZ-RODRÍGUEZ, J. L., SÁNCHEZ-SOTO, P. J. 1993: Thermal study of vermiculites and mica-vermiculite interstratifications. — *Journal of Thermal Analysis* 40 (1), pp. 59–65.
543. KAISERSBERGER, E. 1979: Gas analytical methods of thermal analysis in comparison. — *Thermochimica Acta* 29 (2), pp. 215–220.
544. KAISERSBERGER, E. (ed.) 1997: *Thermochimica Acta* 295 (1–2), pp. 1–186. [The complete issue with papers of Coupling Thermal Analysis and Gas Analysis Methods.]
545. KALMÁR, J., KOVÁCS-PÁLFFY, P., FÖLDVÁRI, M. 1997: Magureni Hill, Preluca Veche: a new occurrence of hydrothermal sepiolite. — *Romanian Journal of Mineralogy* 78, pp. 97–106.
546. KALOUSTIAN, J., PAULI, A. M., PIERONI, G., PORTUGAL, H. 2002: The use of thermal analysis in determination of some urinary calculi of calcium oxalate. — *The Journal of Thermal Analysis and Calorimetry* 70 (3), pp. 959–973.
547. KALYUVEE, T., VEIDERMA, M., TYNSUAADU, K., VILBOK, H. 1988: Physico-chemical transformations during heating of phosphorites. — *Journal of Thermal Analysis* 33 (3), pp. 839–844.

548. KANARI, N., MISHRA, D., GABALLAH, I., DUPRE, B., Mineral Processing and Environmental Engineering Team. 2004: Thermal decomposition of zinc carbonate hydroxide. — *Thermochimica Acta* 410 (1–2), pp. 93–100.
549. KANTINARIS, N., CHRISAFIS, C., FILIPPIDIS, A., PARASKEVOPOULOS KONSTANTINOS, M. 2006: Thermal distinction of HEU-type mineral phases contained in Greek zeolite-rich volcanoclastic tuffs. — *European Journal of Mineralogy* 18 (4), pp. 509–516.
550. KARAKASSIDES, M. A., GOURNIS, D., PETRIDIS, D. 1999: An infrared reflectance study of Si-O vibrations in thermally treated alkali-saturated montmorillonites. — *Clay Minerals* 34 (3), pp. 429–438.
551. KAROLEVA, V., GEORGIEV, G., SPASOV, N. 1974: Dissociation of potassium, sodium and ammonium jarosite. — *Thermal Analysis Vol. 2. Proceedings of the fourth ICTA, Budapest*, pp. 601–610.
552. KASHAKI, M. A., BABAEV, I. A. 1969: Thermal investigations on alunite and its mixtures with quartz and dickite. — *Mineralogical Magazine* 37 (285), pp. 128–134.
553. KAUFFMAN, A. J. JR., DILLING, E. D. 1950: Differential thermal curves of certain hydrous and anhydrous minerals, with a description of the apparatus used. — *Economic Geology* 45 (3), pp. 222–244.
554. KEATTCH, C. J., DOLLIMORE, D. 1991a: Studies in the history and development of thermogravimetry. I. Early development. — *Journal of Thermal Analysis* 37 (9), pp. 2089–2102.
555. KEATTCH, C. J., DOLLIMORE, D. 1991b: Studies in the history and development of thermogravimetry. II. Hannay's "Time Method". — *Journal of Thermal Analysis* 37 (9), pp. 2103–2107.
556. KEATTCH, C. J., DOLLIMORE, D. 1993: Studies in the history and development of thermogravimetry III. The influence of Kotaro Honda and the Japanese school. — *Journal of Thermal Analysis* 39 (1), pp. 97–118.
557. KELLER, P. 1976: Thermogravimetrische Untersuchungen von Goethit und Lepidokrokit und von deren Synthesenprodukten á FeOOH und á-FeOOH. — *Neues Jahrbuch für Mineralogie, Monatshefte* 3, pp. 115–127.
558. KELLY, W. C. 1956: Application of differential thermal analysis to identification of the natural hydrous ferric oxides. — *The American Mineralogist* 41 (3–4), pp. 353–355.
559. KENNEDY, T., STURMAN, B. T. 1975: The oxidation of iron (II) sulphide. — *Journal of Thermal Analysis* 8 (2), pp. 329–337.
560. KENYERES, S., GADÓ, P., SAJÓ, M., SOLYMÁR, K. 1974: Thermal gas analysis of Bauxites. — *Thermal Analysis. Vol 2. Proceedings of the fourth ICTA Budapest*, pp. 531–539
561. KENYERES-SÜKE, S., SOLYMÁR, K., TÓTH, P. 1982: Thermogravimetric examination of sideritic and pyritic bauxites. — *Erzmetall* 35 (11), pp. 564–568.
562. KERR, P. F., KULP, J. L. 1947: Notes and news: Differential thermal analysis of siderite. — *The American Mineralogist* 32 (11–12), pp. 678–679.
563. KERR, P. F., KULP, J. L. 1948: Multiple differential thermal analysis. — *The American Mineralogist* 33 (7–8), pp. 387–419.
564. KHORAMI, J., CHOQUETTE, D., KIMMERLE, E. M., GALLAGHER, P. K. 1984: Interpretation of EGA and DTG analyses of chrysotile asbestos. — *Thermochimica Acta* 76 (1), pp. 89–96.
565. KHOSLA, S. N., KOUL, V. K. 1985: Chemical, dehydration, differential thermal and X-ray analysis of Salal bauxite deposits. — *Journal of Thermal Analysis* 30 (1), pp. 137–143.
566. KIM, J. J., KIM, S. J. 2003: Environmental, mineralogical, and genetic characterization of ochreous and white precipitates from acid mine Drainages in Taebaeg, Korea. — *Environmental Science & Technology* 37 (10), pp. 2120–2126.
567. KIM, S. J. 1975: Mineralogical and genetic significances of nsutite in supergene manganese oxide ores. — *Fortschritte der Mineralogie* 52 (Special issue), pp. 361–368.
568. KIM, Y., KIRKPATRICK, R. J. 1998: High-temperature multi-nuclear NMR investigation of analcime. — *The American Mineralogist* 83 (3–4), pp. 339–347.
569. KIRILOV, P. P., GRUNCHAROV, I. N., PELOVSKI, Y. G. 1994: Enthalpy of thermal-decomposition of pyrite concentrate. — *Thermochimica Acta* 244, pp. 79–83.
570. KISS, A. N., TÓTH, M., TAKÁCS, M., MORVAI, B., WIESZT, Z. 1997: Effects of copper adsorption on the line profile of first basal reflection of montmorillonite. — *Acta Mineralogica et Petrographica Szegediensis* 38, pp. 25–36.
571. KISS, L., TAKÁTS, T. 1963: Mineralogical investigations of the material of the Füzérradvány illite mines with respect to the fine ceramic industry. — *Építésanyagipari Központi Kutató Intézet, Tudományos Közlemények* 10, pp. 1–62. (in Hungarian)
572. KISSINGER, H. E. 1957: Reaction Kinetics in Differential Thermal Analysis. — *Analytical Chemistry* 29 (11), pp. 1702–1706.
573. KIYOHIO, T., OTSUKA, R. 1989: Dehydration mechanism of bound water in sepiolite. — *Thermochimica Acta* 147 (1), pp. 127–138.
574. KLEBER, W., WILDE, W., FRENZEL, M. 1965: On the thermal transformation and the oxidation of divalent iron in vivianite. (Über die thermische Zersetzung und die Oxydation des zweiwertigen Eisens beim Vivianit). — *Chemie der Erde* 24 (1), pp. 77–93.
575. KLEVTSOV, D. P., LOGVINENKO, A. V., ZOLOTOVSKII, B. P., KRIVORUCHKO, O. P., BUYANOV, R. A. 1988: Kinetics of kaolinite dehydration and its dependence on mechanochemical activation. — *Journal of Thermal Analysis* 33 (2), pp. 531–535.
576. KLOPROGGE, J. T., FROST, R. L.: 1999: Infrared emission spectroscopic study of the thermal transformation of Mg-, Ni- and Co-hydro-talcite catalysts. — *Applied catalysis A: General*, 184 (1), pp. 61–71.
577. KLOPROGGE, J. T., FROST, R. L. 2000a: Study of the thermal behaviour of rectorite by in-situ infrared emission spectroscopy. — *Neues Jahrbuch für Mineralogie, Monatshefte* 4, pp. 145–157.
578. KLOPROGGE, J. T., FROST, R. L. 2000b: Thermal decomposition of Ferrian chamosite: an infrared emission spectroscopic study. — *Contributions to Mineralogy and Petrology* 138 (1), pp. 59–67.
579. KLOPROGGE, J. T., RUAN, H. D., FROST, R. L. 2002: Thermal decomposition of bauxite minerals: infrared emission spectroscopy of gibbsite, boehmite and diasporite. — *Journal of Materials Science* 37 (6), pp. 1121–1129.
580. KLOPROGGE, J. T., BOSTRÖM, T. E., WEIER, M. L. 2004: In situ observation of the thermal decomposition of weddellite by heating stage environmental scanning electron microscopy. — *The American Mineralogist* 89 (1), pp. 245–248.
581. KNELLER, W. A. 1986: Physicochemical characterization of coal and coal reactivity: a review. — *Thermochimica Acta* 108, pp. 357–388.
582. KNOWLTON, G. D., WHITE, T. R., MCCAGUE, H. L. 1981: Thermal study of types of water associated with clinoptilolite. — *Clay and Clay Minerals* 29 (5), pp. 403–411.

583. KOCH, CRH. J. W. 1985: Differential thermal analysis — evolved gas analysis of synthetic goethite. — *Thermochimica Acta* 95 (2), pp. 395–400.
584. KOCMAN, V., GAIT, R. I., RUCKLIDGE, J. 1974: The crystal structure of bikitaite. — *The American Mineralogist* 59 (1–2), pp. 71–78.
585. KODAMA, H. 1966: The nature of component layers of rectorite. — *The American Mineralogist* 51 (7), pp. 1035–1055.
586. KODAMA, H., BRYDON, J. E. 1966: Interstratified montmorillonite-mica clays from subsoils of the Prairie provinces, western Canada. — *Clays and Clay Minerals* 13 (1), pp. 151–173.
587. KODAMA, H., BRYDON, J. E. 1968: Dehydroxylation of microcrystalline muscovite. — *Transactions of the Faraday Society* 64 (11), pp. 3112–3119.
588. KOGA, N., TANAKA, H. 2005: Thermal decomposition of copper(II) and zinc carbonate hydroxides by means of TG-MS. Quantitative analyses of evolved gases. — *Journal of Thermal Analysis and Calorimetry* 82 (3), pp. 725–729.
589. KOHLS, D. W., RODDA, J. L. 1967: Iowaite, a new hydrous Mg-hydroxide-ferric-oxychloride from the Precambrian of Iowa. — *The American Mineralogist* 52 (9–10), pp. 1261–1271.
590. KOHYAMA, N. S., SHIMODA, T., SUDO, T. 1973: Iron rich saponite (ferrous and ferric form). — *Clays and Clay Minerals* 21 (4), pp. 229–237.
591. KOIZUMI, M. 1953: Studies on water in minerals I. The differential thermal analysis curves and dehydration curves of zeolites. — *Mineralogical Journal (Japan)*, 1 (1), pp. 36–47.
592. KOIZUMI, M., ROY, R. 1960: Zeolite studies I. Synthesis and stability of calcium zeolites. — *Journal of Geology* 68 (1), pp. 41–53.
593. KÖK, M. V., SMYKATZ-KLOSS, W. 2001: Thermal characterisation of dolomite. — *Journal of Thermal Analysis and Calorimetry* 64 (3), pp. 1271–1275.
594. KOLTERMANN, M., RASCH, H. 1964: Die thermische Umwandlung der Serpentinminerale. — *Schweizerische Mineralogische und Petrographische Mitteilungen* 44 (2), pp. 499–511.
595. KOMUSIŃSKI, J., STOCH, L. 1984: Dehydroxylation of kaolinite-group minerals: An ESR study. — *Journal of Thermal Analysis* 29 (5), pp. 1033–1040.
596. KONRAD, G., CHESTERS, G., KEENEY, D. R. 1970: Determination of organic- and carbonate-carbon in freshwater lake sediments by a microcombustion procedure. — *Journal of Thermal Analysis* 2 (2), pp. 199–208.
597. KONTA, J. 1955: Dillnite — ein spezifisches Tonmineral. — *Chemie der Erde* 17 (4), pp. 223–232.
598. KONTA, J. 1956: Trioktaedričeskij illit iz Templštejna v zapadnoj Moravii (“parasepiolit Fersmana”). — *Izvestiya Akademii Nauk, SSSR. Seriya Geologiya* 11, pp. 109–113.
599. KONTA, J., MRAZ, L. 1961: Dillnite and its relation to zunyite. — *The American Mineralogist* 46 (5–6), pp. 629–636.
600. KÓNYA, J., NAGY, N. M., FÖLDVÁRI, M. 2005: The formation and production of nano and micro particles on clays under environmental-like conditions. — *Journal of Thermal Analysis and Calorimetry* 79 (3), pp. 537–543.
601. KÓNYA, P., FÖLDVÁRI, M. 2008: Thermoanalytical investigation of cavity filling natrolite group minerals of basalts from Balaton Highland, Hungary. — *Journal of Thermal Analysis* 94 (1), pp. 209–218.
602. KOPP, O. C., HARRIS, L. A. 1984: Initial volatilization temperatures and average volatilization rates of coal — their relationship to coal rank and other characteristic. — *International Journal of Coal Geology* 3 (4), pp. 333–348.
603. KOPP, O. C., KERR, P. F. 1957: DTA of sulphides and arsenides. — *The American Mineralogist* 42 (7–8), pp. 445–454.
604. KOPP, O. C., KERR, P. F. 1958a: Differential thermal analysis of sphalerite. — *The American Mineralogist* 43 (7–8), pp. 732–748.
605. KOPP, O. C., KERR, P. F. 1958b: Differential thermal analysis of pyrite and markasite. — *The American Mineralogist* 43 (11–12), pp. 1079–1097.
606. KORANYI, DE A. 1987: Coal characterisation by thermal analysis. — *Thermochimica Acta* 110 (1), pp. 527–533.
607. KORNEVA, T. A., STOLPOVSKAYA, V. N., PALCHIK, N. A., MASUROV, M. P. 1995: The thermal behaviour of chlinochlores of different polytypes (Korshunovsk ore deposit). — *Geologica Carpathica, Series Clays* 4 (2), p. 99.
608. KORNEVA, T. A., YUSUPOV, T. S., LUKJANOVA, L. G., GUSEV, G. M. 1975: Thermal analysis of mechanically activated bauxites. — *Thermal Analysis V. 2. Proceedings of the fourth ICTA Budapest 1974*, pp. 659–666.
609. KORZHINSKI, A. F. 1956: Nekotorije novie dannie ob uzomorfizme i polimorfizme uglekislovo strontia i kalcia. — *Zapiski Vsesoyuznogo Mineralogicheskogo Obshchestva* 85 (4), pp. 535–542.
610. KORZHINSKI, A. F. 1956: O zavisimosti termiceseszkij szvoisztv amfibolov ot soderzsanyijja v nih cselocsej. — *Doklady Akademii Nauk SSSR* 111 (2), pp. 445–447.
611. KOSTER VAN GROSS, A. F., GUGGENHEIM, S. 1989: Dehydroxylation of Ca- and Mg-exchanged montmorillonite. — *The American Mineralogist* 74 (5–6), pp. 624–636.
612. KOTSIS, T. 1964: Derivatographische Untersuchungen von Bauxitmineralien. — *Geologie* 13 (2), pp. 159–167.
613. KOVÁCS-PÁLFFY, P., FÖLDVÁRI, M. 2004: Hydrothermal minerals and phenomena in the Mórágý Granite Formation. — *Annual Report of the Geological Institute of Hungary of 2003*, pp. 319–332.
614. KOVÁCS-PÁLFFY, P., FÖLDVÁRI, M., RÁLISCH FELGENHAUER, E., BARÁTH, I.-né 2000: Mineralogical characterisation of the fissure filling in the Üveghuta granite. — *Annual Report of the Geological Institute of Hungary of 1989*, pp. 353–368.
615. KOVÁCS-PÁLFFY, P., KÓNYA, P., FÖLDVÁRI, M., KÁKAY-SZABÓ, O., BODORKÓS, Zs. 2007: The cavity filling minerals of the basalt from Karikás-tető (Prága Hill, Balaton Highland, Transdanubia). — *Annual Report of the Geological Institute of Hungary of 2005*, pp. 95–118.
616. KRESTEN, P., CHYSSLER, J. 1978: The thermal decomposition of gorceixite — *Geologiska Föreningens i Stockholm Förhandlingar* 100 (1), pp. 105–106.
617. KRISTÓF, E., JUHÁSZ, A. Z. 1993: The effect of intensive grinding on the crystal structure of dolomite. — *Powder technology* 75 (2), pp. 145–152.
618. KRISTÓF-MAKÓ, É., JUHÁSZ, A. Z. 1999: The effect of mechanical treatment on the crystal structure and thermal decomposition of dolomite. — *Thermochimica Acta* 342 (1–2), pp. 105–114.
619. KRISTÓF, É., JUHÁSZ, A. Z., VASSÁNYI, I. 1993: The effect of mechanical treatment on the crystal structure and thermal behavior of kaolinite. — *Clays and Clay Minerals* 41 (5), pp. 608–611.

620. KRISTÓF, J., INCZÉDY, J. 1993: Continuous determination of carbon-dioxide evolved during thermal-decomposition reactions. — *Journal of Thermal Analysis* 40 (3), pp. 993–998.
621. KRISTÓF, J., INCZÉDY, J., PAULIK, J., PAULIK, F. 1979: A simple device for continuous and selective detection of water vapour evolved during thermal decomposition reaction. — *Journal of Thermal Analysis* 15 (1), pp. 151–157.
622. KRISTÓF, J., INCZÉDY, J., PAULIK, J., PAULIK, F. 1982: Application of a continuous and selective water detector in thermoanalytical investigations — *Thermochimica Acta* 56 (3), pp. 286–290.
623. KRISTÓF, J., VASSÁNYI, I., NEMECZ, E., INCZÉDY, J. 1985: Study of the dehydroxylation of clay minerals using continuous selective water detector. — *Thermochimica Acta* 93, pp. 625–628.
624. KRISTÓF, J., INCZÉDY, J., MOHÁCSI, G. 1990: Continuous determination of carbon monoxide evolved during thermal decomposition reactions. — *Journal of Thermal Analysis* 36 (4), pp. 1401–1409.
625. KRISTÓF, J., TÓTH, M., GÁBOR, M., SZABÓ, P., FROST, L. R. 1997: Study of the structure and thermal behavior of intercalated kaolinites. — *Journal of Thermal Analysis* 49 (3), pp. 1441–1448.
626. KRISTÓF, J., FROST, R. L., KLOPROGGE, J. T., HORVÁTH, E., MAKÓ, É. 2002: Detection of four different OH-groups in ground kaolin-ite with controlled-rate thermal analysis. — *Journal of Thermal Analysis and Calorimetry* 69 (1), pp. 77–83.
627. KRS, M., NOVÁK, F., KRISOVÁ, M., PRUNER, P., JANSÁ, J. 1993: Magnetic properties, self-reversal remanence and thermal alteration products of smyhtite. — *Studia Geophysica et Geodaetica* 37 (4), pp. 382–400.
628. KRÜGER, T. M., SMYKATZ-KLOSS, W. 1985: Differential thermal analysis as an indicative method for the determination of soil mineral damage. — *Thermochimica Acta* 83 (1), pp. 107–112.
629. KUANG, W. X., FACEY, G. A., DETELLIER, C. 2004: Dehydration and rehydration of palygorskite and the influence of water on the nanopores. — *Clays and Clay Minerals* 52 (5), pp. 635–642.
630. KUDO, H., MIURA, H., HARIYA, Y. 1990: Tetragonal-monoclinic transformation of cryptomelane at high temperature. — *Mineralogical Journal* 15 (2), pp. 50–63.
631. KULBICKI, G. 1959: High temperature phases in sepiolite, attapulgite and saponite. — *The American Mineralogist* 44 (7–8), pp. 752–764.
632. KULBICKI, G., GRIM, R. E. 1959: A new method for thermal dehydration studies of clay minerals. — *Mineralogical Magazine* 32 (244), 53–62.
633. KULP, J. L., ADLER, H. H. 1950: Thermal study of jarosite. — *American Journal of Science* 248 (7), pp. 475–487.
634. KULP, J. L., KERR, P. F. 1949: Improved differential thermal analysis apparatus. — *The American Mineralogist* 34 (11–12), pp. 839–845.
635. KULP, J. L., PERFETTI, J. N. 1950: Thermal study of some manganese oxide minerals. — *Mineralogical Magazine* 29 (210), pp. 239–252.
636. KULP, J. L., TRITES, A. F. 1951: Differential thermal analysis of natural hydrous ferric oxides. — *The American Mineralogist* 36 (1), pp. 23–44.
637. KULP, J. L., WRIGHT, H. D., HOLMES, R. J. 1949: Thermal study of rhodochrosite. — *The American Mineralogist* 34 (3–4), pp. 195–219.
638. KULP, J. L., KENT, P., KERR, P. F. 1951: Thermal study of the Ca-Mg-Fe carbonates minerals. — *The American Mineralogist* 36 (9–10), pp. 643–670.
639. KURILENKO, C. 1950: Differential thermal analysis of tourmaline. — *Bulletin de la Société Française de Minéralogie et de Cristallographie* 73 (1–3), pp. 49–54.
640. L'VOV, B. V. 2002: Mechanism and kinetics of thermal decomposition of carbonate. — *Thermochimica Acta* 381 (1), pp. 1–16.
641. LA IGLESIA, A., DOVAL, M., LOPEZ-AGUAYO, F. 1977: Thermal behavior of valleriite. — *The American Mineralogist* 62 (9–10), pp. 1030–1031.
642. LAMPPHAM, D. L. 1958: Structural and chemical variation in chromium chlorite. — *The American Mineralogist* 43 (9–10), pp. 921–956.
643. LANG, B., GRODZINSKI, A., STOCH, L. 1983: Thermoanalytical curves for Yamato-74013 and -74010 diogenites. — *Memoirs of National Institute of Polar Research* 30 (Special issue), pp. 378–388.
644. LANGELLA, A., PANSINI, M., CERRI, G., CAPPELLETTI, P., DE'GENNARO, M. 2003: Thermal behavior of natural and cation-exchanged clinoptilolite from Sardinia (Italy). — *Clays and Clay Minerals* 51 (6), pp. 625–633.
645. LANGER, A. M., KERR, P. F. 1967: Evaluation of kaolinite and quartz differential thermal analysis curves with a new high temperature cell. — *The American Mineralogist* 52 (3–4), pp. 509–523.
646. LANGER, K., FLÖRKE, O. W. 1974: Near infrared absorption spectra (4000–9000 cm<sup>-1</sup>) of opals and the role of “water” in these SiO<sub>2</sub>·nH<sub>2</sub>O minerals. — *Fortschritte der Mineralogie* 52 (1), pp. 17–51.
647. LANGIER-KUŹNIAROWA, A. 1967: *Termogramy mineralow ilastych*. — Wydaw. geologiczne, Warszawa, 316 p.
648. LANGIER-KUŹNIAROWA, A. 1969: On the thermal analysis of mineral components in clays. — *Journal of Thermal Analysis* 1 (1), pp. 47–52.
649. LANGIER-KUŹNIAROWA, A. 1989: The present state of thermal investigations of clays. — *Thermochimica Acta* 148, pp. 413–420.
650. LANGIER-KUŹNIAROWA, A., INCZÉDY, J., KRISTÓF, J., PAULIK, F., PAULIK, J., ARNOLD, M. 1990: Simultaneous TG, DTG, DTA and EGA examination of argillaceous rock. Part II. — *Journal of Thermal Analysis* 36 (1), pp. 67–83.
651. LANTOS, Z., VETŐ, I., FÖLDVÁRI, M., KOVÁCS-PÁLFFY, P. 2003: On the role of remote magmatic source and intrabasalt redeposition in the genesis of the Toarcian Úrkút Manganese Ore, Hungary. — *Acta Geologica Hungarica* 46 (4), pp. 321–340.
652. LAPIDES, I. L. 1994: The influence of composition and fine structure on a thermographical characteristic of micas. — *Journal of Thermal Analysis* 42 (1), pp. 197–206.
653. LAPIDES, I. L. 1997: Evaluation of kinetic parameters from a single TG curve based on the similarity theory and process symmetry. — *Journal of Thermal Analysis* 50 (1–2), pp. 269–277.
654. LASKOU, M., MARGOMENOU-LEONIDOPOULOU, G., BALEK, V. 2006: Thermal characterization of bauxite samples. — *Journal of Thermal Analysis and Calorimetry* 84 (1), pp. 141–146.

655. LAUER JR., H. V., MING, D. W., GOLDEN, D. C., LIN, I-C., BOYNTON, M. W. 2000: Thermal and evolved gas analysis of hydromagnesite and nesquehonite: implications for remote thermal analysis on Mars. — *Lunar and Planetary Science. 31st Annual Lunar and Planetary Science Conference, March 13–17, 2000, Houston, Texas, abstract no.* 2102.
656. LAUREIRO, Y., JEREZ, A., PICO, C., VEIGA, M. L. 1991: Controlled decomposition rate thermal analysis of  $\text{Mg}(\text{OH})_2$  and  $\text{Cd}(\text{OH})_2$ . Kinetic study. — *Thermochimica Acta* 182 (1), pp. 47–56.
657. LAUREIRO, Y., JEREZ, A., ROUQUÉROL, F., ROUQUÉROL, J. 1996: Dehydration kinetics of Wyoming montmorillonite studied by controlled transformation rate thermal analysis. — *Thermochimica Acta* 278 (1–2), pp. 165–173.
658. LEHMANN, H., RÖSSLER, M. 1975: A contribution to the nature of water-binding in perlites. — *Thermal Analysis. Vol. 2. Proceedings fourth ICTA Budapest*, pp. 619–628.
659. LEMAITRE, J., LÉONARD, A. J., DELMON, B. 1982: Le mécanisme de la transformation thermique de la métakaolinite. — *Bulletin de Mineralogy* 105 (5), pp. 501–507.
660. LENGAUER, C. L., GIESTER, G., TILLMANN, E. 1997: Mineralogical characterization of paulingite from Vinaricka Hora, Czech Republic. — *Mineralogical Magazine* 61 (407), pp. 591–606.
661. LEPESHKOV, I. N., SEMENDYAEVA, N. K. 1975: Thermal analysis of natural salts. — *Thermal Analysis V.2. Proceedings of the fourth ICTA, Budapest*, pp. 677–683.
662. LEPP, H. 1957: Stages in the oxidation of magnetite. — *The American Mineralogist* 42 (9–10), pp. 679–680.
663. LEVY, C. 1958: Analyse thermique différentielle des minéraux sulfures. — *Bulletin de la Société Française de Mineralogie et de Cristallographie* 81 (1–3), pp. 29–34.
664. LIFEROVICH, R. P., SOKOLOVA, E. V., HAWTHORNE, F. C., LAJOKI, K. V. O., GEHÖR, S., PAKHOMOVSKY, Y. A., SOROKHTINA, N. V. 2000: Gladiusite, ideally  $\text{Fe}^{3+}_2(\text{Fe}^{2+}, \text{Mg})_4(\text{PO}_4)_6(\text{OH})_{11}(\text{H}_2\text{O})$ , a new hydrothermal mineral species from the phoscorite–carbonatite unit, Kovdor complex, Kola Peninsula, Russia. — *The Canadian Mineralogist* 38 (6), pp. 1477–1485.
665. LIMA-DE-FARIA, J., A. LOPES-VIEIRA, A. 1964: The transformation of groutite ( $\alpha\text{-MnOOH}$ ) into pyrolusite ( $\text{MnO}_2$ ). — *Mineralogical Magazine* 33 (266), pp. 1024–1031.
666. LIPPMANN, F. 1954: Über einen Keuperton von Zaiserweiher bei Maulbronn. — *Heidelberger Beiträge zur Mineralogie und Petrographie* 4, pp. 130–134.
667. LIPPMANN, F. 1956: Clay minerals from the Rot Member of the Triassic near Gottingen, Germany. — *Journal of Sedimentary Petrology* 26 (2), pp. 125–139.
668. LISK, M., RODGERS, K. A., BROWN, P. R. L. 1991: Instrumental and preparative factors influencing measurement of  $\alpha$ -quartz inversion temperatures. — *Thermochimica Acta* 175 (2), pp. 293–298.
669. LJUNGGREN, P. 1955: Differential thermal analysis and x-ray examination of Fe and Mn bog ores. — *Geologiska Föreningens i Stockholm Förhandlingar* 77 (2), pp. 135–147.
670. LJUNGGREN, P. 1960: Todorokite and pyrolusite from Vermlands Taberg, Sweden. — *The American Mineralogist* 45 (1–2), pp. 235–238.
671. LOMBARDI, G. 1977: For better thermal analysis. — *International Confederation for Thermal Analysis, Istituto di Mineralogia e Petrografia Dell' Università Di Roma, Rome*, 36 p.
672. LÄRNVIK, K., SMYKATZ-KLOSS, W. 1984: Comparative studies of structural transformations of carbonate and silica minerals by means of thermosonimetry and differential thermal analysis. — *Thermochimica Acta* 72 (1–2), pp. 159–163.
673. LOUCKS, R. R. 1991: The bound interlayer  $\text{H}_2\text{O}$  content of potassic white micas: Muscovite-hydromuscovite-hydropyrophyllite solutions. — *The American Mineralogist* 76, pp. 1563–1579.
674. L'VOV, B. V., UGOLKOV, V. L. 2005: Kinetics and mechanism of dehydration of kaolinite, muscovite and talc analyzed thermogravimetrically by the third-law method. — *Journal of Thermal Analysis and Calorimetry* 82 (1), pp. 15–22.
675. MACKENZIE, K. J. D., BEREZOWSKI, R. M. 1980: Thermal and Mossbauer studies of iron-containing hydrous silicates. II. Hisingerite. — *Thermochimica Acta* 41 (3), pp. 335–355.
676. MACKENZIE, K. J. D., BEREZOWSKI, R. M. 1981: Thermal and Mössbauer studies of iron-containing hydrous silicates. III. Cronstedtite. — *Thermochimica Acta* 44 (2), pp. 171–187.
677. MACKENZIE, K. J. D., BEREZOWSKI, R. M. 1984: Thermal and Mössbauer studies of iron-containing hydrous silicates. V. Berthierine. — *Thermochimica Acta* 74 (1–3), pp. 291–312.
678. MACKENZIE, K. J. D., MCGAVIN, D. G. 1994: Thermal and Mössbauer studies of iron-containing hydrous silicates. Part 8. Chrysotile. — *Thermochimica Acta* 244, pp. 205–221.
679. MACKENZIE, K. J. D., MEINHOLD, R. H. 1993: Thermal decomposition of brucite,  $\text{Mg}(\text{OH})_2$ : a  $^{25}\text{Mg}$  MAS NMR study. — *Thermochimica Acta* 230, pp. 339–343.
680. MACKENZIE, K. J. D., MEINHOLD, R. H. 1994a: The thermal reactions of talc studied by  $^{29}\text{Si}$  and  $^{25}\text{Mg}$  MAS NMR. — *Thermochimica Acta* 244, pp. 195–203.
681. MACKENZIE, K. J. D., MEINHOLD, R. H. 1994b: Thermal reactions of chrysotile revisited: A  $^{29}\text{Si}$  and  $^{25}\text{Mg}$  MAS NMR study. — *The American Mineralogist* 79 (1–2), pp. 43–50.
682. MACKENZIE, K. J. D., BEREZOWSKI, R. M., BOWDEN, M. E. 1986: Thermal and Mössbauer studies of iron-containing hydrous silicates. VI. Minnesotait. — *Thermochimica Acta* 99, pp. 273–289.
683. MACKENZIE, K. J. D., BROWN, I. W. M., CARDILE, C. M., MEINHOLD, R. H. 1987: The thermal reactions of muscovite studied by high-resolution solid-state  $^{29}\text{Si}$  and  $^{27}\text{Al}$  NMR. — *Journal of Materials Science* 22 (7), pp. 2645–2654.
684. MACKENZIE, K. J. D., CARDILE, C. M., BROWN, I. W. M. 1988: Thermal and Mössbauer studies of iron-containing hydrous silicates. VII: Glauconite. — *Thermochimica Acta* 136, pp. 247–261.
685. MACKENZIE, K. J. D., MEINHOLD, R. H., SHERRIFF, B. L., XU, Z. 1993:  $^{27}\text{Al}$  and  $^{25}\text{Mg}$  solid-state magic-angle spinning nuclear magnetic resonance study of hydrotalcite and its thermal decomposition sequence. — *Journal of Material Chemistry* 3 (12), pp. 1263–1269.
686. MACKENZIE, K. J. D., TEMUJIN, J., OKADA, K. 1999: Thermal decomposition of mechanically activated gibbsite. — *Thermochimica Acta* 327 (1–2), pp. 103–108.

687. MACKENZIE, R. C. 1957a: Saponite from Allt Ribhein, Fiskavaig Bay, Skye. — *Mineralogical Magazine* 31 (239), pp. 672–680.
688. MACKENZIE, R. C. 1957b: *The differential thermal investigation of clays*. — Mineralogical Society, London, 456 p.
689. MACKENZIE, R. C. 1962: *Scifax Differential Thermal Data Index*. — Cleaver-Hume Press, London.
690. MACKENZIE, R. C. 1970: *Differential thermal Analysis. I*. — Academic Press, London-New York. 775 p.
691. MACKENZIE, R. C. 1978: Nomenclature in thermal analysis, Part IV. — *Journal of Thermal Analysis* 13 (2), pp. 387–392.
692. MACKENZIE, R. C. 1981: Nomenclature in thermal analysis, Part V: Symbols. — *Journal of Thermal Analysis* 21 (1), pp. 173–175.
693. MACKENZIE, R. C., BERGGREN, G. 1970: Oxides and hydroxides of higher-valency elements. — In: MACKENZIE, R. C. (ed.): *Differential Thermal Analysis*. Academic Press, London – New York, pp. 272–302.
694. MACKENZIE, R. C., CAILLÈRE, S. 1979: Thermal Analysis DTA, TG, DTG. — In: VAN OLPHEEN, H., FRIPIAT, J. J. (eds): *Data handbook for clay materials and other non-metallic minerals*. Pergamon Press, Oxford, pp. 243–284.
695. MACKENZIE, R. C., MILNE, A. A. 1953a: The effect of grinding on micas. — *Clay Minerals Bulletin* 2 (9), pp. 57–62.
696. MACKENZIE, R. C., MILNE, A. A. 1953b: The effect of grinding on micas. I. Muscovite. — *Mineralogical Magazine* 30 (222), pp. 178–185.
697. MACKENZIE, R. C., RAHMAN, A. A. 1987: Interaction of kaolinite with calcite on heating: I. instrumental and procedural factors for one kaolinite in air and nitrogen. — *Thermochimica Acta* 121 (20), pp. 51–69.
698. MACKENZIE, R. C., KEATTCH, C. J., DOLLIMORE, D., FORRESTER, J. A., HODGSON, A. A., REDFERN, J. P. 1972: Nomenclature in thermal analysis, part II. — *Journal of Thermal Analysis* 4 (3), pp. 343–347.
699. MACKENZIE, R. C., PATERSON, E., SWAFFIELD, R. 1981: Observation of surface characteristics by DSC and DTA. — *Journal of Thermal Analysis* 22 (2), pp. 269–274.
700. MACKENZIE, R. C., RAHMAN, A. A., MOIR, H. M. 1988: Interaction of kaolinite with calcite on heating: II. mixtures with one kaolinite in carbon dioxide. — *Thermochimica Acta* 124, pp. 119–127.
701. MACKENZIE, R. C., HELLER-KALLAI, L., LACHOWSKI, E. E. 1991: An unusual kaolinite-calcite interaction. — *Applied Clay Science* 7 (1), pp. 69–77.
702. MADARÁSZ, J., POKOL, G., NOVÁK, C., MOSELHY, H., GÁL, S. 1993: Comprehensive kinetic studies on isothermal and non-isothermal reactions of some aluminium compounds. — *Journal of Thermal Analysis* 40 (3), pp. 1367–1378.
703. MADEJOVÁ, J., ARVAIOVÁ, B., KOMADEL, P. 1999: FTIR spectroscopic characterization of thermally treated Cu<sup>2+</sup>, Cd<sup>2+</sup>, and Li<sup>+</sup> montmorillonites — *Spectrochimica Acta Part A: Molecular and Biomolecular Spectroscopy* 55 (12), pp. 2467–2476.
704. MAFTULEAC, A., DRANCA, I., LUPASCU, T. 2002: Study of interlayer water on the active sites of mineral sorbent: Thermal Analysis. — *Journal of Thermal Analysis and Calorimetry* 69 (2), pp. 589–598.
705. MAINLY, R. L. 1950: The differential thermal analysis of certain phosphates. — *The American Mineralogist* 35 (1–2), pp. 108–115.
706. MAKUDOV, S. A. 1961: Apophyllite from the Kedabel district. — *Izvestiya Akademii Nauk Azerbaydzhanskoy S.S.R. Seriya Geologo-geografičeskikh Nauk i Nefti* 5, pp. 33–38.
707. MAKÓ, É., JUHÁSZ, A. Z. 2000: In situ XRD study of the thermal decomposition of dolomite. — *European Powder Diffraction* 321 (3), pp. 380–385.
708. MAKSIMOVIC, Z., BISH, D. L. 1978: Brindleyite, a nickel-rich aluminous serpentine mineral analogous of berthierite. — *The American Mineralogist* 63 (5–6), pp. 484–489.
709. MALEK, Z., BALEK, V., GARFINKEL-SHWEKY, D., YARIV, S. 1997: The study of the dehydration and dehydroxylation of smectites by emanation thermal analysis. — *Journal of Thermal Analysis* 48 (1), pp. 83–92.
710. MANCEAU, A., GATES, W. 1997: Surface structural model for ferrihydrite. — *Clays and Clay Minerals* 45 (3), pp. 448–460.
711. MANCEAU, A., GORSHKOV, A. I., DRITS, V. A. 1992: Structural chemistry of Mn, Fe, Co, and Ni in Mn hydrous oxide. II. Information from EXAFS spectroscopy, electron and X-ray diffraction. — *The American Mineralogist* 77 (11–12), pp. 1144–1157.
712. MANSOUR, S. A. A. 1994: Thermoanalytical investigations of decomposition course of copper oxysalts. I: Basic copper carbonate. — *Journal of Thermal Analysis* 42 (6), pp. 1251–1263.
713. MARCOS, C., ARGÜELLES, A., RÚIZ-CONDE, A., SÁNCHEZ-SOTO, P. J., BLANCO, J. A. 2003: Study of the dehydration process of vermiculites by applying a vacuum pressure: formation of interstratified phases. — *Mineralogical Magazine* 67 (6), pp. 1253–1268.
714. MAREL VAN DER H. W. 1956: Quantitative differential thermal analyses of clay and other minerals. — *The American Mineralogist* 41. 3–4. pp. 222–244.
715. MARINCEA, S., CONSTANTINESCU, E., LADRIERE, J. 1997: Relatively unoxidized vivianite in limnic coal from Capeni, Baraolt Basin, Romania. — *The Canadian Mineralogist* 35 (3), pp. 713–722.
716. MARSI, I., DON, GY., FÖLDVÁRI, M., KOLOSZÁR, L., KOVÁCS-PÁLLFY, P., KROLOPP, E., LANTOS, M., NAGY BODOR, E., ZILÁHI-SEBESS, L. 2004: Quaternary sediments of the north-eastern Mórág Block. — *Annual Report of the Hungarian Geological Institute of 2003*, pp. 343–370.
717. MARTIN, C. J. 1977: The thermal decomposition of chrysotile. — *Mineralogical Magazine* 41 (320), pp. 453–459.
718. MARTIN, R. T., 1958: Clay-carbonate-soluble salt interaction during differential thermal analysis. — *The American Mineralogist* 43 (7–8), pp. 649–655.
719. MARTIN VIVALDI, J. L., CANO RUIZ, J. 1956: Algunas consideraciones acerca de la formula mineralogica de la sepiolita. — *Anales de la Real Sociedad Espanola de Fisica y Química, Ser. B. Química* 52 (B), (718), pp. 499–508.
720. MARTIN VIVALDI, J. L., FENOLL HACH-ALI, P. 1970: Palygorskite and sepiolite. — In: MACKENZIE, R. C. (ed.): *Differential Thermal Analysis*. Academic Press. London – New York pp. 553–573.
721. MASON, B., SAND, L. B. 1960: Clinoptilolite from Patagonia; the relationship between clinoptilolite and heulandite. — *The American Mineralogist* 45 (3–4), pp. 341–350.
722. MAUREL, P. C. 1964: Types de reaction d' oxydation observes au cours de l' analyse thermique differentielle dans l' air de mineraux sulfures et arsenies de Fe, Co, Ni, Cu, Zn, Ag et Pb. — *Bulletin de la Société Française de Mineralogie et de Cristallographie* 87 (3), pp. 377–385.
723. MAZZETTI, L., THISTLETHWAITE, P. J. 2002: Raman spectra and thermal transformations of ferrihydrite and schwertmannite. — *Journal of Raman Spectroscopy* 33 (2), pp. 104–111.

724. MCADIE, H. G. 1967: Recommendation for reporting thermal analysis data. — *Analytical Chemistry* 39 (4), p. 543.
725. MCADIE, H. G. 1972: Recommendation for reporting thermal analysis data. Evolved gas techniques. — *Analytical Chemistry* 44 (3), pp. 640–641.
726. MCADIE, H. G. 1977: Environmental applications for thermal analysis. — *Thermochimica Acta* 18. 1. pp. 3–13.
727. MCADIE, H. G., GARN, P. D., MENIS, O. 1972: Standard reference materials: selection of differential thermal analysis temperature standards through a cooperative study. — *NBS Special Publication 260-40 U.S. Department of Commerce National Bureau of Standards*, 61 p.
728. MCCONNELL, J. D. C. 1954: The hydrated calcium silicates riversideite, tobermorite, and plombierite. — *Mineralogical Magazine* 30 (224), pp. 293–305.
729. MCINTOSH, R. M., SHARP, J. H., WILBURN, F. W. 1990: The thermal decomposition of dolomite. — *Thermochimica Acta* 165 (2), pp. 281–296.
730. MCLAUGHLIN, R. J. W. 1957: Other Minerals. — In: MACKENZIE, R. C. (ed.): *The differential thermal investigation of clays*. Mineralogical Society, London. pp. 373–374.
731. MCRAE, S. G. 1972: Glauconite. — *Earth Science Reviews* 8 (4), pp. 397–440.
732. MEHTA, S. K., KALSOTRA, A. 1991: Kinetics and hydrothermal transformation of gibbsite. — *Journal of Thermal Analysis* 37 (2), pp. 267–275.
733. MEHTA, S. K., KALSOTRA, A., MURAT, M. 1992: A new approach to phase transformations in gibbsite: the role of the crystallinity — *Thermochimica Acta* 205, pp. 191–203.
734. MELDAU, R., ROBERTSON, R. H. S. 1953: Thermal decomposition of dolomite. — *Nature* 172 (4387), pp. 998–999.
735. MELKA, K., CÍLEK, V. 2000: Recent allophane coatings form the karst and pseudokarst caves. — *Scripta Faculta Sciences University of Masaryk, Brun*, 28–29. pp. 19–26.
736. MENDELOVICI, E., YARIV, S., 1981: Interactions between the iron and the aluminum minerals during the heating of Venezuelan lateritic bauxites. I. Infrared spectroscopy investigation. — *Thermochimica Acta* 45 (3), pp. 327–337.
737. MENDIOROZ, S., BELZUNCE, M. J., PAJARES, J. A. 1989: Thermogravimetric study of diatomites — *Journal of Thermal Analysis* 35 (7), pp. 2097–2104.
738. MERKLE, A. B., SLAUGHTER, M. 1968: Determination and refinement of the structure of heulandite. — *The American Mineralogist* 53 (7–8), pp. 1120–1138.
739. MEYER, K. 1968: Phisikalisch-chemische Kristallographie. — Leipzig, 337 p.
740. MEYER, K. S., SPEYER, R. F. 2003: Thermal analysis of clays. — In: BROWN M.E., GALLAGHER P. K. (eds): *Handbook of thermal analysis and calorimetry. Vol. 2: Application to Inorganic and miscellaneous Materials*. — Elsevier, pp. 261–306.
741. MIDGLEY, H. G., GROSS, K. A. 1956: Thermal reactions of smectites. — *Clay Minerals Bulletin* 3 (16), pp. 79–90.
742. MIFSUD, A., RAUTUREAU, M., FORMES, V. 1978: Etude de l'eau dans la palygorskite a l'aide des analyses thermiques (Study of water in palygorskite by thermal analysis). — *Clays and Clay Minerals* 13 (4), pp. 367–374.
743. MIHAJLOVIĆ, I. M. 2005: Kinetic study and mechanism of chalcocite and covellite oxidation process. — *Journal of Thermal Analysis and Calorimetry* 79 (3), pp. 715–720.
744. MILLER, A. K., GUGGENHEIM, S., KOSTER VAN GROOS, A. F. 1991a: The incorporation of “water” in a high-pressure 2:1 silicate. A high pressure differential thermal analysis of the 10 Å phase. — *The American Mineralogist* 76 (1–2), pp. 106–112.
745. MILLER, A. K., GUGGENHEIM, S., KOSTER VAN GROOS, A. F. 1991b: Bond energy of adsorbed and interlayer water: kerolite dehydration at elevated pressures. — *Clays and Clay Minerals* 39 (2), pp. 127–130.
746. MIŁODOWSKI, A. E., MORGAN, D. J., WARNE, S. ST. J., 1989: Thermal analysis studies of the dolomite-ferroan dolomite-ankerite series. II. Decomposition mechanism in flowing CO<sub>2</sub> atmosphere. — *Thermochimica Acta* 152 (2), pp. 279–297.
747. MINATO, H. 1988: Dehydration energy of halloysite by means of D. S. C. methods with the relationships of its mineralogy and modes of occurrence. — *Thermochimica Acta* 135, pp. 279–283.
748. MIRWALD, P. W. 1976: A differential thermal analysis study of the high-temperature polymorphism of calcite at high pressure. — *Contributions to Mineralogy and Petrology* 59 (1), pp. 33–40.
749. MIRZA, I., GHERGARIU, L. 1963: Bentonitul de la Valea Chioarului (Regiunea Maramures). — *Revista Minelor*, 14 (1), pp. 41–43.
750. MIRZAI, J. I., GASHIMOV, F. A., PRIBYLOV, A. A., SERPINSKII, V. V., MAMEDOV, KH. S. 1987: Dehydration of desmine. — *Russian Chemical Bulletin* 36 (2), pp. 221–224.
751. MITOV, I., PANEVA, D., KUNEV, B. 2002: Comparative study of the thermal decomposition of iron oxyhydroxides. — *Thermochimica Acta* 386 (2), pp. 179–188.
752. MIURA, H., HARIYA, Y. 1988: Gas analysis of manganese wad from Hokkaido. — *Kobutsugaku Zasshi (Journal of the Mineralogical Society of Japan)*, 18 (4), pp. 247–254.
753. MIURA, Y., KATO, T., RUCKLIDGE, J., MATSUEDA, H. 1981: Natroapophyllite, a new orthorhombic sodium analog of apophyllit. II. Crystal structure. — *The American Mineralogist* 66 (3–4), pp. 410–423.
754. MOHAPATRA, B. K., MISHRA, S. K., SAHOO, R. K. 1989: Characteristics of marine ferromanganese concretions at elevated temperature. — *Thermochimica Acta* 145, pp. 33–49.
755. MOLNÁR, B., MURVAI, M. I., HEGYI PAKÓ, J. 1976: Recent lacustrine dolomite formation in the Great Hungarian Plain. — *Acta Geologica Hungarica* 20 (3–4), pp. 179–198.
756. MONTROYA, C., LANAS, J., ARANDIGOYEN, M., NAVARRO, I., GARCÍA CASADO, P. J., ALVAREZ, J. L. 2001: Characterization of ancient dolomitic binding materials from Zamarce, in Navarre (Spain). — *Symposium II, Materials Issues in Art and Archaeology VI, Nov. 26–30th, Boston, MA, USA*, Paper II3.2
757. MOORE, G. S. M. 1993: The  $\alpha$ - $\beta$  inversion in submilligram particles of natural quartz. — *Journal of Thermal Analysis* 40 (1), pp. 115–120.
758. MOORE, G. S. M., ROSE, H. E. 1979: Thermal effect of contamination, adsorbed water and annealing on the DTA of powdered quartz. — *Journal of Thermal Analysis* 15 (1), pp. 37–45.
759. MORGAN, D. J. 1977: Simultaneous DTA-EGA of minerals and natural mineral mixtures. — *Journal of Thermal Analysis* 12 (2), pp. 245–263.

760. MORGAN, D. J., WARNE, S. ST. J., WARRINGTON, S. B., NANCARROW, PH. A. 1986: Thermal-decomposition reactions of caledonite and their products. — *Mineralogical Magazine* 50 (357), pp. 521–526. Part 3.
761. MORGAN, D. J., MIŁODOWSKI, A. E., WARNE, S. ST. J., WARRINGTON, S. B. 1988a: Atmosphere dependence of the thermal decomposition of manganite,  $\gamma$ -MnOOH. — *Thermochimica Acta* 135, pp. 273–277.
762. MORGAN, D. J., WARRINGTON, S. B., WARNE, S. ST. J. 1988b: Earth sciences applications of evolved gas analysis: A review. — *Thermochimica Acta* 135, pp. 207–212.
763. MOSKALEWICZ, R. 1975: Application of derivatograph (with the 1500 °C furnace) for Curie point  $T_c$  measurement based on magnetic interaction between heating current and a ferromagnetic sample. — *Thermal Analysis III. Proceedings of the IV. ICTA, Budapest 1974*, pp. 873–880.
764. MÜLLER, F., DRITS, V., PLANCON, A., BESSON G. 2000a: Dehydroxylation of  $\text{Fe}^{3+}$ , Mg-rich dioctahedral micas: (I) structural transformation. — *Clay Minerals* 35 (3), pp. 491–504.
765. MÜLLER, F., DRITS, V., PLANCON A., ROBERT J. L. 2000b: Structural transformation of 2:1 dioctahedral layer silicates during dehydroxylation-rehydroxylation reactions. — *Clays and Clay Minerals* 48 (5), pp. 572–585.
766. MÜLLER, G. 1970: High-magnesian Calcite and Protodolomite in Lake Balaton (Hungary) Sediments — *Nature* 226 (5247), pp. 749–750.
767. MÜLLER-VONMOOS, M., SCHINDLER, C. 1973: Palygorskit im helvetischen Kieselkalk des Bürgenstocks. — *Schweizerische Mineralogische und Petrographische Mitteilungen* 53 (3), pp. 395–403.
768. MUMPTON, F. A. 1960: Clinoptilolite redefined. — *The American Mineralogist* 45 (3–4), pp. 351–369.
769. MURAD, E., WAGNER, U. 1996: The thermal behaviour of an Fe-rich illite. — *Clay Minerals* 31 (1), pp. 45–52.
770. MURRAY, P., WHITE, J. 1949: Kinetics of the thermal dehydration of clays. — *Transactions of the British Ceramic Society* 48, pp. 187–206.
771. MUSIC, S., POPOVIĆ, S., RISTIĆ, M. 1992: Thermal decomposition of pyrite. — *Journal of Radioanalytical and Nuclear Chemistry* 162 (2), pp. 217–226.
772. NAGASAWA, K., OHKOCHI, N. 1988: X-ray studies on dehydration and rehydration of expansible clay minerals. — *Thermochimica Acta* 135, pp. 285–290.
773. NAGATA, H., SHIMODA, S, SUDO, T. 1974: On dehydration of bound water in sepiolite. — *Clays and Clay Minerals* 22 (3), pp. 285–293.
774. NAGY, B., BRADLEY, W. F. 1955: The structural scheme of sepiolite. — *The American Mineralogist* 40 (9–10), pp. 885–892.
775. NAGY, B., FAUST, G. T. 1956: Serpentine: natural mixtures of chrysotile and antigorite. — *The American Mineralogist* 41 (11–12), pp. 817–838.
776. NAGY, N. M., KÓNYA, J., FÖLDVÁRI, M., KOVÁCS-PÁLFFY, P. 2003: The adsorption of caesium-137 on clay rocks from the Carpathian Basin. — *Czechoslovak Journal of Physics* 53 (1), Suppl. A. pp. 103–111.
777. NAKAGAWA, M., MATSUURA, T. 1994: Hydrothermal alteration at the Denbekova deposit of Amakusa pottery stone. — *Clay Science, (Society of Japan)*, 9 (3), pp. 123–136.
778. NAKAHIRA, M., KATO, T. 1964: Thermal transformations of pyrophyllite and talc as revealed by X-ray and electron diffraction studies. — *Clays and Clay Minerals, Proceedings of the 12th Natl. Conf. Atlante*, pp. 21–27.
779. NAKAI, I., ADACHI, H., MATSUBARA, S., KATO, A., MASUTOMI, K., FUJIWARA, T., NAGASHIMA, K. 1978: Sarabauite, a new oxide sulfide mineral from the Sarabau mine, Sarawak, Malaysia. — *The American Mineralogist* 63 (7–8), pp. 715–719.
780. NASEDKIN, V. V., NASEDKINA, V. H. 1967: Svravnitel'nāa harakteristika obrazcov prirodnoġo i sintetičeskogo mordenitov. — In: PETROV V. P. (ed.) 1967: *Vodnye vulkaničeskie stekla i post vulkaničeskie mineraly*. Nauka, Moskow. pp. 158–170.
781. NASEDKIN, V. V., PILOYAN, G. O., 1983: Investigations of perlites by modified differential thermogravimetry. — *Journal of Thermal Analysis* 27 (2), pp. 341–352.
782. NAUER, G., STRECHA, P., BRINDA-KONOPIK, N., LIPTAY, G. 1985: Spectroscopic and thermoanalytical characterization of standard substances for the identification of reaction products on iron electrodes. — *Journal of Thermal Analysis* 30 (4), pp. 813–830.
783. NAUMANN, A. W., DRESHER, W. H. 1966: The influence of sample texture on chrysotile dehydroxylation. — *The American Mineralogist* 51 (7), pp. 1200–1211.
784. NAUMANN, R., KÖHNKE, K., PAULIK, J., PAULIK, F. 1983: Kinetics and mechanism of the dehydration of hydrargillites. Part. II. — *Thermochimica Acta* 64 (1–2), pp. 15–26.
785. NAZAROVA, G. S., OSTASHCHENKO, B. A., MITROFANOV, V. YA., SHILOVA, O. YU., ZARIPOVA, L. D. 1990: Nature of the color of prehnite. — *Journal of Applied Spectroscopy* 53 (2), pp. 890–894.
786. NEMECZ, E., VARJÚ, GY. 1970: Chemical and structural investigation of Sárospatakites (illite/montmorillonite). — *Bulletin of the Hungarian Geological Society* 100 (1), pp. 11–22. (in Hungarian with English summary)
787. NEMECZ, E., VARJÚ, GY., BARNÁ, J. 1965: Allevardite from Királyhegy, Tokaj Mountains, Hungary. — In: ROSENQUIST, I. TH., GRAFF-PETERSEN, P. (eds): *Proceedings of the International Clay Conference, Stockholm 1963*. Pergamon Press, Oxford, 2. pp. 51–67.
788. NÉMETH, T. 2003: Crystalstructural, chrystalchemical and mineralogical characteristic of montmorillonites as reflected by metal-ion adsorption studies. — *Doctoral Thesis, Manuscript University Eötvös Loránd, Budapest*.
789. NEUHOFF, P. S., BIRD, D. K. 2001: Partial dehydration of laumontite: thermodynamic constraints and petrogenetic implications. — *Mineralogical Magazine* 65 (1), pp. 59–70.
790. NICKEL, E. H., DAVIS, C. S. S., BUSSELL, M., BRIDGE, P. J., DUNN, J. G., MACDONALD, R. D. 1977: Eardleyite as a product of the supergene alteration of nickel sulfides in Western Australia. — *The American Mineralogist* 62 (5–6), pp. 449–457.
791. NICOLAS, J., DE ROSEN, A. 1963: Phosphates hydrothermaux de basse température et kaolinisation. La gorgeixite du massif Colettes (Allier) et les minéraux associés (hinsdalite). — *Bulletin de la Société Française de Minéralogie et des Cristallographie* 86 (4), pp. 379–385.
792. NIEDERMEYER, R. O., SCHOMBURG, J. 1984: Phosphoritic nodules from the Late Cretaceous of Mielnik (Poland) and some aspects of the genesis of phosphorites. — *Chemie der Erde* 43 (2), pp. 139–148.
793. NORRISH, K., ROGERS, L. E. R., SHAPTER, R. E. 1957: Kingite, a new mineral. — *Mineralogical Magazine* 31 (236), pp. 351–357.

794. NOVÁK, C., POKOL, G., TOMOR, K., KÓMÍVES, J., GÁL, S. 1988: Studies on the thermal reactions of aluminium oxides and hydroxides. — *Journal of Thermal Analysis* 33 (3), pp. 765–769.
795. NOVÁK, C., POKOL, G., IZVEKOV, V., GÁL, T. 1990: Studies on the reactions of aluminium oxides and hydroxides. — *Journal of Thermal Analysis* 36 (5), pp. 1895–1909.
796. NOVÁK, F. 1959: Tetradrit z ložiska Mária u Rožňavy. — *Geologické Práce, Zoš. Bratislava* 56., pp. 217–246.
797. NOVÁK, F., POVONDRA, P., VTĚLENSKY, J. 1967: Bukovskyt,  $\text{Fe}^{3+}_2(\text{AsO}_4)(\text{SO}_4)\text{OH}\cdot 7\text{H}_2\text{O}$ , from Kaňk, near Kutná Hora a new mineral. — *Acta Universitatis Carolinae — Geologica, Prague*, 4, pp. 297–325.
798. NUKUI, A., NAKAZAWA, H. 1978: Thermal changes in monoclinic tridymite. — *The American Mineralogist* 63 (11–12), pp. 1252–1259.
799. OGORODOVA, L. P., KISELEVA, I. A., MELCHAKOVA, L. V., SCHURIGA, T. N. 2005: Thermodynamic properties of lithium mica: Lepidolite. — *Thermochimica Acta* 435 (1), pp. 68–70.
800. ONAC, B. P., ZAHARIA, L., KEARNS, J., VERES, D. 2006: Vashegyite from Gaura cu Muscă Cave (Locvei Mountains, Romania): a new and rare phosphate occurrence. — *International Journal of Speleology, Bologna (Italy)*, 35 (2), 67–73.
801. ONDRUS, P., SKÁLA, R., CÍSAROVÁ, I., VESELOVSKY, F., FRYDA, J., CEJKA, J. 2002: Description and crystal structure of vajdakite,  $[(\text{Mo}^{6+}\text{O}_2)_2(\text{H}_2\text{O})_2\text{As}^{3+}_2\text{O}_5] \cdot \text{H}_2\text{O}$  — a new mineral from Jáchymov, Czech Republic. — *The American Mineralogist* 87 (7), pp. 983–990.
802. ONDRUS, P., SKÁLA, R., VITI, C., VESELOVSKY, F., NOVÁK, F., JANSÁ, J. 1999: Parascorodite,  $\text{FeAsO}_4\cdot 2\text{H}_2\text{O}$  — a new mineral from Kank near Kutná Hora, Czech Republic. — *The American Mineralogist* 84 (9), pp. 1439–1444.
803. ORCEL, J., CAILLÈRE, S., HÉNIN, S. 1951: O nouvel essai de classification des chlorites. — *Mineralogical Magazine* 29 (211), pp. 329–340.
804. OTSUKA, R. 1986: Recent studies on the decomposition of the dolomite group by thermal analysis. — *Thermochimica Acta* 100 (1), pp. 69–80.
805. OTSUKA, R., YAMAZAKI, A., KATO, K. 1991: Kinetics and mechanism of dehydration of natrolite and its potassium exchanged form. — *Thermochimica Acta* 181, pp. 45–56.
806. ÓZACAR, M., ALP, A., AYDIN, A. O. 2000: Kinetics of thermal decomposition of plumbo-jarosite. — *Journal of Thermal Analysis and Calorimetry* 59 (3), pp. 869–875.
807. OZAO, R., OTSUKA, R. 1985: Thermoanalytical investigation of huntite. — *Thermochimica Acta* 86, pp. 45–56.
808. PADILLA, R., FAN, Y., WILKOMIRSKY, I. 2001: Decomposition of enargite in nitrogen atmosphere. — *Canadian Metallurgical Quarterly* 40 (3), pp. 335–342.
809. PALOMBA, M., PORCU, R. 1988: Thermal behaviour of some minerals. Differential thermal analysis and determination of PA curves for different heating rates. — *Journal of Thermal Analysis* 34 (3), pp. 711–722.
810. PANEŠ, V. I., NASEDKINA, V. H., NASEDKIN, V. V. 1967: Mineralogo-petrografičeskââ charakteristika i osobennosti degidracii mineralov gruppy ceolitov. — In: PETROV, V. P. (ed.) 1967: *Vodnye vulkaničeskie stekla i post vulkaničeskie mineraly*. Nauka, Moscow, pp. 56–92.
811. PAPP, G., DÓDONY, I., LOVAS, GY., FÖLDVÁRI, M. 1999: “Hidroantigorite” from Csódi Hill, Visegrád Mts., Hungary. — *Topographia Hungarica Hungariae, Miskolc*, 6, pp. 127–136.
812. PARTHASARATHY, G., CHETTY, T. R. K., HAGGERTY, S. E. 2002: Thermal stability and spectroscopic studies of zemkorite: A carbonate from the Venkatampalle kimberlite of southern, India. — *The American Mineralogist* 87 (10), pp. 1384–1389.
813. PASHKEVICH, L. A. 1975: Thermographic study of low quality bauxites. — In: *Mineralogical and Technological Evaluation of Bauxites*. VÁMI-FKI. Budapest.
814. PASSAGLIA, E. 1969: Roggianite, a new silicate mineral. — *Clay Minerals* 8 (1), pp. 107–111.
815. PASSAGLIA, E. 1970: The crystal chemistry of chabasites. — *The American Mineralogist* 55 (7–8), pp. 1278–1301.
816. PASSAGLIA, E., VEZZALINI, G. 1985: Crystal chemistry of diagenetic zeolites in volcanoclastic deposits of Italy. — *Contributions to Mineralogy and Petrology* 90 (2–3), pp. 190–198.
817. PASSAGLIA, E., GALLI, E., RINALDI, R. 1974: Levynites and erionites from Sardinia, Italy. — *Contributions to Mineralogy and Petrology* 43 (4), pp. 253–259.
818. PASSAGLIA, E., GALLI, E., GOTTARDI, G., VEZZALINI, G. 1985: An anomalous phillipsite from Saint-Jean-Le-Centenair, Ardeche. — *Bulletin de Mineralogie* 108 (5), pp. 719–724.
819. PASSE-COUTRIN, N., N’GUYEN, P., PELMARD, R., OUENSANGA, A., BOUCHON, C., 1995: Water desorption and aragonite–calcite phase transition in scleractinian corals skeletons. — *Thermochimica Acta* 265, pp. 135–140.
820. PATNAIK, N., PATIL, R., SAKTIVELU, R., BHIMA, R. R. 1999: Thermal and structural study of low grade graphite ore from Shivaganga, India — Its implications in beneficiation process. — *Journal of Thermal Analysis and Calorimetry* 57 (2), pp. 541–549.
821. PAULIK, F. 1999: Thermal analysis under quasi-isothermal–quasi-isobaric conditions. — *Thermochimica Acta* 340–341, pp. 105–116.
822. PAULIK, F., ARNOLD, M. 1993: Simultaneous TG, DTG, DTA and EGA technique for the determination of carbonate, sulphate, pyrite and organic materials in minerals, soils and rocks. Part IV. Reproducibility and accuracy of the determination of sulphur trioxide and carbon dioxide. — *Journal of Thermal Analysis* 39 (8–9), pp. 1079–1090.
823. PAULIK, F., PAULIK, J. 1972: Kinetic studies of thermal decomposition reactions under quasi-isothermal and quasi-isobaric conditions by means of the derivatograph. — *Thermochimica Acta* 4 (3–5), pp. 189–198.
824. PAULIK, F., PAULIK, J. 1973: Investigations under quasi-isothermal and quasi-isobaric conditions by means of the derivatograph. — *Journal of Thermal Analysis* 5 (2–3), pp. 263–270.
825. PAULIK, F., PAULIK, J. 1978: Simultaneous techniques in thermal analysis. — *Analyst* 103 (1226), pp. 417–437.
826. PAULIK, F., PAULIK, J. 1986: Thermoanalytical examination under quasi-isothermal and quasi-isobaric conditions. — *Thermochimica Acta* 100 (1), pp. 23–59.
827. PAULIK, F., PAULIK, J. 1992: Role of heat and gas transport processes in thermal analysis. — *Journal of Thermal Analysis* 38 (1–2), pp. 197–211.
828. PAULIK, F., WELTNER, M. 1958: Über die derivative thermogravimetrische Analyse von Torfen und Torfbestandteilen. — *Acta Chimica Academiae Scientiarum Hungaricae, Budapest*, 16 (2), pp. 159–184.

829. PAULIK, F., PAULIK, J., ERDEY, L. 1961: Einfluss der im Inneren der Probe sich ausbildenden Atmosphäre bei den derivatographischen Untersuchungen. — *Acta Chimica Academiae Scientiarum Hungaricae, Budapest*, 26 (1–4), pp. 143–148.
830. PAULIK, F., GÁL, S., ERDEY, L. 1963a: Determination of the pyrites content of bauxites by thermal methods. — *Analytica Chimica Acta* 29, pp. 381–394.
831. PAULIK, F., LIPTAY, GY., ERDEY, L. 1963b: Die Bestimmung von Kalcit, Magnesit und Dolomit nebeneinander mit Hilfe des Derivatographen. — *Periodica Polytechnica* 7 (3), pp. 177–184.
832. PAULIK, F., PAULIK, J., ERDEY, L. 1966: A complex method in thermal analysis. — *Talanta* 13, pp. 1405–1430.
833. PAULIK, F., PAULIK, J., ERDEY, L. 1968: Combined thermo-dilatometric and derivatographic examination of hydrargillite and barium dihydrate. — *Analytica Chimica Acta* 41, pp. 170–172.
834. PAULIK, F., PAULIK, J., ARNOLD, M. 1982a: Kinetics and mechanism of the decomposition of pyrite under conventional and quasi isothermal-quasi isobaric thermoanalytical conditions. — *Journal of Thermal Analysis* 25 (2), pp. 313–325.
835. PAULIK, F., PAULIK, J., ARNOLD, M. 1982b: Simultaneous TG, DTG, DTA and EGA Technique for the determination of carbonate, sulphate, pyrite and organic materials in minerals, soils and rocks. Part I. Principles of the method. — *Journal of Thermal Analysis* 25 (2), pp. 327–340.
836. PAULIK, F., PAULIK, J., NAUMANN, R., KÖHNKE, K., PETZOLD, D. 1983: Mechanism and kinetics of the dehydration of hydrargillites. Part I. — *Thermochimica Acta* 64 (1–2), pp. 1–14.
837. PAULIK, F., PAULIK, J., ARNOLD, M. 1984a: Simultaneous TG, DTG, DTA and EGA Technique for the determination of carbonate, sulphate, pyrite and organic materials in minerals, soils and rocks. Part II. Operation of the thermo-gas-titrimetric device and examination procedure. — *Journal of Thermal Analysis* 29 (2), pp. 333–344.
838. PAULIK, F., PAULIK, J., ARNOLD, M. 1984b: Simultaneous TG, DTG, DTA and EGA Technique for the determination of carbonate, sulphate, pyrite and organic materials in minerals, soils and rocks Part III. Operation of the thermo-gas-titrimetric equipment and the examination procedure in special cases. — *Journal of Thermal Analysis* 29 (2), pp. 345–351.
839. PAULIK, F., PAULIK, J., ARNOLD, M., INCZÉDY, J., KRISTÓF, J., LANGIER-KUŹNIAROWA, A. 1989: Simultaneous TG, DTG, DTA and EGA examination of argillaceous rocks. Part I — *Journal of Thermal Analysis* 35 (6), pp. 1849–1860.
840. PAULIK, F., PAULIK, J., ARNOLD, M. 1992: Thermal decomposition of gypsum. — *Thermochimica Acta* 200, pp. 195–204.
841. PAULIK, F., BESSENYEY-PAULIK, E., WALTHER-PAULIK, K. 2004: Differential thermal analysis under quasi-isothermal, quasi-isobaric conditions (Q-DTA): Part II. Water evaporation and the decomposition mechanism of compounds with structural and crystal water. — *Thermochimica Acta* 424 (1–2), pp. 75–82.
842. PAULIK, J., PAULIK, F. 1970: Role of experimental conditions in thermal studies III. Calibration of DTG and DTA galvanometer flow curves on the derivatograph. — *Periodica Polytechnica; Chemical Engineering* 14, pp. 141–147.
843. PAULIK, J., PAULIK, F. 1971a: “Quasi-isothermal” thermogravimetry. — *Analytica Chimica Acta* 56 (2), pp. 328–331.
844. PAULIK, J., PAULIK, F. 1971b: Complex thermoanalytical method for the simultaneous recording of T, TG, DTG, DTA, TGT, DTGT, TD and DTD curves Part I. Development and characterization of equipment. — *Thermochimica Acta* 3 (1), pp. 13–15.
845. PAULIK J., PAULIK F. 1972: “Quasi-isothermal” and “quasi-isobaric” thermogravimetry. — *Analytica Chimica Acta* 60 (1), pp. 127–130.
846. PAULIK, J., PAULIK, F., ERDEY, L. 1966: Standardization of experimental conditions in thermal analysis: A new polyplate sample holder. — *Analytica Chimica Acta* 34, pp. 419–426.
847. PAULIK, J., PAULIK, F., ARNOLD, M. 1981: Dehydration of magnesium-sulfate heptahydrate investigated by quasi isothermal — quasi isobaric TG. — *Thermochimica Acta* 50 (1–3), pp. 105–110.
848. PAULIK, J., PAULIK, F., ARNOLD, M. 1982: Simultaneous TG, DTG, DTA and EGA technique for the determination of carbonate, sulphate, pyrite and organic materials in minerals, soils and rocks. Part I. Principles of the method. — *Journal of Thermal Analysis* 25 (2), pp. 327–340.
849. PAULIK, J., PAULIK, F., ARNOLD, M. 1986: Derivatograph-c. A microcomputer automated equipment for simultaneous TG, DTG, DTA, EGA and TD — *Thermochimica Acta* 107, pp. 375–378.
850. PAULIK, J., PAULIK, F., ARNOLD, M. 1987: The Derivatograph-c. A microcomputer-controlled simultaneous TG, DTG, DTA, TD and EGA apparatus. I. — *Journal of Thermal Analysis* 32 (1), pp. 301–309.
851. PAULIK, J., PAULIK, F., ARNOLD, M. 1988: Dependence of the thermal decomposition of  $\text{CuSO}_4 \cdot 5\text{H}_2\text{O}$  on the experimental conditions. — *Journal of Thermal Analysis* 34 (5–6), pp. 1455–1466.
852. PÉCSI DONÁTH, É. 1962: Investigation of the thermal decomposition of zeolites by the DTA method. — *Acta Geologica Hungarica* 6 (3–4), pp. 429–442.
853. PÉCSI DONÁTH, É. 1965: On the individual properties of some Hungarian zeolites. — *Acta Geologica Hungarica* 9 (3–4), pp. 234–257.
854. PÉCSI DONÁTH, É. 1966: On the relationships between lattice structural and “zeolite water” in gmelinite, heulandite and scolecite. — *Acta Mineralogica et Petrographica Universitatis Szegediensis* 17 (2), pp. 143–148.
855. PÉCSI-DONÁTH, É. 1968: Some contributions to the knowledge of zeolites. — *Acta Mineralogica et Petrographica, Universitatis Szegediensis* 18 (2), pp. 127–141.
856. PEKENC, E., SHARP, J. H. 1975: Quantitative mineralogical analysis of alunitic clays. — *Thermal Analysis Vol. 2. Proceedings of the fourth ICTA, Budapest*, pp. 585–597.
857. PELOVSKI, Y., PETKOVA, V. 1999: Investigation on thermal decomposition of pyrite: Part I. — *Journal of Thermal Analysis and Calorimetry* 56 (1), pp. 95–99.
858. PENG, C. J. 1955: Thermal analysis study of natrolite group. — *The American Mineralogist* 40 (9–10), pp. 834–856.
859. PÉREZ RODRIGUEZ, J. L., SÁNCHEZ SOTO, P. J. 1991: The influence of the dry grinding on the thermal behaviour of pyrophyllite. — *Journal of Thermal Analysis* 37 (7), pp. 1401–1413.
860. PÉREZ-RODRÍGUEZ, J. L., POYATO, J., JIMÉNEZ DE HARO, M. C., PÉREZ-MAQUEDA, L. A., LERF, A. 2004: Thermal decomposition of  $\text{NH}_4^+$ -vermiculite from Santa Olalla (Huelva, Spain) and its relation to the metal ion distribution in the octahedral sheet. — *Physics and Chemistry of Minerals* 31 (7), pp. 415–420.

861. PÉREZ-RODRÍGUEZ, J. L., FRANCO, F., RAMÍREZ-VALLE, V., PÉREZ-MAQUEDA, L. A. 2005: Modification of the thermal dehydroxylation of antigorite by ultrasound treatment. — *Journal of Thermal Analysis and Calorimetry* 82 (3), pp. 769–774.
862. PERIĆ, J., KRSTULOVIĆ, R., VUČAK, M. 1996: Investigation of dehydroxylation of gibbsite into boehmite by DSC analysis. — *Journal of Thermal Analysis* 46 (5), pp. 1339–1347.
863. PERLAKI, E., SZŐÖR, GY. 1973: The perlites of the Tokaj Mountains. — *Acta Geologica Hungarica* 17 (1–3), pp. 85–106.
864. PERSEIL, E. A., PINET, M. 1976: Contribution à la connaissance des romanéchites et des cryptomélanes — coronadites — hollandites. Traits essentiels et paragenèses. — *Contributions to Mineralogy and Petrology* 55 (2), pp. 191–204.
865. PETERS, TJ. 1961: Differenzialthermoanalyse von Vesuvian. — *Schweizerische Mineralogische und Petrographische Mitteilungen* 41 (2), pp. 325–334.
866. PETERS, TJ. 1963: Mineralogie und Petrographie des Totalserpentins bei Davos. — *Schweizerische Mineralogische und Petrographische Mitteilungen* 43 (2), pp. 529–685.
867. PETERSON, M. N. A. 1961: Expandable chloritic minerals from upper Mississippian carbonate rocks of the Cumberland plateau in Tennessee. — *The American Mineralogist* 46 (11–12), pp. 1245–1269.
868. PETRO, N. SH., GIRGIS, B. S. 1988: Dehydration kinetics of hydrated iron oxide from dynamic thermogravimetry. — *Journal of Thermal Analysis* 34 (1), pp. 37–45.
869. PETZOLD, D., NAUMANN, R. 1980: Thermoanalytische Untersuchungen zur Zersetzung von  $\text{MgCl}_2 \cdot 6\text{H}_2\text{O}$  unter quasiisobaren Bedingungen. — *Journal of Thermal Analysis* 19 (1), pp. 25–34.
870. PHADKE, A. V., APTE, A. 1997: Thermal behaviour of fibrous zeolites of the natrolite group. — *Journal of Thermal Analysis* 50 (3), pp. 473–486.
871. PHILLIPS, W. R. 1954: The differential thermal study of chlorites. — *Mineralogical Magazine* 33 (260), pp. 404–414.
872. PIÈCE, R. 1961: Analyse thermique différentielle et thermogravimétrie simultanées du gypse et de ses produits de déshydratation. — *Schweizerische Mineralogische Petrographische Mitteilungen* 41 (2), pp. 303–310.
873. PIGA, L. 1995: Thermogravimetry of a kaolinite-alunite ore. — *Thermochimica Acta* 265, pp. 177–187.
874. PIGA, L., VILLIERAS, F., YVON, J. 1992: Thermogravimetric analysis of a talc mixture. — *Thermochimica Acta* 211, pp. 155–162.
875. PLAS, L. VAN DER HÜGI, TH. 1961: A ferrian sodium-amphibole from Vals, Switzerland. — *Schweizerische Mineralogische und Petrographische Mitteilungen* 41 (2), pp. 371–393.
876. PLÖTZE, M., EMMERICH, K. 2004: EPR Studies of Copper Exchanged Smectite and the Behaviour upon Heating — *Proceedings of the Clay Minerals Society 41st Annual Meeting 2004 jun. 19–24. Richland, Washington*, 113 p.
877. POKOL, GY., GÁL, S. 1985: Description of the shape of thermoanalytical curves. Part I. Empirical parameters for the characterization of peaks in differential scanning calorimetry. — *Analytica Chimica Acta* 167, pp. 183–192.
878. POKOL, GY., VÁRHEGYI, G., VÁRADY, L. 1984: Studies on the kinetics of the gibbsite @ k-alumina reaction. — *Thermochimica Acta* 76 (1–2), pp. 237–247.
879. POKOL, GY., GÁL, S., PUNGOR, E. 1985: The application of empirical quantities describing the shape of thermoanalytical curves. — *Proceedings of the 8th ICTA, Thermochimica Acta*, pp. 89–92.
880. POKOL, G., HEVESI TÓTH, F., PÉTER, I., MADARÁSZ, J., KOCIS, T., GÁL, S. 1990: Description of the shape of Thermoanalytical curves. — *Journal of Thermal Analysis* 36 (5), pp. 1867–1888.
881. POST, J. E., HEANEY, P. J., HANSON, J. 2003: Synchrotron X-ray diffraction study of the structure and dehydration behavior of todorokite. — *The American Mineralogist* 88 (1), pp. 142–150.
882. POST, J. L., CUPP, B. L., MADSEN, F. T. 1997: Beidellite and associated clays from the DeLamar Mine and Florida Mountain area, Idaho. — *Clays and Clay Minerals* 45 (2), pp. 240–250.
883. POVONDRA, P., SLANSKY, E. 1966: Occurrence of gorceixite in argillized phonolites of Northwestern Bohemia. — *Acta Universitatis Carolinae — Geologica, Prague* 1, pp. 61–76.
884. POWELL, D. H., FISCHER, H. E., SKIPPER, N. T. 1998: The structure of interlayer water in Li-montmorillonite studied by neutron diffraction with isotopic substitution. — *Journal of Physical Chemistry B*, 102 (52), pp. 10899–10905.
885. PRASAD, S. V. S., SITAKARA RAO, V. 1984: Thermal transformation of iron (III) oxide hydrate gel. — *Journal of Materials Science* 19 (10), pp. 3266–3270.
886. PREISINGER, A. 1979: Neusiedlersee: The Limnology of a shallow lake in Central Europe. — *Monographie Biologicae* 37, pp. 131–138.
887. PREWITT-HOPKINS, J., FRONDEL, C. 1950: Thermal decomposition of zinc sulfide polymorphs. — *The American Mineralogist* 35 (1–2), p. 116.
888. PRIETO, A. C., LOBÓN, J. M., ALÍA, J. M., RULL, F., MARTIN, F. 1991: Thermal and spectroscopic analysis of natural trioctahedral chlorites — *Journal of Thermal Analysis* 37 (5), pp. 969–981.
889. PROUVOST, J. 1963: Etude des transformations de la bornite ( $\text{Cu}_5\text{FeS}_4$ ) par élévation de la température. — *Annales de la Société Géologique du Nord* 93 (2), pp. 143–144.
890. PUSZTASZERI, L. 1969: Etude pétrographique du massif du Chenaillet (Hautes-Alpes, France). — *Schweizerische Mineralogische und Petrographische Mitteilungen* 49 (3), pp. 425–466.
891. PYSIAK, J., PACEWSKA B. 1980: Thermal dissociation of basic aluminium ammonium sulfate in vacuum. Part I. Stages of decomposition. — *Journal of Thermal Analysis* 19 (1), pp. 79–88.
892. QUAKERNAAT, J. 1970: A new occurrence of a macrocrystalline form of saponite. — *Clay Minerals* 8 (4), pp. 491–493.
893. QUERALT, I., JULIÁ, R., PLANA, F., BISCHOFF, J. L. 1997: A hydrous Ca-bearing magnesium carbonate from playa lake sediments, Salinas Lake, Spain. — *The American Mineralogist* 82 (7–8), pp. 812–819.
894. QUIRK, J. P., MARCELI, A. S. 1997: The Application of double layer theories to the extensive crystalline swelling of Li-montmorillonite. — *Langmuir* 13 (23), pp. 6241–6248.
895. RAADE, G., MLADECK, M. H., KRISTIANSEN, R., DIN, V. K., 1984: Kaatjalaite, a new ferric arsenate mineral from Finland. — *The American Mineralogist* 69 (3–4), pp. 383–390.
896. RAHDEN, VON H. V. R., RAHDEN, VON M. J. E. 1972: Some aspects of the identification and characterization of 14 Å chlorites. — *Minerals Science and Engineering* 4 (3), pp. 43–66.

897. RANDALL, B. A. O. 1959: Stevensite from the Whine Skill in region of the North Tyne. — *Mineralogical Magazine* 32 (246), pp. 218–225.
898. RAUTUREAU, M., MIFSUD, A. 1977: Etude par microscope electronique des differents etats d'hydratation de la sepiolite. — *Clay Minerals* 12 (4), pp. 309–318.
899. RAZ, S., TESTENIERE, O., HECKER, A., WEINER, S., LUQUET, G. 2002: Stable amorphous calcium carbonate is the main component of the calcium storage. Structures of the Crustacean *Orchestia cavimana*. — *The Biological Bulletin* 203 (3), pp. 269–274.
900. REEUWIJK, VAN L. P. 1971: The dehydration of gismondite. — *The American Mineralogist* 56 (9–10), pp. 1655–1659.
901. REEUWIJK, VAN L. P. 1972: High temperature phases of zeolites of the natrolite group. — *The American Mineralogist* 57 (3–4), pp. 499–510.
902. REISZ, K., INCZÉDY, J. 1979: Investigation of complete oxidation of organic materials by means of derivatograph. — *Journal of Thermal Analysis* 16 (2), pp. 421–432.
903. REISZ, K., INCZÉDY, J. 1986: Thermoanalytical and thermogravimetric investigation of oil-shales. — *Journal of Thermal Analysis and Calorimetry* 31 (3), pp. 611–619.
904. RIESENKAMPF, W., ZABINSKI, W. 1975: Application of thermal analysis in the investigation of phase composition of some materials in the hydrometallurgy of zinc. — *Thermal Analysis III. Proceedings of the IV. ICTA, Budapest 1974*, pp. 647–655.
905. RIMSAITE, J. 1970: Structural formulae of oxidized and hydroxyl-deficient micas and decomposition of the hydroxyl group. — *Contributions to Mineralogy and Petrology* 25 (3), pp. 225–240.
906. RINCÓN, J. MA., ROMERO, M., HIDALGO, A., LIS, MA. J. 2004: Thermal behaviour and characterization of an iron aluminum arsenate mineral. — *Journal of Thermal Analysis and Calorimetry* 76 (3), pp. 903–911.
907. ROBERTSON, R. H. S., BRINDLEY, G. W., MACKENZIE, R. C. 1954: Mineralogy of kaolin clays from Pugu, Tanganyika. — *The American Mineralogist* 3 (1–2), pp. 118–139.
908. ROBIE, R. A., HEMINGWAY, B. S., FISHER, J. R. 1978: Thermodynamic properties of minerals and related substances at 298.15 K and 1 Bar (105 Pascals) pressure and at higher temperatures. — *Geological Survey Bulletin*, 456 p.
909. RODGERS, K. A., CURRIE, S. 2000: A thermal analytical study of some modern and fossil resins from New Zealand. — *Thermochimica Acta* 326 (1–2), pp. 143–149.
910. RODGERS, K. A., HENDERSON, G. S. 1986: The thermochemistry of some iron phosphate minerals: vivianite, metavivianite, baracite, ludlamite and vivianite/metavivianite admixtures. — *Thermochimica Acta* 104, pp. 1–12.
911. ROGHI, G., RAGAZZI, E., GIANOLLA, P. 2006: Triassic amber of the Southern Alps (Italy). — *Palaios* 21 (2), pp. 143–154.
912. ROSEBOOM, E. JR. 1966: An investigation of the system Cu-S and some natural copper sulfides between 25 and 700 °C. — *Economic Geology* 61 (4), pp. 641–672.
913. ROSS, G. J., KODAMA, H. 1967: Properties of a synthetic magnesium-aluminum carbonate hydroxide and its relation ship to magnesium-aluminum double hydroxide, manasseite and hydrotalcite. — *The American Mineralogist* 52, pp. 1036–1047.
914. ROSS, G. J., KODAMA, H. 1974: Experimental transformation of chlorite into vermiculite. — *Clays and Clay Minerals* 22 (3), pp. 205–211.
915. ROSSMAN, G. R. 1996: Studies of OH in nominally anhydrous minerals. — *Physics and Chemistry of Minerals* 23 (4–5), pp. 299–304.
916. ROSSMAN, G. R., AINES, R. D. 1991: The hydrous components in garnets: Grossular-hydrogrossular. — *The American Mineralogist* 76 (7–8), pp. 1153–1164.
917. ROUQUEROL, J. 1970: L'analyse Thermique a vitesse de decomposition constante. — *Journal of Thermal Analysis* 2 (2), pp. 123–140.
918. ROUQUEROL, J. 1973: Critical examination of several problems typically found in the kinetic study of thermal decomposition under vacuum. — *Journal of Thermal Analysis* 5 (2–3), pp. 203–216.
919. ROUQUEROL, J., GANTEAUME, M. 1977: Thermolysis under vacuum: Essential influence of the residual pressure on thermoanalytical curves and the reaction products. — *Journal of Thermal Analysis* 11 (2), pp. 211–219.
920. ROUQUEROL, J., BORDÈRE, S., ROQUEROL, F. 1990: Kinetic study of mineral reactions by means of controlled transformation rate thermal analysis (CRTA). — In: Application of Thermal Analysis in Mineral Technology. — In: SMYKATZ-KLOSS, W., WARNE, S. ST. J. (eds): *Thermal Analysis in the Geosciences. Series of Lecture Notes in Earth*. Springer Verlag, pp. 134–151.
921. ROUSSET, A., CLERC, L., VAJEI, A.C., GILLOT, B. 1987: Thermoanalytical studies on cation distribution in submicronic titanomagnetites. — *Journal of Thermal Analysis* 32 (3), pp. 845–855.
922. ROWLAND, R. A., JONAS, E. C. 1949: Variations in differential thermal analysis curves of siderite. — *The American Mineralogist* 34 (7–8), pp. 550–558.
923. ROWLAND, R. A., LEWIS, D. R. 1951: Furnace atmosphere control in differential thermal analysis. — *The American Mineralogist* 36 (1–2), pp. 80–91.
924. ROY, D. M., MUMPTON, F. A. 1956: Stability of minerals in the system ZnO–SiO<sub>2</sub>–H<sub>2</sub>O. — *Economic Geology* 51 (5), pp. 432–443.
925. ROY, D. M., ROY, R. 1954: An experimental study of the formation and properties of synthetic serpentines and related layer silicate minerals. — *The American Mineralogist* 39 (11–12), pp. 957–975.
926. ROY, P. D., SINHA, R., SMYKATZ-KLOSS, W. 2001: Mineralogy and geochemistry of the evaporitic crust from the hypersaline Sambhar Lake playa, Thar Desert, India. — *Chemie der Erde – Geochemistry* 61 (4), pp. 241–253.
927. RUAN, H. D., GILKES, R. J. 1995: Dehydroxylation of aluminous goethite: unit cell dimensions, crystal size and surface area. — *Clays and Clay Minerals* 43 (2), pp. 196–211.
928. RUAN, H. D., GILKES, R. J. 1996: Kinetics of thermal dehydroxylation of aluminous goethite. — *Journal of Thermal Analysis* 46 (5), pp. 1223–1238.
929. RUE, J. W., OTT, W. R. 1974: Scanning electron microscopic interpretation of the thermal analysis of kaolinite. — *Journal of Thermal Analysis* 6 (4), pp. 513–519.
930. RUIZ, R., DEL MORAL, J. C., PESQUERA, C., BENITO, I., GONZÁLEZ, F. 1996: Reversible folding in sepiolite: study by thermal and textural analysis. — *Thermochimica Acta* 279 (1–2), pp. 103–110.
931. RULE, A. C., RADKE, F. 1988: Baileychlorite, the Zn end member of the trioctahedral chlorite series. — *The American Mineralogist* 73 (1–2), pp. 135–139.

932. RUNKEL, R. L., BENCALA, K. E. 1995: — Chapter 5: Transport of reacting solutes in rivers and streams. — In: SINGH, V. P. (ed.): *Environmental Hydrology*. Dordrecht, The Netherlands, Kluwer Academic Publishers, pp. 137–164.
933. RUSSEL, J. D. 1979: Infrared spectroscopy of ferrihydrites: Evidence for the presence of structural hydroxyl groups. — *Clay Minerals* 14 (2), pp. 109–114.
934. RYKL, D., PECHAR, F. 1991: Thermal decomposition of natural phillipsite. — *Zeolites* 11 (7), pp. 680–683.
935. SABATIER, G. 1950: Influence of particle size on differential thermal analysis curves of chlorites. — *Bulletin de la Société Française de Minéralogie et de Cristallographie* 73 (1–3), pp. 43–48.
936. SABATIER, G. 1956: Analyse thermique différentielle de quelques sulfures. — *Bulletin de la Société Française de Minéralogie et de Cristallographie* 79 (1–3), pp. 172–174.
937. SAIZ-DÍAZ, C. I., ESCAMILLA-ROA, E., HERNÁNDEZ-LAGUNA, A. 2005: Quantum mechanical calculations of trans-vacant and cis-vacant polymorphous in dioctahedral 2:1 silicates. — *The American Mineralogist* 90 (11–12), pp. 1827–1834.
938. SAKURAI, K., HAYASHI, A. 1952: “Yugawaralite,” a new zeolite. — *Scientific Reports of the Yokohama National University Sect. II*, 1, pp. 69–77.
939. SAKURAI, K., HAYASHI, A. 1962: card A-0534 — In: MACKENZIE, R. C. 1962: *Scifax Differential Thermal Data Index*. Cleaver-Hume Press, London.
940. SAMTANI, M., DOLLIMORE, D., ALEXANDER, K. 2001: Thermal decomposition of dolomite in an Atmosphere of Carbon Dioxide: The effect of procedural variables in thermal analysis. — *Journal of Thermal Analysis and Calorimetry* 65 (1), pp. 93–101.
941. SÁNCHEZ-SOTO, P. J., PÉREZ-RODRÍGUEZ, J. L., 1989a: Formation of mullite from pyrophyllite by mechanical and thermal treatments. — *Journal of the American Ceramic Society* 72 (1), pp. 154–157.
942. SÁNCHEZ-SOTO, P. J., PÉREZ-RODRÍGUEZ, J. L., 1989b: Thermal analysis of pyrophyllite transformations. — *Thermochimica Acta* 138 (2), pp. 267–276.
943. SÁNCHEZ-SOTO, P. J., SOBRADOS, I., SANZ, J., PÉREZ-RODRÍGUEZ, J. L. 1993: 29-Si and 27-Al magic-angle spinning nuclear magnetic resonance study of the thermal transformations of pyrophyllite. — *Journal of the American Ceramic Society* 76 (12), pp. 3024–3028.
944. SÁNCHEZ-SOTO, P. J., JUSTO, A., PÉREZ-RODRÍGUEZ, J. L. 1994: Grinding effect on kaolinite-pyrophyllite-illite natural mixtures and its influence on mullite formation. — *Journal of Materials Science* 29 (5), pp. 1276–1283.
945. SÁNCHEZ-SOTO, P. J., PÉREZ-RODRÍGUEZ, J. L., SOBRADOS, I., SANZ, J. 1997: Influence of grinding in pyrophyllite-mullite thermal transformation assessed by <sup>29</sup>Si and <sup>27</sup>Al MAS NMR spectroscopies. — *Chemistry of Materials* 9 (3) pp. 677–684.
946. SANDERS, J. P., GALLAGHER, P. K. 2003a: Kinetics of the oxidation of magnetite using simultaneous TG/DSC. — *Journal of Thermal Analysis and Calorimetry* 72 (3), pp. 777–789.
947. SANDERS, J. P., GALLAGHER, P. K. 2003b: Thermomagnetometric evidence of  $\alpha$ -Fe<sub>2</sub>O<sub>3</sub> as an intermediate in the oxidation of magnetite. — *Thermochimica Acta* 406 (1–2), pp. 241–243.
948. SARDA, C. MATHIEU, F., VAJPEL, A. C., ROUSSET, A. 1987: Size- and surface-dependence of enthalpy of oxidation of submicronic magnetites. — *Journal of Thermal Analysis* 32 (3), pp. 865–871.
949. SASVÁRI, K., HEGEDŰS, A. J. 1955: Röntgen- und thermoanalytischen Beitrag zum thermischen Abbau von Aluminiumoxyhydraten. — *Naturwissenschaften* 42 (9), pp. 254–256.
950. SASVÁRI, K., ZALAI, A. 1957: The crystal structure and thermal decomposition of alumina and alumina hydrates as regarded from the point of view of lattice geometry. — *Acta Geologica Hungarica* 4 (3–4), pp. 415–466.
951. SATO, H., ONO, K., JOHNSTON, C. T., YAMAGISHI, A. 2004: First-principle study of polytype structures of 1:1 dioctahedral phyllosilicates. — *The American Mineralogist* 89 (11–12), pp. 1581–1585.
952. SATO, M., OINUMA, K., KOBAYASHI, K. 1965: Interstratified mineral of illite and montmorillonite. — *Nature* 208 (5006), pp. 179–180.
953. SATO, T. 1986: Thermal transformation of aluminum hydroxides to aluminas. — *Shizuoka Daigaku Kogakubu Kenkyu Hokoku (Report of the Faculty of Engineering, Shizuoka University)* 37, pp. 9–16.
954. SATO, T. 1987: Thermal decomposition of aluminium hydroxides. — *Journal of Thermal Analysis* 32 (1), pp. 61–70.
955. SCHEFFER, F., WELTE, E., LUDWIG, F. 1957: Zur Frage der Eisenoxidhydrate im Boden. — *Chemie der Erde* 19 (1), pp. 51–56.
956. SCHELZ, J. P. 1974: The detection of chrysotile asbestos at low levels in talc by differential thermal analysis. — *Thermochimica Acta* 8 (1–2), pp. 197–204.
957. SCHELZ, J. P. 1976: The detection of quartz in clay minerals by differential thermal analysis — *Thermochimica Acta* 15 (1), pp. 17–28.
958. SCHMIDT, C. M., HEIDE, K. 2001: Thermal Analysis of Hydrocarbons in Paleozoic Black Shales. — *Journal of Thermal Analysis and Calorimetry* 64 (3), pp. 1297–1302.
959. SCHMIDT, E. R., HEYSTEK, S. B. 1953: Saponite from Krugersdorp District, Transvaal. — *Mineralogical Magazine* 30 (222), pp. 201–210.
960. SCHMIDT, E. R., VERMAAS, F. H. S. 1955: Differential thermal analysis and cell dimensions of some natural magnetites. — *The American Mineralogist* 40 (5–6), pp. 422–431.
961. SCHOMBURG, J. 1982: Kombinierte thermische Untersuchungen an eisenarmen trioktaedrischen Chloritmineralen. — *Proceedings of the Ninth Conference on Clay Mineralogy and Petrology Zvolen*, pp. 159–166.
962. SCHOMBURG, J. 1984: Kombinierte thermoanalytische Untersuchungen an Muskovit-Montmorillonit-Wechselagerungsmineralen (Combined thermoanalytical investigations of mixed-layers of muscovite-montmorillonite). — *Zeitschrift für Geologische Wissenschaften, Berlin* 12 (4), pp. 457–468.
963. SCHOMBURG, J. 1985: Thermal investigations of pyrophyllites. — *Thermochimica Acta* 93, pp. 521–524.
964. SCHOMBURG, J. 1986: Zur Systematik thermischer Umwandlungsprozesse von Tonmineralstoffen. — *Zeitschrift für Angewandte Geologie* 32 (9), pp. 231–233.
965. SCHOMBURG, J. 1987: Kombinierte thermische Untersuchungen an eisenarmen trioktaedrischen Chloritmineralen. — *Chemie der Erde* 46 (3–4), pp. 337–344.
966. SCHOMBURG, J. 1988: Trioctahedral smectite — results of thermal studies. — *Proceedings of the tenth Conference on Clay Mineralogy and Petrology Ostrava 1986*, pp. 343–349.

967. SCHOMBURG, J. 1991: Thermal investigations in Technical Mineralogy. — In: SMYKATZ-KLOSS, W., WARNE, S. ST. J. (eds): *Thermal Analysis in the Geosciences*. Series of Lecture Notes in Earth. Springer Verlag, pp. 224–232.
968. SCHOMBURG, J., STÖRR, M. 1978: Kombinierte thermische Analyse an Dreischichttonmineralen. — *Thermochimica Acta* 25 (3), pp. 313–324.
969. SCHOMBURG, J., ZWAHR, H. 1997: Thermal differential diagnosis of mica mineral group. — *Journal of Thermal Analysis* 48 (1), pp. 135–139.
970. SCHÜLLER, K. H. 1968: Mineralogische und chemische Untersuchungen am Göpfersgrüner Spechstein. — *Neues Jahrbuch für Mineralogie, Monatshefte* 10, pp. 363–376.
971. SCHULTZ, L. G. 1969: Lithium and potassium absorption, dehydroxylation temperature and structural water content of aluminous smectites. — *Clays and Clay Minerals* 17 (3), pp. 137–150.
972. SCHULTZE, D., STEINKE, U., KUSSIN, J., KRETZSCHMAR, U. 1995: Thermal oxidation of ZnS modifications sphalerite and wurtzite. — *Crystal research and technology* 30 (4), pp. 553–558.
973. SCHWANDER, H., HUNZIKER, J. C., STERN, W. 1968: Zur Mineralchemie von Hellglimmern in den Tessiner Alpen. — *Schweizerische Mineralogische und Petrographische Mitteilungen* 48 (2), pp. 357–390.
974. SCHWERTMANN, U. 1984: The double dehydroxylation peak of goethite. — *Thermochimica Acta* 78, pp. 39–46.
975. SCHWERTMANN, U., CORNELL, R. M. 2000: *Iron oxides in the laboratory. Preparation and characterization*. — Wiley-VCH. Weinheim, New York, Chichester, Brisbane, Singapore, Toronto, 188 p.
976. SCHWERTMANN, U., FISCHER, W. R. 1973: Natural “amorphous” ferric hydroxide. — *Geoderma* 10 (3), pp. 237–247.
977. SCORDARI, F., MILELLA, G. 1982: Metasideronatrite: a mixture of coexisting compounds. — *Neues Jahrbuch für Mineralogie, Monatshefte* 6, pp. 255–264.
978. SEGUIN, M. K. 1972: Study of the stability of  $\text{MnCO}_3$  in inert atmospheres and in air. — *The American Mineralogist* 57 (3–4), pp. 511–523.
979. SEILLER, W. 1970: Zur Frage der quantitativen Differentialthermoanalyse Cristobalithaltiger Staubproben. — *Journal of Thermal Analysis* 2 (3), pp. 251–257.
980. SELMECZI, B. 1970: Determination of pyrite and calcite side by side by derivatograph. — *Hungarian Journal of Chemistry (Magyar kémiai Folyóirat)* 76 (9), pp. 472–477. (in Hungarian)
981. SELMECZI, B. 1971: Application of the derivatograph in rock analysis. — *Hungarian Scientific Instruments* 21, pp. 39–52.
982. SERNA, C. J., AHLDRICH, J. L., SERRATOSA, J. M. 1975: Folding in sepiolite crystals. — *Clays and Clay Minerals* 23 (6), pp. 452–457.
983. SERNA, C. J., VAN SCOYOC, G. E., AHLDRICH, J. L. 1977: Hydroxyl groups and water in palygorskite. — *The American Mineralogist* 62 (7–8), pp. 784–792.
984. SHADID, K. A., GLASSER, F.P. 1970: Thermal properties of trydimite 25 °C – 300 °C. — *Journal of Thermal Analysis* 2 (2), pp. 181–190.
985. SHARP, J. H., WILBURN, F. W., MCINTOSH, R. M. 1991: The effect of procedural variables on TG, DTG and DTA curves of magnesite and dolomite. — *Journal of Thermal Analysis* 37 (9), pp. 2021–2029.
986. SHAYAN, A. 1984a: Strontium in huntites from Geelong and Deer Park, Victoria, Australia. — *The American Mineralogist* 69 (5–6), pp. 528–530.
987. SHAYAN, A. 1984b: Hisingerite material from a basalt quarry near Geelong, Victoria, Australia. — *Clays and Clay Minerals* 32 (4), pp. 272–278.
988. SHIMODA, S., SUDO, T., OINUMA, K. 1969: Differential thermal analysis of mica clays. — *Proceedings of the International Clay Conference, 1969. Sept. 5–10. (Tokyo)*, I, pp. 197–206.
989. SHIROZU, H. 1962: Thermal reaction of iron chlorites. — *Clay Science, (Society of Japan)* 1 (5), pp. 108–112.
990. SHKODIN, V. G., ABISHEV, D. N., KOBZHASOV, A. K., MALYSHEV, V. P., MANGUTOVA, R. F. 1978: The question of thermal decomposition of pyrite. — *Journal of Thermal Analysis* 13 (1), pp. 49–53.
991. SHLYAPKINA, E. N. 1978: Quantitative thermogravimetry of multicomponent zeolite-bearing rocks. — *Journal of Thermal Analysis* 13 (3), pp. 553–561.
992. SHOVAL, S., YOFE, O., NATHAN, Y., 2003: Distinguishing between natural and recarbonated calcite in oil shale ashes. — *Journal of Thermal Analysis and Calorimetry* 71 (3), pp. 883–892.
993. SHUALI, U., YARIV, S., STEINBERG, M., MULLER VONMOOS, M., KAHR, G., RUB, A. 1988: Thermal analysis study of the adsorption of  $\text{D}_2\text{O}$  by sepiolite and palygorskite. — *Thermochimica Acta* 135, pp. 291–297.
994. SIDDIQUI, M. K. H. 1967: Palygorskite clays from Andhra Pradesh, India. — *Clay Minerals* 7 (1), pp. 120–123.
995. SIEVERT, CH. 2004: Rapid screening of soil properties using thermogravimetry. — *Soil Science Society of American Journal* 68 (5), pp. 1656–1661.
996. SILEO E. E., RAMOS A. Y., MAGAZ G. E., BLES A. M. A. 2004: Long-range vs. short-range ordering in synthetic Cr-substituted goethites. — *Geochimica and Cosmochimica Acta* 68 (14), pp. 3053–3063.
997. SINGH, B., MERRINGTON, G., WILSON, M. J., KURODA, W. J. B., FRASER, A. R., MERRINGTON, G. 1999: Mineralogy and chemistry of ochre sediments from an acid mine drainage disused mine in Cornwall, UK. — *Clay Minerals* 34 (2), pp. 301–317.
998. SINHA, R., SMYKATZ-KLOSS, W. 2003: Thermal characterisation of lacustrine dolomites from the Sambhar Lake playa, Thar desert, India. — *Journal of Thermal Analysis and Calorimetry* 71 (3), pp. 739–750.
999. SLOVENEC, D., HALLE, R. 1979: Unusual thermal behaviour of biotites Mt. Papuk. — *Journal of Thermal Analysis* 17 (1), pp. 177–179.
1000. SMYKATZ-KLOSS, W. 1964: Differential Thermo-Analysen von einigen Karbonat-Mineralen. — *Beiträge zur Mineralogie und Petrographie* 9 (5), pp. 481–502.
1001. SMYKATZ-KLOSS, W. 1966: Sedimentpetrographische und geochemische Untersuchungen an Karbonatgesteinen des Zechsteins. Teil I: Methodischer Teil. — *Contributions to Mineralogy and Petrology* 13 (3), pp. 207–231.
1002. SMYKATZ-KLOSS, W. 1969: Über die Genese der Quarze von Dietlingen in Baden und von Suttrop in Westfalen. — *Neues Jahrbuch für Mineralogie, Monatshefte* 12, pp. 563–567.

1003. SMYKATZ-KLOSS, W. 1970: Die Hoch-Tiefquarz-Inversion als petrologisches Hilfsmittel. — *Contributions to Mineralogy and Petrology* 26 (1), pp. 20–41.
1004. SMYKATZ-KLOSS, W. 1971: Petrologische Anwendung der Inversionstemperatur-Bestimmung von Quarzen. — *Thermal Analysis. Vol. 3. Proceedings of the III. ICTA, Davos 1971*, pp. 637–648.
1005. SMYKATZ-KLOSS, W. 1972: Das Hoch-Tief-Umwandungsverhalten mikrokristalliner Quarzen. — *Contributions to Mineralogy and Petrology* 36 (1), pp. 1–18.
1006. SMYKATZ-KLOSS, W. 1974a: *Differential thermal Analysis. Application and Results in Mineralogy*. — Springer Verlag, Berlin – Heidelberg – New York, 185 p.
1007. SMYKATZ-KLOSS, W. 1974b: The determination of the degree of (dis)order of kaolinite by means of DTA. — *Chemie der Erde* 33 (4), pp. 358–364.
1008. SMYKATZ-KLOSS, W. 1975: DTA as a tool for the measurement of disorder in kaolinites and for the classification of montmorillonites. — *Thermal Analysis. Vol. 2. Proceedings of the fourth ICTA, 1974. Budapest*, pp. 561–567.
1009. SMYKATZ-KLOSS, W. 1982: Application of differential thermal analysis in mineralogy. — *Journal of Thermal Analysis* 23 (1–2), pp. 15–44.
1010. SMYKATZ-KLOSS, W. 2002: Differential Thermal Analysis of Mg-bearing carbonates and sheet silicates. — *Journal of Thermal Analysis and Calorimetry* 69 (1), pp. 85–92.
1011. SMYKATZ-KLOSS, W., HAUSMANN, K. 1993: Differential Thermal Analysis of polymorphic copper and silver sulfides. — *Journal of Thermal Analysis* 39 (8–9), pp. 1209–1232.
1012. SMYKATZ-KLOSS, W., HEIDE, K. 1988: Progress of Thermal-Analysis in earth Sciences. — *Journal of Thermal Analysis* 33 (4), pp. 1253–1257.
1013. SMYKATZ-KLOSS, W., KLINKE, W. 1997: The high-low quartz inversion. Key to the petrogenesis of quartz-bearing rocks. — *Journal of Thermal Analysis* 48 (1), pp. 19–38.
1014. SMYKATZ-KLOSS, W., ISTRATE, G., HÖTZL, H., KÖSSL, H. 1985: Vorkommen und Entstehung von Bassanit,  $\text{CaSO}_4 \cdot 1/2\text{H}_2\text{O}$ , im Gipskarstgebiet von Fom Tathouine, Südtunesien. — *Chemie der Erde – Geochemistry* 44 (1), pp. 67–77.
1015. SMYKATZ-KLOSS, W., HEIDE, K., KLINKE, W. 2003: Chapter 11. Applications of the thermal methods in the Geosciences. — In: BROWN M. E., GALLAGHER, P. K. (eds): *Handbook of thermal analysis and calorimetry, Vol. 2*. — Elsevier, pp. 451–593.
1016. SOKOLOVA, L. A. 1967: Šabazit (fakolit) iz Baženovskogo mestoroždeniâshrizotil-azbesta. — In: PETROV, V. P. (ed.) 1967: *Vodnye vulkaničeskie stekla i post vulkaničeskie mineraly*. Nauka, Moskow, pp. 151–157.
1017. ŠOLC, Z., TROJAN, M., BRANDOVÁ, D., KUCHLER, M. 1988: A study of thermal preparation of iron (III) pigments by means of thermal analysis methods. — *Journal of Thermal Analysis* 33 (2), pp. 463–469.
1018. SOLYMÁR, K., KENYERES-SÜKE, S. 1970: Recent results in derivatographic phase analysis of bauxites and red muds. — *Proceedings of the III. Analytical Chemical Conference, Budapest*, pp. 401–409.
1019. SREBRODOL'SKII, V. I. 1974: On the problem of alumohydrocalcites. (Ob alûmogidrocal'citah). — *Izvestiya Akademii Nauk SSSR, Seria Geologicheskaja* 10, pp. 88–96.
1020. SRODON, J. 1984: X-ray powder diffraction identification of illitic materials. — *Clays and Clay Minerals* 32 (5), pp. 337–349.
1021. SRODON, J., ELSASS, F., MCHARDY, W. J., MORGAN, D. J. 1992: Chemistry of illite-smectite inferred from TEM measurements of fundamental particles. — *Clay Minerals* 27 (2), pp. 137–158.
1022. STADLER, H. A. 1964: Petrographische und mineralogische Untersuchungen im Grimselgebiet. — *Schweizerische Mineralogische Petrographische Mitteilungen* 44 (1), pp. 187–399.
1023. STADLER, M., SCHINDLER, P.W. 1993: Modeling of  $\text{H}^+$  and  $\text{Cu}^{2+}$  adsorption on calcium-montmorillonite — *Clays and Clay Minerals* 41 (3), pp. 288–296.
1024. STÄHL, ARTIOLI, G., HANSON, J. C. 1996: The dehydration process in the zeolite laumontite: a real-time synchrotron X-ray powder diffraction study. — *Physics and Chemistry of Minerals* 23 (6), pp. 328–336.
1025. STELZNER, T., HEIDE, K. 1996: Study of weathering products of meteorites by means of evolved gas analysis. — *Meteoritic and Planetary Science* 31 (2), pp. 249–254.
1026. STEVENS, S. J., HAND, R. J., SHARP, J. H. 1997: Temperature dependence of the cristobalite  $\alpha$ - $\beta$  inversion. — *Journal of Thermal Analysis* 49 (3), pp. 1409–1415.
1027. STOCH, L. 1984: Significance of structural factors in dehydroxylation of kaolinite polytypes. — *Journal of Thermal Analysis* 29 (5), pp. 919–931.
1028. STOCH, L. 1991: Internal thermal reactions of minerals. — In: SMYKATZ-KLOSS, W., WARNE, S. St. J. (eds): *Thermal Analysis in the Geosciences. Series of Lecture Notes in Earth Sciences* 38. Springer Verlag, pp. 118–133.
1029. STOCH, L., WACLAWSKA, I. 1981a: Dehydroxylation of kaolinite group minerals. I. Kinetics of dehydroxylation of kaolinite and halloysite. — *Journal of Thermal Analysis* 20 (2), pp. 291–304.
1030. STOCH, L., WACLAWSKA, I. 1981b: Dehydroxylation of kaolinite group minerals. II. Kinetics of dickite dehydroxylation. — *Journal of Thermal Analysis* 20 (2), pp. 305–310.
1031. STOCH, L., ŁACZKA, M., WACLAWSKA, I. 1985: DTA and x-ray diffraction study of the phase transformation of silica minerals. — *Thermochimica Acta* 93, pp. 533–536.
1032. STRACZEK, J. A., HOREN, A., ROSS, M., WARSHAW, E. M. 1960: Studies of the manganese oxides: IV. todorokite. — *The American Mineralogist* 45 (11–12), pp. 1174–1184.
1033. STRASZKO, J., OLSZAK-HUMIENIK, M., MOŹEJKO, J. 1997: The kinetic parameters of thermal decomposition hydrated iron sulphate. — *Journal of Thermal Analysis* 48 (6), pp. 1415–1422.
1034. STRAWN, D. G., PALMER, N. E., FURNARE, L. C., GOODELL, C., AMONETTE, J. E., KUKKADAPU, R. K. 2004: Copper sorption mechanisms on smectites. — *Clays and Clay Minerals* 52 (3), pp. 321–333.
1035. ŠTRBAC, N., ŽIVKOVIC, Z., ŽIVKOVIC, D., MIHAJLOVIĆ, I., VELINOVSKI, V. 2002: Thermal analysis of the copper sulfide minerals oxidation process. — *Proceedings of the 34th International October Conference on Mining and Metallurgy; Bor Lake; Yugoslavia; 30 Sept. – 3 Oct. 2002*, pp. 389–395.

1036. STRUNZ, H., TENNYSON, C. 1982: *Mineralogical Tables*. — Akademische Verlagsgesellschaft Geest & Portig K.-G., 621 p.
1037. STRUNZ, H., NICKEL, E. H. 2001: Tectosilicates with Zeolitic H<sub>2</sub>O; Zeolite Family. — In: *Strunz Mineralogical Table*. Chemical-Structural Mineral Classification System. Ninth Edition — Schweizerbart'sche Verlagsbuchhandlung, Stuttgart pp. 701–712.
1038. ŠUBRT, J., HANOUSEK, F., ZAPLETAL, V., LIPKA, J., HUCL, M. 1981: Dehydration of synthetic lepidocrocite (̑-FeOOH). — *Journal of Thermal Analysis* 20 (1), pp. 61–69.
1039. ŠUBRT, J., VINŠ, J., ZAPLETAL, V., BALEK, V., ŠAPLYGIN, I. S. 1988: Reactivity of finely dispersed iron (III) oxides and oxide hydroxides in solid-state reactions. — *Journal of Thermal Analysis* 33 (2), pp. 455–461.
1040. SUDO, T. 1954: Iron-rich saponite found from tertiary iron sand beds of Japan. (Reexamination on “Lembergite”). — *Journal of the Geological Society of Japan, (Tokyo)* 60 (700), pp. 18–27.
1041. SUDO, T., NAKAMURA, T. 1952: Hisingerite from Japan. — *The American Mineralogist* 37 (7–8), pp. 618–621.
1042. SUDO, T., SHIMODA, S. 1970: Interstratified Phyllosilicates. — In: MACKENZIE, R. C. (ed.): *Differential Thermal Analysis*. Academic Press. London – New York 539–551.
1043. SUDO, T., SHIMODA, S., NISHIGAKI, S., AOKI, M. 1966: Energy changes in dehydration processes of clay minerals. — *Clay Minerals* 7 (1), pp. 33–42.
1044. SUGAKI, A., KITAKAZE, A. 1998: High form of pentlandite and its thermal stability. — *The American Mineralogist* 83 (1–2), pp. 133–140.
1045. SUQUET, H., MALARD, C., QUARTON, M., DUBERNAT, J., PEZERAT, H. 1984: Etude du biopyribole forme par chauffage des vermiculites magnésiennes. — *Clays and Clay Minerals* 19 (2), pp. 217–227.
1046. SUTTON, R., SPOSITO, G. 2001: Molecular simulation of interlayer structure and dynamics of 12.4 Å Cs-smectite hydrates. — *Journal of Colloid and Interface Science* 237 (2), pp. 174–184.
1047. SUTTON, R., SPOSITO, G. 2002: Animated molecular dynamics simulations of hydrated caesium-smectite interlayers. — *Geochemical Transactions* 3 (9), pp. 73–80.
1048. SWAMY, M. S. R., PRASAD, T. P. 1982: Thermal decomposition of iron(II) sulphate heptahydrate in the presence of alkali metal carbonates. — *Journal of Thermal Analysis* 25 (2), pp. 347–354.
1049. SZAKÁLL, S., FÖLDVÁRI, M. 1995: New minerals of Hungary III. Ferro-axinite and chrysocolla from Miskolc-Lillafüred (Bükk Mts.). — *Bulletin of the Hungarian Geological Society* 125 (3–4), pp. 433–442. (in Hungarian)
1050. SZAKÁLL, S., FÖLDVÁRI, M., KOVÁCS, Á. 1994: Phosphate minerals from Recsk and Paráđ-Parádfüřdő ore deposits. (N-Hungary) — *Folia Historico Naturalia Musei Matraensis* 19, pp. 23–36. (in Hungarian)
1051. SZAKÁLL, S., FÖLDVÁRI, M., PAPP, G., KOVÁCS-PÁLFFY, P., KOVÁCS, Á. 1997: Secondary Sulphate Minerals from Hungary. — *Acta Mineralogica et Petrographica Szegediensis* 38 (Supplementum), pp. 7–63.
1052. SZAKÁLL S., FÖLDVÁRI M., KOVÁCS-PÁLFFY P. 2000: Kankite from Nagyörzsöny, Börzsöny Mts., a new mineral for Hungary. — *Acta Mineralogica-Petrographica, Szeged XLI, Supplementum*. p. 103
1053. SZEGEDI, Á. 1988: Mixed layer character of “illites” from Füžéradvány, Hungary. — In: KONTA J. (ed.): *Proceedings of the tenth Conference of Clay Mineralogy and Petrology 1986 August 26–29, Ostrava*. — Praha, Univerzita Karlova, pp. 249–254.
1054. SZENTPÉTERY, I., FÖLDVÁRI, M., FARKAS, L. 1989: Occurrence of gorceixite in Hungary. — *Bulletin of the Hungarian Geological Society* 119 (2), pp. 167–172. (in Hungarian)
1055. SZÖÖR, GY. 1971a: Possibilities of facies indication through physical and chemical analyses of mollusc shells. — *Acta Geographica Debrecina* 15–16, pp. 73–83.
1056. SZÖÖR GY. 1971b: The instrumental analysis of modern vertebrate tooth as fossil model material. — *Acta Mineralogica et Petrographica Szegediensis* 20 (1), pp. 149–167.
1057. SZÖÖR GY. 1972: Analysis of Molluscan shells by the derivatographic fingerprint method. — *Geologica Carpathica* 23 (1), pp. 15–38.
1058. SZÖÖR GY. 1975: Sedimental correlations. A possibility for the determination of relative chronology on the basis of the thermoanalytic (derivatograph) investigation of the organic material content of fossils. — *Acta Mineralogica et Petrographica Szegediensis* 22 (1), pp. 67–71.
1059. SZÖÖR GY. 1978: Thermogravimetric examination of soils for soil mechanical and construction-geological application. — *Bulletin of the Hungarian Geological Society* 108 (4), pp. 577–581. (in Hungarian)
1060. SZÖÖR GY. 1981: Age determination of Quarternary and Pliocene Terrestrial Strata in Hungary by a thermoanalytical method. — *Hungarian Symposium on Thermal Analysis Budapest, Abstracts* p. 89.
1061. SZÖÖR GY. 1982: Chronostratigraphic interpretation of Hungarian karstic Quarternary and Pliocene vertebrata finds. — *Bulletin of the Hungarian Geological Society* 112 (1), pp. 1–18.
1062. SZÖÖR GY. 1982: Fossil age-determination by thermal-analysis. — *Journal of Thermal Analysis* 23 (1–2), pp. 83–91.
1063. SZÖÖR GY. 1983: Comparative derivatographic analysis, chronological and taxonomic evaluation of the malacological material of pannonian localities. — *Acta Geographica Debrecina, Communications from the department of mineralogy and geology of Lajos Kossuth University* 21 (49), pp. 121–134.
1064. SZÖÖR GY., BOHÁTKA S. 1985: Derivatograph-Qms System in Geochemical Research. — *Thermochimica Acta* 92, pp. 395–398.
1065. SZPILA, K., WIEWIORA, A., GADOMSKI, M. 1972: Preliminary Investigation of Kaolinite-Smectite from Jęglowa, Lower Silesia. — *Bulletin de l'Académie Polonaise des Sciences. Serie des Sciences de la Terre* 20 (1), pp. 19–24.
1066. TABOADELA, M., FERRANDIS, V. A. 1957: The mica minerals. — In: MACKENZIE, R. C. (ed.) 1957: *The differential thermal investigation of clays*. Mineralogical Society, London, pp. 165–190.
1067. TATSUKA, K., MORIMOTO, N. 1977: Tetrahedrite stability relations in the Cu-Fe-Sb-S system. — *The American Mineralogist* 62 (11–12), pp. 1101–1109.
1068. TSUCHIDA, T. 1994: ETA-DTA study of mechanically ground gibbsite. — *Thermochimica Acta* 231, (1–2), pp. 337–339.
1069. TAMAS, T., GHERGARI, L. 2003: Hydronium Jarosite from Iza Cave (Rodnei Mts., Romania). — *Acta Mineralogica et Petrographica Szegediensis, Abstract Series* 1, p. 102.
1070. TÁNAGO DEL, J. G., LA IGLESIA, Á., RIUS, J., SANTÍN, S. F. 2003: Calderonite, a new lead-iron-vanadate of the brackebuschite group. — *The American Mineralogist* 88 (11–12), pp. 1703–1708.

1071. TAYLOR, H. F. W. 1962a: Homogeneous and inhomogeneous mechanisms in the dehydroxylation of minerals. — *Clay Minerals Bulletin* 5 (28), pp. 45–55.
1072. TAYLOR, H. F. W. 1962b: The dehydration of hemimorphite. — *The American Mineralogist* 47 (7–8), pp. 932–944.
1073. TEDJAR, F., GUITTON, J. 1991: Structural modification on heat treatment of  $\alpha$ -MnO<sub>2</sub>. — *Thermochimica Acta* 181, pp. 13–22.
1074. THENG, B. K. G., HAYASHI, S., SOMA, M., SEYAMA, H. 1997: Nuclear magnetic resonance and X-ray photoelectron spectroscopic investigation of lithium migration in montmorillonite. — *Clays and Clay Minerals* 45 (5), pp. 718–723.
1075. THOMAS, P. S., HIRSCHAUSEN, D., WHITE, R. E., GUERBOIS, J. P., RAY, A. S. 2003: Characterisation of the oxidation products of pyrite by Thermogravimetric and Evolved Gas analysis. — *Journal of Thermal Analysis and Calorimetry* 72 (3), pp. 769–776.
1076. THREADGOLD, I. M. 1959: Hydromuscovite with 2M2 structure, from Mount Lyell, Tasmania. — *The American Mineralogist* 44 (5–6), pp. 488–494.
1077. TIEN, P. L. 1968: Hydrobasaluminite and basaluminite in Cabanis Formation (Middle Pennsylvanian), Southeastern Kansas. — *The American Mineralogist* 53 (5–6), pp. 722–723.
1078. TIEN, P. L., WAUGH, T. C. 1969: Thermal and X-ray studies on earthy vivianite in Graneros Shale Upper Cretaceous, Kansas. — *The American Mineralogist* 54 (9–10), pp. 1355–1362.
1079. TINSLEY, D. M., SHARP, J. H. 1971: Thermal analysis of manganese dioxide in controlled atmospheres. — *Journal of Thermal Analysis* 3 (1), pp. 43–48.
1080. TKÁČOVÁ, K., BALÁŽ, P., BASTL, Z. 1990: Thermal characterization of changes in structure and properties of chalcopyrite after mechanical activation. — *Thermochimica Acta* 170, pp. 277–288.
1081. TODOR, D. N. 1972: *Analiza Termica a Mineralelor*. — Editura Tehnica, Bucuresti, 279 p.
1082. TOMANEC, R., POPOV, S., VUČINIČ, D., LAZIČ, P. 1997: Vermiculite from Kopaonik (Yugoslavia) Characterization and Processing. — *Fizykochemiczne Problemy Mineralurgii* 31, pp. 247–254.
1083. TÖNSUAADU, K., PELT, J., BORISSOVA, M. 2005: Monitoring of the evolved gases in apatite-ammonium sulfate thermal reactions. — *Journal of Thermal Analysis and Calorimetry* 80 (3), pp. 655–658.
1084. TOWE, K., BRADLEY, W. F. 1967: Mineralogical constitution of colloidal “hydrous ferric oxides”. — *Journal of Colloid Interface Science* 24 (3), pp. 384–392.
1085. TRAUTH, N., LUCAS, J. 1968: Apport des Methodes thermiques dans l’étude des Minéraux argileux. — *Bulletin du Groupe Francais des Argiles* 19 (2), pp. 11–24.
1086. TRDLÍČKA, Z., HOFFMAN, V. 1965: Skorodit von Kutná Hora (Kuttenberg), Tschechoslowakei. — *Chemie der Erde* 24 (3–4), pp. 223–229.
1087. TROCHIM, H. D. 1967: Chlorite Minerale. — In: TRÖGER, P., BRATSCH, O. (eds): *Optische Bestimmung der gesteinsbildenden Minerale, Teil II*. Schweizerische Verlagsbuchhandlung, pp. 564–583.
1088. TSUSUE, A. 1967: Magnesian kutnahorite from Ryujima mine, Japan. — *The American Mineralogist* 52 (11–12), pp. 1751–1761.
1089. TSVETKOV, A. I., VALYASHIKHINA, E. P. 1953: Fibroferrite and melanterite. — *Doklady Akademii Nauk SSSR* 93 (2), pp. 343–346.
1090. TSVETKOV, A. I., VALYASHIKHINA, E. P. 1955: Termoanalitičeskie harakteristiki sulfatnih mineralov II. — *Trudy Instituta Geologičeskikh Nauk* 157, Petrografičeskaja Serija 45, pp. 30–107.
1091. TSVETKOV, A. I., VALYASHIKHINA, E. P. 1958: Termoanalitičeskie harakteristiki nekotoryh sulfidov železa i medi. — *Trudy Instituta Geologii Rudnykh Mestorozhdeniy Petrografii, Mineralogii i Geokhimii* 30, pp. 3–36.
1092. TSVETKOV, A. I., VALYASHIKHINA, E. P., PILOYAN, G. O. 1964: *Differentsialny termicheskii analiz karbonatnykh mineralov*. (Differential Thermal Analysis of Carbonate Minerals). — Nauka, Moscow, 167 p.
1093. TUTTI, F. L., DUBROVINSKY, L. S. L., NYGREN, M. L. 2000: High-temperature study and thermal expansion of phlogopite. — *Physics and Chemistry of Minerals* 27 (9), pp. 597–603.
1094. TUTTLE, O. F. 1949: The variable inversion temperature of quartz as a possible geologic thermometer. — *The American Mineralogist* 34 (9–10), pp. 723–730.
1095. UEHARA, M., VANZAKI, A., TSUTSUM, S. 1997: Surite: its structure and properties. — *The American Mineralogist* 82 (3–4), pp. 416–422.
1096. ULLRICH, B., ADOLPHI, P., SCHOMBURG, J., ZWAHR, H. 1987: Kombinierte thermoanalytische Untersuchungen an Zeolithen. Teil I.: Minerale der Natrolith-Gruppe. — *Chemie der Erde* 47 (3–4), pp. 283–293.
1097. ULLRICH, B., ADOLPHI, P., SCHOMBURG, J., ZWAHR, H. 1988a: Kombinierte thermoanalytische Untersuchungen an Zeolithen. Teil II.: Heulandit-Stilbit-Gruppe. — *Chemie der Erde* 48 (2.), pp. 141–154.
1098. ULLRICH, B., ADOLPHI, P., SCHOMBURG, J., ZWAHR, H. 1988b: Kombinierte thermoanalytische Untersuchungen an Zeolithen. Teil III: Mordenit, Laumontit, Chabasit, Faujasit. — *Chemie der Erde* 48 (3), pp. 245–253.
1099. UNDABEYTIA, T., NIR, S., RYTWO, G., SERBAN, C., MORILLO, E., MAQUEDA, C. 2002: Modeling adsorption-desorption processes of Cu on edge and planar sites of montmorillonite. — *Environmental Science and Technology* 36 (12), pp. 2677–2683.
1100. VEBLEN, D. R., GUTHRIE, JR. G. D., LIVI, K. J. T., REYNOLDS, JR. R. C. 1990: High-resolution transmission electron microscopy and electron diffraction of mixed-layer illite/smectite: experimental results. — *Clays and Clay Minerals* 38 (1), pp. 1–13.
1101. VEDDER, W., WILKINS, R. W. T. 1969: Dehydroxylation and rehydroxylation, oxidation and reduction of micas. — *The American Mineralogist* 54 (3–4), pp. 482–509.
1102. VENIALE, F. 1962: Effetto delle fibre sul comportamento all A.T.D. di un minerale de gruppo serpentino. — *Rendiconti della Società Mineralogica Italiana* 18, pp. 277–290.
1103. VENIALE, F., VAN DER MAREL, H. W. 1963: An intersratified saponite-swelling chlorite mineral as a weathering product of lizardite rock from St. Margherita Staffora (Pavia Province), Italy. — *Beiträge zur Mineralogie und Petrographie* 9 (3), pp. 198–245.
1104. VENIALE, F., VAN DER MAREL, H. W. 1968: A regular talc-saponite mixed-layer mineral from Ferriere, Nure Valley (Piacenza Province, Italy). — *Contributions to Mineralogy and Petrology* 17 (3), pp. 237–254.
1105. VICZIÁN, I. 1997: Hungarian investigation on the “Zempleni” illite. — *Clays and Clay Minerals* 45 (1), pp. 114–115.
1106. VICZIÁN, I. 2000: History of mineralogical investigations of the Füžerradvány “illite”, near Sárospatak, Hungary. — *Acta Geologica Hungarica* 43 (4), pp. 493–500.

1107. VINCENT, E. A., WRIGHT, J. B., CHEVALLIER, R., MATHIEW, S. 1957: Heating experiments on some natural titaniferrous magnetites. — *Mineralogical Magazine* 31 (239), pp. 624–655.
1108. VIZCAYNO, C., CASTELLÓ, R., RANZ, I., CALVO, B. 2005: Some physico-chemical alterations caused by mechanochemical treatments in kaolinites of different structural order. — *Thermochimica Acta* 428 (1–2), pp. 173–183.
1109. VOCHTEN, R., DE GRAVE, E., PELSMAEKERS, J. 1984: Mineralogical study of bassettite in relation to its oxidation. — *The American Mineralogist* 69 (9–10), pp. 967–978.
1110. VYAZOVKIN, S., LINERT, W. 1995: Kinetic analysis of reversible thermal decomposition of solids. — *International Journal of Chemical Kinetics* 27 (1), pp. 73–84.
1111. WACŁAWSKA, I., PIECZKA, A., OLKIEWICZ, St., ŻABIŃSKI, W. 1998: Thermal decomposition of axinite. — *Journal of Thermal Analysis and Calorimetry* 52 (2), pp. 413–423.
1112. WACŁAWSKA, I., STOCH, L., PAULIK, J., PAULIK, F. 1988: Thermal decomposition of colemanite. — *Thermochimica Acta* 126, pp. 317–328.
1113. WAGNER-BEEGER S. 1961: Zur Charakterisierung von Niederlausitzer Weichbraunkohlen durch Differentialthermoanalysen. Beitrag zur kritischen Beurteilung von Differetialthermoanalysen an organischen Substanzen. — *Freiberger Forschungshefte, A* 194, pp. 1–68.
1114. WALENTA, K. 1972: Grimselit, ein neues Kalium-Natrium-Uranylkarbonat aus dem Grimselgebiet (Oberhasli, Kt. Bern, Schweiz). — *Schweizerische Mineralogische Petrographische Mitteilungen* 52 (1), pp. 93–108.
1115. WALKER, G. F., COLE, W. F. 1957: The vermiculite minerals. — In: MACKENZIE, R. . (ed.): *The differential thermal investigation of clays*. Mineralogical Society, London, pp. 191–206.
1116. WALTER, D., BUXBAUM, G., LAQUA, W. 2001: The mechanism of the thermal transformation from goethite to hematite. — *Journal of Thermal Analysis and Calorimetry* 63 (3), pp. 733–748
1117. WAMBEKE, L. VAN 1971: The uranium-bearing mineral bolivarite: new data and a second occurrence. — *Mineralogical Magazine* 38 (296), pp. 418–423.
1118. WANG, L., ZHANG, M. REDFERN, S. A. T., ZHANG, Z. 2002: Dehydroxylation and transformations of the 2:1 phyllosilicate pyrophyllite at elevated temperatures: An infrared spectroscopic study. — *Clays and Clay Minerals* 50 (2), pp. 272–283.
1119. WARDLE, R., BRINDLEY, G. W. 1972: The crystal structures of pyrophyllite 1Tc, and of its dehydroxylate. — *The American Mineralogist* 57 (5–6), pp. 732–750.
1120. WARNE, S. St. J. 1976: Siderite, differential thermal analysis — curve modifications with progressive dilution and furnace atmosphere changes. — *Chemie der Erde* 35 (3), pp. 251–255.
1121. WARNE, S. St. J. 1977: Carbonate mineral detection by variable atmosphere differential thermal analysis. — *Nature* 269 (5630), p. 678.
1122. WARNE, S. St. J. 1978: Proben-Abhängigkeit (PA) curves and simple anhydrous carbonate minerals. — *Journal of Thermal Analysis* 14 (3), pp. 325–330.
1123. WARNE, S. St. J. 1980: Predictable curve modifications and variable atmosphere DTA: uses in diagnostic mineralogy, particularly for carbonates. — *Proceedings of the Sixth International Conference on Thermal Analysis, Bayreuth 1980. July 6–12*, pp. 283–288.
1124. WARNE, S. St. J. 1981: Improvements and comments on the method of “Quantitative estimation of magnesite by differential thermal analysis”. — *Journal of Thermal Analysis* 20 (1), pp. 225–228.
1125. WARNE, S. St. J. 1985: The assessment of the coal-organic matter contents of geological materials by differential thermal analysis. — *Thermochimica Acta* 86, pp. 337–342.
1126. WARNE, S. St. J. 1986: Applications of variable atmosphere DTA in CO<sub>2</sub> to improved detection and content evaluation of anhydrous carbonates in mixtures. — *Thermochimica Acta* 109 (1), pp. 243–252.
1127. WARNE, S. St. J. 1987: Applications of thermal analysis to carbonate mineralogy. — *Thermochimica Acta* 110, pp. 501–511.
1128. WARNE, S. St. J., 1990: Fossil fuels: an overview of trends, methods and applications of thermal analysis. — *Thermochimica Acta* 166, pp. 343–349.
1129. WARNE, S. St. J., 1991: Thermal analysis — a resurgence in the earth sciences: With applied, industrial and environmental aspects. — *Thermochimica Acta* 192, pp. 19–28.
1130. WARNE, S. St. J., 1996: Thermal analysis and coal assessment: an overview with new developments. — *Thermochimica Acta* 272, pp. 1–9.
1131. WARNE, S. St. J., BAYLISS, P. 1962: DTA of cerussite. — *The American Mineralogist* 47 (9–10), pp. 1011–1023.
1132. WARNE, S. St. J., DUBRAWski, J. V. 1988: Potential for coal calorific value corrections, dependent on the carbonate mineral type present. — *Journal of Thermal Analysis* 33 (2), pp. 435–440.
1133. WARNE, S. St. J., FRENCH, D. H. 1984a: Siderite, pyrite and magnesite identification in oil shale by variable atmosphere DTA. — *Thermochimica Acta* 79, pp. 131–137.
1134. WARNE, S. St. J., FRENCH, D. H. 1984b: The application of simultaneous DTA and TG to some aspects of oil shale mineralogy. — *Thermochimica Acta* 76 (1–2) pp. 179–200.
1135. WARNE, S. St. J., FRENCH, D. H. 1984c: The decomposition of anhydrous carbonate minerals in coal and oil shale ashes produced at temperatures of 400 and 575 °C. — *Thermochimica Acta* 75 (1–2), pp. 139–149.
1136. WARNE, S. St. J., MACKENZIE, R. C. 1971: The thermal dissociation of some carbonate minerals. — *Journal of Thermal Analysis* 3 (1), pp. 49–55.
1137. WARNE, S. St. J., MITCHELL, B. D. 1979: Variable atmosphere DTA in identification and determination of anhydrous carbonate minerals in soils. — *European Journal of Soil Science* 30 (1), pp. 111–116.
1138. WARNE, S. St. J., MORGAN, D. J., MIŁODOWSKI, A. E. 1981: Thermal analysis studies of the dolomite, ferroan dolomite, ankerite series. Part I: Iron content recognition and determination by variable atmosphere DTA. — *Thermochimica Acta* 51 (2–3), pp. 105–111.
1139. WEBB, J. A., FINLAYSON, B. L. 1987: Incorporation of Al, Mg, and water in opal-A; evidence from speleothems. — *The American Mineralogist* 72 (11–12), pp. 1204–1210.
1140. WEBER, J. N., GREER, R. T. 1965: Dehydration of serpentine: heat of reaction and reaction kinetics at p<sub>H<sub>2</sub>O</sub> = 1 atm. — *The American Mineralogist* 50 (3–4), pp. 450–464.

1141. WEIR, A. H., GREENE-KELLY, R. 1962: Beidellite. — *The American Mineralogist* 47 (1–2), pp. 137–146.
1142. WEISSENBORN, P. K., DUNN, J. G., WARREN, L. J. 1994: Quantitative thermogravimetric analysis of hematite, goethite and kaolinite in Western Australian iron ores. — *Thermochimica Acta* 239 (1), pp. 147–156.
1143. WEISZBURG, T. G., SZŐÖR, GY., VINCZE, P., LOVAS, GY., BALLA, M. 2000: Mellite ( $\text{Al}_2\text{C}_{12}\text{O}_{12} \cdot 16\text{H}_2\text{O}$ ) from Csordakút Mine, Bicske, Hungary: a new mineral for the Carpathian–Pannonian Region. — *Acta Mineralogica et Petrographica Szegediensis* 41 (Supplementum), (*Abstracts, Minerals of the Carpathians International Conference, Miskolc, March 9–10, 2000.*) p. 125.
1144. WELLS, M. A., GILKES, R. J., SINGH, B., FITZPATRICK, R. W. 1992: Differential X-Ray Diffraction (DXRD) of poorly crystalline materials in synthetic, metal-substituted goethite and hematite. — *Zeitschrift für Pflanzenernährung und Bodenkunde* 155 (5), pp. 423–429.
1145. WELLS, N., CHILDS, C. W. 1988: Flow behaviour of allophane and ferrihydrite under Shearing Forces. — *Australian Journal of Soil Research* 26 (1), pp. 145–152.
1146. WELTNER, M. 1959a: Derivatographische investigation of the anthracite of the Don. — *Nature* 183 (4670), pp. 1254–1256.
1147. WELTNER, M. 1959b: Über die derivative thermogravimetrische Analyse von Ligniten, Braun- und Steinkohlen II. — *Acta Chimica Academiae Scientiarum Hungaricae (Budapest)* 21 (1), pp. 1–33.
1148. WELTNER, M. 1961: Die derivatographische Analyse der thermischen Zersetzung von Kohlen. — *Brennstoff Chemie* 42 (2), 40–46.
1149. WELTNER, M. 1962: Über die derivatographische Untersuchung des Extraktionsvorganges von unbehandelten und thermisch vorbehandelten Steinkohlen. — *Acta Chimica Academiae Scientiarum Hungaricae (Budapest)* 31 (4), pp. 449–472.
1150. WELTNER, M. 1965: Über die derivatographische Untersuchung der Verbrennung von Kohlen. — *Acta Chimica Academiae Scientiarum Hungaricae (Budapest)* 43 (1), pp. 89–98.
1151. WESOŁOWSKI, M. 1984: Thermal decomposition of talc: A review. — *Thermochimica Acta* 78 (1–3), pp. 395–421.
1152. WETZEL, R. 1973: Chemismus und physikalische Parameter einiger Chlorite aus der Grünschieferfazies. — *Schweizerische Mineralogische und Petrographische Mitteilungen* 53 (2), pp. 273–298.
1153. WHITE, W. A. 1953: Allophanes from Lawrence County Indiana. — *The American Mineralogist* 38 (3–4), pp. 279–281
1154. WICKS, F. J. 2000: Status of the reference X-ray powder-diffraction patterns for the serpentine minerals in the PDF database – 1997. — *Powder Diffraction* 15 (1), pp. 42–50.
1155. WIECZOREK-CIUROWA, K., PAULIK, J., PAULIK, F. 1980: Influence of foreign materials upon the thermal decomposition of dolomite, calcite and magnesite. Part I. Influence of sodium chloride. — *Thermochimica Acta* 38 (2), pp. 157–164.
1156. WIEDEMANN, H. G., BAYER, G. 1987: Note on the thermal decomposition of dolomite. — *Thermochimica Acta* 121, pp. 479–485.
1157. WIEDEMANN, G., BAYER, G. 1988: Kinetics of the formation of whewellite and weddellite by displacement reactions. — *Journal of Thermal Analysis* 33 (3), pp. 707–718
1158. WIEGMANN, J., HORTE, C. H., KRANZ, G. 1966: Mineralanalytische Untersuchungen an Gliedern der Montmorillonitgruppe. — *Berichte der Deutschen Gesellschaft für Geologische Wissenschaften, Reihe B: Mineralogie und Lagerstättenforschung* 11 (3), pp. 317–342.
1159. WIEWIORA, A., SZPILA, K. 1975: Nickel containing regularly interstratified chlorite-saponite from Szklary Lower Silesia, Poland. — *Clays and Clay Minerals* 23 (2), pp. 91–96.
1160. WILBURN, F. W., SHARP, J. H. 1993: The bed-depth effect in the thermal decomposition of carbonates. — *Journal of Thermal Analysis* 40 (1), pp. 133–140.
1161. WILBURN, F. W., SHARP, J. H., TINSLEY, D. M., MCINTOSH, R. M. 1991: The effect of procedural variables on TG, DTG and DTA curves of calcium carbonate. — *Journal of Thermal Analysis* 37 (9), pp. 2003–2019.
1162. WILSON, L. J., MIKHAIL, S. A. 1989: Investigation of the oxidation of skutterudite by thermal analysis. — *Thermochimica Acta* 156 (1), pp. 107–115.
1163. WILSON, M. J. 1970: A study of weathering in a soil derived from a biotite-hornblende rock. I. Weathering of biotite. — *Clay Minerals* 8 (3), pp. 291–303.
1164. WILSON, M. J., BAIN, D. C., MITCHELL, W. A. 1968: Saponite from the Dalradian metalimestone of N-E Scotland. — *Clay Minerals* 7 (3), pp. 343–349.
1165. WILSON, M. J., BERROW, M. L., MCHARDY, W. J. 1970: Lithiophorite from the Lecht mines, Tomintoul, Bannffshire — *Mineralogical Magazine* 37 (289), pp. 618–623.
1166. WITTELS, M. 1951: The structural desintegration of some amphiboles. — *The American Mineralogist* 36 (11–12), pp. 851–858.
1167. WITTELS, M. 1952: The structural desintegration of some amphiboles. — *The American Mineralogist* 37. (1–2), pp. 28–36.
1168. WŁODYKA, R., BZOWSKA, G., WRZALIK, R. 2004: The thermal behaviour of fluorapophyllite from the Międzyrzecze sill near Bielsko-Biała in the Polish Carpathians. — *Neues Jahrbuch für Mineralogie, Monatshefte* 8, pp. 337–356.
1169. WOJCIECHOWSKA, R., WOJCIECHOWSKI, W., KAMIŃSKI, J. 1988: Thermal decompositions of ammonium and potassium alums. — *Journal of Thermal Analysis* 33 (2), pp. 503–509.
1170. WOLSKA, E. 1981: The structure of hydrohematite. — *Zeitschrift für Kristallographie* 154 (1–2), pp. 69–75.
1171. WOLSKA, E., SCHWERTMANN, U. 1989: Nonstoichiometric structures during dehydroxylation of goethite. — *Zeitschrift für Kristallographie* 189 (3–4), pp. 69–75.
1172. WOLSKA, E., SZAJDA, W., PISZORA, P. 1992: Determination of solid solution limits based on the thermal behaviour of aluminium substituted iron hydroxides and oxides. — *Journal of Thermal Analysis* 38 (9), pp. 2115–2122.
1173. WULFSBERG, G. 1987: *Principles of Descriptive Inorganic Chemistry*. — Brooks/Cole Publishing, Monterey CA 464 p.
1174. XIA, M. S., HU, C. H., XU, Z. R., YE, Y., ZHOU, Y. H., XIONG, L. 2004: Effects of copper-bearing montmorillonite (Cu-MMT) on *Escherichia coli* and Diarrhea on Weanling Pigs. — *Asian-Australasian Journal of Animal Sciences* 17 (12), pp. 1712–1716.
1175. YAMAZAKI, A., MATSUMOTO, H., OTSUKA, R. 1988: Fibrous zeolite. Thermal stability of fibrous zeolites. — *Nendo Kagaku* 28 (3), pp. 143–154.
1176. YAMAZAKI, A., INOUE, Y., KOIKE, M., SAKAMOTO, T., OTSUKA, R. 1993: Preparation and dehydration behaviour of thomsonite with ideal chemical composition — *Journal of Thermal Analysis* 40 (1), pp. 85–97.
1177. YARIV, S. 1992: Wettability of Clay Minerals. — In: SCHRADER, M. E., LOEB, G. I. (eds): *Modern approaches to wettability: Theory and applications*. Plenum Publishing Corporation, New York, pp. 279–3 26.

1178. YARIV, S., SHOVAL, S. 1975: Nature of Interaction between water-molecules and kaolin-like layers in hydrated halloysite. — *Clays and Clay Minerals* 23 (6), pp. 473–474.
1179. YARIV, S., MENDELOVICI, E., VILLALBA, R. 1981: Interactions between the iron and the aluminum minerals during the heating of Venezuelan lateritic bauxites. II. X-ray diffraction study. — *Thermochimica Acta* 45 (3), pp. 339–348.
1180. YEN, F. S., CHEN, W. C., YANG, J. M., HONG, C. T. 2002: Crystallite size variations of nanosized  $\text{Fe}_2\text{O}_3$  powders during  $\alpha$ - to  $\alpha'$ -phase transformation. — *Nano Letters* 2 (3), pp. 245–252.
1181. YENER, N., ÖNAL, M., ÜSTÜNÝTYK, G., SARÝKAYA, Y. 2007: Thermal behavior of a mineral mixture of sepiolite and dolomite. — *Journal of Thermal Analysis and Calorimetry* 88 (3), pp. 813–817.
1182. YESKIS, D., KOSTER VAN GROOS, A. F., GUGGENHEIM, S. 1985: The dehydroxylation of kaolinite. — *The American Mineralogist* 70 (1–2), pp. 159–164.
1183. YU, J. Y., PARK, M., KIM, J. 2002: Solubilities of synthetic schwertmannite and ferrihydrite. — *Geochemical Journal* 36 (2), pp. 119–132.
1184. ŻABIŃSKI, W., WACŁAWSKA, I., PALUSZKIEWICZ, C. 1996: Thermal decomposition of vesuvianite. — *Journal of Thermal Analysis* 46 (5), pp. 1437–1447.
1185. ZAGHIB, K., SONG, X., KINOSHITA, K. 2001: Thermal analysis of the oxidation of natural graphite: isothermal kinetic studies. — *Thermochimica Acta* 371 (1–2), pp. 57–64.
1186. ŽÁŮÁK, L., POVONDRA, P. 1977: Sedimentary rhodochrosite from the Upper Proterozoic of chvaletice (Czechoslovakia). — *Acta Universitatis Carolinae – Geologica, Slavik* 1 (3–4), pp. 199–211.
1187. ZHAO, J., HUGGINS, F. E., FENG, Z., HUFFMAN, G. P. 1994: Ferrihydrite: surface structure and its effects on phase transformation. — *Clays and Clay Minerals* 42 (6), pp. 737–746.
1188. ŽIVKOVIĆ, Ž. D., BLEČIĆ, D. 1988: Comparative thermal analysis of commercial and low-grade bauxites. — *Journal of Thermal Analysis* 33 (2), pp. 413–419.
1189. ŽIVKOVIĆ, Ž. D., MILOSAVLJEVIĆ, N., ŠESTÁK, J. 1990: Kinetics and mechanism of pyrite oxidation. — *Thermochimica Acta* 157 (2), pp. 215–219.
1190. ZODROW, E. L., WILTSHIRE, J., MCCANDLISH, K. 1979: Hydrated sulfates in the Sidney coalfield of Cape Breton, Nova Scotia. II. Pyrite and its alteration products. — *The Canadian Mineralogist* 17 (1), pp. 63–70.
1191. ZWAHR, H., SCHOMBURG, J., SCHMIDT, D. 1978: Mineralogische Untersuchungen am Variscit vom Pansberg bei Horschach (Lausitz). — *Chemie der Erde* 37 (2), pp. 165–171.
1192. ZWICKER, W. K., GROENEVELD MEIER, W. O. J., JAFFE, H.W. 1962: Nsutite — a widespread manganese oxide mineral. — *The American Mineralogist* 47 (3–4), pp. 246–266.
1193. ICTAC Nomenclature of Thermal Analysis 2004 — <http://www.ictac.org>.
1194. Nomenclature Committee of the ICTA 1972: Nomenclature in thermal analysis. Part II. — *Journal of Thermal Analysis* 4 (3), pp. 640–641.
1195. webside [www.igw.uni-jena.de/mineral/start.html](http://www.igw.uni-jena.de/mineral/start.html) 2005-09-26



## MINERAL AND ROCK INDEXES

- abucumalite — 132
- acanthite — 44, 51, 55
- actinolite — 95
- adamite — 132
- adamsite — 120
- akaganeite — 67
- alabandite — 50, 55
- allanite — 93
- allevardite — 86, 88
- allophane — 37, 44, 59, 71
- alstonite — 45, 120
- aluminite — 36, 40, 46, 121, 128, 129, 130
- alumogel — 37, 67
- alumo-goethite — 65, 66, 137
- alumohydrocalcite — 120
- alums — 130
- alunite — 121, 124, 127, 128, 129, 130
- alunogen — 40, 121, 124, 129, 130
- amblygonite — 132
- ameghinite — 133
- amicite — 106, 107
- ammonioalunite — 129
- ammonioleucite — 107
- ammoniojarosite — 129
- amosite — 95
- amphibole — 94, 95
- analcime — 36, 98, 99, 107
- anapaite — 132
- ancylite — 120
- anglesite — 40, 45, 121, 130
- anhydrite — 40, 121, 129, 130
- ankerite — 41, 43, 111, 114, 115, 120
- annabergite — 132, 133
- anorthite — 44
- anthracite — 135
- antigorite — 68, 72, 73, 74
- antimonite — 54
- antophyllite — 95
- aphrosiderite — 85
- apophyllite — 89, 90, 91
- aragonite — 38, 45, 107, 108, 113, 120
- arcaneite — 45, 130
- arfvedsonite — 95
- argentite — 44, 45, 50, 54, 55
- argentojarosite — 129, 130
- arrojadite — 132
- arsenopyrite — 50, 54, 55
- artinite — 119, 120
- asbolane — 67
- ascharite — 133
- astrachanite — 129, 130
- atacamite — 134
- augelite — 132, 133
- aurichalcite — 119, 120
- autunite — 132, 133
- axinite — 93, 94
- azurite — 40, 117, 119, 120
- bakerite — 93
- baraëite — 132
- barbertonite — 120
- barite — 37, 130
- baritocalcite — 120
- barrandite — 132
- barrerite — 106
- basaluminite — 121, 129, 130
- bassanite — 62, 129, 130
- bassetite — 133
- bastnäsité — 119, 120
- bauxite — 23, 62, 64, 65, 66, 67, 137
- beidellite — 42, 74, 80
- belovite — 132
- bentonite — 29, 80
- berbankite — 120
- berlinite — 132, 133
- bermanite — 132
- bernalite — 40, 42, 61, 63
- berthierine — 74
- beyerite — 119, 120
- bieberite — 40, 130
- bikitaite — 106, 107
- biotite — 75, 81, 82, 83
- biotite-chlorite — 88
- birnessite — 60, 61
- birôza — 132
- bischofite — 45, 133, 134
- bismuthinite — 54, 55
- bismutite — 40, 50, 119, 120
- bixbyite — 60
- bloedite — 45, 121, 129, 130
- bobierrite — 132, 133
- boehmite — 23, 42, 43, 61, 62, 64, 65, 66, 67, 129, 137
- bolivarite — 132, 133
- boracite — 133
- borax — 133
- bornite — 44, 51, 54, 55
- bosporite — 133
- botryogen — 130
- boulangerite — 54
- bournonite — 51, 55
- brasilianite — 132
- braunite — 60, 61, 93
- breunnerite — 110, 119, 120
- brewsterite — 106, 107
- britholite — 132
- brochantite — 130
- brucite — 40, 42, 61, 63, 68
- brugnatellite — 120
- brushite — 132
- buddingtonite — 107
- bukovskyite — 132
- buserite — 60, 61
- calcite — 22, 40, 41, 42, 43, 46, 61, 63, 64, 65, 67, 76, 84, 88, 92, 107, 108, 110, 111, 112, 113, 114, 115, 116, 120, 125, 131
- calderonite — 133
- caledonite — 120
- cancrinite — 120
- caoxite — 135
- carbocernaite — 120
- carbonate-apatite — 132
- carletonite — 120
- carnallite — 45, 133, 134
- carrboydite — 120
- carrollite — 55
- cefarovite — 132
- celadonite — 75, 84, 109
- celestine — 40, 130
- cerussite — 40, 45, 107, 108, 110, 111, 120
- chabasite — 36, 44, 105, 106, 107
- chalcantite — 38, 40, 41, 42, 45, 121, 122, 129, 130
- chalcocite — 44, 50, 51, 54, 55
- chalcophanite — 60
- chalcopyrite — 44, 49, 50, 51, 54, 55
- chalcostibite — 51
- chamosite — 42, 85
- charoite — 94, 95
- chiavennite — 107
- chlorite — 42, 44, 82, 85, 86, 88, 91, 112, 114
- chlorite-vermiculite — 87, 88
- chloromagnesite — 45
- chrysocolla — 94
- chrysotile — 68, 72, 73, 74
- cinnabar — 22, 43, 50, 51, 53
- clausenthalite — 50
- clinochlore — 85
- clinoptilolite — 36, 103, 107
- coal — 43, 135, 136
- cobaltite — 50, 54, 55
- colemanite — 40, 133
- collinsite — 132
- cookeite — 85
- copiapite — 129, 130

coquimbite — 130  
 cordierite — 76, 78, 89, 94  
 cordilyte — 120  
 coronadite — 60, 61  
 cotsubeite — 85  
 covellite — 44, 50, 51, 54, 55  
 cowlesite — 106  
 crandallite — 25, 132  
 cristobalite — 44, 55, 56, 74, 75, 76, 78, 80, 89, 90, 94  
 crocidolite — 95  
 cronstedtite — 68, 74  
 cryolite — 45, 134  
 cryptomelane — 60, 61  
 chrysocolla — 44  
 cubanite — 55  
 cyanotrichite — 130  
 dachiardite — 106  
 dahlite — 132  
 dawsonite — 44, 45, 117, 119, 120  
 deficient boehmite — 62  
 delessite — 85  
 desmite — 107  
 destinezite — 132  
 deweylite — 74  
 diadochite — 44, 131, 132, 133  
 diaspora — 64, 65, 66, 137  
 dickite — 53, 68, 69, 70  
 digenite — 50, 51, 55  
 diopside — 94  
 djurleite — 51  
 dolomite — 41, 43, 52, 62, 84, 111, 112, 113, 114, 115, 120  
 donbassite — 85  
 dufrenite — 132  
 dundasite — 119, 120  
 dypingite — 118  
 eardleyerite — 120  
 edingtonite — 98, 107  
 elisavetite — 67  
 elite — 132  
 enargite — 55  
 enstatite — 44  
 epidesmine — 107  
 epidote — 91, 93  
 epistilbite — 106, 107  
 epsomite — 38, 45, 121, 129, 130, 133  
 erionite — 105, 107  
 erythrite — 132, 133  
 eucairite — 54  
 evansite — 132, 133  
 ezcurrite — 133  
 falcondoite — 42, 68  
 faujasite — 106, 107  
 felsőbányaite — 121  
 ferroxyhyte — 67  
 ferrierite — 106  
 ferrihydrite — 37, 57, 58, 59, 60  
 ferroselite — 54  
 fibroferrite — 90, 129, 130  
 fireclay — 68, 69, 70  
 florencite — 132  
 fluorite — 134  
 forsterite — 44  
 fossil resins — 140  
 frankeite — 54  
 gadolinite — 93  
 galena — 50, 54, 111  
 garnierite — 42  
 garronite — 106  
 gaylussite — 119, 120  
 germanite — 55  
 gersdorffite — 50, 54, 55  
 gibbsite — 23, 27, 34, 40, 42, 61, 62, 65, 66, 67, 137  
 gismondine — 100, 107  
 glaserite — 45, 121, 129, 130  
 glauberite — 45, 121, 129, 130  
 glauconite — 35, 75, 84  
 glaucophane — 95  
 glaudiusite — 132  
 gmelinite — 104, 105, 107  
 gobbinsite — 106  
 goethite — 27, 42, 57, 62, 64, 65, 66, 79, 94, 109, 112, 128  
 gonnardite — 96, 97, 107  
 gorgeixite — 131, 132, 133  
 görgeyte — 121  
 goslarite — 38, 40, 129, 130  
 graphite — 43, 48, 49, 120  
 greenalite — 42, 74  
 greenockite — 50, 55  
 greigite — 55  
 grimselite — 120  
 guanajuatite — 54  
 gypsum — 39, 45, 112, 121, 125, 129, 130  
 haidingerite — 132, 133  
 halite — 45, 113, 133, 134  
 halloysite — 34, 68, 69, 71  
 halotrichite — 126, 130  
 harmotome — 101, 107  
 hauerite — 54, 55  
 hausmannite — 44, 60, 61  
 heazlewoodite — 50  
 hectorite — 74  
 hematite — 44, 46, 57, 58, 65, 74, 80, 94, 109  
 hematogelite — 44, 57  
 hemimorphite — 44, 93, 94  
 herzenbergite — 44, 45, 51  
 heulandite — 102, 103, 107  
 hexahydrite — 121, 124, 125, 130  
 hibschite — 93  
 hillebrandite — 95  
 hinsdalite — 132  
 hisingerite — 71  
 hollandite — 61  
 hornblende — 95  
 hornesite — 132, 133  
 humboldtine — 134, 135  
 huntite — 111, 113, 120  
 hurlbutite — 132  
 hyalophane — 107  
 hydroantigorite — 73, 74  
 hydrobasaluminite — 121, 129, 130  
 hydrobiotite — 81, 82  
 hydroboracite — 133  
 hydrocalcite — 120  
 hydrocerussite — 119, 120  
 hydrogrossular — 93  
 hydrohonessite — 120  
 hydromagnesite — 118, 120  
 hydromica — 31, 41, 44, 83, 84  
 hydromuscovite — 83, 84  
 hydroniumjarosite — 129, 130  
 hydrotalcite — 118, 120  
 hydroxylapatite — 132  
 hydrozincite — 119, 120  
 illite — 35, 42, 52, 64, 75, 83, 84, 87, 88, 112, 114, 124  
 illite-montmorillonite — 87  
 inderite — 133  
 interstratified chlorite-saponite — 88  
 inyoite — 133  
 iowaite — 120, 134  
 iquiqueite — 133  
 jalpaite — 51, 55  
 jamesonite — 54  
 jarosite — 40, 121, 128, 129, 130  
 jokukoite — 130  
 kaatialaite — 132  
 kaemmererite — 85  
 kainite — 45, 130, 134  
 kaliborite — 133  
 kalicinite — 45, 108, 116, 120  
 kaňkite — 132, 133  
 kaolinite — 17, 23, 24, 25, 26, 34, 41, 42, 43, 44, 52, 61, 62, 65, 66, 68, 69, 70, 71, 72, 91, 112, 124, 128, 131, 137, 139, 140  
 kaolinite-smectite — 88  
 katoite — 93  
 kemmlitzite — 132  
 kernite — 133  
 kershenite — 132  
 kieserite — 38, 39, 40, 121, 129, 130  
 kingite — 132  
 kintoreite — 132  
 kischtymite — 119, 120  
 klockmannite — 54  
 konyaite — 129  
 kutnahorite — 41, 109, 111, 115, 116, 120  
 langbeinite — 45, 121, 130  
 lansfordite — 119, 120  
 laumontite — 99, 100, 107  
 lavendulaite — 133  
 lazulite — 44, 45, 130, 131, 132  
 leadhillite — 120  
 ledikite — 42, 75  
 leonhardite — 99, 100, 107  
 leonite — 45, 129, 130  
 lepidocrocite — 64, 65  
 lepidolite — 75, 83  
 leuchtenbergite — 85  
 leucite — 45, 82, 83, 99  
 levyne — 106, 107  
 libethenite — 132  
 lindbergite — 135  
 linnaeite — 54  
 lithiophorite — 67  
 lithiophyllite — 132  
 lizardite — 72, 74  
 loewigite — 45, 130  
 löllingite — 54, 55  
 loweite — 121, 129, 130  
 ludlamite — 132  
 luneburgite — 132  
 macallisterite — 133  
 maghemite — 46

magnesite — 40, 41, 107, 109, 111, 112, 113, 120  
 magnetite — 43, 44, 46, 57  
 malachite — 117, 119, 120  
 mallardite — 40, 121, 130  
 manasseite — 120  
 manganite — 42, 60, 64, 65  
 manganocalcite — 108, 120  
 manganosiderite — 120  
 manganosite — 60, 61  
 mansfieldite — 132  
 marcasite — 44, 50, 51, 53, 54, 55  
 mascagnite — 40, 121, 122, 130  
 massicote — 45  
 matildite — 54  
 mckinstryite — 51  
 melanterite — 38, 40, 121, 123, 129, 130  
 mellite — 135  
 merlionite — 106  
 mesolite — 96, 107  
 meta-aluminite — 121  
 meta-alunogen — 121  
 meta-basaluminite — 121, 129  
 metasideronatrite — 130  
 metastrengite — 132  
 metatorbernite — 132  
 metavariscite — 132  
 metavivianite — 132  
 metazeunerite — 132  
 meteorite — 140  
 miargyrite — 54  
 millerite — 44, 45, 50, 51, 54, 55  
 mimetesite — 132  
 minnesotaite — 74  
 mirabilite — 45, 129, 130  
 molybdenite — 50, 54, 55  
 monacite — 132  
 monetite — 132  
 monheimite — 120  
 montebrasite — 132  
 montmorillonite — 29, 30, 31, 32, 33, 34, 35, 42, 52, 64, 65, 74, 76, 77, 78, 79, 92, 112, 114  
 moolooite — 135  
 moraesite — 132  
 mordenite — 36, 101, 102, 107  
 morenosite — 38, 40, 45, 121, 129, 130  
 mounanaite — 132  
 mountainite — 107  
 mullite — 44, 68, 70, 74, 75, 76, 78, 82, 83, 91  
 muscovite — 35, 42, 52, 75, 82, 83, 84, 138  
 nacholite — 120  
 nacrite — 69  
 nahcolite — 119, 120  
 natrite — 40, 45, 107, 108  
 natrolite — 36, 95, 96, 97, 98, 107  
 natural glasses — 139  
 naumannite — 54  
 nepheline — 107  
 nephrite — 95  
 nesquehonite — 117, 120  
 newberyite — 132  
 niccolite — 50, 55  
 nickeline — 54, 55  
 nickolsonite — 119, 120  
 nimitite — 85  
 niter — 45  
 nitratine — 45  
 nontronite — 42, 74, 80  
 nordstrandite — 34, 62  
 norsethite — 45, 120  
 nsutite — 60, 61  
 offretite — 106  
 oligonite — 120  
 olivenite — 132, 133  
 olivine — 44  
 opal — 37, 55, 56  
 orpiment — 50, 54, 55  
 otavite — 40, 107, 120  
 oxalite — 134  
 oxammite — 135  
 oxikersheinite — 132  
 palygorskite — 36, 39, 40, 88  
 pandermite — 133  
 paragonite — 82, 83  
 parascorodite — 132  
 parasepiolite — 75  
 parasite — 120  
 paratacamite — 134  
 paravauxite — 132  
 pargasite — 95  
 parisite — 119, 120  
 partheite — 107  
 paulingite — 106, 107  
 pectolite — 95  
 peisleyite — 132  
 pennantite — 85  
 pennine — 85  
 pentahydrate — 121  
 pentlandite — 50, 51, 54, 55  
 perlite — 37, 38, 136, 137  
 phillipsite — 100, 101, 107  
 phlogopite — 42, 75, 83  
 phosphates — 44  
 phosgenite — 120  
 phosphorite — 132  
 pickeringite — 129, 130  
 picromerite — 45, 130  
 picropharmacolite — 132  
 piemontite — 93  
 pinnoite — 133  
 pirrsonite — 120  
 pisanite — 130  
 pistomesite — 110, 119, 120  
 plombierite — 91  
 plumbocalcite — 120  
 plumbogummite — 132  
 plumbojarosite — 129, 130  
 plumbonacrite — 120  
 podolite — 120  
 polyhalite — 45, 129, 130  
 portlandite — 40, 41, 42, 61, 63  
 potassium-alum — 126, 127  
 prehnite — 90, 91  
 prochlorite — 85  
 protodolomite — 113, 120  
 proustite — 54, 55  
 pseudoboehmite — 34  
 pseudomalachite — 132  
 pseudothuringite — 85  
 psilomelane — 60, 61  
 pumpellyite — 91  
 pyrrargyrite — 54  
 pyrite — 46, 50, 52, 53, 77, 79, 90, 91, 92, 131  
 pyroaurite — 120  
 pyrochroite — 61  
 pyrolusite — 43, 44, 60, 65  
 pyrophyllite — 42, 43, 74, 75, 76  
 pyrrhotite — 44, 46, 50, 51, 53, 54, 55  
 quartz — 17, 19, 20, 44, 55, 56, 59, 80, 87, 138  
 rabdophane — 132  
 rammelsbergite — 51  
 rancieite — 60, 61  
 realgar — 51, 54, 55  
 rectorite — 86, 88  
 reevesite — 120  
 rhodosite — 107  
 rhodochrosite — 40, 41, 43, 107, 108, 109, 120  
 rhodonite — 95  
 richterite — 95  
 ripidolite — 85  
 rivadavite — 133  
 riversideite — 91  
 roggianite — 106, 107  
 romanechite — 60, 61  
 rosasite — 120  
 roselite — 132  
 rozenite — 121, 123, 129  
 römerite — 125, 126, 129, 130  
 rusakovite — 133  
 rutherfordine — 119, 120  
 sampleite — 132  
 sanderite — 121  
 sanjuanite — 132  
 santabarbaraite — 133  
 saponite — 42, 74, 80, 81  
 saponite-swelling chlorite — 87  
 sarabauite — 55  
 sárospatakite — 87, 88  
 sárospatite — 87, 88  
 sassolite — 40, 42, 61, 63, 133  
 sauconite — 74  
 scarbroite — 120  
 scawtite — 120  
 schoenite — 45, 129, 130  
 schröckingerite — 119, 120  
 schroderite — 132  
 schroedingerite — 120  
 scolecite — 98, 107  
 scorodite — 132, 133  
 scorzalite — 132  
 scutterudite — 54, 55  
 sepiolite — 88, 89  
 sericite — 35, 84  
 serpentine — 42, 44, 72, 73, 74  
 shandite — 51  
 siderite — 23, 24, 40, 41, 43, 107, 108, 109, 110, 115, 120  
 sideronatrite — 130  
 siderotile — 121  
 siegenite — 55  
 sigolite — 132  
 silver — 31, 45  
 sjögrenite — 120

skutterudite — 55  
 slavikite — 129  
 smectite — 29, 30, 33, 34, 42, 44, 76, 78, 79, 81, 84  
 smithsonite — 40, 107, 120  
 smythite — 55  
 soda — 24, 45, 120  
 soil, palaeosoil — 57, 108, 112, 125, 137, 138, 139, 140  
 sphalerite — 50, 51, 54  
 spinel — 44  
 spherocobaltite — 120  
 stannite — 54, 55  
 starkeyite — 121, 130  
 steigerite — 133  
 stellerite — 106  
 stephanite — 51, 55  
 stewartite — 132  
 stibnite — 43, 45, 51, 55  
 stichtite — 120  
 stilbite — 36, 50, 104, 106  
 strengite — 132  
 stromeyerite — 51, 55  
 strontianite — 40, 45, 107, 108, 120  
 strunzite — 132  
 struvite — 132  
 sudoite — 42, 85  
 sulphates — 40, 41, 50, 121, 129  
 sulphides — 27, 43, 44, 49, 50, 51, 52, 54  
 sulphur — 22, 43, 44, 45, 48, 52  
 surite — 120  
 svanbergite — 132  
 sylvite — 45, 134  
 syngenite — 45, 121, 129, 130,  
 synhysite — 120  
 szájbelyite — 133  
 szomolnokite — 121, 124, 130  
 tachyhydrite — 133, 134  
 takovite — 120  
 talc — 42, 74, 75, 76  
 talc-saponite — 87, 88  
 takanelite — 60  
 taranakite — 132  
 teallite — 51  
 tennantite — 51, 54, 55  
 teruggite — 133  
 teschemacherite — 116, 120  
 tetradymite — 45, 50, 51, 54  
 tetrahedrite — 49, 54, 55  
 tetranatrolite — 95, 96, 107  
 thaumasite — 120  
 thenardite — 45, 130  
 thermonatrite — 120  
 thomsonite — 97, 107  
 thuringite — 42, 85  
 titanohematite — 46  
 tobermorite — 90, 91  
 todorokite — 60, 61  
 topaz — 91, 93  
 torbernite — 132  
 tosudite — 86  
 tourmaline — 94  
 tremolite — 95  
 tridimite — 44, 55, 56  
 triphyllite — 132  
 troilite — 54, 55  
 trona — 45, 108, 119, 120  
 tschermigite — 127, 129, 130  
 tungstenite — 54  
 turquoise — 132  
 tuzlaite — 133  
 tyrolite — 132, 133  
 tysonite — 119, 120  
 ulexite — 133  
 ullmannite — 45, 50  
 uranothallite — 119, 120  
 vaesite — 51, 92, 93  
 vajdakite — 132  
 valleriite — 55  
 vanthoffite — 45, 121, 130  
 variscite — 132, 133  
 vashegyite — 132  
 vaterite — 45, 120  
 vermiculite — 81, 82  
 vernadite — 60, 61  
 vesuvianite — 91, 92, 93  
 violarite — 55  
 vivianite — 43, 130, 132, 133  
 voglite — 120  
 volkonskoite — 74  
 voltaite — 126  
 wad — 60, 61  
 wagnerite — 132  
 wairakite — 44, 106  
 wardite — 132  
 wavellite — 132, 133  
 weddellite — 135  
 wellsitite — 106  
 whewellite — 134, 135  
 wiartite — 120  
 witherite — 40, 45, 107, 108, 120  
 willemite — 44  
 woodhouseite — 132  
 wurtzite — 55  
 yugawaralite — 106, 107  
 zaratite — 120  
 zemkorite — 120  
 zeolites — 22, 26, 38, 44, 95, 96, 98, 100, 101, 102, 104, 106, 107  
 zepharovichite — 132  
 zincdibraunite — 61  
 zinwaldite — 75, 83  
 zoizite — 91, 93  
 zunyite — 91, 92, 93  
 zykaite — 132